Ground Improvement and Geosynthetics

Geotechnical Special Publication No. 207

Edited by
Anand J. Puppala
Jie Huang
Jie Han
Laureano R. Hoyos

ASCE
G-I GEO-INSTITUTE

GEOTECHNICAL SPECIAL PUBLICATION NO. 207

GROUND IMPROVEMENT AND GEOSYNTHETICS

PROCEEDINGS OF SESSIONS OF GEOSHANGHAI 2010

June 3–5, 2010
Shanghai, China

HOSTED BY
Tongji University
Shanghai Society of Civil Engineering, China
Chinese Institution of Soil Mechanics and Geotechnical Engineering, China

IN COOPERATION WITH
Alaska University Transportation Center, USA
ASCE Geo-Institute, USA
Deep Foundation Institute, USA
East China Architectural Design & Research Institute Company, China
Georgia Institute of Technology, USA
Nagoya Institute of Technology, Japan
Transportation Research Board (TRB), USA
The University of Newcastle, Australia
The University of Illinois at Urbana-Champaign, USA
The University of Kansas, USA
The University of Tennessee, USA
Vienna University of Natural Resources and Applied Life Sciences, Austria

EDITED BY
Anand Puppala
Jie Huang
Jie Han
Laureano R. Hoyos

ASCE

G-I GEO-INSTITUTE

Published by the American Society of Civil Engineers

Library of Congress Cataloging-in-Publication Data

GeoShanghai International Conference (2010)
Ground improvement and geosynthetics : proceedings of the GeoShanghai 2010 International Conference, June 3-5, 2010, Shanghai, China / edited by Anand Puppala ... [et al.].
p. cm. -- (Geotechnical special publication ; 207)
Includes bibliographical references and index.
ISBN 978-0-7844-1108-7
1. Soil stabilization--Congresses. 2. Geosynthetics--Congresses. 3. Earthwork--Materials--Congresses. I. Puppala, Anand J. II. Title.

TA749.G46 2010
624.1'51363--dc22 2010012100

American Society of Civil Engineers
1801 Alexander Bell Drive
Reston, Virginia, 20191-4400

www.pubs.asce.org

Any statements expressed in these materials are those of the individual authors and do not necessarily represent the views of ASCE, which takes no responsibility for any statement made herein. No reference made in this publication to any specific method, product, process, or service constitutes or implies an endorsement, recommendation, or warranty thereof by ASCE. The materials are for general information only and do not represent a standard of ASCE, nor are they intended as a reference in purchase specifications, contracts, regulations, statutes, or any other legal document. ASCE makes no representation or warranty of any kind, whether express or implied, concerning the accuracy, completeness, suitability, or utility of any information, apparatus, product, or process discussed in this publication, and assumes no liability therefore. This information should not be used without first securing competent advice with respect to its suitability for any general or specific application. Anyone utilizing this information assumes all liability arising from such use, including but not limited to infringement of any patent or patents.

ASCE and American Society of Civil Engineers—Registered in U.S. Patent and Trademark Office.

Photocopies and reprints.
You can obtain instant permission to photocopy ASCE publications by using ASCE's online permission service (http://pubs.asce.org/permissions/requests/). Requests for 100 copies or more should be submitted to the Reprints Department, Publications Division, ASCE, (address above); email: permissions@asce.org. A reprint order form can be found at http://pubs.asce.org/support/reprints/.

Copyright © 2010 by the American Society of Civil Engineers.
All Rights Reserved.
ISBN 978-0-7844-1108-7
Manufactured in the United States of America.

Preface

Ground improvement has been practiced for years as civil and transportation infrastructures often need to be constructed on unstable ground. Unstable ground included soft soils, expansive soils, collapsible soils, reclaimed soils, contaminated soils and others. Improvement methods include mechanical and hydraulic methods, chemical stabilization methods in both shallow and deep ground, reinforcement methods using geosynthetics and others. This Geotechnical Special Publication (GSP) "Ground Improvement and Geosynthetics" is one of the several official proceedings of the GeoShanghai 2010 Conference and contains technical papers that address several of these issues. It includes the full-length, peer-reviewed papers accepted for this conference.

More than four hundred abstracts were received for this conference in response to the Call for Papers, of which sixty-one abstracts were submitted to the Ground Improvement track. The abstracts were reviewed by the Organizing Committee and fifty-three invitations were extended to the authors to prepare and submit full-length papers for the Ground Improvement track.

All papers were reviewed following the same procedure and at the same technical standards of practice of the Geo-Institute of the American Society of Civil Engineers. All papers received a minimum of two full reviews coordinated by various track chairs and supervised by the GSP editors. Standard editorial review forms and checklists were applied to maintain uniform technical standards of the papers. As a result, 47 papers and one keynote lecture were accepted and published in this GSP designated for the Ground Improvement track. The authors of the accepted papers have addressed all the comments of the reviewers to the satisfaction of the session chairs. It is hoped that readers of *Ground Improvement and Geosynthetics* will be stimulated and inspired by the wide range of papers written by a distinguished group of national and international authors. The papers are eligible for discussion in the *Journal of Geotechnical and Geo-environmental Engineering* and for ASCE award nominations.

Publication of this quality of technical papers would not have been possible without the dedication and professionalism of the paper reviewers. The names of these reviewers appear in the acknowledgment that follows. For any additional reviewers whose names were inadvertently missed, we offer our sincere apologies.

We are thankful to Professor Maosong Huang, Chair and Professor Baoshan Huang, Co-chair of the technical committee of the GeoShanghai 2010 Conference. Appreciation is extended to the authors and track chairs for their significant contributions. Thanks are also extended to ASCE Geo-Institute staff, especially Carol

Bowers, Director, ASCE-GI, and Lauren Tighe, Board and meeting Specialist, for their coordination and enthusiastic support to this conference. All of the submission activities of the papers for this conference were managed online by Conference Manager and we thank Dr. Sireesh Saride, Aravind Pedarla, Richard Williammee, and Nagasreenivasu Talluri of the University of Texas at Arlington for their help with additional reviews and help with the final preparations of GSP. The editors also acknowledge the assistance of Ms. Donna Dickert at ASCE Geo-Institute in the final production of this Geotechnical Special Publication.

Anand J. Puppala, PhD, PE, Professor, The University of Texas at Arlington, Arlington, Texas, USA

Jie Huang, PhD, PE, California Department of Transportation, Los Angles, California, USA

Jie Han, PhD, PE, Associate Professor, The University of Kansas, Lawrence, Kansas, USA

Laureano R. Hoyos, PhD, PE, Associate Professor, The University of Texas at Arlington, Arlington, Texas, USA

January 2010

Acknowledgements

The editors would like to specially thank the following individuals who reviewed one or more papers for this Geotechnical Special Publication.

Anand Puppala
Anil Misra
Antonio Marinucci
Aravind Pedarla
Baolin Wan
Baoshan Huang
Bin Zhang
G. Cai
Chang-Yu Ou
Ching Tsai
Chunling Li
Curt Basnett
Deren Yuan
Der-Wen Chang
Ekarut Archeewa
Eng Choon Leong
Giovanni Bonita
Guojun Cai
Guoqiang Li
Haifang Wen
Hani Titi
Harry Moore
Heather Brown
Huang Baoshan
James Niehoff
Jenny Liu
Jianfeng Chen
Jie Han
Jie Huang
Junjie Zheng
Kunnawee Kanitpong
Kyle Rollins
Laureano Hoyos
Manuel Celaya
Ming Xiao
Muhannad Suleiman
Murali Krishna Adapa
Nagasreenivasu Talluri
Nasser Massoudi
Peter Wu
Qiao Dong
Rafiqul Tarefder
Raja Sekhar Madhyannapu
Richard Williammee
Robert Liang
Robert Mokwa
Sadik Oztoprak
Samer Rababah
Scott Anderson
Sireesh Saride
Soheil Nazarian
Songyu Liu
Srinivas Chittoori
Suksun Horpibulsuk
Tanner Blackburn
Thornchaya Wejrungsikul
Venkata S Dronamraju
Vijay Ganne
JS Vinod
Virgil Ping
Vishnu Diyaljee
Vivek Tandon
Wei Lee
William Camp
Xian Liu
Yongqi Li
Zhanping You

This page intentionally left blank

Contents

Keynote Lecture Paper

Durability of Cement Treated Clay with Air Foam Used in Water Front Structures 1
Yoshiaki Kikuchi and Takeshi Nagatome

Ground Improvement

Mechanical and Hydraulic Modification Methods

An Economical, Practical, and Environmental Friendly Surcharge Preloading Method to Improve Soft Ground of Municipal Road 31
Heping Yang, Jie Xiao, and Yufei He

Estimation of Strength Gain Due to Consolidation 38
Raghvendra Singh, Debasis Roy, and Himanshu Dubey

Numerical Study on the Deformation and Failure of Reinforced Sand Retaining Walls Subjected to the Vertical Load 44
Yanbo Cao, Fangle Peng, Ke Tan, and M. S. A. Siddiquee

Development of Reinforced Soil Structure with Pile Foundation: Piled Geo-Wall 53
Takashi Hara, Shinichiro Tsuji, Naoki Tatta, Atsushi Yashima, and Kazuhide Sawada

Limit Analysis of Reinforced Soil Slopes Based on Composite Reinforcement Mechanism 59
Yong-liang Lin, Xin-xing Li, and Meng-xi Zhang

Comparison of Performance between Cross Shaped and Conventional Deep Mixed Columns for Three-Layered Soft Ground Improvement under Embankment Load 65
Yaolin Yi, Songyu Liu, Yanjun Du, Fei Jing, and Nenghe Gong

A New Method for Settlement Calculation of Long-Short Piles Combined Composite Foundation 71
Chuang Yu, Linyou Pan, and Xiaobing Li

Experimental Study on Vertical Bearing Behavior of Composite Foundation with Tapered Rigid Pile 79
Jie He, Jie Liu, Ke-neng Zhang, Chang-qing Min, and Da Hu

Implementation of Optimized Soil Improvement Techniques for a Giga Project 87
Babak Hamidi, Serge Varaksin, and Hamid Nikraz

Experimental Study on Shear Strength Behavior of Shredded Tyre-Reinforced Sand 93
V. Vinot and Baleshwar Singh

Numerical Analysis of Lateral Behavior of Rigid Piles to Support Embankments 99
Li Liu, Gang Zheng, and Jie Han

Settlement Behavior of Highway Transition Sections on Soft Clay Foundation 107
Yongfeng Deng, Songyu Liu, Fei Jing, and Weijiang Feng

Consolidating Dredge Soil by Combining Vacuum and Dynamic Compaction Effort 113
An Deng and Shi-long Xu

Chemical Modification Methods

Optimization of Deep Mixed Shear Walls for Stabilization of a Pile-Supported Flood Wall on Level Ground 119
Tiffany E. Adams, George M. Filz, Peter R. Cali, Mark L. Woodward, and Neil T. Schwanz

Heavy Structures Supported by Soil-Cement Columns 125
Lisheng Shao and Ken Ivanetich

Mechanical Properties of Used Tire Granulates, Sand, and Cement Mixtures 131
Berrak Teymur and B. Alp Atapek

Fly Ash As a Dispersing Material in Cement Stabilization 137
Suksun Horpibulsuk and Yuttana Raksachon

Strength Characteristics of a Local Red Soil Blended with Class F Fly Ash and Cement 143
Ajanta Kalita and Baleshwar Singh

Mechanical Behavior of Compacted Geomaterial Changed from the Dredged Soil in Nagoya Port by Mixing with Some Stabilizers 149
Kai Sun, Masaki Nakano, Eiji Yamada, and Akira Asaoka

Effects of Organics on Stabilized Expansive Subgrade Soils 155
Sireesh Saride, Srujan R. Chikyala, Anand J. Puppala, and Pat J. Harris

Application of Gypsum Waste Plasterboard and Waste Plastic Trays to Enhance the Performance of Sandy Soil 165
Aly Ahmed, Keizo Ugai, and Takeshi Kamei

Effect of Placement Water Content on Strength of Temperature Cured Lime Treated Expansive Soil 174
Amir Asad Nasrizar, M. Muttharam, and K. Ilamparuthi

Utilization of Shredded Rubber Tires for Cement-Stabilized Soft Clays 181
Mohamed A. Shahin and Liao S. Hong

Other Modification Methods

Analysis on Load Transfer for Single Pile Composite Foundation under Embankments Based on Elastic Theory 187
Xiao Ming Lou, Geng Bo Jiang, and Hong Yue Xu

A Review of the Settlement of Stone Columns in Compressible Soils 197
Bryan A. McCabe and Derek Egan

Field Test and Numerical Analysis on Performance Upgrade of Existing Rockfall Protection Fence by Using High Energy Absorption Net 205
Shinichiro Tsuji, Takashi Hara, Atsushi Yashima, and Masaki Yoshida

Numerical Modelling for Ground Improvement of Batter Micropiles on Liquefiable Soils 212
Mingwu Wang and Jinping Han

Slope Stability Analysis for Embankment on Wash Pond Sediments with Prefabricated Wick Drains and Staged Construction 220
J. Ding, R. Vester, and R. Knott

Bridge Approach Settlements: Lessons Learned from Present Case Studies and Ground Improvement Solutions 228
Anand J. Puppala, Sireesh Saride, Ekarut Archeewa, Soheil Nazarian, and Richard Williammee, Jr.

Analysis of the Influence of Embankment Widening on Soft Ground with Differential Settlements on Pavement Structure 239
Yekai Chen, Yimin Wang, and Chao Ren

Improving Reinforced Soil Performance Incorporating Vertical Reinforcement 249
Binod Shrestha and Hadi Khabbaz

Safety Problem of Freezing Projects in Saline Soils 255
Xiang-Dong Hu, Fei Zhao, and Rui-Zhi Yu

Large Scale Test on Improving Ultra Soft Soil Using Electro-Osmotic Method 263
Yonghua Cao, Jingfang Yang, and Dongdong Cheng

Geosynthetics

Finite Element Modeling of a Field-Scale Shored Mechanically Stabilized Earth Wall 269
Cheng Chen, Louis Ge, and Jia Sheng Zhang

Bearing Capacities of Geogrid-Reinforced Sand Bases under Static Loading 275
Yan-Li Dong, Jie Han, and Xiao-Hong Bai

Performance Study of Geosynthetic Reinforced Soil Retaining Structures 282
Sao-Jeng Chao

Stability Analysis of Geobelt-Reinforced Cushion Foundations 287
Xian-Zhi Huang, Jie Han, Feng-Xiang Yan, and Jian-Zhou Fan

Noise Barriers by Steep Vegetated Walls Reinforced with Geosynthetics –An Economical Alternative? 295
Harald Schoen, Franz Aschauer, and Wei Wu

Geosynthetics and Pavement Life Cycle: An Analysis through the M-E PDG 302
Filippo G. Praticò, Domenico Tramontana, Antonio Casciano, and Antonella Attinà

Mechanical Behavior of Geosynthetic-Reinforced Soil Retaining Wall 310
Mamoru Kikumoto, Teruo Nakai, Shahin Md. Hossain, Kenji Ishii, Asami Watanabe, and Feng Zhang

3D Parametric Study of Geosynthetic-Reinforced Column-Supported Embankments **318**
Jie Huang, Jie Han, and Junjie Zheng

Prediction of Settlements of Geocell Reinforced Sand Foundations **328**
Sireesh Saride, T. G. Sitharam, and Anand J. Puppala

Investigation of Tire Chips-Sand Mixtures As Preventive Measure against Liquefaction **338**
Hemanta Hazarika, Masayuki Hyodo, and Kazuya Yasuhara

Design Method for Flat Geotextile Tubes **346**
Yue Yan, Shuwang Yan, Changlin Qiu, and Gang Zheng

Laboratory Model Tests for a Strip Footing Supported on Geocell Reinforced Sand Bed **353**
S. N. Moghaddas Tafreshi and A. R. Dawson

Macro-Mesoscopic Study of the Interface between Sand and Geogrid **361**
J. Q. Wang, J. Zhou, and Y. B. Deng

Triaxial Compression and Extension Tests for Fiber-Reinforced Silty Sand **367**
Cheng-Wei Chen

Indexes

Author Index **377**

Subject Index **379**

Durability of Cement Treated Clay with Air Foam Used in Water Front Structures

Yoshiaki Kikuchi[1] and Takeshi Nagatome[2]

[1]Director, Geotechnical and Structural Engineering Department, Port and Airport Research Institute, 3-1-1 Nagase, Yokosuka 239-0826, Japan; kikuchi@pari.go.jp

[2] Senior Researcher, Geotechnical and Disaster Prevention Technology Group, Research and Development Center, Toa Corporation, 1-3 Anzen-cho, Tsurumi-ku, Yokohama 230-0035, Japan; t_nagatome@tao-const.co. jp

ABSTRACT: Durability of cement treated clay with air foam, Super Geo-Material (hereafter referred to as "SGM"), was investigated in this paper. When SGM is used for the backfill of a quay wall or reclamation of a man-made island, this material will be used under water or under the water table. In this case, hydraulic conductivity and water absorption characteristics are important characteristics for the durability of this material. From a series of several permeability tests, air foam in SGM is an impermeable medium if the air volume ratio is less than 25%. However, when the air volume is higher, the air foam makes bleeding channels and the coefficient of permeability dramatically increases. From a series of absorption tests in the laboratory, the absorption properties of SGM under the wet sand condition were different from those under the water condition. The absorption velocity of SGM under the wet sand condition was more than 10 times slower than that under the water condition. And this conclusion was supported by a ten year investigation of a SGM used in the field.

INTRODUCTION

Effective use of dredged clay has been one of the most important issues for port construction engineers, due to the maintenance of navigation channels producing a large amount of dredged clay. On the other hand, light weight geo-material has been needed to reduce earth pressure to water front structures which are deteriorated or are being improved. Light weight geo-materials, which are made from dredged clay, cement, and lightening materials such as air foam or expanded polystyrol (EPS) beads, were developed for these circumstances. Total settlement will be decreased when it is used for reclamation, and earth pressure to the retaining structure will be reduced when this material is used for backfilling. The mechanical properties of the material were studied and the mixing method of the material along with the construction method using the material were also studied (Tsuchida et al., 1996). The preliminary manual for using the

material was published (Tsuchida et al., 2004).

Recently, at Tokyo International Airport, which is usually called Haneda Airport, a fourth runway is being constructed. Since this runway is to be located at the mouth of the Tama River, one third of this runway will be constructed on an open pier to prevent flooding from the river. The rest of the runway is to be constructed on reclaimed land. The retaining structure at this conjunction point should be able to sustain large earth pressure and minimize settlement of reclaimed land next to the structure. Super Geo-Materials (SGM), which is one of the light weight geo-materials made from cement treated clay with air foam, were discussed for possible use. The durability of this material was one of the biggest issues at that time. In particular, the increment of the density of the material and the reduction of strength were among the biggest issues.

As SGM is applied to waterfront construction, the characteristics of this material can be influenced by seawater when it is used in coastal areas. There is a risk that some air in the SGM may be replaced with water over time and a prediction of the change of unit weight with time is required. This phenomenon is affected by the permeability and absorption properties of the material.

Much knowledge has been accumulated on making the strength of the clay higher. Yet, there is much uncertainty about the increasing of the unit weight. Furthermore, the hydraulic conductivity of SGM is unknown. Conventional permeability tests and theoretical analysis (Kikuchi et al., 1998) have demonstrated the principle of hydraulic conductivity of this material, but much uncertainty about its mechanism remains, and the mechanism of absorption of water to SGM is completely unknown. A visualizing technique using an X-ray CT scanner has the potential to resolve these problems.

It is usually considered that X-ray CT scanners are unsuitable for observing the inner density structure of clay, because clay particles are too small and specimens made of clay are too homogeneous. However, such materials as lightweight artificial mixed materials are inhomogeneous in density, and so changes of the inner structure with environmental changes can be observed with an X-ray CT scanner.

MICRO-FOCUS X-RAY CT SCANNER

The basic specifications of the X-ray CT scanner used in this research are shown in Table 1. As shown, the voltage and current can be changed and the distances between the X-ray tube and test piece or image intensifier can be changed in this apparatus. Therefore, the micro-focus X-ray CT scanner can be used for scanning a wide variety of specimens. A very small focus of this scanner achieves a high resolution that enables small parts to be easily observed, and its maximum magnification is about 80. To get precise data, 6000 views can be taken in a full scan of the specimen for one cross section.

Figure 1 shows an overview of the apparatus. The shield box is designed so that triaxial tests can be performed in the box: water tubes, air tubes and electric cables are inserted from the outside, and the object mounting table can be moved about 50 cm in the vertical direction.

Table 1. Specifications of micro-focus X-ray CT used in this study

X-ray unit	Type	Non-enclosed
	Voltage	30 – 225 kV
	Current	10 – 1000 μA
	Maximum output	135 W
	Minimum focus size	4 μm
	X-ray irradiation angle	60 deg. In cone shape
Image intensifier	Field-of-view diameter	9/7.5/6/4.5 inches
Test samples	Maximum mounting	ϕ 250 × 800 mm
	Maximum weight	600 N
X-ray shield box	Dimensions	2150 × 1310 × 2400
	Weight	45100 N

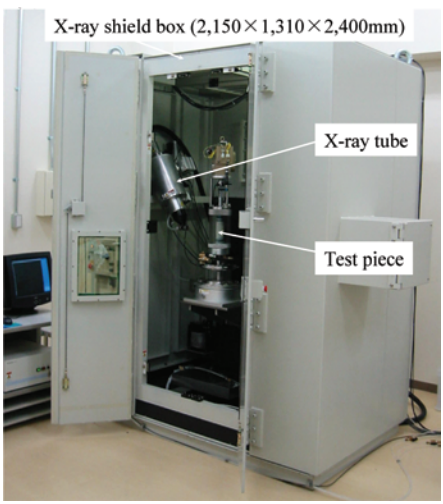

FIG. 1. Overview of micro-focus X-ray CT scanner used in this study.

In this apparatus, one slice of the specimen can be divided into a 4096 × 4096 matrix at maximum. In each voxel (volumetric pixel), a gray level (GL) value is allocated by CT analysis. The GL-value is a kind of contrasting parameter used for imaging processing, and is basically a linear parameter for estimating the density of the specimen.

Although GL-values depend on the scanning conditions, some materials of different density were scanned under the same scanning condition. Figure 2 shows the average GL-values of the test results against the average density of the materials. This figure shows that there is a linear relation between the GL-value and the density.

The materials discussed in this report are high-water-content clay with cement, and air foam. The density of the high-water-content clay, cement slurry, and air are 1.25 g/cm^3, 2.0 g/cm^3, and 0.0 g/cm^3, respectively. It is necessary to distinguish differences

of these material densities. Several test results show that a density change of about 4% can be easily distinguished.

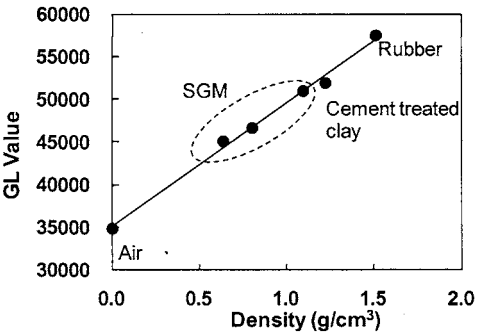

FIG. 2. Relationship between the gray level and average density of some materials.

The voxel size can be changed as required according to the purpose (Fig. 3). For example, in this study, the scanning space was divided into 512 × 512 or 2048 × 2048 voxels. In scans of the entire cross section of specimens, 512 × 512 voxels were used, and the size of one voxel was 0.12 mm × 0.12 mm × 1 mm. Microscopic scans of the cross section were performed using 2048 × 2048 voxels, giving a voxel size of 0.01 mm × 0.01 mm × 0.01 mm. Three-dimensional images were reconstructed by superposing 2-dimensional images.

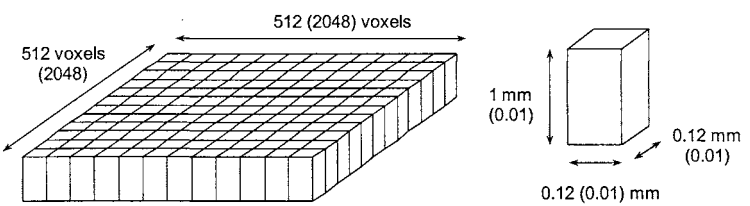

(a) X-ray CT image (b) Voxel size

FIG. 3. Voxels in an X-ray CT image in a cross section and size of a voxel.

HYDRAULIC CONDUCTIVITY OF SUPER GEO-MATERIAL (SGM)

Although the permeability of cement-mixed clay is known to be decreased (Terashi et al., 1983), little information is available on the permeability of SGM. SGM is a new material composed of saturated clay, cement, and air foam. The air in SGM is in the form of bubbles, and each bubble retains its position after the SGM solidifies. Since the unsaturated condition of the SGM differs from that of unsaturated natural soils, its permeability mechanism may also differ from that of unsaturated natural soil.

The purpose of this study was to clarify the hydraulic conductivity characteristics of the SGM and find the effect governing the hydraulic conductivity. First, permeability tests with a triaxial apparatus and constant-rate-of-consolidation tests were conducted. From the results, a hypothesis of the hydraulic conductivity mechanism was proposed. In the first series of permeability tests, only one mixing condition was used. Other permeability tests of several SGMs prepared under different mixing conditions were conducted with observation by a micro-focus X-ray CT scanner.

Permeability tests

Permeability tests with a triaxial apparatus and constant-rate-of-consolidation tests were conducted to clarify the macroscopic permeability of the SGM.

Marine clay dredged from Kawasaki Port (ρ_s = 2.678 g/cm^3, w_L = 52.1%, w_P = 23.0%) was used in a series of these tests. Specimens were prepared as follows: 1) Liquefied clay of 2.5w_L was prepared (1016 kg/m^3). The water used for controlling the water content ratio was fresh water. 2) Air foam made of a surfactant (238 l/m^3) and blast furnace cement B (75 kg/m^3) were mixed with the clay for 3 minutes. The target wet density of the SGM was 1.1 g/cm^3. 3) Molds of ϕ50 mm × h120 mm were filled with the mixture. 4) The molds were placed in water and the specimens were allowed to cure for about 28 days. The target unconfined compressive strength at 28 days of curing time qu_{28} was 200 kN/m^2.

Two types of permeability tests were conducted. The first series consisted of permeability tests using the triaxial apparatus. The second was a series of constant-rate-of-consolidation tests performed to estimate the permeability of the geotechnical materials.

The procedure of the permeability tests using the triaxial apparatus was as follows: First, the specimen was trimmed to ϕ50 mm × h100 mm and was placed in the triaxial cell. A cell pressure of 50 kPa was then applied to initiate consolidation. No back pressure was applied to prevent the shrinkage of air in SGM during consolidation. The consolidation period was 3 days. Following consolidation, a pressure of 20 kPa was applied to the volume change burette connected to the bottom of the specimen. Water was introduced into the specimen, and the influent and effluent water volumes were measured using volume change burettes connected to the bottom and top of the specimen during the water flow. The water flow was continued for one week. The permeability of a specimen made of the same amount of cement treated clay without air foam (CTC) was also measured in order to investigate the effect of the air foam.

The mixing conditions of the SGM used in the constant-rate-of-consolidation tests were the same as those used in the triaxial permeability tests. The SGM filled a consolidation ring of ϕ6 cm × h2 cm. The specimen used in this test was cured for 28 days. After curing, the specimen was placed in the consolidation apparatus. A back pressure of 100 kPa was applied to measure the pore water pressure change. The consolidation rate was 0.05%/min.

Figure 4 shows the relationship between the time and the influent/effluent water volume in the triaxial permeability tests. The water content ratio of the two specimens was substantially the same. The water pressure gradients were approximately 20 in both tests.

Figure 4 shows that when the specimen did not include air foam (CTC), the influent

and effluent water volumes were virtually the same, and the influent and effluent speeds were basically constant. On the other hand, when the specimen included air foam (SGM), the speed of the influent water was very fast and the water content increased initially, but then became constant. The water effluent rate with air foam was smaller than that without air foam. These two test results showed that the permeability determined from the difference in the influent and effluent water volumes, that is "apparent" permeability, was larger without air foam than with air foam. This shows that air foam is a less permeable medium than the basic mixture of clay and cement.

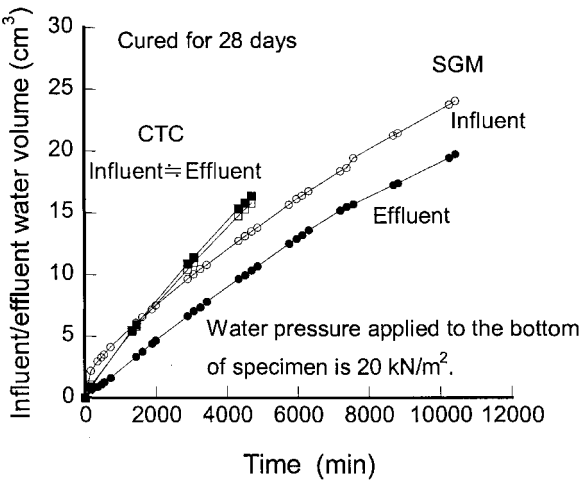

FIG. 4. Difference in influent/effluent water volume due to existence of air foam.

Figure 4 shows that the volume of air in the SGM changed during the test. In this case, the flow of the water in the specimen was affected by the compressibility of the pore fluid. The consolidation of soil containing compressive fluid is expressed as follows:

$$\alpha \frac{\partial u}{\partial t} = \frac{k}{m_v \rho g} \frac{\partial^2 u}{\partial z^2} \tag{1}$$

where $\alpha = 1 + n(C'_w / m_v)$, ρ: density of pore fluid, z: distance, t: time, n: porosity (= e/(1+e)), k: coefficient of permeability, u: absolute pressure of pore fluid, g: gravitational acceleration, C'_w: volumetric compressibility of pore fluid ($= (1 - S_r)/u + S_r C_w$) (Verruijt, 1969), m_v: coefficient of volume change for saturated soil, C_w: compressibility of water, and S_r: rate of saturation.

This equation is valid if the entrapped air is in a bubble state in the pore water and the coefficient of permeability is approximately the same as that of the saturated clay (Zen, 1993). Considering the method of specimen preparation, the air in the SGM used here exists separately and does not pass through the specimen. It is therefore reasonable

to treat the SGM as a material containing a compressible fluid when considering the permeability of SGM.

Simulation of the influent volume using Eq. (1) showed that the air in the foam was pressurized even though the foam was produced under atmospheric pressure. It is reasonable to assume that the diameter of each bubble was about 0.1 mm and small bubbles can be pressurized by surface tension (Kikuchi et al., 1998). The change in the influent volume during flow testing was also simulated using Eq. (1).

Figure 5 shows the corrected relationship between permeability and the void ratio. The volume of air foam was excluded from the plotted void ratio in the figure because air foam in the SGM is less permeable than voids. The permeability of the SGM shown in Fig. 5 was calculated using Eq. (1) in accordance with the results of the constant rate of consolidation test. It was also calculated considering that the cross-sectional area of air foam was excluded when calculating the effective cross-sectional area for water flow. Here, we define this permeability as "true" permeability. Furthermore, the volume of air was excluded when calculating the effective void ratio of SGM. Figure 5 shows that the relationship between the coefficient of true permeability and the effective void ratio of SGM and CTC estimated by the triaxial apparatus test are in good agreement. This result indicates that this kind of correction can represent the permeability of SGM from the macro viewpoint.

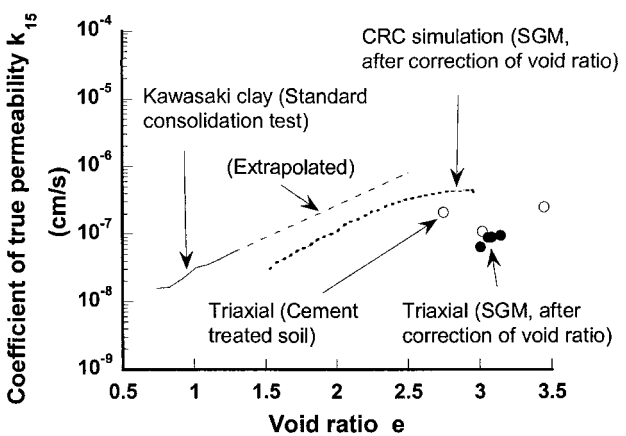

FIG. 5. Coefficient of true permeability of SGM.

Figure 5 also shows the relationship between the permeability and void ratio of the Kawasaki clay used in the SGM. The permeability of Kawasaki clay is extrapolated in the figure because a linear relationship exists between the logarithm of permeability and the void ratio (Kobayashi et al., 1990). The relationship estimated by the constant-rate-of-consolidation test is basically parallel to the relationship in Kawasaki clay. Furthermore, from the relationship in the SGM shown in Fig. 5, the permeability of the SGM is rather small due to inclusion of cement in the mixture. The results in the present study showed that the reduction of permeability ranges from 1/30 to 1/4. These

results agree with the results reported by Terashi et al. (1983).

Permeability test with micro-focus X-ray CT scanner

The dredged clay used in the SGM in this series of tests was Tokyo Bay clay (ρ_s = 2.758 g/cm^3, w_L = 104%). Air foam made of a surfactant and blast furnace cement B were used to lighten and solidify the SGM, respectively.

Four mixing conditions were used in this series to obtain different target densities as shown in Table 2. The composition volume of air foam was 13%, 38%, and 59% with the 1.10, 0.80, and 0.60 g/cm^3 target densities, respectively. Thus, specimens with 0.6 and 0.8 g/cm^3 target densities included a large amount of air.

Table 2. Mixing compositions for SGM for micro-focus X-ray CT scanner.

Target density (g/cm^3)		Dry soil	Sea Water	Cement	Air	Total
1.25	Mass (kg/m^3)	283	904	60	-	1247
	Volume (l/m^3)	103	878	20	-	1000
1.10	Mass (kg/m^3)	246	787	61	6	1100
	Volume (l/m^3)	89	764	20	127	1000
0.8	Mass (kg/m^3)	152	561	69	19	800
	Volume (l/m^3)	55	544	23	378	1000
0.6	Mass (kg/m^3)	94	347	130	29	600
	Volume (l/m^3)	34	337	43	586	1000

Samples were poured into molds of ϕ50 mm × h120 mm. The top surface of the molds was sealed with wrap and the molds were placed in a curing box in which the temperature and humidity were maintained at 20°C and 95%, respectively, for about 28 days.

Permeability tests were conducted with a triaxial apparatus made for the X-ray CT scanner. The specimens were consolidated under a confining pressure of 50 kPa for 3 days. A water pressure of 20 kPa was then applied to the bottom of the specimens to create a water pressure gradient. The influent and effluent water volumes were measured using volume change burettes. The specimens were scanned with the X-ray CT scanner several times during the permeability tests.

Table 3 shows the density change during the permeability tests and the coefficient of permeability for each case. The permeability of the specimen with the 1.1 g/cm^3 target density is smaller than that of the specimen without air foam (target density is 1.25 g/cm^3), and the permeabilities of the specimens with the 0.8 and 0.6 g/cm^3 target densities were very high compared to that of the specimen without air foam. With 0.6 and 0.8 g/cm^3 target densities, air emerged from the specimens in the early stage of the permeability tests. And Table 3 shows that wet density increased with the 0.6 and 0.8 g/cm^3 target densities and a partial amount of the air was replaced by water in these specimens. This means that bleeding channels through which water could easily flow were formed in these specimens.

These results show that bleeding channels will tend to form if the air content is

These results show that bleeding channels will tend to form if the air content is excessive, and as a result, the wet density and coefficient of permeability will tend to increase. On the other hand, when the air content is small, the air functions as an impermeable medium.

Table 3. Wet densities before and after permeability tests and coefficients of permeability.

Target density (g/cm^3)	Wet density (g/cm^3)		Coefficient of permeability (cm/s)
	Before test	After test	
1.25	1.232	1.229	$1.47X10^{-6}$
1.10	1.114	1.122	$8.33X10^{-7}$
0.80	0.816	0.894	$3.47X10^{-6}$
0.60	0.676	0.951	$1.87X10^{-3}$

Figures 6 to 9 show X-ray CT images of the specimen at a height of around 50 mm during the permeability tests. The difference in the brightness of (a) in each figure corresponds to the difference in average density caused by the difference in the fraction of air volume. Figures 6 and 7 show no apparent density changes during the permeability tests. On the other hand, Figures 8 and 9 show that the densities of the specimen changed during the tests. In both cases, the density increments did not occur uniformly, but occurred in some parts of the specimens at the beginning of the tests. However, at the end of the tests, the density increments had become rather uniform.

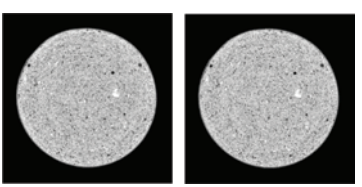

(a) Initial (b) After 40 hours

FIG. 6. Cross-sectional X ray CT image (without air).

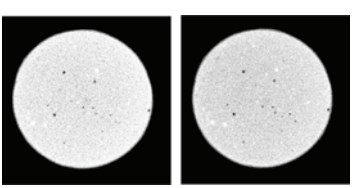

(a) Initial (b) After 72 hours

FIG. 7. Cross-sectional X ray CT image (1.1 g/cm^3 target density).

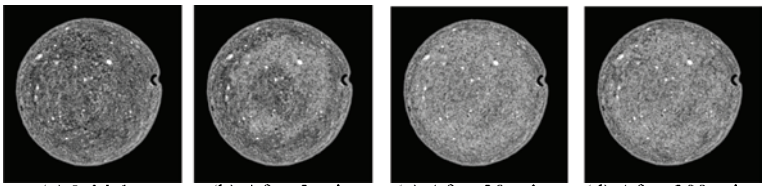

(a) Initial (b) After 3 min (c) After 30 min (d) After 300 min

FIG. 8. Cross-sectional X ray CT image (0.8 g/cm^3 target density).

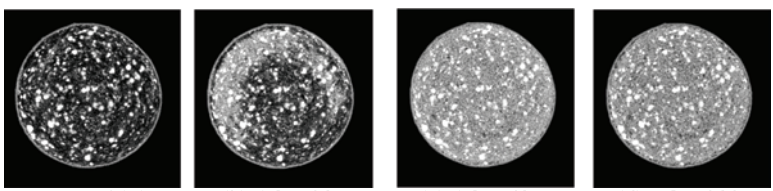

(a) Initial (b) After 30 s (c) After 60 s (d) After 300 s

FIG. 9. Cross-sectional X ray CT image (0.6 g/cm^3 target density).

Figures 10 and 11 show the vertical cross section of the specimen during the permeability tests with the 0.6 and 0.8 g/cm^3 target densities. These figures show that density increments occurred from the bottom to the top, and occurred only at the beginning of the test. For example, the average density became uniform in 30 minutes with the 0.8 g/cm^3 target density and in approximately 90 seconds with the 0.6 g/cm3 target density.

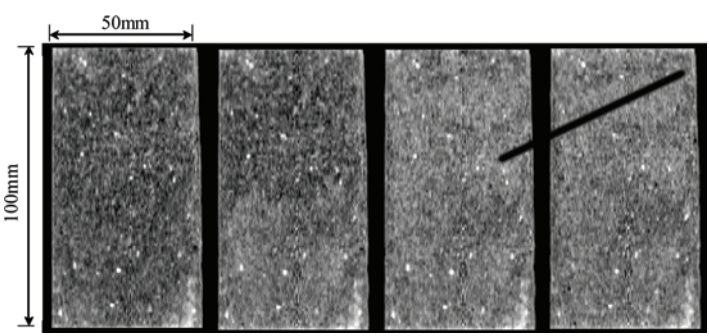

Initial After 3 min After 30 min After 300 min

FIG. 10. Vertical cross sectional CT image (0.8 g/cm^3 target density).

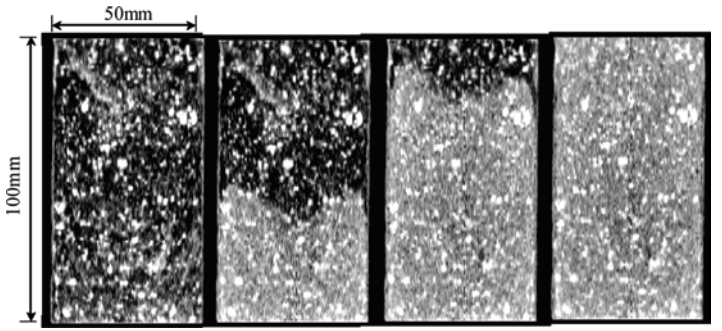

FIG. 11. Vertical cross sectional CT image (0.6 g/cm^3 target density).

Figures 12 to 14 show close-ups of the central part of the cross section an approximate height of 50 mm of each specimen. In each figure, (a) was taken before the test and (b) was taken after the test. The pictures compared in each figure are not the same cross section, but are similar sections. The black circles in the figures are bubbles. It is apparent that the number of black circles decreased in the tests, but not all of the black circles disappeared. This means that the air in some bubbles was replaced with water, which may produce channels facilitating water flow, but in others, the air remained as an impermeable medium.

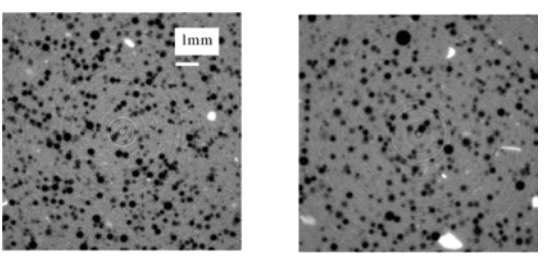

(a) Before test (b) After test

FIG. 12. Micro CT image (1.1 g/cm^3 target density).

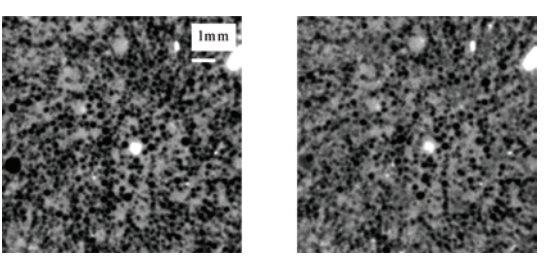

(a) Before test (b) After test

FIG. 13. Micro CT image (0.8 g/cm^3 target density).

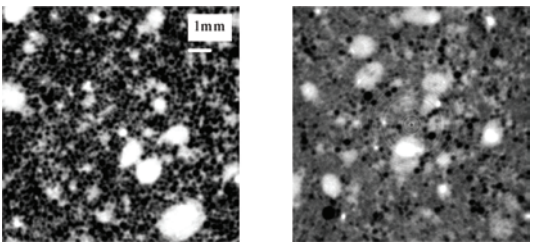

(a) Before test (b) After test

FIG. 14. Micro CT image (0.6 g/cm^3 target density).

Figure 15 shows the calculated results of the water substitution ratio relative to the initial air volume. This calculation is based on two assumptions. First, the clay slurry with cement is assumed to be uniform in the specimen. This means that variances in density are attributable to variances in air volume. The second assumption is that density change is attributable to the substitution of water for air. Although there may be some degree of error, there is an overall tendency shown of the actual phenomena which occurs in the specimen.

Figure 15 shows that some amount of air will be replaced by water. The substitution speed is very high in the early stage, but slows down dramatically with time. If the target density is low, which means the initial volume of air is large it would mean that approximately half of the air will be replaced by water, while half of the air will remain in the specimen. In such cases, bleeding channels which facilitate water flow may exist, while the remaining air zone acts as an impermeable zone.

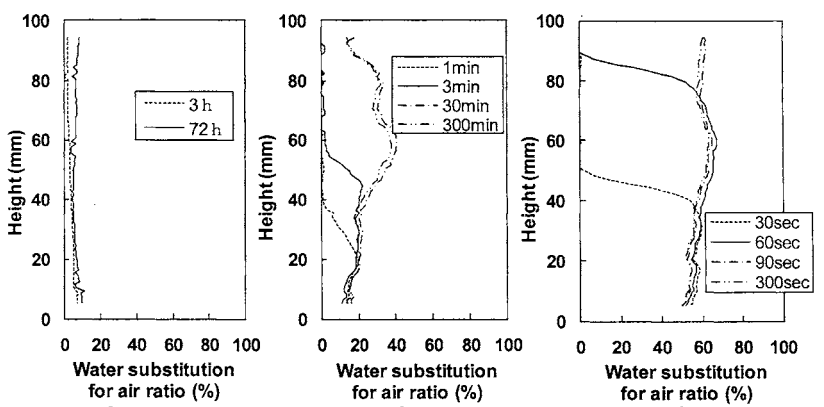

(a) 1.1 g/cm^3 target density (b) 0.8 g/cm^3 target density (c) 0.6 g/cm^3 target density

FIG. 15. Water substitution for air ratio.

Figure 16 shows the change of the coefficient of permeability of SGM according to the change of air fraction. The vertical axis of the figure is the coefficient of apparent

permeability normalized by that of CTC. The coefficients of apparent permeability of SGM with less than 25% air are lower than that of CTC. However, the coefficients of apparent permeability of SGM with more than 30% air are quite large compared to that of CTC. It is likely that this difference is due to the ease of bleeding channelization.

In this sense, the permeability of SGM is governed by the material permeability, the amount of impermeable air, and by the possibility of forming bleeding channels. Although the possibility of bleeding channelization is difficult to assess, bleeding channels will tend to form if the distance between the bubbles is short. Considering the fact that the mean diameter of air bubbles is approximately 0.3 mm and assuming that the bubbles are distributed regularly, the average surface distance between the bubbles would be 0.24 mm, 0.07 mm, and 0.03 mm with air fraction of 13%, 35%, and 50%, respectively. It is likely that this distance is the controlling factor for the possibility of bleeding channelization and permeability. Admittedly, this discussion is oversimplified for consideration of actual phenomena, as there are great variations in both the diameters of bubbles and the distances between bubbles in actual materials. Further experimental work and discussion are needed to resolve this problem.

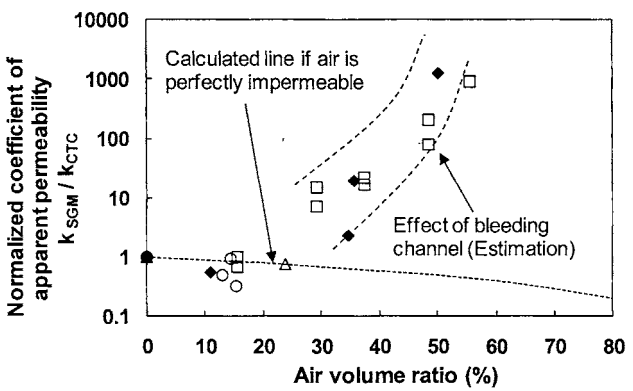

FIG. 16. Relation between air volume ratio and apparent coefficient of permeability.

ABSORPTION OF SUPER GEO-MATERIAL (SGM)

As discussed in the previous section, bubbles in the SGM act as an impermeable medium when the air volume fraction is less than around 30%. On the other hand, there is still the problem that air bubbles are replaced by water over a long period, but there is no information on the speed or extent of this displacement. This absorption phenomenon was therefore examined experimentally.

The first series of absorption tests using the X-ray CT scanner was conducted in Kumamoto University (Otani et al., 2001). The sample used in this test was in-situ SGM that was sampled at a trial construction site at Kumamoto Port. The dredged slurry used for the SGM was Ariake clay ($\rho_s = 2.619$ g/cm^3, $w_L = 119\%$). The mixing condition was 991 kg/m^3 of clay with 2.5 w_L and 100 kg/m^3 of cement and 225 l/m^3 of air foam. The

water used for controlling the water content ratio was sea water. The SGM was mixed using the mixing plant at the construction site, and the air foam was made with a surfactant. The sampling depth varied from 0.9 to 1.0 m. The target density after construction was 1.1 g/cm^3, and the actual density was 1.17 g/cm^3, slightly higher than expected.

The sample was trimmed to ϕ50 mm × h100 mm. The specimen was soaked in distilled water at a constant temperature of 20°C. Therefore, water could absorb into the specimen not only from the sides, but also from the bottom and top ends. In this test, the specimen was measured according to its weight and volume, and the specimen was scanned by X-ray CT scanner at scheduled times. This test continued for 19 months.

During the absorption test, the wet density of the specimen increased with elapsed time. Its initial wet density was 1.17 g/cm^3, but this increased to 1.32 g/cm^3 over the 19-month test period.

Figure 17 shows X-ray CT images of the specimen at mid-height at several different elapsed times from the beginning of the test to 19 months. The light parts of the image show a relatively high density and the dark parts show a relatively low density. As illustrated here, gradual concentrated circular expansion of the absorbed zone from the surface to the center of the specimen was observed.

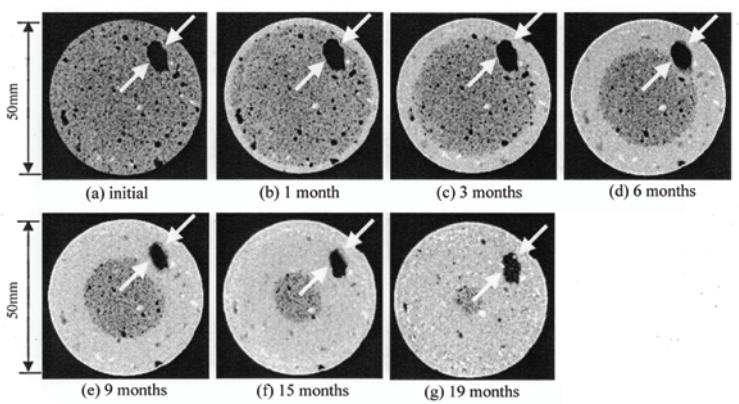

FIG. 17. Change in X-ray image according to seepage duration.

As seen in Fig. 17, a white ring appeared on the surface and it expanded toward the inside with time. This brightness change is a change of density and the close-up image shows that the air was replaced by water. As shown in Fig. 18, no air voids were observed in the white ring and all the air voids within the white ring remained. This observation means that there is a distinct boundary between the absorbed zone and non-absorbed zone and the front of the absorbed zone can be defined.

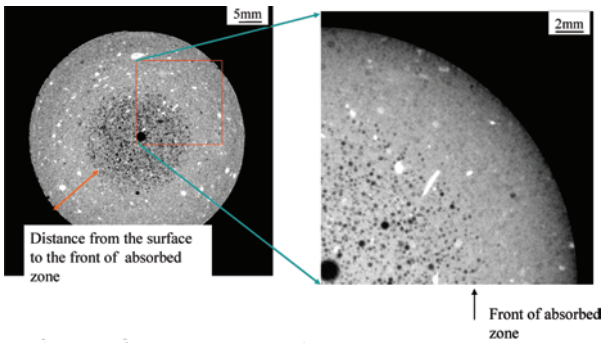

FIG. 18. Close-up image of absorbed zone with X-ray CT.

Effect of the amount of the air to the absorption

An absorption test was performed with the specimens for the target densities of 1.25, 1.1, 0.8 and 0.6 g/cm^3, respectively. The dredged clay used in this series of test was the same as the clay used in the **Permeability test with micro-focus X-ray CT scanner**. The mixing condition is shown in Table 4. The specimen was soaked in water at a constant temperature of 20 °C. Therefore, the water could be absorbed into the specimen not only from the side surface, but also from the bottom surface and top surface. In this test, the weight and volume of each specimen were measured over an elapsed period, and specimen was scanned by an X-ray CT scanner. This test was continued for 282 days.

Figure 19 shows the relationship between the wet density and elapsed days with each specimen. It was found that the density of each specimen of SGM increased with the increment of elapsed days. The specimens of 0.8 and 0.6 g/cm^3 target densities were especially increased. In contrast, the density of CTC showed no large change.

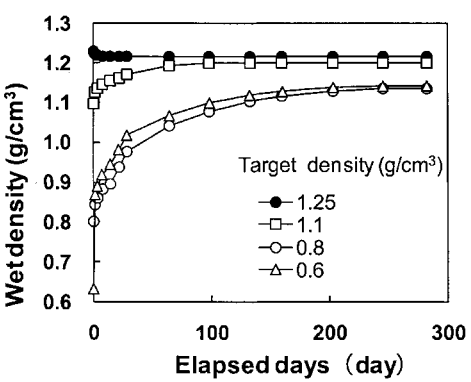

Fig. 19. Relationship between wet density and elapsed days.

Figure 20 shows cross-sectional images of each specimen during the absorption test. These images were chosen at the middle height of each specimen. The images of CTC showed no large change. Meanwhile, the images of SGM showed extended lighter parts from the water contact surface with the elapsed time. These lighter parts were absorption zones. It was observed that the absorption front was extended gradually to the center of the specimens for the target densities of 1.1 and 0.8 g/cm^3. From the image of 0.6 g/cm^3 target density after 1 day, it was observed that lighter parts were sparse across the board. And then, the lighter parts were extended gradually from the side surface like the target densities of 1.1 and 0.8 g/cm^3. Furthermore, it was found that the more air foam there was in the specimen, the slower the absorption speed.

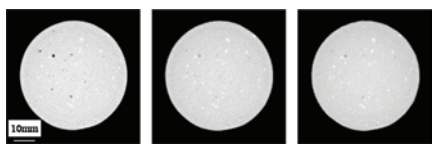

Initial 28 days 98 days

(a) 1.25 g/cm^3 target density

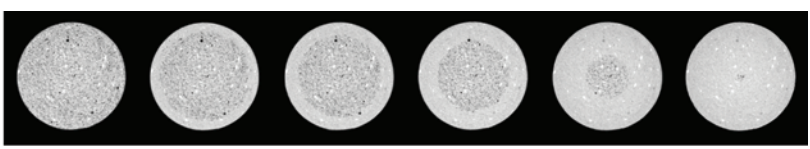

Initial 7 days 14 days 28 days 64 days 98 days

(b) 1.1 g/cm^3 target density

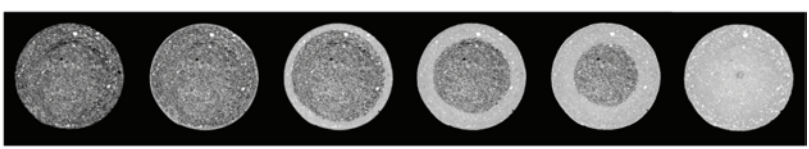

Initial 7 days 28 days 64 days 98 days 282 days

(c) 0.8 g/cm^3 target density

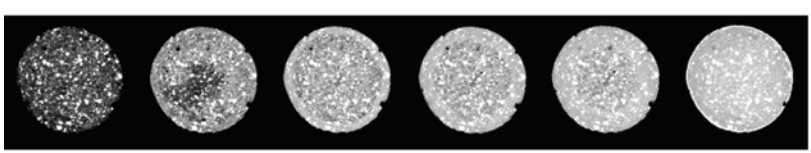

Initial 1 day 28 days 64 days 98 days 282 days

(d) 0.6 g/cm^3 target density

FIG. 20. Cross-sectional CT image.

Figure 21 shows the vertical cross section of the specimen during the absorption tests with the 1.1, 0.8 and 0.6 g/cm^3 target densities. The images of the target densities of 1.1 and 0.8 g/cm^3 were extended as lighter parts from the water contact surface to the

center. It was similar to the tendency of the absorption process in the cross-sectional images. In the image of 0.6 g/cm^3 target density after 1 day, it was observed that the lighter parts were extended from the specimen bottom. It was thought that the specimen of 0.6 g/cm^3 had many water-bleeding channels. Since water flowed from the bottom to the top surface at an early stage. After the bleeding channels were filled with water, the absorption process was no different from that without bleeding channels.

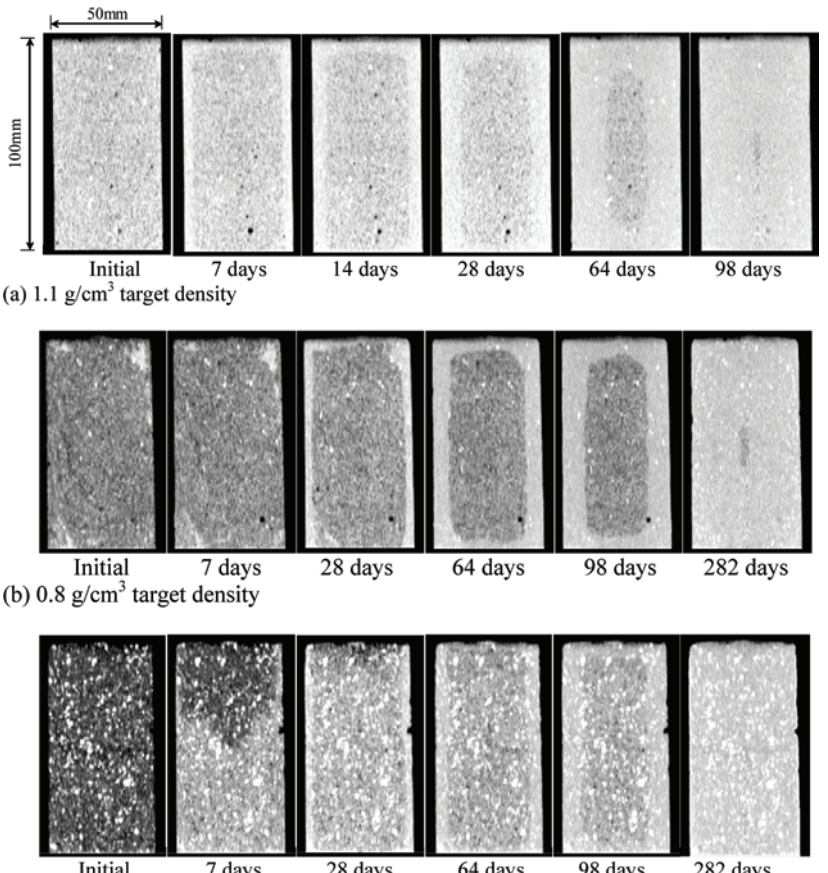

FIG. 21. Vertical cross-sectional CT image.

Figure 22 shows an example of the distribution of density in the submerged regions by cross-sectional CT data. These data were from the middle height of the specimen. The saturated density was expressed in this figure. The saturated density was calculated by the measured density and mixing condition. The density was increased from the

water contact surface and the density increase position progressed to the center of the specimen. In the density increased area, it was mainly due to saturated density. So it was considered that most air foam in these specimens was replaced by water.

Figure 23 shows the relationship between the absorbed distance from the surface and the elapsed days. Here, the absorbed parts are shown where the air foam was replaced by water. The absorbed distance was calculated using the cross-sectional X-ray CT data. The absorption speed of each specimen was almost constant irrespective of the number of elapsed days. The absorption speed of 1.1 g/cm^3 was higher than that of 0.8 and 0.6 g/cm^3.

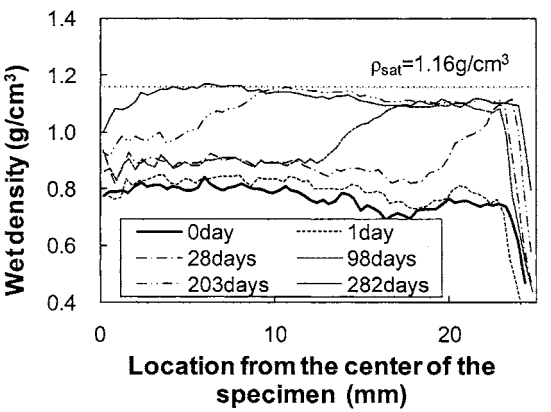

FIG. 22. Change of density distribution of the soaked specimen with 0.8 g/cm^3 target density.

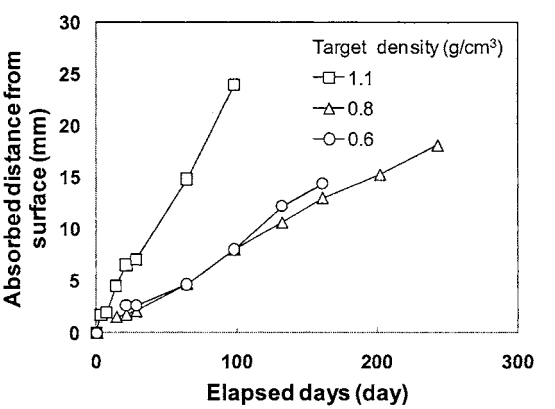

FIG. 23. Relationship between elapsed days and absorbed distance from the surface.

Effect of the water condition to the absorption

When SGM is used in a port area, it is used under groundwater to prevent drying; it will never be used in direct contact with free water but will always be used in the ground. The difference in the absorption phenomenon of SGM in the ground from that in free water is investigated below.

The dredged clay used in the SGM was Tokyo Bay clay (ρ_s = 2.663 g/cm^3, w_L = 104%). The cement used was blast furnace cement B, the particle density of which was 3.04 g/cm^3. Air foam was made of surfactant.

SGM was made by mixing dredged clay (the water content of which was controlled), cement, and air foam. In this series, the target density was designed to be 1.05 g/cm^3, and the target unconfined compression strength at 28 days of curing was 400 kPa. The water content ratio of the dredged clay was controlled to 3.46 w_L. The mixing conditions of SGM are shown in Table 4.

Table 4. Mixing conditions for SGM.

	Mass (kg)	Volume (L)
Soil	211.5	78.4
Sea water	760.4	741.8
Cement	70.0	23.0
Lightweight agent	8.1	156.8
Total	1050	1000

These mixtures were filled to a height of 10 cm in plastic containers of 5 cm inner diameter and 12 cm height. The containers were sealed and put into a curing container under the conditions of 20°C and relative humidity of more than 95%. The samples were cured for 28 days, then the cured specimens were removed from the plastic containers and the top and bottom surfaces trimmed to 5 cm in diameter and 10 cm in height. The specimens were exposed under given environments. Wet densities of SGM were 1.06 g/cm^3 at the beginning of exposure.

In this research, five exposed conditions were considered: soaked in water, in sand with three water levels, and saturated gravel. Under the soaked condition, specimens were soaked in distilled water as shown in Fig. 24. Under the wet sand condition, three water levels (water level higher than specimen, middle height of the specimen, bottom of the specimen) were used. Figures 25 and 26 show these conditions. In these cases, water levels were controlled with an observation well as shown in Fig. 26. The sand used in these cases was Sagami river sand. The particle distribution of the sand is shown in Fig. 27. Relative density was selected to be 40%. Under the saturated gravel condition, gravel was fully saturated. The gravel used was Sagami sand with particles under 2 mm sieved and removed. The particle distribution of the gravel is also shown in Fig. 27. In each condition, the water used was distilled water and the water temperature was controlled to 20°C.

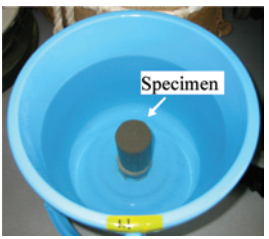

FIG. 24. Specimen soaked in water.

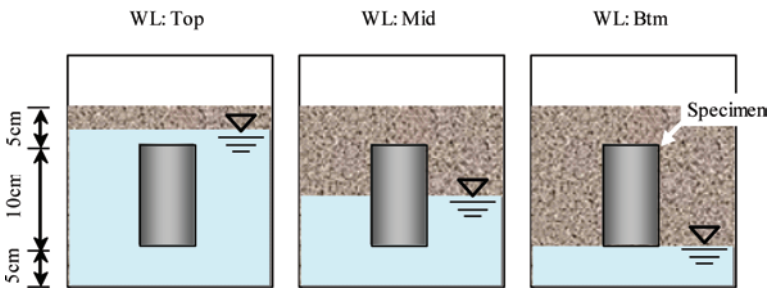

FIG. 25. Three cases of the wet sand condition with different water levels. Left: The water level is higher than the specimen's top (WL: Top). Middle: The water level is at the middle (WL: Middle). Right: The water level is at the bottom (WL: Bottom).

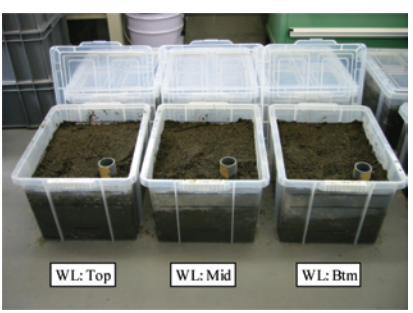

FIG. 26. Wet sand condition.

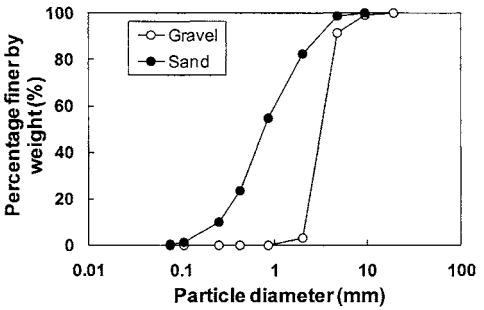

FIG. 27. Particle distributions of sand and gravel.

During the exposure, the densities of specimens were measured and X-ray CT scanning was performed to evaluate the inner density distributions of the specimens at given dates.

Figure 28 (a) shows the change of wet density of the specimen soaked in water. The wet density of the specimen of SGM increased from 1.06 g/cm^3 to 1.20 g/cm^3. Figure 28 (b) shows the air volume change of SGM during exposure. Air volume change was evaluated by assuming that the wet density change occurred only by the exchange of air in SGM for water. It was found that the change of air volume was very large in the early stage of exposure and air included in the SGM was almost entirely replaced by water in 150 days.

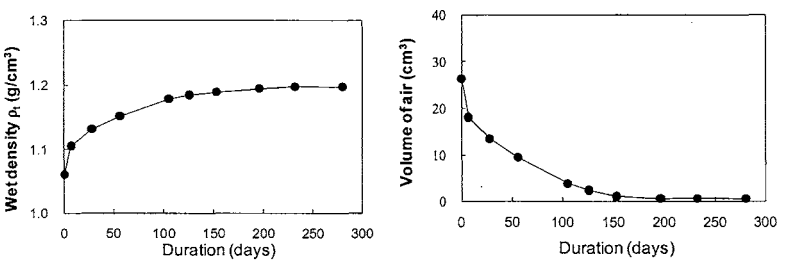

(a) Wet density (b) Air volume

FIG. 28. Wet density and air volume change during exposure when soaked in water.

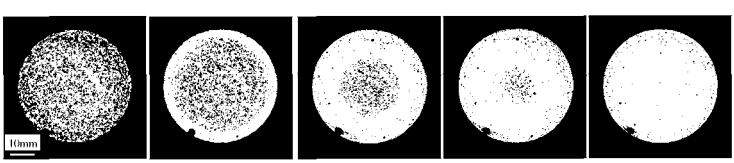

FIG. 29. Horizontal cross sectional X-ray CT image at the middle height of the specimen soaked into water.

Figure 29 shows X-ray CT scanning images of these specimens. These images are cross sections of the specimen at the middle height.

Figure 30 shows the change of absorbed distance with time. The absorbed distance expanded inside very rapidly at the beginning and its velocity was almost constant later. The average velocity of the movement of the front of the absorbed zone was about 4 cm/year. This means that air in the SGM with less than 2 m depth from the surface will be completely replaced by water in 50 years. If this happens, the change of bulk density cannot be ignored.

The absorbed zone of SGM will expand toward the inside very rapidly under the soaked in water condition. Usually, SGM is not directly exposed to water but is used in wet sand. This situation was simulated by exposing SGM to wet sand.

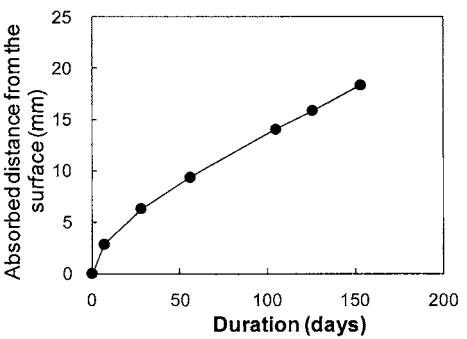

FIG. 30. Change of absorbed distance against time in SGM when soaked in water.

Figure 31 shows the change of wet density under the wet sand condition. From the figure, the increase in density was rapid and large when the water level was low, and vice versa. In all the cases, the increase in density was slower than in the case of soaked in water.

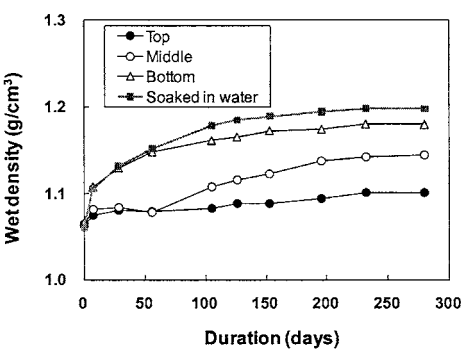

FIG. 31. Wet density change under wet sand condition.

The absorbed zone of SGM in these cases expanded from the surface to the inside in concentric circle similar to Fig. 11 or 29 by observation of the horizontal cross section of the X-ray CT image. Figure 32 shows the vertical cross section image taken by X-ray CT. These vertical cross sections were on the central axis of the specimen. The results for the lowest water level are shown in (c). From these figures, air was uniformly replaced by water from the side, top, and bottom surfaces. The results when the water level was higher than the specimen's top are shown in (a). No exchange or less exchange occurred in this case, and air was replaced by water only at the upper part of the specimen after 105 days of exposure. The results for the water level at the middle height of the specimen are shown in (b). The absorbed zone expanded rapidly in the upper part of the specimen and slowly in the lower part as can be estimated from the results of (a) and (c).

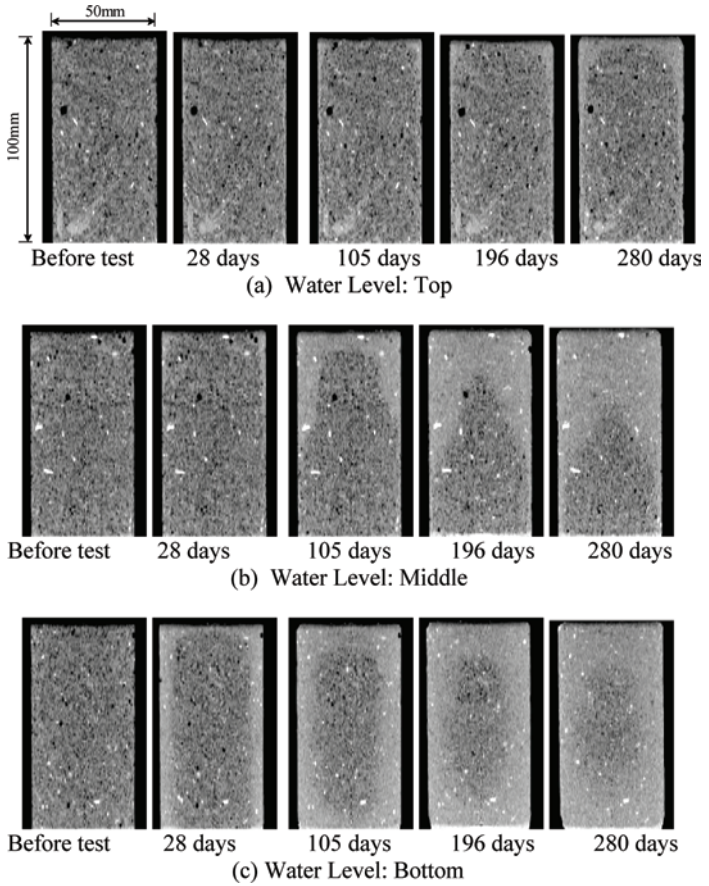

FIG. 32. Vertical cross sectional image by X-ray CT under wet sand condition.

Figure 33 shows the change of absorbed depth against time in SGM under the wet sand condition. The data shown in this figure were measured at the specimen's middle height and the water level height was at the top and at the bottom of the specimen. The absorbed zone was limited to near the surface when the water level was at the top of the specimen, while the absorbed zone expanded toward the inside when the water level was at the bottom of the specimen. When the water level was at the bottom of the specimen, the expansion velocity of the absorbed zone was almost the same as when soaked in water at the beginning and was slower than in the case of the specimen soaked in water.

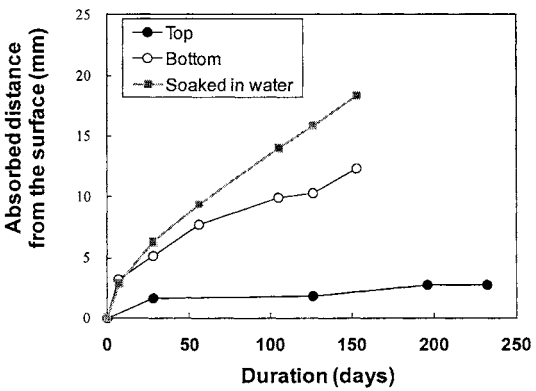

FIG. 33. Change of absorbed depth against time in SGM under wet sand condition.

Figure 34 shows the change of absorbed depth against time at 25 mm, 50 mm, and 75 mm heights of the specimen when the water level was at the specimen's middle height. The absorbed depth at 50 mm height of the specimen when the water level was at the top and bottom of the specimen are also shown in Fig. 34. The amount of air replaced by water in the lower part of the specimen in the case of the middle water level was almost the same as that of the high water level case. On the other hand, the higher part of the specimen in this case was almost the same as in the low water level case, and the middle height specimen was an intermediate value of these two cases.

The above results show that air is rapidly replaced by water when the SGM is located higher than the water table but air is slowly replaced by water when SGM is located lower than the water table. This conclusion is somewhat inconsistent with the results of the soaked water condition, because the specimen below the water table in wet sand was surrounded by more water than in the case when it was higher than the water table.

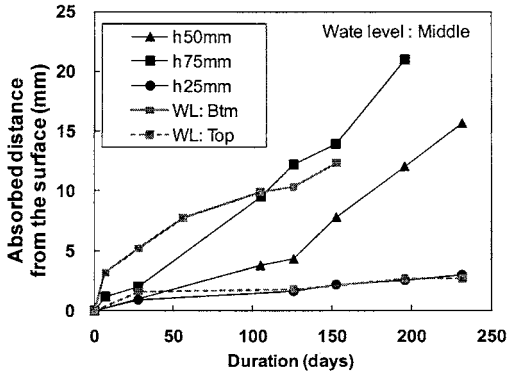

FIG. 34. Change of absorbed depth against time in SGM in the wet sand condition with middle water level.

In the wet sand condition, the sand surrounding the specimen was not saturated as shown in Fig. 35. This may have affected the test results. Therefore, the specimen was exposed to the saturated gravel layer. X-ray CT images of the cross section of the middle height of the specimen are shown in Fig. 36. The same as the above results, the absorbed zone expanded toward the inside in a concentric way. Figure 37 shows the absorbed depth in this case. The expansion velocity of the absorbed zone was almost the same as when soaked in water, though the exposure duration was rather short in the case of saturated gravel.

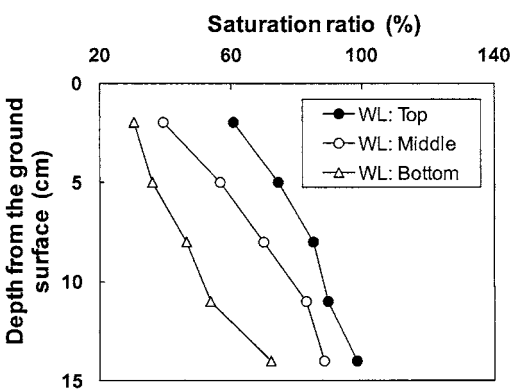

FIG. 35. Saturation ratio of wet sand surrounding SGM specimens.

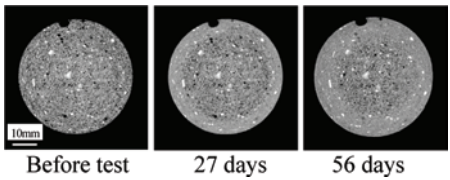

FIG. 36. X-ray CT images of the middle height of the specimen under saturated gravel condition.

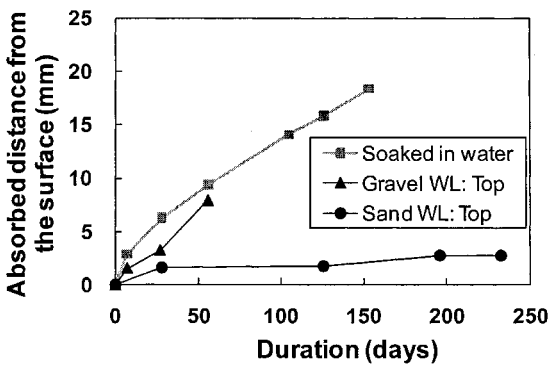

FIG. 37. Change of absorbed depth against time in SGM under saturated gravel condition.

The expansion velocity of the absorbed zone was not exactly constant, but the evaluation of this velocity had some errors. All the data showed that the velocity was rapid at the beginning of the experiment and became constant later. The long-term velocity such as longer than a year is unknown, but we assumed it to be constant, and the velocities were defined from the data after 20 days of exposure.

Figure 38 shows the relationship between the estimated expansion velocity of the absorbed zone and the saturation ratio of the surrounding ground. In this figure, the case when soaked in water is considered to be in the saturated condition. The velocity was high when the ground was fully saturated. The velocity was higher when the saturation ratio of the surrounding ground was lower and when the ground was unsaturated, at which time the saturation ratio was more than 50%. The velocity was low or negligible when the saturation ratio of the surrounding ground was about 80 to 90%.

It is still uncertain whether the velocity is directly related to the saturation of the surrounding ground and what drives the replacement of air by water in the SGM.

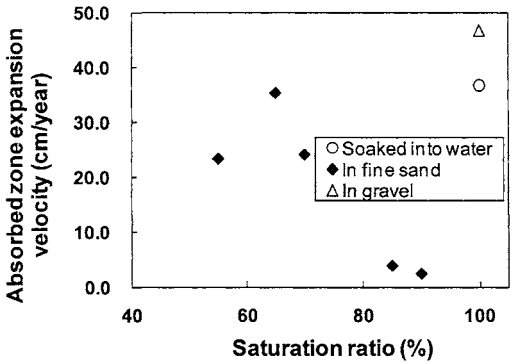

FIG. 38. Relationship between absorbed zone expansion velocity and saturation ratio.

Field observation

The SGM for backfilling a quay wall was sampled at Kobe Port Island in 2005. This site was destroyed by the Kobe earthquake in 1995, and SGM was then used for the restoration construction work.

Figure 39 shows the cross section of a reconstructed quay wall at Kobe Port Island at that time. The top surface of SGM was covered by wet sand to a thickness of 65 cm. The soil particle density was 2.70 g/cm^3, and the natural water content of the wet sand was about 10%. The top of the wet sand was covered by a 22 cm thick pavement. The top surface of SGM was D.L. +3.4 m and the bottom surface of SGM height was D.L. -1.0 m. The high water level of the front quay was D.L. +1.7 m and the low water level was D.L. $\pm$0.0 m.

The dredged clay was Kobe Bay clay, the physical properties of which are summarized in Table 5. The water content of the clay was controlled to 2.79 w_L by adding seawater. The cement was blast furnace slag cement B, and the foaming agent was surfactant. SGM was made by mixing these materials in the designated mixing condition as shown in Table 6.

This study used the X-ray CT scanner to confirm the stability of the internal structure of the field SGM that had been cast 10 years earlier. The top surface of the SGM was sampled as a 300 mm cubic block at the site. Then, this block was cut into a column of 50 mm in diameter and 100 mm in height in the laboratory. The specimens were taken at 0-100 mm and 120-220 mm from the top surface of the SGM. The density of the 0-100 mm specimen was 1.12 g/cm^3 higher than the design density of 1.00 g/cm^3, and the density of the 120-220 mm specimen was 1.02 g/cm^3.

Figure 40 shows the vertical cross section of each specimen. The image of the 0-100 mm specimen shows lighter parts extending from the top to the middle height. These lighter parts are considered to be absorption zones. The bottom of this specimen showed some black parts such as air foam. The image of the 120-220 mm specimen revealed that it was almost entirely air foam.

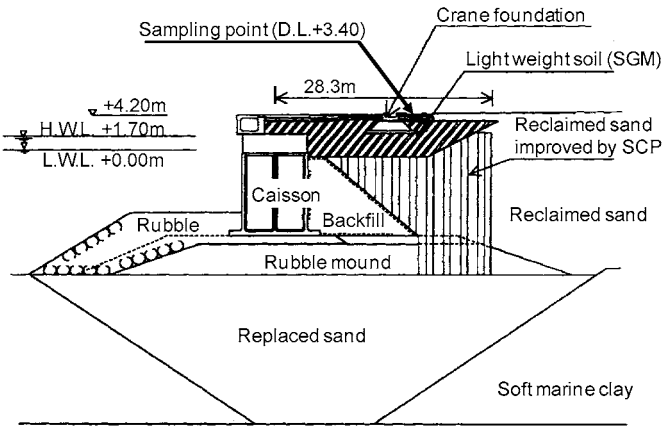

FIG. 39. Cross section of reconstructed quay wall at Kobe Port Island.

Table 5. Physical properties of Kobe Bay clay

Particle density (g/cm^3)	Liquid limit (%)	Plastic limit (%)	Grain size distribution (%)			
			Gravel	Sand	Silt	Clay
2.709	97	41	3	14	54	28

Table 6. Mixing condition of SGM

Controlled clay (kg/m^3)	Cement (kg/m^3)	Air foam (l/m^3)	Target density (g/cm^3)
849	140	279	1.0

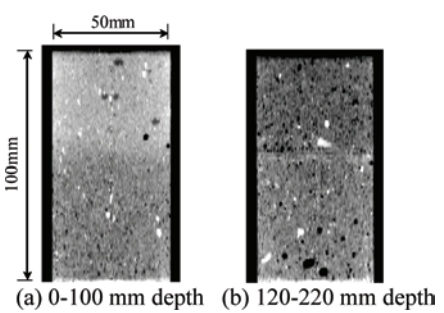

FIG. 40. Vertical cross-sectional images.

Figure 41 shows the density distribution of the SGM specimens estimated from CT data. The density from the top surface to 30 mm depth was constant at about 1.20 g/cm^3. The density from 30 mm to 70 mm depth decreased with the increasing of the depth, and the density from 70 mm depth was about 1.03 g/cm^3. The area of complete absorption was to 30 mm deep from the SGM surface after 10 years, so the absorption velocity under this condition was about 0.01 mm/day.

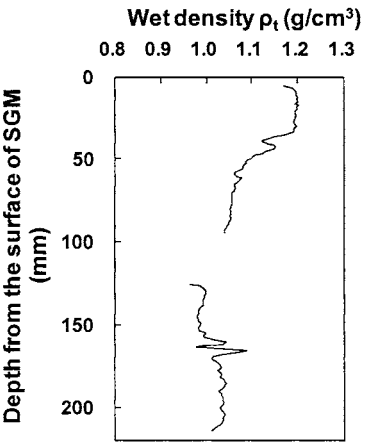

FIG. 41. Density distribution.

Another specimen from this site was cut from a 30 cm cubic block sample, and was soaked in water. The specimen size was 50 mm in diameter and 100 mm in height, and the depth from the top surface of the SGM was 120-220 mm. The conditions of this test were the same as those shown in Fig. 24. Figure 42 shows horizontal cross-sectional images of the specimen during the absorption test. These images were chosen from the middle height of the specimen. The images reveal extension of lighter parts from the water contact surface after 93 days; these lighter parts were absorption zones. The absorption velocity under the water condition was about 0.1 mm/day. This result was almost the same tendency as the laboratory test results. It is considered that the absorption velocity in the field was very slow, because the field SGM was surrounded by wet sand.

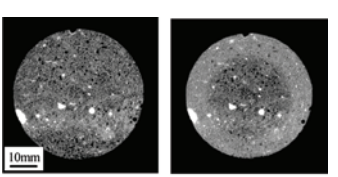

FIG. 42. Horizontal cross-sectional images.

CONCLUSIONS

In this paper, durability of cement treated clay with air foam, SGM, was investigated. When SGM is used for the backfill of the quay wall or reclamation of the man-made island, this material will be used under water or under the water table. In this case, hydraulic conductivity and water absorption characteristics are important characteristics for the durability of this material. This paper discussed these issues. The main conclusions are as follows;

1) The permeability and absorption properties of SGM are affected by air volume.
2) Air foam in SGM is an impermeable medium if bleeding channels are not made. However, when the air volume is higher, the air foam makes bleeding channels and the coefficient of permeability dramatically increases.
3) The absorption property of SGM is governed by the amount of air volume.
4) The absorption properties of SGM under the wet sand condition were different from those under the water condition. The absorption velocity of SGM under the wet sand condition was more than 10 times slower than under the water condition.
5) Ten years experience of the SGM used for backfilling quay walls certified that the absorption velocity of the SGM was as low as SGM covered by wet sand.

REFERENCES

Kikuchi, Y. and Yoshino, H. (1998). "Permeability of light-weight soil made of dredged slurry mixed with air foam", *Report of Port and Harbour Research Institute*, Vol. 37(1): 33-56. (in Japanese)

Kobayashi, M., Mizukami, J., and Tsuchida, T. (1990). "Determination of the horizontal coefficient of consolidation c_h", *Report of Port and Harbour Research Institute*, Vol. 29(2): 63-83. (in Japanese)

Otani, J., Mukunoki, T., Nagatome, T., Kikuchi, Y., and Sato T. (2001). "Characterization of seepage and drying on lightweight soil with air foam using X-ray CT method", *J. Geotech. Eng.*, JSCE, No. 701/III-58: 293-302. (in Japanese)

Terashi, M., Tanaka, H., Mitsumoto, T., Honda, S., and Ohashi, T. (1983). "Fundamental properties of lime and cement treated soils (3rd Report)." *Report of the Port and Harbour Research Institute*, Vol. 22(1): 69-96. (in Japanese)

Tsuchida, T., Takeuchi, D., Okumura, T. and Kishida, T. (1996). "Development of light-weight fill from dredgings." *Proc. of Environmental Geotechnics*, : 415-420.

Tsuchida, T., and Egashira, K. (2004). *The lightweight Treated Soil Method*: 120.

Zen, K. (1993). "Study on wave-induced liquefaction in seabed", *Technical Note of the Port and Harbour Research Institute*, No. 755: 17-31. (in Japanese)

An Economical, Practical and Environmental Friendly Surcharge Preloading Method to Improve Soft Ground of Municipal Road

Heping Yang[1], Jie Xiao[2] and Yufei He[3]

[1]Professor, School of Traffic and Transportation Engineering, Changsha University of Science and Technology, Changsha, Hunan Province, 410076, China; cscuyang@163.com
[2]Doctoral candidate, School of Traffic and Transportation Engineering, Changsha University of Science and Technology, Changsha, Hunan Province, 410076, China; xiaojie324@sina.com.cn
[3]Engineer, Dongguan Honggao Construction Engineering Corporation limited, Dongguan, Guangdong Province, 523507, China; hyf196209@163.com

ABSTRACT: The conventional surcharge materials are soils, sands and other building materials. According to local environment and construction conditions, this paper presents a case applying water as surcharge to treat soft ground of a western main road in Dong Guan city in the Pear River Delta alluvial plain. With the comparison to the vacuum preloading and deep soil mixing, the necessity and feasibility of this method were analyzed. In addition, a number of settlement plates and multi-point extensometers were installed for real-time monitoring of the embankment during construction. The in-situ vane plate shear test and geotechnical parameters testing of the soft ground were carried out after the removal of surcharge to evaluate the effect of improvement on soft ground. The results indicate that the effectiveness of improvement on soft soil is good. It is a cost-effective and environmental friendly method to consolidate soft ground especially in areas where it is lack of available fill but abound in water.

INTRODUCTION

Because of low bearing capacity and large settlements when subject to load, it is therefore inevitable to treat soft soil deposits prior to construction activities in order to prevent differential settlement, post-construction settlement and subsequently potential damages to structures.

At present, many soft ground improvement techniques are available. Every technique should lead to an increase in shear strength of soil, a reduction in soil compressibility and a reduction in soil permeability. The choice of ground improvement technique depends on geological formation of the soil, soil characteristics, cost, availability of backfill material and experience in the past. According to Bergado et al. (1996), they can be divided broadly into two categories. The first category includes techniques, which require foreign materials, and utilization of reinforcements, such as stone

columns, creep piles, deep stabilization. The second category includes methods that are strengthening the soil by dewatering, i.e. preloading techniques often combined with vertical drains.

When in comparison to the conventional surcharge preloading, the vacuum preloading method is more complex and needs complicated construction equipments. Vacuum consolidation is particularly applicable to very soft soils and the soft ground adjacent to critical slopes (Charles and Ali, 2004). The lack of understanding of its basic principles is a major obstacle to the development of vacuum-based consolidation. According to Masse et al., (2001), unsuccessful attempts have been recorded in the past for technological reasons.

Conventional surcharge preloading (physical surcharge) method is simple, mature and extensive application. This method involves the placement and removal of fill of similar to or greater than the permanent load. In order to reduce the post-construction settlement, the height of fill is usually higher than the desired final height, so that usually a large proportion of the fill is left behind after the surcharge has been removed. Because of the low strength of soft ground, the rate of increase in loading needs to be limited so that the ratio of load to the available strength of the subsoil is within the acceptable factor of safety. Therefore, this method requires a longer construction period.

The surcharge fills are usually soils, sands and other building materials. After the consolidation satisfied, the surcharge fill is often needed to remove. For the large-scale road construction in the Pear River Delta area where it is lack of available fill, the project cost is high if all surcharge fill are hauled from far away from the project sites. Furthermore, account should be taken to the impact on environment and to deal with the surcharge fill. According to local environmental and constructional condition, this paper presents an innovative method utilizing water as surcharge instead of part of surcharge soil to accelerate the soft ground consolidation. Several settlement plates and multi-point extensometers were installed in the subsoil for real-time monitoring of the embankment during construction. After construction, the in-situ vane plate shear tests were carried out to assess the effect of improvement on the geotechnical parameters of soft ground.

PROJECT DESCRIPTION

The western main road (the total length of 16.1Km) in Dong Guan city near Shenzhen Municipality is located in the Pear River Delta alluvial plain where there are many rivers and canals. The groundwater level is high. The geologic conditions are described as four layers. The upper layer is artificial soil of 0.5-4.7m. The mid layer is quaternary alluvium of 5.0-14.7m mainly consisting of clay, silt, silt soil, sand silt, clay sand, mid fine sand, mid coarse sand, etc. The third layer is the quaternary alluvial clay course. The bottom layer is bedrock of highly weathered, moderately weathered and slightly weathered mudstone. One typical section of geologic conditions is shown in FIG.1.

According to the initial design requirements, the average width and depth of embankment treated were 66 and 2m, respectively. The soft ground of embankment was consolidated by surcharge preloading combined with vertical drains. The freight of surcharge soil was as high as 5.2 dollars per cubic meter due to the average

transportation distance being more than 30km across more than four towns. It would produce a large amount of dust and a lot of noise in transit. That would disturb the people and cause serious environmental pollution. In addition, the contractual construction period of two and a half years was sufficient for soft ground consolidation according to the design requirement. Therefore, the contractor and the owner negotiated to change the initial design scheme from soil as surcharge material to water instead of part of soil to save project costs, accelerate the construction schedule and reduce the environmental pollution.

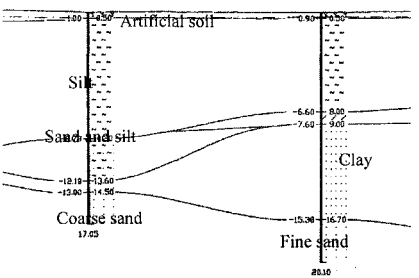

FIG. 1. Typical section of geologic conditions

This method has been successfully conducted in the third contract section of 3.4km. At the beginning of October in 2005, the first layer of embankment was filled after the continuously completion of installation of geotextiles, drainage layer and plastic vertical pipes. The first settlement sensor was installed in October 13 in 2005, and 34 settlement plates were sequentially installed at different stages of construction. The removal of water and surcharge fill started at July 30 in 2007, after which was completed the in-situ vane plate shear test was carried out to assess the effectiveness of improvement on soft soil.

CONSTRUCTION TECHNIQUES

Construction procedures

The surcharge preloading with water instead of part of surcharge fill was undertaken in following steps: (1) Placing a sand filled drainage layer (not less than 0.5m thickness) above the soft ground to provide a suitable working platform as well as an efficient draining layer; (2) Installing the plastic vertical drain pipes to accelerate the speed of consolidation of the subsoil by reducing the drainage path lengths and utilizing the naturally higher horizontal permeability of clay deposits, at a spacing of from 1.1 to 1.3m center to center, in a regular triangular array and the length determined by actual conditions; (3) Making infiltration ditch and collector well; (4) Installing the settlement plates and multi-point extensometer after the completion of embankment (shown in FIG.2); (5) Compacting the embankment fill by layers in the same thickness; (6) Placing surcharge fill (h=1.0m) over the embankment and compacting as (5); (7) Building cofferdam; placing waterproof geomembrane; adding water that was directly

pumped from a river not far from the road as the surcharge load; (8) Monitoring the total settlement and horizontal displacement at different depths to control the rate of load and preloading time and determine the removal time of surcharge.

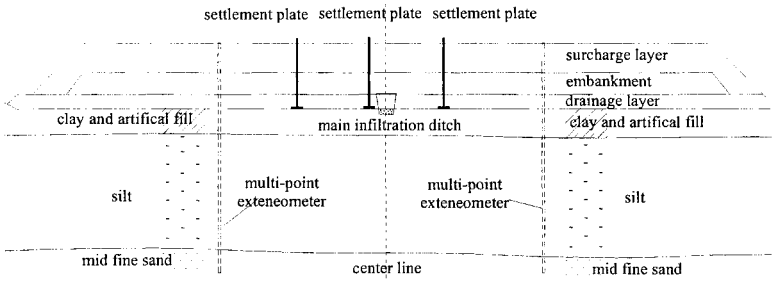

FIG. 2. Typical instrumentation profile

Implementation of the surcharge water

The high toughness plastic membranes were used to segregate the water and soil to resist infiltration. The cofferdam was continuously set up along the road. The length varied from 30 to 50m. The width was identical to that of the treated soft ground (shown in FIG. 3). In order to protect the settlement plates and observe the settlement conveniently, protection facility with the width not less than 1.0m and height equal to the cofferdam was built.

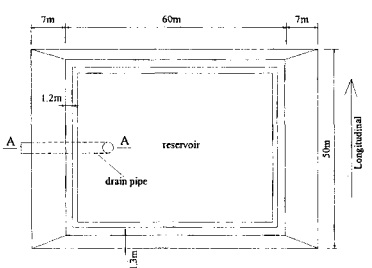

FIG. 3. General layout plan of cofferdam

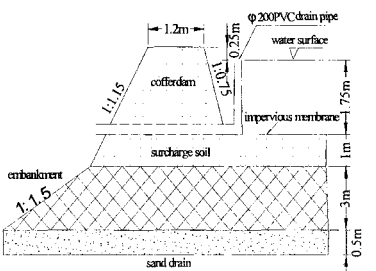

FIG. 4. A-A cross section profile of cofferdam

FIG. 4 shows the A-A cross-section profile of cofferdam. In order to ensure the cofferdam's stability after adding water, the width of top cofferdam, the outer slope rate and inner slope rate were 1.2m, 1:1.15 and 1:0.75, respectively. According to the simple Bishop method, the factor of safety was 1.585 calculated by that the maximum height of embankment fill, the height of surcharge fill and cofferdam height were 4.0m, 1.0m and 2.0m, respectively. Therefore, the overall stability of embankment should be satisfied

during construction. In order to prevent water over the top of cofferdam when raining, three to six overflow weirs in each pond were placed. One drainpipe (Φ 200 PVC tube, 1.75 m height) was installed in each pond to maintain the water at a constant level.

ESTIMATION OF GROUND IMPROVEMENT TECHNIQUE

In order to research the effects of improvement on the soft ground by this method, the rational construction scheme of loading was established. A large mount of in-situ settlement plates and multi-point extensometers were installed to monitor the total settlement and lateral displacement, respectively.

The settlement-time relationship is not only an important index of the embankment construction schedule, but also one criterion for assessing the effectiveness of improvement on soft soil. The settlement plates were placed at the bottom of the centerline of drainage layer to monitor the total settlement and settlement rate during construction. One representative values of monitoring point A (K6+903) selected from 32 monitoring points was analyzed as illustrated in FIG. 5, which was relatively higher than others.

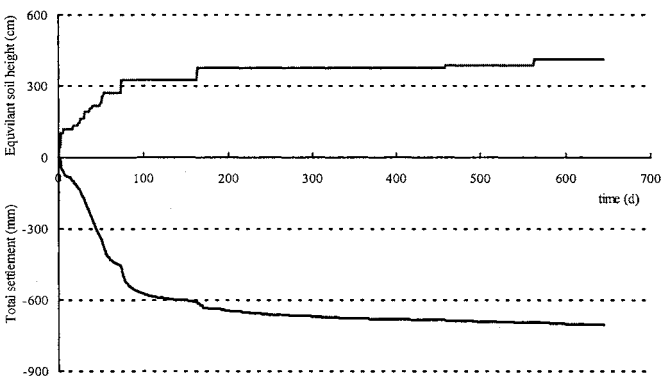

FIG. 5. Relationship of settlement versus time at monitoring point A

The initial settlement was large. The maximum total settlement of monitoring point A treated after 644 days was 812.12 mm. The total settlement changed very little one month before the removal of surcharge, which indicated that the effectiveness of treatment with surcharge preloading using water instead of part of surcharge soil on the soft ground achieved the desired objective.

The lateral displacements at different depths of monitoring point A at different times are shown in FIG. 6. It could be seen that the lateral displacements of soft ground were all outward displacements, gradually convergent with the depth increasing and equal to zero at the depth of 12m. The maximum of lateral displacement at monitoring point A was 42.4mm taking place at the surface of soft ground 3.0m under the surcharge (soil) surface. Meanwhile, the initial lateral displacement was large, but the increment of the

lateral displacement gradually became smaller with time.

In order to evaluate the effects of consolidation on the soft ground, the shear strengths of soft ground before and after consolidation were tested by the in-situ vane shear plate. The representative results are illustrated in FIG. 7. It could be seen that the shear strengths of consolidated soft ground were larger than that of unconsolidated soft ground, the increments of which were between 35%~80%.

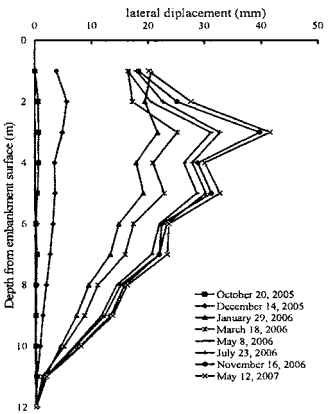

FIG. 6. Lateral displacements at point A

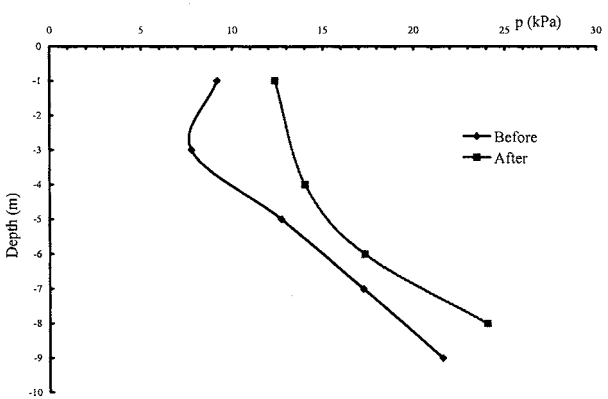

FIG. 7. Shear strengths with different depths at A

Properties index of soil before and after treatment

A large amount of geotechnical tests on various kinds of soils (mainly mud and mud soils) were carried out to analyze the effects of consolidation. The results of physical

and mechanical properties test on soft soils before and after consolidation at different depths at point A are presented in Table 1.

Table 1. Physical and Mechanical Properties on Various Soils

properties of soil		Depth (m)	Density (kN/m^3)	Water content (%)	Void ratio (e)	Modulus of compressibility (E_s)	Coefficient of compressibility $\alpha_{(1-2)}(MPa)^{-1}$	Quick direct shear test	
								c(kPa)	$\varphi(°)$
K6+903	Before	5.5~5.7	1.48	85.2	2.216	1.90	1.689	5.5	2.5
		12.8~13.0	1.55	70.0	1.830	1.69	1.677	7.7	5.0
	After	4.7~4.9	1.61	62.0	1.616	1.56	1.279	8.8	5.0
		6~6.2	1.73	47.7	1.228	2.91	0.746	13.2	5.0
		9.7~9.9	1.59	64.9	1.696	1.45	1.350	9.0	5.6

It can be seen that the effects of improvement on the soft ground were obvious from the results of physical and mechanical properties on soils before and after consolidation.

CONCLUSIONS

It was for the first time utilizing water instead of part of surcharge soil to treat the soft ground of a municipal road under the design and construction stages. According to local environmental and constructional condition, it took the advantage of water instead of part of soils as surcharge materials to make the surcharge soil height only a little higher than the total settlement of the soft ground in Dongguan City, so that the removal volume of surcharge soil was much less than that by conventional surcharge preloading method. For the treatment road of 3.4km, it totally saved 0.6 million dollars at least for reducing removal of 0.15 million cubic meters of soils. It protected the natural environment for reducing soil erosion, noises and emissions of exhaust gas. It has proven that utilizing water as part of surcharge fill to treat soft ground where are abounded in water but lack of available soil is an effective way. It is a simple technique, fast construction progress, low cost and practical method.

REFERENCES

Bergado, D. T., Anderson, L. R., Miura, N. and Balasubramaniam, A. S. (1996). "Soft ground improvement in lowland and other environments." America: *ASCE Press*.

Spaulding, C. and Porbaha, A. (2004). "Embankment Construction on Marshland using Vacuum Consolidation Technology." *Geotechnical Engineering for Transportation Projects*. 1943-1950.

Masse, F., et al. (2001). "Vacuum consolidation: A review of 12 years of successful development." Geo-Odessey-ASCE/ Virginia Tech-Blacksburg. VA USA.

Qian, J.H. and Yin, Z.Z. (1996). "Geotechnical Theory and Calculation (the first edition)." *Water and Electric Power Press*. (in Chinese).

Hao, B.Y. and Zhang, S.D. (1995). "Soft Ground Treatment." *China Railway Press*. (in Chinese)

Xia, C.C, and Pan, G.R, etc. (2001). "Civil Engineering Monitoring Technology." *China Architecture Industry Press*. (in Chinese).

Estimation of Strength Gain Due to Consolidation

Raghvendra Singh[1], Debasis Roy[2] and Himanshu Dubey[3]

[1]Research Student, Department of Civil Engineering, Indian Institute of Technology, Kharagpur, WB, INDIA 721302; rsingh@civil.iitkgp.ernet.in
[2]Associate Professor, Department of Civil Engineering, Indian Institute of Technology, Kharagpur, WB, INDIA 721302; debasis@civil.iitkgp.ernet.in
[3]Graduate Student, Department of Civil Engineering, Government Engineering College, Rewa MP, 486001; himansh.dubey@gmail.com

ABSTRACT: The undrained shear strength of foundation soils often increase substantially with consolidation due to staged construction and ongoing consolidation. In staged construction embankments on soft soil sites the rate of filling is mainly governed by the increase in soil strength as a result of consolidation. If the shear strength gain is not appropriately accounted for in the design, the design is unlikely to be economical or even feasible. However, a simple frame work for assessing the gain in undrained shear strength due to staged construction and ongoing consolidation is rare. The objective of this study is to validate the procedure proposed by Roy and Singh (2008) to estimate the undrained shear strength in stage construction embankments on soft soil sites using the two case histories. Use of undrained shear strengths in limit equilibrium slope stability assessments was found to provide results that were in qualitative agreement with the observed embankment behavior at the sites.

INTRODUCTION

Generally the gain in shear strength during stage construction of embankments on soft soil sites is estimated from poorly documented local experience database and an elaborate scheme of construction monitoring is implemented to ensure the pace of construction does not lead to remolding and progressive failure. The rate of fill placement is controlled by the rate of increase of the undrained shear strength of the underlying soil layers as a result of consolidation in the staged construction embankments. A slow rate of construction is maintained so as to reduce the possible instability at any stage of construction. If the shear strength gain is not appropriately accounted for in the design, the design is unlikely to be economical or even feasible. If the rate of consolidation-related strength gain of the foundation soils is overestimated, the instability could be triggered during construction. A simple framework for assessing the gain in undrained shear strength due to staged

construction and ongoing consolidation is therefore preferable. The objective of this study is to validate the proposed method that accounts for consolidation-related strengthening of soils for assessing the stability of earth structures founded at soft soil sites by Roy and Singh (2008).

ROY AND SINGH (2008) PROCEDURE

A simple procedure to estimate the shear strength gain during stage construction of embankments on soft soil sites was developed by Roy and Singh (2008) and outline of his procedure are discussed below.

Firstly, for estimating the undrained shear strength after the development of a certain amount of settlement a fictitious surcharge that would give an ultimate settlement equal to the observed settlement was back figured first assuming the fictitious surcharge to have an identical footprint as that of the preload fill and from the result the stress increments within the layers of foundation soils were estimated assuming the 2 (vertical) on 1 (horizontal) load-dispersion or using the elastic solution, e.g., the Newmark's influence chart. Then the apparent over consolidation ratio was computed for foundation soil layers using the Equation 1.

$$OCR = (\sigma_v' + \Delta\sigma_v')/\sigma_v' \tag{1}$$

where OCR is the apparent over-consolidation ratio, σ_v' is the original effective vertical stress and $\Delta\sigma_v'$ is the effective vertical stress increment within a certain soil layer due to the fictitious surcharge.

Secondly, the undrained shear strength was estimated following the SHANSEP (Ladd et al., 1977) approach in which

$$s_u/\sigma_v' = S \times OCR^m \tag{2}$$

where s_u is the un-drained shear strength, and SHANSEP parameters S and m are obtained from test data. s_u/σ_v', is the undrained shear strength ratio. For estimating s_u values of OCR obtained from Equation 1 was used if these values exceed those obtained from consolidation test. Otherwise, the estimates from laboratory consolidation tests were used. A similar approach is used for shear strength forecasting.

Thirdly, the parameters S and m (Equation 2) were obtained using the plot between s_u/σ_v' values obtained from field vane shear testing or laboratory UU testing of undisturbed or high quality soil samples and over-consolidation ratios obtained from one dimensional incrementally loaded consolidation testing of undisturbed or high quality soil samples conducted in the laboratory those were corrected for the sample disturbance. The soil properties of the various clays used for the plot are presented in the Table 1.

Table 1. Soil parameters of various clays

Site	S, m	Goodness of Fit (r^2)	Source
Marine Organic Clay	0.29, 0.81	-	Ladd et al. 1977
Bangkok clay	0.28, 0.76	-	Ladd et al. 1977
Atchafalaya clay	0.24, 0.79	-	Ladd et al. 1977
AGS CH clay	0.27, 0.70	-	Ladd et al. 1977
Boston Blue clay	0.22, 0.70	-	Ladd et al. 1977
Connecticut valley varved clay	0.17,0.71	-	Ladd et al. 1977
West Breakwater	0.21, 0.96	0.84	Chung et al. 2006
East Breakwater	0.20, 1.08	0.97	Chung et al 2006
Muar	0.20, 0.80	0.95	Indraratna et al. 1992
Suvarnabhumi	0.15, 1.04	0.95	Bergado et al. 2001
K18 (CL/CH)	0.34, 0.62	0.62	Roy and Singh 2008
K26 (CL/CH)	0.15, 1.08	0.84	Roy and Singh 2008

Using such $s_u / \sigma'_v - OCR$ relationships and the over-consolidation ratio estimated for a given stage of embankment construction obtained according to the procedure outlined in the preceding section, the undrained shear strength ratio for that stage of embankment construction is estimated.

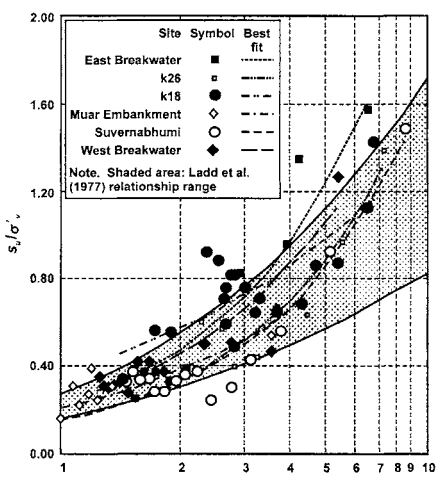

FIG. 1. $s_u / \sigma'_v - OCR$ relationships (from Roy and Singh 2008)

VALIDATION

The proposed relationship between $s_u / \sigma'_v - OCR$ was used to predict the response of two sites. The detailed description of the sites and the performance of these two sites are discussed in the following sub sections.

k26 Embankment

The k26 MSE wall of NH 6 failed near Kolkata, India. The construction of this site was started in July 15, 2003 and the deep seated failure was occurred in the early hour of January 12, 2005 when earth work of the embankment was nearly complete. The heavy rains with 24 h precipitations of 18.4 mm of January 10 and 0.4 mm on January 11 were reported before two days of incident. The height of the affected MSE wall was between 8.9 and 9.8m at the time of the incident. Subsurface investigations at k26 indicated that the site is under-lain by 15m thick, grey, soft to firm, silty clay of Holocene age over stiff, yellow-brown, silty clay of Pleistocene age containing calcareous nodules and silt and sand interbeds.

Using the parameters listed in Table 1 and the construction sequence it was estimated that the effect of the staged construction is equivalent to that of an instantaneously imposed surcharge pressure of 152.40 kPa placed over an identical footprint as those of the rock fill structures. Accordingly, the undrained shear strengths beneath the embankment were computed (Table 2).

The limit equilibrium stability analyses of the k26 MSE wall was conducted with the software package XSTABL Version 5.2 (Interactive Software Designs, Inc. 1994) and GLE method. The analysis indicated that the structure was marginally stable with a factor of safety 0.90 at the time of failure (Figure 2).

Table 2. Estimation of shear strength gain for k26

Depth	σ	σ'	$\Delta\sigma'$	OCR		OCR	s_u
m	kPa	kPa	kPa	Eq. 1	Lab		kPa
0.5	8.50	3.60	124.02	35.50	10.01	35.50	19.00
1.5	25.5	10.79	122.04	12.32	5.96	12.32	17.39
2.5	42.5	17.98	119.46	7.65	4.63	7.65	15.78
3.5	59.5	25.17	116.32	5.62	3.79	5.62	14.75
4.5	76.5	32.36	112.70	4.48	3.21	4.48	14.28
5.5	93.5	39.55	108.66	3.75	2.13	3.75	15.35
6.5	110.0	46.27	104.31	3.25	1.80	3.25	17.96
7.5	126.6	52.99	99.73	2.88	1.76	2.88	24.00
8.5	143.1	59.70	95.00	2.59	1.59	2.59	33.51
9.5	159.6	66.41	90.20	2.36	1.45	2.36	45.13

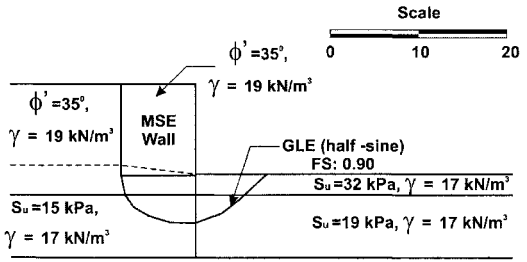

FIG. 2. Stability analysis of k26 embankment

k18 Embankment

The k18 MSE wall was failed at around 11:00 p.m., February 9, 2006, about a month after the northbound lanes became operational near Kolkata, India. During the failure, a section of the newly constructed MSE wall settled vertically by about 3 m and translated outward horizontally by about 4 m. Data from these investigations indicate that the site is under-lain by a sequence of 10 to 12 m thick, Holocene silty clay, over silty clay of Pleistocene age. The upper 5-8 m of the Holocene unit was firm and over consolidated with pre-consolidation pressure of up to 200 kPa, underlain by a 3 to 5 m thick soft, compressible, normally to lightly over-consolidated layer containing organics and peat inclusions.

Using the parameters listed in Table 1 and the construction sequence it was estimated that the effect of the staged construction is equivalent to that of an instantaneously imposed surcharge pressure of 182.67 kPa placed over an identical footprint as those of the rock fill structures. Accordingly, the undrained shear strengths beneath the embankment were computed (Table 3).

Table 3. Estimation of shear strength gain for k18

Depth	σ	σ'	Δσ'	OCR		OCR	s_u
m	kPa	kPa	kPa	Eq. 1	Lab		kPa
0.5	8.34	3.44	179.974	53.38	28.10	53.38	43.200
1.5	25.06	10.35	174.815	17.89	22.31	22.31	42.100
2.5	41.83	17.30	169.944	10.82	16.45	16.45	40.130
3.5	58.50	24.17	165.336	7.84	10.59	10.59	37.770
4.5	75.15	31.01	160.972	6.19	6.86	6.86	35.420
5.5	91.78	37.83	156.832	5.15	5.71	5.71	33.060
6.5	108.40	44.63	152.900	4.43	4.56	4.56	30.710
7.5	125.00	51.43	149.160	3.90	3.41	3.90	33.060
8.5	141.59	58.21	145.599	3.50	2.80	3.50	41.070
9.5	158.18	64.98	142.204	3.19	2.83	3.19	49.090

The limit equilibrium stability analyses of the k18 MSE wall was conducted with the software package XSTABL Version 5.2 (Interactive Software Designs, Inc. 1994) and Modified Bishop method. The analysis indicated that the structure was marginally

stable with a factor of safety 0.99 at the time of failure (Figure 3).

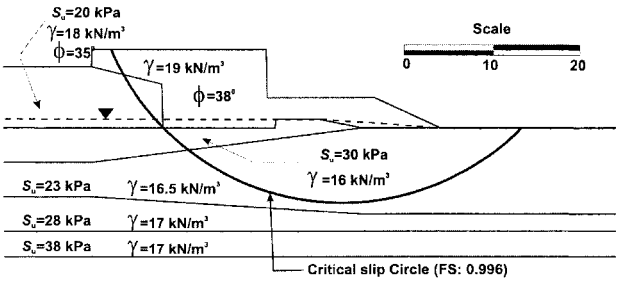

FIG. 3. Stability analysis of k18 embankment

CONCLUSIONS

The procedure proposed by Roy and Singh (2008) to estimate the undrained shear strength in stage construction embankments on soft soil sites that depends on the rate of fill placement was validated with the stability analysis of two embankments constructed over soft sites. The results of limit equilibrium slope stability assessments of these two cases were in qualitative agreement with the observed embankment behavior of these sites.

REFERENCES

Bergado, D.T., Balasubramaniam, A.S., Fannin. R.J. and Holtz, R.D. (2001). "Prefabricated vertical drains (PVDs) in soft Bangkok clay: a case study of the new Bangkok international Airport project." Can. Geotech. J., Vol. 39(2): 304-315.

Chung, S. G., Kim, S. K., Kang, Y.J., Im, J. C. and Nagendra Prasad, K. (2006). "Failure of breakwater founded on thick normally consolidated clay layer." Geotechnique, Vol. 56(6): 393-409.

Indraratna, B., Balasubramanian, A.S. and Balachandran, S. (1992). "Performance of test embankment constructed on failure on soft marine clay." J. of Geotech. Engrg, ASCE, Vol. 118(1): 12-33.

Interactive Software Designs Inc. (1994). "XSTABL User's Manual." Moscow, ID, USA.

Ladd, C.C., Foott, R., Ishihara, K., Schlossar, F. and Poulas, H.G. (1977). "Stress-deformation and strength characteristics." *Proc. 9th Int. Conf. on Soil Mech. And Found. Engg.*, International Society of Soil Mechanics and Geotechnical Engg., London, Vol.: 412-494.

Roy, D. and Singh, R. (2008). "Mechanically stabilized earth wall failure at two soft and sensitive soil sites." J. of Performance of constructed facilities, ASCE, Vol. 22(6): 373-380.

Numerical Study on the Deformation and Failure of Reinforced Sand Retaining Walls subjected to the Vertical Load

Yanbo Cao [1], Fangle Peng [2], Ke Tan [3] and M.S.A.Siddiquee [4]

[1]Department of Geotechnical Engineering, Tongji University, 1239 Siping Road, Shanghai 200092, PRC; email: caoyb2008@yahoo.com.cn

[2]China Key Laboratory of Geotechnical and Underground Engineering of Ministry of Education, Department of Geotechnical Engineering, Tongji University, 1239 Siping Road, Shanghai 200092, PRC; email: pengfangle@tongji.edu.cn

[3]Department of Geotechnical Engineering, Tongji University, 1239 Siping Road, Shanghai 200092, PRC; email: Godisfair_tk@yahoo.com.cn

[4]Department of Civil Engineering, Bangladesh Univ. of Science and Engineering, Dhaka 1000, Bangladesh; email: sid@ce.buet.ac.bd

ABSTRACT : To gain a better insight into the deformation and failure of reinforced sand retaining walls subjected to the vertical load from the crest and their associated reinforcing mechanisms, the model experimental results from well-controlled fully-instrumented load tests of full-scale reinforced sand retaining wall with sand backfill are simulated by making use of a nonlinear elasto-plastic finite element model considering strain localization. In the FEM analysis, the effects of the following factors for the filled sandy soil are taken into account: (a) the non-linear pre-peak work-hardening and post-peak work-softening; (b) effects of stress history and stress path; (c) the confining pressure dependency and strength anisotropy; (d) the stress-dilatancy characteristics; and (e) strain localization into a shear band(s) with a width proportional to the particle size. The load-settlement relationship obtained from FEM analysis is generally in good agreement with the physical experimental result. It is also found that the progressive failure with a development of shear bands and the horizontal earth pressure on the back of facing and the tensile force in the reinforcement layers can be reasonably simulated by the proposed FEM analysis.

INTRODUCTION

The current stability analysis of reinforced soil retaining walls is basically by the limit equilibrium method. It is usually assumed that the strain-stress behavior of soil is rigid perfectly plastic, and therefore the peak strength is mobilized simultaneously along the potential failure plane while the active zone inside the failure plane remains rigid. However, this method neglects the progressive nature of failure and the essential strength and deformation characteristics of the reinforced sands, including stress history and stress-path, pressure level-dependency and inherent anisotropy. Also, the reinforcing mechanism associated with generation and development of shear band in reinforced soil structures cannot be solved in the current design method.

In view of the above, Tatsuoka et al. (1989) performed a series of plane strain model tests of reinforced sand retaining walls, making the model fail by loading with a strip footing on the wall crest. The results show that the failure pattern of the retaining walls is progressive along with the development of shear bands. Kotake et al. (1999) and Peng et al. (2000, 2002a, 2002b and 2008) successfully simulated a series of physical model tests of reinforced sand under plane strain condition by the elasto-plastic FEM analysis with considering strain localization. They showed that FEM analysis was able to predict realistically the progressive failure of unreinforced and reinforced sand only when based on realistic constitutive models of the sand. Therefore, the objective of this study is to simulate the reinforced sand retaining wall model tests (Tatsuoka et al. 1989) by the elastic-plastic FEM analysis with one energy-based hardening and softening constitutive model (Peng et al. 2002a, 2002b, and 2009). The load-settlement relationship and the failure pattern with progressive development of shear bands obtained from the physical model test will be compared and examined. In addition, the horizontal earth pressure on the back of facing and the tensile force in the reinforcement layers from the FEM analysis are presented.

MODEL TEST REVIEW

FIG. 1 shows the setup of the laboratory reinforced sand retaining wall model test under a plane strain condition (Tatsuoka et al. 1989). The model wall is constructed in a sand box by the following construction sequences. The surface of the previous sand layer is made flat and then a reinforcement layer is placed on it. Subsequently, on the previous block with being supported by a temporary support. The reinforcement is connected to the block. Then, a layer of air-dried Toyoura sand is placed by pluviating through air at a controlled fall height. The model wall is 84cm in width (including 3cm wide facing), 39.5cm in length and 52cm in height (see FIG. 1(a)). The side walls of the sand box consists of 3cm thick transparent acrylic plates with outside steel stiffeners to ensure the plane strain condition. The inside surface of the acrylic plates is well lubricated by means of a 0.5mm-thick silicone grease layer placed between the

plate and a 0.2mm-thick latex rubber membrane sheet in contact with sand.

A rigid 10cm wide and 39.5cm long footing with a lubricated base is loaded at an axial displacement rate of 0.10mm/min (see FIG. 1(b)). The footing load is measured by means of two two-component load cells located at the central third of the footing. The footing is located behind the reinforced zone with the toe of footing above the back of reinforced zone. The model facing is made by pilling up eleven wooden blocks which are tightly connected to each other by means of both the steel bars penetrating them and the outside stiffeners (see FIG. 1(b)). The bottom of the facing is hinged on the rigid base of the sand box, preventing the facing from sliding out. The model reinforcement members are of grid-type, made of phosphor-bronze strips (see FIG. 1(c)). Each strip is 3mm wide, 0.1mm thick and 15cm long. The model wall is reinforced with 10 layers of phosphor-bronze strips. The detail of laboratory model test has been described in Tatsuoka et al. (1989).

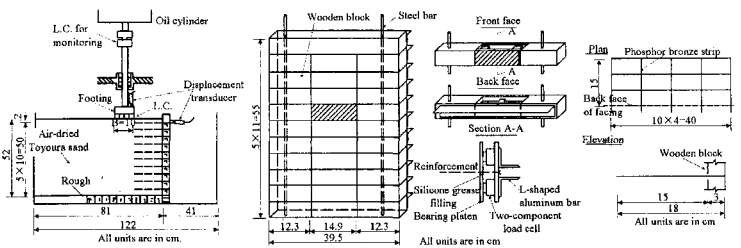

FIG. 1. Set-up of the laboratory model loading tests on reinforced sand retaining wall: (a) cross-section of model wall and loading arrange; (b) details of model facing; (c) model reinforcement (Redrawn according to Tatsuoka et al. 1989).

FEM MODELING FOR REINFORCED SAND RETAINING WALL

FEM mesh

As shown in FIG. 2, the whole domain of the model wall is discretised into four node quadrilateral plane strain elements. The critical zone in the vicinity of the footing base is discretized into fine square elements (1.0cm×1.0cm) to better capture the deformation and failure mode. The total numbers of elements and nodal points are 1262 and 1233, respectively. Rollers are placed along the left lateral and bottom boundaries of the analysis domain, except the bottom of facing which is hinged.

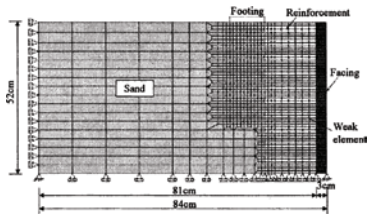

FIG. 2. Finite element mesh for the present simulation.

Constitutive model for sand

As the details of the sand constitutive model have been reported in several previous papers by authors (Peng et al. 2002a, 2002b and 2009), only the essence will be described below. This model is developed based on the modified plastic strain energy concept, represented by a unique relationship between the modified plastic strain energy and a stress parameter, which is independent of stress history. The modified plastic strain energy concept is developed based on results from a series of drained plane compression tests along various stress paths on saturated dense Toyoura sand with accurate stress and strain measurements. The proposed model is coupled with an isotropic work-hardening and softening, non-associated, elasto-plastic material description. The yield function and the plastic potential function are of Mohr-Coulomb and Drucker-Prager type, respectively. It is assumed that the deformation of a given sand element under uniform boundary stress conditions is homogeneous in the pre-peak regime, while strain localization into a shear strain starts suddenly at the peak stress state. This model considers the effects of the following factors for sands: (a) non-linear pre-peak work-hardening and post-peak work-softening; (b) effects of stress history and stress path; (c) the confining pressure dependency and strength anisotropy; (d) the stress-dilatancy characteristics; and (e) strain localization into a shear band(s) with a width proportional to the particle size. Due to the paper page limitation, more details about this constitutive model and its parameter identification can be found in Peng et al. (2002a, 2002b and 2009).

Modeling of reinforcement

The reinforced soil retaining wall with metal strips has a three-dimensional geometry that cannot be modified directly with a two-dimensional model in a plane strain condition. Therefore each reinforcement layer, consisting of phosphor bronze strips, is modeled as a planar reinforcement layer by using beam elements in the present FEM analysis. The axial and bending stiffness values of each planar reinforcement layer are set equal to the respective average value of the original reinforcement layer, consisting of 5 phosphor bronze strips with a covering ratio CR=3% in a width of 40cm. The beam element has a cross sectional area A= 2.9×10^{-4}cm^2, a moment of inertia I=2.4×10^{-9}cm^4 per unit length in the ε_2 direction, and a Young's modulus E=1.22×10^{8}kN/m^2 for phosphor bronze material. This E value is

evaluated assuming linear elasticity based on tensile loading test results.

Modeling of facing and footing

The facing platen, having two-dimensional nature, is modeled by four node quadrilateral plane elements. The behavior of the facing is simply assumed to be linearly elastic. The Young's modulus of the facing E is taken equal to 10^5kN/m^2, the Possion's ratio of the facing ν is taken equal to 0.28.

The footing adopted in the physical model test, having a lubricated base, is modeled by applying prescribed uniform vertical displacements at the nodal points along the footing allowing horizontal displacements, without introducing a model footing directly.

Modeling of interface between sand and reinforcement

In the present study, no interface elements is used since neither pronounced slippage between sand and reinforcement nor pull-out failure of reinforcement is observed in the physical model tests. However, the sand elements adjacent to the reinforcement are assumed as weak elements (Kotake et al. 1999 and Peng et al. 2000) which are easier to fail (see Fig. 2). The weak element has the same constitutive law with the surrounding sand, but has the upper limit of internal friction angle ϕ_{peak}, corresponding to the peak interface friction angle. Thus, an equivalent interface friction angle mobilized between the soil and the reinforcement models in the two-dimensional analysis, ϕ_{mob}, has a relation with ϕ_{peak} as:

$$\phi_{mob} = \arctan(\tau_s / \sigma_n)_{\max} \le \phi_{peak} \tag{1}$$

Where, τ_s is shear stress between soil and reinforcement; σ_n is normal stress on the reinforcement. In the present study, no weak element is used between sand and facing.

Numerical procedure

By incorporating the energy-based constitutive model for sand, a FEM procedure is developed (Peng, 2000). A set of non-linear equations are solved by the dynamic relaxation (DR) technique, which has a reputation in solving highly non-linear equations, especially for high friction angle materials as used in the present case. The details have been introduced in Siddiquee et al. (1995) and Peng (2000).

In the same way as the physical model test, a central and vertical load is applied to a rigid footing with smooth base under displacement control. Uniform vertical displacements are prescribed to the nodal points of the sand retaining wall model, which is in contact with the footing base, while horizontal displacements of those nodal points are free to model the smooth base footing condition. The displacement rate in the analysis is 0.004mm/step, i.e., 0.004%/step of the footing width B, which is found to be small enough to keep accuracy and numerical stability with an equilibrium iteration tolerance of a force norm and an energy norm of 10^{-6}.

FEM RESULTS AND DISSCUSSIONS

Load-settlement relationship

The relationships between the average footing pressure q and the footing settlement S obtained from the model test and the FEM analysis are compared in FIG. 3. It is found that the present FEM analysis can reasonably simulate the load-settlement relationship from the physical model test not only the pre-peak but also the post peak regime. However, the peak footing load and the pre-peak stiffness in the present simulation are slightly larger than that in the model test.

Strain field and progressive failure

FIG. 4 shows the strain field (contours of maximum shear strain $\gamma_{max} = \varepsilon_1 - \varepsilon_3$) from the model test observed at a footing settlement of 15mm. It is found that the shear band starting from the footing heel goes downwards and then heads for the heel of the reinforced zone, while the other shear band from the footing toe along the back of reinforced zone which goes downwards vertically is not clearer than the first.

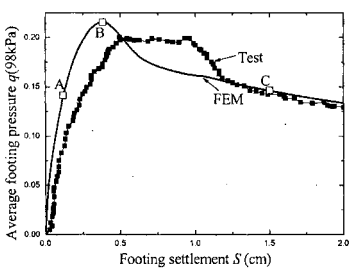

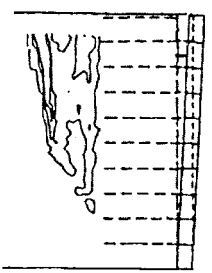

FIG. 3. (left) Measured and simulated load-settlement relationships.

FIG. 4. (right) Contours of maximum shear strain γ_{max} from the model test at a footing settlement of 15mm (from Tatsuoka et al. 1989).

FIG. 5 shows the contours of the maximum shear strains γ_{max} at three loading stages obtained from the FEM analysis, in which the representative loading stages selected are "before peak (A)", "around peak (B)" and "after peak to residual (C)" (corresponding to the stage of the footing settlement of 15mm) as denoted in FIG. 3.

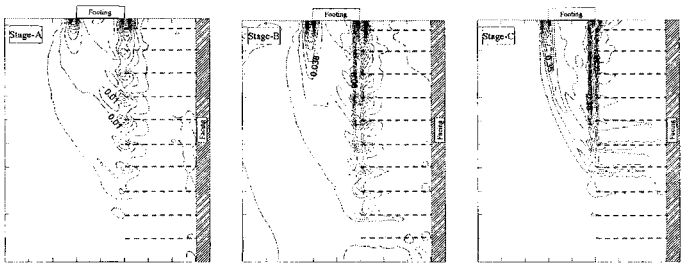

FIG.5. Contours of maximum shear strain γ_{max} from the FEM analysis.

It can be seen in FIG. 4 and FIG. 5 that the shear bands in the model test is well simulated by the present FEM analysis. In addition, it is found in the FIG. 5 that the FEM analysis can well simulate the development of the shear bands which affect the load-settlement behavior, that is: (1) at the pre-peak stage (A), the zone beneath the footing toe and heal are more intensely strained; (2) around the peak stage (B), the shear bands from the footing heel and toes go downwards and the shear strains in the reinforced zone are highly restrained by the reinforcement layers and the rigid facing; (3) at the post-peak stage (C), the two shear bands go deeper and the shear band from the footing toe heads for the heal of the reinforced zone. These results indicate that the failure of reinforced retaining wall is highly progressive examined well by the FEM.

Horizontal earth pressure and reinforcement force

FIG. 6 shows the distribution of the horizontal earth pressure on the back of facing at the peak footing load stage from the FEM analysis (q_u is the peak average footing pressure, p_f is the horizontal earth pressure at the peak footing load stage). It may be seen that the earth pressure generally increases as the height of the retaining wall increases and the largest earth pressure locates at the bottom of facing.

FIG. 7 shows the distributions of the tensile force in the reinforcing members at the peak footing load stage from the FEM analysis. It is found that the peak value of tensile force in each reinforcement occurs near the back face of facing, while the minimum tensile force locates at another end of the reinforcement. In addition, the tensile forces are mobilized in the lower reinforcement layers such as the 8th and 10th reinforcement, while little tensile forces are mobilized in the higher reinforcement layers such as the 2nd and 4th reinforcement.

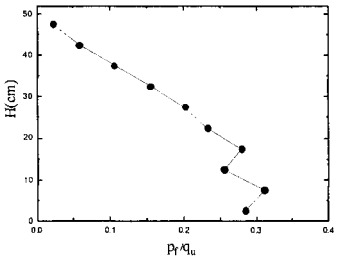

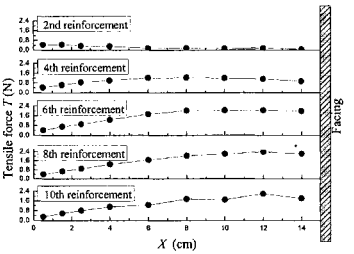

FIG. 6. (left) Distribution of the horizontal earth pressure on the back of facing at the peak footing load stage from the FEM analysis.

FIG. 7. (right) Tensile force in the reinforcement at peak footing load stage from the FEM analysis.

CONCLUSIONS

(1) The proposed FEM analysis can well simulate the footing load-settlement relationship and strain fields of the laboratory reinforced sand retaining wall model test, and reasonably examine the horizontal earth pressure and reinforcement force.

(2) The failure of reinforced retaining wall is highly progressive with the development of shear bands, which is examined well by the proposed FEM analysis. By an insight into the strain fields, the reinforcing mechanism is clearly understood in relation to the load-settlement relationship.

(3) The peak footing load and the pre-peak stiffness in the present simulation are slightly larger than that in the model test. These discrepancies may be partially attributed to some intrinsic limitations in the FEM analysis and no interface elements used between sand and facing.

ACKNOWLEDGMENTS

The authors acknowledge gratefully the support provided by China National Key Technology R&D Program (2006BAJ27B02-02), Shuguang Project (No.05SG25), NSFC (No.50679056 and No.40972176), NCET (06-0378), and Shanghai Leading Academic Discipline Project (B308).

REFERENCES

Kotake, N., Tatsuoka, F., Tanaka, T., Siddiquee M S A. and Yamauchi, H. (1999). " An insight into the failure of reinforced sand in plane strain compression by FEM simulation." *Soils and foundations*, 39(5):103-129.

Peng, F.L. (2000). "Constitutive modeling and finite element analysis of reinforced soils." *Doctoral thesis*, University of Tokyo, Japan.

Peng, F. L., Kotake, N., Tatsuoka, F., Hirakawa, H. and Tanaka, T. (2000). "Plane strain compression behavior of geogrid-reinforced sand and its numerical analysis." *Soils and Foundations*, 40(3):55-74.

Peng, F. L., Tatsuoka, F., Siddiquee, M S A. and Kotake, N. (2002a). " FEM simulation of failure of reinforced sand in plane strain compression." *Geosynthetics-7th ICG*:1273-1276.

Peng, F.L., Tatsuoka, F. and Siddiquee, M.S.A. (2002b). "An energy-based modeling of sand and its FEM application." *IN:PROC. Of the 15th ASCE Engineering Mechanics Conference*.New York: ASCE, 2002. in CD-ROM.

Peng, F.L., Siddiquee, M. S. A. and Tatsuoka, F. (2008). "Elasto-viscoplastic simulation of bearing capacity characteristics of strip footing on reninforced sand." *Geosynthetics in Civil and Environmental Engineering-Geosynthetics Asia 2008, Proceedings of the 4th Asian Regional Conference on Geosynthetics* : 305-310.

Peng, F.L., Siddiquee, M.S.A., Tatsuoka, F., Yasin, S.J.M. and Tanaka, T. (2009). "Strain energy-based elasto-viscolastic constitutive modeling of sand for numerical simulation." *Soils and Foundations.*, Vol. 49 (4):611-630.

Siddiquee, M.S.A. Tanaka, T. and Tatsuoka, F. (1995). "Tracing the equilibrium path by dynamic relaxation in materially nonlinear problems." *International Journal for Numerical and Analytical Methods in Geomechanics*, 19:749-767.

Tatsuoka, F. Tateyama, M. and Murata, O. (1989). "Earth retaining wall with a short geotextile and a rigid facing." *Proc. 12th ICSMFE*, 2:1311-1314.

Development of Reinforced Soil Structure With Pile Foundation - Piled Geo-Wall -

Takashi Hara[1], Shinichiro Tsuji[2], Naoki Tatta[3], Atsushi Yashima[4] and Kazuhide Sawada[5]

[1]Associate Professor, Department of Civil Engineering, Gifu Unicersity, 1-1 Yanagido, Gifu, Japan, 501-1193; t_hara@gifu-u.ac.jp
[2]Assistant Professor, Department of Civil Engineering, Gifu Unicersity, 1-1 Yanagido, Gifu, Japan, 501-1193; s_tsuji@gifu-u.ac.jp
[3]Chief Engineer, Technical Department, MAEDA KOSEN CO., LTD., 38-3 Okinunome Harue-cho Sakai-city, Fukui, Japan, 919-0422; tatsu@mdk.ac.jp
[4]Professor, Department of Civil Engineering, Gifu Unicersity, 1-1 Yanagido, Gifu, Japan, 501-1193; yashima@gifu-u.ac.jp
[5]Associate Professor, River Basin Research Center, Gifu Unicersity, 1-1 Yanagido, Gifu, Japan, 501-1193; sawada@gifu-u.ac.jp

ABSTRACT: This study aims to achieve independent reinforced soil structure with pile foundation, which can apply to earth retaining wall, rockfall protection structure and others that can built on narrow construction site, such as on a sloped foundation or beside mountainous road. In this study, in order to confirm the effectiveness of the application of pile foundation to reinforced soil structure for improvement of the lateral resistance and investigate interaction between pile and reinforced soil structure, a dynamic centrifuge model test (25G) was carried out. And a numerical simulation of the experiment was conducted to propose a design method of the structure.

INTRODUCTION

High ductility of soil structure reinforced by geogrid is well known and it is also possible to build independent soil structure. The independent reinforced soil structure, which is termed "Geo-wall" in this paper, can be applied to earth retaining wall, rockfall protection structure and others, as reasonable one, because it can be built by using soil existing at the construction site.

However, wide Geo-wall with spread foundation is designed in general, thus the application to narrow construction site, such as on a sloped foundation or beside mountainous road, is too difficult. If pile foundation can be applied to Geo-wall, wide-range narrow width Geo-wall can be achieved. Therefore, a study on the application of pile foundation to Geo-wall, which is termed "Piled Geo-wall" in this paper, as shown in Figure 1, has been conducted by authors.

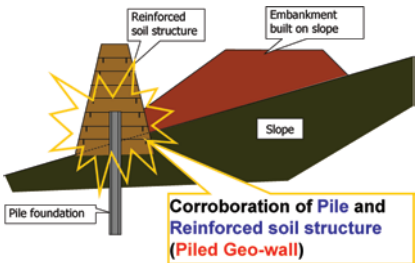

FIG. 1. Piled Geo-wall.

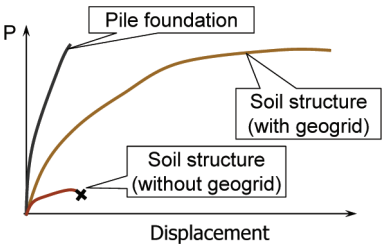

FIG. 2. Assumption of interaction between pile and Geo-wall.

In this study, the effectiveness of the applicability of the pile foundation to Geo-wall in order to improve lateral resistance and the assumption in relation to interaction between pile and Geo-wall, which reinforced soil structure with high ductility can transmit the lateral force to the pile foundation, as shown in Figure 2, were confirmed from a dynamic centrifuge model test (25G), and a numerical simulation of the experiment was carried out to propose a design model of the structure.

EFFECTIVENESS OF THE APPLICATION OF PILE FOUNDATION TO GEO-WALL FOR IMPROVEMENT OF LATERAL RESISTANCE

A dynamic centrifuge model test (25G) was carried out to confirm the effectiveness of application of pile foundation to Geo-wall, and dynamic interaction between pile and Geo-wall. In this test, the difference of the behaviors between a piled Geo-wall and normal one (without pile), which are used as a seismic countermeasure to restrict deformation of road embankment built on sloped foundation, as shown in Figure 3, was compared. Table 1 and 2 show the geotechnical and the structural parameters adopted in this test.

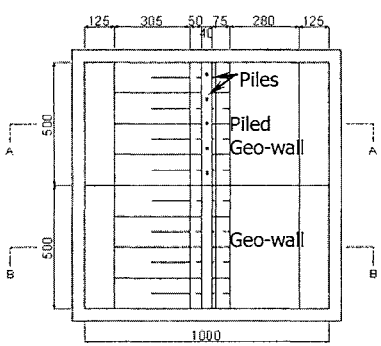

(a) top view

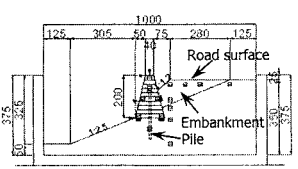

(b) A-A section

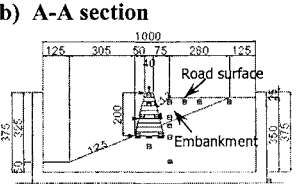

(c) B-B section

FIG. 3. Experiment model (1/25 scale model).

Table 1. Geotechnical parameter*

	Elastic modulus (kPa)	Cohesion (kPa)	Internal friction angle (Deg.)
Slope	3.26×10^5	55	0
Embankment	3.0×10^4	0	40
Geo-wall	3.0×10^4	0	40

Table 2. Structural parameter*

	Elastic modulus (kPa)	Sectional area (m^2/m)	Moment of inertia (m^4)
Pile	2.0×10^8	4.79×10^{-3}	2.04×10^{-5}
Geogrid	8.0×10^5	1.0×10^{-3}	-

* converted value to actual scale

Where, the Geogrid that has equivalent initial elastic modulus to actual geogrid, which is converted by EA, was adopted. Geo-wall was built at every step as same as actual Geo-wall execution as shown in Figure 4. Figure 5 shows specific longitudinal additional geogrid, which aims to transmit the load to pile from Geo-wall body smoothly, were installed at every layer. An earthquake wave observed in Kobe earthquake (1995) was input in this test, because this wave has large acceleration, as shown in Figure 6, and it was considered that the effect of large acceleration to the structure can be confirmed.

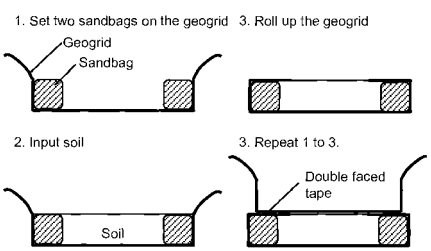

FIG. 4. Procedure for building Geo-wall.

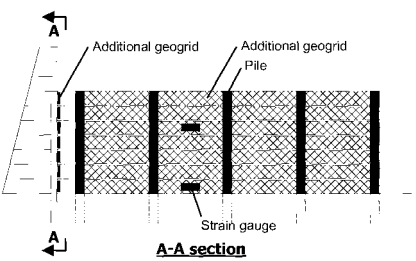

FIG. 5. Additional Geogrid.

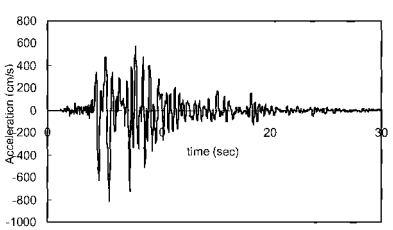

FIG. 6. Input wave.

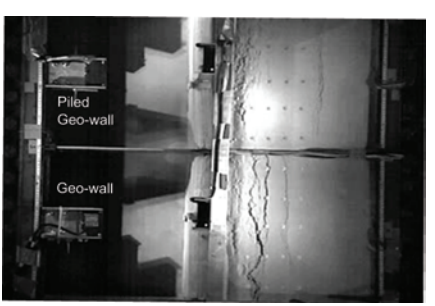

FIG. 7. State of road surface after shaking.

Effectiveness of pile foundation for improvement of lateral resistance of Geo-wall

Figure 7 shows the state of road surface after shaking. And residual deformation of the Geo-walls, transition of earth pressure at the back of the Geo-walls, and distribution of the strain in depth occurring in the pile are shown in Figure 8 to Figure 10, respectively. According to the results, the effectiveness of the application of the pile foundation to Geo-wall was confirmed as follows;

a. The load of embankment was transmitted to the piles from the view point of strain occurring in the piles as shown in Figure 10.

b. As the above result, the Piled Geo-wall received larger earth pressure than the normal one without pile as shown in Figure 9.

c. And, the residual displacement of the Piled Geo-wall is smaller than the normal one without pile as shown in Figure 8.

Conclusively, the deformation of the road surface could be reduced as shown in Figure 7.

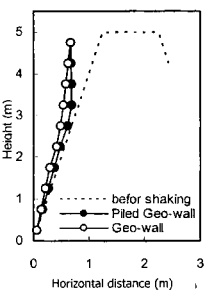

FIG. 8. Deformation of Geo-grid.

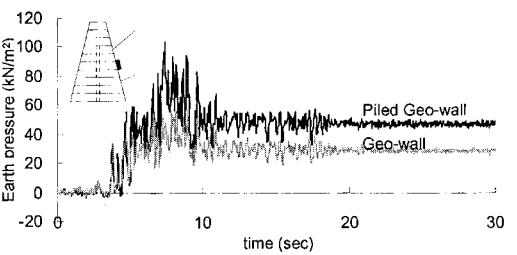

FIG. 9. Transition of earth pressure on back of Geo-wall.

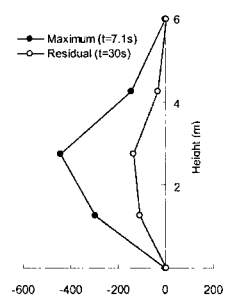

FIG. 10. Strain occurring in the pile.

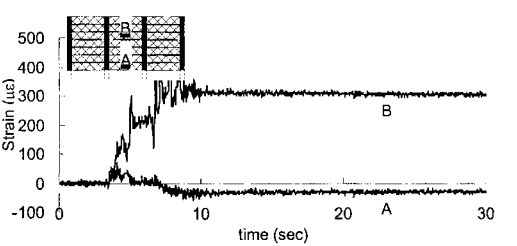

FIG. 11. Transition of strain occurring in the additional geogrid.

Figure 11 shows the transition of the strain occurring in the longitudinal additional geogrid. According to the result, it was confirmed that the geogrid is effectiveness to transmit the load of the back embankment to the piles through the Geo-wall from the result that large strain occurs in the geogrid.

Interaction between pile and Geo-wall

The distribution of the displacements in depth of the pile and the Geo-wall is shown in Figure 12. According to the result, because of high ductility of reinforced soil structure, relative deformation between pile and Geo-wall is not small though; it was considered that Geo-wall can transmit the force to pile foundation predictably shown in Figure 2.

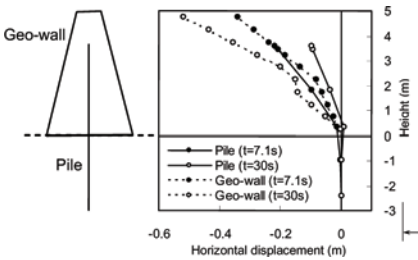

FIG. 12. Displacement distribution of pile and Geo-wall.

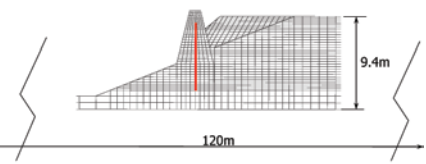

FIG. 13. Analysis model.

A NUMERICAL SIMULATION OF THE EXPERIMENT

A numerical simulation was carried out in order to propose a design model. From the view point of practical design, two-dimensional elasto-plastic dynamic FEM (UWLC, Wakai et al. 2004) was adopted for the simulation. Figure 13 shows the FEM mesh.

Three dimensional effect of pile foundation

In case of adopting two-dimensional (2D) FEM for design of Piled Geo-wall, three-dimensional (3D) effect of pile for modeling of the piles as a continuous wall in 2D analysis has to be considered. More specifically, the 3D effect can be established by the flexural stiffness of the continuous wall (2D modeling of pile) from the comparison with static 3D and 2D analysis (Hara et al. 2009), which the Geo-wall deformation analyzed by 3D analysis (each pile modeling) can be reproduced by 2D analysis (continuous wall modeling). Figure 14 shows the example of 3D effect study for the experiment's case. According to the result, 0.2 times of flexural stiffness (EI) of the equivalent continuous wall of the actual piles was established as 3D effect of piles for 2D modeling in this case.

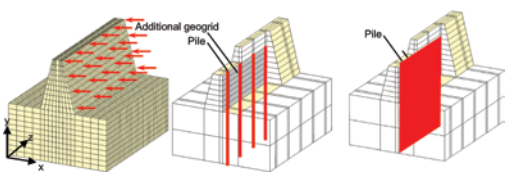

(a) 3D modeling **(b) 2D modeling**

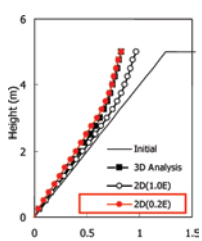

FIG. 14. An example of 3D effect study. **(c) Geo-wall deformation**

Reproducibility of the design method

Comparisons of the results obtained from the numerical simulation and the experiment, residual deformation of Geo-wall and road surface, maximum deformation and bending moment of the pile, are shown in Figure 15 to 17, respectively. According to the results, the analyzed responses comparatively good reproduce the observed ones.

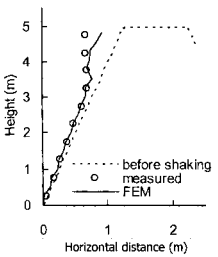

FIG. 15. Geo-wall deformation.

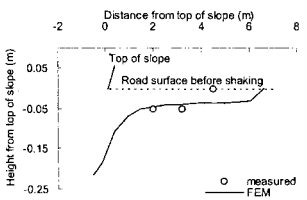

FIG. 16. Road surface deformation.

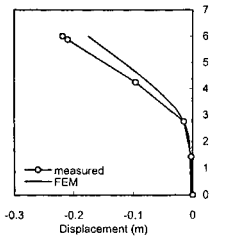

(a) Deformation

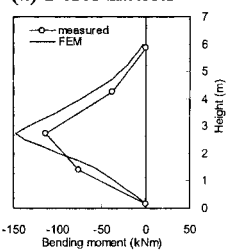

(b) Bending moment

FIG. 17. Maximum response of pile.

CONCLUSION

This paper can be concluded as follows; (1) application of pile foundation to Geo-wall with high ductility is effectiveness to improve lateral resistance, (2) the longitudinal geogrid installed in front of piles in each layer is availableness to transmit the load to piles from Geo-wall body, (3) seismic response of Piled Geo-wall can be estimated by using 2D dynamic elasto-plastic FEM with considering of 3D effect of pile for 2D modeling, (4) the 3D effect can be established by comparison with static 3D and 2D analyses.

REFERENCES

Wakai, A. and Ugai, K. (2004). "A simple constitutive model for the seismic analysis of slopes and its applications." *Soils and Foundations* (Japanese Geotechnical Society) Vol.44 No.4, pp.83-97.

Hara, T., Tsuji, S., Yashima, A., Sawada, K. and Tatta, N. (2009). "Dynamic interaction between pile and reinforced soil structure." *Proceeding of the International Symposium on Prediction and Simulation Methods for Geohazard Mitigation (IS-Kyoto 2009)*: 457-463.

Limit Analysis of Reinforced Soil Slopes Based on Composite Reinforcement Mechanism

Yong-liang Lin[1], Xin-xing Li[2] and Meng-xi Zhang[1]

[1] Civil department of Engineering, Shanghai University, Shanghai, China; lin_yliang@163.com
[2] R&D Department, Shanghai Tunnel Engineering and Rail Transit Design & Research Institute, Shanghai, China; lxxxinyue@163.com

ABSTRACT: In this paper, the composite reinforcement mechanism is proposed, and it considers the interaction of quasi-cohesion and friction-bar theory. The validity of the proposed method is demonstrated through the previous experimental results of critical height for the reinforced slope. And it is introduced into pseudo-static seismic analysis of reinforced slopes. A kinematical approach based on the framework of limit analysis is applied for evaluation the stability. A rotational failure mechanism is used and the failure surface is assumed to be a log-spiral surface. Results of analysis of simple cases have been presented for the design of reinforced slopes in seismically active areas.

INTRODUCTION

Construction of earth structures reinforced with geosynthetics has expanded extensively in the last twenty years. To date, several analytical methods have been formulated and many parametric studies have been carried out to show the importance of the main design parameters (Radoslaw, 1997). The finite element method is certainly the most comprehensive approach to analyze the performance of soil structures subjected to seismic loading. However, its use usually requires high numerical costs and accurate measurements of the properties of the component materials, which are often difficult to achieve. The pseudo-static approach, in which a safety factor for the stability of the soil structure is introduced, is widely applied (Bathurst et al., 1995; Ling et al., 1997; Michalowski, 1998). As we know, the interaction of soil-reinforcement is rather complex. So the composite reinforcement mechanism is proposed, and it considers the interaction of quasi-cohesion and friction-bar theory (Lin, 2009). The validity of the proposed method is demonstrated through the previous experimental results of critical height for the reinforced slope. Finally, a suitable procedure based on the assessment of earthquake-induced stability is proposed for the design of reinforced slopes.

VALIDITY OF COMPOSITE REINFORCEMENT MECHANISM

To prove the versatility of the proposed method, the previous experimental results of critical height for the reinforced slope are adopted (Porbaha et al., 1996). The log-spiral failure mechanism is used in this study. The seismic force is not considered in the experiment. The work ratio induced by soil deadweight was derived by Chen et al. (1990), and is given as follows for completeness:

$$\dot{W}_\gamma = \gamma r_0^3 (f_1 - f_2 - f_3)\omega \tag{1}$$

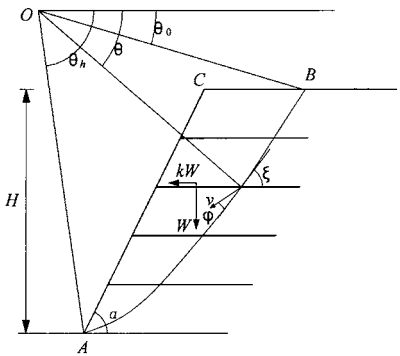

FIG.1 Collapse mechanism for a reinforced soil slope.

Where γ is the unit weight, r_0 is the radius at initial angle θ_0 as shown in FIG.1, functions f_1, f_2 and f_3 are shown by Chen et al. (1990). The layers are assumed to be uniformly spaced. According to the friction-bar theory, the energy dissipation rate by geosynthetic reinforcement along the entire log-spiral slip surface is calculated by integrating the unit energy dissipation given:

$$\dot{D}_R = \frac{1}{2} K_t r_0^2 \omega f_8 \tag{2}$$

Where K_t is tensile strength of reinforcement per unit cross-section, the expression of function f_8 is given by Porbaha (2000). Based on the quasi-cohesion mechanism, the rate of energy dissipation by reinforcement can be calculated as follows:

$$\dot{D}_c = \frac{(c + \Delta c) r_0^2 \omega}{2 \tan \varphi} f_7 \tag{3}$$

Where

$$f_7 = e^{2(\theta_h-\theta_0)\tan\varphi} - 1 \qquad \Delta c = \frac{R_f}{2S_v}\sqrt{K_p} \tag{4}$$

Where Δc is the additional cohesive strength, R_f is the tensile strength of a single reinforcement layer(per unit width), S_v is the vertical interval of reinforcements, K_p is the coefficient of passive earth pressure. For unloaded slopes, the following formulation for the solution of the critical height of a reinforced slope is as follows:

$$H = \frac{(c+\Delta c)}{\gamma} f(\theta_h, \theta_0) \tag{5}$$

$$f(\theta_h, \theta_0) = \frac{\sin\theta_h e^{(\theta_h-\theta_0)\tan\varphi} - \sin\theta_0}{2(f_1 - f_2 - f_3)} \cdot \left(f_7 \cot\varphi + \frac{K_t f_8}{(c+\Delta c)} \right) \tag{6}$$

The prototype equivalent height is obtained by multiplying model height by the centrifugal acceleration. Table 1 summarizes the prototype equivalent heights of different reinforcement mechanism and the results of model experiment. The value of critical height through the conventional reinforcement mechanism is lower than H_f and the maximum variations are up to 20%. However, the predicted height H_{cr} is in good agreement with the previous experimental results. It shows that the composite mechanism is available and efficient.

Table 1. Comparison of critical height

Model No.	α (°)	c (kPa)	φ (°)	K_t (kPa)	H_f(m)	H_c(m)	H_K(m)	H_{cr}(m)
M-11	90	24.7	19.3	2.816	9.2	8.1	8.1	8.7
M-28	90	20.2	20.8	2.804	8.2	7.0	7.0	7.6
M-32	80.5	22.7	21.3	2.776	11.4	9.7	9.6	10.6
M-35	80.5	23.8	20.6	2.796	11.1	9.6	9.5	10.3
M-41	63.4	17.3	20.7	2.575	11.7	10.6	10.4	11.5

Note: H_f = equivalent height of the experiment result
H_c = prototype equivalent height through the quasi-cohesion mechanism
H_K = prototype equivalent height through the friction-bar mechanism
H_{cr} = prototype equivalent height through the composite mechanism

UPPER BOUND ANALYSIS FOR STABILITY OF REINFORCED SOIL SLOPES

The work rate of inertia force is equal to the sum of the work rate by soil deadweight and by the seismic force. According to the previous method, the work rate by soil deadweight

is same with Eq.(1). The work rate by the seismic force is given by Chen et al. (1990), and the reinforcement strength is given as:

$$\frac{K_t}{\gamma H} = \frac{2\gamma_0 (f_1 - f_2 - f_3 + k(f_4 - f_5 - f_6)) - 2f_7\, c/\tan\varphi}{\gamma H\left(f_8 + f_7\sqrt{K_p}/\tan\varphi\right)} \tag{7}$$

Where k is the coefficient of seismic force, functions f_4, f_5 and f_6 are shown by Chen et al. (1990). An optimization scheme needs to be used in order to find the best lower bound to the required reinforcement. The proposed method can be simplified into quasi-cohesion theory, friction-bar theory and composite reinforcement mechanism.

As known, design based on pseudo-static analysis is generally considered conservative, since even when the safety factor drops below one the soil structure could experience only a finite displacement rather than a complete failure. A design procedure based on a tolerable displacement against sliding was proposed by Ling et al (1997). In this method, the evaluation of yield acceleration is the most important. The yield acceleration is defined, as the horizontal ground acceleration in the downhill direction required to bring the safety factor with respect to slope failure to one. The yield acceleration, k_y, can be given as:

$$k_y = \frac{(c + \Delta c) f_7/\tan\varphi + K_t f_8 - 2\gamma_0 (f_1 - f_2 - f_3)}{2\gamma_0 (f_4 - f_5 - f_6)} \tag{8}$$

The critical seismic coefficient is obtained by minimizing k_y with respect to θ_0 and θ_n. This critical value of k_y will be indicated in the following text as k_c.

RESULTS AND DISCUSSIONS

Required reinforcement strength remarks

Several plots have been recently published by Ling et al.(1997) and by Ausilio (2000) to illustrate the effect of seismic forces on the stability of reinforcement slopes. A comparison of the results based on friction-bar theory with those presented by Ling et al and Ausilio is given in Fig. 2(a), for the coefficient of earthquake(k=0.2)and two different slope angles ($\alpha = 45°$). As can be seen from these figures, the equations derived in this work provide values for $K_t/\gamma H$ that are in close agreement with those read from the graphs by Ling et al. The proposed method can be simplified into the method presented by Michalowski et al (1998). To explore the influence of different reinforcement mechanism on ultimate reinforcement strength, the example presented by Michalowski et al (1998) is introduced and the results (k = 0.2) are shown in Fig.2(b). It is found that the ultimate

reinforcement strength derived from composite reinforcement mechanism is les than that of quasi-cohesion or friction-bar theory.

Yield acceleration remarks

To illustrate the effect of different reinforcement mechanism on the yield acceleration of a

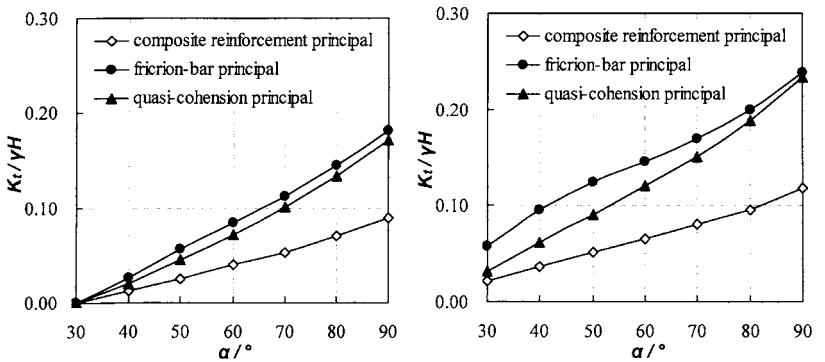

FIG.2 Reinforcement strength (dimensionless) necessary to prevent slope collapse associated with reinforcement rupture.

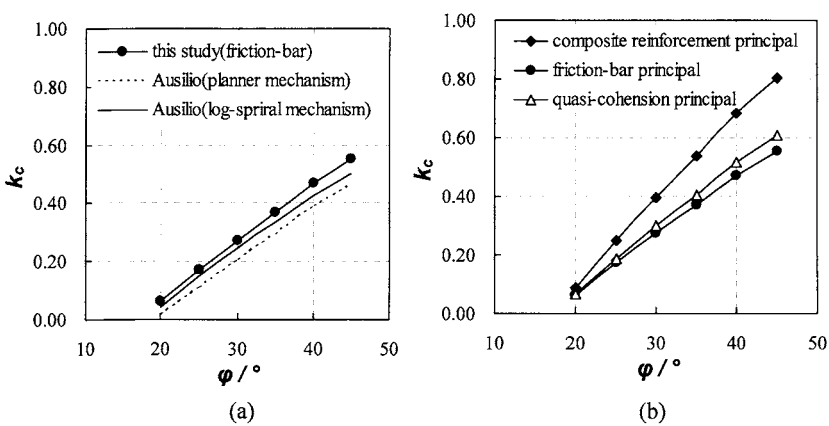

FIG.3 Results of the yield acceleration.

reinforced slope, it is assumed that the soil is cohesionless with unit weight $\gamma = 18$ kN/m^3, $K_t/\gamma H = 0.35$, $H = 5$m, $\alpha = 75°$ and angle of soil shearing resistance φ ranging from 20 to 45°. The validity of the proposed method is demonstrated through the previous results as shown in Fig.3(a). As can be seen from the figure, when the friction-bar theory is only considered the results agree very well with those obtained from Ausilio(2000). Similarly, the influence of different reinforcement mechanism on the yield acceleration is investigated in Fig.3(b). As can be noted that the value of k_c derived from the reinforcement mechanism of quasi-cohesion or friction-bar is rather less than that of composite reinforcement mechanism.

CONCLUSION

In the current study, a new version of reinforcement mechanism for slopes which has been firstly suggested for reinforced soil slopes, was developed. The validity of the proposed method is demonstrated through the previous experimental results of critical height for the reinforced slope. Then, it is introduced into the seismic stability of reinforced slopes. The calculations carried out by the pseudo-static approach indicate that it is more reasonable to reduce the amount of the reinforcement. The evaluation of permanent displacement will be discussed in the future. It will provide some beneficial guidance for seismic stability of reinforced slope.

REFFERENCES

Ausilio E, Conte E and Dente G. (2000). "Seismic stability analysis of reinforced slopes." *Soil Dynamics and Earthquake Engineering*, Vol.19(2):159-172.

Bathurst R.J and Cai Z.(1995). "Pseudo-static seismic analysis of geosynthetic reinforced segmental retaining walls." *Geosynthetics International*, Vol.2(5):789-832.

Chen W.F and Liu X.L.(1990). "Limit analysis in soil mechanics." Elsevier Sciences Publishers B.V.

Lin Y.L.(2009) "Upper bound method for stability reinforce slope based on composite reinforcement mechanism." *Journal of Yangtze river scientific research institute*, Vol.26(9):44-46.

Ling H.I, Leshchinsky D and Perry E.B.(1997). "Seismic design and performance of geosynthetic-reinforced soil structures." *Geotechnique*, Vol.47(5):933-952.

Michalowski R.L.(1998). "Soil reinforcement for seismic design of geotechnical structures." *Computers and Geotechnics*, Vol.23(1):1-17.

Porbaha A, Goodings D.J. (1996). "Centrifuge modeling of geotextiles- reinforced steep clay slopes." *Canadian Geotechnical Journal*, Vol.33 (5):696-704.

Porbaha A, Zhao A, Kobayashi M, et al.(2000). "Upper bound estimate of scaled reinforced soil retaining walls." *Geotextiles and geomembranes*, Vol.18(6):403-413.

Radoslaw L.M.(1997). "Stability of uniformly reinforced slopes." *Journal of Geotechnical and Geoenviormental Engineering*, Vol.123 (6):546-556.

Comparison of Performance between Cross Shaped and Conventional Deep Mixed Columns for Three-layered Soft Ground Improvement under Embankment Load

Yaolin Yi[1], Songyu Liu[2], M. ASCE, Yanjun Du[3], Fei Jing[4] and Nenghe Gong[5]

[1]Ph.D candidate, Institute of Geotechnical Engineering, Southeast University, 2# Sipailou, Nanjing, China, 210096; Academic Visitor, Department of Engineering, University of Cambridge, Cambridge, UK, CB2 1PZ; yy331@cam.ac.uk

[2]Professor, Institute of Geotechnical Engineering, Southeast University, 2# Sipailou, Nanjing, China, 210096; liusy@seu.edu.cn

[3]Professor, Institute of Geotechnical Engineering, Southeast University, 2# Sipailou, Nanjing, China, 210096; duyanjun@seu.edu.cn

[4] Associate professor, Institute of Geotechnical Engineering, Southeast University, 2# Sipailou, Nanjing, China, 210096; jingfei9212@sohu.com

[5]Manager, Nanjing LUDING Special Deep Mixing Technology Co.Ltd, Building 57, North Ruijin Village, Baixia, Nanjing, China, 21009; gnh1234@163.com

ABSTRACT: Soil-cement deep mixing method is one of the most widely used soft ground improvement methods. For most of the soil-cement deep mixed columns (DM columns), the diameter of a single column is a constant along column depth. In this study, a diameter-varied (cross shaped) DM column is presented to improve a three-layered soft ground where a soft soil layer with high compressibility is overlain and underlain by medium compressible soil layers. A 3D numerical analysis is carried out to investigate the performance of three-layered soft ground improved by cross shaped DM columns, as well as by conventional DM columns for comparison. The results indicate that the proposed cross shaped DM column has higher performance than the conventional one under embankment load.

INTRODUCTION

Deep Mixing Method (DMM), a deep in-situ soil stabilization technique, was developed in Japan and in the Scandinavian country in 1970's (CDIT 2002). As DMM has many merits, such as relatively lower noise, lower vibration, lower cost, faster construction, and smaller impact on the nearby existing structures, it spreads into the other part of the world. The DMM was introduced to China in the early 1980s, and then spread rapidly throughout the country in the 1990s (Han *et al.* 2002). In China, the group soil-cement deep mixed columns (DM columns) are often used to increase the

bearing capacity and to reduce the settlement of soft ground for highway embankment application (Han *et al.* 2002; Liu and Hryciw 2003).

For most of the DM columns put into practice, the diameter of a single column is a constant. In this study, a diameter-varied deep mixed column (cross shaped DM columns) is presented to improve a three-layered soft ground where a soft soil layer with high compressibility is overlain and underlain by medium compressible soil layers. A 3D numerical analysis is carried out to compare the performance of three-layered soft ground improved by cross shaped DM columns with conventional DM columns.

FUNDAMENTALS OF CROSS SHAPED DM COLUMN

For DM columns improved ground, the area replacement ratio (a_s) is a basic parameter to design, which is defined as the ratio of the single column area over the whole area of the influence unit cell (Bergado *et al.* 1996). For square column arrangement, the area replacement can be calculated from the equation as follow:

$$a_s = \frac{\pi}{4}\left(\frac{D}{S}\right)^2 \tag{1}$$

Where D is the column diameter and S is the column spacing.

In engineering practice, a relatively high value of a_s is usually chosen for relatively soft soil, while relatively low value is chosen for relatively stiff soil. The a_s is a constant for a conventional DM columns improved ground. A three-layered soft ground is encountered when constructing a highway embankment in Xuzhou area, China, where a soft soil layer with high compressibility is overlain and underlain by medium compressible soil layers. For this case, the conventional deep mixed columns may not be the optimum solution, since a_s may be lower than required in the high compressible layer, while it may be larger than required in the medium compressible layers. In order to improve this three-layered soft ground effectively and economically, a diameter-varied deep mixed column is developed, which has relatively large diameter in high compressible layer and relatively small diameter in medium compressible layers. With this type of DM columns, a_s in the high compressible layer is larger than that in medium compressible layers. This new DM column is called cross shaped DM column.

Cross shaped DM column can be installed by a new deep mixing machine with an automatic spreading mixing blades developed by Liu *et al.* (2007). The mixing blades can spread outwards and shrink inwards at any position under ground in order to form a diameter-varied DM column. Yi *et al.* (2008) presented the construction of a T-shaped DM column, of which the diameter at shallow depth is larger than that at deep depth, using the new deep mixing machine. Similar to the T-shaped DM column installation, the cross shaped DM column can also be installed using this deep machine. In other words, the mixing blades shrink inwards when the small diameter column in medium compressible layers is installed, while the mixing blades shrink inwards when the large diameter column in high compressible layer is installed.

NUMERICAL MODELING

To investigate the performance of the three-layered soft ground improved by cross shaped DM columns comparing with conventional DM columns, a 3D numerical

analysis was carried out with the finite difference software (FLAC 3D). The ground consists of four soil layers. The first layer and the third layer have relatively low compressibility (medium soil). A soft soil layer with high compressibility is overlain and underlain by medium soil layers. The fourth layer is a firm soil layer. It is pointed out that this study is preliminary attempt, so the simple calculation method is chosen. Only the mechanical calculation, not coupled fluid, was taken in the numerical analysis. Mohr-Coulomb failure criteria are used for embankment fill, medium soil, soft soil, firm soil, and DM columns. The material properties are shown in Table 1. Two cases of numerical analysis were conducted, one is the cross shaped DM columns improved ground and another is conventional DM columns improved case, as shown in FIG. 1.

Table 1. Material properties for numerical analysis

Material	E (MPa)	ν	γ (kN/m^3)	c (kPa)	φ '(°)
Medium soil	8	0.30	18	0	35
Soft soil	1	0.35	16	0	28
Firm soil	30	0.28	20	0	30
Fill	20	0.28	22	0	35
Column	60	0.25	22	156	35

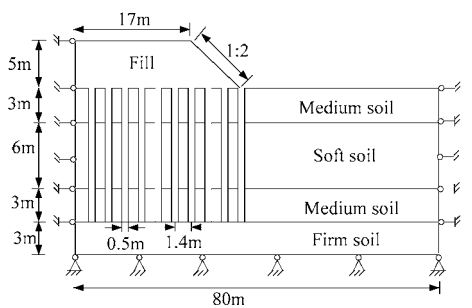

(a) Conventional DM columns

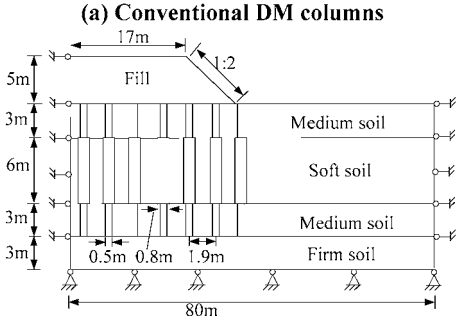

(b) Cross shaped DM columns

FIG. 1. Numerical analysis model (not to scale)

Based on Equation (1), the value of a_s in FIG. 1(a) is calculated, which is 0.100. For cross shaped DM columns improved ground, there are two values of a_s corresponding to the larger diameter and smaller diameter. In this study, the cross shaped DM column is equivalent to a conventional DM column with equal column volume and column length (see FIG. 2.), and the equivalent column diameter D_e is then calculated. The equivalent a_s can be calculated from Equation (1) by replacing D with D_e. The equivalent a_s in FIG. 1(b) is 0.097, which is slightly less than that of conventional DM columns improved ground (0.100).

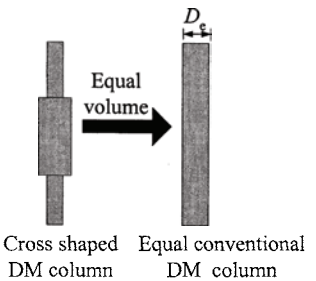

FIG. 2. Cross shaped column and conventional column with equal column volume

ANALYSIS OF RESULTS

The calculated ground surface settlement under the embankment load is presented in FIG. 3. When the distance from road center is less than 20 m, the surface settlement of the cross shaped DM columns improved ground is much less than that of the conventional DM columns improved ground. The maximum surface settlement of the cross shaped and the conventional DM columns improved ground are 178 mm and 244 mm respectively, which means the latter is 37.1% larger than the former.

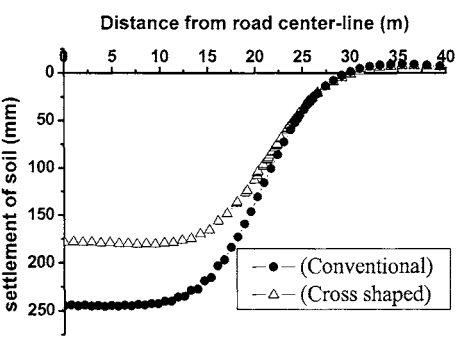

FIG. 3. Settlement of soil at ground surface

FIG. 4 shows the calculated settlement of layered soil at the road center-line under the embankment load. In the soft soil layer (3 m to 9 m depth), the vertical deformation of conventional DM columns improved ground is much larger than that of cross shaped DM columns improved ground. However, in the medium compressible soil layers, the vertical deformation of the former is only slightly less than that of the latter. As a result, the total settlement at the ground surface of the conventional DM columns improved ground is much larger than that of the cross shaped DM columns improved ground.

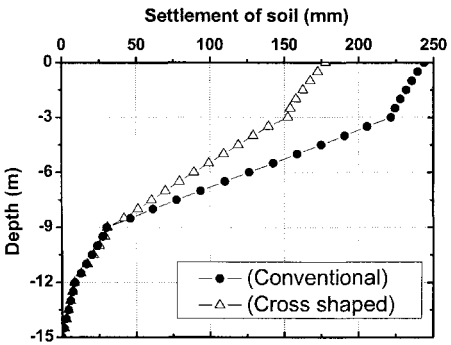

FIG. 4. Calculated settlement of layered soils at road center-line

The lateral movement of the soil under the embankment toe is shown in FIG. 5. It is found that the difference of the lateral movement between these two types of DM columns improved ground is not as significant as the surface settlement. In the soft soil layer, the lateral movement of the cross shaped DM columns improved ground is slightly less than the conventional one. The maximum lateral movements under the embankment toe of cross shaped and conventional DM columns improved ground are 78 mm and 83 mm respectively, and both appear at the interface between the first medium layer and the soft layer.

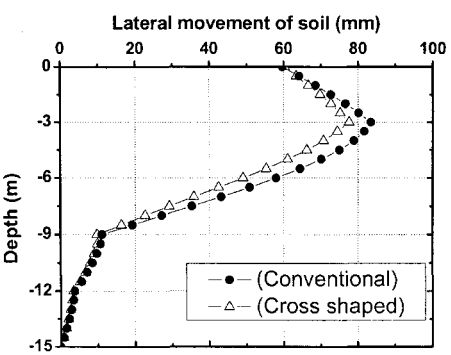

FIG. 5. Lateral movement of soil under embankment toe

CONCLUSIONS

When the equivalent area replacement ratios are almost the same, the maximum ground settlement of cross shaped DM columns improved ground is much less than that of the conventional one. The maximum lateral movement under the embankment toe of the former is slightly less than that of the latter. It can be concluded that the proposed cross shaped DM column has higher performance than the conventional one for this three layered soft ground under embankment load.

ACKNOWLEDGMENTS

The authors appreciate the financial support of the National Natural Science Foundation of China (Grant No. 50879011), Scientific Research Innovation Program for Graduate Students in Jiangsu Province (Grant No. CX08B_101Z) and the Scientific Research Foundation of Graduate School of Southeast University (Grant No. YBJJ0914). The authors also appreciate the reviewers' excellent comments, which improved the quality of the paper.

REFERENCES

Bergado, D. T., Anderson, L. R. and Miura, N. et al. (1996). "Soft ground improvement in lowland and other environments." *ASCE*, New York.

CDIT. (2002). "The deep mixing method: Principle, Design and Construction." *A.A. Balkema Publishers*, Tokyo.

Han, J., Zhou, H.T. and Ye, F. (2002). "State of practice review of deep soil mixing techniques in China". *Journal of the Transportation Research Board*, No.1808: 49-57.

Liu, S.Y., Chu, H.Y. and Gong N.H. et al. (2007). "Automatic spreading mixing blade." *Chinese Patent*: ZL 2004 10065862.9. (in Chinese)

Liu, S.Y. and Hryciw, R.D. (2003). "Evaluation and quality control of dry-jet-mixed clay soil-cement columns by standard penetration test". *Journal of the Transportation Research Board*, No.1849: 47-52.

Yi, Y.L., Liu, S.Y., Zhang, D.W. et al. (2008). "Experimental study on T-shaped soil-cement deep mixing column composite foundation." *Slope stability, Retaining Walls and Foundations* (GSP 197), ASCE, Reston/VA: 1-7.

A New Method for Settlement Calculation of Long-Short Piles Combined Composite Foundation

Yu Chuang[1] , Pan Linyou[2] and Li Xiaobing[3]

[1]Lecturer, Doctor, College of Architecture and Civil Engineering, Wenzhou University, Zhejiang Wenzhou, China, 325035; geoyuchuang@hotmail.com
[2]Professor, Doctor, College of Architecture and Civil Engineering, Wenzhou University, Zhejiang Wenzhou, China, 325035; ply51204@yahoo.com.cn
[3]Lecturer, PhD candidate, College of Architecture and Civil Engineering, Wenzhou University, Zhejiang Wenzhou, China, 325035; lxb@wzu.edu.cn

ABSTRACT: In the past ten years, China has seen great development of infrastructure construction, most of which are built on soft ground. Infrastructure constructions such as road and railway embankments, bridge approach and flood protection dam on soft soils have raised several concerns related to excessive total and differential settlements, bearing capacity failures, lateral pressure and movement and stability of the foundation These challenges have led to a significant development of soil improvement, which show economic solutions for the constructions on soft soils. One of the techniques is long-short piles combined composite foundation. Long-short piles combined composite foundation is referred to as a composite foundation supported by long piles and short piles. The composite foundation system utilizes the advantages of long piles and short piles individually, which is already applied in ground improvement widely in China . Nevertheless, there is no good method to calculate the settlement of this foundation .On basis of the performance of ground compression of the long-short piles combined composite foundation , a new settlement calculation method is presented. The method takes the different work condition of different part of the foundation into account, simplifies the additional stress distribution versus depth and presents the compression index . Finally, this new method is applied to investigate the settlement of one case. The computed results have good agreements with measured data, which shows the advantage over other existing methods in calculating the settlement of long-short piles combined composite foundation.

INTRODUCTION

Soft ground is widely distributed in China especially along the east coastal area, where most of economically developed areas are located over soft marine clayey deposits. The increasing need of infrastructure development has often forced civil engineers to deal with buildings on soft soils. Infrastructure constructions such as road

and railway embankments, bridge approach and flood protection dam on soft soils have raised several concerns related to excessive total and differential settlements, bearing capacity failures, lateral pressure and movement and stability of the embankment (Kempfert et al. 2004). These challenges have led to a significant development of soil improvement and reinforcement techniques, which show economic solutions for the constructions on soft soils. According to Technical Code for Ground Treatment of Building (JGJ79-2002) , basic ground treatment method mainly include Removal and Replacement, Dynamic Consolidation, Vibro-Compaction, Vibro-Replacement, Preloading, Vacuum Preloading, Sand Column, Cement-Flyash-Gravel (CFG) column, Rammed-Cemented-Soil Pile, Rammed-Soil Pile, Lime Column, Lime-Soil Compaction Pile, Grouting, Solution Injection, Deep Mixing, Jet Grouting, Lime-soil Pile. Among them Deep Mixing columns are mostly used for the treatment of building foundation soil. Moreover, there are still some other methods, which are used in the treatment of soft subgrade under highway and railway although seldom used in the build foundation soil treatment.

There have been more than ten kinds of ground treatment methods adopted in the construction of highway, railway and high speed railway in China including preloading compaction, dynamic compaction, deep mixing method (including DMM and DJM), jet grouting method, vacuum preloading, combined preloading and vacuum preloading, composite ground with different reinforcement elements, piled embankment. For composite ground, rigid piles are sometime used as ground reinforcement elements besides DM column, sand column or gravel column, which are called flexible pile composite foundation. It is often called rigid pile composite ground when rigid pile is introduced as ground reinforcement element to form composite ground. However, the improvement depth is limited when using deep mixing columns(called short piles in this paper). Nevertheless, the cost is too high when using rigid pile foundation(called long piles in this paper). On the basis of above analysis, a multi-piles foundation is presented. A new settlement method for the long-short piles combined composite foundation , is presented.

BEHAVIOR OF LONG-SHORT PILES COMBINED COMPOSITE FOUNDATION

With the development of ground improvement, more and more individual technologies are combined in practice. For example, in China, combinations of cement–fly ash–gravel (CFG), soil–cement (SC), and lime columns are often used as ground improvement to support highway embankments overlying soft soils. This system consists of installing different column types with different lengths and diameters to support the embankment fill and to mobilize the strength and stiffness of the soil at shallow depths. Fig. 1 shows an example of such a composite foundation, where the embankment is supported by long piles , such as CFG columns or SC columns and short piles such as lime columns. The long piles are generally much stiffer than the short piles and they are used much like piles to mobilize the bearing capacity of the deeper soil strata. The more flexible lime columns strengthen and stiffen the shallower soil strata, thereby allowing the latter to be utilized as a load-supporting system. This type of foundation is called as long-short piles combined composite foundation. In many areas

around China, this kind of ground improvement is being increasingly adopted. In recent years, a substantial amount of research has been conducted on such multi-column composite foundations.

Many researchers have investigated the behavior of long-short piles combined composite foundation through field tests (Liu 2003, Chen 2004), numerical simulations (Liang 2003, Abusharar2009) and theoretical methods(Zheng 2002) . However, there are very few studies on the settlement calculation of this composite foundation.

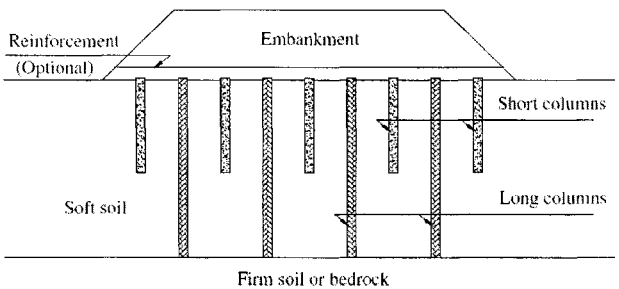

FIG.1. Long-short piles combined composite foundation (Abusharar 2009)

The long-short piles combined composite foundation, as shown in Figure 1, is consisting of five elements: long piles, short piles, ground between short piles, ground between long piles, and ground under long piles. The interactions among short piles, long piles and ground can be described as follows. The load is carried by ground, short piles and long piles. The compression of ground is composed of the following three components, compression of soils between short piles, compression of soils between long piles, and compression of soils between under long piles. In order to compute the settlement , the additional stress should be obtained firstly.

A NEW SETTLEMENT CALCULATION METHOD FOR LONG-SHORT PILES COMBINED COMPOSITE FOUNDATION

THE ADDITIONAL STRESS IN THE GROUND

For the calculation of settlement in the ground, the determination of additional stress is the first step, at the same time the calculation is very complicated. Zai (1993) gave some expressions that the additional stress is composed of self-weight stress, additional stress and construction stress. Among them the additional stress is made up of the pressure under the raft, the skin friction along the pile and the pressure of pile bottom. And the determination of additional stress is a very difficult problem. The usual calculated method are elastic analysis, finite element method, shear deformation (displacement) method and so on. If the details of pile foundation need simulating, the coupling of soil and pile must be considered. The finite element method is a powerful solution to the above coupling issue. The finite element method has its unique advantage in its ability to treat the complicated configurations of structures and soil

media and it has gotten popular application in civil engineering including pile foundations (Ottavianvi, 1975; Liu, 1991; Poulos, 2001). The three-dimensional finite element can take all influenced factors into account, but too many calculated parameters and the long time-consuming make its limitations. the complicated three-dimensional problem of pile foundation is simplified as a plane strain model and the plane strain finite element is presented to simulate the additional stress distribution and the deformation, then the simplified distribution of additional stress is presented (Yu,2006). In this paper, based on the simplification of additional stress in long-short piles combined composite foundation a new method of calculating the settlement is presented.

Li (1993) has presented the curve showing the change trend of σ_z at the central line of the pile cap with 100 piles along the depth, which is calculated with the method of both Boussinesq and Mindlin's solution, moreover it has done a comparison with σ_z of the pile cap without pile (curve 3), please refer to Figure 2. The curve 2 in the Figure.2 is the sum of σ_z produced respectively by the pile and the pile cap. Comparing it with Curve 3 we can find that just because of the pile σ_z within the depth of the pile is similarly a constant and nearly equal to the σ_z at the same place of the raft foundation without pile. Based on the above analysis we can draw the conclusion that the soil additional stress in the composite pile foundation has the following characters: the additional stress of the soil between piles is even along the pile shaft and the number value of the additional stress equals to the σ_z at the same place of the pile foundation without pile, moreover, the distribution feature of the additional stress of the soil under the pile bottom is similar with that of Boussinesq's solution.

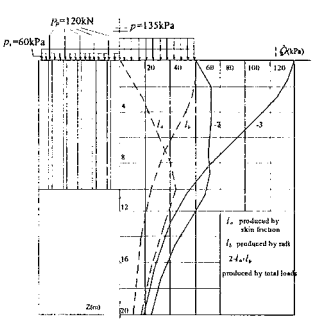

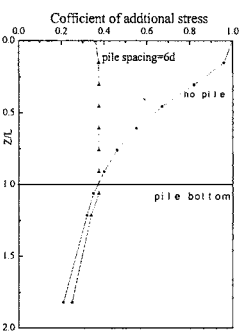

FIG.2. Soil additional stress of 100 piles foundation

FIG.3 .Soil additional stress coefficient of pile foundation

For long-short piles combined composite foundation, the additional stress can be obtained as the previous results. The additional stress is composed of self-weight stress, additional stress and imposed loads. the additional stress is made up of the pressure under the raft, the pressure of pile bottom and the skin friction along the pile, which is

affected by the longer and shorter piles. Among them the additional stress under the bottom of shorter piles, is different from traditional ones. The additional stress over there is influenced by the shorter piles bottom's pressure. It's found to be that the distribution of additional stress is different from conventional pile foundation. From the above analysis, the additional stress distribution along depth in longer piles range can be simplified as trapezoid form, which is shown in figure.4.

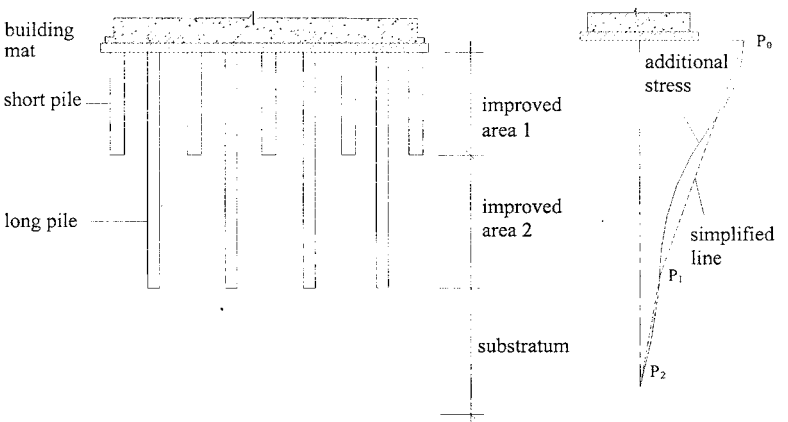

FIG.4. Additional stress in long-short piles combined composite foundation

SETTLEMENT CALCULATION

The total settlement is divided into two parts, one is S_1, which is the soil compression between piles, the other one is S_2, which is the compression of soils under pile bottoms. S_1 is expressed as follows,

$$S_1 = \frac{P_0 + P_1}{2 \times \overline{E_{sp}}} \times H$$

whereP_0 is additional stress at the raft bottom ; P_1 is additional stress at the long piles' bottom ; $\overline{E_{sp}}$ is the average compression modulus of ground treatment ; H is the length of long piles.

For the second part, S_2 is computed using the conventional layer-summation method. The total settlement S is

$$S = S_1 + S_2$$

SETTLEMENT CALCULATION WITH THE PRESENTED METHOD

INTRODUCTION

The project of Hangzhou Baihaidang Dwelling house is located over soft ground in Hangzhou City, where is very close to Shanghai East China**(Gong, 2006)**. All of the houses are 12 stairs and in frame structure, the dimension of one tower building is $30.84m \times 14.7m$.

TABLE.1. SOIL PARAMETERS

Soil layer	Thickness/m	Water content /W(%)	E_s/MPa	ρ/ kN/m^3
1 peat	2	-	-	16.5
2 silty clay	1.5	30.4	4.43	19.2
3-1mucky clay	4.2	42.1	2.48	18.4
3-2 mucky silty clay	5.1	37.1	3.11	19.6
3-3 mucky silty clay	11.5	42.5	2.65	17.8
3-4 mucky silty clay	11	38.3	2.79	18
3-5conch soil	2.2	44.8	2.81	-
6 pudding stone	3	-	20	-

APPLICATION OF LONG-SHORT PILES COMBINED COMPOSITE FOUNDATION

If the common pile foundation is used, in order to meet the requirements in terms of the foundation bearing capability and settlement, 200 or so piles per house must be constructed, however, if it is designed with the theory of long-short piles combined composite foundation, the bearing capability of the foundation soil can be fully utilized and the number of the piles and the cost for the project can be decreased largely, furthermore the requirements in terms of foundation bearing capability and settlement can also be met.

The long-short piles combined composite foundation is adopted for the foundation design. The longer piles are concrete piles with diameter of 500mm and length of 40 m. the amount used in this project is 44. The shorter piles are deep mixing columns with diameter of 500mm and length of 9 m. The compression modulus for longer piles is 30000 MPa and 60 MPa for shorter piles. The additional stress under the foundation bottom is 163.6 MPa.

CONVENTIONAL METHOD FOR THE SETTLEMENT CALCULATION

The area replacing ratio for long piles, m_1=8.64/453.35=0.0191,the settlement is computed via conventional method as follows,

TABLE .2. SETTLEMENT CALCULATION

Layer	Z_i (m)	E_{spi}(kPa)	σ_z (kPa)	S(mm)
3-1	4.2	147.8	162.5	4.172
3-2	5.1	148.4	156.1	4.867
3-3	11.5	145.8	129.2	8.688
3-4	11	146.0	90.5	6.362

3-5	2.2	146.0	70.9	0.953
6-2	3	162.9	65.1	1.193

The total settlement is 26.235mm.

THE NEW METHOD FOR THE SETTLEMENT CALCULATION

According to the presented settlement calculation in this paper, S_1 the settlement in the range of ground improvement is obtained as the following equation.

$$S_1 = \frac{P_0 + P_1}{2 \times \overline{E}_{sp}} \times H = \frac{163.6 + 65.1}{2 \times 149.48} \times 37 = 28.3\text{mm}$$

Due to the reason of that there is no compression soil under the longer piles bottom, the total settlement is: $S = S_1 + S_2 = 28.3$ mm, which is very close to the measure data of 27 mm.

CONCLUSIONS

On basis of the performance of ground compression of the long-short piles combined composite foundation , a new settlement calculation method is presented in this paper. The method takes the work condition of different part of the foundation into account, simplifies the additional stress distribution versus depth and presents the compression index. This new method is applied to investigate the settlement of one case. The computed results keep good agreements with measured data, which shows the advantage over other existing methods in calculating the settlement of long-short piles combined composite foundation. It is helpful for the engineers who are working on the field of foundation engineering.

ACKNOWLEDGMENTS

The authors appreciate the support of the Qianjiang Talent Program of Zhejiang Province (No. 2009R10047).

REFERENCES

Abusharar SW et al.(2009). "Finite element modeling of the consolidation behavior of multi-column supported road embankment". *Computers and Geotechnics*, Vol.36(4): 676-685

Chen, L.Z., Liang, F.Y. and Yan, P. (2004). "Experimental study on behavior of rigid-flexible piles raft foundation with cushion". *Journal of Building Structure*, Vol.25(3): 125-129.

Gong X.N.(2006) . "Theory and application of composite foundation". Beijing: China Architecture & Building press.

H.G. Poulos. (2001)."Piled raft foundations: design and applications" .*Geotechnique*, Vol.51(2): 95-113.

JGJ79-2002. (2002). "Technical code for ground treatment of buildings". Beijing: China Architecture & Building Press.

Kempfert, H.-G., et al. (2004)."German recommendations for reinforced embankments on pile-similar elements". *EuroGeo3 - Third European Geosynthetics Conference, Geotechnical Engineering with Geosynthetics*: 279-284.

Li, J.W. (1993). "The additional stress in soil under piled raft foundation produced by Boussinesq and Mindlin's solution". *Chinese Foundation Treatment*,13(4):15-21.

Liang, F.Y., Chen, L.Z. and Shi, X.G. (2003). "Numerical analysis of composite piled raft with cushion". *Computers and Geotechnics*, Vol.30(2):443-453.

Liu, F.Y., Yang, X.B. and Liu.X. (2003). "Field tests of a composite foundation including mixed pile". *Chinese Journal of Geotechnical Engineering*, Vol.25(1):71-75.

Liu,W.M and Milos Novak. (1991). "Soil-pile-cap static interaction analysis by finite and infinite elements". *Can.Geotech.J.* , Vol.28,771-783.

Ottavianvi, M.(1975). "Three-dimensional finite element analysis of vertical loaded pile group". *Geotechnique*, Vol.25(2):159-174.

Yu C, et al.(2005). "Research on the additional stress and deformation in the soil of composite pile foundation under vertically uniform loads". *Geotechnical Special Publication*(GSP142),ASCE, Geo-Frontiers:881-890.

Zai J.M. and Zai J.Z.(1993). "Analysis and design of pile foundation". Beijing:Chinese Building Engineering Publishing House.

Zheng, J.J. and Ou, J.H. (2002). "Theory and practice of multi-element composite ground". *Chinese Journal of Geotechnical Engineering*, Vol.24(2): 208-212.

Experimental study on vertical bearing behavior of composite foundation with tapered rigid pile

HE Jie[1,2], LIU Jie[2], ZHANG Ke-neng[1], MIN Chang-qing[2], HU Da[2]

[1] School of Geosince and Environmental Engineering, Central South University, Lu Shan South Road, Changsha, Hunan, 410083, People's Republic of China (Tel:+86-731-28182108; Email: hjhlhjy@yahoo.com.cn) ;

[2] School of Civil Engineering, Hunan University of Technology, Wenhua Road, Zhuzhou, Hunan, 412008, People's Republic of China

ABSTRACT: In order to study the vertical bearing behavior of composite foundation with tapered rigid pile, three static load model tests of composite foundation with 5 different tapered rigid piles were performed as well as a static model test of composite foundation with 5 cylindrical rigid piles under the same geological conditions. The test results indicated that the average pile-soil stress ratio of composite foundation with tapered pile is lower than that of cylindrical rigid piles. Tapered pile was beneficial to take full advantage of the bearing capacity of natural foundation and could effectively relief pile-tip stress concentration in composite foundation. The axial forces decay gradually along pile depth under load. However, the axial force attenuation grads of tapered pile are larger than that of cylindrical rigid piles. The axial force attenuation speed of the center pile, which increases along pile depth with the increase of the obliquity, is much faster than that of corner pile in composite foundation with tapered rigid pile. The skin frictions of the piles mostly focus on the range from pile top to L/3 of the pile length.

1. INTRODUCTION

Tapered pile that originated from the Soviet Union is a new type of pile with high unit bearing capacity, which not only save material but also make the construction simpler. Tapered pile takes full advantage of the interaction between pile and soil by its side surface. The side wall of the tapered pile was subjected to tangential frictions as well as the normal resistance provided by soil, which can greatly enhance the bearing capacity of the tapered pile. The data at home and abroad show that unite volume bearing capacity of tapered piles is 0.5 to 2.5 times higher than that of cylindrical pile in the same geological conditions. Compared with cylindrical pile, the foundation cost of the tapered piles decreases by 40%~60%, and the tapered piles have some advantages such as saving material, convenient production and transportation [1]. Based on experimental results, some researchers [2~9] have investigated the bearing behavior and

load transfer of tapered pile, and they reported that compared with cylindrical piles with same volume, tapered pile can increase 60% bearing capacity and foundation settlement decrease about 65% in the same condition. The interaction between tapered pile and surrounding soil was studied by numerical analysis [10] and the corresponding results showed that the taper sidewall is beneficial to utilize the interaction between pile and soil, which resulted in the increase of the unite volume bearing capacity of tapered pile. The interaction between tapered piles, soil and pile-cap was studied by FEM [11]. Based on composite summation method and layer-wise summation method, the bearing capacity and settlement of composite foundation with tapered rigid piles were analyzed, and calculation and measured result were also compared [12]. The systematic theory analysis on tapered short piles was conducted, but the study was only limited to deformation performance of single pile [13].

As discussed above, in the past several years, the study on tapered pile and composite foundation with tapered rigid piles had gained some development. However, compared with other fields, the research on composite foundation with tapered pile was less and there are many problems to be solved. In order to improve the use of the composite foundation with tapered pile in soft clay, based on the model test, the average pile-soil stress ratio and load transfer of the composite foundation was discussed in the paper.

2. MODEL TEST

Model test was carried out in a large size steel box (model box).

2.1 Test program:

1) Filling: Soil was filled into model box and rammed by 3 layers, and compacted uniform to predetermined elevation. During this process, some earth pressure cells were placed on predetermined place.

2) Pressing pile: Model piles were pressed into predetermined place of model foundation by static load.

3) Setting cushion: sandstone was layed over the foundation surface.

4) Erecting loading device (shown in **Fig.1**)

5) Loading: The static load test was conducted strictly according to the "technical code for ground treatment of building (JGJ79-2002)".

2.2 Model introduction and test parameters:

The model test was conducted in a steel box with 1500 mm×1500 mm×1500 mm and 10mm thick walls. The model walls were stiffened by steel rim every 500 mm in longitudinal and transverse direction to satisfy experimental requirement.

The loading plate size was $10d \times 10d \times 20$ mm (d is the average diameter of model pile). The soil was clay, the physical and mechanical parameters of soil are given in Table 1.The cushion was comprised of dry sandstone, and the corresponding thickness was 50 mm. The model pile material is steel. The size, and physical and mechanical parameters of the model pile was presented in Table 2.

The sidewall roughness of the model pile was increased to simulate the interaction between pile and surrounding soil during engineering practice, the mixture of sand and

epoxy resin was attached over the pile sidewall.

To discuss the load transfer and bearing behavior of composite foundation with tapered piles and investigate the difference between composite foundation with cylindrical piles and that with tapered piles, four static load tests with different model pile were carried out in four model boxes. The horizontal distance between pile and pile is equal to 4*d*. The earth pressure cells were installed at the pile top and the soil surface to measure soil stress as shown in Fig.1 (*a*).

Table 1. Physical and Mechanical Parameters of the Soil

Modulus of Compressibility /MPa	Friction Angle / (^{0})	Cohesion /kPa	Weight /kN·m^{-3}	Water Content /%
3.24	11.53	4.52	19.18	25.75

Table 2. Test Parameters of the Model Pile

Model No.	Pile Type	Diameter /cm		Pile Length /cm	Taper Angle / (^{0})	Elastic Modulus /GPa
		Pile top	Pile tip			
1#	Cylindrical pile	1.5		35.0	0	200.9
2#	Tapered pile	2.0	1.0	35.0	0.82	
3#	Tapered pile	3.0	1.0	35.0	1.64	
4#	Tapered pile	4.0	1.0	35.0	2.45	

Test device was shown in Fig.1 (*b*). The loading system was consisted of lever and weight, the ratio of force arm is 3:1. The measure equipment was consisted of Micro-Measurements and dial indicator. Seven pairs of strain gauges were attached to the external surface of model pile. The strain gauges were measured by DH-3815N Micro-Measurements System.

After completing all test preparation, the foundation was preloaded for 2 h at pressure equal to 5.0kPa. After preloading 4 h, static test began by slow maintaining load method.

3. EXPERIMENTAL RESULTS AND ANALYSIS

3.1 Pile-soil stress ratio

Fig.2 shows that average pile-soil stress ratio varies at different value of load. From Fig.2, we can find that the pile-soil stress ratio in the composite foundation with rigid piles decreases with the increase of load. The stress ratio in the composite foundation with tapered piles is much less than that with cylindrical piles. The stress ratio in the composite foundation with tapered piles decreases gradually with the increase of the taper angle. The squeezing effect of tapered piles to surrounding soil results in that soil around pile shares more load. When the taper angle increases, the squeezing effect was more obvious and the soil around piles shares more loads. Hence, the tapered piles in the

composite foundation can make full use of bearing capacity of natural foundation and decrease pile-soil stress ratio stress concentration. As the taper angle increases, the decreasing amplitude of average pile-soil stress ratio in the composite foundation with tapered piles become smaller, which shows that the effect of increasing taper angle on bearing capacity of natural foundation is very limited. Besides, the optimum angle of tapered pile is need to be studied further.

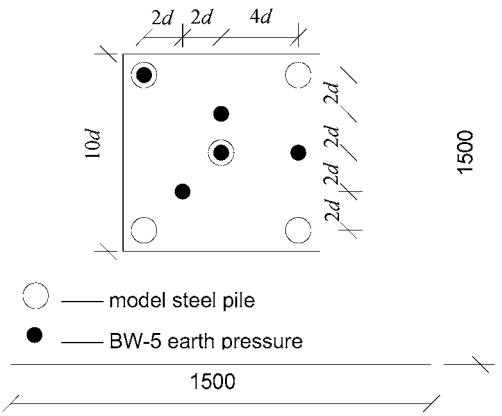

(*a*) Plane Layout of Foundation Surface

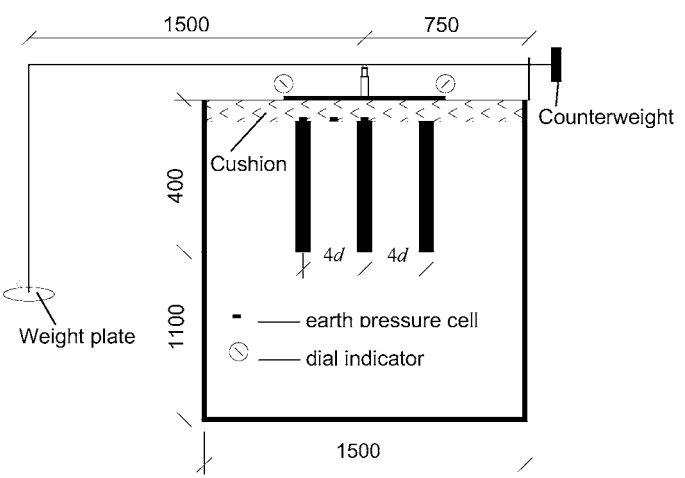

(*b*)Axial Loading Equipment

FIG.1 Installation of Experimental Equipments

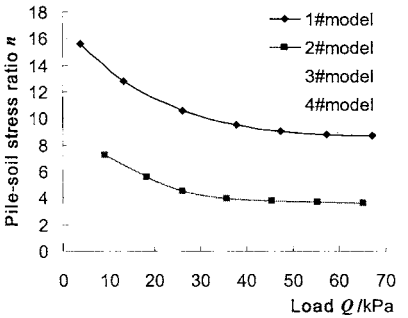

FIG.2 Relation between Average Pile-Soil Stress Ratio and Load

3.2 Axial forces distribution along pile

Based on 4 groups of composite foundation model, the axial forces distribution of central and corner piles were obtained from experimental study (shown in Fig.3~6). From Fig.3~6, we can find that the axial force of the pile decreases along the depth gradually, and the attenuation gradient of axial force of tapered piles is much greater than that of cylindrical piles, showing that the resistance of tapered pile subjected is bigger that of cylindrical piles. The skin friction becomes bigger gradually with the increase of the taper angle. The mutual action between piles and soil was strengthened. In the composite foundation with tapered pile or cylindrical piles, the attenuation gradient of axial force of central piles is greater than that of corner piles. In the composite foundation with tapered pile, attenuation gradient of the central pile above (0~3L, L is the length of the pile) is larger the other section with the increase of the taper angle of the pile sidewall, indicated that the large taper angle resulted in the large mutual interaction between pile and surrounding soil, which make the resistance of pile sidewall increased.

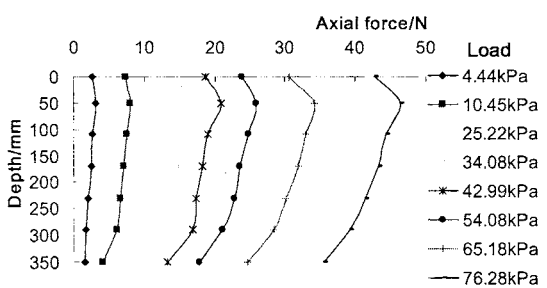

(*a*) Corner Pile

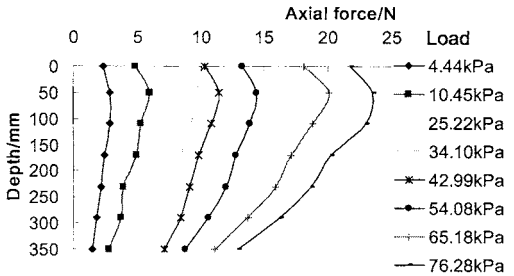

(*b*) Central Pile

FIG. 3 Distribution of the axial force in No.1 model composite foundation

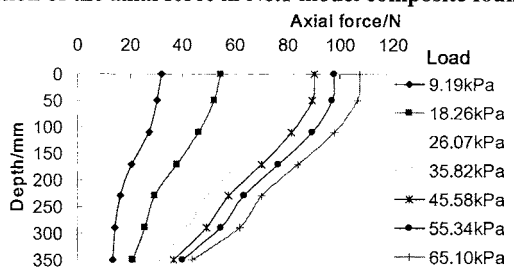

(*a*) Corner Pile

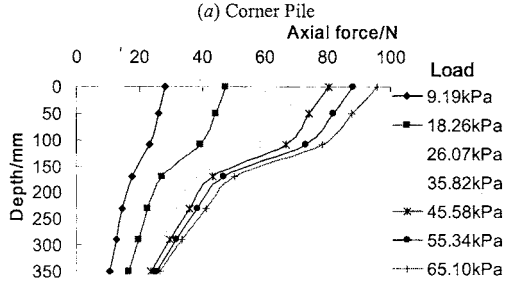

(*b*) Central Pile

FIG. 4 Distribution of the axial force in No.2 model composite foundation

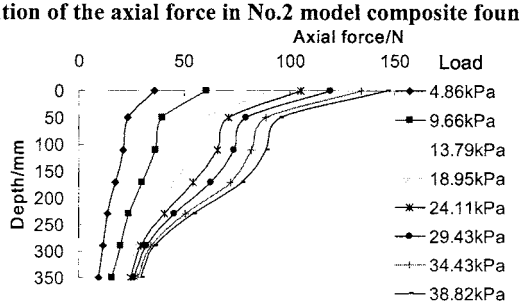

(*a*) Corner Pile

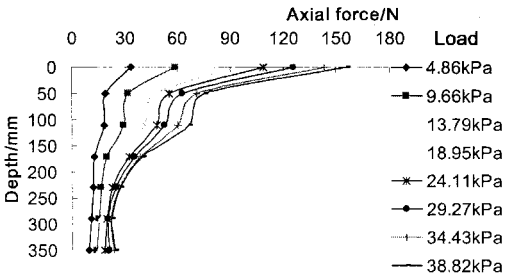

(*b*) Central Pile

FIG. 5 Distribution of the axial force in No.3 model composite foundation

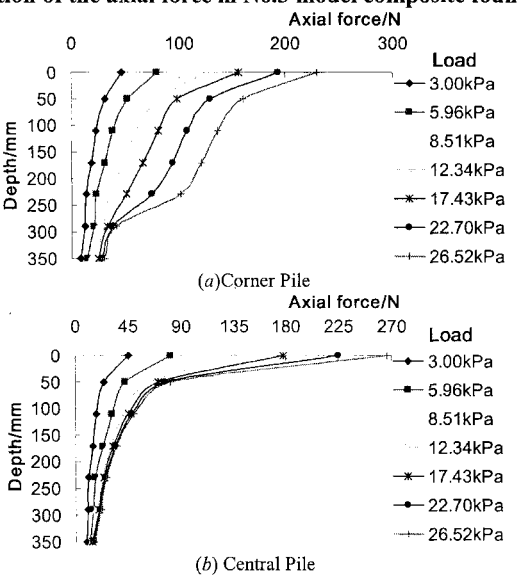

(*a*)Corner Pile

(*b*) Central Pile

FIG. 6 Distribution of the axial force in No.4 model composite foundation

CONCLUSIONS

1. The stress ratio in the composite foundation with tapered piles is much less than that with cylindrical piles. The tapered piles in the composite foundation can make full use of bearing capacity of natural foundation and decrease pile-soil stress ratio stress concentration. However, the optimum angle of tapered pile is needed to be studied further.

2. Under load, the axial force of the pile decreases along the depth gradually, and the attenuation gradient of axial force of tapered piles is much greater than that of cylindrical piles.

3. In the composite foundation with tapered pile or cylindrical piles, the attenuation

gradient of axial force of central piles is greater than that of corner piles, and attenuation speed increase with the increase of the taper angle, The resistance of the pile sidewall focused on the pile above (0~3L, L is the length of the pile) .

ACKNOWLEDGMENTS

The research data in this paper was obtained from the research project sponsored by the National Nature Science Fund of China (Project No. 50878084).

REFERENCES

Jiang, Jian-ping. (2006). "Introduction of study and application of tapered piles." *Construction Technology*, Vol. 35(1): 37-40. (in Chinese)

Wei J. Q. , EI Naggar M. H. (1998). "Experimental study of axial behaviour of tapered piles." *Canadian Geotechnical Journal*. Vol. 35(4) : 641-654

EI Naggar M. H. , Wei J. Q. (2000). "Uplift behaviour of tapered piles established from model tests." *Canadian Geotechnical Journal*. Vol. 37(1) : 56-74

M. Hesham EI Naggar , Mohammed Sakr. (2000). "Evaluation of axial performance of tapered piles from centrifuge tests." *Canadian Geotechnical Journal* , Vol. 37(6): 1295-1308

Jin Qi Wei. (1998). "Experimental investigation of tapered piles." Ontario: The University of Western Ontario

Jiang Jian-ping, GAO Guang-yun. (2003). "Comparison of belled pile, tapered pile and equal-diameter pile." *Chinese Journal of Geotechnical Engineering*, Vol. 25(6): 764-766. (in Chinese)

He Jie , Liu Jie , Min Chang-qing, Ding Bang-ying. (2008). "Experimental study on characteristic of behavior of tapered rigid pile." *Highway Engineering*, Vol. 33(1): 7-9. (in Chinese)

Cheng Li-qin, Xu De-liang. (2003). "Pilot study of taper peg in Tianjin." *Jour. of Northwest Sci-Tech Univ. of Agri. and For.(Nat. Sci. Ed.)*, Vol. 31(1): 135-138. (in Chinese)

Liu Jie, WANG Zhong-hai. (2002). "Experimental Study on the Bearing Capacity of Wedge Pile." *Journal of Tianjin University*, Vol. 35(2): 257-260.(in Chinese)

Take W. A , Valsangkar A. J. (2002). "The Elastic Analysis of Compressible Tin-Piles and Pile Groups." *Geotechnique*, Vol. 31: 456-474

Yahia E-A. Mohamedzein , Muzamil G. Mohamed. (2001). "Finite Analysis of Axially Tin-Pile groups." *Computers and Geotechnics*, Vol. 26: 231-243

Hu Xiang-kui, QING Feng. (2001). "Engineering application of rigid composite foundation with tapered pile." *Coal Engineering*, (12): 47-50.(in Chinese)

Хазин, В. И. (1981). "Tapered short pile." Bejing: China Agricultural Mechanical Press(in Chinese)

Implementation of Optimized Soil Improvement Techniques for a Giga Project

Babak Hamidi[1], Serge Varaksin[2] and Hamid Nikraz[3]

[1]PhD Candidate, Curtin University of Technology, 5/531Hay Street, Subiaco 6008 WA, Australia; babak.hamidi@postgrad.curtin.edu.au

[2]Deputy General Manager, Menard; Chairman, ISSMFE TC17, 2 rue Gutenberg, BP 28, 91620 Nozay France; serge.varaksin@menard-mail.com

[3]Professor and Head of Civil Engineering Department, Curtin University of Technology, GPO Box U1987 Perth WA, Australia; h.nikraz@curtin.edu.au

ABSTRACT: One of the world's largest ground improvement projects that has ever been carried out in one phase by a single specialist ground improvement contractor is the 2,600,000 m^2 King Abdulla University of Science and Technology in Jeddah. What has made this project perhaps one of the most unique ground improvement accomplishments ever is not only its size but also the ability to interpret the ground conditions based on limited geotechnical investigation and the ground's behavior during the treatment, the know-how to adapt the solution to late architectural and structural changes, and the capacity to execute the works by an optimized combination of Dynamic Compaction, Dynamic Replacement, High Energy Dynamic Replacement and Dynamic Surcharging.

INTRODUCTION

The 5.6 million m^2 King Abdulla University of Science and Technology (KAUST) is located in Rabigh on the Red Sea coast and near the city of Jeddah in Saudi Arabia. KAUST, originally anticipated to have buildings with at most two to three stories, includes the university campus and academic administration core, a desalination plant, wind turbines, residential neighborhoods, a research park, a commercial center, a waste water treatment plant and a beach club.

The concept of the project was developed in 2006. According to the schedule, master planning, architectural and structural design and construction had to be completed in less than three years and handover date was set at September 2009.

The preliminary geotechnical investigation that was carried out in a relatively wide grid indicated that the ground was very heterogeneous and composed of a

combination of loose or soft soils with rapid variations within short distances. This investigation and further testing during the works revealed that more than 2.6 million m^2 of the construction area was to be built on soil consisting of up to 9 m of loose silty sand or soft sandy silt (locally called sabkah). A generalized profile of the ground and a summary of the test results for each soil layer are respectively shown in Fig. 1 and Table 1.

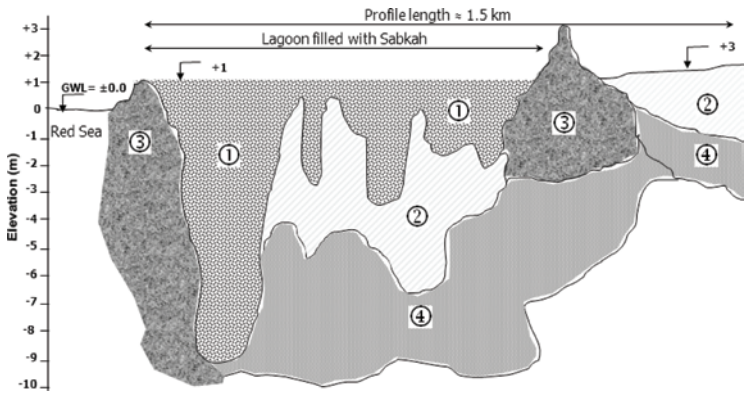

Fig. 1. Ground profile in KAUST

As groundwater table was less than 1 m below in-situ ground level it was decided that the final ground level (FGL) had to about 3 m above original levels to be safely above high tide levels.

It was evident that only a well worked out schedule that incorporated design and construction could meet the project's deadline. However, the problematic soil posed a serious threat to this program as it was not possible to design the foundations without the finalization of the buildings' locations and architectural drawings. Thus a delay in construction seemed inevitable.

Table 1. Ground conditions in KAUST

Layer & USC	Water Content	Fines Content	N_{SPT}	CPT		PMT	
				q_c (MPa)	f_r (%)	P_L (kPa)	E_p (MPa)
1- Sabkah (SM+ML)	35-48%	28-56%	0-2	0-0.2	1.2-4.0	40-190	0.4-1.7
2- Silty Sand (SM)	-	15-28%	3-9	1.2-4.5	0.5-1.2	210-400	1.8-3.5
3- Coral	26-35%	-	6-12	-	-	510-720	3.5-6.0
4- Sand (SM)	-	12-37%	3-18	1.5-1.8	0.5-1.8	400-1200	2.8-8.5

DEVELOPMENT, EXECUTION AND TESTING OF THE FOUNDATION SOLUTION

All possible foundation solutions were considered. Piling was immediately deemed as infeasible because without architectural and structural design it was not possible to define the pile locations. Thus, only ground improvement remained as a potential solution.

The design and construct (D&C) ground improvement proposal that met the project manager's technical requirements, schedule and budget was based on the below design criteria:

- Footing location: Any place within the treatment area
- Maximum footing load: 1,500 kN
- Allowable bearing capacity: 200 kPa
- Maximum total settlement: 25 mm
- Maximum differential settlement between two adjacent footings: 1/500
- Liquefaction mitigation for an earthquake with PGA= 0.07g
- Level: 0.8 m below final ground level, but in any case at least 2 m above sabkah level

The construction method was composed of a combination of *Dynamic Compaction (DC)* (Menard, 1972, 1974; Chu et al, 2009), *Dynamic Replacement (DR)* (Menard and Broise, 1975), and *High Energy Dynamic Replacement (HDR)*. Changes to the height (and consequently footing loads) of some buildings later introduced the need to also utilize *Dynamic Surcharging (DS)* (Al Hamoud, 2005).

The working platform was constructed by dumping and leveling 1 to 1.5 m of granular fill. Roller compaction was not necessary as the platform material was to be compacted in the process of soil improvement works. This of course, was advantageous because not only was the cost of watering, removal of oversize material, mixing and roller compaction eliminated, but more importantly since precious construction time was saved.

In DC, granular soil is compacted using impact energy that is delivered by dropping a heavy weight or pounder from a significant height (Hamidi et al, 2009). In KAUST this technique was used to compact soils with fines content up to about 30 to 35% using pounders weighing up to 21 tons.

In DR, a heavy pounder is dropped to create a cavity in soft soils which is then backfilled with granular material that dynamically driven to the bottom of the soft soil layer or down to a depth of about 5 to 6 m. DR technique was used in areas where the maximum depth of sabkah was 5 m. HDR was used when the sabkah layer's depth was more than 5 m. In such a case, a 3 m surcharge, in addition to the engineered fill required for reaching FGL, was placed over the area for 3 weeks.

After the completion of ground treatment in specific areas, it became known that the revised master plan incorporated 20 six-story. Consequently and as shown in Fig. 2, DS was also used to consolidate the deep sabkah layers. In this technique the combination of preloading and vibration is used to re-introduce pore pressure in the soil-water system and consequently to accelerate settlement rates (Menard and Broise, 1975). Hence, in addition to the engineered fill required for reaching FGL a 3 m high surcharge was place and DC was performed on top of it.

Fig. 2. Dynamic Surcharging in KAUST

Differences in ground behavior due to pounder impact enabled the site supervisors to assess the rapidly varying ground conditions and to apply the appropriate ground improvement technique as needed. It was observed that while the first DC pounder impact penetrated the ground by about 0.25 m, the DR pounder penetration was substantially more and in the range of about 1 m. Also, performing DC frequently resulted in the seepage of groundwater to the surface, but this phenomenon was rarely encountered in the DR areas. Ground rest periods in between DC phases were 1 to 3 days. However, this period was considerably longer and from 7 to 21 days when DR was utilized. Furthermore, ground heave due to pounding was not observed in DC areas but was quite evident in DR zones.

The allocated time frame for mobilization, execution and testing of ground improvement works was set at 10 months. Ground improvement was carried out basically over a period of 8 months using a total of 13 DC/DR/HDR-DS rigs working two shifts per day. To the knowledge of the authors, this is the world record for the number of DC rigs working at the same time on a single project. A review of the treatment rates shows that at its peak, about 600,000 m^2 of ground was treated in one month.

In all, a total of 180 PMT tests were carried out to confirm that the bearing and settlements had been achieved. Several CPT tests were also performed for verification of liquefaction mitigation.

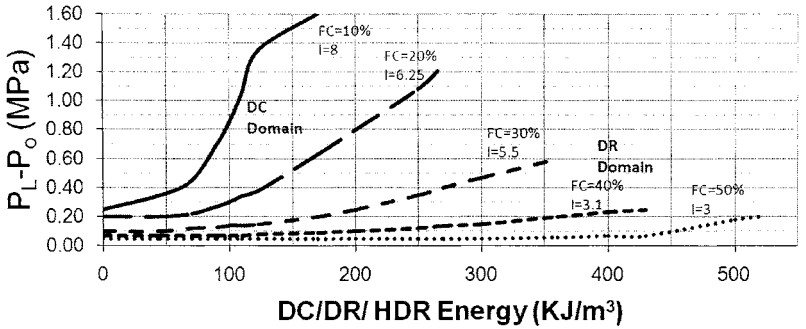

Fig. 3. The relationship between net limit pressure and improvement energy

Due to the wide range of ground conditions, including soil classification, strength, and thickness of layers, test results showed a wide range of results. Although the results clearly demonstrated that design criteria had been satisfied, it is interesting to note that it is possible to classify the test results according to the amount of dynamic energy applied to the ground and the amount of improvement. Fig. 3 shows the relation between the net pressuremeter limit pressure (P_L-P_o) and the energy per volume of improved soil. As expected, it can be observed that the improvement factor (I) or the post to pre soil improvement net limit pressure ratio (only the in situ soil without the DR columns) is higher and more efficient when the soil is more granular and contains lesser fines. Furthermore, it can be noted that the DR columns play a vital role in providing the required ground properties in the sabkah soils, and their exclusion will result in failure of satisfying the design criteria.

LESSONS LEARNED

In this paper it has been demonstrated that classical solutions are not able to meet the requirements of special projects in which the site is unusually large, preliminary field tests are most probably insufficient, design and construction period is relatively short, and construction must commence parallel to the preparation of the architectural and structural drawings. However it is possible to construct such a project successfully if:

- Design and construction phases are merged smartly and efficiently.
- Design criteria are specified based on the actual project requirements rather than copy and pasting specifications from past projects.
- A combination of ground improvement techniques are used for treating different ground conditions rather than forcefully trying to implement one technique to a variety of different conditions. Furthermore, it may be more efficient to provide different amounts of treatment for each technique.
- The limits of each technique are well understood.

- Possible production rates are well understood and sufficient amounts of plant and equipment are mobilized.
- Site observations are given value and changes in actual ground conditions are taken into account during the process of the works.

CONCLUSION

In KAUST, the combination of DC, DR and HDR was able to provide safe foundations at any undefined location. Last moment changes in the master plan and the introduction of heavier loads were taken into account by additionally implementing DS.

The heterogeneity of the site and rapid variations of ground conditions would have normally required excessive amounts of field testing which would have inevitably forced considerable delays in the completion date of the project. Alternatively, field observations of the ground behavior during the works proved to be the ultimate method for defining an optimized treatment area for each technique.

Professional project management skills and planning allowed the allocation of sufficient numbers of equipment and rigs, and ground improvement production rates as high as 600,000 m^2/month permitted the works to be completed in due time and in accordance to the construction schedule.

ACKNOWLEDGMENT

The authors would like to express their gratitude and appreciation to Menard for providing the project information.

REFERENCES

Al Hamoud, A. S. (2005) An Innovative Soil Improvement Under Raft Foundation by a Combination of Dynamic Surcharging and Dynamic Replacement. *Association of Engineering Geologists Conference*, Las Vegas, 19-24 September 2005.

Chu, J., Varaksin, S., Klotz, U. & Menge, P. (2009) State of the Art Report: Construction Processes. *17th International Conference on Soil Mechanics & Geotechnical Engineering: TC17 meeting ground improvement.* Alexandria, Egypt, 130.

Hamidi, B., Nikraz, H. & Varaksin, S. (2009) A Review on Impact Oriented Ground Improvement Techniques. *Australian Geomechanics Journal,* 44, 17-24.

Menard, L (1972). "La Consolidation Dynamique des Remblais Recents et Sols Compressibles", *Travaux*, (November): 56-60

Menard, L (1974). "La Consolidation Dynamique des Sols de Fondations." *Revue des Sols et Fondations* : 320

Menard, L and Broise, Y (1975). "Theoretical and Practical Aspects of Dynamic Compaction." *Geotechnique*, Vol. 25 (3): 3-18

Experimental Study on Shear Strength Behavior of Shredded Tyre-Reinforced Sand

V.Vinot[1] and Baleshwar Singh[2]

[1] Post-graduate Student, Department of Civil Engineering, Indian Institute of Technology, Guwahati – 781039, India; v.vinot@iitg.ernet.in
[2]Associate Professor, Department of Civil Engineering, Indian Institute of Technology, Guwahati – 781039, India; baleshwar@iitg.ernet.in

ABSTRACT: End-of-life tyres are a disposal problem due to large volumes produced every year. This has prompted interest in finding ways to reuse or recycle them. To this aim, the present study demonstrates how the shear strength characteristics of a locally available sand are altered by reinforcing with various percentages of shredded waste car tyres. The tyres were shredded in different sizes of 10x10 mm, 10x20 mm and 10x30 mm, and then added to the sand in various proportions by dry weight. To assess the variation of dry density and shear behavior, vibratory and large scale direct shear tests were carried out. The dry density decreases with shred content, as expected. The inclusion of shredded tyres in sand increases the shear resistance. During shearing, the mixes display both dilatancy and contraction depending on the mixing ratio. There is a noticeable increase of both cohesive intercept and internal friction angle of the mixes due to shred addition. Finally, statistical analysis shows that the normal stress and shred content mainly influence the measured shear strength values.

INTRODUCTION

The increasing number of vehicles on the roads of industrialized and developing nations generates millions of used and worn-out tyres every year. In industrialized countries, approximately one waste tyre per capita is generated every year. Waste tyres are also generated plentifully in quickly growing markets like India.

Wherever large volumes of earthen materials are used, applications of wastes tyres can emerge. Based on the literature available, the addition of shreds influences the properties of sand considerably. Shredded tyre influences the shear resistance of sand (Foose et al. 1996; Zornberg et al. 2004; Gotteland et al. 2005). Inclusion of shreds to sand influences significantly the variation of cohesion intercept with marginal variation in frictional angle (Ghazavi 2004; Rao and Dutta 2006). Tyre shreds placed below the water table appear to have a negligible adverse effect on water quality (Humphrey and Katz 2001). Thus, the use of waste tyres and their components in highway and non-highway applications hold great promise for consuming large

quantities of tyres in an environmentally acceptable manner, at significant economic benefits. In view of the above, the objective of study is to investigate the influence of shredded waste tyres on the shear strength characteristics of a locally available sand.

MATERIALS AND METHODS

The experimental programme in this study was conducted with sand collected from the deposits of the nearby Brahmaputra River. The sand can be designated as SP as per the Unified Soil Classification Systems (USCS). The specific gravity of sand is 2.70 with a uniformity coefficient of 1.47 and coefficient of curvature of 0.89. The maximum and minimum void ratios sand are 0.86 and 0.57. Waste car tyres were shredded into three different sizes (10x10 mm, 10x20 mm, and 10x30 mm). The shreds had thickness ranging from 5 to 7 mm. The specific gravity of shreds ranged from 1.01 to 1.19 depending on the nylon fibre content. The shreds were uniformly mixed with sand of various proportions ranging from 0% in steps of 10% by dry weight and varying aspect ratio (shred length/shred width) of 1, 2, and 3.

Vibratory tests were run to determine the maximum and minimum dry density of the sand alone and mixtures with various shred aspect ratios and contents. The tests were conducted in accordance with ASTM Standard Test Methods for Maximum Index Density and Unit Weight of Soils Using a Vibratory Table (D 4253-06).

Direct shear tests were performed as per ASTM Test Method for Direct Shear Test for Soils under Consolidated Drained Conditions (D 3080-04). The shear behavior of the mixtures was investigated in a large scale direct shear box consisting of two halves of size 30x30x15 cm. Five normal stresses (σ_n) of 25, 50, 75, 100, and 125 kN/m^2 were used to cover the stress range in field applications of lightweight fill embankments.. The shear rate was kept at 0.5 mm/min for all tests to simulate a rapid, quasi-undrained condition in the field (Tatlisoz et al. 1997). The tests were continued until the shear stress became essentially constant or until a maximum shear deformation of 25 mm was reached. When no peak stress was observed, the shear stress at 25 mm displacement was taken as the ultimate shear stress.

TEST RESULTS AND DISCUSSION

Typical variations of dry density versus shredded tyre content at dense and loose states are presented in Figure 1. The figure indicates that the dry density decreases with shred content for all sizes, which is due to reduction of sand content and lower specific gravity of shreds.

Figure 2 illustrates the typical variation of shear stress-displacement curves at a normal stress of 75 kPa for mixtures with shred inclusion of size 10x20 mm. The shear resistance of the mixtures is an improvement over sand alone up to 30% shreds content. During the shearing, compressional prestress is overcome after sufficient shear distortion and then the interaction between shred and sand starts. The shred inclusion in different proportions leads to a decrease in the loss of post-peak shear strength. The behavior for other cases showed similar trends.

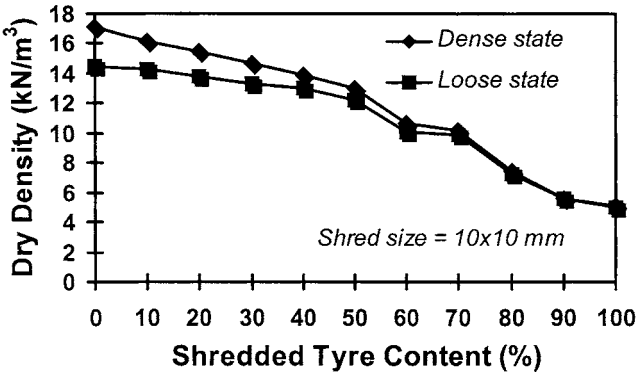

FIG. 1. Variation of Dry Density with Shred Content

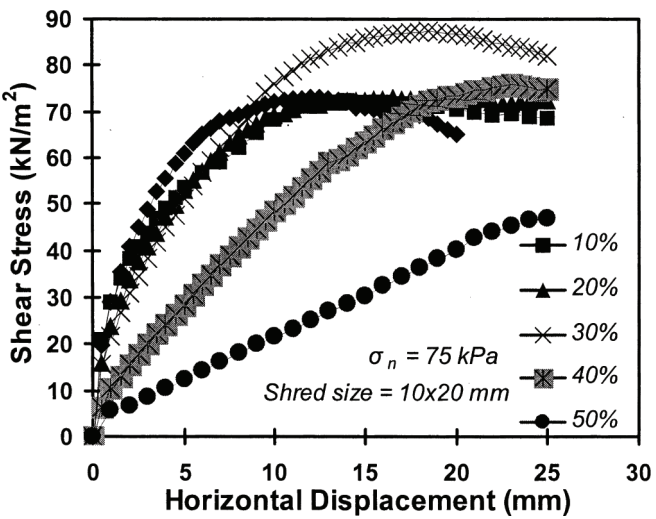

FIG. 2. Variation of Shear Stress with Horizontal Displacement for Different Shred Contents

The typical variation of volume change curves at a normal stress of 50 kPa for mixtures with shred inclusion of size 10x10 mm are reported in Figure 3 along with those of sand alone. The variation in shear vs. vertical displacement indicates an initial contraction followed by dilation, but the transition is at a higher displacement than for the unreinforced sand. This is due to the effect of shreds causing a decrease in initial density of the mixture. It is also observed that the dilation decreases with increase in

normal stress. Similar trends were noticed in all the other cases.

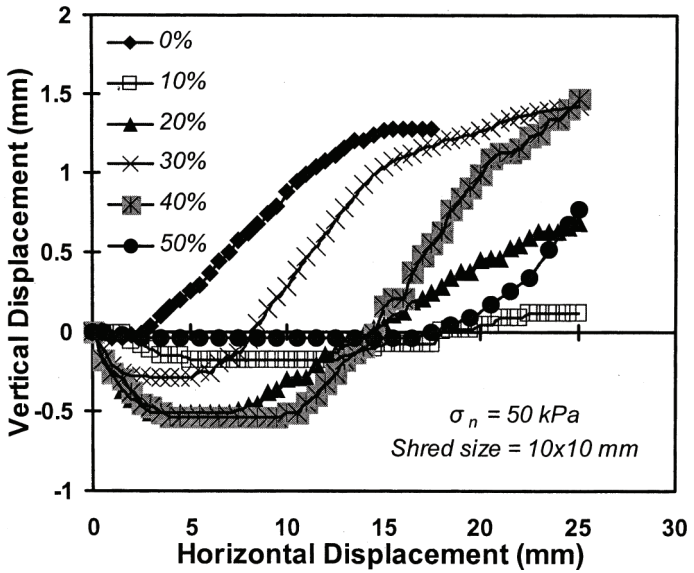

FIG. 3. Variation of Vertical Displacement with Horizontal Displacement for Different Shred Contents

The effective stress strength parameters (φ' and c') have been derived from the Mohr-Coulomb failure envelopes. The value of φ' increases marginally by 2° to 6° with shred inclusion compared to 36.6° of sand alone. The variation of cohesion with shred content is almost linear, and the maximum increase is of the order of 3 times at 50% shred content due to interlocking effect when compared with 12.1 kPa of sand alone.

The increase in shear strength achieved by adding shreds can be described in terms of shear efficiency, E_t, which is defined as

$$E_t = \tau_{st} / \tau_s \quad \text{..... (1)}$$

were τ_{st} is the composite shear strength of the sand-shred mixtures and τ_s is the shear strength of the sand.

Figure 4 shows variation of shear efficiency with shred content of size 10x20 mm. An increase of normal stress leads to considerable decrease of the shear efficiency at a shred content higher than 30% due to less dilatancy. As the normal stress is increased, the efficiency decreases and asymptotically approaches 1.0 for all shred contents regardless of size.

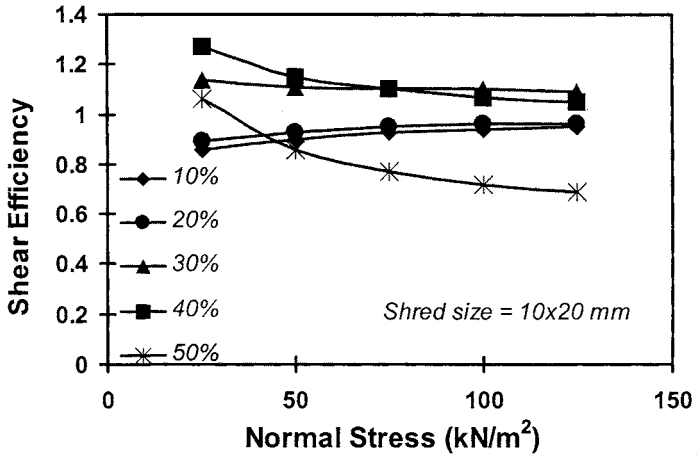

FIG. 4. Shear Efficiency of Sand-Shred Mixtures for Different Shred Contents

REGRESSION ANALYSIS

Regression analyses were carried out to assess the correlation of independent variables (normal stress, shred content, shred aspect ratio) with the dependent variable (composite shear strength) based on t-ratio tests. The independent variables used in the prediction of composite shear strength are statistically significant at 95% confidence limits. The results of regression analysis as presented in Table 1 are based on 104 tested samples.

Table 1. Results of Regression Analysis

Property	Variables	Coefficients	t–statistic (t_{as})	t-critical (t_{ac})	Statistically significant (t_{as}) > (t_{ac})
Composite shear strength	Normal stress	0.560	10.686	1.660	yes
	Shred content	-0.591	14.520		yes
	Shred aspect ratio	-0.305	2.850		yes

The following regression model resulted:

$$\tau_{st} = 41.437 + 0.560\,(\sigma) - 0.591\,(\chi) - 0.305\,(Ar) \quad \ldots\ldots (2)$$

in which τ_{st} is the calculated composite shear strength (in kPa), σ is the applied normal stress, χ is the shred content, and Ar is the shred aspect ratio. From the t-statistic

analysis, it is observed that normal stress and shred content mainly contribute to the composite shear strength. The shred aspect ratio is less significant than the other two factors.

CONCLUSIONS

The results of this study indicate that the addition of shredded waste car tyres to sand in a dry condition showed improvement in the strength behavior due to interlocking effect. A shred content of 30% is found to be the most beneficial. Practical field applications will be in a moist condition.

REFERENCES

Foose, G. J., Benson, C. H. and Bosscher, P. J. (1996). "Sand Reinforced with Shredded Waste Tires." *J. Geotech. Eng.*, ASCE, 122(9):760-767.

Ghazavi, M. (2004). "Shear Strength Characteristics of Sand-Mixed with Granular Rubber." *Geotechnical and Geological Engineering*, 22(3): 401- 416.

Gotteland, P., Lambert, S. and Balachowski, L. (2005). "Strength Characteristics of Tyre Chips–Sand Mixtures." *Studia Geotechnica et Mechanica*, 27(1-2): 55-66.

Humphrey, D. N, and Katz, L. E. (2001). "Field Study of Water Quality Effects of Tyre Shreds Placed Below the Water Table." *Proc. Conf. on Beneficial Use of Recycled Materials in Transportation Applications,* Air and Waste Management Association, pp. 1-10.

Rao, G.V. and Dutta, R.K. (2006). "Compressibility and Strength Behaviour of Sand-Tyre Chip Mixtures." *Geotechnical and Geological Engineering,* 24: 711-724.

Tatlisoz, N., Bensob, C. and Edil, T. (1997. "Effect of Fines on Mechanical properties of Soil-Tire Chip Mixtures." *Testing Soil Mixed with Waste or Recycled Materials*, ASTM STP 1275, pp. 93-108.

Zornberg, J. G., Cabral, A. R. and Chardphoom, V. (2004). "Behaviour of Tire Shred-Sand Mixtures." *Can. Geotech. J.*, 41(1): 227-241.

Numerical Analysis of Lateral Behavior of Rigid Piles to Support Embankments

Li Liu[1], Gang Zheng[2], and Jie Han[3]

[1]PhD. Candidate, Department of Civil Engineering, Tianjin University, Tianjin 300072, China, liulitumu@yahoo.com.cn
[2]Professor, Department of Civil Engineering, Tianjin University, Tianjin 300072, China, zhengzige2004@yahoo.com.cn
[3]Associate Professor, The Civil, Environmental, & Architectural Engineering (CEAE) Department, the University of Kansas, Lawrence, Kansas 66045-7609, U.S. jiehan@ku.edu

ABSTRACT: The stability of embankments constructed on soft soil is one of the most important issues concerned especially for rapid embankment construction. In practice, piles are increasingly introduced to reinforce the soft soil to achieve the stability of the embankment. Limited research has been conducted so far on the stability of piled-embankments on soft soil especially the failure mechanism. Three-dimensional FDM numerical analyses were performed in this study for an embankment supported by rigid piles. The lateral behavior of piles at different locations relative to the toe of the embankment was investigated. To evaluate possible soil flow, a single pile was placed under the embankment subjected to an additional load up to a limit equilibrium state. The numerical results showed that an increase of the applied load on the top of the embankment increased the soil deformation under the embankment, and eventually caused the soil flow around the pile.

INTRODUCTION

When embankments are constructed on soft ground, excessive settlement and stability often become a challenge to the engineers, various reinforcement elements including stone columns, deep mixed columns, cement fly-ash gravel piles, and even concrete piles have been used to support the embankment. Rigid piles, such as cement fly-ash gravel piles and concrete piles, are increasingly used in China.

Terashi et al. (1983) found the extrusion of the unstabilized soil between the column rows in the centrifuge tests. Centrifuge tests of embankments supported by deep mixed columns showed that possible failure modes include bending, tilting, translation, shearing, and crushing of the columns, and the flowing of the soil around the columns (Miyake et al., 1991a, b; Kitazume et al., 2000, 2005).

Han et al. (2005a, b) and Navin et al. (2006) performed numerical analyses on the stability of the embankments on deep mixed columns and concluded that assuming shear failure for deep mixed columns tends to be unsafe.

3D numerical analysis was conducted to investigate the lateral behavior of rigid piles at different locations to support embankments. To evaluate the phenomenon of soil flow, a single pile was placed under the embankment subjected to an additional load up to a limit equilibrium state.

LATERAL BEHAVIOR OF PILES UNDER AN EMBANKMENT

Numerical Model

A typical cross section and a plan view of the embankment were selected and shown in Fig. 1, and Fig. 2, respectively. The embankment was supported by columns of 0.5 meter in diameter and 28 meters in length at center-to-center spacing of 2.0 meters. No basal reinforcement was placed at the base of the embankment. The typical soil profile in Tianjin, China was selected according to Zheng *et al.* (2008). The embankment was 23 m wide on the crest and 5 m high, and had a side slope of 1(V):1.5(H). The embankment was constructed in 5 lifts of fill with 1.0 meter each lift. A surcharge of 15kPa was applied to simulate the traffic load. Half of the embankment was modeled considering its symmetry.

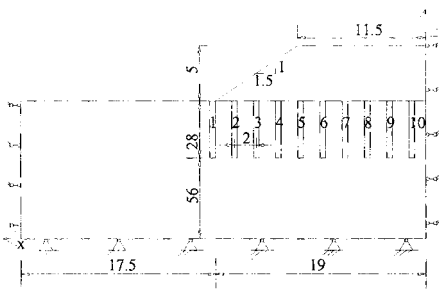

Fig. 1 Cross section of the column supported embankment (unit: m)

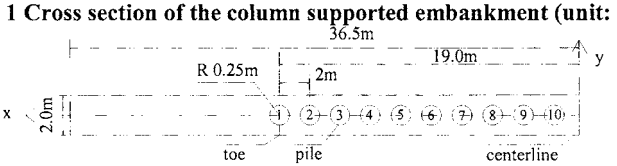

Fig. 2 Plan view of the column supported embankment

Material Properties

The soil profile and properties are shown in Table 1. All the soil layers were modeled as linearly elastic perfectly plastic materials with Mohr-Coulomb failure criteria. Poisson's ratios of all the soil layers were taken as 0.35. The cohesion, the friction angle, the elastic modulus, and Poisson's ratio of the embankment fill were taken as 15kPa, 28^0, 30MPa, and 0.3, respectively. The piles were modeled as pile elements with the elastic modulus of 60GPa and Poisson's ratio of 0.2, respectively. The soil-pile interaction was reflected by the normal stiffness, k_n, and the shear stiffness, k_s, of 10^9 kN/m^2.

The 3D model shown in Fig. 2 contained one row of piles. The thickness of the foundation soil beneath the pile tip was two times the pile length as shown in Fig.1. The bottom boundary was fixed in both vertical and horizontal directions and two side boundaries were fixed in the horizontal but free in the vertical direction.

Pile Lateral Behavior

The lateral behavior of piles including pile deflection and pile moment were analyzed by changing the positions of the piles under the embankment from Positions No. #1 to #10 as shown in Fig. 2.

Table 1. Properties of foundation soils

No.	(1)	(2)	(3)	(4)	(5)	(6)
Soil layer	Fill	Clay	Soft Clay	Very soft clay	Soft Clay	Silt
Bottom depth (m)	1.5	2.5	7	12	16.5	84
E (MPa)	10	6.8	6	4.2	6	24.2
w (%)	-	33	39.6	54.6	40.3	21.6
c (kPa)	10	20	8.6	9.4	14.6	13
φ (°)	5	4.25	6.2	5.9	11.2	33.5

Pile deflection

The lateral deflections of the piles at Positions No. #1 to #9 are shown in Fig. 3. All the piles had similar shapes of deflections along the length of the pile. However, the piles close to the center of the embankment had the smallest deflections. When the piles located near the center of the embankment, the piles were mainly subjected to vertical load. The piles under the slope and close to the shoulder were more severely affected by the lateral deformation of the foundation soil. The piles at Positions No. #1 and #6, #2 and #5, #3 and #4 had similar deflections, respectively. The piles at Positions No. #3 and #4 had the largest deflections while those at Positions No. #1 and #6 had the least deflections. The maximum deflections for most of the piles occurred at the top of the piles.

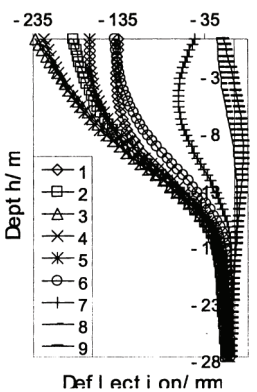

Fig.3 Lateral deflections of piles

Bending moment

Figure 4 presents the distributions of bending moment along all the piles. The bending moment increased from the central piles to the outer piles. The maximum bending moments among all the piles occurred at the lower part of the piles (i.e., at a depth of 16m, near the interface between the soft clay and the relatively firm silt layer). Figure 4 shows that the peak moment and the depth of the peak moment are different for the piles at different locations. The bending moments of the piles at Positions No. #1 and #5 were the largest at the upper part of the piles while those of the piles at Positions #3 and #4 were the largest at the lower part of the piles.

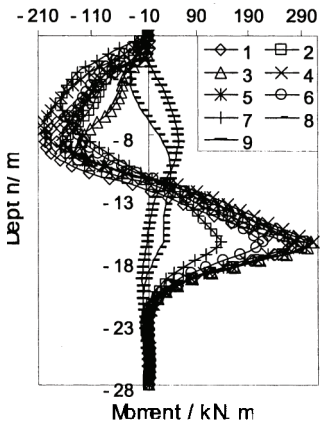

Fig. 4 Moments of piles

SOIL FLOW AROUND THE PILE

Background

An embankment on the Guang-Zhu highway was supported by two layers of geogrid above pipe piles in soft soils. The embankment failed when the height of the embankment reached 7m due to the collapse of the piles under the embankment. The measured lateral displacement of soil in the midway between the piles was larger than the lateral deflections of the piles. This case study implied that the soils might flow around the piles, when rigid piles were installed at large spacing, and thus lead to the instability of the embankment.

Numerical Model

To investigate the possible soil flow around piles, a single rigid pile was employed under the embankment in the 3D numerical model. The numerical model had the same cross section of the embankment (geometry and dimensions) as shown in Fig. 1. However, the number and diameter of the piles and the thickness of the soft soils were different from those in Fig. 1. Figure 5 shows the 3D numerical model. The plan view

of the single pile under the embankment is shown in Fig. 6. The soil thickness below the pile tip was 2.0m. The pile had a length of 28m, a diameter of 1.0m, and a pile spacing of 3.0m along the centerline. The Young's modulus of the pile was 60GPa and the Poisson's ratio was 0.2. The interface between the pile and the soil had both normal stiffness, k_n, and shear stiffness, k_s, of 10^9 kN/m^2.

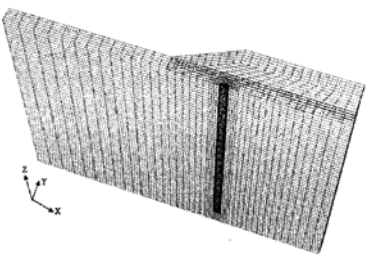

Fig.5 Numerical model

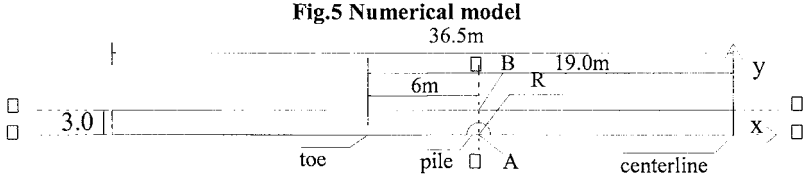

Fig.6 Plan view of the column supported embankment (unit: m)

Numerical results

The plan view of the numerical model is shown in Fig. 6. The pile in Figs. 5 and 6 was located at the same position as No. #4 as shown in Fig. 2. Additional load was applied as a uniform pressure on the top of the embankment up to a state close to limit equilibrium to observe the soil flow. Figure 6 shows that the I-I section goes through the center of the pile, the II -II section is the midway of two adjacent piles along the length of the embankment, and the III-III section goes through the center of the pile and is perpendicular to the I-I and II -II sections. The III-III section intersects with the I-I section at Point A, the III-III section intersects with the II -II section at Point B. The soil flow around the pile could be illustrated by comparing the deflection of the pile at Point A with the lateral deformation of the soil at Point B.

The relative displacement of Point B to Point A along the x direction is shown in Fig. 7. The negative value represents the displacement of the soil was larger than the displacement of the pile. The relative displacement increased with the increase of the applied load.

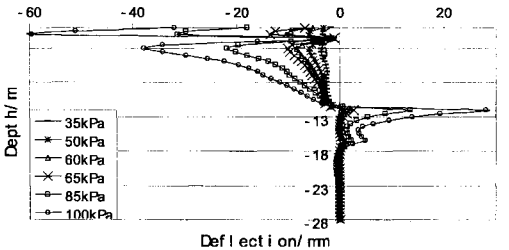

Fig.7. Relative displacement between the soil and the pile along the x direction under a different additional load on the top of the embankment

Figure 8 shows the soil displacement vectors in the x-z section at the additional load of 100kPa on the top of the embankment. The vertical displacement contours of the soil in the x-y section at the depth of -1m and -3m under the additional load of 100kPa are shown in Fig. 9. The positive value represents the soil moving upward while the negative value represents the soil moving downward. It is shown that the soil in front of the pile moved upward and toward the midway of the pile spacing while the soil behind the pile moved downward and also toward the midway of the pile spacing. This result implies that the soil in front of the pile was flowing around the pile. Figure 10 shows that the largest relative displacement of Point B to Point A along the x direction increased with the increase of the applied load. The position for the largest vertical displacement did not change much. This phenomenon could only be observed in a 3D analysis. The soil flow around the pile may be affected by the pile stiffness, pile spacing, soil strength and stiffness, interface roughness, which will be studied in the future.

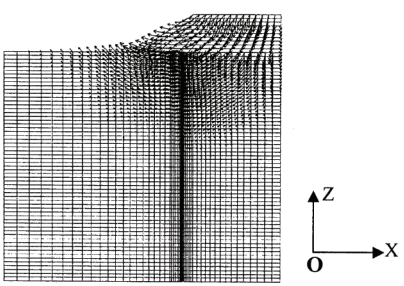

Fig.8. Soil displacement vectors in the x-z section at the additional load of 100kPa on the top of the embankment

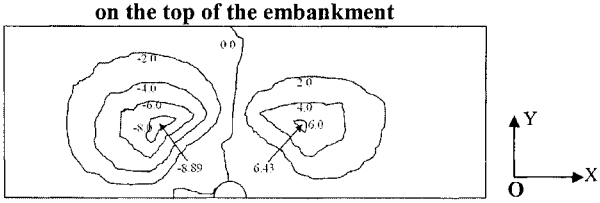

(a) at the depth of -1m

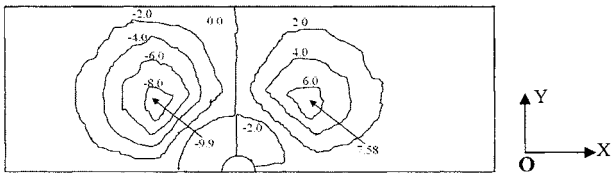

(b) at the depth of -3m

Fig.9. The contours of vertical displacement under the additional load of 100kPa (unit: cm)

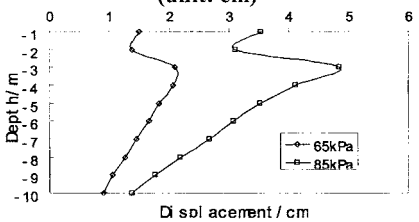

Fig.10. The largest vertical displacements of the soil under two different additional loads

CONCLUSIONS

Through the 3D numerical analysis of pile supported embankments, the following conclusions can be drawn:

(1) The construction of the embankment may induce lateral deformation of the foundation soil and induce pile deflection and bending moment. The pile lateral behavior, including pile deflection and pile moment, are different for piles at different positions. The deflection and moment of the pile at the inner and outer positions under the embankment are larger than the pile near the centerline of the embankment.

(2) For large diameter rigid pile supported embankment of large pile spacing, the soil may flow around the pile. The displacement of soil midway between the piles is larger than the deflection of the pile. When the lateral stiffness of pile is large enough to prevent the pile from occurring bending failure, soil may flow around the pile for embankment constructed on soft ground.

ACKNOWLEDGMENTS

The authors gratefully acknowledge the financial support for this study provided by the National Science Foundation under the contract No. 50678115 and the Tianjin National Science Foundation under contract No. 07JCZDJC09800.

REFERENCES

Terashi, M., Tanaka, H., Kitazume, M. (1983). "Extrusion failure of the ground improved by the deep mixing method." *Proceedings of the 7th Asian Regional Conference on Soil Mechanics and Foundation Engineering*, Haifa, Israel, 1,

313-318.

Miyake, M., Wada, M., and Satoh, T. (1991a). "Deformation and strength of ground improved by cement treated soil columns." *Proceedings of the International Conference on Geotechnical Engineering Coastal Development.* GeoCoast'96, Yokohama, Japan, 1, 369-372.

Miyake, M., Akamoto, H. and Wada, M. (1991b). "Deformation characteristics of ground improved by a group of treated soil." *Centrifuge 91*, Balkema, Rotterdam, 295-302.

Kitazume, M., Okano, K., and Miyajima, S. (2000). "Centrifuge model tests on failure envelope of column type mixing method improved ground." *Soils and Foundations*, 40(4). 43-55.

Kitazume, M. and Maruyama, K. (2005). "Collapse failure of group column type deep mixing improved ground under embankment." *Proc. of the International Conference on Deep Mixing 05*, 245-254.

Han, J., Huang, J, and Porbaha, A. (2005a). "2D numerical modeling of a constructed geosynthetic-reinforced embankment over deep mixed columns." ASCE Geotechnical special publication (GSP) No. 131: *Contemporary Issues in Foundation Engineering*, ASCE GeoFrontiers, Austin, TX, Jan. 24-26.

Han, J., Parsons, R.L., and Huang, J. (2005b). "Factors of safety against deep-seated failure of embankments over deep mixed columns." *Proc. of the International Conference on Deep Mixing 05*. Sweden, 1.2, May 23-25, 231-236.

Navin, M.P. and Filz, G.M. (2006). "Numerical stability of embankments supported on deep mixed columns." *Ground Modification and Seismic Mitigation*, (GSP 152), ASCE.

Zheng, G., and Wang, L. (2008). "Load transfer and bearing capacity of inclined pile under vertical load." *Chinese Journal of Geotechnical Engineering*, 2008, 30(3), 323-330. (In Chinese)

Settlement Behavior of Highway Transition Sections on Soft clay foundation

Deng Yongfeng[1], Liu Songyu[2], Jing Fei[3], Feng Weijiang[4]

[1]Transportation College, Southeast University, Nanjing, P.R.China, 210096, noden@163.com

[2]Transportation College, Southeast University, Nanjing, P.R.China, 210096, liusy@seu.edu.cn

[3]Transportation College, Southeast University, Nanjing, P.R.China, 210096, jingfei9212@sohu.com

[4]East china investigation and design institute, Hangzhou, P.R.China, 310014, feng_wj@ecidi.com

ABSTRACT: When highways were constructed on the soft clay foundations, the ground improvement methods such as deep mixing column, preloading and gravel column, were alternately used, and the transition sections were generated. When the different settlement between two methods was large enough after operations, the crack or bumping on the pavement probably happened. In the paper, a transition case between the preloading method and the deep mixing method was studied. Later the three dimension finite element method (3DFEM) was adopted to analyze its different settlement behavior. The results showed that the different settlement just happened in a small zone near the border of two ground improvement methods instead of the whole transitional zone.

INTRODUCTION

There alternately existed the embankment, bridge, culvert and other structures along the highway. Among the embankment and structures, the approach or the transition section was set to reduce the different settlement for the driving comfort and safety of the highway. If the different settlement of the approach or the transition wasn't deposed well, the hump or pavement crack would occur as FIG. 1 and FIG. 2. In FIG. 1, there was a hump located at a culvert, which was supported by piles, and whose two borders were embankment supported by grounds. FIG. 2 was a case in a highway located at the marine clay zone where many ground improvement methods were used such as the preloading method and the deep mixing method.

About the different settlement of the approach between the bridge and embankment (Shown as FIG. 1), there were some researches (Zhang, 1999) where

the different settlement were produced by embankment settlement on the foundation because the settlement of the curvet and bridge supported by the piles was considered as zero.

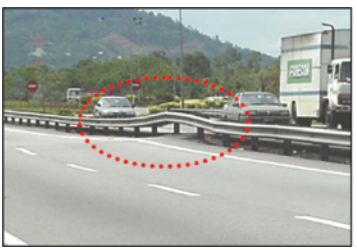

FIG. 1. Hump over culvert supported by pile

FIG. 2. Pavement crack

In the highway engineering on the soft clay foundation, there was another kind of transitions caused by the different ground improvement methods for example, the preloading method and deep mixing method. In this kind of transitions, the different settlement was brought out by the properties of the two foundations (or the modified foundations) which sometimes would lead to the pavement crack (as FIG. 2).

Hence it was important to understand the settlement behavior of the transition. Han et al. (2007) analyzed the settlement behavior of the foundation with the bedrock inclination on the flexible strip loading, which gave a method to analyze the settlement behavior of the transition. In this paper, the settlement behavior of the transition between the preloading and deep mixing method was analyzed by a case and numerical simulation to understand how the different settlement happened.

CASE STUDY

In this analysis, a case was selected from a highway at Lian-Yun-Gang city, East china near the East Sea where the marine clay was sedimented. The stratigraphic section, embankment height and ground modification method of the transition K21 +200-K21+400 were shown as FIG. 3 and soil basic properties are shown as Table 1.

In Table 1, e was the initial void ratio; C and ϕ were the cohesion and friction angle by the CU tests; E_s was the compression modulus by the odometer test; and k was the hydraulic conductivity. In FIG. 3 and Table 1, it showed that the transition's foundation of highway constructed near Lian-Yun-Gang city was composed of three layers: the upper layer (a crust about 1.3 m), the soft clay (the thickness of 10.3 m) and the sub layer. The modulus of the soft clay is very small about 1.2 MPa. In the highway design, the foundation near K21+200 was improved by the preloading method for the low embankment height was just 2.9 m and the foundation near

K21+400 was improved by the deep mixing method for the embankment height was 3.9 m, where the length of deep mixing columns was 12.0 m with 0.5 m in diameter, 1.4 m in column spacing and 0.8 MPa in the design strength.

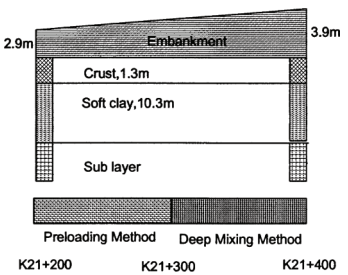

FIG. 3. Sketch of the ground and embankment

Table 1. Basic properties of the foundation and embankment

Soil	Thickness (m)	Density (kN/m^3)	e	C (kPa)	ϕ (°)	E_s (MPa)	k (10^{-7}cm/s)
Crust	1.3	18	1.079	17.6	18.0	3.69	16.0
Soft clay	10.3	15.3	1.853	4.6	10.0	1.21	7.48
Sub layer	14	18.8	0.876	18.8	15.0	4.19	12.9
Embankment		21.0		28.0	29.8	31.2	

The embankment height curve near K21+200 could be separated as three stages: (1) To fill the embankment to 3.6 m, which was 0.7m higher than the design height of the embankment; (2) To excavate the embankment, (3) To refill the embankment and pavement to design height. There was a preloading period (220 days) during the first stage. It showed that the settlement of the section K21+200 was more than that of the section K21+400, and at the end of construction (after 1000 days in the FIG. 4) the settlement speed of the section K21+200 was higher than that of K21+400 which probably caused the pavement crack shown as FIG. 2.

The time dependent curve of two sections was presented in FIG. 4. In the FIG. 4, the relation between the settlement and embankment height could be redrawn as FIG. 5 where it showed that the settlement of the K21+400 was almost rising linearly with the embankment height but the settlement of K21+200 was rising nonlinearly with

the embankment height, where the settlement increased rapidly with the embankment height when the embankment height was more than 1.5 m.

According to FIG. 4 and FIG. 5, the total different settlement was 61 cm and the different settlement after construction was 6.3 cm.

If the different settlement after construction was considered as 6.3cm along the transition in 200 m length (From K21+200 to K21+400), the slope change of pavement after construction was just 0.032 %, which could not generate crack of the pavement. But in fact, it was found that the slope change of pavement was larger than that and changing area was just near the border between two improvement methods. Hence the different settlement behavior of the transition should be reinvestigated.

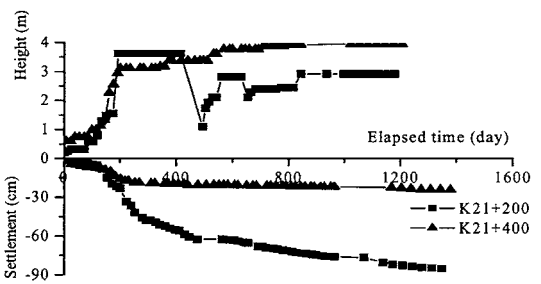

FIG. 4. Time dependent curve of Sections K21+200 and k21+400

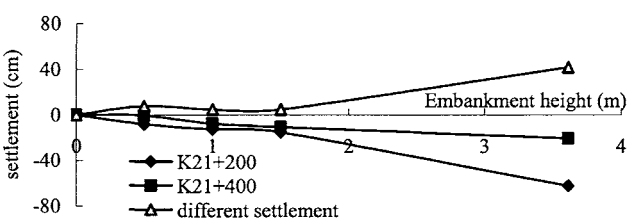

FIG. 5. Curve of settlement versus embankment height

NUMERICAL SIMULATION OF THE CASE

The numerical simulation method was adopted to analyze the different settlement of the transition. FIG. 6 was the simplified numerical simulation model of the transition. In the simulation, the x direction deformation of the surfaces at x=25

m and x=-25 m was fixed; the y direction deformation of the surfaces at y=0 m and y= 100 m was fixed; the x, y and z direction deformation of the surface at z= 30.6 m was fixed. The surfaces at x=25 m, x=-25 m, y=0 m, y=100 m and z=0 m were considered as drainage surface. The water level was set as z=0. The modulus E_c of the deep mixing zone was calculated by $E_c=mE_p+(1-m)E_s$, where E_p was the column modulus, equal to 100 times of the unconfined strength (0.8 MPa), m was the area replacement ratio, equal to $0.91D^2/L^2$,where D was the column diameter and L was the column spacing (Liu, 2000).

The Mohr-Coulomb model was used for the soils and embankments, but the deep mixing zone was considered as elastic zone. FIG. 7 was the idealized embankment filling curve. With the parameters in Table 1, numerical simulation model and embankment filling curve, the settlement curve of the transition at the top, y=50 m and z=0 m of the foundation was drawn as FIG. 8, which showed that the settlement of the transition along the highway is 'S' shape curve, and the settlement on the soft clay foundation was more than that on the deep mixing zone. FIG. 8 also showed that the settlement at the deep mixing zone changed smoothly and when the distance from the border was more than 5 m, where there was almost no change. While the settlement at the soft clay zone changed rapidly, especially near the border of the transitions, and when the distance from the boundary is more that 15m, there was almost no change too. In others words, the different settlement of the transition zone occurred in the 20 m around the boundary for this case.

For this case, if the different settlement of the pavement after operation was 3.6 cm and the distance of the influence zone was just 20 m, the slope change of pavement after construction was just 0.32 %, about 10 times larger than that calculated before, which probably generated the pavement crack.

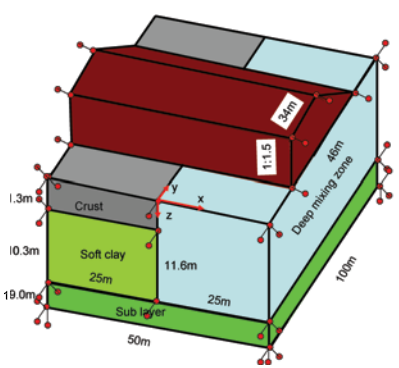

FIG. 6. Numerical simulation models

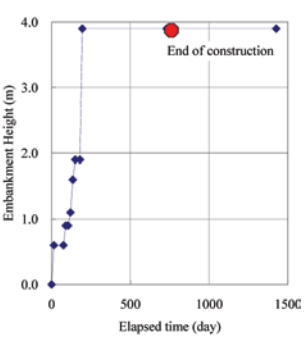

FIG. 7. Filling curve

The A and B points in FIG. 8 were two turning points of the settlement curve with 'S' shape. The top of pavements at A point was compressed while at B point was tensed for the transition's different settlement. So it was more possible that the pavement cracked at the deep mixing zone if the different settlement was large enough. In facts, the slope change and pavement crack happened longitudinally mostly at the 5-10 m area of the deep mixing zone according to the pavement investigation of the whole highway after operation, which was similar to the simulation result.

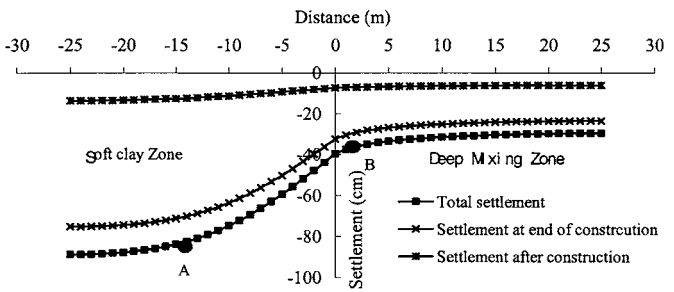

FIG. 8. Simulation settlement of the transition

CONCLUSIONS

The settlement behavior of the transitions between two ground improvement methods was analyzed by a case and numerical simulation to understand how the different settlement happened which would generate the pavement crack. The results of the case showed that the settlement curve of the transition was 'S' shape and the settlement curve changed rapidly after operation at the range of 15 m near the soft clay zone and 5 m near the deep mixing zone from the border between two methods. In others words, the different settlement just happened in a small zone near the border of two ground improvement methods instead of the whole transitional zone.

REFERENCES

Han J., Huang J., Parsons R.L., (2007). "Influence of bedrock inclination on elastic settlements of flexible shallow strip foundations." *Computers and Geoctechnics*, Vol.34: 53-56.

Liu S.Y., (2009). "Ground improvement in highway engineering", Nanjing: *Press of Southeast University*, 370 pp.

Zhang L.M., (1999). "Settlement patterns of soft soil foundations under embankments." *Canadian Geotechnical Engineering*, Vol.36: 774–781.

Consolidating Dredge Soil by Combining Vacuum and Dynamic Compaction Effort

An Deng[1] and Shi-long Xu[2]

[1] Associate Professor, Key Laboratory of MOE for Geomechanics and Embankment Engineering, Hohai University, Nanjing 210098, China;
Geotechnical Research Institute, Hohai University, Nanjing 210098, China; a_deng@hhu.edu.cn
[2] Shanghai GeoHarbor Group, Shanghai 200092, China

ABSTRACT: Escalating lands are being reclaimed at coastal areas by dredging soils from sea or rivers. Such formed lands are often characterized as presenting high water content, high void ratio, high compression, worst disturbance and weak bearing capacity, and thus cannot be directly used as a bearing deposit. It is time consuming to consolidate such lands by relying on naturally occurring evaporation and hydraulic dissipation. Enhanced engineered technology has to be introduced to expedite the dredge consolidation process. A technology, known as high vacuum densification method (HVDM), was developed to treat the dredge soil in a time-efficient and cost-effective means. Its principle is to consolidate the soil by combining vacuum effort and dynamic compaction. The vacuum effort is used to pump the moisture out of the soils in steps; and the drained soils are densified by dynamic compactions. Soils amenable to HVDM can be treated to favorable conditions meeting both strength and deformation requirements. Besides the principles and the construction procedures of HVDM, cases studies were also presented in this paper, which demonstrates the attractive merits of HVDM in contrast to comparable soil treatment methods.

INTRODUCTION

In the past decade, land reclamation from sea or river waterway has been escalating at coastal areas of China, which brings forth challenging soil treatment issues pressing geotechnical communities. Once dredged from sea and waterway, the dredge soil is characterized presenting high water content, high void ratio, high compression, worst disturbance and weak bearing capacity, which leads the dredge land unqualified for the use as a jobsite or a bearing deposit where buildings shall be rested on. To consolidate a large-scale dredge land using a time- and cost-effective means is challenging the current available soil treatment technologies.

Dynamic compaction may be unanimously chosen as the first option to implement the land consolidation. This technology, however, is limited to treatments of unsaturated sandy soils of low water content (Zheng et al. 2000, Shi et al. 2006). The dredge soil

often comprises saturated silty and/or clayey soil of high water content and low hydraulic conduction, which impedes the efficient dissipation of excess pore water pressure resulted due to compactions. As a result, a rubber soil phenomenon may be incurred if the dynamic compaction is used to treat the dredge soil. Additional related but limited soil treatment technologies include composite foundation (e.g., in-place mixing columns), which is relatively high in cost, and drainage-consolidation methods (e.g., vacuum-surcharge preloading), which often takes relatively long duration to consolidate the jobsite and extra expenditure if backfilling is required (Editor Committee 1994).

In this study, a soil treatment technology, known as high vacuum densification method (HVDM), is described. HVDM was developed to efficiently consolidate dredge soil by combining vacuum and dynamic compaction effort. The principles, procedures and practices of HVDM are presented in brief.

DESCRIPTION OF METHOD

Principles

Soil dry density is regarded as one the soil properties indicating the relative compaction of the soil. The higher the dry density, the more compacted the soil. HVDM is a method to compact the soil into its maximum dry density, and equivalently, the most densified condition. Fig. 1 demonstrates the soil densification progress in relation to compaction implementation and moisture content variation occurred to a jobsite treated by HVDM. The jobsite soil starts from state A, which presents a relatively high moisture content and low dry density. By reducing the moisture content, the soil is converted into state B, where the soil is subjected to N1 blows at its optimal moisture content and densified into state C. By alternating the two steps, i.e., moisture reduction and dynamic compaction, the soil would further follow routes C-D-E and E-F-G. After three runs, the jobsite soil is converted into state G, which presents significantly low moisture content and high dry density, relative to its initial state A. That is, a substantial consolidation is completed.

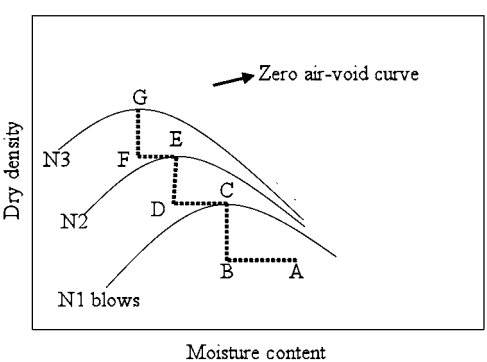

FIG. 1. Schematic of soil compaction.

The above concept is implemented by construction procedures of HVDM. Each HVDM run consists of two steps, i.e., moisture reduction and dynamic compaction. In the steps of moisture reduction (i.e., A-B, C-D and E-F), HVDM employs vacuum effort to suck or drain the soil moisture out (Fig. 2). In the steps of dynamic compaction (i.e., B-C, D-E and F-G), HVDM employs conventional dynamic compaction procedures to densify the soil (Fig. 2). In each HVDM run, the vacuum effort leads to negative pore pressure in the soil around the vacuum pipes, whereas the dynamic compaction leads to positive pore pressure. The two opposite pore pressures form a lateral pressure gradient in influenced soils if the vacuum and compaction spacing are well designated on the jobsite. The pressure gradient is generated to expedite the pore pressure dissipation and moisture discharge.

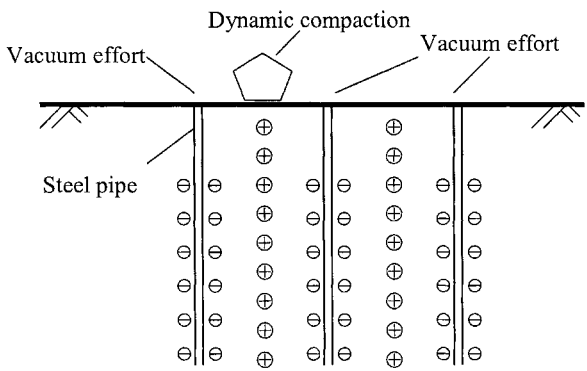

FIG. 2. Diagram of HVDM operation.

Most often, a restoration break is allowed between HVDM runs (i.e., at states C and E), during which the soil strength gains to eliminate the occurrence of a rubber soil. The number of HVDM run is dependent on the compaction energy and the influential depth of the machinery, the construction time allotted, and most importantly, the bearing capacity required for the jobsite or individual section of the jobsite. Generally, for a newly dredge soil, three runs are needed to attain a soil bearing capacity of 80-100 kPa and a consolidation degree of 80-90%.

Facilities and Procedures

The facilities used in HVDM treatments include vacuum facilities, compaction facilities, monitoring devices and sometimes, prefabricated vertical drain (PVD). Vacuum facilities mainly include vacuum system, tubular perforated steel pipes and horizontal main collection pipes. Compaction facilities include crane compactors, bulldozers, rollers or vibrators, etc. Monitoring devices are used to measure the pore water pressure variation in the HVDM progress. PVD is used as an aid facilitating the moisture discharge.

Fig. 3 shows a construction flow chart in a typical HVDM treatment. The treatment starts with the jobsite preparation, in which the site is leveled off, cleaned, and exposed to a site shallow exploration. The perforated steel vacuum pipes are installed in array to depth of 6-8 m. Discharge system is hooked up on the ground. Vacuum systems are laid out independently to charge designated portions of the jobsite.

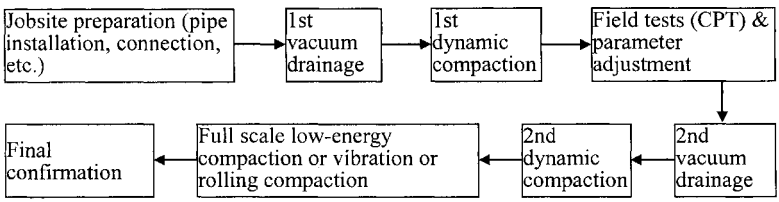

FIG. 3. Construction flow chart in a typical HVDM treatment.

The 1st HVDM run starts with the 1st vacuum drainage, which lasts until the soil moisture content of the treated stratums is close to the 1st optimal moisture content (i.e., the abscissa of state B in Fig. 1). Uninstall the steel pipes, and run the 1st dynamic compaction. Certainly, the energy of the dynamic compaction is decided by trial-and-error via indoor and field compaction tests. After the 1st HVDM run, field confirmation tests (e.g., CPT) are conducted. In terms of the monitoring data and CPT data, a restoration break is estimated and allowed prior to the next HVDM run. Likewise, one or two more HVDM runs are carried out to eventually consolidate the subsurface into a hard shell.

Merits

HVDM enables the dredge soil consolidated in a time-efficient and cost-effective means. Firstly, a pressure gradient is repetitively yielded between the positive pressure (i.e., excess pore water pressure by dynamic compactions) and the negative pressures (i.e., vacuum effort), and being over 1 atm (i.e., over 101 kPa), which is equivalent to a backfill surcharge of 5 m high. Such pressure is able to force out pore moisture in relatively impermeable soils at an expedited rate. Plus, vacuum effort help reduces moisture content in an active manner, instead of the passive manner imposed by conventional methods (e.g., the surcharge preloading method). As a result, the time elapse on water discharge and soil restoration is favorably saved from 3-4 weeks (e.g., in a vacuum-surcharge preloading method) to 5-10 days. According to the experiences, only 10-25 days are required for a treatment unit, which is merely 1/3 to 1/2 of the construction time a general method needs. Meanwhile, low-cost energy machinery, saved labor force, and reduced procedure and time yield substantial saving in cost, which is around 40% to 80% the cost of comparable methods.

Secondary, the influential depth of HVDM leads to the formation of a hard shell of 6-8 m deep in the subsurface. The hard shell is over-consolidated and firm, which helps improve stress distribution conditions (i.e., hardness, thickness and angle). As a result, the post-treatment settlement and differential settlement are controlled. Furthermore,

the soil moisture content and saturation degree is decreased in steps. Plus, the soil strength gains via the moderate compaction effort. Occurrence of rubber soils is eliminated. Concurrently, HVDM is a mechanical process which neither uses chemical additions nor discharge environmental unsafe emissions or effluents.

Lastly, a jobsite subjected to HVDM treatment favors a further foundation formation. For instances, the treated jobsite can be formed into an enhanced composite foundation by backfilling stones or gravels, i.e., stone columns. The over-consolidated soils of 6-8 m deep lead to the increased friction between columns and soils. The field test data indicated that the site bearing capacity reached up to 210 kPa.

CASE STUDIES

A jobsite for a port lies close to the Yangtze River in eastern China. The jobsite consisted of the reclamation formation of farmland and dredge soil. The water level was about 0.6 m beneath the ground surface. The main soil profile of the jobsite included: 1) top layer, drained silty fine sand, 1-3 m thick, 2) clay and silty clay, on average 1-2 m thick and 34% water content, void ratio of 0.9, 3) silt and mucky soil with siltage, 0-6 m thick, 43% water content and 1.16 void ratio, and 4) fine sand, medium compaction, good bearing capacity. Deposits beneath were the inter-layers of soft soil and sandy soil.

The end use of the jobsite was to stack steel products and freight containers. According to designs, the soil bearing capacity needed to attain 120 kPa, and 150 kPa for some locations.

A pilot treatment was conducted by using HVDM on a trial patch of 20×20 m. Vacuum pipes were arranged in array of 3.5×4.0 m. The 1st vacuum drainage lasted 11 d. The 1st compact energy was 3000 kN-m at a drop spacing of 7.0×7.0 m and 8 blows each drop location. The drop penetration depth should be less than 2 m. After leveling off the ground, the 2nd vacuum drainage was conducted immediately with identical drainage layout. After 10 d drainage, the 2nd compaction was performed at the energy of 1800 kN-m. The drop spacing was 2.5-3.5 m in quincunx layout. Six blows were conducted each drop location, and the drop penetration depth should be less than 1 m. The ground leveling procedure should be done again after compaction. In order to increase the soil bearing capacity to 150 kPa and form a homogeneous hard subsurface shell, a third HVDM run was conducted. A high energy vibratory roller was finally used to further compact the subsurface of the jobsite.

The site elevations prior to the treatment and after the 1st, 2nd and 3rd compaction were monitor to measure the ground settlement. The segmental settlements were 23.2 cm following the 1st HVDM run, 32.2 cm following the 2nd HVDM run, 10.4 cm following the 3rd HVDM run. The cumulative settlement was 65.8 cm. It is indicated the majority of the consolidation was complemented in the first two HVDM runs in this jobsite.

Field CPT tests and laboratory soil tests were conducted prior to and after soil treatments. Table 1 shows the results of main soil physical and mechanical parameters. It is indicated that the physical and mechanical properties of clayey soils were improved clearly. But the parameter values for sandy soil were decreased, which is associable with the un-accessibility of undisturbed sandy soil samples. Based on the increase of void ratio Δe and the formula $\Delta\sigma' = \Delta e / a = E_s \Delta e / (1 + e_0)$, the effective stress were estimated to increase in the order of over 120 kPa for both silty clay and muddy clay

with silty sand, which met the working load of 120 kPa. Meanwhile, the specific penetration resistance increased obviously for the soil deposit up to 10 m, in particular, the deposit of 3-5 m deep. The increase is more effective in sandy soil than in clayey soil. Based on the experience relating CPT test data to soil bearing capacity, the bearing capacity of the shallow deposit was increased from 80-100 kPa to 160 kPa, which met the design requirement.

Table 1. Soil Physical and Mechanical Properties Before and After Treatment.

Layer	Status	Water content w (%)	Specific gravity r_d (kN/m^3)	Void ratio e	Compression modulus Es (MPa)	Specific penetration resistance Ps (MPa)
Alluvial sand	Before	29 4	14 40	0 841	16 53	3 02
	After	32 0	13 86	0 911	16 78	7 18
Silty clay	Before	32 1	14 32	0 898	8 29	1 51
	After	28 5	14 91	0 807	10 15	2 95
Muddy clay with silty sand	Before	41 1	12 91	1 110	4 15	1 05
	After	38 0	13 30	1 050	5 45	1 65
Silty sand	Before	32 7	14 36	0 896	11 56	4 46
	After	31 9	14 31	0 906	10 72	6 81

CONCLUSIONS

HVDM is an enhanced dredge soil treatment method, which expedites the soil consolidation process by coupling two mutual and alternate efforts, i.e., vacuum drainage and dynamic compaction. High moisture content of dredge soils can be decreased in steps, and concurrently, the soil strength gains by the densification effect. Principles and practices indicate that HVDM is able to consolidate high water content dredge soil in a time-efficient and cost-effective means.

ACKNOWLEDGEMENTS

The study presented in this paper was supervised under Hohai Talent Program (2009).

REFERENCES

Editor Committee of Soil Treatment Manual (1994). *Soil Treatment Manual.* Beijing, China, Architecture & Building Press.

Shi, G., Zhi, X.L., Xie, Y.L. et al. (2006). "Effect analysis of percussive compaction and dynamic compaction on roadbed reinforcement." *Journal of Traffic and Transportation Engineering*, Vol. 6(4): 52-56.

Zheng, Y.R. and Lu, X. et al. (2000). "Research on theory and technology of improving soft clay with DCM." *Chinese Journal of Geotechnical Engineering*, Vol. 22(1): 18-22.

Optimization of Deep Mixed Shear Walls for Stabilization of a Pile-Supported Flood Wall on Level Ground

Tiffany E. Adams[1], M. ASCE, P.E., George M. Filz[2], Ph.D., F. ASCE, P.E., Peter R. Cali[3], Ph.D., M. ASCE, P.E., Mark L. Woodward[4], P.E., and Neil T. Schwanz[5], P.E.

[1]Via Fellow and IGERT Trainee, Department of Civil and Environmental Engineering, Virginia Tech, Blacksburg, VA 24061; teadams@vt.edu
[2]Professor, Department of Civil and Environmental Engineering, Virginia Tech, Blacksburg, VA 24061; filz@vt.edu
[3]Geotechnical Engineer - Contractor, U.S Army Corps of Engineers, Hurricane Protection Office, P.O. Box 60267, New Orleans, LA 70160, peter.r.cali@mvn02.usace.army.mil
[4]Supervisory Geotechnical Engineer, U.S Army Corps of Engineers, P.O. Box 60267, New Orleans, LA 70160, mark.l.woodward@mvn02.usace.army.mil
[5]Geotechnical Engineer and Regional Technical Specialist, U.S Army Corps of Engineers, St. Paul District, 190 Fifth Street East, St. Paul, MN 55101, neil.t.schwanz@usace.army.mil

ABSTRACT: In 2006, the U.S. Army Corps of Engineers installed deep mixing method (DMM) shear walls on the protected side of a pile-supported flood wall at the Gainard Woods Pump Station. Numerical analyses indicated that a primary benefit of the DMM shear walls at this site was to stabilize a slope on the protected side. To investigate optimization of DMM shear walls for pile-supported flood walls on level ground, a cross-section based on the conditions at the Gainard Woods site, but with level ground, was developed and analyzed using a range of DMM shear wall configurations. The results show that DMM shear walls centered underneath the flood wall are most efficient for stabilizing the wall.

INTRODUCTION

As part of an ongoing research project on the stability of levees and floodwalls stabilized using deep mixed shear walls, stability analyses were performed for a pile-supported, reinforced-concrete flood wall (a T-wall) constructed by the U.S. Army Corps of Engineers at the Gainard Woods Pump Station in Plaquemines Parish, Louisiana (Adams et al 2008). A zone of deep-mixed shear walls was installed on the protected side of the T-wall, between the wall and an existing drainage canal, to improve the stability of the system. The shear walls, which are oriented perpendicular to the T-wall alignment, were constructed using the deep-mixing method (DMM). The shear walls are 9.1 m long, 16.8 m deep, and located 9.1 m away from the toe of the T-wall at the ground surface in order to provide a minimum

clearance of 3.0 m between the bottom of the shear walls and the battered piles. This geometry leaves a gap between the DMM shear walls and the pile-supported T-wall, which created uncertainty about the effectiveness of the shear walls in improving stability of the T-wall. Numerical analyses were completed to evaluate the performance of the T-wall and to calculate the factor of safety for the system. The analysis results showed that the increase in factor of safety due to the addition of DMM shear walls was primarily due to stabilization of a shallow slope near the existing drainage canal. Subsequently, additional analyses were performed to investigate optimum DMM shear wall configurations for stabilizing pile-supported T-walls on approximately level ground. Results of the level-ground analyses are presented in this paper. Additional details are in a report by Adams and Filz (2008).

ANALYSIS SECTION AND MATERIAL PROPERTIES

The design cross section for the Gainard Woods Pump Station project (Adams et al 2008) was adjusted to create a level ground analysis section for the optimization study. The height of the flood wall and the tip elevation of the piles were increased until the factor of safety for the level ground analysis section, using the same material properties as for the Gainard Woods analyses, but without DMM shear walls, was about 1.2. The resulting analysis section is shown in Figure 1, in which "Stratum 1" is the floodwater on the left-hand side, "Stratum 2" is a low-height embankment near the T-wall, and "Stratum 3" through "Stratum 13" are existing layers of soil at the site. The top of the flood wall is at El +8.2 m and the tip elevation for both piles is at El -21.3 m. The location of the DMM zone relative to the T-wall for the configuration at the Gainard Woods Pump Station T-wall is also shown in Figure 1.

The material property values used for this optimization study, which are listed in Table 1, are the same as those used for the Gainard Woods stability analyses.

NUMERICAL ANALYSES

Numerical analyses were performed using the finite difference computer code FLAC (ITASCA 2005) with its automated factor of safety analysis procedure. The results for the DMM zone configuration in Figure 1 resulted in a factor of safety of 1.34 and showed substantial shearing in the soil between the T-wall and the DMM zone. Alternate DMM zone configurations were then identified to limit the amount of shear strain in the soil between the DMM zone and the T-wall. This paper presents the results for a DMM zone located entirely on the protected side of the T-wall piles, as well as a centered DMM zone located underneath the flood wall. These two configuration options are illustrated by the schematic diagrams in Figure 2. For the centered DMM zone, pile alignment would need to be carefully controlled.

The DMM arrangement in Figure 2a incorporates a stepped face next to the protected-side piles to limit the amount of shear strain in the soil between the DMM zone and the T-wall, and the top of the DMM zone was raised to the ground surface at El +0.6 ft. The minimum horizontal clearance between the protected side pile and the DMM zone was reduced to 1.5 m. Analyses were completed for DMM zone widths of 15.2 m, 21.2 m, and 27.6 m with base elevations of -5.5 m, -10.7 m, -16.8 m, and

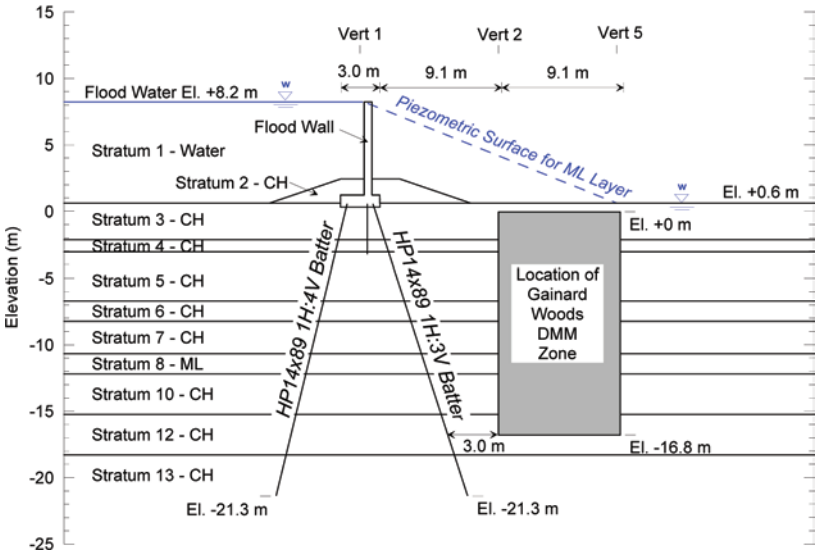

FIG. 1. Design Cross-Section

Table 1. Summary of Material Property Values

Stratum	γ_t (kN/m^3)			c[b] (kN/m^2)			ϕ (deg)	G/s_u
	Vert 1	Vert 2	Vert 5	Vert 1	Vert 2	Vert 5		
1	9.8			0			0	0
2	17.3			19			0	130
3	13.5			14	10	7.2	0	100
4	15.4	13.5	15.4	14	10	7.2	0	130
5	15.7	14.5	15.7	14 to 20	10 to 16	7 to 13	0	130
6	18.1	15.7	15.7	20 to 23	16 to 18	13 to 15	0	130
7	18.1	15.7	15.7	23 to 26	18 to 22	15 to 19	0	130
8	18.4			200			15	130
10	18.1	15.7	15.7	29 to 34	25 to 29	22 to 26	0	160
12	16.5			34 to 38	29 to 34	26 to 31	0	160
13	16.5			38+	34+	31+	0	160
DMM	Varies[a]			48[c]			0	103

[a] The unit weight equals that assigned to the corresponding existing soil layers.

[b] Cohesion for CH strata increases with depth below El -3.05 m at a rate of 1.57kN/m^2/m. Linear interpolation was used to model the horizontal variation in strengths and unit weights between verts 1 and 2 and between verts 2 and 5.

[c] Representative DMM cohesion is a weighted average for the column/soil matrix within the DMM zone.

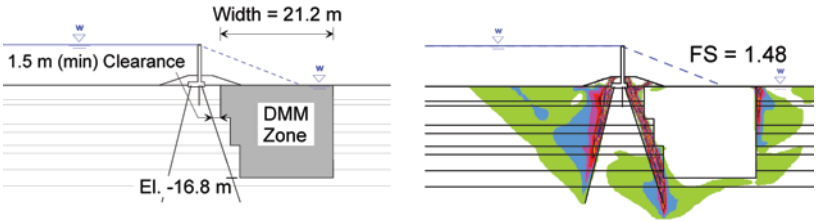

FIG. 2a. Protected Side 21.2 m Wide DMM Zone with Base El -16.8 m

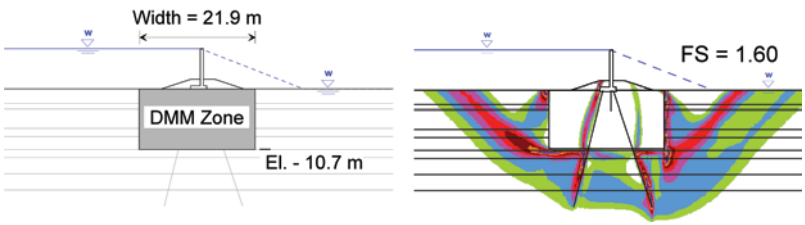

FIG. 2b. Centered 21.9 m Wide DMM Zone with Base El -10.7 m

FIG. 2. DMM Zone Configurations and Shear Strain Contours at Failure

-21.6 m. The configuration of the DMM zone and the shear strain contours at failure for the 21.2 m wide DMM zone with a base elevation of -16.8 m are shown in Figure 2a. The strain contours indicate a significant amount of shear strain in the soil between the protected-side piles and the DMM zone. The factors of safety for each of the protected side DMM zone configurations are presented in Figure 3. The factor of safety increases with increasing DMM zone width and depth, although the benefit of additional depth below El -16.8 m is relatively small.

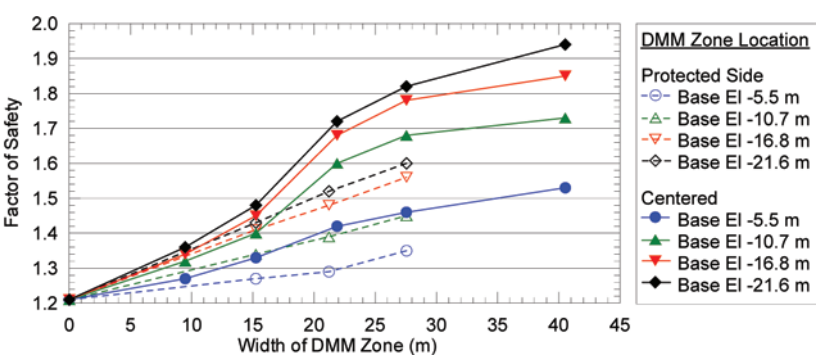

FIG. 3. Comparison of Factors of Safety

Analyses for configurations with a centered DMM zone were completed for DMM zone widths of 9.5 m, 15.2 m, 21.9 m, 27.5 m, and 40.5 m and base elevations of -5.5m, -10.7 m, -16.8 m, and -21.6 m. The configuration of the DMM zone and the shear strain contours at failure for the 21.9 m wide DMM zone with a base elevation of -10.7 m are shown in Figure 2b. The contours indicate a complex failure mode with a sliding/rotational failure underneath the DMM zone, shearing around the piles, and shearing in the DMM zone. The factors of safety for each of the centered DMM zone configurations are presented in Figure 3. For base elevations of -10.7 m and below, there is a sharp increase in the factor of safety as the DMM zone width increases from 15.2 m to 21.9 m. As was noted for the protected side DMM zone, the benefit of additional depth below El -16.8 m is relatively small. The factors of safety for the centered DMM zone configurations are significantly greater than those for the protected side DMM zone configurations.

OPTIMIZATION OF THE DMM ZONE CONFIGURATION

An optimized DMM zone configuration would meet the design criteria for factor of safety with the smallest DMM zone, considering that the cost of installing the DMM zone is a function of the total treated volume. The efficiency of each DMM zone configuration can be evaluated by dividing the increase in factor of safety by the volume of improved ground. For this study, the increase in factor of safety is determined by subtracting the factor of safety of 1.21 for the T-wall without a DMM zone from the factor of safety obtained for each DMM configuration. Because the replacement ratio is assumed to be constant for this study, the cross-sectional area of the DMM zone is used instead of the volume of improved ground. For the centered DMM zone that is 21.9 m wide with a tip elevation at -10.7 m, the resulting calculation for the efficiency of the DMM zone is $(1.60 - 1.21)/((21.9\text{ m})(0.6\text{ m} + 10.7\text{ m})) = 15.8 \times 10^{-4} / \text{m}^2$.

The efficiencies for each of the configurations are presented in Figure 4. For protected-side DMM zone configurations with base elevations below -5.5 m, the

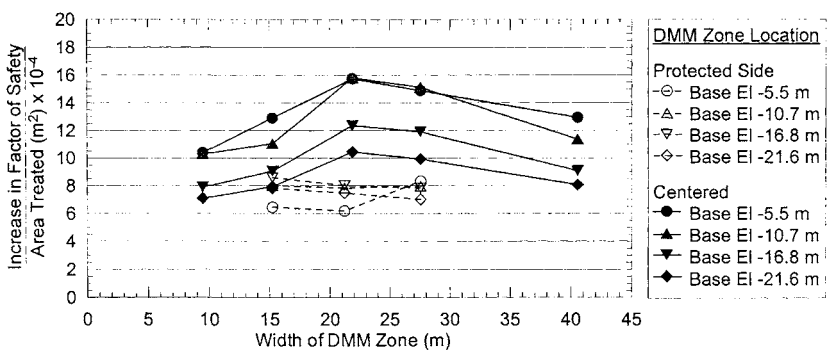

FIG. 4. Comparison of Efficiencies

efficiency of the DMM zone decreases with increasing width. For centered DMM zone configurations, the efficiency decreases with increasing depth, with peak efficiencies occurring for all DMM zone depths at a zone width of about 22 m. The efficiencies for the centered DMM zone configurations are significantly greater than those for the protected side DMM zone configurations, indicating that a DMM zone centered underneath the wall is the most effective at stabilizing the T-wall.

While the trends shown in Figure 4 provide a basis for comparing the efficiency of different DMM zone configurations, they do not reflect the ability of the different configurations to achieve acceptable factors of safety. Selecting an optimum DMM section for a given design would require considering both the desired factor of safety and the efficiency. For example, if the desired factor of safety is 1.6, Figures 3 and 4 indicate that the optimum DMM configuration is a centered zone with a width of about 22 m and a base elevation of about -11 m, for the site conditions analyzed.

CONCLUSIONS

The following conclusions can be drawn from this study, for the conditions used to represent the level ground T-wall section.

- Of the configurations included in this study, a continuous DMM zone centered underneath the T-wall is the most efficient configuration for stabilizing the wall.
- For the continuous DMM zones centered underneath the T-wall, the highest efficiency is produced by a 22 m wide zone. Both efficiency and achieving the desired factor of safety should be considered when selecting an optimum design configuration.

ACKNOWLEDGMENTS

The information presented in this paper is based on work supported, in part, by the U.S. National Science Foundation under grant No. DGE-0504196. Any opinions, findings, conclusions, and recommendations in this paper are those of the authors and do not necessarily reflect the views of the U.S. National Science Foundation.

REFERENCES

Adams, T.E. and Filz, G.M. (2008). *"Technical Memorandum: Stability of a T-Wall on Level Ground with Deep-Mixed Soil-Cement Columns"*, Report prepared for the New Orleans District, U.S. Army Corps of Engineers.

Adams, T.E. Filz, G.M., Cali P.R. and Woodward, M.L. (2008). *"Deformation and Stability Analyses of a Pile Supported T-Wall with Deep Mixed Shear Panels In Plaquemines Parish, Louisiana"*, Proc. 2nd Int. Conf. Geotechnical Engineering for Disaster Mitigation & Rehabilitation (GEDMAR08), Science Press Beijing and Springer Berlin, pp. 481-486.

ITASCA Consulting Group (2005). *FLAC2D Fast Lagrangian Analysis of Continua, ITASCA Consulting Group*, Minneapolis.

Heavy Structures Supported by Soil-Cement Columns

Lisheng Shao[1], M.ASCE, Ken Ivanetich[2], M.ASCE

[1]Chief Engineer, Ph.D, PE, GE – Hayward Baker Inc. Western Region, 1780 Lemonwood Drive, Santa Paula, CA, 93060, LShao@HaywardBaker.com
[2]Area Manager, PE, Hayward Baker Inc., 2322 Bates Avenue, Concord, CA, 94520, KBIvanetich@HaywardBaker.com

ABSTRACT

Deep soil mixing and jet grouting have been widely used to construct soil-cement columns for the support of heavy structures such as tanks, cement silos, and storage buildings. Although the installation methods may vary with deep soil mixing or jet grouting, the end product of soil-cement columns will behave similarly under the heavy structure loads. In many cases, the soil-cement mass treatment option offers the owner substantial savings over driven/drilled pile programs, and will allow some projects to become financially feasible, that may have otherwise been disregarded due to the excessive costs encountered with conventional foundation systems

This paper covers design methodology, production work, and quality control and testing, with supporting figures for three recent ground improvement projects. The design considerations include the static settlement, and column group bearing capacity under the structure static and seismic loads. Extensive field and laboratory tests were performed to investigate the soil-cement strength and modulus. The ground improvement programs on these three projects were proven successful under real operational loads.

INTRODUCTION

Heavy structures such as tanks, cement silos, and storage buildings apply high soil pressures over very large areas and often require deep foundations or site ground improvements for support. Deep foundations for these applications can become very costly. Thus, deep soil mixing and jet grouting are two ground improvement techniques that have been used to provide the necessary bearing capacity. Soil-cement mass treatment programs can offer owners a substantial savings over driven/drilled pile programs, and can allow some projects to become financially feasible. Three recent projects in northern California are covered: Soil mixing for a cement dome, soil mixing combined with vibro replacement for ethanol plant structures, and jet grouting for an aggregate storage/loading facility.

CEMENT DOME, PORT OF STOCKTON, CALIFORNIA, USA

A 190-ft diameter, 97 ft high cement storage dome capable of holding 65,000 metric tons of cement was slated for construction at the Port of Stockton. The dome design consisted of a vertical base wall supported on a cast-in-place concrete ring beam, and

capped with a hemispherical dome constructed of reinforced shotcrete. The dome floor was a reinforced concrete mat slab. When fully loaded with dry cement, the dome floor loads would range from 4,500 psf to 9,500 psf, as shown in Figure 1.

Problem

The soft to medium stiff clay deposits underlying the site would not provide adequate foundation support for the dome. The settlement due to the consolidation of the soft to medium stiff clayey soils was the primary concern. Additionally, the high earthquake-induced lateral loads could not be practically resisted with a pile supported foundation.

Solution

The geotechnical contractor developed a site improvement program using 8-ft diameter end-bearing soil mix columns to provide the required bearing capacity and reduce the consolidation settlement in the clay layers. These soilcrete columns, with replacement ratios ranging from 55% to 79%, would transfer the loads, as shown in Figure 1, to the underlying very stiff clay or dense sands. Post-construction settlement within the improved soil matrix under full dome load was specified at 1-inch. Maximum differential settlement of improved soil across the dome diameter (exclusive of settlement in soils below the treatment zone) was also specified at 1-inch. A soilcrete ring wall under the dome perimeter was designed as an oversized shear wall. This would transfer the dome lateral seismic load to the deep soils (Figure 1). This ring wall consisted of two concentric rows of overlapping soil mix columns, providing nearly 100 percent replacement of existing soils with soil-cement.

Construction

The geotechnical contractor predrilled through the top desiccated clay layer in order to install each column. A total of 427 soil mix columns were installed throughout the floor plan and the ring foundation. Two concentric rings of overlapping columns beneath the ring foundation were on a 7.5 ft triangular spacing. Beneath the floor center, an 8-ft square spacing pattern was utilized. Elsewhere beneath the slab, an 8- to 9-ft square spacing pattern was used. Column depths ranged from 20 to 38 ft. A total of 19,211 cy of soilcrete was installed with a minimum unconfined compressive strength of 100 psi.

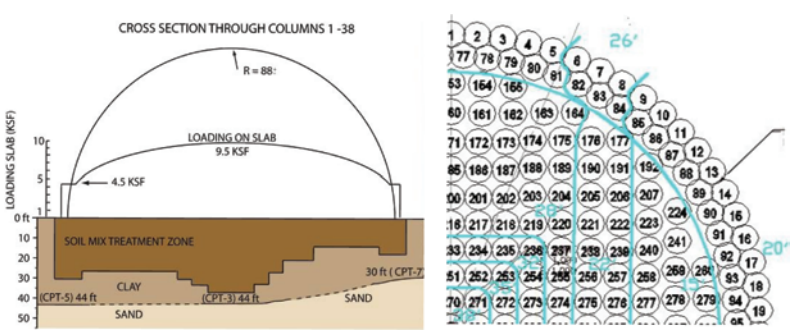

Figure 1. Sketch of the cement dome load distribution and soil mixing column layout.

QA/QC

Individual column installation parameters were recorded by computer during the construction for quality control. Grout slurry density, flow rate, total grout volume, rotation rates and penetration/withdrawal rates were monitored continuously at the rig to ensure that the design cement content and mixing energies were achieved. An independent laboratory tested soilcrete samples taken from columns, and determined that the minimum 28-day unconfined compressive strength of 100 psi had been obtained. The soil mixing treated foundation has been performed very well in the past eight years, and no floor distress was detected.

ETHANOL PLANT, STOCKTON, CALIFORNIA, USA

A new ethanol plant was planned for construction in Stockton, California. The heavy structures, including grain towers, large ethanol storage tanks, boilers, and main processing tanks and facilities exerted heavy foundation loads over large areas.

Problem

Without soil improvement, part of the site would be susceptible to liquefaction during the design seismic event. In addition to the liquefaction hazard, the storage tanks and other heavy production facilities would exert large dead and sustained live loads on the soils, which would result in substantial settlements due to primary and secondary consolidation of the soft to medium stiff clays, as shown in Figure 2.

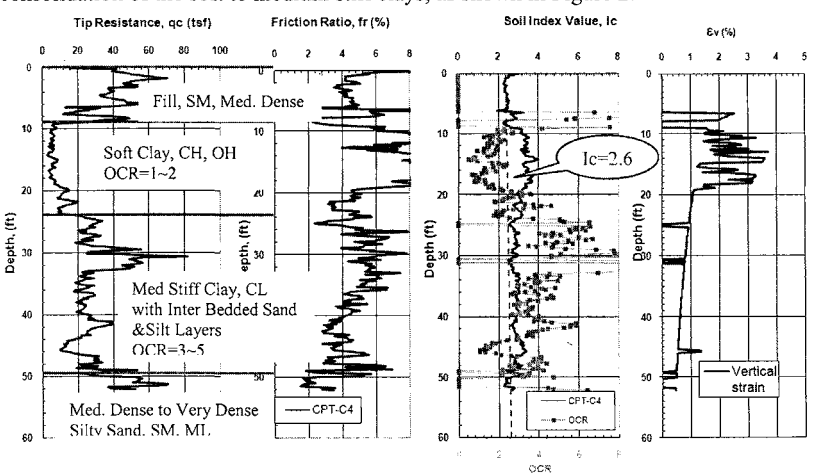

Figure 2. Typical site CPT profile; under 1500 psf static load, the 110'x297' processing building will settle over 6 inch without ground improvement.

Solution

The geotechnical contractor proposed wet soil mix columns to support the ethanol tanks and grain handling structures, and Vibro replacement stone columns to increase bearing

support of light load structures and mitigate the liquefaction hazard over part of the plant. Based on an extensive site exploration program, including 36 CPTs, 6 SPTs and related laboratory tests, the author proposed a treatment depth of approximately 28-34 ft, and a total treatment area of approximately 175,000 square feet. Soil mixing and Vibro replacement was designed to limit differential static and dynamic settlement to 1-inch in 40 ft at applied loads ranging from 5,000 psf to 1,500 psf.

Design Considerations

Based on pre-construction site investigations and laboratory testing, a soilcrete design average Unconfined Compressive Strength (UCS) of 150 psi was specified. Design foundation loads ranged from 3,000 to 5,000 psf for the tanks and grain structures, and 1,500 psf for the remaining structures. The design assumed load transfer through the soil mix columns and Vibro replacement stone columns to the underlying dense silty clay/sands.

Soil mix column spacing consisted from 8-ft by 8-ft to 16-ft by 16-ft resulting in area replacement ratios from 78.5% to 19.6%, respectively. The soil mix columns working stress was around 50 psi; about 1/3 of the soilcrete design average UCS. This factor of safety of 3 was used in order to prevent the column progressive failure mode, as recommended by Burke and Sehn (2005). In order to obtain densification of the potentially liquefiable soils in part of the plant site, the Vibro replacement stone column spacing was 10-ft by 10-ft, resulting in an area replacement ratio of 7.1%

Soil Mix Column Installation

Initially, each column location was predrilled to depth and backfilled. The mixing rig was then moved into position and the ground improvement process commenced. As the 8-ft-diameter soil mixing tool penetrated the ground, grout slurry was pumped through the hollow stem of the shaft and injected into the soil through nozzles located on the backside of the rotating mixing blades. The auger flights and mixing blades on the tool mixed the soil with the grout slurry. Injection and soil mixing continued to design depth. After reaching design depth, tool rotation with reduced grout injection continued as the tool was withdrawn, leaving behind stabilized soilcrete columns.

QA/QC

The soil mixing rig was fitted with a real time data acquisition system that continuously monitored RPM or blade rotation number, depth, penetration rate, withdrawal rate, pumping rate, and binder content. For each soil mix column, the data log displayed location identification and the measured parameters as a continuous function of the penetration depth, including any special comments. This ensured proper dosage rates and mixing energies at all times. Quality control also consisted of UCS testing by an independent laboratory of wet and core samples, which confirmed that the design criteria were met, as shown in Figure 3.

The soilcrete core strength was typically higher than the corresponding wet sample at the same age. This is typically attributed to the in-situ confinement during curing.

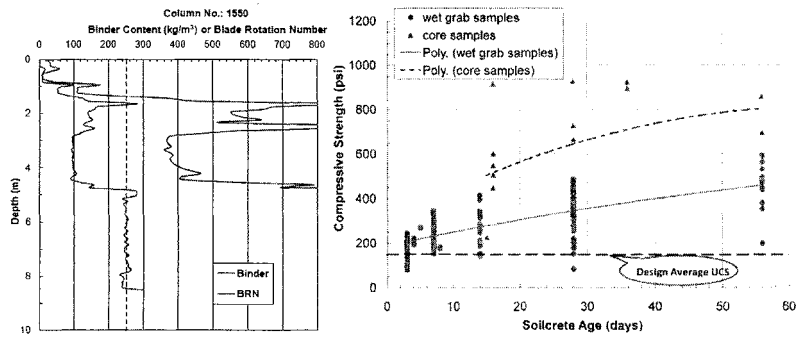

Figure 3 Real time soil mixing records and soilcrete sample test results.

AGGREGATE STORAGE/HANDLING FACILTY, PORT OF RICHMOND, CALIFORNIA

A gravel storage building and distribution facility was planned for construction at the West Parr yard located at the Port of Richmond, near the San Francisco Bay in California. This building, 640 ft long and 145 ft wide, has 80,000 tons of gravel storage capacity. The floor loads from the peak gravel storage were anticipated to be on the order of 3,500 psf at the center of the stockpile. The combined dead load, live load, and seismic loads under the footings were calculated at up to 4,600 psf.

The general subsurface profile consisted of a fill layer overlying a lens of soft to medium stiff silty clay and clayey silt, locally termed as Young Bay Mud. Below that lied a dense clayey sand and stiff clay layer (Old Bay Clay). The ground water table elevation observed in borings was approximately 7 to 10 feet below the ground surface.

Problem

The high floor loads over the very large building footprint would be applied to relatively poor soils extending as deep as 30 feet. Relatively tight settlement tolerances were necessary to maintain functionality of the building's conveyor systems and thus ruled out the used of spread footings. Deep pile foundations were considered. But due to the excessive costs associated with the quantity of piles, ground modification was considered instead. The site also had high potential for undocumented in situ obstructions such as timber piles, trash, marine debris, and other construction debris since the site had been host to numerous industrial facilities for over 50 years.

Solution

The geotechnical contractor implemented a ground modification system consisting of 9-ft-diameter jet grouted soilcrete columns to transfer the loads through the undocumented fill and Young Bay Muds, to the more competent, stiff clay layer below. Since jet grouting uses high velocity/energy fluid jets to erode and mix the soil instead of a bladed mixing tool as with soil mixing, the obstructions could more easily be

negotiated and thus did not pose a serious imposition to the construction method, as reported by Ivanetich & Shao (2008).

Design Considerations

First, pretreatment CPTs and laboratory testing of the native materials mixed with several specific cement dosages were performed. This testing provided the necessary parameters to develop the geotechnical construction program. To minimize the potential costs, the geotechnical contractor divided the area into three typical loading scenarios with three different replacement ratios ranging from 16 to 32% (Figure 4). This resulted in 317 Jet Grout columns extending up to 30 feet deep to socket into the more competent stiff clays (aka "Old Bay Mud"). The design average UCS was 150 psi and the design column average diameter was 9 ft.

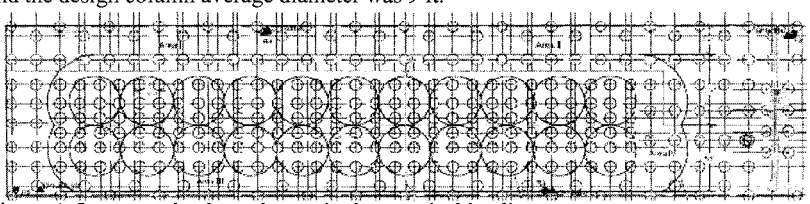

Figure 4. Jet grouted column layout in three typical loading zones.

QA/QC

Prior to construction a test section was performed using three separate groups of parameters to assess which selection would prove most efficient while meeting the specified strengths and diameters. After the parameters were established in the test section, they were monitored throughout construction using real time instrumentation.

The soil cement strength was documented by both wet sample testing (daily) and through coring the cured in-situ elements (5% of columns installed). Additionally, the coring was used to assess the treatment diameter of the installed jet grouted columns.

CONCLUSION

Since construction of the structures at these three projects, settlements have remained within design limits. Ground improvement by wet soil mixing and jet grouting offers an efficient and cost-effective means to stabilize soft soils globally as well as to support substantial loads. Both deep soil mixing and jet grouting offer flexible construction methodologies to adapt to soil conditions and site constraints. Additionally, the techniques can easily adapt to the building load patterns. These points in many cases can lead to a more cost effective and time saving solution for the owner.

REFERENCES

Ivanetich, K, & Shao L, "Jet Grouting for Mass Treatment to Support an Aggregate Stockpile Building over Very Soft Clays", 6th International Conference on Case Histories in Geotechnical Engineering, Arlington, VA, August 11~16, 2008

Burke, G. K. & Sehn, A.L. "An Analysis of Single Axis Wet Mix Performance", Deep Mixing 2005, May 23-25, 2005, Stockholm, Sweden.

Mechanical Properties of Used Tire Granulates, Sand and Cement Mixtures

Berrak Teymur[1] and B. Alp Atapek[2]

[1]Assistant Professor, Faculty of Civil Engineering, Istanbul Technical University, Ayazaga Campus, Maslak, 34469, Istanbul; teymurb@itu.edu.tr
[2]Former MSc Student, Faculty of Civil Engineering, Istanbul Technical University, Ayazaga Campus, Maslak, 34469, Istanbul; atapek@gmail.com

ABSTRACT: One of the soil improvement and ground modification techniques is soil stabilization by mixing soil with admixtures. Cement is increasingly used as a stabilizing material as it helps increase the strength of soils and its strength increases with the curing time. Used tire granulates can be used as an admixture to stabilize soils. Many studies have been made on the use of shredded tires as a lightweight fill material. In this paper, results of direct shear test and permeability tests done on mixtures of granulated tires and sand to find their properties are presented. These samples are then mixed with different ratios of cement and a composite soil is achieved. CBR and unconfined compression tests are done on this composite soil. Composite soils have high unconfined compression strengths and CBR values. Finally, results of each experiment are discussed and comments over usages of composite soil and its efficiency are made.

INTRODUCTION

Soil improvement techniques became more important with respect to the ever growing demand to use less than desirable soils for highway constructions. Soil improvement techniques usually focus on composite soils and soil substitutions. The recycling of used consumer products is an important issue and used tires are one of the consumer products suitable for recycling. Recycling used tires is very important for the economy, and for reducing energy demand and pollution. Many studies and researches about usage possibilities of recycled tires have been made. Some of these are; use of shredded tires as an ingredient for asphalt production, as a lightweight fill material and as a possible substitution for drainage materials. Recycling of used tires is a major issue for environmental preservation of developed countries. Around three percent of total waste materials are formed from used tires in Turkey. (MEFRT, 2008)

Elasticity, strength, toughness and high resistance to friction are some of the advantageous properties of used tires. They have been used successfully in road embankments over weak soil and as lightweight fill waste material, since they reduce weight and lateral earth pressure to retaining walls. (Bosscher et al, 1997) Used tires

can be classified in four categories as whole, cut, scrapped and chipped. Used tires' properties are affected by variations of types of used tires and tire shredders. Specific gravity of used tires varies between 1.08 - 1.27. (Humphrey and Manion, 1992; Foose et al., 1996; Edil and Bosscher, 1994; Yang et al., 2002; Zornberg et al., 2004)

Unit weight of composite soils with sand and used tire mixtures depend only on the amount of sand in the mixture. Shear strengths of mixtures are found to be greater than those of sand. Internal friction angles of composite soils differ between 25° to 41°. On the other hand, cohesions of mixtures vary between 0 to 30 kPa. (Foose et al., 1996) Strength of composite soils increases up to 40 % depending on the amount of used tire chips. Also the compressibility of the mixture increases when the used tire chips content is more than 20 %.

Lightly cemented used tire chips have excellent geotechnical performance under both static and dynamic conditions. Interlocking design of construction blocks also allows blocks to be self standing with a high degree of internal stability without the use of a mechanical fastening. As a result, retaining and foundation requirements of earth structures are reduced. In slope stability, very little cutting and excavation is required for construction when used tire shreds are used as a fill. The risk due to human modification of slope areas and construction time can also be reduced significantly. (Lee et al, 2002)

Used tire granulates are used tire particles which are 1 to 10 mm in width, and have specific gravities varying between 1.08 to 1.18 and internal friction angles varying between 6° to 32°. When used tire granulates are added to sand, they decrease the internal friction angle of sand. Finally, used tire granulates have high damping property under low frequency vibrations which are caused by traffic loads, machine loads or small earthquakes.

In this study, physical and mechanical properties of tire granulate and possible usage area of composite soil which includes sand, used tire granulates and cement is examined. For this purpose, several laboratory tests are performed on these samples.

TESTS AND RESULTS

Direct shear, permeability, California Bearing Ratio (CBR) and unconfined compression tests are performed on sand, used tire granulates and composite soil. Sand used in this study was obtained from river and creek beds in Sakarya. Used tire granulates used are from one of the three used tire regeneration plants of Turkey. The used tire granulates used in this study match the ASTM D6270 - 98 (1998) standard.

Portland cement is used as a binding material with water for preparing composite soil. Sieve analysis is done on sand and used tire granulates. Figure 1 shows the particle size distribution curve for these samples. Particle size distribution curves show that sand and used tire granulates samples are poorly graded. Specific gravities of sand and used tire granulates are found to be 2.66 and 1.10 respectively. Dry unit weights of sand and used tire granulates are 16.80 kN/m^3 and 4.66 kN/m^3 respectively.

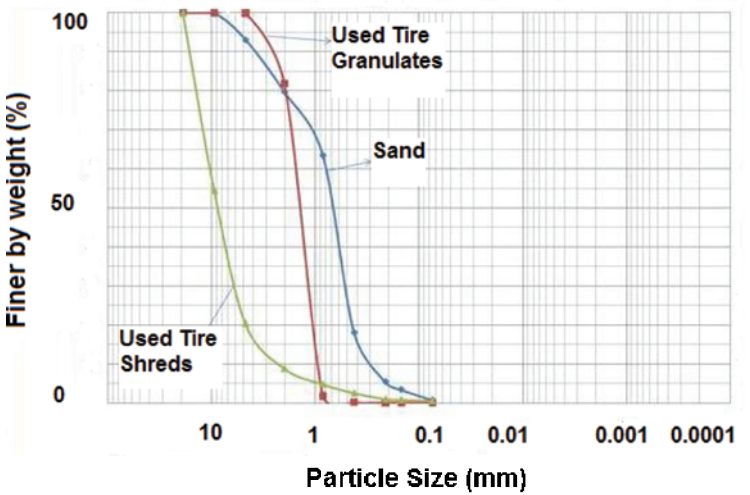

FIG. 1. Particle size distribution curves of sand, used tire granulates and used tire shreds.

Preparation of the samples

Composite soil samples are casted with reference to Turkish standard TS 802 T2 (1996). In this standard, weakest concrete class is C16 which is selected for upper limit for composite soil samples. This limitation is chosen as it is easier and practical to determine mixture ratios of sand and used tire granulates by volume on field. Five different samples were prepared with different ratios of sand to used tire granulates. The ratios are 90 to 10, 80 to 20, 70 to 30, 60 to 40 and 50 to 50. In these samples, cement content was kept volumetrically constant.

The results of the permeability test carried on sand, used tire granulates, sand and used tire granulates mixtures are $2.2x10^{-2}$ cm/s, $4.3x10^{-2}$ cm/s and varies between 2.4 to $3x10^{-2}$cm/s for the mixtures respectively. It can be concluded that all the samples have medium to high degree of permeability. Also as the amount of sand increases, the permeability decreases. The results of direct shear tests show that the internal friction angles of the mixtures varied from 31° to 46° depending on the amount of sand in the mixtures. The values have decreased as the amount of used tire granulates increased.

In this study, composite soil samples with sand, used tire granulates, water and cement are casted to conduct the unconfined compression test. Sand and used tire granulates mixtures are mixed with constant amount of cement and water, and casted into PVC casings with constant dimensions. The materials are mixed in a plastic bowl with a spatula for 15 minutes until a homogeneous mixture is obtained. Each sample is cured for 7 and 28 days. Curing is made in a traditional way where the concrete curing method is to expose the mixture to repeated water sprinkling and constant coverage

with moist fabrics. Figure 2 gives the unconfined compression strength for 7 and 28 days for each composite soil sample in correlation with the ratio of used tire granulates. Increasing the amount of used tire granulates in the composite soil decreases the strength of the mixture.

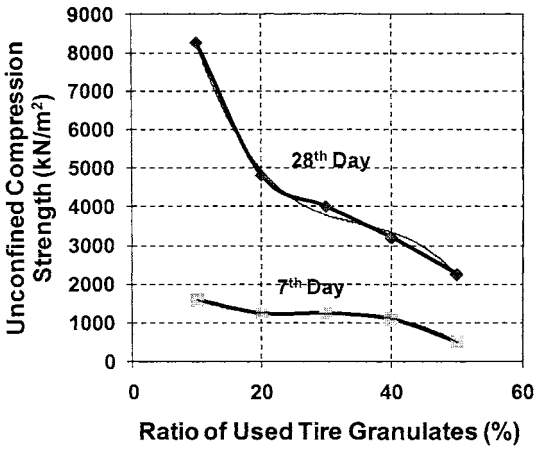

FIG. 2. Correlation between unconfined compression strength and ratio of used tire granulates in the composite soil.

An unsaturated CBR test is performed for each composite soil sample which is prepared like the unconfined compression test samples. They are also casted in PVC casings, but with larger dimensions. Curing is done for 28 days. The results of CBR tests for each sample vary between 125 to 282% depending on the amount of sand in the sample. All samples are found to be an excellent base material. It was observed that increasing the amount of used tire granulates in the composite soil, have decreased the CBR value.

DISCUSSION

In this paper, geotechnical properties of sand and used tire granulate mixtures and composite soil made with used tire granulates, sand and cement are investigated. Whether composite soils can be used as a ground modification material is explored. Shear modulus is calculated from the direct shear test results. The initial shear modulus for each loading step is calculated and then the average of these values is taken. The average shear modulus is considered as the exact value for the mixture. Figure 3 gives the correlation between the shear modulus and the ratio of used tire granulates to sand in used tire granulates mixtures. Increasing the amount of used tire granulates in sand and used tire granulates mixtures, decreases the shear modulus of the mixture.

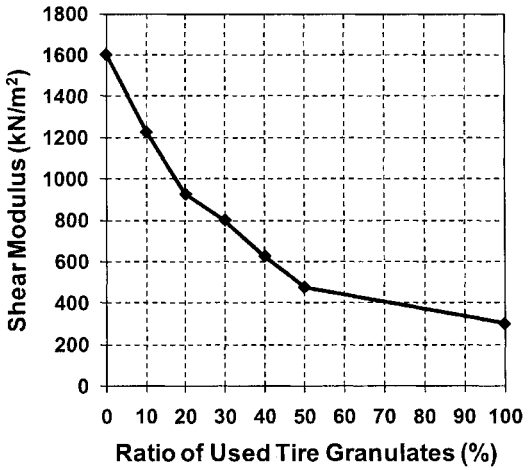

FIG. 3. Correlation between shear modulus and ratio of used tire granulates in the mixture.

The equations for the curves given in Figure 2 can be represented by Equation 1 and Equation 2 for 7^{th} and 28^{th} day respectively where x is the ratio of used tire granulates in the composite soil expressed as a percentage and q_u is the unconfined compression strength in kN/m^2

$$q_u = -0.07x^3+5.5x^2-153x+2640 \quad (1)$$
$$q_u = -0.20x^3+25x^2-900x+15000 \quad (2)$$

CONCLUSIONS

One of the soil improvement and ground modification techniques is the soil stabilization by mixing soil with admixtures. The main purposes of soil stabilization are to modify the soil, accelerate construction, and improve the strength and durability of the soil. Cement is increasingly used as a stabilizing material for soil, particularly for the construction of highways and earth dams. Cement helps increase the strength of soils and its strength increases with the curing time. Some typical values of the unconfined compression strength of various types of untreated poorly graded sands and cement mixtures made with approximately 10 % cement by weight differ from 280 to 700kPa and 700 to 1730kPa respectively. (Das, 1999) As can be seen treating soil increases its compressive strength almost twice.

It is possible to improve the local soil class with used tire granulates. Composite soils with sand, used tire granulates and cement has high unconfined compression strengths. However sand and used tire granulates mixtures have lower shear modulus than sand. Used tire granulates are not economically important for used tire

regeneration plants today. Mixing used tire granulates with sand may decrease the cost of the fill operation in construction areas where sand is costly. Increasing demand on used tire granulates eventually will affect their economical value.

REFERENCES

ASTM D6270-98, (1998). "Standard practice for use of scrap tires in civil engineering applications". *American Standard for Testing and Materials*, West Conshohocken, Pennsylvania.

Bosscher, P.J., Edil, T.B. and Kuraoka, S. (1997). "Design of highway embankments using tire chips". *J. Geotechnical & Geoenv. Engrg*, Vol. 123 (4): 295-304.

Das, B. M. (1999). "Principles of foundation engineering". Brooks/Cole Publishing Co., Pacific Grove, California.

Edil, T.B. and Bosscher, P.J. (1994). "Engineering properties of tire chips and soil mixtures". *Geotechnical Testing Journal*, Vol. 17 (4): 453-464.

Foose, G.J., Benson, C.H. and Bosscher, P.J. (1996). "Sand reinforced with shredded waste tires". *J. Geotechnical Engineering*, Vol. 122 (9): 760-767.

Humphrey, D.N. and Manion, W.P. (1992). "Properties of tire chips for lightweight fill grouting soil improvement and geosynthetics". *Geotechnical Special Publication*, Vol. 2 (30): 1344-1355.

Lee, K. M., Cheng, B. K. W. and Yip, C. L. Y. (2002). "Lightly cemented scrap rubber tire chips as lightweight geomaterials". *Proceedings of the International Workshop on Lightweight Geomaterials*, 26 - 27 March, Tokyo, Japan.

MEFRT (2008). http://www.cevreorman.gov.tr, Ministry of Environment and Forestry of Republic of Turkey, Ankara, Turkey.

TS 802 T2 (1996). "Design concrete mixes". *Turkish Standards Institution*, Ankara, Turkey.

Yang, S., Lohnes, R.A. and Kjartanson, B.H. (2002). "Mechanical properties of shredded tires". *Geotechnical Testing Journal*, Vol. 25 (1): 44-52.

Zornberg, J.G., Cabral, A.R. and Viratjandr, C. (2004). "Behavior of tire shred sand mixtures". *Canadian Geotechnical Journal*, Vol 41 (2): 227-241.

Fly Ash as a Dispersing Material in Cement Stabilization

Suksun Horpibulsuk[1], and Yuttana Raksachon[2]

[1]Associate Professor, School of Civil Engineering, Suranaree University of Technology, Nakhon-Ratchasima, THAILAND; suksun@g.sut.ac.th
[2]Engineer, Office of Chonburi Provincial Rural Road, Chonburi, THAILAND

ABSTRACT: This paper presents the role of fly ash on strength development in cement stabilized clay. The microstructure (fabric and cementation bond) of cement stabilized clay is investigated by a scanning electron microscope (SEM), and thermal gravity (TG) analysis. It is found that the reactivity of fly ash (pozzolanic reaction) is minimal, which is different from concrete technology. This is possibly due to less amount of $Ca(OH)_2$ to be consumed. The role of fly ash in cement stabilization is to disperse the large clay-cement clusters into smaller clusters. Consequently, the reactive surfaces to be interacted with water increase, and hence the cementitious products (inter-cluster cementation bond). It is concluded that the strength development in the blended cement stabilized clay is controlled by cementitious products due to combined effect: hydration and dispersion.

INTRODUCTION

One of the extensively used soil improvement techniques for subgrade is cement stabilization since adequate strength can be achieved in a short time. There has been an attempt to use waste pozzolanic materials from industries to reduce the input of cement. It was possible to utilize fly ash in geotechnical and geoenvironmental works (Cokca, 1997). Kawasaki et al. (1981) used fly ash mixed with cement in the construction of a man-made island for the Hakucho Bridge in Hokkaido. Laboratory investigation demonstrated that fly ash can control the volume change of expensive clay (Kehew, 1995). Fly ash-cement admixture can reduce swelling, compressibility and increase strength of soil. The incorporation of fly ash as partial replacement of cement might refine the microstructure (fabric and cementation bond) of the cement stabilized clay, resulting in the improvement of engineering properties (strength, compressibility, permeability, and durability). Its role on the microstructure development has not been well established so far. It is however fundamental to be examined for better understanding and analyzing the engineering properties of the blended cement stabilized clay.

The present paper attempts to explain the role of fly ash in cement stabilization on

refining the microstructure, and hence the strength improvement. The parameters involved in this investigation are curing time, and replacement ratio. The microstructural analyses have been conducted in this paper via scanning electron microscope, and thermal gravity tests.

LABORATORY INVESTIGATION

Soil sample is silty clay collected from the campus of Suranaree University of Technology, Nakhon Ratchasima, Thailand at 3 meter depth. The soil is composed of 2% sand, 45% silt and 53% clay. Its specific gravity is 2.74. The liquid and plastic limits are in the order of 74 and 27 percent, respectively. Based on the Unified Soil Classification System (USCS), the clay is classified as high plasticity (CH).

Type I Portland cement (PC), fly ash from Mae Moh power plant in the north of Thailand, and tap water were used in this study. Total amount of the major components SiO_2, Al_2O_3, and Fe_2O_3 in fly ash are 81.54% and 79.44%, respectively. They are thus classified as class F fly ash in accordance with ASTM C 618. The cement is irregular in shape whereas the fly ashes are spherical.

The silty clay was passed through a 16-mm sieve to remove coarser particles. It was air-dried for at least three days and then thoroughly mixed with 10% binder (cement and fly ash) and water to attain water content of 1.2OWC where OWC is the optimum water content of cement-clay mixture. This water content is proved as suitable for the stabilization (Horpibulsuk et al., 2009). The clay-cement mixture was compacted under modified Proctor energy. The percentages of fly ash to replace the cement (replacement ratio) are 0, 10, 20, 30, and 40% by weight of binder. After 24 hours of compaction, the blended cement stabilized samples were dismantled from the mold, wrapped in vinyl bags and stored in a humidity chamber of constant temperature (25±2°C). Unconfined compression test was run on the samples after 7, 28, 60, 90, and 120 days of curing. The rate of vertical displacement was fixed at 1 mm/min. Microstructure development of the samples was investigated by scanning electron microscope (SEM), and thermal gravity (TG) analyses. Details of microstructural tests can be referred to Horpibulsuk et al. (2009).

TEST RESULTS

Influence of replacement ratio on the strength development of the blended cement stabilized clay for the five curing times is presented in Figure 1. For all curing times, the samples with 20% replacement ratio exhibit almost the same strength as those with 0% replacement ratio. The 30 and 40% replacement samples exhibit lower strength than 0% replacement samples. The samples with 10% replacement ratio exhibit the highest strength since early curing time. The sudden strength development with time is not found for all replacement ratios. This finding is different from concrete technology where the role of fly ash as a pozzolanic material comes into play after a long curing time (generally after 60 days). In other words, the strength of concrete mixed with fly ash is higher than that without fly ash after about 60 days of curing.

Figure 2 shows SEM photos of the blended cement stabilized clay and cured for 60 days at different replacement ratios. The fly ash particles are clearly shown among

clay-cement clusters especially for 30% replacement ratio (C:F = 70:30) (Figures 2a). It is noted that the hydration products growing from the cement grains connect fly ash particles and clay-cement clusters together. Some of the surfaces of fly ash particles are coated with layers of amounts of hydration products. However, they are still smooth with different curing times. This finding is different from concrete technology where the precipitation in the pozzolanic reaction is indicated by the etching on fly ash surface (Fraay et al., 1989; Berry et al., 1994; and Xu and Sarker, 1994; and Chindapasirt, 2006). This is because the input of cement in concrete is high enough to produce a relatively high amount of $Ca(OH)_2$ to be consumed for pozzolanic reaction. From this observation, it is thus possible to conclude that the pozzolanic reaction is minimal for strength development in the blended cement stabilized clay.

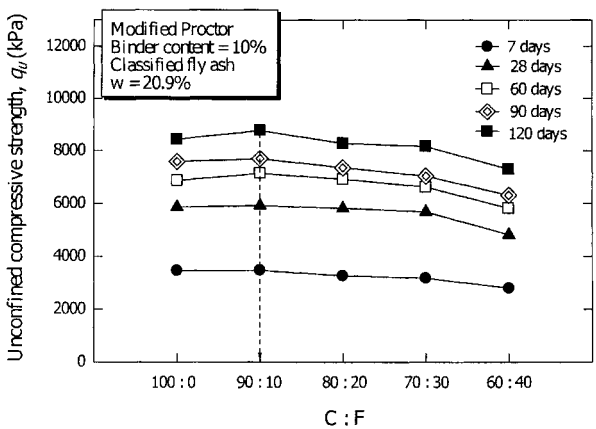

FIG. 1. Relationship between strength development and replacement ratio of the CFA blended cement stabilized silty clay at different curing times.

Table 1 shows $Ca(OH)_2$ of the blended cement stabilized clay for different replacement ratios and curing times. For a particular water content and curing time, $Ca(OH)_2$ decreases with replacement ratio only when the replacement ratio is in excess of a certain value. This finding is different from concrete technology in which $Ca(OH)_2$ decreases significantly with the increase in replacement ratio (Sybertz and Wiens, 1991; Harris et al., 1987; Chindapasirt, 2006; and others) due to pozzolanic reaction. The highest $Ca(OH)_2$ is at 10% replacement ratio (C:F = 90:10) for all curing times. For replacement ratios higher than 10%, $Ca(OH)_2$ decreases with replacement ratio. $Ca(OH)_2$ at 20% replacement ratio is almost the same as that at 0% replacement ratio. This finding is associated with the strength test results that the 10% replacement ratio gives the highest strength and the strengths for 0% and 20% replacement ratios are practically the same for all curing times. It is thus concluded that cementitious products mainly control the strength development. In other words, the strengths of the blended cement stabilized clay having different mixing condition (binder content, replacement ratios, and curing time) could be identical as long as cementitious products are the same.

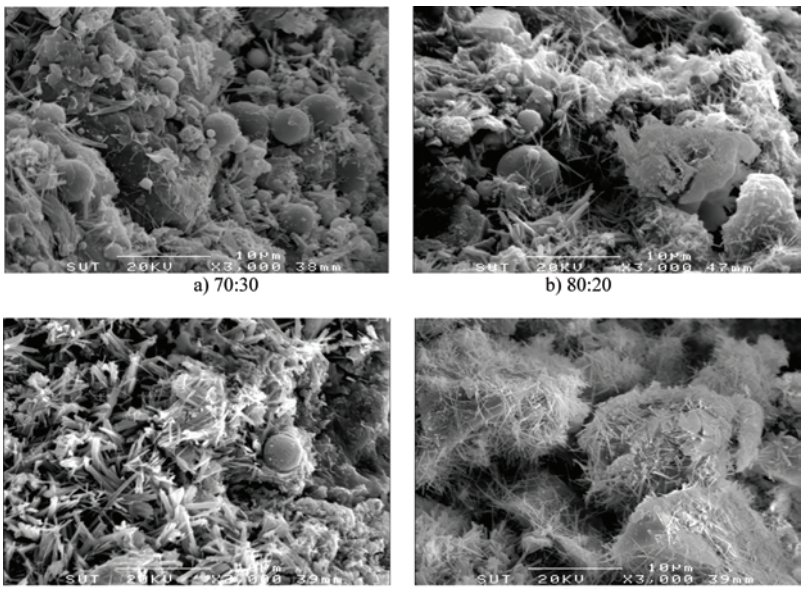

FIG. 2. SEM photos of the CFA blended cement stabilized clay at different replacement ratios after 60 days of curing

From SEM observation, it is possible to mention that the role of fly ash is to disperse large clay-cement clusters formed when interacted with water into smaller clusters. The higher the replacement ratio, the better the dispersion. Consequently, the reactive surfaces increase, resulting in the increase in cementitious products as illustrated by dispersion induced $Ca(OH)_2$ (*vide* Table 1). It is the difference in $Ca(OH)_2$ of the blended cement stabilized clay due to the combined effect (hydration and dispersion) and due to hydration. $Ca(OH)_2$ due to combined effect is directly obtained from TG test on the blended cement stabilized sample. $Ca(OH)_2$ due to hydration is also obtained from TG test on the cement stabilized sample having the same cement content as the blended cement stabilized sample. For simplicity, $Ca(OH)_2$ due to hydration at any cement content can be estimated from known $Ca(OH)_2$ of cement stabilized clay at a specific cement content by assuming that the change in the cementitious products is directly proportional to the input of cement (Sinsiri et al., 2006). Thus, $Ca(OH)_2$ due to hydration (H) for any replacement ratio at a particular curing time is approximated in the form.

$$H = T \times \left(1 - \frac{F}{100}\right) \tag{1}$$

where T is known $Ca(OH)_2$ of the cement stabilized clay (0% replacement ratio) obtained from TG test, and F is the replacement ratio expressed in percentage. Sinsiri et al. (2006) have shown that $Ca(OH)_2$ of the cement paste with fly ash is always

lower than $Ca(OH)_2$ of the cement paste without fly ash, resulted from $Ca(OH)_2$ consumption for pozzalanic reaction. The same is not for the blended cement stabilized clay. It is found that $Ca(OH)_2$ due to combined effect is higher than that due to hydration for all replacement ratios and curing times. The dispersion induced $Ca(OH)_2$ increases with replacement ratio for all curing times.

Table 1. $Ca(OH)_2$ of the blended cement stabilized clay at different replacement ratios and curing times.

Curing time (days)	Replacement ratio C : F	$Ca(OH)_2$ (%)		
		Test (Combined effect)	Hydration	Induced (dispersing effect)
7	100:0	6.67	6.67	0.00
	90:10	6.97	6.00	0.97
	80:20	6.79	5.34	1.45
	70:30	6.39	4.67	1.72
28	100:0	6.79	6.79	0.00
	90:10	6.96	6.11	0.85
	80:20	6.81	5.43	1.38
	70:30	6.57	4.75	1.82
60	100:0	6.82	6.82	0.00
	90:10	7.16	6.14	1.02
	80:20	6.92	5.46	1.46
	70:30	6.68	4.77	1.91
90	100:0	7.07	7.07	0.00
	90:10	7.28	6.36	0.91
	80:20	6.94	5.66	1.28
	70:30	6.67	4.95	1.72
120	100:0	7.08	7.08	0.00
	90:10	7.29	6.37	0.92
	80:20	6.96	5.66	1.30
	70:30	6.70	4.96	1.74

CONCLUSIONS

This paper presents the role of fly ash on the strength and microstructure development in the blended cement stabilized clay. The following conclusions can be advanced from this study.

1. The surfaces of fly ash in the blended cement stabilized clay are still smooth for different curing times, suggesting that pozzolanic reaction is minimal. Fly ash is considered as a dispersing material in the blended cement stabilized clay. This is different from the application of fly ash as a pozzolanic material in concrete structure in which $Ca(OH)_2$ from hydration is much enough to be consumed for pozzolanic reaction.
2. From the microstructural investigation, it is concluded that the role of fly ash as a non-interacting material is to disperse the cement-clay clusters into smaller

clusters. The dispersing effect by fly ash increases the reactive surfaces, and hence the increase in degree of hydration as clearly illustrated by the increase in the induced $Ca(OH)_2$ with replacement ratio.

ACKNOWLEDGEMENT

The authors would like to acknowledge the financial support provided by the Commission on Higher Education (CHE) and the Thailand Research Fund (TRF). Facilities, equipments and financial support provided from Suranaree University of Technology are appreciated.

REFERENCES

Berry, E.E., Hemmings, R.T., Zhang, M.H., and Cornelious, B.J. and Golden, D.M. (1994). "Hydration in high-volume fly ash binders." *ACI Material Journal*, Vol. 91: 382-389.

Chindaprasirt, P., Jaturapitakkul, C., and Sinsiri, T. (2006). "Effect of fly ash fineness on microstructure development of blended cement plates." *Construction and Building Materials Journal*, Vol.21: 1534-1541.

Cokca, E. (1997). "Frost Susceptibility Properties of Soma-B Fly Ash." *Journal of Energy Engineering*, ASCE, Vol.123(1): pp.1-10.

Fraay, A.L.A, Bijen, J.M., and de Haan, Y.M. (1989). "The reaction of fly ash in concrete: A critical examination." *Cement and Concrete Research*, Vol.19: 235-246.

Harris, H.A., Thompson, J.L., and Murphy, T.E. (1987). "Factor affecting the reactivity of fly ash from western coals." *Cement and Concrete Aggregate*, Vol.9: 34-37.

Horpibulsuk, S., Rachan, R., and Raksachon, Y. (2009). "Role of fly ash on strength and microstructure development in blended cement stabilized silty clay." *Soils and Foundations*, Vol.49 (1): 85-98.

Kawasaki, T., Niina, A., Saitoh, S., Suzuki, Y. and Honjo, Y. (1981). "Deep mixing method using cement hardening agent." *Proceedings of 10th International Conference on Soil Mechanics and Foundation Engineering*: 721-724.

Kehew, E.A. (1995), *Geology for Engineers and Environmental Scientists*, 2nd Ed. Prentice Hall Englewood Cliffs, New Jersey: 295-302.

Sinsiri, T., Jaturapitakkul, C., and Chindaprasirt, P. (2006). "Influence of fly ash fineness on calcium hydroxide in blended cement paste." *Proceedings of Technology and Innovation for Sustainable Development Conference (TISD2006), Khon Kaen University, Thailand.*

Sybert, F., and Wiens, U. (1991). "Effect of fly ash fineness on hydration characteristics and strength development." *Proceedings of International Conference on Blended Cement in Construction*, University of Sheffield, UK.: 152-165.

Strength Characteristics of a Local Red Soil Blended with Class F Fly Ash and Cement

Ajanta Kalita[1] and Baleshwar Singh[2]

[1]Research Scholar, Department of Civil Engineering, Indian Institute of Technology, Guwahati – 781039, India; ajanta@iitg.ernet.in
[2]Associate Professor, Department of Civil Engineering, Indian Institute of Technology, Guwahati – 781039, India; baleshwar@iitg.ernet.in

ABSTRACT: An experimental program was undertaken to study the individual and combined effects of fly ash and cement stabilization on the geotechnical characteristics of a local red soil. The soil was blended with a class F fly ash in proportions up to 50% by weight and with Portland cement up to 4%. Compacted specimens were prepared at optimum moisture content and maximum dry density, and then cured for different durations up to 28 days, prior to unconfined compression (UC) tests. California bearing ratio (CBR) tests were also carried out both with no soaking and with soaking for 4 days. The replacement of the soil by 20-35% fly ash gives the best long-term results along with minimum cement treatment.

INTRODUCTION

At several sites during construction of embankments for roads, large amounts of soil are required. Available local soils which do not meet the requirements can be amended with lime or cement for use in the subgrade and sub-base layers of the road. Fly ash for soil stabilization has been a research focus for many years mainly due to the possibility of its bulk utilization.

Kaniraj and Havanagi (1999) added cement to stabilize fly ash-soil mixtures and established correlations for unconfined compressive strength and secant modulus as functions of curing time, fly ash content, and cement content. Lo and Wardani (2002) conducted an experimental work to study the strength and dilatancy of a silt stabilized with the addition of a cement and fly ash mixture in a slurry form. Kaniraj and Gayathri (2003) conducted a laboratory experimental study to investigate the effect of cement content, curing period, and curing conditions on the development of the strength of stabilized Class F fly ashes with reference to their use as pavement base courses. Schnaid et al. (2007) studied the stress-strain-strength behavior of an artificially cemented sandy soil produced through the addition of cement.

Pandian et al. (2001) investigated the effect of different percentages of fly ash addition to black cotton soil on California Bearing Ratio value and found that proper

proportions of black cotton soil and fly ash improved the CBR values. Pandian and Krishna (2002) studied the effect of the addition of ordinary Portland cement on the California Bearing Ratio of fly ash-black cotton soil mixes for different curing periods.

The aim of the present study is to investigate the strength behavior of a local red soil when mixed with a class F fly ash and cement.

MATERIALS & METHODS

The red soil was lateritic soil that was obtained from the hills near our institute campus. It can be classified as silt of intermediate plasticity. The fly ash was collected from a thermal power plant located in the state of West Bengal. The fly ash can be classified as Class F fly ash. Ordinary Portland cement (53 grade) was used in the study.

For preparing test specimens, first the measured quantities of soil, fly ash and cement were mixed together in a dry state, and then water equal to the corresponding optimum moisture content of the mix was added. Fly ash up to 50% and Portland cement up to 4% were used. The UC specimens were then statically compacted in moulds to achieve their respective maximum dry densities. Three specimens for each mix and curing period were prepared in order to provide an indication of repeatability. They were then stored at 100% humidity in desiccators kept at room temperature, and then cured for 3, 7, 14, and 28 days. For soaking CBR specimens, they were loaded with surcharge weights and then immersed under water in buckets for 4 days. In the mix designations, RS and FA indicate red soil and fly ash, respectively. 20FA means 20% by weight is fly ash. Similarly, 2C means that 2% cement by weight has been added.

UNCONFINED COMPRESSION TESTS

Unconfined compression test was performed as per ASTM Test Method for Unconfined Compressive Strength of Cohesive Soil (D 2166-06). Each specimen was loaded until complete failure was reached. Stress-strain plots for soil-fly ash and soil-cement mixes after 28 days curing are shown in Figs. 1 and 2, respectively. It can be noted that when only fly ash is added, the strength is seen to be the maximum with 35% fly ash content. For the soil-35FA mix, the strength is 624 kPa, and it reduces drastically to 264 kPa at 50% fly ash content, which is less than that of the soil alone. Hence, no benefit is achieved if more fly ash is added. The effect of adding only cement to the soil is more pronounced. Peak stresses are noticed with the failure strain less than 2.5% for all the mixes. Very limited ductility can be seen for all the mixes.

Stress-strain plots of soil-35%fly ash-cement and soil-50%fly ash-cement mixes for 28 days curing are shown in Figs. 3 and 4, respectively. It can be noted that when cement is added, the gain in strength of soil-50% fly ash mixes is generally greater than that of soil-35% fly ash mixes. For the soil-50FA mix, the strength increases from 264 kPa with no cement to a value of 744 kPa at 4% cement content. For the soil-35FA mix, the corresponding strength values are 624 kPa and 808 kPa. From a comparison of Figs. 3 and 4, it is evident that the initial stiffnesses of the soil-35% fly ash-cement mixes are higher than those of the soil-50% fly ash-cement mixes.

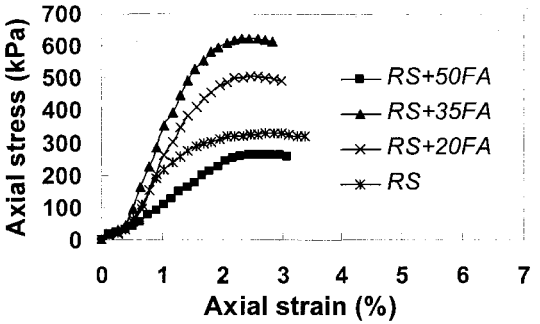

FIG. 1. Stress-strain plots of soil+fly ash mixes (28 days curing)

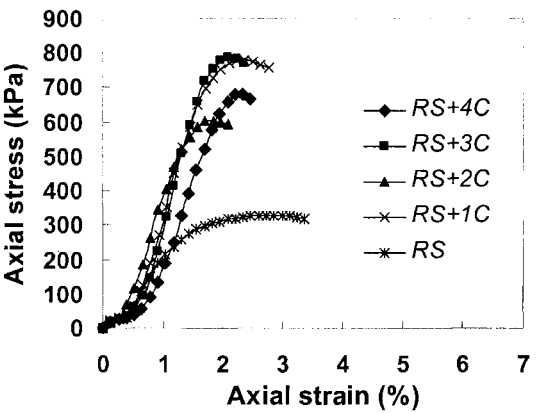

FIG. 2. Stress-strain plots of soil+cement mixes (28 days curing)

CALIFORNIA BEARING RATIO TESTS

CBR tests were conducted as per ASTM Test Method for California Bearing Ratio of Laboratory Compacted Soils (D 1883-07). These tests were done to investigate the strength under confined conditions, which were different from the UC tests. First, the CBR of the separate materials were obtained. The unsoaked and soaked CBR values of soil and fly ash are 6.6%, 4.7% and 39.7%, 2.9%, respectively. Figure 5 shows comparison of unsoaked and soaked CBR values of soil-fly ash mixtures. Under unsoaked condition, as fly ash is added, improved CBR values are obtained for all the red soil-fly ash mixes. The CBR value increases from 6.6% with no fly ash to a value of 37.2% at 50% fly ash content. In contrast, in case of soaked condition, the corresponding CBR values are 4.7% and 9.7%.

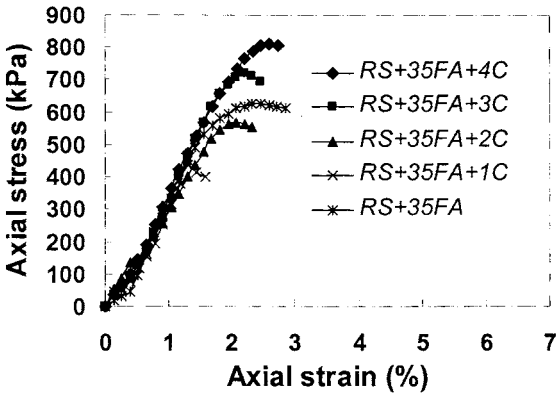

FIG. 3. Stress-strain plots of red soil+35FA+cement mixes (28 days curing)

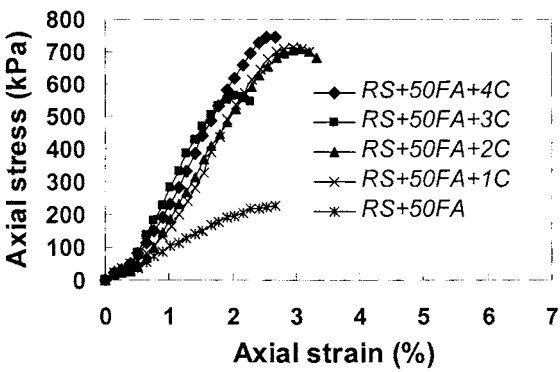

FIG. 4. Stress-strain plots of red soil+50FA+cement mixes (28 days curing)

Figure 6 presents unsoaked and soaked CBR values of soil-cement mixes for comparison. The unsoaked CBR value varies from 18.4% with 1% cement to a value of 13.4% at 4% cement content. Under unsoaked condition, as cement is added, CBR value decreases due to incomplete hydration. In soaked condition, the CBR values are 15.1% and 29.1% at 1% and 4% cement contents, respectively. Figures 7 and 8 depict comparison of unsoaked and soaked CBR values of soil-20%fly ash-cement and soil-35%fly ash-cement mixes. The CBR value is observed to have increased with cement content. For soil-20% fly ash mix, the CBR value increases from 19.6% with no cement to a value of 24.5% at 2% cement content in unsoaked condition. The corresponding soaked CBR values are 6.7% and 31.8%. Similarly, for soil-35% fly ash mix, the unsoaked and soaked CBR values at 0% and 2% cement contents are 25%, 5.2% and 31.9%, 42.2%, respectively. Thus for soil-fly ash mixes, when no

cement is added, the soaked value is smaller. However, even with 1% cement, the soaked value is found to be greater.

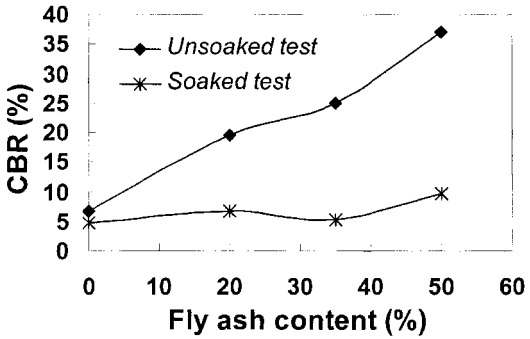

FIG. 5. Unsoaked and soaked CBR values of soil-fly ash mixes

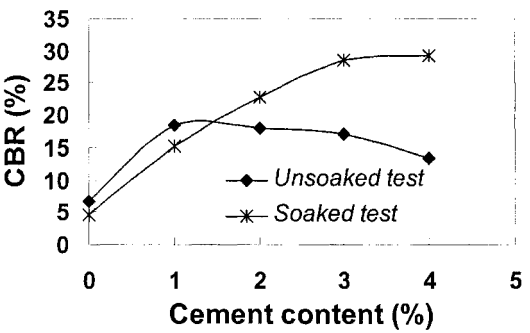

FIG. 6. Unsoaked and soaked CBR values of soil-cement mixes

A minimum soaked CBR of 6% and 20% are generally recommended for use in the subgrade and sub-base layers of strong and durable road pavements. From Figs. 5 and 7, it can be noted that the soil-20% fly ash mix is suitable for subgrade layer and when this mix is blended with only 1% cement content, it becomes suitable for sub-base layer.

CONCLUSIONS

The results of this experimental study reveal that only proper portions of fly ash added to the red soil can improve the compacted strength and CBR values. The replacement of the soil by 20 to 35% fly ash gives the best long-term results. A small percentage of cement when added will be sufficient for construction of the topmost layers of new embankments for roads.

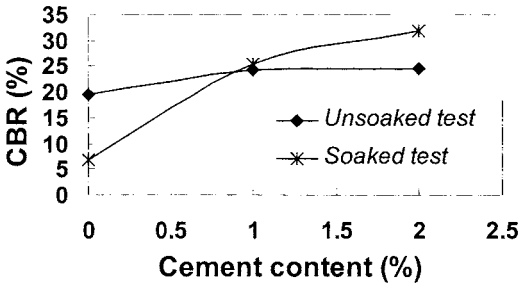

FIG. 7. Unsoaked and soaked CBR values of soil-20FA-cement mixes

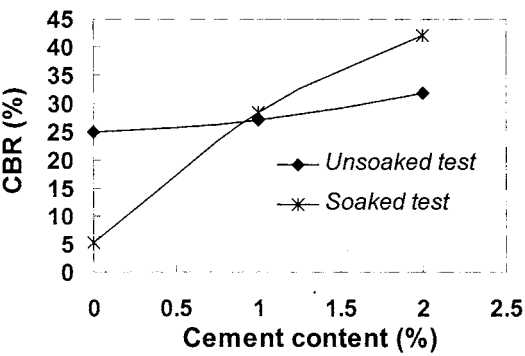

FIG. 8. Unsoaked and soaked CBR values of soil-35FA-cement mixes

REFERENCES

Kaniraj, S. R. and Havanagi, V. G. (1999). "Compressive Strength of Cement Stabilized Fly Ash-Soil Mixtures." *Cem. Concr. Res.*, 29: 673-677.

Kaniraj, S. R. and Gayathri, V. (2003). "Factors Influencing the Strength of Cement Fly Ash Base Courses." *J. Transp. Eng.*, ASCE, 129(5): 538-548.

Lo, S. R. and Wardani, S. P. R. (2002). "Strength and Dilatancy of a Silt Stabilized by a Cement and Fly ash Mixture." *Can. Geotech. J.*, 39:77-89.

Pandian, N. S., Krishna, K. C. and Sridharan, A. (2001). "California Bearing Ratio Behavior of Soil/ Fly Ash Mixtures." *J. Testing and Evaluation,* ASTM, 29(2): 220-226.

Pandian, N. S. and Krishna, K. C. (2002). "California Bearing Ratio Behavior of Cement-Stabilized Fly Ash - Soil Mixtures." *J. Testing and Evaluation,* ASTM, 30(6): 1-5.

Schnaid, F., Prietto, P. D. M. and Consoli, N. C. (2001). "Characterization of Cemented Sand in Triaxial Compression." *J. Geotech. and Geoenv. Eng.*, ASCE, 127(10): 857-868.

Mechanical behavior of compacted geomaterial changed from the dredged soil in Nagoya Port by mixing with some stabilizers

Kai Sun[1], Masaki Nakano[2], Eiji Yamada[3] and Akira Asaoka[4]

[1]Doctral student, Department of civil engineering, Nagoya University, Furo, Chikusa, Nagoya, 464-8603, JAPAN; sun@soil.civil.nagoya-u.ac.jp

[2,4]Professor, ditto; nakano@civil.nagoya-u.ac.jp, asaoka@civil.nagoya-u.ac.jp

[3]Assistant professor, ditto; e-yamada@civil.nagoya-u.ac.jp

ABSTRACT: To solve the problem of accumulation of huge amount of dredged soil (DS) in Nagoya Port Island, some kinds of stabilizers are mixed with the dredged soil to improve the mechanical properties, and then the treated soils can be used as geomaterial. A series of laboratory tests were carried out to investigate the mechanical behaviors of these soils, and also SYS Cam-clay model was adopted to interpret these behaviors by evolutions of soil skeleton structure theoretically. It is suggested that DS behaves like typical clay, which is difficult to decay structure and easy to lose overconsolidation. Compared with DS, these treated soils are in highly-structured and heavily-overconsolidated state. Moreover, the treated soils change to be new materials with slow rate in both decay of structure and loss of overconsolidation. The strength of treated soils is therefore promoted compared with DS and can be used as a new kind of construction material.

INTRODUCTION

To maintain the function of Nagoya Port, about 1.3 million m^3 soil is annually dredged from the ship channel and then reclaimed on Nagoya Port Island (PI), which is an artificial island used as storage for dredged soil. Because of the low strength and high water content of the dredged soil (DS) in natural condition, it can not be used directly as a construction material. The accumulation of DS caused PI reached its limit capacity. Consuming this huge amount of dredged soil, as a new kind of construction material by mixing with soil stabilizer, is an effective solution for this problem.

In this study, two kinds of soil stabilizers, blast furnace cement B type (cement) and gypsum neutral stabilizer (GS), are separately used to improve the mechanical properties of the dredged soil. With the development of hydration reaction between the water in DS and the mineral in stabilizers, the physical and mechanical properties

of the soil are gradually changed. The chemical reaction is very complex and is not discussed in this study.

A series of laboratory tests are carried out to investigate the physical and mechanical behaviors of the soils. Moreover, an elasto-plastic constitutive model, SYS Cam-clay model (Asaoka et al., 2000, 2002), is adopted to reproduce the behaviors of the soils in triaxial test and oedometer test and to interpret the mechanical behaviors based on the evolutions of soil skeleton structure. The SYS Cam-clay model is the model in which the concept of the soil skeleton structure (soil structure, overconsolidation and anisotropy) is introduced into the Cam-clay model. The details of the model can be found in the references (Asaoka et al., 2000, 2002).

EXPERIMENT INFORMATION

Basic properties of DS

The dredged soil used here is assumed to be in deep layer in PI, of which the water content is about 40%. With the development of consolidation, its water content decreased and was not as high as the one of the soil in shallow layer. Therefore, it is possible to be used as "compaction material" after further treatment.

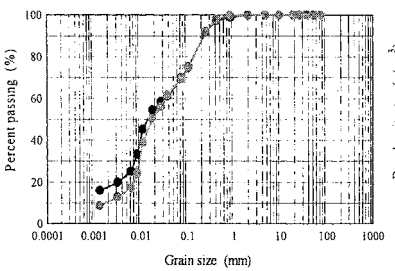

FIG. 1 Grain size distribution of DS

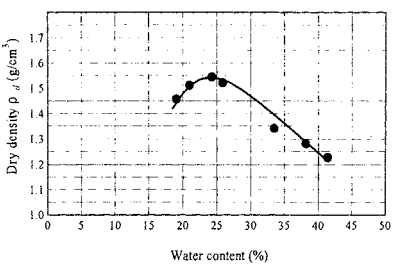

FIG. 2 Compaction curve of DS

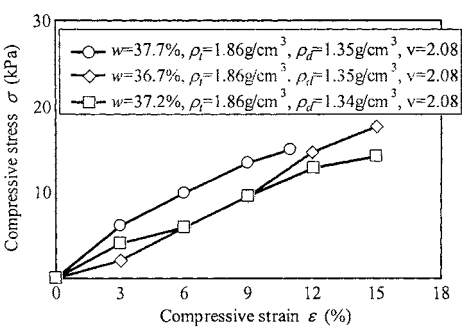

FIG. 3 Unconfined compression test results of DS

Figure 1 shows the grain size distribution curves of DS. The percentage of clay, silt and sand in DS is 35.1%, 34.2% and 30.7% respectively. It can be classified to be a kind of clay-like material physically. Figure 2 is the compaction curve of DS and Figure 3 shows the unconfined compression test results, in which w, ρ_t, ρ_d, v is water content, wet density, dry density and void ratio respectively. According to Figs. 1 and 2, for this kind of fine-grained dredged soil with the natural water content of about 40%, which is much higher than the optimum water content w_{opt}=24.3%, it is difficult to be compacted to dense state and therefore its strength is too low to be used as geomaterial, as shown in Fig 3. Therefore, two kinds of stabilizers, which are cement and GS, are used to improve the mechanical properties of DS.

Optimum mix proportion of stabilizer

To guarantee the quality of the treated soils, the target unconfined compression strength is required to achieve 100kPa, which is corresponds to the standard strength of the 3rd type of construction geomaterial defined by Ministry of Land, Infrastructure and Transport of Japan (MLIT). The unconfined compression test is used to determine the optimum mix proportions of stabilizers. The stabilizers are firstly mixed with DS at the mix proportions of 10%, 20%, 30% and 40%. The optimum mix proportions are then obtained by linear fitting between unconfined compression strength q_u and the proportion, which are 2% for cement and 10% for gypsum neutral stabilizer (GS) (Nakano et al 2009). For simplicity, the treated soils, cement-treated soil and GS-treated soil, are renamed as CS2 and GS10 respectively in the following.

Specimen making and laboratory test condition

"Chain rotary crusher-mixer" is used to homogenously mix the dredged soil and stabilizer (Ninomiya et al 2002). In this machine, the soil is crushed and mixed with the stabilizer to turn the soil into an aggregate of soil granules in an unsaturated state. For this kind of "clay pebble", the water content is easy to decrease, and therefore the assembly can be compacted to high density. And the soil is then compacted in mold immediately.

After a curing period of 28 days, the specimens are taken out for oedometer test and triaxial compression test, which are used to investigate the compression/shear responses of the soils. Oedometer test follows the standard of JIS Designation A 1217: 2000, in which specimen is loaded from 39.4kPa to 1255.7kPa and then unloaded to 39.4kPa. Moreover, undrained triaxial compression test is carried out, in which the shear speed slows to 0.014mm/min with 2 kinds of confined pressure of 98.1kPa and 294.3kPa.

INTERPRETATION OF THE MECHANICAL BEHAVIORS

The experimental results and analytical results are shown in Figures 4 to 6, in which the bold lines or points are experimental results and the thin lines are analytical results. In each figure, the first two are triaxial test results and the last one is the oedometer test result. In Fig.4, the analytical results obtained by using SYS Cam-clay model are in good agreement with the experiment results of DS (Sun et al. 2009).

In order to interpret the improvement effect of stabilizer on the mechanical properties based on the concept of decay of structure and loss of overconsolidation, the analytical results of CS2 and GS10 were obtained by using the same elasto-plastic parameters as DS. However, in the calculation, the evolution parameters and initial conditions are different from these of DS. It implies that the improvement effect of stabilizer on the mechanical behavior can be explained by initial soil structure, initial overconsolidation ratio and evolution parameters, which mean the changes of the soil structure and overconsolidation ratio with the development of plastic deformation. The parameters used in calculation are listed in Table 1 and 2.

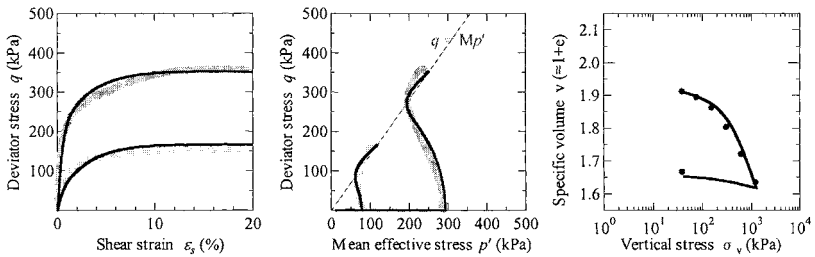

FIG. 4 Undrained triaxial test and simulation result of DS

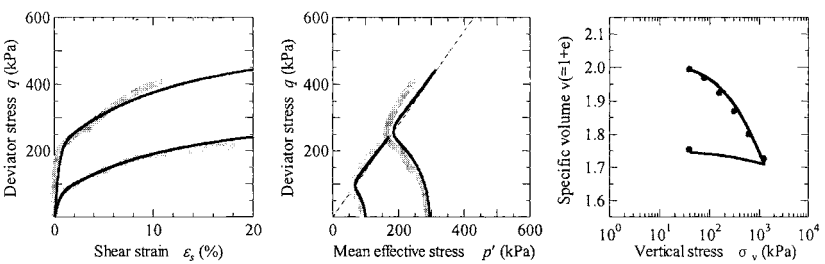

FIG. 5 Undrained triaxial test and simulation result of CS2

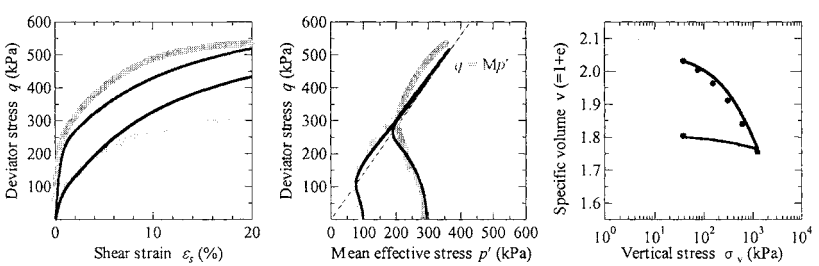

FIG. 6 Undrained triaxial test and simulation result of GS10

Table 1. Elasto-plastic parameters and evolution parameters

Elasto-plastic parameters		Evolution parameters			
Compression index $\tilde{\lambda}$	0.18		DS	CS2	GS10
Swelling index $\tilde{\kappa}$	0.02	m	1.5	0.15	0.15
Critical state constant M	1.4	a	0.3	0.18	0.18
NCL intercept N (at p'=98.1kPa)	2.15	b	1	1	1
		c	1	0.1	0.1
Possion's ratio ν	0.3	c_s	0.3	0.3	0.3

m: Degradation parameter of overconsolidation state
a, b, c: Degradation parameters of structure
c_s: Ratio of plastic shear to plastic compression

Table 2. Initial conditions

	Oedometer test				Triaxial test					
	DS	CS2	GS10		DS		CS2		GS10	
σ'_{v0}	39.2	39.2	39.2	p'_0	98.1	294.3	98.1	294.3	98.1	294.3
v_0	1.91	1.99	2.03	v_0	1.98	1.91	1.79	1.84	1.91	1.89
$1/R_0$	7.87	20.83	23.26	$1/R_0$	3.41	1.77	7.25	3.92	14.04	4.72
$1/R_0^*$	1.6	7.0	10.0	$1/R_0^*$	1.58	1.53	2.0	5.0	8.0	8.0

σ'_{v0} (kPa): Initial vertical stress $1/R_0$: Overconsolidation ratio

p'_0 (kPa): Confined stress $1/R_0^*$: Degree of structure

v_0: Specific volume (v_0=1+e_0, e_0: initial void ratio)

By using the parameters in Tables 1 and 2, the mechanical properties can be described by SYS Cam-clay model based on the concept of decay of structure and loss of overconsolidation in Figure 7. The degree of the structure is expressed by the similarity ratio between the Cam-clay yield surface and superloading surfaces as R^* ($0<R^*\leq 1$), while the overconsolidation by the similarity ratio between the subloading surface and superloading surfaces as R ($0<R\leq 1$). With the development of plastic deformation, the soil structure decays, when R^* closes to 1, while the overconsolidation loses, when R closes to 1 (Asaoka et al., 2000, 2002).

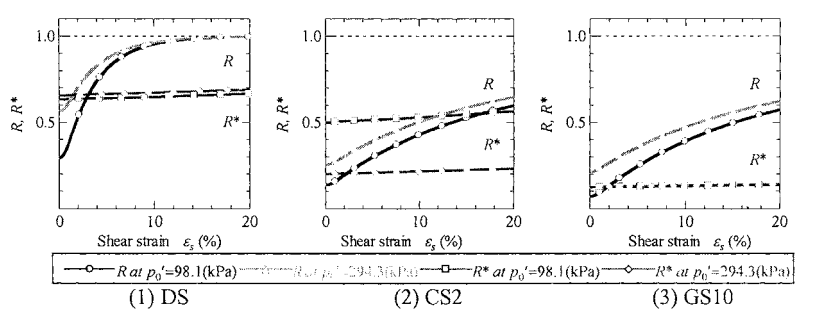

(1) DS (2) CS2 (3) GS10

FIG. 7 Initial soils skeleton state, decay of structure and loss of overconsolidation

According to the definition of R and R^*, the dotted line where R and R^* equal to 1 represents no-structured and normally-consolidated state. As shown in Fig.7 (1), for DS, it behaves as typical clay, which is hard to decay the structure and loss of overconsolidation is relatively easily. For treated soils, as shown in Fig.7 (2) and Fig.7 (3), they are in high-structured and heavily-overconsolidated state compared with DS. It is difficult to decay structure; however, it is also difficult to lose overconsolidation.

CONCLUSIONS

In this study, the compression and shear behaviors of DS and the treated soils were studied through a series of laboratory tests. The SYS Cam-clay model is adopted to interpret the improvement effect of the stabilizers on the behaviors as the action of the soil skeleton structure. The main conclusions are as follows:

1) The DS is in lowly structured and lightly overconsolidated state, and it behaves like typical clay, which is easy to lose overconsolidation and difficult to decay the structure.

2) After mixing with stabilizers under the optimum mix proportion, the strength of DS is highly promoted and the treated soils can achieve the strength standard of construction geomaterial.

3) By using the same elasto-plastic parameter as DS, the improvement effect is well interpreted by SYS Cam-clay model based on the concept of decay of structure and loss of overconsolidation. For the initial conditions, the treated soils are in high-structured and heavily-overconsolidated state. Moreover, for the evolution parameters, the treated soils are new kinds of materials with slow rate in both decay of structure and loss of overconsolidation.

ACKNOWLEDGMENTS

This work was supported by JSPS KAKENHI (21560519).

REFERENCES

Asaoka, A., Nakano, M. and Noda, T. (2000). Superloading yield surface concept for highly structured soil behavior, *Soils and Foundations*, Vol.40, No. 2, pp.99-110.

Asaoka, A., Noda, T., Yamada, E., Kaneda, K. and Nakano, M. (2002). An elasto-plastic description of two distinct volume change mechanisms of soils. *Soils and Foundations*, Vol.42, No.5, pp.47-57.

Nakano, M. et al. (2009). Compression and shear behavior on treated soils of the dredged soil through laboratory tests, *Japanese Geotechnical Society, The 44th JNCGE* pp.591-592 (in Japanese).

Ninomiya, K. et al. (2002). Example in use of an industrial method for pre-mixing of soils using a rotary crushing and mixing procedure, *JSCE, Proc. of 1st Symposium for Civil Engineering Construction Technology*, pp.225-232 (in Japanese).

Sun K., Nakano, M., Yamada, E., Asaoka, A. (2009). Elasto-plastic description of mechanical behavior on treated soils of the dredged soil of Nagoya Port, *Journal of Applied mechanics, JSCE*, vol.12, pp.413-420.

Effects of Organics on Stabilized Expansive Subgrade Soils

Sireesh Saride[1], A.M. ASCE, Srujan R. Chikyala[2], Anand J. Puppala[3], M. ASCE, Pat J. Harris[4]

[1]Lecturer (adjunct), Department of Civil Engineering, The University of Texas at Arlington, Arlington, Tx 76019; sireesh@uta.edu
[2]Former Masters Student, Department of Civil Engineering, The University of Texas at Arlington, Texas 76019, srujanchikyala@gmail.com
[3]Professor, Department of Civil Engineering, The University of Texas at Arlington, Texas 76019, anand@uta.edu
[4]Associate Research Scientist, Texas Transportation Institute, TAMU, College Station, Texas 77843, Pat-Harris@tamu.edu

ABSTRACT: Organic soils are the combination of decayed plant matter and weathered rock material. These soils are known for their inferior engineering behavior. In order to get the precise control over the engineering behavior of organic rich soils, they are often stabilized either with lime or cement. However, transportation agencies in the United States reported that these stabilized soils bearing organic content less than 1 percent have never achieved the desired improvement or the improvement disappeared over a period of time. Therefore, a laboratory investigation was initiated to understand the mechanisms when calcium-based additives (lime and/or cement) are amended with organic rich expansive soils. Two soils having high and low organic content were considered for detailed investigation. Firstly, optimum dosage of the stabilizer was determined for the selected soils. The strength of control (untreated) and stabilized soils were determined at different curing periods. In this paper, the influence of organic matter on the engineering behavior of the lime and cement stabilized organic rich soils are discussed in detail.

INTRODUCTION

Organic soils are a mixture of finely divided particles of organic matter. In some instances, visible fragments of partly decayed vegetable matter and shells are also present in the organic matter (Terzaghi et al., 1996). Organic soils undergo large amount of secondary settlements depending on the amount of organic matter present in the soil (Terzaghi et al., 1996). In order to reduce these secondary settlements, organic soils are often treated with different stabilizing agents. It is well understood that the strength gain in stabilized soft soil are due to hydration products formed by reactions between binding materials and water, and also reaction between the binding material, water and soil particles (Hampton and Edil, 1998). In addition, it also depends on the type of binding material chosen, type of soil and water-binder ratio and curing conditions. This school of

theory appears to be valid for inorganic soils and this understanding is no longer reasonable for organic soils.

The difficulties associated with organic soils arise when they are treated with cement or lime stabilizers, as organic matter inhibits cementitious reactions responsible for strength gain. There is a need to understand the fundamentals behind the chemical reactions contributing to the changes in geotechnical properties of stabilized organic soil beds (Hampton and Edil, 1998). In this paper, the influence of organic matter on the engineering properties of lime and cement stabilized soils collected from two different places in Texas viz. Bryan and Corpus Christi will be discussed in detail.

BACKGROUND

In Civil Engineering nomenclature, a soil is said to be an organic if it has a sufficient organic content to affect the engineering properties of the material but does not have to have the spongy structure of peat or muck (Schmidt, 1965). The organic matter and its relevance is widely diversified from discipline to discipline, the geotechnical engineering deals with the engineering properties such as secondary consolidation effects, shear strength parameters and the hydraulic conductivity of the organic soils.

Even though the organic content of the most soils ranges from 0.5 to 5 % by mass, colloidal behavior of organic matter has a negative influence on the chemical and engineering properties of soil (Bohn et al, 1985; Edil and Wang, 2000). Geotechnical engineers categorize the organic soils as one of the problematic soils because of their high compressibility and moisture content (Mitchell & Soga, 2005). Many transportation agencies have addressed the occurrence of settlements after the pavement construction on organic soils (Mitchell & Soga, 2005).

Many researchers reported that the engineering behavior of soft or organic soils could be improved by stabilizing the soils either with lime or cement (Hampton and Edil, 1998; Edil and Wang, 2000; Chen and Wang, 2005). The major reactions results in increase in shear strength of soft soil when quick lime is used as a binding material are as follows:

1. Isomorphous substitution of calcium in the clay particles decreases the interlayer spacing and causes coagulation of the clay particles, thus reducing the plasticity of the soil.
2. Calcium hydroxide will be formed when the quicklime reacts with water.
3. The increase in pH in the system promotes the dissolution of silica in the clay particles which then reacts with the calcium oxides to form calcium silica hydrate (C-S-H) cementing compounds.

These compounds form bonds either between the binder particles and soil particles or between the binder particles to form a stiff matrix. The composition and structure of the C-S-H gel and the type and amount of other hydration products can alter due to the presence of organic matter in the soil (Hampton and Edil, 1998). They also demonstrated that the characteristics of the solid soil particles dominate the stabilization potential of the organic soil. Since there is a small fraction of clay minerals in the peats and organic soils, adding lime will not induce a pozzalonic reaction. Calcium hydroxide is the only hydration product forms in this reaction.

Bonomaluwa and Palutnicowa (1987) stated that 'the black humic acid present in organic matter has a strong chemical affinity to calcium and hence where calcium is

present in solution, the humic acid may react with the calcium and form insoluble calcium humic acid'. Organic matter forms complexes with alumino-silicates and metal ions which can interfere with hydration reactions of cement. The lag in gaining in strength of the organic soil-cement mixture is due to the retention by the organic matter of the calcium ions liberated during the hydrolysis of the cement grains (Clare and Sherwood, 1954; Maclean and Sherwood, 1962). Besides, the organic matter binds the calcium ions, and alters the system chemistry so the calcium silica hydrate gel cannot form.

To visualize the changes in chemical bonds as a cement paste hydrated, and to track the changes in an organic soil treated with a binder, Fourier Transform Infrared Spectroscopy (FTIR) studies were performed at Delft Geotechnics by Hampton and Edil, (1998). FTIR scans depicts that polymerization of silicates was greatly hampered in soils with highly decomposed organic matter. Increase ettringite formation was also found in stabilized organic soils. Ettringite is not as strong as C-S-H gel, and in certain environments it may not be stable (Hampton and Edil, 1998).

It is well understood from the above discussion that when organic rich soils are treated with chemical stabilizers such as lime or cement, the organic content inhibits the cementitious reactions between the stabilizers and the soil. The fundamentals behind this phenomenon are yet to be understood. In addition, it is also important to obtain the qualitative and quantitative measures of the organic content present in the soil to decide upon the type and amount of admixtures to accelerate the process of chemical stabilization. Therefore, a laboratory investigation was initiated to understand the mechanisms when calcium based additives are amended with organic rich soils and to evaluate the strength of these stabilized soils. Two soils with high and low organic content were considered for the detailed investigation.

EXPERIMENTAL PROGRAM

The soils used in the present study are natural clays obtained from highway construction project sites in two districts, Bryan and Corpus Christi, Texas. These soil samples were taken at a depth of 0.3 m from an open pit excavation since in highway projects, the top few centimeters of subgrade soils are of interest.

A series of laboratory tests were performed on both the samples to classify them and to determine optimum dosages of stabilizers prior to the stabilization tests. The laboratory tests include organic content determination, Grain size distribution, Atterberg limits, optimum lime/cement content determination, unconfined compressive strength (UCS) tests and pH concentration tests. Grain size analysis was conducted only on control soils. Atterberg limits tests were performed on both control and treated samples at zero days curing period. In a series of stabilization tests, UCS tests were conducted on lime and cement stabilized soils cured at 7, 28 and 56 days. Type II cement and quick lime were used as stabilizers in this research study.

Organic content (o/c) of the soils were determined by loss on ignition method. The amount of organic content present in the soil samples obtained from Bryan and Corpus Christi are respectively 6.0% and 1.5%. According to Karlson and Hansbo (1981), soils having organic content in the range of 2% to 6% are termed as low organic soils, and soils having organic content in the range of 6% to 20% are termed as medium organic

soils. However, the organic content present in these soils are typical for most of the Texas soils.

The grain size distribution curves are presented in Figure 1. Bryan soil has 50% fines and Corpus Christi soil has about 30% fines. Atterberg tests were conducted to measure the consistency of the control and treated soils. The liquid limit (LL), plasticity index (PI) and specific gravity of the Bryan soil are 60%, 38 and 2.37 respectively. The LL, PI and specific gravity of the Corpus Christi soil are 30%, 10 and 2.52 respectively. It can be illustrated that the plasticity index of the soil has increased with an increase in the organic content of the soil. According to Jenny (1941), soils with a high plasticity index should have a higher organic content than soils with a low plasticity index. This observation confirms that the present soils follow the same trend of results. These specific gravity values are low compared to the inorganic soils, which are usually in the range between 2.5 to 2.7. These low values are attributed to the amount of light weight organic content present in these control soils. Several researchers have reported similar results in the literature (Mitchell and Soga, 2005).

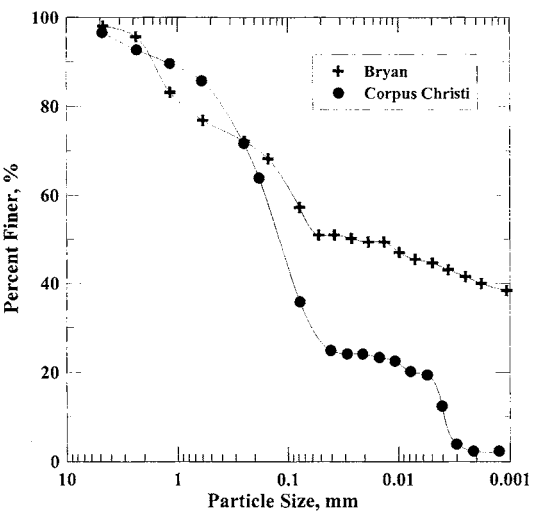

Figure 1 Grain size Analysis Curve

Proctor compaction tests were conducted on the control soils to determine the optimum moisture content (OMC) and dry unit weight (MD) relationships. Table 1 shows the optimum moisture content and dry unit weight of both the soils. From Table 1 it can also be illustrated that soil having high organic content has high optimum moisture content. This can be explained from the fact that the organic matter has high water retention capacity (Terzaghi et al., 1996). Dry unit weight of the soil decreases with increase in organic content. This decrease is due to an increase in organic content that decreases the soil unit weight.

STABILIZATION STUDIES

Optimum Lime Content Determination

Optimum lime content for the soils was determined using the procedure given by Eades and Grim (1966) and Tex-121-E methods. The soils were first air dried and passed through a 4.75 mm size sieve (US sieve # 40). Lime dosages calculated in percentage by dry weight in the order of 2, 4, 6, 8 and 10% were then added to the 20 g of soil. These lime-soil mixtures were transferred into a 250 ml plastic container with an appropriate lid. Then 100 ml distilled water (free of CO_2) in a ratio of 1:5 was added to these mixtures and the samples were shaken in an Eberbach shaker for 30 seconds. This process of shaking is repeated for every 10 minutes and was continued for at least one hour to ensure proper mixing of the binder and soil. The sample was then removed from the shaker and the pH of the mixture was measured. The pH concentrations versus the binder dosage in percentage were plotted and the threshold value of dosage was determined beyond which any further addition of the binder doesn't change the pH of the soil-binder mixture. Figure 2 shows the graph between pH value and percent dose of lime. The optimum lime contents obtained from this procedure for Bryan and Corpus Christi soils are respectively 6% and 4%.

Table 1 Summary of Control and Stabilized Test Results

Sample	o/c (%)	LL (%)	PI	OMC (%)	MD (kN/m^3)	pH
Control Specimens						
Bryan	6.0	60	38	31.0	12.4	5.0
Corpus Christi	1.5	30	10	16.3	16.3	8.5
Lime Stabilized Specimens						
Bryan	6.0	58	30	33.6	11.8	12.3
Corpus Christi	1.5	32	8	16.5	15.6	12.3
Cement Stabilized Specimens						
Bryan	6.0	68	34	29.0	10.9	12.14
Corpus Christi	1.5	35	7	15.9	16.0	12.13

Optimum Cement Content Determination

Optimum cement content of the organic soils was determined using the Texas Department of Transportation's (TXDOT) test procedure: Tex-120-E. The optimum cement dosage is a percent of cement in a soil specimen that gives the UCS value of 1035 kPa (150 psi) for a treated subgrade soil at a 7 days curing period. Higher strengths are not recommended because they can lead to cracking. Cement dosages of 2, 4, 6, 8 and 10% were used to prepare UCS specimens. Samples were first cured for 7 days prior to the UCS testing. The cement dosage (%) that gives the UCS value of 1035 kPa was

selected as optimum cement dosage. The optimum cement dosage for Bryan and Corpus Christi respectively are 6.5% and 5.5%.

After obtaining the optimum dosages of lime and cement stabilizers, Atterberg limits, compaction characteristics and pH tests were repeated to obtain the modified properties of the soils. The modified compaction characteristics were used to prepare the UCS specimens for the stabilization studies. It was noticed that both lime and cement treatments reduced the plasticity index of the organic soils by respectively 22% and 11% for Bryan soils and 20% and 30% for Corpus Christi samples. The moderate reduction in PI could be attributed to the presence of organic matter in these soils.

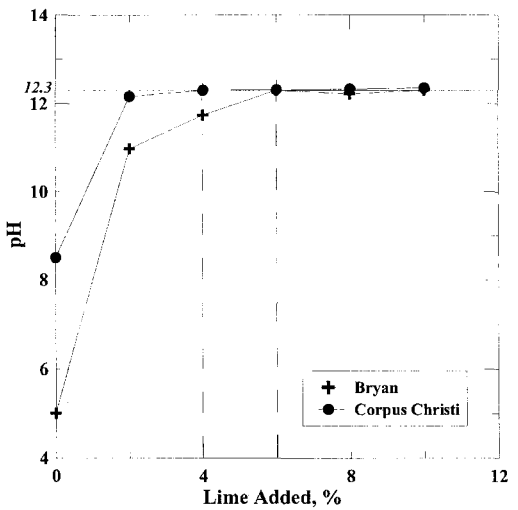

Figure 2 pH versus Percent Lime added

Unconfined Compressive Strength (UCS) Tests

Unconfined compressive strength tests were conducted on samples treated with optimum lime and cement content at curing intervals of 7, 28 and 56 days. These curing periods were chosen to understand the influence of organic matter on the UC strength of treated specimens. To compare the results, tests were also conducted on control (untreated) specimens at zero days curing period. The compressive strength of soil samples treated with lime and cement at different curing periods is presented in Figure 3. The strength has drastically improved with the curing period until 28 days in lime treated specimens. The strength gain is marginal from thereafter. In contrary, the gain in strength of cement treated specimens is moderate even from 7 to 28 days curing period. A reduction in UCS value is noticed after a curing period of 28 days in cement treated specimens. Besides, soils having high organic content loose more strength than soils having low organic content after 56 days. Further analysis is very necessary to quantify these reductions in strength at prolonged curing periods.

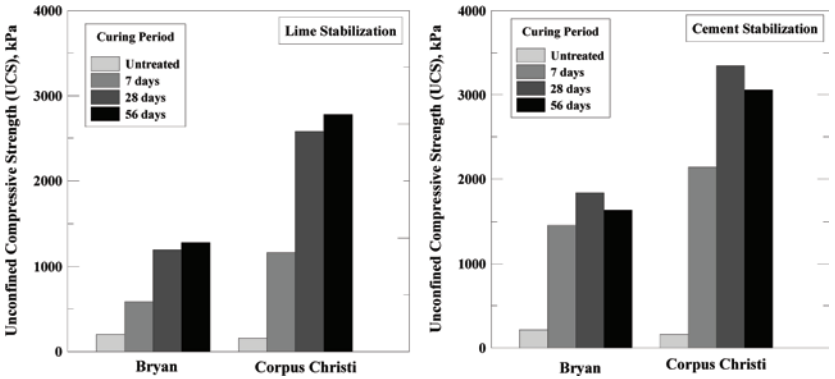

Figure 3 UCS of Lime and Cement Treated Samples at Different Curing Periods

Variation of pH of the lime- and cement-stabilized soils with a curing period (days) is shown in Figure 4. It can be seen that the pH of the soil decreases with curing periods. In general, when calcium-based additives are used to stabilize soils, the pH of the stabilized soil mixture increases and leads to the formation of calcium-silica-hydrate (CSH) gel by dissolving the silica present in the clay (Eades and Grim, 1966). The CSH gel is known to be the basic hydration product that contributes to the increase in strength of the stabilized soil. In contrary, the pH of the lime/cement-stabilized organic soil is decreased with an increase in the curing period. This drop in pH concentration retards the dissolution of silica in the clay, which inhibits the formation of CSH gel and thus the strength of the stabilized soil.

Another factor contributing to the reduction in strength is attributed to the formation of insoluble calcium humic acid. To understand this phenomenon, a brief history of organic soil formation in Texas is needed. The main soil formations in Texas are either grassland soils or forest soils (Soil Taxonomy, 2006). These soils are rich in both humic and fulvic acids. The present sampled soils geographically obtained from the locations having dominant soil orders as Alfisols, Ultisols, Vertisols, and Mollisols.

According to Tindall and Kunkel (1999), alfisols, spodosols, and ultisols are generally high in fulvic acids classified as forest soils; mollisols are high in humic acids classified as grassland soils. However, vertisol is neither a grassland soil nor forest soil. In addition, Stevenson (1994) reported that forest soils consist of fulvic acid, whereas grassland soils consist of humic acid in which the major portion is gray humic acid, as shown in the pie chart in Figure 5. Among these acids, humic acid has a higher affinity towards calcium if present in the soil (Bonomaluwa and Palutnicowa, 1987). Besides, the half life of humic acid present in any soil formation is reported as more than 100 years (Brady and Weil, 1999). Hence, when calcium-based additives, such as lime or cement, are used to stabilize humic acid rich organic soils, the humic acid will react with the calcium present in the stabilizer and form insoluble calcium humic acid. This compound formation utilizes most of the calcium present in the stabilizer and hence no formations of required amount of CSH gel.

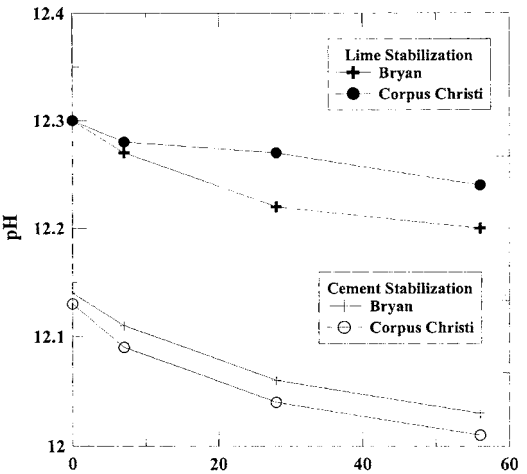

Figure 4 Variation of pH of Cement Treated Samples

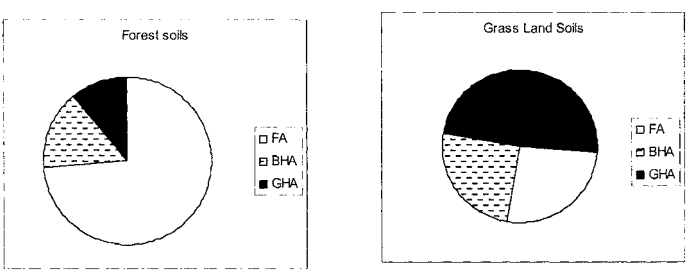

NOTE: FA - Fulvic acid; BHA - Brown humic acid; GHA - Gray humic acid

Figure 5 Pie chart showing the relationship of Humic acid and Fulvic acid (Stevenson, 1994)

Strength Improvement Factors

To explain the strength improvement in stabilized soils, a non-dimensional parameter is introduced as explained below:

Strength Improvement Factor, $SIF = \dfrac{UCS\ of\ stabilized\ specimen\ at\ n\ days}{UCS\ of\ unstabilized\ specimen\ at\ n\ days}$

Strength improvement factors are calculated for 7, 28, and 56 days curing periods and presented the results between the improvement factors and organic content in Figure 6. It is noticed that the strength improvement factors are reduced with increase in organic content for both lime and cement stabilized soils. Cement stabilized soils exhibit more improvement factors than lime stabilized soils.

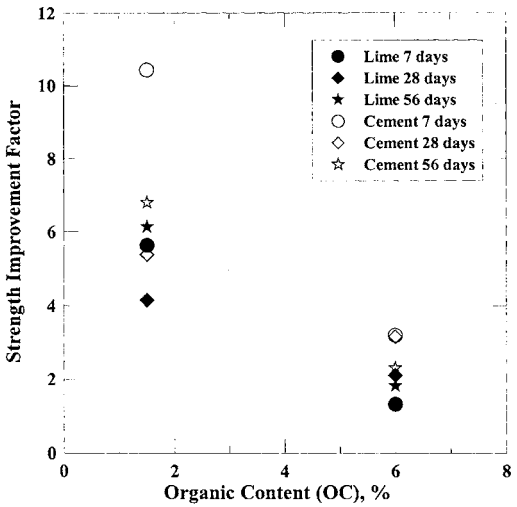

Figure 6 Strength Improvement Factors

CONCLUSIONS

Based on a series of stabilization studies performed on two organic soils collected from Texas, the following major conclusions were drawn from this research:

- The optimum moisture content of soils increases with an increase in the organic content. This increase is due to high water retention capacity of organic soils.
- The dry unit weight of the soil decreases with an increase in organic content. This decrease is attributed to the increase in organic content that decreases the soil unit weight.
- Organic content has moderate influence on the UCS of the present control soils. This influence is expected as the strength of the soil is dependent of soil type and clay mineralogy.
- The improvement in unconfined compressive strength of the soil is either negligible or reduced after 28 days of curing, when the soil is stabilized with lime and cement. This reduction could be due to 1) Moderate reduction of pH in the stabilized soils as the curing period progresses, and 2) Formation of inorganic calcium humic acid when calcium present in the stabilizer is reacted with humic acid present in the soil.
- The strength improvement factors of the soil are decreased with an increase in the organic content, when stabilized with lime or cement.

REFERENCES

Bohn, H. L., McNeal, B. L., & O'Connor, G. A. (1985). Soil chemistry. John wiley & sons.

Bonomaluwa BB, Palutnicowa TA [USSR](1987).The formation of soil and humus. Translated by Wei KZ. Agricultural Publishing House, Beijing, pp 140–141 (in Chinese)

Brady, N.C., and Weil, R.R. (1999) The Nature and Properties of Soils. 12th ed., Upper Saddle River, NJ; Prentice Hall.

Chen, H., and Wang, Q. (2006) The behavior of organic matter in the process of soft soil stabilization using cement, *Bulletin of Engineering Geology and the Environment.*, 65(4): 445-448.

Clare, K.E., and Sherwood, P.T. (1954) The Effect of Organic Matter on the Setting of Soil-Cement Mixtures. *Journal of Applied Chemistry*, vol. 4, no. 11, pp. 625-630.

Eades, J. L., and Grim, R. E. (1966) A Quick test to determine lime requirements for lime stabilization. Transportation Research Board., 139: pp. 61-72.

Edil, T.B., & Wang, X. (2000). Shear strength and Ko of peats and organic soils, Geotechnics of highwater content materials: ASTM Special technical publication, 1374(2000), pp. 209-225.

Hampton, M. B., and Edil, T. B. (1998) Strength gain of organic ground with cement-type Binders. *Soil improvement for big digs, 81,* pp. 135-148.

Jenny, H. (1941) Factors of Soil Formation. New York; McGraw-Hill.

Karlsson, R., & Hansbo, S. (1981). (in collaboration with the laboratory committee of the Swedish geotechnical society) soil classification and identification. Swedish council for building research. D8: 81. Stocckholm.

Maclean, D.J., and Sherwood, P.T. (1962) Study of the occurrence and effects of organic matter in relation to the stabilisation of soils with cement, In Proceedings of the 5th International Conference on Soil Mechanics and Foundation Engineering (ICSMFE), Paris, 17–22 July 1961. Dunod, Paris. pp. 269–275.

Mitchell, J. K & Soga, K (2005). Fundamentals of soil behavior. John Wiley & Sons, Inc. 3rd ed., p. 577

Schmidt, N. O. (1965). A study of the isolation of organic matter as a variable affecting Engineering properties of soil, thesis presented to the university of Illinois, at Urbana, III., in partial fulfillment of the requirements for the degree of Philosophy.

Soil taxonomy. (2006). Chapter 2, Differentiate between mineral soils and organic soils. Soil taxonomy, pp. 3-5.

Stevenson, F. J. (1994) *Humus chemistry genesis, composition, reactions.* New York, A Wiley Interscience publication.

Terzaghi, K., Peck, R. B., and Mesri, G. (1996) *Soil Mechanics in Engineering Practice.* John Wiley & Sons, Inc. 3rd ed., pp.549.

Tindall, J.A., and Kunkel, J.R. (1999) Unsaturated Zone Hydrology for Scientists and Engineers. New Jersey; Prentice Hall.

Application of Gypsum Waste Plasterboard and Waste Plastic Trays to Enhance the Performance of Sandy Soil

Aly Ahmed[1], Keizo Ugai[2] and Takeshi Kamei[3]

[1]Visiting scholar, Gunma University, Japan; aly_76@hotmail.com
[2]Professor, Gunma University, Japan; ugai@ ce.gunma-u.ac.jp
[3]Professor, Miyazaki University, Japan; kamei@civil.miyazaki-u.ac.jp

ABSTRACT: This paper presents the results of a research project that evaluated the use of recycled gypsum obtained from waste plasterboard along with strips of waste plastic trays to enhance the performance of tested soil. Recycled gypsum was used as a stabilizing agent for stabilized soil to improve the compressive strength, whereas the waste plastic trays were used to improve the tensile strength. The effects of waste gypsum content, size, aspect ratio and waste plastic trays content were investigated to determine the mechanical behavior of soil treated with such waste materials. Experimental test results showed that unconfined compressive and splitting tensile strengths increased with increasing waste gypsum content. The increase in waste gypsum has a more significant effect on the unconfined compressive strength than on the tensile strength. Adding strips of waste plastic trays to samples treated with waste gypsum enhanced the splitting tensile strength. The size, aspect ratio and content of waste plastic trays have significant effect on the enhancement of soil strength

INTRODUCTION

Nowadays, most studies are directed to protect environment by using waste materials as alternative materials in civil and industrial engineering applications. Gypsum waste plasterboard and waste plastic trays are considered two examples of such wastes. Approximately 1.5 million tons of gypsum waste plasterboard is sent to landfills annually in Japan (Ugai and Ahmed 2009). To avoid the increase amount of gypsum waste plasterboard that is disposed in landfill, it is necessary to find alternative ways to reduce the disposed waste, as they increase the cost of disposal in landfill and decrease the available ground spaces that are specified for landfills sites.

Waste plastic trays are wastes that have not progressed in the recycling process due to the difficulty of making separation and most of such plastic products used as one way products. For example, the amount of waste plastic produced annually in the United State is approximately 11 million tons (EPA 2003) while in UK is approximately 3 million tons (PRIS, 2001). An estimated 56% of all plastics waste is

used in packaging, which is mainly considered waste plastic trays that are used in preservation and distribution of food (EPA 2003).

Generally, recycled gypsum which is derived from gypsum waste plaster has a potential to be used as a cementation material because gypsum is the main key of cementation products. In order to resist the weakness of stabilized soil-cement against tension, it is necessary to introduce another material that has a power to resist tensile stresses. Plastic is made of synthetics polymers that are comparable to plastic fibers that are commonly used to resist tensile stress in soil improvement. Therefore, the main objective of this research is to investigate the use of gypsum waste plaster as a stabilizing agent, along with strips of waste plastic trays as a reinforcing material to improve the performance of sandy soil.

PREVIOUS RESEARCH

Several researchers have conducted investigations to improve the physical and mechanical properties of soil by using different types of waste materials. Their research includes, for example, waste tire, waste plastic, cement kiln dust, fly and bottom ashes, blast furnace slag, stone dust, recycled carpet wastes, factory-waste roof shingles and sewage sludge ash (Baghdadi et al. 1995, Montardo et al. 2002, Sbhan and Mashnad 2003, Ghiassian 2004, Ahmed 2004, Dutta 2007, Ahmed et al. 2008, Chen and Lin 2009).

The use of recycled gypsum which is derived from gypsum waste plasterboard, which is reported in most previous studies, is related to agriculture applications (Ugai and Ahmed 2009). A few studies have been directed to the use of recycled gypsum in civil engineering applications. Laboratory and field investigations were conducted to develop effective novel cementation mixes using recycled gypsum for road foundation construction. Therefore, a series of laboratory trials were carried out to determine the optimum proportions of recycled gypsum-mineral wastes used as a binder paste in order to achieve the higher compressive strength. Results indicated that recycled gypsum can be used in low-strength concrete mixes for the foundations of minor roads and car parks (WRAP 2007). The bassanite which is derived from gypsum waster plasterboard was used as a soil improvement material by Kamei et al. (2007). The results indicated that adding of bassanite improved the unconfined compression strength for tested soil.

Waste plastic milk packages, which are considered one of waste plastic trays, were used to improve the strength and CBR for tested soil. Results showed that the use pieces of waste plastic enhanced the strength and increased the value of CBR for sandy soil (Benson and Khire, 1994). Waste plastic have been used also to improve the behavior of sand soil using a series of triaxial tests. Results confirmed that waste plastic can be used for ground improvement. Waste plastic bottles were used were used to improve the properties of fine sand. Results showed that the use of fibers which produced from waste plastic bottles increased the strength of tested sand specimens (Montardo et al., 2002).

MATERIALS AND METHODS

Four different types of materials were used in this research: silty sand soil, recycled gypsum which is derived from waste plaster, waste plastic trays, and Portland cement. The soil type used in this research was brought from Gunma Prefecture in Japan. It is classified as silty sand soil (A-2-4) according to ASSHTO. All physical and mechanical properties of tested soil are shown in Table 1. The grain size distribution for the tested soil composed of 99.8%, 53.2%, 27.3% and 11.3% passing sieves No. 60, No.100, No.140 and No.200, respectively.

Table 1. Physical and mechanical properties of tested soil

Property	Value	Property	Value
Effective diameter, (D10), (mm)	0.06	Max. dry unit weight, (N/mm^3)	1.428 e-5
Nominal mean size, (D50), (mm)	0.15	Optimum moisture content, (%)	20.00
Uniformity coefficient, (Cu)	2.72	Specific gravity, Gs	2.67
Curvature coefficient, (Cc)	1.02	Max. void ratio	1.28
Passing from sieve No. 200	11.30	Min. void ratio	0.79

Recycled gypsum used in this research was produced by heating of crushed gypsum waste plasterboard, chemically named hydrate calcium sulphate ($CaSO_4.2H_2O$). This process was done at temperature which ranged from 130°C to 160°C for a certain time resulting in a hemi-hydrate calcium sulphate ($CaSO_4.0.5H_2O$) with three quarters of the water removed. The preparation of waste plasterboard was done in local construction company in Gunma prefecture in Japan. The x-ray results indicated that the content of calcium hemi-hydrate is bassanite with 99.80% with respect to the whole tested sample. Figure 1 shows the produced recycled gypsum used in this research. Four different contents of recycled gypsum of 5%, 10%, 15%, and 20% per mass of the soil were investigated. The grain size distribution for the produced recycled gypsum composed of 88.5%, 76.28%, 61.17%, 24.69%, 2.1 % and 0.2 % passing sieves No. 10, No. 20, No.40, No.60, No.140 and No.200, respectively.

A) Before crushing (solid state) **B) After crushing and heating**

FIG. 1. The recycled gypsum used as stabilizing agent

A small content of ordinary Portland cement, 3% by soil mass, was added to the mixture of soil and waste plaster. The main reason of adding cement is to prevent the solubility of recycled gypsum when water is introduced because hydrate calcium sulphate is soluble material in water.

The waste plastic trays used in this research were brought from the cleaning center in Kiryu city, Gunma Prefecture in Japan. The waste plastic trays were cut by shredder machine in three different width strip sizes 2.5, 5 and 10 mm. The average thickness of waste plastic trays used in this research is approximately 1 mm. The content, size and aspect ratio of plastic strips were investigated to evaluate their effects on the behavior of treated soil based gypsum waste plaster. Four different contents of plastic strips were used by soil mass, 0.25, 0.5, 1, and 2%, also four varied aspect ratios (L/B) were considered: 1, 2, 3, and 4. Table 2 shows the testing program for different investigated parameters in this study.

SAMPLE PREPARATION

The effect of using waste plaster along with waste plastic trays on the strength of tested soil was evaluated by conducting a series of unconfined compression and splitting tensile strength tests. Cylindrical samples having a 50-mm diameter and 100-mm height were used. All samples were prepared at optimum moisture content and maximum dry unit weight. A moisture content-density relationship for tested soil treated with different plaster waste content is shown in Figure 2. The soil sample was mixed firstly with the recycled gypsum and cement in dry condition after that the plastic strips was added to the dry mixture and then the required optimal water content was added. The samples were placed in the molds and compacted statically using a static method till reached to the desired density according to the method which is illustrated by Ahmed et al. (2008). All samples were subjected to curing for seven days at temperature (21 ± 1 °C) and relative humidity above 90% before testing.

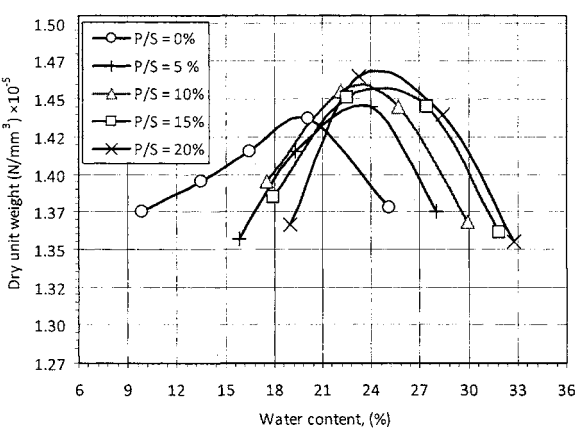

FIG.2. Optimal moisture-density relationships for tested soil with different recycled gypsum contents.

Table 2. Experimental Program

Group No.	Test No.	Unconfined Compression Test				Splitting Tensile Test			
			Plastic Strips				Plastic Strips		
		Bassanite Content, %	Content %	Size, mm	Aspect ratio, L/B	Bassanite Content, %	Content %	Size, mm	Aspect ratio, L/B
A	A-1	0	--	--	--	0	--	--	--
	A-2	5				5			
	A-3	10				10			
	A-4	15				15			
	A-5	20				20			
B	B-1	10	0.25	2.50	4	10	0.25	2.5	4
	B-2		0.50				0.50		
	B-3		1.00				1.00		
	B-4		2.00				2.00		
C	C-1	10	0.50	2.50	2	10	0.50	2.5	2
	C-2			5.00				5.00	
	C-3			10.00				10.00	
D	D-1	10	2.5	5	1	10	0.50	2.50	1
	D-2				2				2
	D-3				3				3
	D-4				4				4

RESULTS AND ANALYSIS

As aforementioned, the feasibility of using different contents of waste plaster to enhance the strength of tested soil was proposed. A series of unconfined and splitting tests were conducted on soil samples treated with waste plaster and untreated samples. The results of unconfined compression tests for samples treated with different contents of waste plaster are shown in Figure 3. Noticeably, the compressive strength values increase with the increase of waste plaster content volume. These data confirmed that gypsum waste plasterboard can be used as an alternative cementation material for soil stabilization in earthwork projects. Figure 4 shows the maximum peak of stress for compressive and splitting tensile tests. Both unconfined and splitting tests, the strength of treated soil increases with the increase of waste plaster content compared with untreated identical sample. Also, it is noted that the increase of waste plaster content up to 15% did not result in significant increase in the tensile strength compared with the enhancement of compressive strength. This result concurs with the results of several research which confirmed that cement stabilized soil is weak in tension comparing to its behavior under compression (Ahmed et al. 2008, Sobhan and Mashnad 2003). Generally, it can be stated that the use of recycled gypsum, which is derived from waste plaster to enhance the strength of soil, is acceptable especially in the case of compressive strength.

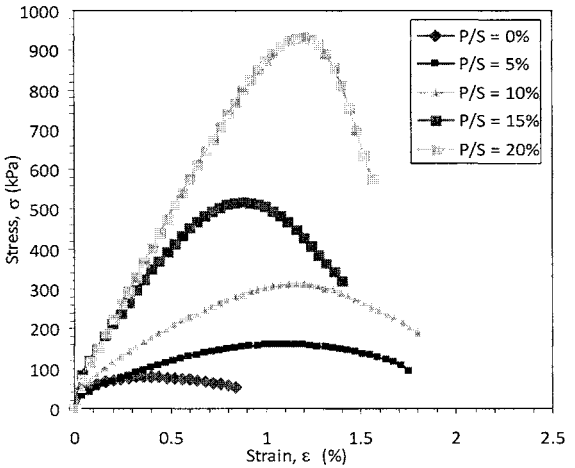

FIG.3. Effect of plaster content on compressive strength

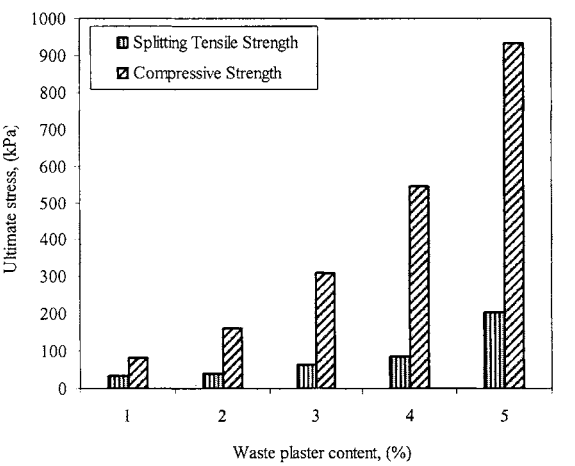

FIG.4. Effect of plaster content on compressive and splitting strengths

To overcome the shortage of recycled gypsum to resist tensile strength especially when this system is used in projects subjected to repeated loading, as in highway, using another material maybe is needed. In this research, strips of waste plastic trays were used as an alternative reinforced material to enhance the resistance of treated soil against tensile stresses. As mentioned, three different sizes, four different contents, and four aspect ratios of waste plastic strips were used to investigate their effect on the

enhancement of tensile and compressive strengths of treated soil. All tests were conducted on samples having 10% of waste plaster content in addition to strips of waste plastic with different sizes, contents and aspect ratios. Figure 5 shows the improvement stress ratio for both compressive and splitting tensile strengths with different waste plastic contents. Improvement stress ratio is defined as the stress of treated soil specimen with wastes divided by the stress of untreated identical sample (control sample).

Both compressive and tensile strengths increased with the presence of strips of waste plastic compared with treated sample with waste plaster alone. This result agrees with the results of previous studies which used different types of waste plastic or plastic fibers (Montardo 2002, Dutta and Venkatappa 2004, Dutta 2007). The increase of plastic strips content has a more significant effect on the enhancement of splitting strength compared to the compressive strength. The maximum improvement in compressive and splitting strength was obtained at plastic strips content of 0.5 and 1%, respectively. The improvement of tensile strength is attributed to increasing the number of plastic strips elements. The performance of reinforced soil treated with any inclusions such as elements of waste plastic strips depends on the number of reinforcing elements, and orientation in the favorable directions of tensile strain directions (Ahmed 2004). Thus increasing the number of plastic elements will result in a greater chance of a large number of plastic elements oriented in the principal tensile strain; as such, an improvement might be developed. While in the case of compressive strength, increasing the number of plastic elements up to a specified content will result in an increasing in the compressibility of treated soil. Thus, the improvement ratio in compressive strength decreases. This was the case that occurred in this study, beyond 0.5% content of plastic strips, the improvement in compressive strength declined.

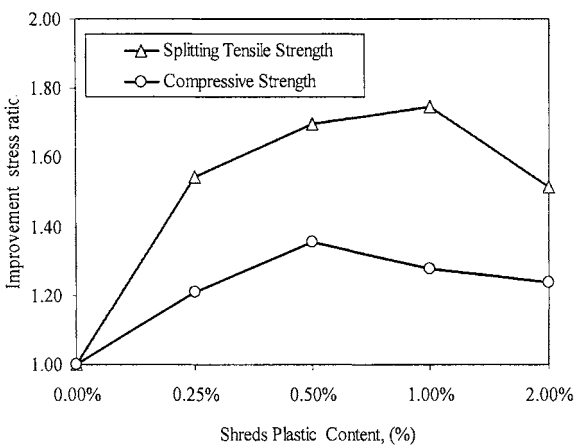

FIG.5. Effect of content of waste plastic strips on the strength of treated soil

The effect of aspect ratio and size of waste plastic strips on the strength of treated soil are shown in Figures 4 and 5, respectively. Figure 6 shows that the effect of aspect

ratio is much pronounced on splitting strength compared to compressive strength. The effect of aspect ratio for waste plastic strips on compressive strength is not significant while splitting strength increased with the increase of aspect ratio. The increase of splitting strength with increasing of aspect ratio is related to increase of the length of plastic strips, and gives a greater chance to resist the shear plane of the plastic failure compared to small length of strips. The best improvement in compressive strength was obtained with strips of 2.5 mm size compared to other different strips sizes used as shown in Figure 7. The increase of compressive strength with the small strips size is attributed to the number of plastic elements for small size is more than the number of elements in the case of large size for the same weight. Thus, increasing the number of plastic elements within soil mass, up to the specified limit, is associated with increasing the friction between soil particles and elements of plastic strips.

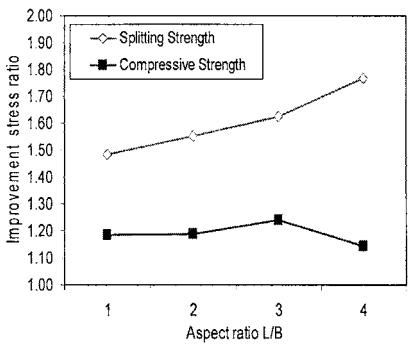

FIG.6. Effect of aspect ratio of waste plastic strips on the strength

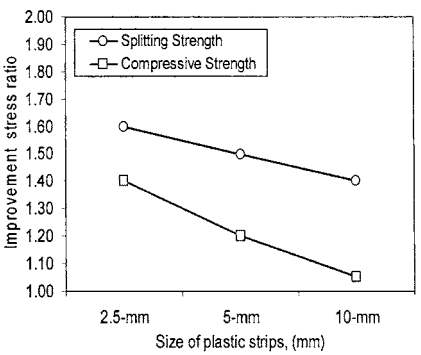

FIG.7. Effect of size of waste plastic strips on the strength of treated soil

CONCLUSIONS

The use of recycled gypsum along with waste plastic trays enhanced the performance of tested soil. Based on test results, the following conclusions can be drawn:

1. Increasing of waste plaster content in soil mixture is associated with the increase of optimum moisture content and insignificant increase in dry unit weight.

2. The compressive and splitting strengths increased with the increase of waste plaster content. The use of waste plaster in ground improvement had a more significant effect on the compressive strength compared to the splitting tensile strength.

3. Adding strips of waste plastic trays to soil treated with waste plaster had a more significant effect on the enhancement of splitting strength compared to the compressive strength.

4. The content, size and aspect ratio of waste plastic strips have significant effects on the splitting tensile strength. Splitting strength increased with the increase of content and aspect ratio of waste plastic strips.

REFERENCES

Ahmed A, Shehat M and Easa S., (2008). "Enhancing the Strength of Roadway Subgrades Using Factory-waste Roof Shingles" The proceeding of CSCE 2008 Annual Conference, 10-13 June, Québec, Canada.

Ahmed, A. (2004). "Utilization of Shredded Waste Tires in the Strengthening of Unpaved Roads Over soft Clay" Ph.D. Thesis, Civil Eng. Dept., Faculty of Engineering, El-Mina University, El-Minia, Egypt.

Baghdadi ZA, Fatani MN, Sabban NA, (1995). "Soil modification by cement kiln dust" Material Civil Eng. J., 7(4), 218-222.

Benson, C.H. and Khire, M.U., (1994). "Reinforcing Sand with Strips of Reclaimed High-Density Polyethylene" Journal of Geotechnical Eng., 120(5): 838-855.

Chen L. and Lin, D. (2009). "Stabilization treatment of soft subgrade soil by sewage sludge ash and cement." Journal of Hazardous Materials, 162(1), 321-327.

Dutta, R. K. and Venkatappa Rao, G., (2004). "Engineering Properties of Sand Reinforced with Strips from Waste Plastic", Proceedings of International Conference on Geotechnical Engineering, Sharjah, UAE, 186-193, 2004.

Dutta, R.K., (2007), "Regression Models for Predicting the Behavior of Sand Reinforced with Waste Plastic", Turkish J. Eng. Env. Sci. 31: 119 – 126.

EPA, 2003, Report on Plastics, USA.

Ghiassian H. (2004). "Soil Reinforcement with Recycled Carpet Wastes" Waste Management & Research J., 22(2): 108-114.

Kamei T., Kato T. and Shuku T. (2007). "Effective Use for Bassanite as Soil Improvement Materials- Recycling of Waste Plasterboard –" Geotechnical Society Electronic Journals, 2(3): 245-252 (in Japanese)

Montardo J.P., Prietto P.D. M. and Pasa G.S. (2002). "Engineering behavior of a sand reinforced with plastic waste." J. Geotech. and Geoenvir. Eng., 128(6): 462-472.

Plastic Recycling Information Sheet (PRIS), UK. (2001) <www.wasteonline.org.uk/resources/information/sheets/plastics/htm>

Sobhan K. and Mashnad M. (2003). "Mechanical stabilization of cement soil-fly ash mixtures with recycled plastic strips." J. Envir. Eng., ASCE, 129(10): 943-947.

Ugai K. and Ahmed A. (2009). "Evaluation of Using Gypsum Waste Plasterboard in Ground Improvement" In Proceeding of the Workshop on Recycling Waste Plasterboard, March 13, 2009, Memorial Hall, Chuo University, Tokyo, Japan

Waste & Resources Action Programme, (WRAP), (2007-b). "Plasterboard case study: Recycled gypsum in a novel cementations material" The Old Academy, 21 Horse Fair, Banbury, Oxon, UK. www.wrap.org.uk.

Effect of Placement Water Content on Strength of Temperature Cured Lime Treated Expansive Soil

Amir Asad Nasrizar[1], M. Muttharam[2], K. Ilamparuthi[3]

[1]Research scholar, aans50@yahoo.com
IAU Sanandaj, Kurdistan, Iran
[2]Assistant professor, muttharam@annauniv.edu
[3]Professor and Head, kanniilam@gmail.com
Division of Soil Mechanics and Foundation Engineering, Anna University, Chennai 600025

ABSTRACT: In this study the effect of initial moisture content on the strength of thermally cured lime treated expansive soil is examined. The soil of CH type was selected and stabilized with 5% and 7% lime. The effect of placement water content is brought out by conducting UCC tests on lime stabilized samples compacted at OMC of 5% lime (26%) and other two water contents representing wet of OMC (30%) and dry of OMC (21%). The samples thus prepared are cured for 7, 14 and 28 days at temperatures of 5°C, 30°C, and 50°C. The strength of wet side compacted sample is almost equal to the strength of sample compacted at OMC irrespective temperature of curing, curing period and lime content though it has 4% higher moisture content. Further, the rate of strength gain is higher for higher temperature but this effect is a function of initial moisture content and is pronounced much in sample moisture contents of OMC and wet side OMC. To derive maximum benefit from lime stabilization of expansive clay, the sample should be compacted at OMC or slightly higher than OMC and cured at elevated temperatures.

INTRODUCTION

Lime is the most widely used chemical for stabilizing clayey soils. Design of lime-stabilized mixtures is usually based on laboratory analysis of desired engineering properties. Several approaches to mix design currently exist. In addition to engineering design criteria, users must consider whether the laboratory procedures adequately simulate field conditions and long-term performance. Laboratory testing procedures include determination of optimum lime requirement, placement moisture content, and curing of sample under simulated field conditions. Curing is important for chemically stabilized soils particularly lime-stabilized soils because lime-soil reactions are time and temperature dependent and they continue for longer period, even years (Petry and Little 2002). The three main factors that control the curing of lime stabilized soils are moisture content, curing temperature and curing time. The reactivity of the lime is a function of the temperature and time of curing; temperature

having the greatest effect on reactivity (Gillot 1987). On the other hand it is well known that water is a critical component of the lime-soil stabilization process. Water is necessary to hydrate the quicklime (CaO) to form hydrated lime ($CaOH_2$) which can react with the clay components of the soil. Water also serves as the medium to mobilize the calcium ions (Ca^{++}) that exchange with cations at the surface of the clay, and hydroxyls (OH^-) that raise the pH of the soil system, which solubilizes silica and alumina to react with the lime. Water is an important component of the calcium-silicate hydrates (CSH) and calcium-aluminate-hydrates (CAH) that contribute to the long-term strength of lime stabilized soil (Petry and Berger 2006).

Though several researchers (Thompson 1966, Ranganatham & Pandian 1971, Wild et al. 1986, George et al. 1992, Bell 1996, Boardman et al. 2001, Rao & Shivananda 2005, Nasrizar et al. 2008) have worked on the effect of curing temperature on strength of lime stabilized expansive soils. Studies considering curing temperature and placement moisture content together are limited (Bell 1996, Petry and Berger 2006) and there is no protocol to use lime in regions of different climates (i.e. cooler climates, semi-arid and arid regions). Hence this paper aims to examine how the curing conditions prevalent in cooler, semi-arid and arid regions and the placement water content affect the strength of lime stabilized expansive clay.

TESTING MATERIAL

A black cotton soil from Siruseri, Chennai in India was used in this study. The properties of the soil are presented in Table 1. As per Unified Soil Classification System the soil is classified as clay of high plasticity (CH). Laboratory grade hydrated lime with assay more than 95% was used in the present study for the stabilization of expansive soil.

Table 1. Physical Properties of Soil

Description	Value
Sand (%)	30
Silt (%)	34
Clay (%)	36
Specific gravity, G_s	2.72
Liquid limit, LL (%)	80
Plastic limit, PL (%)	25
Plasticity index, PI (%)	55
Shrinkage limit, SL (%)	12
Maximum dry unit weight (kN/m³)	15.50
Optimum moisture content (%)	23
Differential Free Swell Index (%)	85
Unified Soil Classification System (USCS)	CH

TESTING METHOD

The air dried natural soil sieved through 425 μm for was used for index properties test. Proctor compaction and UCC tests were conducted on soil passed through 4.75 mm sieve.

Determination of Initial Consumption of Lime (ICL)

Two independent methods were used to determine the initial consumption of lime for the soil. First method is suggested by Eades & Grim (1966) (ASTM D 6276-99a, Reapproved 2006). As per this method the ICL of the soil is found to be 3%. Second method is based on plastic limit values (Nelson & Miller 1992), which resulted a minimum percentage of lime required to modify the plasticity characteristics of the soil used in the present study is 3%. The lime addition in excess of initial consumption of lime is mainly involved in the pozzolanic reaction; hence 2% and 4% higher than ICL of 3% of the soil have been used in this research. Thus the lime contents used for stabilizing soil is 5% and 7% by weight of soil.

Compaction Characteristics

The compaction characteristics of soil were determined as per ASTM D 698 – 07 and presented in Table 1. Standard Proctor compaction test was performed for soil-lime mix with 5% and 7% lime content. The standard Proctor maximum dry unit weights(MDD) for 5% and 7% lime mixed soil are 14.5 and 14.3 kN/m^3 respectively and the corresponding Optimum Moisture Contents (OMC) are 26% and 27.4% respectively. The increase in the lime content reduced the maximum dry unit weight and increased the optimum moisture content. However the reduction in the unit weight is marginal.

Preparation of Samples for Strength Test

Soil in the field is usually compacted to achieve relative compaction of more than 95%. To achieve the given relative compaction, placement water content may correspond to either dry or wet of OMC. Hence in the present study to take this aspect into account the placement water content is varied and the strength is determined. Three different water contents are considered such that one is OMC and the other two are water contents corresponds to 97% of maximum dry unit weight taken from the Proctor compaction curve. For 5% lime treated soil the OMC is 26% and the water contents correspond to 97% relative compaction for the dry and wet side of OMC are 21% and 30% respectively. Since the difference in compaction characteristics of 5% and 7% lime treated soil is marginal; for comparison purpose soil treated with 7% lime is also compacted to have same dry unit weights and water contents as that of soil treated with 5% lime content. However the natural soil was compacted at its MDD and OMC, which are 15.5 kN/m^3 and 23% respectively and tested for its strength.

Cylindrical samples of diameter 51 mm and length 102 mm were prepared as per ASTM D 5102-04 at the required dry unit weights and water contents. All these samples were prepared at room temperature of 25°C to 27°C and tested for their compressive strength after curing for 7,14 and 24 days at temperatures of 5°C, 30°C, and 50°C.

Experimental Program

To understand the effect of initial moisture content at different curing temperature on strength of thermal cured lime treated soils, curing temperatures of 5°C, 30°C, and 50°C (to represent temperatures of cooler, semi-arid and arid regions) and curing periods of 7, 14 and 28 days were chosen for the study. Cylindrical soil specimens

prepared with 5% and 7% lime were sealed in air tight polythene covers and cured at 5°C, 30°C, and 50°C in a thermo controlled humidity chamber. Enough care was taken to maintain humidity of 100% inside the containers around the sealed samples to prevent moisture loss. The samples thus cured were tested for UCC strength. Samples were also tested after 2 hours of curing, which are taken as strength of 0 days curing.

RESULTS AND DISCUSSION

Effect of Initial Moisture Content on Strength

Figure 1 shows the variation of UCC strength with curing period for 5% (Fig.1a) and 7% (Fig.1b) lime treated soils compacted at 26% (OMC), 21% (dry of OMC) and 30% (wet of OMC) moisture contents and cured at 5°C. The unit weight of specimen compacted at 26% moisture content is 14.5 kN/m^3 and compacted at moisture contents of 21% and 30% is 14.1 kN/m^3 which is equal to 97.2% of Proctor density (γ_{dmax}). The UCC strength of both 5% and 7% lime treated specimens show a trend of increase in strength with curing period. The strength of lime treated soil cured at 5°C is less than the strength of virgin soil despite curing for a period of 14 days. After 28 days of curing the strength of lime treated specimens compacted at OMC and wet of OMC is slightly higher than that of virgin soil. The strength of lime treated specimens compacted at dry of OMC is less than that of specimens compacted at wet of OMC. Further, the strength of specimens compacted at wet of OMC is almost comparable with that of specimens compacted at OMC for 5% lime treated specimens up to 14 days. For 7% lime treated specimens the strength of specimens compacted at OMC is marginally higher than the specimens compacted at wet of OMC for the curing period up to 14 days. However after 28 days of curing both 5% and 7% lime treated specimens compacted at wet of OMC exhibited slightly higher strength than that of OMC. The strength of lime treated specimens compacted at 30% moisture content is nearly 95% more than that of specimens compacted at 21% moisture content both for 5% and 7% lime contents cured for 28 days. Despite the same unit weight, specimens compacted at 30% moisture content showed higher strength than that of specimens compacted at 21% moisture content which indicates that higher moisture content favours soil-lime reactions. The nearly comparable strength at 26% and 30% moisture content (average difference in strength is 8%) may be due to the fact that the unit weight of specimens compacted at 26% moisture content is higher than that of specimens compacted at 30% moisture content. That is though lesser moisture content is not favorable for strength gain, higher unit weight contributed for the strength gain. The UCC strength of 5% and 7% lime treated specimens compacted at different water contents and cured at 30°C for various curing periods are plotted in Figure 2. Specimens compacted at dry of OMC exhibited lesser strength than that of wet of OMC. Strength at wet of OMC is 97% and 155% higher than that at dry of OMC respectively for 5% and 7% lime content. Further, the strength at OMC and wet of OMC are almost comparable for 5% lime treated soil (Fig. 2a) and the similar trend is observed for 7% lime treated specimens curried up to 14 days. After 28 days wet of OMC shows slightly higher strength than OMC (Fig. 2b). Figure 3 presents the strength of specimens cured at 50°C with curing periods. Behavior similar to

specimens cured at 30°C is observed in this case also. After 28 days curing at 50°C, strength of specimens compacted at wet of OMC is 72% and 101% higher than that at dry of OMC for 5% and 7% lime content.

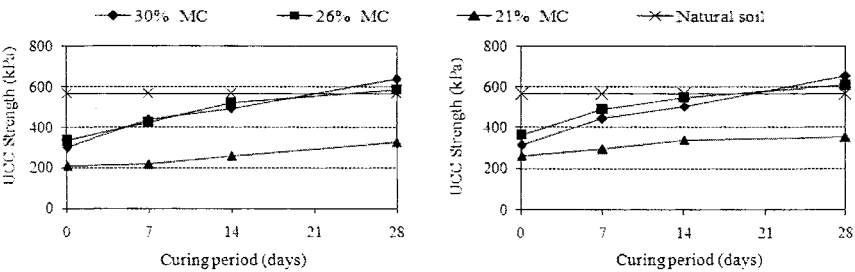

(a) 5% lime content (b) 7% lime content

FIG. 1. Effect of initial moisture content and curing period on UCC Strength of lime treated soil cured at 5°C.

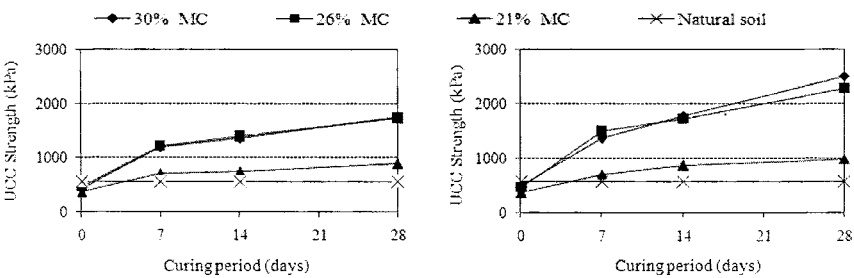

(a) 5% lime content (b) 7% lime content

FIG. 2. Effect of initial moisture content and curing period on UCC Strength of lime treated soil cured at 30°C.

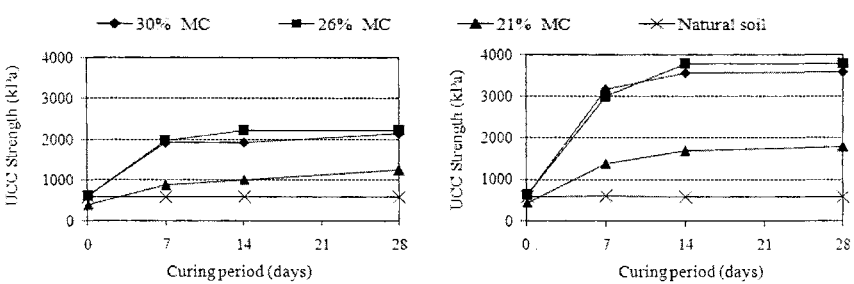

(a) 5% lime content (b) 7% lime content

FIG. 3. Effect of initial moisture content and curing period on UCC Strength of lime treated soil cured at 50°C.

Effect of Lime Content on Strength

It is well established that the strength of clayey soil increases with increases in lime content up to a certain amount of lime content. This has been confirmed in this study also. Comparison of strength between the specimens of 5% and 7% lime contents cured at 30°C (Fig. 2) showed that the strength of specimen of 7% lime compacted at OMC is higher by 22% and 32% for the curing periods of 7 and 28 days respectively over samples stabilized with 5% lime. Similar response is seen in samples cured at 50°C, but the increase in the strength is 51% and 71% for the curing periods of 7 and 28 days respectively. The strength of 7% lime treated specimen is always higher than that of 5% lime treated specimen for specimens cured at temperatures of 5°C, 30°C and 50°C for different curing periods. The increase in strength is more pronounced at higher curing temperatures. All these results clearly indicate the complementary behavior between curing temperature and lime content. The strength of untreated specimen is also included in Figures 1 to 3 for comparison. It is noticed that the curing temperature and period have negligible influence on strength of untreated soil.

Effect of Curing Temperature on Strength

Curing temperature plays a major role in accelerating gain in strength of lime treated soil. From the Figure 1 it is noticed that the strength of lime treated specimens cured at 5°C is lesser than the virgin soil even after 14 days of curing and only after 28 days the lime treated specimens show marginal increase in strength. This brings out the fact that cooler temperature is not conducive for the soil lime reactions. For both 5% and 7% lime treated specimens after 28 days of curing at 5°C the maximum strength achieved is only around 650kPa. In contrast, the lime stabilized specimens cured at 50°C for 28 days exhibited 2215KPa and 3785kPa for 5% and 7% lime content respectively (Fig. 3). Further hotter temperature helps in achieving the strength in less time. From the Figure 3 it can be seen that the slope of line up to 7 days curing is steeper than the slope of line joining curing periods of 7 and 28 days. The rate of strength gain during the first seven days of curing is 198 and 342kPa/day for 5% and 7% lime treated specimens respectively cured at 50°C at a compaction water content of 26%. For samples cured at 30°C the maximum rate of gain in strength is 109kPa/day and 149kPa/day for 5% and 7% lime treated specimens respectively. However, specimens cured at 5°C showed the strength gain of only around 20kPa/day for both 5% and 7% lime treated specimens. These observations bring out the fact that curing temperature plays a major role in governing the strength gain of lime treated soils.

CONCLUSIONS

Based on the experimental results the following conclusions are drawn:

1. Cooler temperature (5°C) is not conducive for lime treatment.
2. Curing the lime stabilized soil at elevated temperature accelerates the soil-lime reaction and increases the strength in a shorter period.
3. For a given period and temperature of curing the soil sample treated with higher percentage of lime gains more strength. If higher percentage of lime is used for stabilization, curing under enhanced temperature and longer curing

period results maximum benefit in strength gain.

4. For a given relative compaction, the compaction water content corresponding to wet of OMC offers considerable strength gain compared to the sample compacted at dry of OMC. Further the soil stabilized with higher lime content is more sensitive to moisture content variation.

REFERENCES

American Society for Testing and Materials (1999). "Using pH to Estimate the Soil-Lime Proportion Requirement for Soil Stabilization." *ASTM, D 6276 – 99a*

American Society for Testing and Materials (2004). "Unconfined Compressive Strength of Compacted Soil-Lime Mixtures." *ASTM, D 5102 – 04.*

American Society for Testing and Materials(2007). "Laboratory Compaction Characteristics of Soil Using Standard Effort." *ASTM, D 698 – 07.*

Bell, F. G. (1996). "Lime stabilization of clay minerals and soils." *Engineering Geology*, 42, 223-237.

Boardman, D. I., Glendinning, S. & Rogers, C. D. F. (2001). "Development of stabilization and solidification in lime-clay mixes." *Geotechnique*, 50, No.6, 533-543.

Eades J.L. & Grim R.E. (1966). "A quick test to determine lime requirements for lime stabilization." *Highway Research Record, Highway Research Board, National Research Council, Washington, DC*, 139, 61-72.

George, S. Z., Ponniah, D. A. & Little, J. A. (1992). "Effect of temperature on lime-soil stabilization." *Construction & Building Materials*, 6, No.4, 247-252.

Nasrizar, A. A., Muttharam, M. & Ilamparuthi, K. (2008). "Effect of curing temperature on strength of lime stabilized expansive soil." *Indian Geotechnical Conference (IGC), Bangalore*, Vol 2, 28-30.

Nelson, J. D. & Miller, D. J. (1992). "Expansive soils, Problem and Practice in Foundation and Pavement Engineering." *Wiley, New York.*

Petry, T. M., and Berger, E. A. "Impact of Moisture Content on Strength Gain in Lime-Treated Soils." *Transportation Research Board 85th Annual Meeting*, Washington DC, United States, p16.

Ranganathan, B. V. & Pandian, N.S. (1971). "Strength gain in thermally cured lime stabilized clays." *4th Conference on Soil Mechanics, Budapest*, 263-272.

Rao, S. M., & Shivananda, P. (2005). "Role of curing temperature in progress of lime-soil reactions." *Geotechnical and Geological Engineering*, 23, 79 –85.

Thompson, M. R. (1966). "Lime Reactivity of Illinois Soils." *Journal of the Soil Mechanics and Foundations Division, ASCE*, 92(SM5).

Thompson M.R. (1968). "Lime stabilization of soils for highway purposes." *Final Summary Rep. civil Engineering Series26, Illinois Cooperative Highway Program.* University of Illinois, Urbana,24.

Utilization of Shredded Rubber Tires for Cement-Stabilized Soft Clays

Mohamed A. Shahin[1] and Liao S. Hong[2]

[1]Senior Lecturer, Department of Civil Engineering, Curtin University of Technology, GPO Box U1987, Perth Western Australia 6845, Australia; m.shahin@curtin.edu.au
[2]Graduate Student, Department of Civil Engineering, Curtin University of Technology, GPO Box U1987, Perth Western Australia 6845, Australia

ABSTRACT: Tire-soil mixtures can be used as good construction materials in many geotechnical engineering applications such as pavement foundations, lightweight fill in road embankments and lightweight backfill behind retaining walls. This paper describes research undertaken to investigate experimentally the impact of shredded rubber tires as reinforcing material on the mechanical properties of cement-stabilized soft clay, in terms of strength and stiffness. A series of laboratory experiments are carried out on cement-stabilized clay mixed with several portions of shredded rubber tires of sizes 440 μm and 4 mm. The tests conducted include compaction, unconfined compression strength and indirect tensile strength. The results demonstrate that the use of shredded rubber tires has a potential in enhancing the ductility of cement-stabilized soft clay but decreases stiffness and ultimate resistance.

INTRODUCTION

The re-use of waste materials is a primitive step in creating a sustainable future, and due to increasing waste disposal cost, the re-use of waste and recycled materials is increasing worldwide and becoming more popular in civil engineering (Edincliler et al. 2004). The literature indicates that the addition of recycled car tires in the form of tire shreds or chips to soil enhances the engineering properties of the mixture. Research into soil-tire mixtures (e.g. Hataf and Rahimi 2006; Madesic et al. 2009; Zornberg et al. 2004) indicates that adding an adequate amount of tire chips/shreds to sand can generally improve the shear strength characteristics of the mixture, even though compressibility increases. However, full understanding of the engineering behavior of these materials is essential so that they can be used safely in civil engineering applications. In Australia, 20 million used car tires are disposed annually, causing fire and environmental health hazard problems. This urges the need for an alternative, environmentally friendly way of tire disposal. The study presented in this paper is part of an ongoing research to provide good means of consuming the millions of scrap tires that are generated annually in Australia so as to save the available land

that would otherwise be taken for stockpiling of used tires. The study also aims to allow construction over poor quality soils (such as soft clay) by solving the technical problems associated with the instability of constructing over such unstable soils and thus reducing quarrying of the natural resources.

Soft clay is a problematic soil that exhibits low bearing capacity and high compressibility under loading and thus, chemical stabilization by the addition of lime or cement is commonly used to improve the geotechnical properties of soft clay. However, while lime-cement treatment enhances the compressibility and shear strength of soft clay, it decreases the ductility of treated soil, leading to brittle material behavior. In order to improve the ductility of chemically stabilized soils, conventional geosynthetics (e.g. strips, geotextile, geogrid, etc.) are usually used as soil reinforcement. More recently, randomly distributed fibers are also used (e.g. Shahin and Harris 2010), which have found to provide more advantages over conventional geosynthetics in terms of workability and simplicity of adding and mixing the fibers with soil. The aim of the current work is to investigate the effects of shredded rubber tires in enhancing the engineering characteristics of cement-stabilized soft clay, especially ductility.

MATERIAL TESTED

The clay used in this study has a specific gravity of 2.6, liquid limit of 51% and plastic limit of 28%. It is classified as CH by the Unified Soil Classification System (USCS). The clay was stabilized with 15% (by weight of dry soil) of general purpose ordinary Portland cement. Two different sizes of shredded rubber tires, i.e. tire powder of 440 μm and tire grains of 4 mm, are added to cement-stabilized clay at 1%, 4% and 7% (by weight of dry soil). The shredded tires are by-products of used vehicle tires that are manufactured by a local company where a series of tire shredders and magnets are used to produce a clean and consistent grade of rubber crumb. The shredded tires have a specific gravity of 1.1, which is lower than the typical values of 2-3 for most materials. Figure 1 shows photographs of the tire grains and powder used.

FIG. 1. Photographs showing the grain (left) and tire powder (right) used.

TESTING PROGRAM AND RESULTS

Sample preparation

As mentioned previously, the clay soil specimens used in this study were stabilized with 15% (by weight of dry soil) of cement and three different amounts by weight of dry soil (i.e. 1%, 4% and 7%) of tire grains and powder. A series of compaction Proctor tests were carried out on all test specimens in accordance with the Australian Standards AS 1289 (2007), and the respective maximum dry densities and optimum moisture contents were obtained. In preparation of all specimens for compressive and tensile strength tests, the sample components were mixed using Hobart mixer with the dough mixing attachment. Specimens were mixed for approximately five minutes or until the water was evenly mixed throughout, and the specimens were cured in a curing room for 7 days at a constant temperature of 35°C.

Unconfined compression tests

The compressive strength characteristics of the specimens used were obtained through a series of unconfined compression strength (UCS) tests that were conducted on samples of 38 mm in diameter and 76 mm high. All specimens were prepared at a constant level of compaction of at least 95% of that achieved by the standard compaction Proctor tests. The UCS tests were strain controlled with axial loads applied at a rate of 0.6 mm/min, and the stress-strain curves obtained are shown in Figures 2 and 3 for clay stabilized with 15% cement and 440 μm tire powder or 4 mm tire grains.

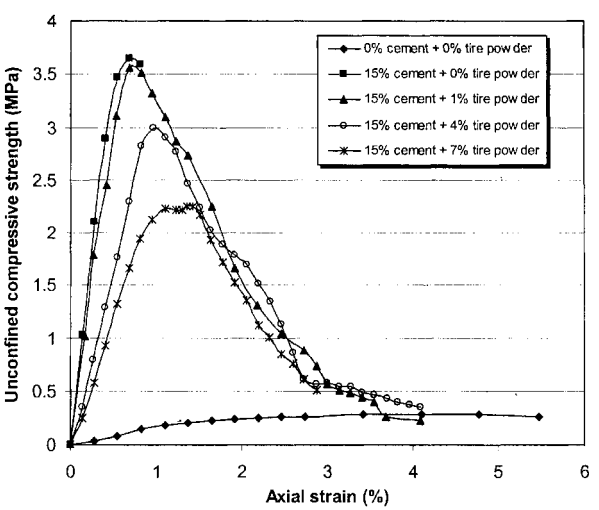

FIG. 2. Results of unconfined compression tests of cement-stabilized soft clay with 440 μm tire powder.

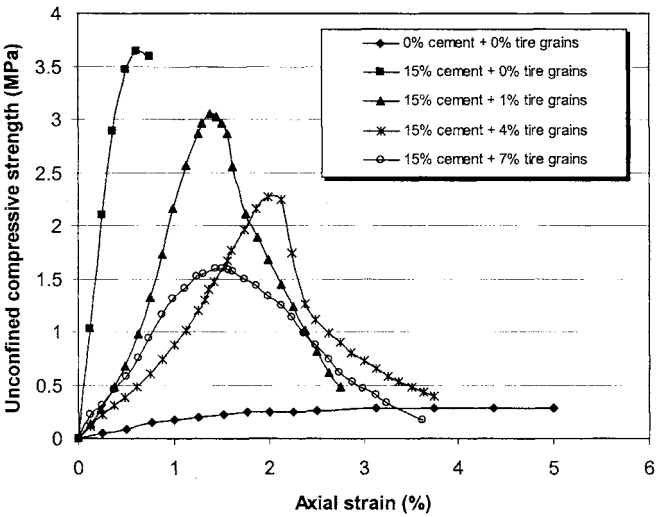

FIG. 3. Results of unconfined compression tests of cement-stabilized soft clay with 4 mm tire grains.

It can be seen from Figures 2 and 3 that the addition of cement alone significantly increases the ultimate strength and stiffness (modulus of elasticity) of clay soil, and decreases the deformation at failure. However, it can also be seen that the addition of cement alone exhibits brittle failure with significant loss of post-peak shear strength. On the other hand, it is shown that the addition of shredded rubber tires to cement-stabilized clay increases soil ductility regardless of the amount of shredded tires added. This is attributed to the reinforcement impact of shredded tires, which enhance soil ability to restrain cracking.

Figures 2 and 3 also show that stiffness and ultimate compressive strength of cement-stabilized clay seems to decrease by the addition of shredded tires. This is because shredded rubber tires carry small amount of load due to their low elastic modulus relative to the surrounding stabilized soil, leading to reduction in the compressive strength and stiffness of the soil matrix. By comparing the results of Figures 2 and 3, it can also be seen that cement-stabilized clay with tire grains seems to be more prone to the reduction in compressive strength than that of cement-stabilized clay with tire powder. For example, the ultimate compressive strength of cement-stabilized clay is decreased by 3% when 1% tire powder was used, whereas the compressive strength of cement-stabilized clay is decreased by 20% when 1% tire grains were added. This may be attributed to the fact that larger tire sizes create larger weak planes in certain areas in soil matrix due to the loss of bonding between tire grains and surrounding stabilized soil, leading to the development of failure paths when load is applied. This phenomenon was also recognized by Turatsinze et al. (2005) who studied the micrograph of bonding between cement paste and rubber

shreds. Based on the above results, it is recommended that 1% tire powder is added to cement-stabilized clay so that the detrimental impact of shredded tire in terms of compressive strength and stiffness is reduced to minimal while keeping better ductility.

Tensile strength tests

Based on the results obtained earlier from the compressive strength tests, it was decided to conduct the indirect tensile strength test only at 1% tire powder. The results of the test are shown in Figure 4, which clearly indicate that the tensile strength of soft clay is significantly increased by the addition of cement. However, it is also obviously shown that the tensile behavior of cement-stabilized clay exhibits brittle failure. As shown in Figure 4, the addition of 1% tire powder significantly enhances the ductility of cement-stabilized clay, even though ultimate tensile strength decreases. Again, this is attributed to the reinforcement impact of rubber tires in increasing the ability of cement-stabilized clay to restrain cracking. It can also be seen from Figure 4 that, on the contrary to the compressive strength tests, the addition of rubber tire to cement-stabilized clay does not reduce the tensile strength modulus of elasticity.

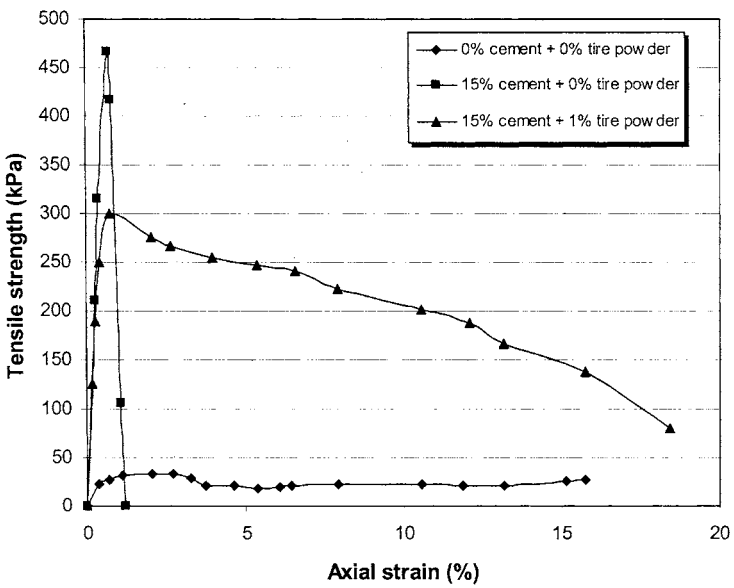

FIG. 4. Results of indirect tensile strength test of cement-stabilized soft clay with 440 μm tire powder.

SUMMARY AND CONCLUSIONS

A series of laboratory tests were conducted to investigate the effects of shredded rubber tires on the strength and stiffness of cement-stabilized soft clay. The tests conducted include the unconfined compression strength and indirect tensile strength. Cement was added by an amount of 15% (by weight of dry soil) and two different sizes of shredded tires, i.e. 440 μm tire powder and 4 mm tire grains, were added in order of 1%, 4% and 7% by weight of dry soil. All experiments were carried out after curing time of 7 days. The study has yielded the following conclusions:

1. The addition of shredded tires increases the compressive strength ductility of cement-stabilized clay regardless of the amount of tire added, but seems to decrease the ultimate compressive strength and compressive modulus of elasticity.
2. The addition of 1% tire powder (by weight of dry soil) seems to reduce the detrimental impact of shredded tires in decreasing the compressive strength and stiffness of cement-stabilized clay, while keeping better ductility.
3. The addition of 1% tire powder increases the tensile strength ductility of cement-stabilized clay and seems not to decrease the tensile strength modulus of elasticity, even though it decreases the ultimate tensile strength.

ACKNOWLEDGEMENT

The authors would like to thank Sim Tire Cycle Pty Ltd. (Melbourne, Australia) for providing the tire grains and powder used in this work.

REFERENCES

Australian Standards AS 1289 (2007). *Method of testing soils for engineering purposes.*

Edincliler, A., Baykal, G., and Dengili, K. (2004). "Determination of static and dynamic behavior of recycled materials for highways." *Resources Conservation and Recycling*, 42, 223-237.

Hataf, N., and Rahimi, N. (2006). "Experimental investigation of bearing capacity of sand reinforced with randomly distributed tire shreds." *Construction and Building Materials*, 20(10), 910-916.

Madesic, T., Shahin, M. A., and Nikraz, H. R. (2009). "Geotechnical properties of red sand mixed with tire grains and powder." *17th International Conference on Soil Mechanics and Geotechnical Engineering*, Alexandria, Egypt, 348-351.

Shahin, M. A., and Harris, L. (2010). "Use of fiber for improving engineering characteristics of cement-stabilized soft clays." *9th International Conference on Geosynthetics*, Brazil, in press.

Turatsinze, A., Bonnet, S., and Granju, J. L. (2005). "Mechanical characterization of cement-based mortar incorporating rubber aggregates from recycled worn tyres." *Building and Environment*, 40, 221-226.

Zornberg, J. G., Cabral, A. R., and Viratjandr, C. (2004). "Behavior of tire shred-sand mixtures." *Canadian Geotechnical Journal*, 41(2), 227-241.

Analysis on Load Transfer for Single Pile Composite Foundation Under Embankments Based on Elastic Theory

Xiao Ming Lou [1], Geng Bo Jiang [2], Hong Yue Xu[3]

[1] Department of Geotechnical Engineering, Tongji University, 1239 Siping Road, Shanghai 200092, People's Republic of China; PH (86-21)6598-3386; email: louhanliang45502@vip.sina.com.cn

[2] Guangzhou City Construction Project Management Co.Ltd, 181 Ti Yu Xi Heng Street, Guangzhou 510620, People's Republic of China; email: hnjgb@126.com

[3] Shanghai Urban Construction Design & Research Institute, 3447 Dongfang Road, Shanghai 200125, People's Republic of China; email: xhy1000@sohu.com

Abstract

A method to analyzing load transfer characteristics is presented for single pile composite foundation under embankment by means of elastic theory coupling with load transfer method. The pile and its above fill can be taken as a column with varied section area. The settlement of soil adjacent to pile caused by frictional resistance is calculated by Mindlin solution, and that induced by the filling load on the ground surface is calculated by Boussinesq solution. Non-linear springs are taken into consideration to simulate the character of pile-soil contact surface. A simplified calculation model for single pile composite foundation under embankment is then established. The pile-soil-cap-embankment interaction can be considered conveniently in this method. The correctness of this method was validated by pile efficacy of model test. The distributions of axial force, frictional resistance and displacement of pile and soil are then compared with those of piles under large area embankment.

INTRODUCTION

Piled embankment can effectively limit the differential settlements, large lateral deformation, overall or local instability, so it is applied in worldwide highway on soft clay or widening of existing roads, as well as embankment adjacent the bridge abutment.

Many scholars have researched the mechanisms of composite foundation of piled embankment.

[1] Department of Geotechnical Engineering, Tongji University, 1239 Siping Road, Shanghai 200092, People's Republic of China; PH (86-21)6598-3386;
email: louhanliang45502@vip.sina.com.cn

[2] Guangzhou City Construction Project Management Co.Ltd, 181 Ti Yu Xi Heng Street, Guangzhou 510620, People's Republic of China; email: hnjgb@126.com

[3] Shanghai Urban Construction Design & Research Institute, 3447 Dongfang Road, Shanghai 200125, People's Republic of China; email: xhy1000@sohu.com

Low (1993), Hewlett (1988), Han (2002) and Chen (2004) have researched the soil arching effect separately through model test, numerical or theoretical analysis. Xu (2005) and Chen (2005) build an approximately closed solution of pile axial force, displacement of pile and soil by load transfer method, in which the load transfer function assumed idealized elastic-plastic model, soil uniform, pile efficacy pre-calculated by approximate method. The distribution of negative friction was also discussed. Lou (2009) presented a more effective method for analyzing the interaction of pile-soil-embankment, where the pile and its above fill, the soil adjacent to pile and its above fill were both taken into as a column. Each column was analyzed one-dimensionally by load transfer method, in which the load transfer function can assumed non-linear model, soil layered, pile efficacy calculated during analyzing.

For all these studies, only the center piles and its surrounding soil under large area embankment were considered, but not the difference between the center piles and corner or edge piles, because of its inherent disregard for the continuity of the soil mass. It is necessary to establish an analytical model based on elastic theory as Poulos 1980) to analyze the settlement of single or group piles.

The main difficulty for analysis of piled embankment is the unknown proportion of vertical load carried by the pile or cap. Based on the research of Lou (2009), the embankment fill are also separated into two parts in this study, the fill above the pile (inside fill) and the fill above the soil (outside fill). The pile and the inside fill are taken into a column, simulated by one dimension compression member, as well as the outside fill. The settlement of soil surrounding pile caused by frictional resistance is calculated by Mindlin solution, and that caused by the load of outside fill is calculated by Boussinesq solution. Springs are taken into consideration to simulate the character of pile-soil interface. A simplified calculation model for single pile composite foundation under embankment is then established, which can take into account the pile efficacy, frictional resistance, and displacement.

ANALYTICAL METHOD

Fundamental assumption. To simplify the analysis, piles are arranged in square, and the fill is considered as having an equivalent domain treated by single pile, with the height of fill assumed to be same. At the pile head elevation, the total load carried by the pile and its surrounding soil is equal to the weight of the fill. The fill and piles are isotropic elastic medium. There are interaction between pile and soil, inside fill and outside fill, as shown in Figure 1. At the same elevation, the settlement of inside fill is considered to be equal, as well as outside fill.

The frictional resistance between pile and soil, inside and outside fill, and the tip resistance of pile are all simulated by springs with the nonlinear or elastic-plastic load transfer model. The elements of pile and springs are shown in Figure 2.

The load carried by pile is transferred into surrounding soil through frictional resistance. The settlement of soil adjacent to pile caused by frictional and tip resistance is calculated by Mindlin solution, and that caused by the load of fill between piled caps is calculated by Boussinesq solution, as shown in Figure 3.

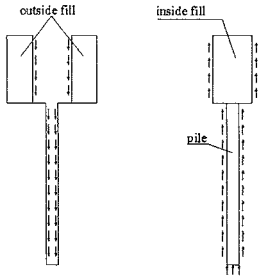

Figure 1. Assumption of pile-soil stress

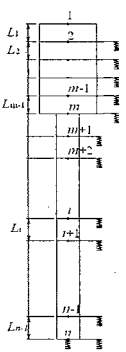

Figure 2. Pile element and spring surface

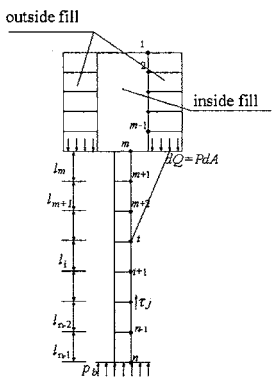

Figure 3. Settlement calculation of soil surrounding pile

Basic equation. The pile and the upper fill on the cap are divided into a series of elements as a generalized pile, The number of node of upper fill is m, and that of pile is u. The total number of node is n, while the element is n-1.

The equations of the pile axial force and settlement can be expressed as follows:

$$\left[K_p\right]\left\{s_p\right\} = \left\{Q_p\right\} - \left\{R\right\} \tag{1}$$

Where $[K_p]$=total stiffness matrix of generalized pile, including pile and its above fill, n×n.

$\{s_p\}$= vector of displacement of all nodes of generalized pile, n×1,

$\{s_p\} = \{\{s_p\}_1 , \{s_p\}_2\}$, while:

$\{s_p\}_1 = \{s_{p1} , s_{p2} , \cdots , s_{pm-1} , s_{pm}\}^T$,

$\{s_p\}_2 = \{s_{pm+1}\ ,\ s_{pm+2}\ ,\ \cdots\ ,\ s_{pn-1}\ ,\ s_{pn}\}^T$

$\{Q_p\}$= vector of load carried by generalized pile, which is the weight of fill above the pile, $n \times 1, \{Q_p\} = \{Q_{p1}\ ,\ Q_{p2}\ ,\ \cdots\ ,\ Q_{pm}\ ,\ 0\ ,\ \cdots\ ,\ 0\}^T$.

$\{R\}$=vector of frictional resistance of generalized pile, n×1. $\{R\} = \{\{R\}_1\ ,\ \{R\}_2\}$,

and: $\{R\}_1=\{R_1\ ,\ R_2\ ,\ ,\ \cdots\ ,\ R_{m-1}\ ,\ R_m\}^T, \{R\}_2 = \{R_{m+1}\ ,\ R_{m+2}\ ,\ ,\ \cdots\ ,\ R_{n-1}\ ,\ R_n\}^T$.

The outside fill is simulated by one dimension compression member, and the equation of the axial force and displacement can also be expressed as follows:

$$[K_s]\{s_s\}_1 = \{Q_s\}_0 + \{R\}_1 \tag{2}$$

Where $[K_s]$=total stiffness matrix of outside fill, m×m.

$\{s_s\}_1$= vector of displacement; $\{s_s\}_1 = \{s_{s1}\ ,\ s_{s2}\ ,\ \cdots\ ,\ s_{sm}\}^T$.

$\{Q_s\}_0$=vector of load carried by outside fill, which is the deadweight of outside fill, $\{Q_s\}_0 = \{Q_{s1}\ ,\ Q_{s2}\ ,\ \cdots\ ,\ Q_{sm}\}^T$.

$\{R\}_1$= the frictional resistance between inside fill and outside fill, m×1,

$\{R\}_1 = \{R_1\ ,\ R_2\ ,\ \cdots\ ,\ R_m\}^T$.

The settlement of soil surrounding pile is composed of two parts, and one part caused by frictional resistance can be calculated by Mindlin solution, another caused by the load of outside fill can be calculated by Boussinesq solution.

The settlement caused by frictional resistance can be shown as:

$$\{s_s\}_{2M} = [I_s]\{R\}_2 \tag{3}$$

Where $\{s_s\}_{2M}$ =settlement of an arbitrary point in the soil surrounding pile caused by frictional and tip resistance, $\{s_s\}_{2M} = \{s_{sm+1}\ ,\ s_{sm+2}\ ,\ \cdots\ ,\ s_{sn-1}\ ,\ s_{sn}\}^T$.

$[I_s]$=flexibility matrix of settlement calculated by Mindlin integral formula, u×u.

$\{R\}_2$=column vector of frictional resistance, u×1, $\{R\}_2 = \{R_{m+1}\ ,\ R_{m+2}\ ,\ \cdots\ ,\ R_{n-1}\ ,\ R_n\}^T$.

The settlement of soil surrounding pile caused by outside fill can be shown as:

$$\{s_s\}_{2B} = [B_s]\{P\} \tag{4}$$

Where

$\{s_s\}_{2B}$ =settlement of an arbitrary point in the soil surrounding pile caused by the weight of outside fill, and the column vector form is the same as that of $\{s_s\}_{2M}$.

$[B_s]$=flexibility matrix of settlement of soil element surrounding pile, which is calculated by

Boussinesq solution, u×m. The settlement is caused by the deadweight of outer fill column and the frictional resistance between inside and outside fill.

$\{P\}$=the sum load of deadweight of outside fill and the frictional resistance at the pile head elevation, and in order to express the equation conveniently, it can be shown as the form of column vector, $\{P\} = (\{Q_s\}_0+\{R\}_1)^T$.

Combining Eq.(3) and (4), the settlement of soil surrounding pile can be given by

$$\{s_s\}_2 = \{s_s\}_{2M} + \{s_s\}_{2B} = [I_s]\{R\}_2 + [B_s](\{Q_s\}_0 + \{R\}_1) \tag{5}$$

Where $\{s_s\}_2$=the total vector of settlement adjacent to pile,

$$\{s_s\}_2 = \{s_{sm+1}\ ,\ s_{sm+2}\ ,\ \cdots\ ,\ s_{sn-1}\ ,\ s_{sn}\}^T.$$

Combining Eqs.(2) and (5), the equations of settlement can be shown as

$$\begin{bmatrix}[K_s] & 0\\ 0 & [E_2]\end{bmatrix}\{s_s\} = \begin{bmatrix}[E_1] & 0\\ [B_s] & 0\end{bmatrix}\{Q_s\} + \begin{bmatrix}[E_1] & 0\\ [B_s] & [I_s]\end{bmatrix}\{R\} \tag{6}$$

Where $[E_1]$=unit matrix, m×m; $[E_2]$=unit matrix, u×u.

$\{Q_s\}$=column vector, n×1, $\{Q_s\} = \{\{Q_s\}_0\ ,\ 0\ ,\ 0\ ,\ \cdots\ ,\ 0\ ,\ 0\}^T$.

$\{s_s\}$=total column vector of settlement, n×1, $\{s_s\} = \{\{s_s\}_1\ ,\ \{s_s\}_2\}^T$.

The calculation of frictional resistance. The frictional resistance between generalized pile and soil (including outside fill) can be calculated through the relative settlement:

$$\{R\} = [K_w]\{w\} \tag{7}$$

Where

$[K_w]$= stiffness matrix of interaction between generalized pile and soil, calculated by load transfer function, n×n.

$\{w\}$=relative settlement between generalized pile and soil,

$$\{w\} = \{s_p\} - \{s_s\} \tag{8}$$

The last equations. Substituting Eq.(7) and (8) into Eq.(1), the matrix equation of generalized pile can be obtained.

$$([K_P] + [K_w])\{s_p\} = \{Q_p\} + [K_w]\{s_s\} \tag{9}$$

Substituting Eq.(7) and (8) into Eq.(6), the settlement matrix equation of outside fill and the elastic half-space ground is expressed as follows:

$$([K_{sf}] + [BI][K_w])\{s_s\} = [EB]\{Q_s\} + [BI][K_w]\{s_p\} \tag{10}$$

Where $[K_{sf}] = \begin{bmatrix}[K_s] & 0\\ 0 & [E_2]\end{bmatrix}$, $[BI] = \begin{bmatrix}[E_1] & 0\\ [B_s] & [I_s]\end{bmatrix}$, $[EB] = \begin{bmatrix}[E_1] & 0\\ [B_s] & 0\end{bmatrix}$.

Solution of the equations and load transfer function. Iterative method is used to solve equations (9) and (10). The solving procedure is same as the depiction by Lou (2009).

The characteristic of pile-soil interface can be simulated by general load transfer function, such as the linear elastic-plastic model, exponential cuve model, hyperbolic model and so on. It can also be referred to the paper by Lou (2009).

CASE STUDIES

Case 1. The model test by Xu (2004) is taken to carry out the contrastive analysis. Table 1 shows the parameters for the case.

Table1. Parameters for Control Case

Material	Parameters
Embankment fill	fine sand, h=0.45m, γ=15.6kN/m^3, compressive modulus=12MPa, φ_u=38°
Model pile	aluminum alloy pipe, diameter=32.3mm, length=9m, wall thickness=1.5mm, E_p=71.4GPa
Pile cap	square armor plate, 90mm×90mm×5mm
Foundation soil	fine sand, γ=15.6kN/m^3, compressive modulus=12MPa, frictional coefficient k=0.30, ultimate end bearing capacity=4000kPa

The efficacy of centre pile calculated under large area embankment is in agreement with that from model test, as shown in Figure 4. The efficacy of center pile is obviously bigger than that of corner pile, which means that the more influence of adjacent piles, the more settlement of soil, and the more embankment load carried by centre pile. Figure 4 also shows that the efficacy of single pile calculated here is a little less than the efficacy of corner pile measured in the model test, because the corner pile measured in the model test is still influenced by the adjacent piles, but the single pile is influenced by no pile. It also can be seen that the calculated pile efficacy decreases with pile spacing increasing, which is similar with that from the model test.

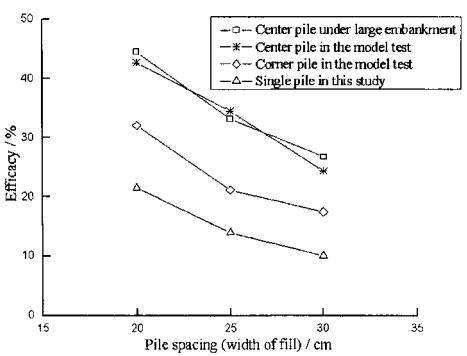

Figure 4. Comparison of pile efficacy

Case 2. In the literature by Lou (2009), the frictional resistance distribution and pile axial force of centre pile under large area embankment are analyzed through load transfer method. In order to contrast with the result in this paper, the same parameters are adopted, which are shown in Table 2. The difference is that the model of the soil adjacent to pile is assumed a half space instead of one dimensional compression column. For the two-layer soil in the Table 2, approximate treatment is referred to the book by Poulos (1980).

Table 2. Parameters for Control Case

Material	Parameters
Embankment fill	Height=4m, 2.5m×2.5m, γ=18kN/m^3, modulus of compressibility=15MPa, c=10kPa.
Pile	Diameter = 0.4m, length = 15m, E_p = 35GPa, pile spacing = 2.5m.
Pile cap	Square, 1m×1m.
First layer of soil	Thickness = 10m, γ = 18kN/m^3, compressive modulus = 3MPa, frictional coefficient k = 0.20, Ultimate frictional resistance=40kPa,relevant relative displacement=0.01m.
Second layer of soil	Thickness =10m,γ = 18kN/m^3, compressive modulus = 6MPa, frictional coefficient k = 0.30, ultimate frictional resistance = 60kPa, ultimate tip resistance = 1000kPa, relevant tip displacement=0.01m.

The main calculated results are shown in Table 3. The efficacy of single pile calculated by this method is obviously less than that of centre pile under large embankment. Because the dispersion of additional stress is not considered under the large area embankment, the compressive deformation of soil surrounding pile and the efficacy of center pile are both the maximum value, while the efficacy of single pile calculate in this study is the minimum value because of the dispersion of superimposed stress and the absent influence of adjacent piles. It also can be seen that the elevation of neutral point of single pile is higher than that of central pile under large embankment, because the different settlement between pile and soil decreases with the consideration of dispersion of additional stress.

Table 3. Main calculation results

	Pile efficacy (%)	Neutral point of pile z_0/L
Central pile under large embankment	69.80	0.50
Single pile under rectangular embankment	39.66	0.29

Figure 5 presents the profile of vertical stress in the outside fill. It can be observed that there is a critical height in the fill, upper which the vertical stress in the outside fill matches with that in the natural ground, while a reduction of the vertical stress in the outside fill exists instead of the

continuing increases in the natural ground in the lower part of fill, due to frictional resistance at inside and outside fill surface, as the arching effect of fill.

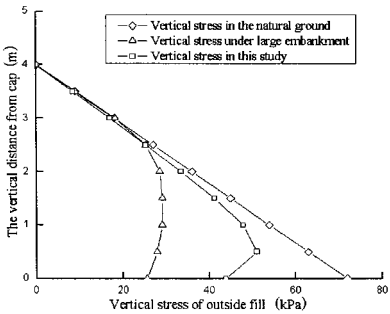

Figure 5. Vertical stress of outside fill

Figure 6 shows the axial force of pile from increasing to decreasing. It is noted in Figure7 that the frictional resistance is negative at the upper part of pile, and positive at the lower part of pile. The value of negative frictional resistance becomes larger with the increase of the width of fill. In addition, the axial force and frictional resistance of pile calculated in this study are both less than those of centre pile under large area embankment.

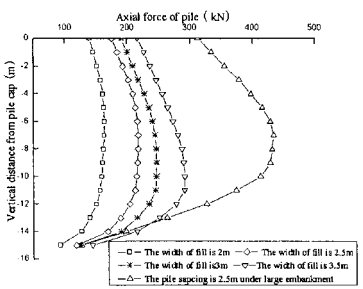

Figure 6. Axial force in pile body

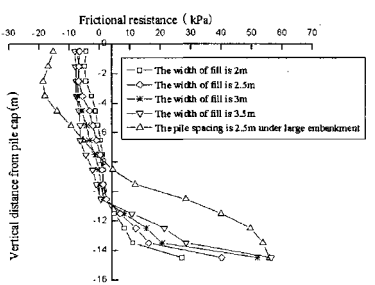

Figure 7. Frictional resistance distribution

As shown in Figure 8, the displacement of soil surrounding pile is more than that of pile at the upper part of pile, while less at the lower part of pile. The elevation of maximum axial force of pile lies where the frictional resistance is zero and the differential settlement is zero. It is also noted that the differential settlement is the maximum value at the pile head elevation or the pile tip elevation. The negative frictional resistance at the upper part of pile and the positive frictional resistance near the pile tip are both larger, which is different from distribution of frictional resistance in the general case.

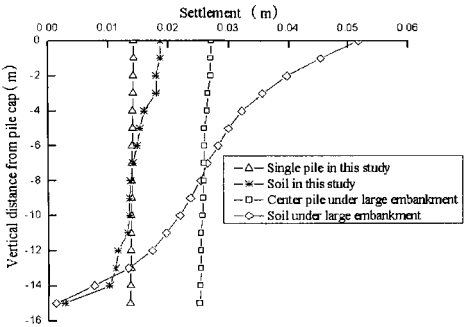

Figure 8. Displacement of pile and soil (width of fill is 2.5m)

Even though soil efficacy of single pile composite is larger than that of large area embankment, less differential settlement and less negative frictional resistance occurs in single pile because of stress dispersion effect.

CONCLUSIONS

This paper presents a study method for the characteristic of single pile composite foundation under embankment by means of elastic theory coupling with load transfer method, including the consideration of the pile-soil interface character, which can be convenient to analyze the pile efficacy and the distribution of pile axial force, frictional resistance and settlement.

The results of the study demonstrate that there are a neutral point in the pile and negative frictional resistance at the shaft of pile, due to the different settlement between pile and soil, and that there is a critical height of fill, upper which the vertical stress in the outside fill matches with that in the natural ground, and the different settlement shall be very small.

The pile efficacy of central pile under large area embankment is obviously larger than that of single pile, because of the influence of adjacent piles.

REFERENCES

Gong Xiao-nan.(2003).Design and construction guide of composite foundation. China Communications Press, Beijing. (in Chinese).

Low B K, Tang S K, Choa V. (1993). "Arching in piled embankments". Journal of Geotechnical Engineering, ASCE, 120(11): 1917–1938.

Hewllet W J, Randolph M F. (1988)."Analysis of piled embankments". Ground Engineering, 21(3):12–18.

Han J, Gabr M .A. (2002). "Numerical analysis of geosynthetic-reinforced and pile-supported earth platforms over soft soil". Journal of Geotechnical and Geoenvironmental Engineering, ASCE, 128(1) : 44–53.

Chen Yun-min. Jia Ning, Chen Ren-peng.(2004). "Soil arch analysis of pile-supported embankments". China Journal of Highway and Transport,, 17(4): 1–6. (in Chinese).

Xu Feng. (2004). Study on pile-supported embankments. Master thesis, Zhejiang University. (in Chinese).

Chen Ren-peng, Xu Feng, Chen Yun-min, Jia Ning. (2005). "Analysis of behavior for rigid pile-supported embankment in soft ground". China Journal of Highway and Transport,18 (3) :7–13. (in Chinese).

Lou Xiao-ming, Sun Xiao-feng, Chen Guang (2009). "Analysis on load transfer for caped pile under large area embankment". China Civil Engineering Journal.42 (2):98-104.

Poulos H G, Davis E H.(1980). "Pile foundation analysis and design". John Wiley and Sons, New York.

A Review of the Settlement of Stone Columns in Compressible Soils

Bryan A. McCabe[1] CEng MIEI and Derek Egan[2] CEng MICE

[1]Lecturer in Civil Engineering, School of Engineering and Informatics, National University of Ireland, Galway, Ireland. bryan.mccabe@nuigalway.ie
[2]Chief Engineer, Keller Foundations, Coventry, England. derek.egan@keller.co.uk

ABSTRACT: The behaviour of Vibro Replacement stone columns has yet to be captured fully by analytical or numerical means, and predicting stone column performance in soft cohesive soils brings specific challenges. In this paper, a new database of settlement improvement factors is developed, drawn from both published and unpublished data. The database illustrates that the improvement is generally predicted quite well by Priebe's (1995) basic improvement factor. Moreover, the extent of improvement reflects the construction method, with the preferred dry bottom feed system performing consistently better than other column construction systems.

INTRODUCTION

Vibro Replacement (VR) has emerged as one of the world's most widely used forms of ground improvement in cohesive soils, as solutions may be tailored to meet specific bearing capacity, settlement magnitude and rate requirements. Mounting pressure nowadays to develop 'marginal' sites has focussed attention on the potential of VR to offer technically and economically viable solutions in these deposits. There are many challenges specific to VR in fine soils. Stress changes and ground movement caused by both the formation of cavities by the poker and the subsequent construction of compacted columns are poorly understood (Egan *et al.*, 2008). The effect of clay sensitivity on stone column performance has not been widely researched, and to date there is no consensus on the extent to which stone columns arrest creep.

The most popular analytical settlement prediction method in European ground improvement practice (Priebe 1995) contains many simplifying assumptions and some empiricism in its formulation. Significant advances have been made in developing constitutive models for soft natural soils for use in conjunction with finite element software to incorporate characteristics such as creep, anisotropy, destructuration and bonding (i.e. Karstunen *et al.*, 2005, Leoni *et al.*, 2008). However, industry practitioners in ground improvement design do not routinely use these models and, in general, finite element approaches are currently limited by their inability to capture installation effects satisfactorily, especially the 3-D formulations.

In light of these uncertainties, it was beneficial to carry out a detailed review of stone column field settlement performance records. A new database of settlement improvement factors for soft cohesive deposits is presented and interpreted herein. The discussion considers the operational friction angle of the stone and the effect of the column construction method, and provides a useful reference for practitioners designing ground improvement schemes in compressible deposits.

STONE COLUMN CONSTRUCTION METHODS

A brief explanation of the main VR systems is given below, where the terms top-feed or bottom-feed describe the stone supply method, and wet or dry relates to the jetting medium. The appropriate choice of construction method and proper on-site implementation is paramount to the successful improvement of soft and very soft soils.

(i) *Dry top feed* is predominantly used for shallow to medium treatment depths of coarse and more competent cohesive deposits. The hole formed by the first penetration of the poker remains stable as the column is constructed. Controlled air flush is often used to aid construction and while commonly used for lightly-loaded to heavily-loaded developments, it is rarely suitable for use in soft cohesive soils.
(ii) *Wet top feed* is used for medium to deep treatment below the water table and treatment of softer cohesive deposits. In cohesive soils, water flush helps remove arisings from the void formed by the poker and maintain its stability. While wet top feed has been used with success in soft cohesive soils (i.e. Munfakh *et al.,* 1983), it is used less frequently nowadays due to difficulty in disposal of the flush arisings, so it is often reserved for larger-scale moderately-loaded to highly-loaded developments.
(iii) *Dry bottom feed* has now largely replaced the wet top feed method since its inception in the late 1970s and is principally used for treatment of water-bearing and soft cohesive deposits. Controlled air flush is used to aid construction and maintain stability of the void formed by the vibrating poker. Now the preferred construction technique in soft soils, there is compelling evidence (i.e. Wehr, 2006) that the dry bottom feed method can successfully treat ground having c_u values well below the 15-20 kPa frequently quoted as the lower practical limit of the system's applicability.
(iv) Alternative construction methods have been used; De Cock and d'Hoore (1994) describe *bottom rammed* columns, which have evolved from the classic Franki pile. A tube is bottom-driven to the required depth. As it is withdrawn, successive charges of stone are introduced and progressively forced into the surrounding soil by intensive ramming. This method is neither practical nor economical for soft soils.

SETTLEMENT IMPROVEMENT DATABASE

Absolute and differential settlement criteria normally govern the design of stone columns in compressible soils. The authors have compiled a new database with settlement information from over 20 case histories in cohesive or predominantly cohesive soils. While the majority of these cases relate to loading of areas that are wide in relation to the stone column length (subsequently referred to as widespread

loading), three of the cases relate to footings supported by small column groups.

A settlement improvement factor (n) is used to quantity the degree of treatment, and is defined as:

$$n = \frac{s_{untreated}}{s_{treated}} \quad [1]$$

where $s_{treated}$ and $s_{untreated}$ are the settlements with and without stone columns respectively for a particular loaded zone. The database necessarily comprises two categories of data, distinguished as follows:

(i) Cases where $s_{treated}$ and a reference value of $s_{untreated}$ have both been measured, so the value of n is entirely measurement-based (Table 1).

(ii) Cases where $s_{treated}$ values have been measured; however $s_{untreated}$ values have not been measured but instead predicted either analytically or from experience of measurements in local of similar ground conditions (Table 2). The values of $s_{untreated}$ used in this paper are those quoted/inferred in the original references.

Priebe (1995) uses the area replacement ratio r =A_c/A to capture the proportion of ground replaced by stone in an infinite array; A_c is the area of one column and A is the plan area of the 'unit cell' attributed to a single column. The value of r may be deduced from the column diameter (D) and spacing (s) according to:

$$r = \frac{A_c}{A} = k\left(\frac{D}{s}\right)^2 \quad [2]$$

Table 1. Case histories in which $s_{untreated}$ and $s_{treated}$ were measured

Reference and Site Location	Material Treated	Avg. Treatment Depth (m)	Treatment Configuration	Treatment Method	Loading Type	Area Replacement Ratio, r	Settlement Impr. Factor, n
Watts *et al.* (2000) Lancashire, U.K.	clay, ash fill	3.50	L	DTF	test strip	0.209	1.47
Greenwood (1970) Bremerhaven, Germany	clay, peat	6.0	TR	WTF	emb.	0.260	1.63
Munfakh et al. (1983) New Orleans, U.S.A.	clay	≈20	TR	WTF	emb.	0.253	1.70
Cooper and Rose (1999) Bristol, U.K.	clay	4.35	TR	BF	emb.	0.075	1.85
		4.35	TR	BF	emb.	0.146	2.55

Legend: L=linear, TR = triangular, DTF = dry top feed, WTF= wet top feed, BF = bottom feed, emb. = embankment

Table 2. Case histories with measured $s_{treated}$ but predicted $s_{untreated}$

Reference and Site Location	Material Treated	Avg. Treatment Depth (m)	Treatment Configuration	Treatment Method	Loading Type	Area Replacement Ratio, r	Settlement Impr. Factor, n
Venmans (1998) Holendrecht-Abcoude, Netherlands	clay	5.2	TR	BF	emb.	0.170	1.67
Greenwood (1991) Canvey Island, U.K.	clay/ silt	10.0	TR	WTF	stg. tank	0.221	2.38
Raju *et al.* (2004) Kajang, Malaysia	silt, fill	13.5	SQ	WTF +BF	emb.	0.240	2.60
De Cock and D'hoore (1994) Antwerp, Belgium	peaty clay	8.5	TR	BR	stg. tank	0.287	3.0
Oreye, Belgium	silt	11.0	TR	BR	stg. tank	0.227	1.83
Baumann and Bauer (1974) Konstanz, Germany	silt	5.5	TR	WTF	raft	0.472	4.03
Watt *et al.* (1974) Teesport 104, U.K.	silt	6.1	TR	WTF	stg. tank	0.296	2.80
Teesport 165, U.K.	silt	6.1	TR	WTF	stg. tank	0.296	3.43
Hedon, U.K.	clay	6.7	TR	WTF	stg. tank	0.269	2.77
Greenwood (1974) Stanlow, U.K.				WTF	stg. tank	0.309	5.47
Raju (1997) Kinrara, Malaysia	silt, fill	17.0	SQ	BF	emb.	0.350	4.0
Kebun, Malaysia	clay	15.0	SQ	BF	emb.	0.196	2.5
Bell (1993) Stockton, U.K.	clay	4.4	TR	WTF	emb.	0.086	1.38
						0.055	1.24
						0.038	1.15
Kirsch (1979) Essen, Germany	silt	5.0	STQ	WTF	stg. tank	0.345	2.35
Kirsch (unpublished) Berlin-B'burg B, Germany	clay/ silt	7.1	SQ	BF	pad	0.070	1.94
Berlin-B'burg C, Germany	clay/ silt	6.8	SQ	BF	pad	0.130	2.1
Keller Foundations (unpubl.) Contract 'B', Scotland	clay	5.5	L	BF	test strip	0.226	1.2
Goughnour and Bayuk (1979) Hampton, U.S.A.	silt, clay	6.4	TR	WTF	emb.	0.339	2.4

Legend: TR = triangular, SQ=square, STQ = staggered square, L=linear, WTF= wet top feed, BF = bottom feed, BR = bottom rammed, emb. = embankment, stg. tank = storage tank.

where k is $\pi/4$ and $\pi/2\sqrt{3}$ for square and triangular column grids respectively. Values of r are also given in Tables 1 and 2, with A_c either measured directly or deduced from stone consumption records. Values of n (Tables 1 and 2) are plotted against r in Figure 1 for the widespread loading cases. In order to provide a frame of reference for the data, Figure 1 also includes Priebe's (1995) basic improvement factor n_0 predictions (eqn 3; assuming Poisson's ratio of the soil ν_s=0.33 as is customary) adopting three different operational friction angles of ϕ'=35^0, ϕ'=40^0 and ϕ'=45^0 for the stone.

$$n_0 = 1 + r\left[\frac{5-r}{4(1-r)\tan^2(45-\frac{\phi'}{2})} - 1\right] \qquad [3]$$

Case-specific values of ϕ' are generally not presented in the literature. Herle *et al.* (2008) advise that $\phi' \approx 40^0$ is conventionally adopted used in European design practice, and this would be especially true for soft soils. Additional parameters needed for predicting Priebe's (1995) n_1 and n_2 factors (amendments to n_0 to account for column compressibility and soil and column unit weights respectively) are not available.

Predicted values of n (n_{pred}) are plotted against measured (n_{meas}) values in Figure 2. Tests plotting below the $n_{pred} = n_{meas}$ line denote measurements which exceed predictions. Much of the data in Figure 2 is taken from Figure 1 (i.e. n_{pred} is n_0 based on $\phi'=40^0$). However, Figure 5 also incorporates data from two test strips (Watts *et al.*, 2001 and Keller Foundations Contract B, unpublished) and two pad footings (Kirsch, unpublished). The Priebe (1995) correction was applied to n_{pred} for the strips to allow for the reduced efficiency of small groups. No such correction was applied for the pads as the loaded columns underneath the footings were surrounded by 'buttressing' columns, so 'unit cell' conditions were assumed for the loaded columns. In Figure 2, Table 1 (true n measurements, filled symbols) and Table 2 data (open symbols) are differentiated, and the different systems used to construct the columns are highlighted.

DISCUSSION

Although some scatter is evident, eqn. [3] with $\phi'=40^0$ provides a good 'average' match to all the measured n-r data in Figure 1. This result is in spite of the fact that there is not enough resolution in the published data to take account of all of the factors that could have influenced the degree of settlement control. Although difficult to quantify, an experienced designer would need to account of the following:

(i) uncertainty in the 'as-constructed' column diameter and spacing
(ii) the time elapsed since loading at which n is measured is not consistent throughout all of the case studies. Due to the drainage effect of stone columns, primary settlement will occur at a faster rate for treated areas than for similarly loaded untreated areas. If the settlement of the untreated area is measured before primary settlement is complete, misleadingly low n values will be obtained.

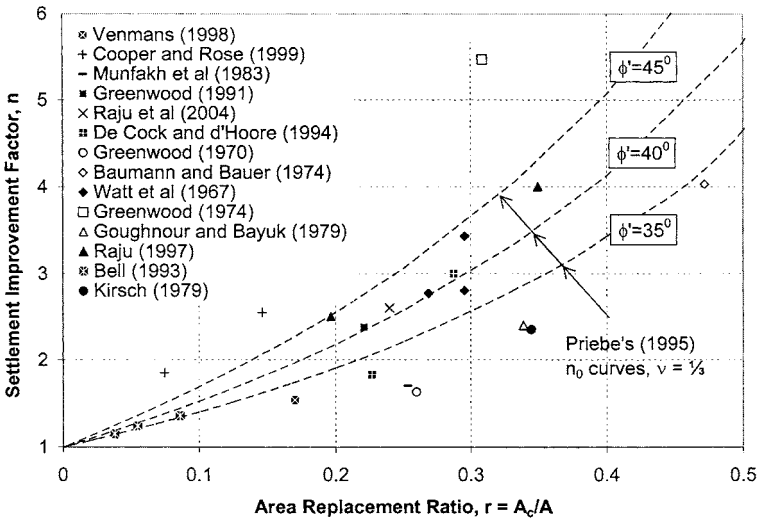

FIG. 1. Settlement improvement factor against area replacement ratio for sites with widespread loading

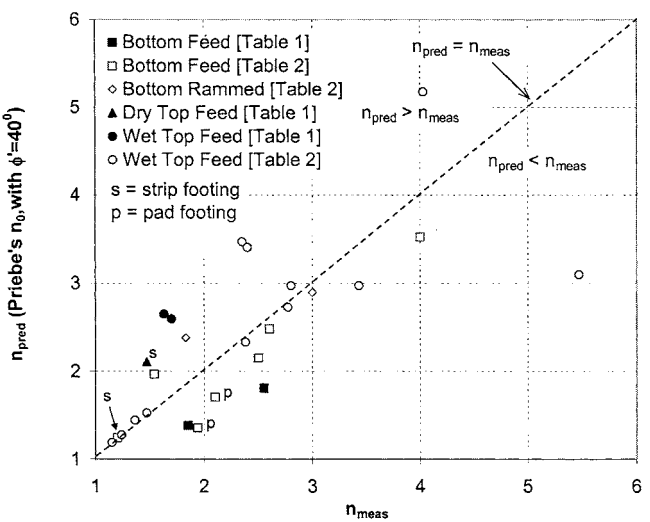

FIG. 2. Predicted versus measured settlement improvement factors (all sites: widespread loading and footings) distinguished by construction method

(iii) the relative contributions to surface settlement from compression over the depth of the treated zone and below the treated zone. It is rarely possible to separate the settlement solely arising from the treated zone in studies carried out on construction projects, hence in such situations the improvement attributed to the installation of the stone columns would probably be underestimated.
(iv) variations in the prediction methods used to determine the n values in Table 2.

Figure 2 implies that a design friction angle of $\phi'=40^0$ may not always give safe settlement predictions for the top feed system, but as already stated, there may be other possible variables besides the friction angle. For example, the deposits within the treatment zone at Bremerhaven (Greenwood, 1970) incorporated some peaty material.

Importantly, the higher n_{meas}/n_{pred} ratios in Figure 2 tend to relate to bottom feed projects, endorsing the use of this system for delivering consistent settlement improvement in soft ground conditions. In these cases, it appears appropriate to adopt a higher friction angle in the range $\phi'= 40\text{-}45^0$ in conjunction with Priebe (1995). Herle *et al.* (2008) advocate the use of higher ϕ' values (i.e. in excess of 50^0), but these are based on shear box tests carried out on stone at high relative density and not with soft soil in mind. Good design practice should consider the degree of stone compaction and the confining strength of the soil, best understood from rig instrumentation.

CONCLUSIONS

The Priebe (2005) design method with conventionally adopted friction angles of 40^0 provides a conservative estimate of the actual performance of the bottom feed system in practice. This method, which continues to be the favoured approach for leading stone column designers, is proved to be reliable even though it does not capture all of the fundamental soil and stress changes that take place during column construction and subsequent loading. More sophisticated approaches, such as finite element analysis, for example, provide another useful tool to geotechnical engineers, although they have not evolved to a stage of readiness for routine design.

The vast majority of published data pertains to large loaded areas and not to strip or pad footings. There remains a need for high quality instrumented field tests to improve our understanding of the factors controlling stone column settlement behaviour.

REFERENCES

Baumann, V. and Bauer, G.E.A. (1974) The performance of foundations on various soils stabilised by the vibro-compaction method, *Canadian Geotech. Jnl.*, Vol. 11, pp. 509-530.

Bell, A.L. (1993) Report on performance of vibro replacement ground improvement beneath embankment at Stockton, *Keller Internal Report*, 21pps.

Cooper, M.R. and Rose, A.N. (1999), Stone column support for an embankment on deep alluvial soils, *Proc. ICE Geotech. Engrg.*, Vol. 137, pp. 15-25.

De Cock, F. and D'Hoore, S. (1994), Deep Soil Improvement by Rammed Stone Columns – Two Case Histories for Large Diameter Storage Tanks, *Proc. 5th Int. Conf. on Deep Fdns.*, Bruges, pp. 5.21.1 – 5.21.9.

Egan, D., Scott, W. and McCabe, B.A. (2008) Installation effects of vibro replacement stone columns in soft clay, *Proc. 2nd Int. Workshop on the Geotechnics of Soft Soils, Focus on Ground Improvement*, Glasgow, pp. 23-29.

Goughnour, R.R. and Bayuk, A.A. (1979) A field study of long term settlements of loads supported by stone columns in soft ground, *C.R. Coll. Int. Renforcement des Sols*, Paris, pp. 279-285.

Greenwood, D.A. (1970) Mechanical improvements of soil below ground surface, *Proc. of Conf. on Ground Engrg.*, Vol. 2, pp. 11-22.

Greenwood, D.A. (1974), Differential settlement tolerances of cylindrical steel tanks for bulk liquid storage, *Conf. on settlement of structures,* Cambridge, pp. 361-367.

Greenwood, D.A. (1991) Load tests on stone columns, *Deep Foundations and Improvements, Design, Construction and Testing*, ASTM 1089, pp. 148-171.

Herle, I., Wehr, J. and Arnold, M. (2008) Soil improvement with vibrated stone columns – influence of pressure level and relative density on friction angle, *Proc. 2nd Int. Conf. on Geotechnics of Soft Soils – Focus on Ground Impr.*, pp. 235-240.

Karstunen, M., Krenn, H., Wheeler, S.J., Koskinen, M. and Zentar, R. (2005). The effect of anisotropy and destructuration on the behaviour of Murro test embankment, *ASCE Int. Jnl. of Geomechanics*, Vol. 5, No. 2, pp. 87-97.

Kirsch, F. (2008) Evaluation of ground improvement by groups of vibro stone columns using field measurements and numerical analysis. *2nd Int. Workshop on the Geotechnics of Soft Soils, Focus on Ground Improvement*, Glasgow, 241-248.

Kirsch, K. (1979) Erfahrungen mit der Baugrundverbesserung durch Tiefenruttler. *Geotechnik* 1, 21-32.

Leoni, M., Karstunen, M. and Vermeer, P. (2008) Anisotropic creep model for soft soils. *Géotechnique*, 58, No. 3, 215-226.

Munfakh, G.A., Sarkar, S.K., and Castelli, R.P. (1983) Performance of a test embankment founded on stone columns, *Proc. Int. Conf. on Advances in Piling and Ground Treatment for Foundations*, London, pp. 259-265.

Priebe, H.J. (1995), The Design of Vibro Replacement, *Ground Engineering*, December, pp. 31-37.

Raju, V.R. (1997) The behaviour of very soft soils improved by vibro-replacement, *Ground Imp. Conf.*, London, Technical paper 12-64E.

Raju, V.R., Yee, Y.W., Tam, E. and Sreenivas, P. (2004) Vibro replacement for the construction of a 15m high highway over a mining pond, *Malaysian Geotech. Conf.*, Kuala Lumpur, Technical paper 12-67E.

Venmans, A.A.J. (1998) Design, construction and lifetime behaviour on a highway widening on stone column improved ground, *Proc. of the Int. Symposium on Problematic Soils*, Tohoku, Japan, pp 105-108.

Watt, A.J., De Boer, J.J. and Greenwood, D.A. (1967) Load tests on structures founded on soft cohesive soils strengthed by compacted granular columns, *Proc. 3rd Asian Conf. on Soil Mech. and Fdn. Engrg*, Haifa, 1, pp. 248-251.

Watts, K.S., Chown, R.C., Serridge, C.J. and Crilly, M.S. (2001) Vibro stone columns in soft clay: a trial to study the influence of column installation on foundation performance, *Proc. 15th ICSMFE*, Vol. 3, pp. 1867-1870

Wehr, J. (2006) The undrained cohesion of the soil as criterion for the column installation with a depth vibrator, *Transvib 2006*, pp. 157-162.

Field Test and Numerical Analysis on Performance Upgrade of Existing Rockfall Protection Fence by using High Energy Absorption Net

Shinichiro Tsuji[1], Takashi Hara[1], Atsushi Yashima[1] and Masaki Yoshida[2]

[1]Department of Civil Engineering, Gifu University, 1-1, Yanagido, Gifu, 501-1193, Japan; s_tsuji@gifu-u.ac.jp
[2]Engineering Department, MAEDA KOSEN CO.,LTD., 38-3, Okinunome, Sakai, 919-0422, Japan; yoshida@mdk.co.jp

ABSTRACT: This paper proposes a new technique, which uses the high energy absorption net, to upgrade the performance of existing rockfall protection fence. The high energy absorption net is installed to mountain side of the existing rockfall protection fence in this technique. In order to confirm the applicability of the proposed technique, field tests and numerical analyses are carried out. This paper describes the detail of the proposed technique and the results of the field tests and the numerical analyses as well as the effectiveness of the high energy absorption net to upgrade the performance of the existing rockfall protection fence.

INTRODUCTION

A great number of rockfall protection fences that protect the road traffic in mountainous area from rockfall impacts have been constructed in Japan. However, there are many cases that a new stone with larger rockfall impact energy than the initial design one was found during the periodic site investigation, hence, many existing rockfall protection fences has not satisfied the performance requirements with respect to absorbing energy of rockfall impacts. Therefore, in order to upgrade the performance of existing rockfall protection fence, a new technique, which uses the high energy absorption net that consists of several members made from synthetic fiber, have been proposed by authors. In this technique, the high energy absorption net is installed to mountain side of the existing fence, and the effect of the rockfall impact to the existing fence can be reduced to smaller one than the initial design rockfall impact with absorbing the energy by high energy absorption net. A field test to confirm the effectiveness of the proposed technique was carried out in this study. This paper describes the detail of the field test and its numerical simulation as well as the effectiveness of the proposed technique to upgrade the performance of the existing rockfall protection fence.

CHARACTERISTICS OF HIGH ENERGY ABSORPTION NET

The structure of the high energy absorption net is illustrated in Figure 1. The net consists of several members made from synthetic fiber, which are knitted net, outer circumferential rope of the net, belt and rope arranged in a double cross. The prime characteristic point of the net is that the net can absorb the large energy of rockfall impacts from its high deformable ability. On the other hand, the characteristic point of the synthetic fiber that is susceptible to the ultraviolet is concerned though, the ability of the synthetic fiber treated anti-ultraviolet shielding, which the net can possess 70% tensile strength after 25 years passed, has been confirmed from a series of accelerated weathering test.

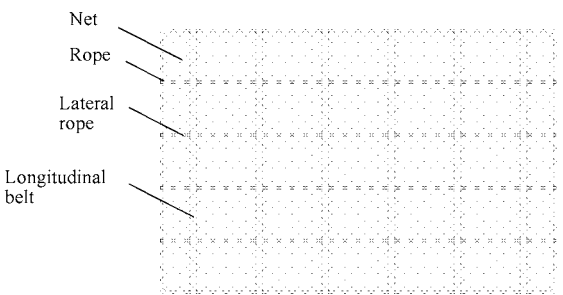

FIG. 1. High energy absorption net.

In order to study the modeling of deformation characteristics of the high energy absorption net for FEM analysis, a field test was carried out previously. Figure 2 shows the summary of the test, where the high energy absorption net was adopted as a member of an independent rockfall protection net. In this test, the target absorptive rockfall energy of the net is 150kJ. According to the test, it was confirmed that the net absorbed the target energy of 150kJ by the deformation of about 4.0m as shown in Figure 3 (Yoshida *et al.* 2008).

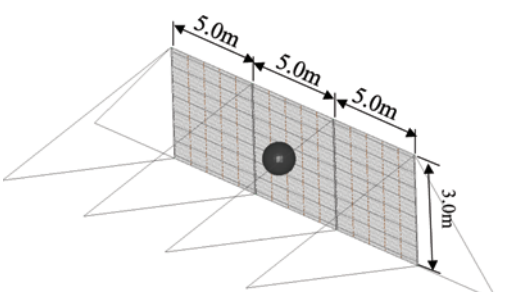

FIG. 2. Field test on high energy absorption net.

A numerical simulation was carried out to study modeling of the deformation characteristics of the net consisting of several members made from synthetic fiber. LS-DYNA was used for the simulation in this study. All members constituting the net are modeled by the cable element, which only resists against the tensile force. Table 1 presents calibrated parameters to simulate the response of the high energy absorption net, where elastic modulus of the members constituting the net are set as 0.2 times of the original parameters of each members. Figure 3 shows the deformation of the net obtained from the numerical analysis. According to the result, the analysis reproduced well the response of the net obtained from the field test; consequently, the parameters adopted in the simulation are used as ones of the net for analysis in this study.

Table 1. Parameters

	Elastic modulus (kN/m^2)	Sectional area (m^2)
Rope making up net	4.27×10^4	6.36×10^{-6}
Longitudinal belt	5.56×10^5	2.40×10^{-4}
Lateral rope	2.12×10^5	3.14×10^{-4}
Stay	2.78×10^6	1.20×10^{-4}

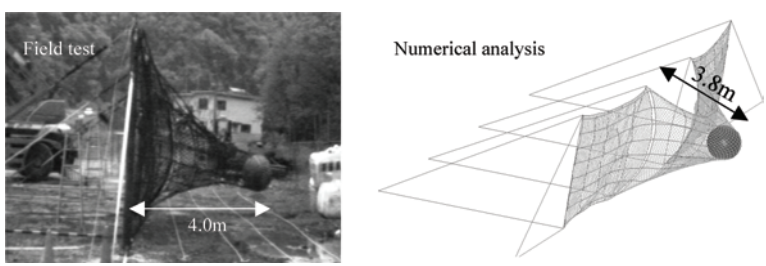

FIG. 3. Deformation of the high energy absorption net.

UPGRADE TECHNIQUE OF EXISTIING ROCKFALL PROTECTION FENCE

Figure 4(a) shows the target existing rockfall protection fence in this study. This type of fence is one of popular rockfall protection facilities in Japan. The fence consists of wire mesh, wire rope and steel post. Figure 4(b) shows the upgrade technique for existing rockfall protection fence using high energy absorption net, which is proposed in this study. The high energy absorption net is installed to mountain side of the existing fence by using rope made from synthetic fiber. Upper and lower ropes are connected with the anchor installed in the back slope. The purpose

of the technique is to reduce the rockfall impact energy to smaller one than the design energy of the existing fence by the absorbable ability of the rockfall energy of the high energy absorption net before the collision with the rockfall and the existing fence.

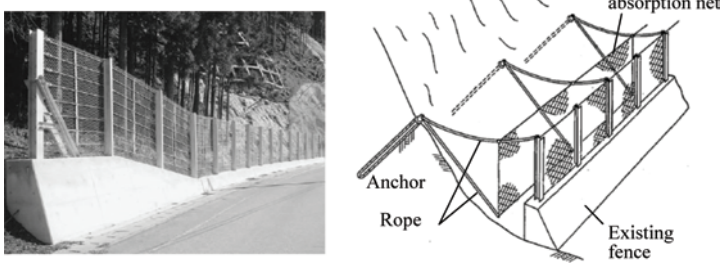

(a) Rckfall protection fence **(b) Upgrade technique**

FIG. 4. Upgrade technique of existing rockfall protection fence.

A field test to confirm the effectiveness of the proposed upgrade technique for existing rockfall protection fences was carried out. Figure 5 shows the summary of the test. The frame structure constructed by H steel members, H200×200×8×12, was adopted to model an existing fence and the back slope of the fence. The existing fence was modeled by putting a wire mesh (mesh size: 50mm square, diameter of wire : 3.2mm) on the front surface of the frame. The high energy absorption net was installed behind the existing fence by using upper and lower ropes. In this test, twice cases, Case 1: a steel ball with the energy of 100kJ hits the wire mesh directly (the case without the high energy absorption net), Case 2: the steel ball hits the wire mesh through the high energy absorption net (the case with the net; the proposed technique), were carried out.

Figure 6 shows the actual responses of the wire mesh, the steel ball and the high energy absorption net after the collision with the wire mesh and the steel ball. According to the results, in Case 1, the steel ball broke the wire mesh and jumped out of the wire mesh, in contrast, in Case 2, the high energy absorption net installed behind the wire mesh reduced the energy of the steel ball before the collision with the steel ball and the wire mesh, consequently, the wire mesh could catch the steel ball with no damage. The applicability of the upgrade technique proposed in this study to actual existing rockfall protection fences was confirmed from the results.

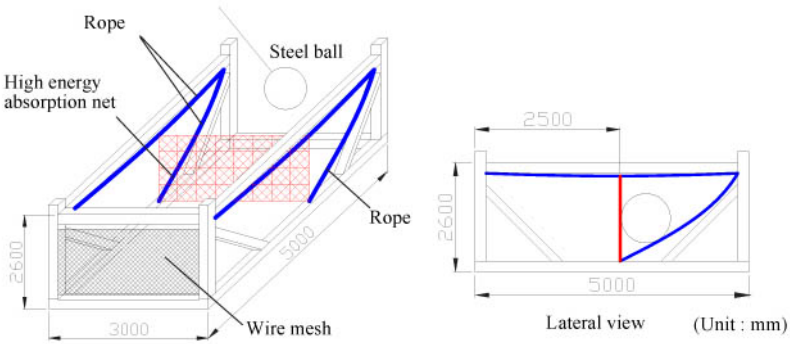

FIG. 5. Experimental model of field test.

FIG. 6. Result of field test.

NUMERICAL ANALYSIS

In order to design the proposed technique, the validity of the numerical analysis was confirmed from the comparison with the results of the field test and analyzed one. The parameters of the high energy absorption net presented in Table 1 was adopted in this analysis. The wire mesh and H steel members are modeled by the beam element. Figure 7 shows the analyzed responses of the high energy absorption net, the steel ball and the wire mesh. Figure 8 shows the comparison with the observed time history of the acceleration of the steel ball and analyzed one. According to the results, the numerical analysis using in this study could reproduce well the obtained results from the field test. Consequently, the usefulness of the analysis to the design of the proposed technique for the actual existing rockfall protection fence was confirmed.

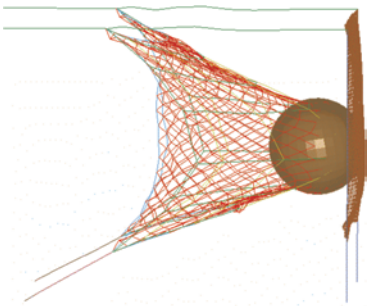

FIG. 7. Calculated behavior of the proposed technique.

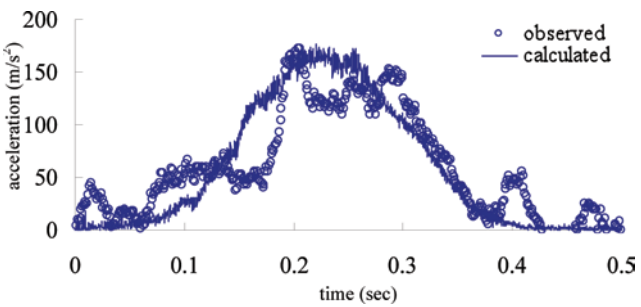

FIG. 8. Time history of acceleration of the weight.

CONCLUSIONS

This paper can be concluded as follows; 1) a new performance upgrade technique for the existing rockfall protection fence, which uses the high energy absorption net, was proposed, 2) the effectiveness of the proposed technique was confirmed from a field test, 3) a design method, which can reproduce the results of the field test, was proposed.

REFERENCES

Yoshida, M., Kobayashi, H., Arakawa, M. and Okumura, H. (2008). "Impact resistance test for rockfall preventing fence using fiber net and rope." *Geosynthetics Engineering Journal*, No.23, 113-118 (in Japanese).

Japan Road Association (2008). Guideline for rockfall countermeasure (in Japanese).
Tsuji, S., Hara, T., Yashima, A., Sawada, K. and Yoshida, M (2009). "Upgrade of stone-guard fence with using high-energy absorption net." *Proceeding of the international symposium on prediction and simulation methods for geohazard mitigation (IS-KYOTO 2009)*, 465-471.

Numerical Modelling for Ground Improvement of Batter Micropiles on Liquefiable Soils

Mingwu Wang[1], Jinping Han[1]

[1]Professor, School of Civil Engineering, Hefei University of Technology, Hefei, China 230009; geotechnics@foxmail.com
[2]School of Civil Engineering, Hefei University of Technology, Hefei, China 230009; hjp13965124601@sina.com

ABSTRACT: The micropiles are widely used in the ground improvement for the liquefiable foundation. However, seismic behavior of batter micropile is not fully understood up to now because the behaviors of micropiles during earthquake are significantly influenced by the nonlinear characteristics of liquefiable soils and soil-pile interaction. Herein the influences of pile inclination and earthquake intensity on seismic response of micropile group on liquefiable soils were investigated by means of an effective stress analysis method. The numerical predications in the simulation model with intensity of 0.1, 0.2 0.3 g, frequency of 2 Hz input sine wave and pile inclination of 15° to the vertical axis, show that the stronger input motion intensity results in higher responses at the micropile top. But in the El Centro earthquake motion model with the pile inclination of 0°, 15°, 25° to the vertical axis, the maximum lateral displacements and maximum bending moments along micropile length decrease with increase of the micropile inclination, the relative micropile-soil lateral displacement increased. The deflection along the micropile in two type models both decreases with increasing the buried depth. The lateral soil-pile relative displacements in liquefiable soils are much more complicated than in non-liquefiable soils. The batter micropile leads to a reduction of bending moment in the micropiles, and accelerations and deflection at pile top.

INTRODUCTION

Micropiles are being increasingly utilized in ground improvement projects in order to increase the bearing capacity and reduce the settlements particularly in strengthening the existing foundations because they are of small diameter, high axial capacities, greater efficiency than tools used for other more conventional foundation types. Micropiles also can be used as foundation support of new structures as well as for seismic retrofitting of structures, which have suffered seismic damage (Misra et al. 2007). The use of micropiles for the improvement of liquefiable soils in seismic zones

requires a dynamic analysis, which takes into account the earthquake-induced pressure and the non-linear pile-soil interaction. However, previous works dealt mainly with the static behaviour of micropiles. Use of micropiles in seismic area suffers from code restrictions issued on piles. In addition, the traditional seismic role of batter piles has been considered detrimental because batter piles may induce large forces to the pile cap, and non-symmetric inclination will result in permanent rotation (Sadek et al. 2006). The current design practice for micropiles is based upon either the methods developed for large diameter pile or simplistic interpretation of micropile load tests similar to the approach used for analyzing tieback anchors (Wang et al. 2008a). In a word, the seismic behavior of batter micropile is not fully understood up to now. Consequently, many issues and considerable research work still need to be done in order to develop and assess seismic design guidelines for proper design of micropile systems. Numerical analysis is an effective way to study the behavior of micropiles as, once a model is verified, conditions can be changed with little effort to conduct a parametric study on the system variables.

The object of this paper is to analyze the influence of micropiles inclination and shaking motion intensity on seismic performances of micropiles on liquefiable soils by means of an effective stress analysis method, then to provide a basis for a rational seismic design of micropiles on liquefiable soils.

NUMERICAL MODELLING

The program FLIP developed by Iai was used to analyze the seismic behaviors of batter micropiles on liquefiable soils. The constitutive model incorporated in the FLIP is composed of a multiple shear plasticity model and a model for generating excess pore water pressure. The more detailed illumination was expounded in references (Iai et al. 1992, Wang et al. 2005; 2008).

Two type models, sine wave model and earthquake wave model were used to conduct numerical simulation. The sine wave models were used to investigate the influence of the input motion intensity on the micropile with inclination of 15° to the vertical axis. The maximum amplitudes of input motion were 0.1, 0.2 and 0.3 g, respectively. The frequency for input sinusoid waves were all 2.0 Hz. For the earthquake models, the El Centro earthquake motion of 30 second shaking duration was used to simulation, and the micropile inclination were 0°, 15°, and 20° respectively.

The stratum for all models was same and composed of a horizontal dry sand deposit and liquefiable sand deposit and dense saturated sand, as shown in the Figure 1. The thickness and factures of the soil were summarized in Table 1. The computed parameters were specified based on a simple method proposed by Iai and Morita. The detailed illumination was expounded in the reference (Iai et al. 1990; Morita et al. 1997). The water table was at the elevation of -2.0 m. The length and diameter of micropile were 5.7 m and 0.2 m. Analysis was carried out with the following characteristics for the micropile material: Shear modulus of the micropile Gs=770 MPa; Poisson's ratio $\mu = 0.3$; the density ρ=2.0 g/cm^3; and I= 7.86×10^{-4} m^{-4}. The parameters, S1, p1, p2, w1 and c1, for the accumulation model of excess pore water pressure (EPWP) were 0.005, 0.5, 1.106, 1.368 and 1.643, respectively.

Five types of elements were used in the numerical simulation. The micropiles were simulated with linear beam elements. The super-structure mass was treated as a rigid body, and is represented by a concentrated mass. The soils were simulated with multiple spring elements. The soil-pile interaction spring element was used to simulate the pile-soil interaction. The pore water pressure was modeled with pore water element.

Table 1. Parameters of Soil Layers

Soil Layer	Thickness (m)	K_{ma} (MPa)	G_{ma} (MPa)	φ_f (°)
Dry Soill	2.0	151.4	58.3	38.59
Saturated Soil	3.0	151.4	58.3	38.59
Dense Saturated Soil	5.0	282.3	108.3	40.56

K_{ma}: initial bulk modulus of soil skeleton at confining pressure of 98 kPa; G_{ma}: initial shear modulus at confining pressure of 98 kPa; φ_f: effective friction angle;

To simulate the conditions of site, the ground motions were applied at the fixed bottom boundary. A viscous condition was assigned for the both side boundaries for dynamic analysis. The numerical integration is done by Wilson-θ method (θ=1.4) at time step of 0.01 seconds. Rayleigh damping (α=0.000, β=0.003) was used for ensure the stability of the numerical solution process. Before the dynamic response analysis conducted under undrained condition, a static analysis was performed with gravity to simulate the initial stress acting in situ.

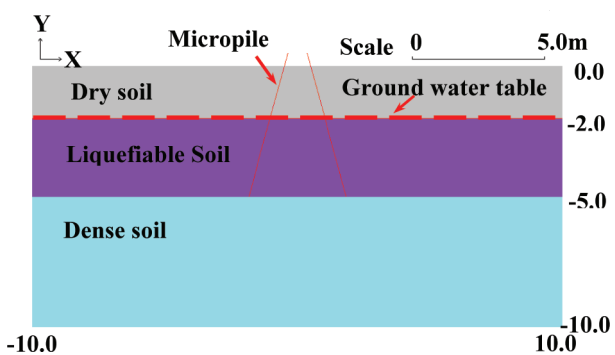

FIG. 1 Sketch of simulation model.

RESULTS AND DISCUSSIONS

The results from numerical predications are presented below in prototype scale and compared with each other.

Acceleration

Figure 2 illustrated the horizontal acceleration responses along the micropile. As expected, the crest acceleration amplitude increased with the increase of shaking intensity in the sine wave models with a pile inclination of 15° to the vertical axis (See Figure 2 (a) and (c)). It was clearly seen in the models subjected to El Centro motion that the amplitude of acceleration decreased in the liquefiable soil layers during the motion, as shown in Figure 2 (b) and (d), and then increased in the non-liquefiable soils. It was observed that the horizontal acceleration was smaller in the batter micropiles than that induced in the vertical micropile case. The peak value of lateral acceleration at the micropile top in the model with an inclination of 25° was about 2.3 m/s^2, which was about 20% smaller than the one induced in vertical micropiles subjected to the El Centro earthquake motion (See Figure 2 (b) and (d)).

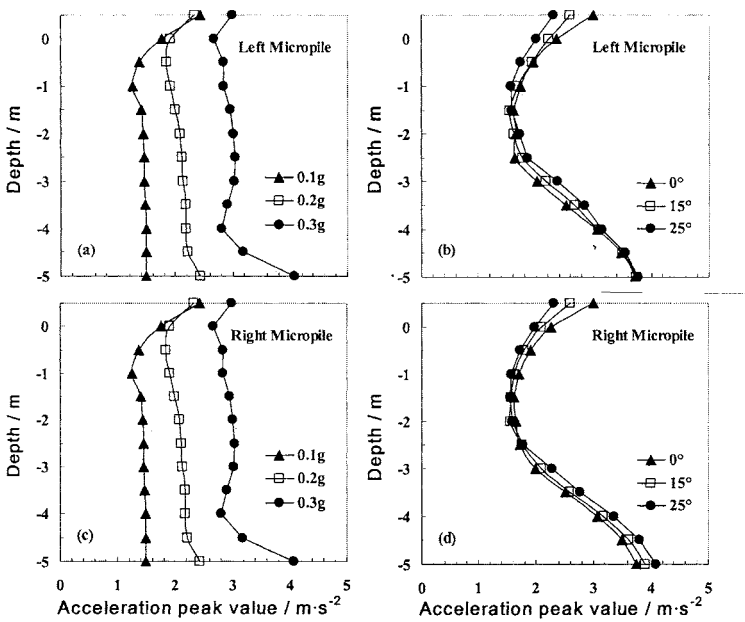

(a), (c) Sine wave (b), (d) El Centro wave

FIG. 2. Peak acceleration value along buried micropile.

Lateral Displacement

The relationship between the maximum lateral displacements of micropile with depth was depicted in Figure 3. It was found that the lateral displacement increased with the increase of shaking intensity (See Figure 3 (a) and (c)). For the earthquake

wave model, the smaller the lateral displacement the bigger pile inclination was (See Figure 3 (b) and (d)). The deflection of micropile all decreased with the buried depth. It was worth noting in Figure 3 that the deflection of micropile changed obviously at the interface between the dry sand and the liquefiable soil. The increasing ratio was larger in liquefiable soil than in dry sand. These results were consistent with the former discussion of accelerations.

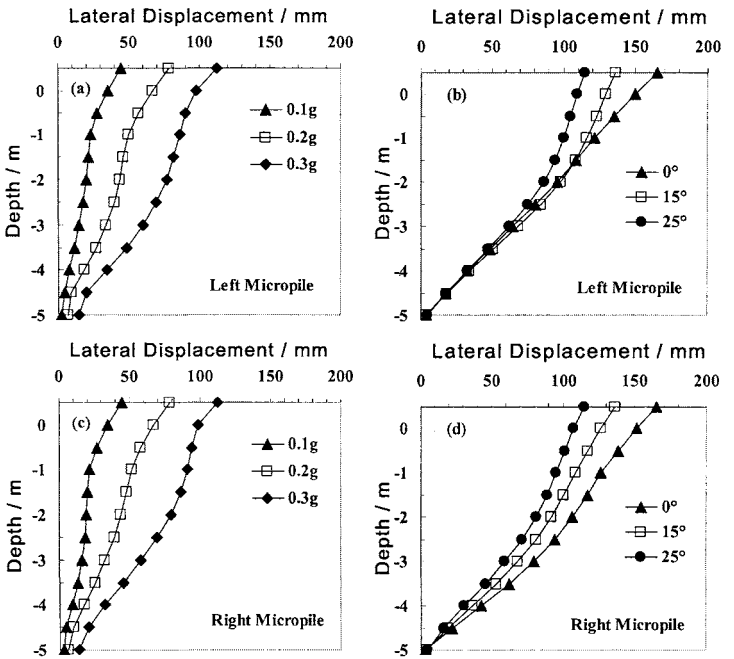

FIG. 3. Lateral displacement along buried length of micropile: (a), (c) Sine wave model; (b), (d) El Centro wave model.

Relative Soil-Micropile Displacement

The relative lateral displacement between the micropile and soil was illustrated in the Figure 4. It may be seen that the larger the value of relative displacement the stronger motion and the larger inclination of micropile were. The relative lateral displacement behaved more complex in liquefiable soil than in the non-liquefiable soil because the nonlinear behavior of the liquefiable soil and the micropile-soil interaction could greatly affect the seismic responses of the micropiles group. In addition, the left micropile and the right micropile behaved different values.

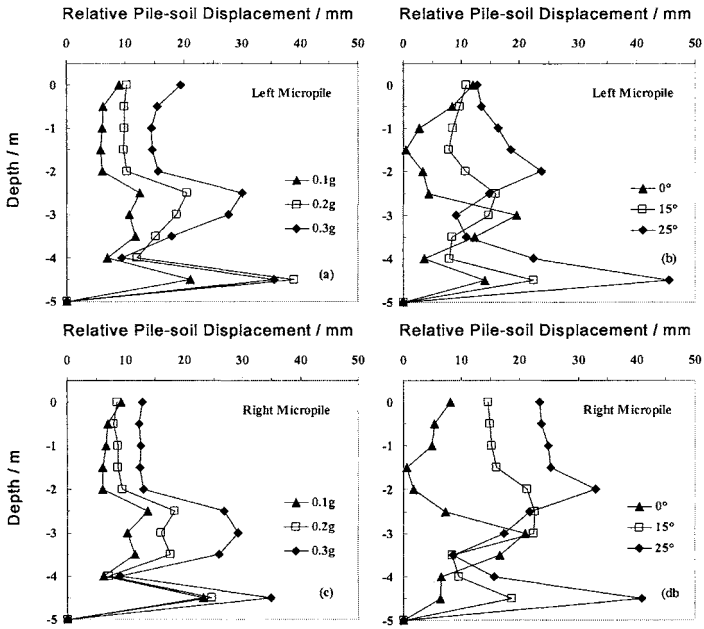

FIG. 4. Relative soil-micropile lateral displacements along buried micropile length: (a), (c) Sine wave model; (b), (d) El Centro wave model.

Bending Moments

The max bending moment profiles along the micropile buried length for various pile inclination and motion intensity were illustrated in Figure 5. The values of bending moments generally increased with increasing intensity (See Figure 5 (a) and (c)). The influence of micropiles inclination on the bending moment was observed in the earthquake wave model. The increase in inclination from 0° to 25° induced a decrease of the bending moment (See Figure 5(b) and (d)). It was also observed that the value of bending moments for the right and the left micropile were not same and not symmetric. This may be due to the inclination of micropile contributed to the unequal distribution of loads.

Figure 6 illustrated the bending moment along the micropile buried length for various pile inclination and motion intensity at the maximum lateral displacement of micropile top. When the lateral displacement of micropile top increased to maximum value, the influence of input motion intensity and pile inclination on bending moment is minor.

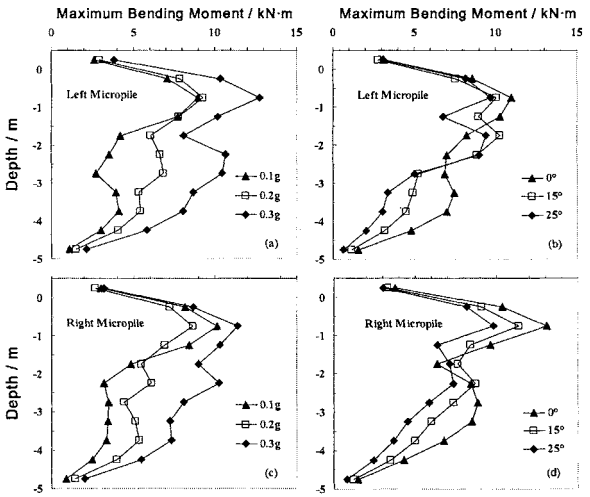

FIG. 5. Relationship between the maximum bending moments and buried length: (a) and (c) sine wave model; (b) and (d) El Centro wave model.

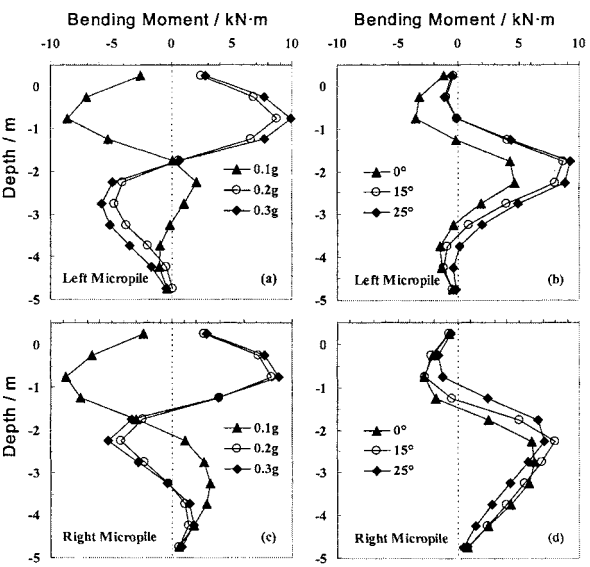

FIG. 6. Bending moments at the maximum lateral displacement of pile top: (a), (c) Sine wave model; (b), (d) El Centro wave model.

CONCLUSIONS

This paper included a numerical analysis of the seismic behaviour of batter micropiles used for the improvement of liquefiable soils. The main results are presented as follow,

1) For the sine wave model of same pile inclination the stronger input motion intensity bigger values of deflection, acceleration and bending moment are. For the El Centro wave model, the bigger pile inclination the smaller values of lateral displacement, bending moment are.

2) The relative soil-micropile displacement increased with the increasing intensity and pile inclination. The micropile-soil interaction during earthquakes is much more complex in liquefiable soils than in non-liquefiable soils.

ACKNOWLEDGMENTS

Financial supports provided by Science and Technological Fund of Anhui Province for Outstanding Youth (No.08040106830) and National Natural Sciences Foundation, China (No.40702049) are gratefully acknowledged.

REFERENCES

Iai, S., Matsunaga Y., Kameoka, T. (1990). "Parameter identification for a cyclic mobility model. *Rep Port Harbour Res Inst*, Vol.29 (4): 57-83.

Iai, S., Matsunaga, Y., Kameoka, T. (1992). "Strain space plasticity model for cyclic mobility." *Soils Foundations*, Vol. 32 (2):1-15.

Misra, A., Roberts, L. A. (2007). "Uncertainty analysis of micropile pullout based upon load test results." *Soil Journal of Geotechnical and Geoenvironmental Engineering*, Vol. 133 (8): 1017-1025.

Morita, T., Iai, S., Liu H. and et al. (1997). "Simplified method to determine parameter of FLIP". *Technical Note of the Port and Harbour Research Institute Ministry of Transport*, No.869: 2-20.

Sadek, M., Shahrour, I. (2006). "Influence of the head and tip connection on the seismic performance of micropiles." *Soil Dynamics and Earthquake Engineering* , Vol. 26 (5): 461-468.

Wang, M., Iai, S. and Tobita, T. (2005). "Numerical modeling for dynamic centrifuge model test of the seismic behaviors of pile-supported structure." *Chinese Journal of Geotechnical Engineering*, Vol. 27(7): 738-741.

Wang M., and Li L. (2008a). "Numerical modelling of seismic performances of passive pile groups adjacent to soil slope". *Geotechnical Engineering for Disaster Mitigation and Rehabilitation*, Science Press Beijing, Springer: 446-451.

Wang, M., and Li L. (2008b). "Effective stress analysis of liquefaction-induced uplift of shallow duct-type underground RC structures." *Journal of Vibration Engineering*, Vol. 21 (3): 286-290.

Slope Stability Analysis for Embankment on Wash Pond Sediments with Prefabricated Wick Drains and Staged Construction

J. Ding[1], P.E., R. Vester[2], P.E., R. Knott[3], P.E.

[1]Senior Principal Engineer, MACTEC Engineering and Consulting, Inc., Richmond, VA 23227, jzding@mactec.com
[2]Senior Engineer, MACTEC Engineering and Consulting, Inc., Richmond, VA 23227, rhvester@mactec.com
[3]Senior Principal Engineer, Vice President, MACTEC Engineering and Consulting, Inc., Kennesaw, GA 30144, raknott@mactec.com

ABSTRACT: Wash Pond Sediments (WPS) are manmade deposits derived from previous gravel pit or other industrial excavation operations. The sediments generally consist of various saturated materials from very soft clay to very loose silty sand. Given the nature of the undesirable engineering properties of WPS, design and construction activities involved in such situations present quite a challenge to engineers and contractors.

This paper presents a case study for a highway embankment constructed over WPS. To improve the engineering properties of the soft soils for the proposed embankment, prefabricated vertical (PV) wick drains in combination with staged construction of the embankment were implemented to accommodate the anticipated settlement and to meet the required minimum factor of safety for the embankment slope stability. With extensive field and laboratory studies of the soil encountered, a relationship between effective overburden pressure and undrained shear strength was established to model the soil shear strength gain from the consolidation in the field. Slope stability analyses were conducted to develop the design in order to provide feasible method for the construction.

INTRODUCTION

The proposed 30 kilometer state-of-the-art Intercounty Connector (ICC) highway is located in the northern suburbs of Washington D.C. The project is currently under construction as a series of design-build contracts and scheduled to be all completed in 2013. With apparent economical benefit after connecting existing and proposed development areas between the I-270/I-370 and I-95/US 1 corridors within central and eastern Montgomery and northwestern Prince George's Counties in Maryland (USA), the ICC has been planned and studied for over 50 years. Its design is being developed with extensive involvement by the local governments and communities. The planned roadway will include the construction of numerous new highway interchanges and bridges. The proposed ICC mainline roadway and associated ramps for the Contract C portion of the ICC project will cross two existing wash ponds of approximately 150 and 350 meters in length, respectively, in a general east-west

direction. The proposed roadway embankment will accommodate six lanes with a 50 meter wide surface. The embankment height ranges from is 2 to 9 meters. Given the poor geotechnical conditions of the WPS, the design and construction of this segment of roadway has been one of the biggest challenges to the ICC engineers and contractors.

The two wash ponds designated as the East Wash Pond and the West Wash Pond are part of previous sand and gravel borrow pit operations. With varying sizes from several thousand square meters to several hectares and varying depths from 5 to 20 meters, these pits, once dewatered to excavate the sands and gravels, were later allowed to refill with groundwater to the current stabilized groundwater level. Later, these pits were used as the depositories for the washings derived from other excavated sand and gravels. These washings, mainly composed of silt and clay size soil particles, were deposited hydraulically through the standing water in the ponds. Some sands and gravels were also included in the washings. As the material settled out through the standing water, a very soft and very loose soil condition resulted as the ponds were filled with the sediment washings. The rising water level was decanted off through hydraulic weirs and exited into nearby streams until the ponds were filled with sediments. The end of the hydraulic pipe bringing the washings into the ponds was likely moved from place to place within the ponds resulting in coarser soil materials dropping out near the end of the pipe and the finer grained sediments suspended in the water being transported further away from the pipe and toward the outlet structures of the pond. This man-made depositional process resulted in layers and lenses of varying soil grain sizes being deposited throughout the pond in a very soft and very loose condition of material of very low strength and density.

Currently, no past engineering records or publications have been found directly related to WPS regarding their geotechnical properties and design parameters.

FIELD AND LABORATORY INVESTIGATIONS

To explore the soil conditions, a total of 85 soil test borings were performed to depths varying from about 5 to 15 meters below the existing ground surface. Split-spoon and thin wall Shelby tube samples were collected in combination with Standard Penetration Tests (SPT). A total of 29 piezocone penetration test (CPT) and 10 flat-plate dilatometer tests (DMT) were also performed to depths ranging from about 2.5 to 17 meters below the existing ground surface. In addition, a total of 42 vane shear tests (VST) were performed at selected depths ranging from about 0.5 to 6 meters below the existing ground surface at five locations. Table 1 presents the engineering properties obtained from the field explorations from different tests.

In general, the soil conditions encountered in the Wash Ponds consisted of the following four materials listed in descending order beginning at the existing ground surface:

A. Formation VM (less than 0.3 meter thickness) – A relatively thin surficial layer of highly organic sandy silt with clay (WPS).
B. Formation I (3.0 to 10.0 meter thickness) – An underlying layer of very soft clayey silt with occasional sandy seams and lenses (WPS).
C. Formation IA (1.0 to 5.0 meter thickness) – Interbedded layers of loose to firm clayey silty sands with some gravel within or below the Formation I (WPS).
D. Formation II (native soil) – Underlying native materials consisting of firm to very dense sands, with some gravel and interbedding of very stiff to hard, fine-grained soils, extending to the boring and sounding termination depths.

The upper three layers of materials are hydraulically deposited sediments from the former open pit mining operations and the lower material is the natural coastal plain sandy deposits of the Patuxent and Brandywine geologic formations. CPT and VST tests indicated a relative crust on the surface and a linear increase of the shear strength to approximately 7 kPa. The friction angles varied from 40 degrees in the silty sand of the upper crust (A) and in the native sandy materials (D) to a few degrees in the clayey sands (C) and clayey silt (B). CPT revealed similar trends to VST for the soil consistency and relative density. Groundwater was encountered at varying depths and elevations from a few centimeters to more than one meter below the existing ground surface. Due to the clayey nature of the hydraulically placed soil deposits, groundwater could temporarily perch at or near the surface following and during precipitation events.

Table 1. Field Test Result Summary

Soil Stratum	A	B	C	D
USCS Classification	SM/CH /ML/CL	ML/SM /SC	SC/SM /SP	GC/SM /SP
SPT (blows per 0.3 meter)	0 -6	0-2	0-4	10-30
Undrained Shear Strength (kPa) from VST	0-15	5-50	0-20	>50
Peak Friction Angle (degree) from CPT	-	20-30	25-30	30-45
Effective Friction Angle (degree) from DMT	30-40	37-45	30-45	35-50

Extensive laboratory tests were conducted for the samples obtained in the field. The laboratory tests included soil index properties, one-dimensional consolidation and consolidated-undrained triaxial compressive strengths. Table 2 lists a summary of the test results.

Table 2. Laboratory Test Result Summary

Soil Stratum	A	B	C	D
USCS Classification	SM/CH /CL/ML	ML/SM/SC	SC/SM/SP	GC/SM/ SP
Moisture Content (%)	8-54	13-72	18-38	3-33
Liquid Limit (LL%)	< 53	<52	< 38	-
Plastic Limit (PL%)	< 31	<35	< 24	-
Plasticity Indices (PI%)	< 24	<37	< 16	-
Compression Index (Cc)	-	0.04-0.4	0.07	-
Initial Void Ratio (e_o)	-	0.44-1.59	0.37	-

SLOPE STABILITY ANALYSIS AND ENGINEERING DESIGN

Slope stability of the embankment was a key issue to the design and construction of the roadway embankments over the WPS due to very low shear strength of the sediments. To increase the shear strength of the WPS, stone column and PV drain were considered as the feasible options for the ground improvement from engineering points of view. PV drain was finally selected for the construction because of its economic advantage over other options and relatively short construction schedule.

PV drains were aligned in a center to center triangular spacing of maximum 1.8 by 1.8 meters and extended to a maximum depth of 10 meters. A horizontal drainage layer consisting of medium to coarse sand and horizontal prefabricated drains was installed to collect the expelled pore water and channel it outside the embankment footprint.

The embankment slope was analyzed assuming a two-dimensional (2-D) cross section and plane strain conditions utilizing limit equilibrium methods with a factor of safety expressed in terms of effective stresses as:

$$F = (c' + (\sigma - u) \tan \phi')/\tau \quad (1)$$

Where:

c', ϕ' – The Mohr-Coulomb cohesion and friction angle, respectively, expressed in terms of total stresses.
τ - Equilibrium shear stress

Simplified Bishop method was incorporated into a computer program to address the static equilibrium by dividing the soil mass above the assumed slip surface into a finite number of vertical slices.

The preliminary analysis indicated that with maximum 3 meters of embankment height, the factor of safety of slope will be less than 1.0 using undrained shear strength of the WPS. Given the nature of the shear strength gain after the consolidation, a total of five stages were considered for the embankment construction in order to maintain a factor of safety greater than 1.3, as required by Federal Highway Administration standards, while maintaining 2H:1V side slopes. Each stage was placed with a controlled maximum thickness based on the results of slope stability analyses. Figure 1 is a sketch of the staged construction.

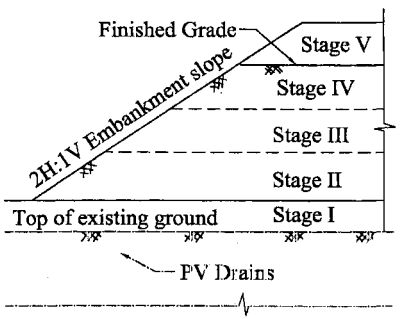

. Stage I (3.0m): Horizontal drains and bridge lift
. Stage II to Stage IV (maximum 3m for each stage): Embankment fill
. Stage V (maximum 4m): Surcharge

FIG.1. PV drains and staged embankment construction

were correlated from laboratory CU test results and similar research by others (Skempton 1957, Army Corp of Engineer, EM 1110-2-1902 2003). Fig. 2 plots the laboratory test results of the shear strength versus effective consolidation pressure. From Fig. 2, a linear regression for the effective stress and shear strength can be summarized as:

$$S_u = 14.5 + 0.75\sigma'_v \qquad (2)$$

Where:

S_u - Shear Strength (kPa)
σ'_v - Effective Consolidation Pressure (kPa)

For the initial undrained shear strength to be considered for the analysis, an in-situ shear strength (S_u) of 6 kPa was selected for the top 3 meters of the WPS based on the field and laboratory test data (McGregor and Duncan, 1998 and Sharma, 2000). Correlations with CPT data (Mayne, 2002) and DMT data (Marchetti, 1980 and 2001, Schmertmann, 1986) were also used to estimate the S_u. The shear strengths at deeper layers were modeled as linearly increasing (Ladd and Foott, 1974) with depth to an estimated maximum S_u of 20 kPa at the interface of the WPS and native soils.

Subsequent stages of fill placement were evaluated using improved undrained shear strength values, which

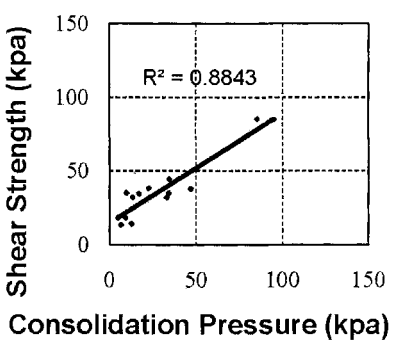

FIG.2. Laboratory test results for shear strength vs. effective consolidation pressure

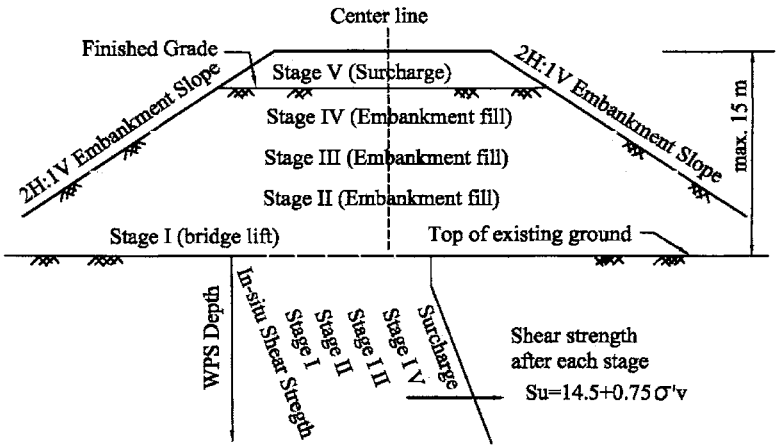

FIG.3. Shear strength modeling for the staged construction

With the application of the shear strength gain at the end of each stage of embankment construction due to the consolidation of the WPS, the entire embankment was construction with a minimum factor of safety of 1.3. Fig. 3 represents the modeling process of the WPS shear strength with relation to each stage of the embankment construction.

GEOTECHNICAL FIELD DATA

The geotechnical instrumentation monitoring program implemented for this project included pore water pressure measurements by piezometers, settlement observation by surface settlement plates and subsurface extensometers, and ground lateral movement measurements by inclinometers. A total of 12 inclinometers, 30 settlement plates, 25 groups of extensometers, and 25 piezometers were installed at critical sections of both wash pond areas. Geotechnical instrumentation data were collected on a weekly basis. The data have provided information for both confirming the engineering analyses and construction control purposes.

Fig. 4 shows field data collected from surface settlement plates over 12 months during construction. As shown in the figures, the magnitude of settlement varied with the embankment height with accelerated settlement occurring at around 60 days after the settlement plate installation at the time of wick drains installation.

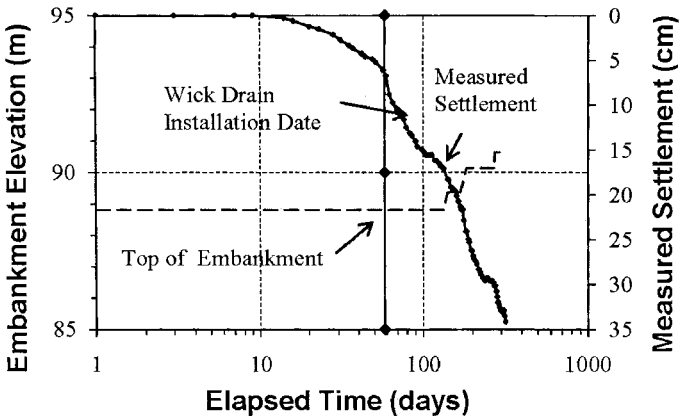

FIG.4. Field measurement of the embankment settlement

CONCLUSIONS

WPS are not common materials encountered by engineers. However, due to the confined and highly developed urban environment and limited land that is available for development, similar materials will probably be encountered with greater frequency in the future.

The final stage of the West Wash Pond embankment construction was placed in May 2009. A total of approximately 40 centimeters of settlement has been measured as compared to the approximately 60 centimeters of total settlement estimated during the design phase of the project. The East Wash Pond is currently in the initial stages of embankment construction with approximately 35 to 45 centimeters of settlement observed as opposed to the approximately 150 centimeters of total settlement estimated during the design phase of the project.

Inclinometer data from both pond sites has generally indicated lateral displacement on the order of less than 12mm at most locations, therefore, it is our opinion that these embankments are currently stable. We believe this stability is attributed to 1) wick drain installation and subsequent increase in shear strength and decrease in excessive pore water pressure, and 2) a staged construction sequence based on the initial design and follow up analysis of the instrumentation monitoring data collected during construction. The staged construction has allowed the wick drains sufficient time to reduce excessive pore pressure build-up and to increase the shear strength of the WPS. The instrumentation monitoring program has greatly helped the engineers and contractor in the decision making process of when to place and compact the next stage of embankment fill.

Another unique feature for this project is the restrictive horizontal limits of the road embankment construction due to encroachment onto environmental regulated areas. During the project planning stages, the state government had imposed very strict limitations for the project Right of Way (ROW) and construction disturbance limits at the environmentally sensitive areas including areas where the wash ponds are located. With the application of the wick drains and staged construction, the engineer is able to effectively design the necessary embankment slopes and at the same time to comply with government regulations on construction and disturbance adjacent to environmentally sensitive areas.

ACKNOWLEDGMENTS

The authors appreciate the support of MACTEC Engineering and Consulting, Inc. in preparing this paper. Special thanks to MACTEC employees Kirk McIntosh, Michael Haith, Scott Stelter, and Ramchandra Mogulla in providing invaluable information and review of this paper.

REFERENCES

Kulhaway, F.H., and Mayne, P.W. (1990). Manual on Estimating Soil Properties for Foundation Design, Electric Power Research Institute, Palo Alto, CA.

LADD, C. C., and Foott, R. (1974). New design procedure for stability of soft clays. ASCE Journal of the Geotechnical Engineering Division, 100(GT7), pp. 763-786.

Marchetti, S. (1980). In Situ Tests by Flat Dilatometer. *ASCE Jnl GED*, Vol. 106, No. 3: 299-321.

Marchetti, S. and G. Totani, S. (2001). "Use of the Flat Dilatometer Test (DMT) in geotechnical design", IN SITU 2001, International Conference on In situ Measurement of Soil Properties, Bali, Indonesia, May 2001

Mayne, P.W., et.al. (2002). "General Report on Ground Property Characterization by In-Situ Tests", Session 1.2, Proceedings, 15th International Conference on Soil Mechanics and Geotechnical Engineering, Istanbul, Vol. 4, 2703-2704.

McGregor, J. A. and Duncan, J. M. (1998). "Performance and use of the standard penetration test in geotechnical engineering practice". Virginia Tech Center for Geotechnical Practice and Research, Blacksburg, VA.

Schmertmann, J., et. al., (1986). CPT/DMT Quality Control of Ground Modification., Proceeding, Use of In Situ Tests in Geotechnical Engineering, ASCE, Special Publication No. 6, Blacksburg, Virginia, pp 985- 1135.

U.S. Army Corps of Engineers (USACE) (2003). "Slope Stability" Engineer Manual EM 1110-2-1902.

Bridge Approach Settlements: Lessons Learned from Present Case Studies and Ground Improvement Solutions

Anand J Puppala[1], Sireesh Saride[2], Ekarut Archeewa[3], Soheil Nazarian[4], and Richard Williammee Jr[5]

[1]Professor, Department of Civil Engineering, The University of Texas at Arlington, Texas 76019, anand@uta.edu
[2]Post Doctoral Fellow, Department of Civil Engineering, The University of Texas at Arlington, Texas 76019; sireesh@uta.edu
[3]Doctoral Student, Department of Civil Engineering, The University of Texas at Arlington, Texas 76019; ekarut@gmail.com
[4]Professor, Department of Civil Engineering, The University of Texas at El Paso, Texas 79968, nazarian@utep.edu
[5]Materials Engineer, Texas Department of Transportation, Fort Worth, Texas 76133, rwillia@dot.state.tx.us

ABSTRACT: Settlement at bridge approaches is a typical problem found between the end of the bridge and highway pavement. This problem creates an uneven transition or a 'bump' in the roadway, and causes not only inconvenience to passengers but also increasing in maintenance and repairing work/costs to the highway agencies. In the United States, state departments of transportations (DOTs) have been spending over $100 million to alleviate the bump problems every year. Many researches had been carried out to study the causes of the bump problem and they are summarized in this paper. To identify factors leading to the bump problem in Texas, a survey questionnaire was send to all twenty five districts in Texas. In addition some field investigations were conducted at bridges in Quanah, Arlington and Cleburne. Results from the study reveal that subsurface void development, erosion and compressibility of fill material were found to be the main contributing factors to the bridge approach settlement in the State of Texas.

INTRODUCTION

Bridge approaches provide smooth and safe transition of vehicles from highway pavements to bridge decks and vice versa. However, settlement and/or heave related movements of bridge approach slabs relative to bridge decks usually create a bump in the roadway (Briaud et al., 1997). This is a typical occurrence at the end of the bridge

decks and requires a solution, because this uneven transition may cause severe damage to bridge decks, inconvenience to passengers, reduced steering control for travelers, distraction to drivers, lower public perception of agency's image, and constant delays to rehabilitate the distressed lanes (Briaud et al., 1997; Puppala et al., 2009). In addition, when heavy trucks travel over these pavement transitions, impact loads created can severely damage the structure, and at the very least, cause an uncomfortable or unsafe ride (Puppala et al., 2009).

The bump problem also increases maintenance work/costs to transportation agencies worldwide. Only in the United States, State Departments of Transportation (DOTs) have been spending over $100 million to maintenance and repair the damaged bridges nationwide (approximately 150,000 bridges) induced by the bridge approach settlement problem every year (Briaud et al., 1997). Additionally, bump repair and maintenance works often result in traffic delays and congestion problems. Federal Highway Administration (FHWA) reported that traffic congestion due to repair works results in 5.7 billion of person-hours of delay. For each person, this delay averages to 36 hours per year (FHWA-HRT-04-053).

There have been many studies employed across the states in the United States to study the causes of the problem and the methodologies to solve it (Hopkins, 1969, 1985; Stewart, 1985; Laguros et al., 1990; Kramer and Sajer, 1991; Jayawikrama et al., 2005; White et al., 2005, 2007; Puppala et al., 2009). The causes can be very variable and are still too complex to identify them easily. Following sections describe the mechanisms causing the bump phenomenon from the available case histories reported in the literature and present case studies carried out in the State of Texas.

MECHANISMS CAUSING THE FORMATION OF THE BUMP

Lessons Learned From Available Case Studies

The bump phenomenon is not a new issue to the State transportation agencies nationwide as well as worldwide. In the United States, this phenomenon was first studied in his pioneered work by Hopkins in late 60's. In a wide survey of existing bridge approaches conducted between 1964 and 1968 in Kentucky, Hopkins (1969) identified and reported that the following factors as causes of differential settlement of the bridge approach problem; (1) type and compressibility of the soil or fill material used in the embankment and foundation, (2) thickness of the compressible foundation soil layer, (3) height of the embankment and (4) type of abutment. The factors were concurred later by Kramer and Sajer (1991) and Briaud et al. (1997) based on extensive surveys of various State DOTs in the USA. Stewart (1985) performed a research study for Caltrans and this study concurred with the finding reported by Hopkins (1969), in particular the observations noting that the original ground and fill materials contribute the maximum settlement to the approach slab.

The consolidation of the foundation soil is further confirmed as the primary factor leading to the formation of the bump later from other studies, such as in Nebraska (Tadros and Benak 1989) and Kentucky (Hopkins 1973; Hopkins 1985; Dupont and Allen 2002).

In 1987, Ardani studied the factors attributed to bridge approach settlement problem in Colorado. Apart from time-dependent consolidation of foundation soil and the approach embankment as reported in earlier works, Ardani (1987) identified several other contributing factors to this problem which include (1) poor drainage and soil erosion around the abutment, and (2) poor compaction of adjacent embankment fill.

According to a wide survey conducted by Laguros et al. (1990) on 758 bridge approaches in Oklahoma State, the age of the approach slab, height of embankment, skewness of the bridge and traffic volume influence the bridge approach settlement. In addition the flexibility of the approach pavements has a considerable influence as well. Laguros et al. (1990) observed greater differential settlement in flexible pavements than rigid pavements during initial stages following construction (short term performance), while both pavement types performed similarly over the long term.

Later in 1995, Stark and his research team conducted a survey on 1181 bridges in Illinois to identify the factors behind the bump problem. Their observations concluded that high embankment experienced more settlement than lower ones. In another study, Arsoy et al. (1999) performed a survey in Staunton district of Virginia to observe the behavior of integral bridges in that area. They stated that for the integral bridge the seasonal temperature changes between summer and winter in a bridge deck cause a void development under the approach slab, which eventually leads to the bump at the end of the bridge as shown in Figure 1. They also concluded that the settlement of the approach fill can be alleviated by using a properly compacted well-drained backfill, but it cannot be eliminated.

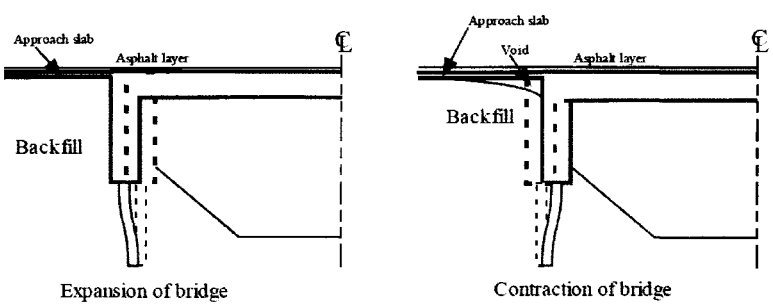

FIG. 1. Expansion and contraction cycle of an integral bridge abutment with an approach slab (Arsoy et al., 1999)

Ha et al. (2002) conducted a detailed investigation of two bridges in Houston, Texas. They could observe that soil near the abutment is more exposed to water than the soil away from the abutment. In this case, the higher water content of soil resulted in the lower strength of soil near the abutment and the higher soil compressibility lead to a bump phenomenon.

Seo (2003) prepared a survey questionnaire on approach settlements and distributed among the 25 districts of the Texas DOT. The responses from TXDOT officials show

that the causes of the bump are the settlement of the embankment fill, followed by the loss of fill by erosion. The results also show that the bump problem will be more serious if the embankment is high and the fill is clay type soil. Seo (2003) also investigated two bridges in Houston, Texas. He concluded that the main causes of bump for bridges were poor compaction, and compression of fill and the natural soil.

Jayawikrama et al. (2005) performed field investigations in four districts in Texas. They reported four major contributors to approach settlement problem which are (1) the time-dependent settlement (primary/secondary consolidation) of foundation soil beneath the embankment and the approach slab embankment, (2) the poor compaction of embankment adjacent to the abutment, (3) erosion of soil at the abutment face, and (4) poor drainage system around the abutment.

White et al. (2005) carried a comprehensive field study of 74 bridges in Iowa to characterize problems leading to poor performance of bridge approach pavement systems. White et al. (2005) claimed that subsurface void development caused by collapse and erosion of the granular backfill, water infiltration through unsealed expansion joints, and poor construction practices were found to be the main contributing factors of the bridge problems including approach slab settlements. Figure 2 shows the problems found from their observation during their study.

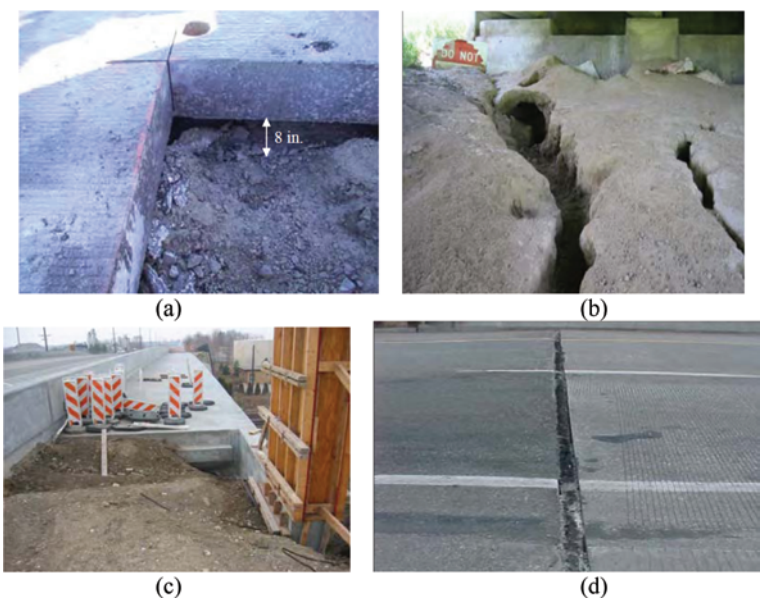

FIG. 2. (a) observed void under the approach slab, (b) soil erosion of granular backfill, (c) non-compacted granular backfill behind the bridge abutment from poor construction practice, (d) unsealed expansion joint (White et al., 2005)

White et al. (2007) summarized the following factors as contributors to differential settlements of the approach slab: (1) backfill materials under poorly performing approach slabs are often loose and under compacted; (2) the foundation soil or embankment fill settles; (3) many bridge approach elevation profiles have slopes higher than 1/200, which is considered a maximum acceptable gradient for bridge approaches; (4) voids develop under bridge approaches within one year of construction, indicating insufficiently compacted and erodible backfill material; and (5) inadequate drainage is a major bridge approach problem. Many abutment subdrains are dry with no evidence of water, are either blocked with soil and debris, or have collapsed. Many expansion joints are not sufficiently filled, allowing water to flow into the underlying fill materials. The problems of the bridge in Iowa from their surveys can be schematized as shown in Figure 3.

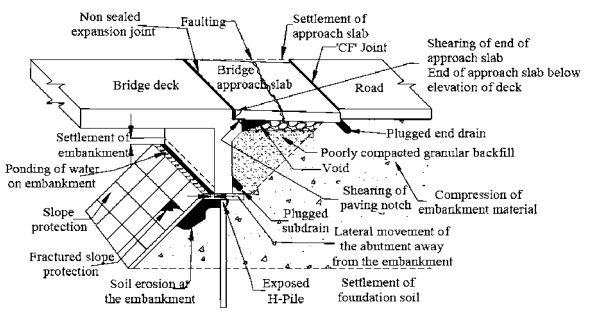

FIG. 3. Schematic diagram summarizing problems observed at bridges in Iowa (White et al., 2007)

Other study from Australia shows that the bump at the end of the bridge is a major concern in highway and freeway constructions. Hsi and Martin (2005) and His (2007) reported that the approach settlement problems were observed due to very soft estuarine and marine clays in subsoils at the construction of the Yelgun-Chinderah Freeway in New South Wales, Australia. Hsi (2007) reported that rapid construction of deep approach embankments over very soft clay subgrade often experienced the long term settlement of the soft subgrade which has attributed to causing settlements at the approach slabs.

Lessons Learned From Present Site Investigations

In a research study supported by Texas Department of Transportation (TxDOT), a survey questionnaire was first prepared and distributed to all 25 District offices in Texas to help identifying the bridge approach problems. Out of 25 district offices, 16 district offices responded immediately to the questionnaire. A majority of respondents (94%) reported that they encountered bridge approach settlement or heaving problems in their districts. The causes for this problem outlined by the respondents are many and a few of them can be listed in the following order: (1) Compaction of the

embankment fill (2) Construction practices (3) Drainage and soil erosion and (4) Void formation. In addition to the information gathered from the questionnaire, the research team also visited a few bridge approaches where bump problems were present. The following sections describe the locations visited and mechanisms observed by the research team

SH 6 Bridge Site, Quanah, Texas

A relatively new bridge along State Highway 6 located in Quanah, Texas has an acute bump problem. The bridge is a non-integral type and the height of embankment is about 40 feet. This high embankment highway bridge crosses a railway line. Locally available low plasticity Sandy Loam) material was used to build the embankment as the fill material was offered to the Department at no cost. During the site visit, uneven settlement of the guardrail on the embankment at the both ends of the bridge showed the obvious settlement problems on this bridge site (Figure 4a). Severe soil erosion and loss of embankment material in the form of gully drains was observed in many locations on the embankments as presented in Figure 4b. The soil erosion problem observed to be severe near the abutments where a void formation and a differential settlement between the bridge deck and the bridge approach slab was noticed (Figure 4c and 4d). Additionally, several longitudinal cracks were observed on the pavement surface which could be attributed to differential settlements of the approach and pavement slab.

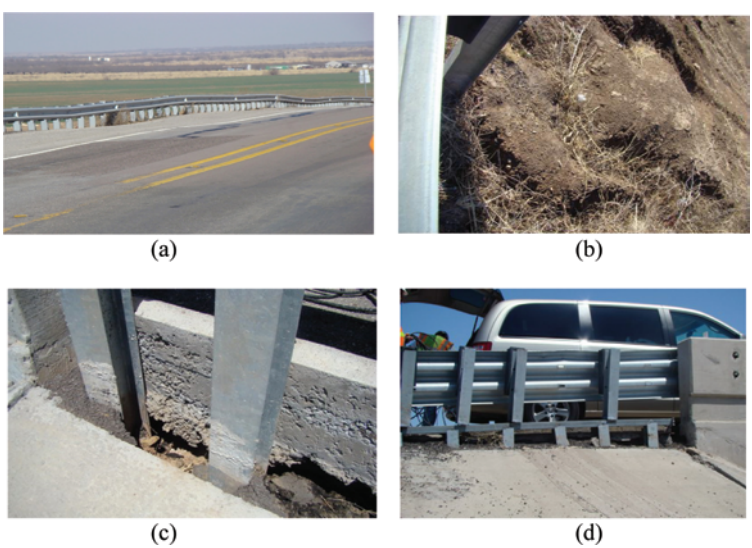

FIG. 4. (a) uneven settlement of guardrail; (b) soil erosion on the embankment; (c) void under the approach slab; (d) differential settlement between the bridge deck and bridge approach – SH 6, Quanah, Texas

From the field investigations, it can be mentioned that the formation of void beneath the approach slab could be attributed to erosion of embankment fill and compaction of the fill and underlying layers. All these factors could lead to the bump problem at the end of the bridge. These erosion problems reveal the possibility of poor drainage conditions for redirecting surface runoff away from the abutment.

Several repair strategies were attempted to reduce the erosion of side slopes of the embankment. These remedial techniques included reseeding, and wire mesh protection along the slopes. Despite these remedial measures, the bump problem is still prevailing. The asphalt overlay of distressed slab is generally a short-term solution and hence the research team has explored possible ground improvement methods for repairing this problem. Additionally, further investigations using non-destructive testing methods are planned to understand the void formation in the embankment fill material.

SH 360 Bridge Site, Arlington, Texas

In a highway extension project on State Highway 360 in south Arlington, Texas, a new bridge was proposed to build on a soft clay subgrade soil. Preliminary geotechnical investigations reveal that the foundation soil is highly expansive and compressible. The report recommended that the weak soil must be excavated and removed or stabilized with lime/cement or to opt for both the alternatives. TXDOT wanted to experiment with a lightweight fill (Expanded Clay Shale, ECS) material on one end of the bridge embankment. The counterpart of the bridge embankment used a normal fill (a low PI material). The subgrade soil was stabilized with 6% lime on both the sides of the bridge. Initially during construction of the embankment with normal fill, erosion issues were noticed as shown in the Figure 5a.

The ECS embankment was instrumented with inclinometers to verify any movements due to traffic loading. Both the embankments were monitored for their settlements using pavement surface profiling with a total station. Results from the pavement surface profiling show that the normal fill embankment has encountered the settlement problems than the ECS embankment. The differential settlement at the end of the bridge was obviously seen under the concrete barrier (Figure 5b). The asphalt overlay was already performed to mitigate the settlement problem observed on the normal fill embankment since the construction of this section. From these observations, it can be concluded that the embankment with normal fill has imposed more pressure on the foundation subsoil which might have lead to settlements in subsoil and eventually on the pavement placed on the embankment. In addition, the soil erosion in normal fill embankment might have also triggered the surface settlements due to loss of embankment material. The approach slab on the embankment with lightweight fill has been performing well without any major settlement distress problems so far.

US Highway 67 Bridge Site, Cleburne, Texas

To divert heavy traffic from downtown Cleburne, Texas, two lane bypass road US highway 67 was constructed in 1995 with four bridges crossing a railroad, two

highways and a creek. All four highway bridges experienced differential movements within six months after construction. This problem is severe on bridge crossing SH 174. The differential settlements were over 12 to 15 inch near approach slabs. This bridge is a non-integral type with a 35 ft. high embankment. The header wall is a geogrid reinforced segemental retaining wall system (also termed as GRS) with concrete block facings. The whole wall and abutment system was founded on the drilled shafts. Pea gravel was used as a backfill for GRS wall system with alternate layers of uniaxial and biaxial geogrids as reinforcement layers in the wall. The flexibility of the GRS wall should allow for any differential settlements expected near the approach slab. However, the flexibility of the GRS wall concurred with the loss of fill material and worsened the bump problem in this case as can be seen from Figure 6a.

Severe subsurface soil erosion and loss of fill material behind the abutment wall caused by water infiltration through surficial joints and cracks into the embankment were also observed (Figure 6a). The eroded material can be seen beneath the openings noted on the GRS wall (Figure 6a). In summary, it is noted that the soil erosion is a major factor causing the bump problem on this bridge site. Due to lack of earlier records of settlements of fill and underlying foundation materials, settlements from these mechanisms are not discussed here. Overall, high density of heavy traffic volume conditions and insufficient erosion and joins design, differential settlements at the end of the bridge on both sides were occurring. This has been distressing this particular bridge for the last few years despite a few ground treatments involving grouting and micropiling measures attempted to correct the settlements.

(a) (b)

FIG. 5. a) soil erosion in normal fill embankment during the construction; (b) differential settlement between the bridge deck and bridge approach - SH 360, Arlington, Texas

(a) (b)

FIG. 6. (a) failure of GRS abutment wall and washout of pea gravel; (b) a transverse crack of the approach slab – US 67, Cleburne, Texas

GROUND IMPROVEMENT REMEDIAL MEASURES

From the detailed field investigations, it can be seen that the asphalt overlay is normally chosen as a mitigation method for the bump problems. However, the asphalt overlay is not a permanent solution and it cannot prevent further settlement and loss of fill material. Therefore, the other ground improvement techniques such as utilization of lightweight fill (ECS), Geofoam and cementitious flowable fill materials for the embankment fill construction, and deep soil mixing (DSM) and any other foundation soil treatment methods could be used to alleviate the approach settlement problems if they are mainly contributors to the overall settlements of approach slabs. Other important criteria include proper fill material type and its resistance to erosion should be evaluated. Also, necessary drainage outlets should be designed to facilitate the surface runoff to move away from the embankment system. Currently this research is looking at some of these techniques for improving foundation and fill materials.

SUMMARY AND CONCLUSIONS

From the available case studies and literature review, it can be summarized that the major contributing factors to the bump phenomenon are the consolidation settlement of foundation soil; poor compaction and consolidation of backfill material; incorrect materials specification; poor drainage and soil erosion; types of bridge abutments. Consolidation of the backfill material, void development under the approach slab due to erosion of the backfill, erosion of slope surface, weak foundation soil and high traffic volume are considered as major causes leading to the bump problem in the State of Texas. It has to be noted that those abovementioned factors can cause the bump at the end of the bridge; however, not all the factors contribute to the formation of the bump concurrently. Also, a few remedial measures including ground improvement strategies to mitigate the bump problems are discussed.

ACKNOWLEDGEMENTS

This study was sponsored by the Texas Department of Transportation (TxDOT) under research project No. 0-6022. The writers would like to thank TxDOT personnel who provided valuable information. Special thanks go to David Head, Bahman Afsheen, Darrell Anglin, Bernie Holder, Jon Holt, Mark McClelland, Taya Retterer, Stanley Yin and German Claros.

REFERENCES

Ardani, A. (1987) "Bridge Approach Settlement." *Report No. CDOT-DTP-R-87-06*, Colorado Department of Highways, Denver, Co.

Arsoy, S., Barker, R. M. and Duncan, J. M. (1999). "The Behavior of Integral Abutment Bridges." *Rep. No. VTRC 00-CR3*, Virginia Transportation Research Council, Charlottesville, Va.

Briaud, J. L., James, R. W., and Hoffman, S. B. (1997) NCHRP synthesis 234: Settlement of Bridge Approaches (the bump at the end of the bridge), Transportation Research Board, National Research Council, Washington, D.C. pp.75.

Dupont, B. and Allen, D. (2002). "Movements and Settlements of Highway Bridge Approches." *Rep. No. KTC-02-18/SPR-220-00-1F*, Kentucky Transportation Center Report, Lexington, Ky.

Federal Highway Administration (2000). "Priority, Market-Ready Technologies and Innovations", *Rep. No. FHWA-HRT-04-053*.

Ha, H.,Seo, J., and Briaud, J-L. (2002). " Investigation of Settlement at Bridge Approach Slab Expansion Joint: Survey and Site Investigations." *Rep. No. FHWA/TX-03/4147-1,* Texas Transportation Institute, Texas A&M University, College Station, TX.

Hopkins, T.C. (1969). "Settlement of Highway Bridge Approaches and Embankment Foundations." *Rep. No. KYHPR-64-17; HPR-1(4)*, Kentucky Transportation Center, Lexington, Kentucky.

Hopkins, T. C. (1973). "Settlement of Highway Bridge Approaches and Embankment Foundations." *Rep. No. KYHPR-64-17; HPR-1(8)*, Kentucky Transportation Center, Lexington, Kentucky, 40.

Hopkins, T.C. (1985). "Long-Term Movements of Highway Bridge Approach Embankments and Pavements". University of Kentucky, Transportation Research Program.

Hsi, J. and Martin, J. (2005). "Soft Ground Treatment and Performance, Yelgun to Chinderah Freeway, New South Wales, Australia." *In Ground Improvement-Case Histories*, Elsevier Geo-Engineering Book Series, Volume 3, 563-599.

Hsi, J. P. (2007). "Managing Difficult Ground-Case Studies." *Proceedings of First Sri Lankan Geotechnical Society International Conference on soil and Rock Engineering*, Colombo.

Jayawickrama, P., Nash, P., Leaverton, M. and Mishra, D. (2005). "Water Intrusion in Base/Subgrade Materials at Bridge Ends." *TxDOT Report, FHWA/TX-06/0-5096-1*, Texas Tech University, Lubbock, Texas.

Kramer, S. L. and Sajer, P. (1991) "Bridge Approach Slab Effectiveness." *Final Report*,
Washington State Department of Transportation, Olympia, Washington.

Laguros, J. G., Zaman, M. M., and Mahmood, I. U. (1990). "Evaluation of Causes of Excessive Settlements of Pavements Behind Bridge Abutments and their Remedies; Phase II." *Rep. No. FHWA/OK 89 (07)*, Oklahoma Department of Transportation.

Puppala, A., Saride, S., Archeewa, E., Hoyos, L. R., Nazarian, S. (2009). "Recommendations for Design, Construction, and Maintenance of Bridge Approach Slabs: Synthesis Report", *Rep. No. FHWA/TX-09/6022-1*, Texas Department of Transportation, 185.

Seo, J. (2003). "The Bump at the End of the Bridge: An Investigation." Dissertation submitted in partial fulfillment of the requirements for the degree of the Doctor of Philosophy, Texas, A&M University, College Station, Texas.

Stark, T. D., Olson, S. M., and Long, J. H. (1995). "Differential Movement at the Embankment/Structure Interface Mitigation and Rehabilitation." *Rep. No. IABH1, FY 93*, Illinois Department of Transportation, Springfield, Illinois.

Stewart, C. F. (1985). "Highway Structure Approaches." California Department of Transportation, Sacramento, CA.

Tadros, M.K., and Benak, J.V. (1989). "Bridge Abutment and Approach Slab Settlement (Phase I Final Report), University of Nebraska, Lincoln.

White, D., Sritharan, S., Suleiman, M., Mohamed M. and Sudhar, C. (2005). "Identification of
the Best Practices for Design, Construction, and Repair of Bridge Approaches." *CTRE. Project 02-118*, Iowa State University. Ames, Iowa.

White, D., Mohamed, M., Sritharan, S. and Suleiman, M. (2007). "Underlying Causes for Settlement of Bridge Approach Pavement Systems." *Journal of Performance of Constructed Facilities*, ASCE, 273-282.

Analysis of the influence of embankment widening on soft ground with differential settlements on pavement structure

Chen Yekai[1], Wang Yimin[1], Ren Chao[2]

[1]School of Civil Engineering and Transportation, South China University of Technology, Guangzhou, China, 510640; chenyekai@163.com
[2]Zhejiang Provincial Plan Design & Research Institute of Communications, Hangzhou, China, 310006; renchao78@126.com

ABSTRACT: Increased traffic volume has made it necessary to increase highway capacities by widening embankments and pavements. Differential settlement may develop between the adding and existing portions of the embankment, especially over soft ground. This differential settlement often causes pavement distress, such as longitudinal cracks or sinking of pavement sections. In this paper, two-dimensional finite method was used to investigate stresses and deformations of the widened embankments over soft ground with or without foundation treatment. The settlements and differential settlements, pavement tensile stress are closely studied.

INTRODUCTION

Increased traffic volume has made it necessary to increase highway capacities by widening embankments and pavements. Adding a new embankment to an existing embankment induces additional stresses and deformations beneath the widened and existing portions of the embankment. Differential settlement may develop between the new and existing portions of the embankment, especially over soft ground. This differential settlement often causes pavement distress, such as longitudinal cracks or sinking of pavement sections. Different techniques have been adopted to remedy these problems, including the use of composite ground, such as deep mixed columns, cast-in-situ concrete thin-wall pipe pile, and lightweight embankment filling.

In this paper, two-dimensional finite method was used to investigate stresses and deformations of the widened embankments over soft ground with or without foundation treatment, the foundation treatment methods is composite ground as deep mixed columns. The relative importance of columns modulus, columns space, foundation treatment range was investigated through a series of parametric studies. The influence of differential settlement between widened and existing embankment on the pavement structure was also presented in this paper.

PROJECT DESCRIPTION

The GS expressway is located at the northwest of Guangzhou in China. It starts from Guangzhou, the capital of Guangdong province, to Sanshui. The total length of

the GS expressway is 30 km, of which about 11.91km is passing though a soft clay deposit. It was constructed in 1996, and it was proposed to widen the embankment and pavement due to the increased traffic volume.

The selected section been analyzed in this study is a embankment constructed on soft soil. The thickness of the soft layers is about 11m. A thin weathered crust (TC) has a thickness of 1-1.5m overlaying a silty clay (SC) approximately 4m thick. The third layer is a very soft mucky clay (MC) with a thickness of approximately 6m. Below the third layer, it is a clayey sand layer (CS). The subsoils are in lightly overconsolidated to normally consolidated States. The overconsolidation ratio at the top crust is about 5. The soft silty clay and mucky clay have a water content greater than the corresponding liquid limit, low hydraulic conductivity, and lower shear strength. The groundwater level is about 1m below the ground surface.

The soft soil beneath the existing embankment was treated by sand drain, 7 cm in diameter triangularly distributed with a spacing of 1.3 m.

NUMERICAL MODELING

A 2D plain strain finite element method, incorporated in ABAQUS, was adopted in this study. The numerical model for this case study is presented in Fig.1. Due to the symmetry of the problem, half of the section was used in the analysis. The element used is an eight-node quadrilateral element.

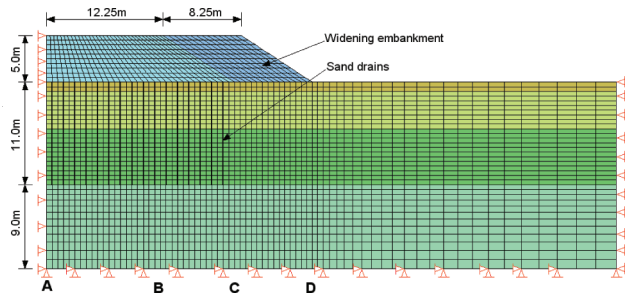

FIG.1. Finite element geometry

2-D modeling of vertical sand drains

Analytical methods developed so far for consolidation analysis of ground improved by vertical drains employ the concept of a "unit cell", wherein a circular domain of influence of a single drain is analyzed. The assumption is that each unit cell works independently and all strains within the soil mass occur in the vertical direction only (Barron, 1948; Hansbo, 1981). In fact, the assumption of no lateral deformation can occur being one of the important signals indicating the instability of the ground. Therefore, it seems more reasonable that the vertical drain installed ground is a three dimensional problem. However, finite element calculations with discrete modeling of vertical drains in a 3-D turn out to be very complicated for routine analysis. Thus, 2-D analysis seems more practical.

Therefore, for consolidation analysis, it is necessary to convert the spatial flow in actual case into the similar one in 2-D plain strain model. By adapting Hansbo's

theory (Hansbo, 1981) for the plain strain case, Hird et al. (1992) showed that the average degrees of consolidation, U, at any depth and times in the two unit cells were theoretically identical. Hird et al. suggested the equivalent permeability as following (Hird et al. 1992):

$$\frac{k_{hp}}{k_h} = \frac{2B^2}{3R^2\left[\ln\left(\frac{R}{r_s}\right)+\left(\frac{k_h}{k_s}\right)\ln\left(\frac{r_s}{r_w}\right)-\frac{3}{4}\right]} \tag{1}$$

where B is the half-width of the plan strain unit cell; R, r_w and r_s are the radius of the axisymmetric unit cell, the drain, and the smear zone, respectively; k_h and k_s are the horizontal permeability of the undisturbed and smeared soil, respectively, and k_{hp} is the converted permeability for the 2-D model.

For drains arranged in a triangular pattern, the equivalent width b_w is expressed as following:

$$b_w = \frac{1.143\pi d_w^2}{2S} \tag{2}$$

where, S is the drain spacing and d_w is the diameter of an actual vertical sand drain.

2-D modeling of vertical composite piles

In 2D FEM model, a row of piles were simplified as a plane strain wall and modeled by 2D plane strain elements. the plane strain wall was assumed to be linear-elastic in the analyses. the stiffness of the plane strain wall was obtained so that the bending stiffness (EI) and compression stiffness (EA) of the plane strain wall was equivalent to that of a row of real piles

Modeling of soil material

In this analyses, the behavior of clay layers was modeled by a modified Cam-clay model (Roscoe and Burland 1968). All soil parameters of clay layers were obtained based on test results, except for Poisson's ratio and hydraulic conductivity of subsoil. During consolidation, the hydraulic conductivity is varied with the void ratio according to Taylor's equation (Taylor, D. W. 1948). The parameter C_k in Taylor's equation was taken as $0.4e_0$ to $0.5e_0$ (e_0 is initial void ratio). The clayey sand layer and embankment fill materials were treated as elastic materials, the Young's modulus E and Poisson's ratio v were assumed empirically (see table 1).

Table 1. Model parameter for subsoil in test site

Layer	E(kPa)	v	λ	κ	M	e_0	γ(kN/m^3)	k(10^{-8}m/s)
TC			0.08	0.016	1.0	0.81	19.3	3.51
SC			0.16	0.032	1.0	1.07	18.5	0.26
MC			0.28	0.056	0.8	1.36	17.3	1.96
CS	20000	0.25					19.5	29.98
Fill	30000	0.25					20.0	6.54

Note: λ=Slope of isotropicconsolidation line; κ=Slope of overconsolidation line.

RESULTS AND DISCUSSION

Current status of existing embankment

The GS expressway was completed the construction at 1996. Until now, it has been under service for 12 years. Fig.2 shows the surface settlement at embankment central line along time. This figure shows that the total settlement from beginning to present is 1.36m, and the settlement after construction is 7.71cm, which is within the limit of specification.

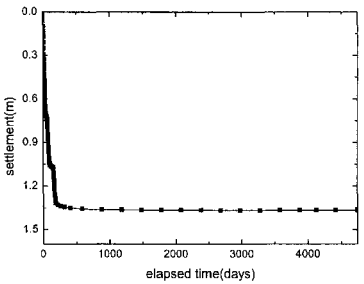

FIG.2. Surface settlement curves

The excess pore pressure distribution in the soft ground due to embankment construction are presented in Fig.3 for different stage. It is shown that the excess pore pressure in the sand drains treatment regional(soft soil) at the end of construction has almost dissipated, but not completed at the underlying regional. The average degree of consolidation is about 93.3% (see Fig.3a). After 12 years consolidation (1996-2008), the disappearance of excess pore pressure has almost completed, only little ones existing far away from the embankment, and the average degree of consolidation is about 98.9% (see Fig.3b).

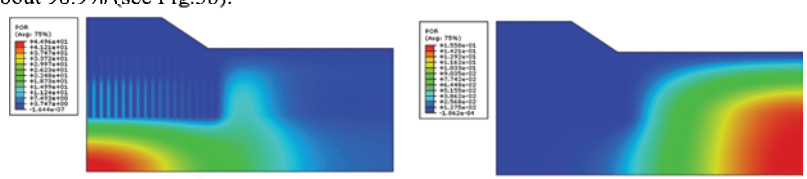

a) End of construction **b) End of 2008**

FIG.3 Excess pore pressure contour in soft ground

Influence for embankment widening

As to widen the embankment and pavement under current status, the widened portion is to been added to the existing embankment (see Fig.1), which will induce additional stresses and deformations beneath the widened and existing portions of the embankment.

The additional vertical stress distribution on the ground surface due to the widened embankment force is presented in Fig.4. It is show that not only there is additional stress in the portion beneath the widened embankment, but also there is considerable additional stress beneath the existing embankment, and the largest stress is located near the toe of the existing embankment. Fig.5 shows the additional vertical

stress distribution at different sections beneath the existing and widened embankment. As show in Fig.1, section A is central line of the embankment, section B is just beneath the top edge of the existing embankment, section C is just beneath the toe of the existing embankment, and section D is just beneath the toe of the widened embankment. It can be seen from this figure that there are considerable additional vertical stress occur at each section of soft soil, especially lager at section C. Therefore, it can be expected that additional vertical settlement will occur in soil both beneath the widened and existing embankment due to embankment widening.

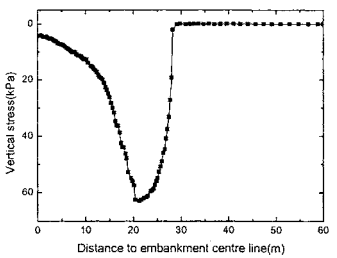

FIG.4. Vertical stress distribution on the ground surface

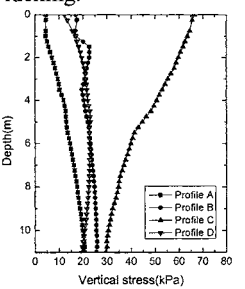

FIG.5. Vertical stress distribution in soft soil

The vertical displacement(settlement) on the top of ground at different stage are presented in Fig.6. As mentioned before, additional settlement developed on the embankment widened portion and existing portion as well due to the embankment widening. Fig.7 shows the additional settlement distribution on the top of soft ground at the end of widened construction and 15 years after widened, the additional settlement distribution features are similar to that of vertical stress. The largest additional settlement is located near the toe of existing embankment, and the maximum additional settlement is 42.73cm. Moreover, differential settlement will develop between the new and existing portions of the embankment. After 15 years serving time, the differential settlement between the adding portion and existing embankment central line will measure up to 31.4cm, which will be bound to cause pavement distress. Therefore, techniques must be adopted to remedy these problems, such as deep mixed columns, cast-in-situ concrete thin-wall pipe pile, and lightweight embankment filling.

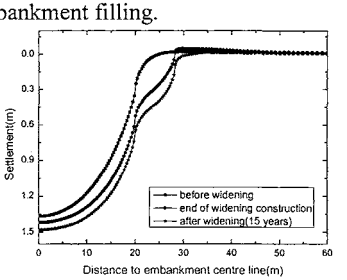

FIG.6. Total settlement distribution on top of ground

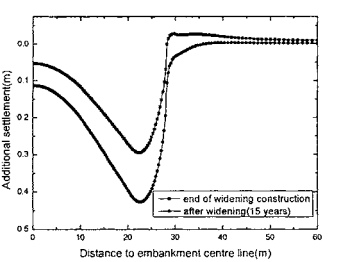

FIG.7. Additional settlement distribution on top of ground

Parametric study of techniques to reduce additional settlement

As mentioned before, embankment widening will cause additional stresses and deformations beneath the widened and existing portions of the embankment. Differential settlement may develop between the new and existing portions of the embankment. This differential settlement often causes pavement distress, such as longitudinal cracks or sinking of pavement sections. Different techniques have been used in practice to avoid, minimize or remedy distresses due to the widening of embankments. In this study, four cases are studied in detail to investigate the effects of different foundation treatment methods supporting widened embankment, also parametric study are presented here. Details of the four cases are presented as follows:(see Fig.8)

Case1: no treatment;

Case2: deep mixed columns beneath only the widened portion, with uniform columns spacing of 1.2 m;

Case3: deep mixed columns beneath both the slope of existing embankment and the widened portion, with uniform columns spacing of 1.2 m;

Case4: deep mixed columns beneath both the slope of existing embankment and the widened portion, with varying columns spacing from Section CC' at 1.2 m towards Sections BB' and DD' at 1.8 m (the average spacing is 1.5 m);

The cross-section and dimensions for the numerical model used for this parametric study are presented in Fig.8. The deep mixed columns were modeled as walls in the plane strain condition. The thickness of the column walls used in this analysis was 0.151 m. All the columns started from the base of the embankment and were embedded into the clayey sand layer (CS) for 1.0 m.

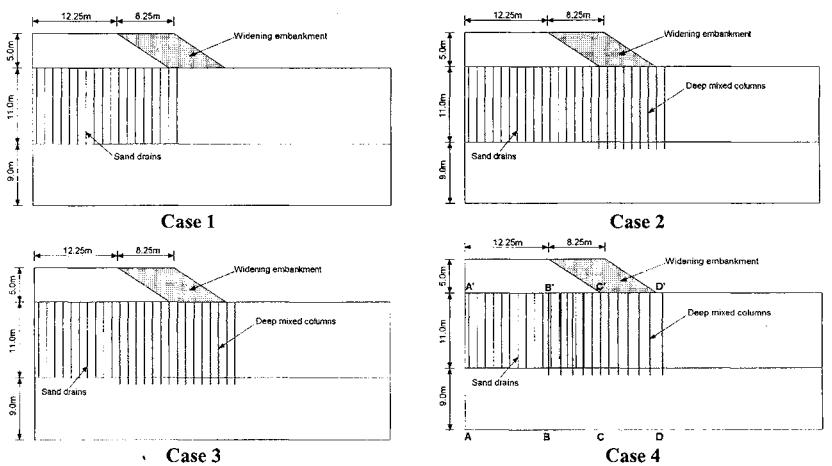

FIG.8. Techniques used in all analyzed cases

The additional settlements of all four cases on the top of the ground induced by embankment widening are presented in Fig. 9. The curve of Case 1 shows the results of no treatment under the widened portion. The curve of Case 2 shows the effect of

deep mixed columns under only the widened portion, as comparing with Case 1, the use of deep mixed columns not only reduces the maximum settlement obviously but also pushes the location of the maximum settlement towards the existing embankment. In other words, the soft soil under the existing embankment plays an important role in the maximum settlement.

Due to the influence of the soft soil under the existing embankment as discussed above, the deep mixed columns installed under the connecting side slope of the existing embankment (Case3) reduce the maximum settlement of the widened embankment as shown in Fig.9. The location of the maximum settlement for Case 3 shifts back to the widened portion. This shift is because the soft soil under the widened portion has lower strength and modulus than that under the connecting side slope of the existing embankment.

The results of Case 4 includes deep mixed columns with varying spacing from Section CC' at 1.2 m towards Sections BB' and DD' at 1.8 m (the average spacing is 1.5 m). This varying spacing makes only slightly difference of the maximum settlement as compared with Case 3 (uniform spacing 1.2m). It is shown that the reduction of the column spacing from varying spacing (1.2m to 1.8m, average spacing is 1.5 m) to uniform spacing (1.2m) only slightly reduces the maximum settlement. This phenomenon results from the fact that the maximum settlement is mostly contributed by the soft soil under the existing embankment. Therefore, the best performance can be obtained by optimizing the deep mixed columns spacing under the connection side slope of both the existing embankment and the widened portion.

Another analysis for Case 3 was performed by changing the column modulus from 80 MPa to 160 MPa (see Fig.10). No obvious difference is found due to the same reason which is related to the soft soil under the existing embankment.

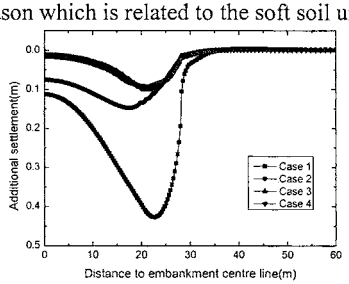

FIG.9. Additional settlement distribution for different treatment techniques

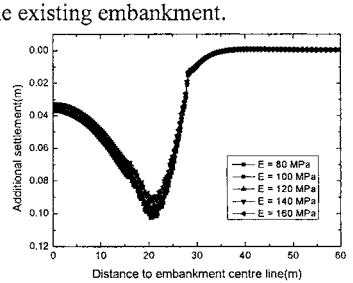

FIG.10. Additional settlement distribution for different columns modulus

When the widened embankment and pavement constructions are finished, the new expressway will delivered to service. Certainly, settlement and differential settlement will continue developed between new and existing embankment due to the consolidation of soft soil. And this differential settlement may causes pavement distress. Fig.11 shows the settlements on top of ground after widening construction for 15 years. The distribution features of settlements after construction are similar to the ones under construction(Fig.9). In Case 1, when no treatment was used, the maximum settlement after construction is 14.0 cm, and the differential settlement between new and existing portion of embankment is 8.0 cm, this may cause more influence on

pavement structure. Techniques as deep mixed columns(Case2, Case 3, and Case4) induce less settlement after construction than Case 1, the maximum settlement of these cases is less than 4.0 cm. There is slightly difference between Case 3 and Case 4, and the maximum settlement after construction is approximately 2.0 cm. Therefore, Case 3 and case 4 may be recommended.

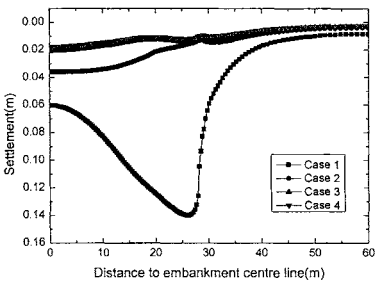

FIG.11. Settlement distribution after construction(15 years)

Influence on pavement stress

As mentioned before, differential settlement between new and existing portions of the embankment may cause pavement distress. The influence of the differential settlement on the pavement structure was investigated in this paper. First of all, the additional settlements on top of the embankment (base of the pavement structure) after widening construction are obtained for all case been analyzed, as seen in Fig.12. The servicing period is supposed to be 15 years. Case 1, with no treatment used to soft ground, has the largest settlement after construction and the largest differential settlement too, and Case 2 is the second one, with deep mixed columns only beneath the widened embankment. The Case with deep mixed columns beneath both the existing and widened embankment have the less additional settlement after construction and differential settlement(Case 3, Case 4).

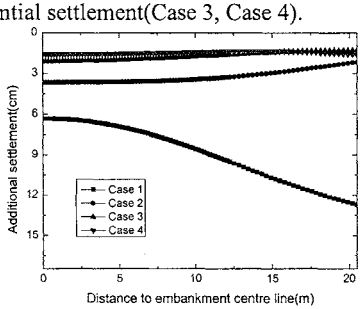

Fig.12 Additional settlement on top of embankment after construction

The existing pavement structure of GS expressway is flexible pavement, including a 18 cm thickness asphalt concrete layer, a 20 cm thickness base layer, and a 20 cm thickness subbase layer, top to bottom. It is designed to exclude a 9 cm thickness old AC layer, then overlay a new 10 cm thickness AC layer on it. The widened pavement structure is also a flexible pavement, including a 18 cm thickness

asphalt concrete layer, a 38cm thickness base layer, and a 18 cm thickness subbase layer, top to bottom. The behavior of the pavement structure is modeled as elastic, the material properties are presented in table 2.

Table 2. Model parameter for pavement structure

	New AC	Old AC	New base	Old base	New subbase	Old subbase
E(kPa)	1200	1000	1500	1200	1000	800
ν	0.3	0.3	0.25	0.25	0.28	0.28

The tension stress distribution in pavement structure are presented in Fig.13 for all four cases been analyzed, the left portion is the existing pavement and right portion is the new pavement. It can be seen that Case 1 causes the largest tension stress, the maximum tension stress is 316 kPa, located on the top of AC layer of existing pavement. When the deep mixed columns are used to treat the soft soil under the widened embankment (Case2, Case 3 and Case 4), The maximum tension stress 46.23kPa, 48.88 kPa and 43.41 kPa respectively, all are under the acceptable level, but the tension region at the subbase bottom is larger in Case 2. Therefore, the best performance can be obtained by optimizing the deep mixed columns spacing under the connection side slope of both the existing embankment and the widened portion.

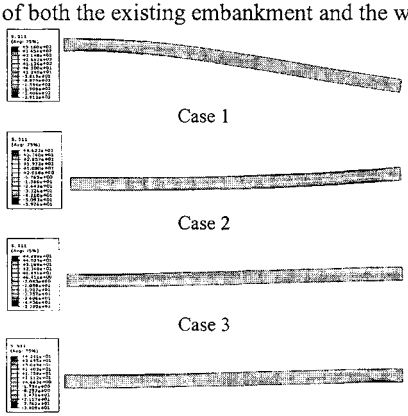

FIG.13 Tension stress (S11) distribution in pavement structure

CONCLUSION

This paper presents the results of a numerical study of the stresses and deformations generated from widened embankments. Based on the results of two-dimensional plane strain finite element analysis, the following conclusions can be drawn:

1. Adding a new embankment to an existing embankment induces additional stresses and deformations beneath the widened and existing portions of the embankment.

2. Composite ground as deep mixed columns can reduces the maximum

settlement caused by widened embankment, These reductions can also be achieved by installing columns under the widened portion and the connecting side slope of the existing embankment. Columns with varying spacing makes only slightly difference of the maximum settlement as compared to uniform spacing, thus the best performance can be obtained by optimizing the column spacing under the connection side slope of both the existing embankment and the widened portion.

3. Deep mixed columns can significantly reduce the tension stress both in the old pavement structure and new adding pavement structure.

REFERENCES

Barron, R. A. (1948). "Consolidation of fine-grained soils by drain wells". *Trans. ASCE*, 113, 718-742.

Chai, J. C., and Miura, N. (1999). "Investigation of factors affecting vertical drain behavior". *J. Geotech. and Geoenviron. Engrg., ASCE*, 125(3), 216–226.

Chai, J. C., Shen, S. L., Miura, N., and Bergado, D. T. (2001). "Simple Method of Modeling PVD-Improved Subsoil". *J. Geotech. and Geoenviron. Engrg., ASCE*, 127(11), 965–972.

Han, J., Oztoprak, S., Parsons, R. C., and Huang, J. (2007). "Numerical analysis of foundation columns to support widening of embankments". *Computers and Geotechnics*, 34, 435-448.

Hansbo, S. (1981). "Consolidation of fine-grained soils by prefabricated drains". *Proc., 10th Int. Conf. Soil Mech. and Found. Engrg.*, Vol. 3, 677-682.

Hibbit, K. and Sorenson. (2004). *ABAQUS Theory and Users Manual Version 6.5*, Inc., Pawttucket, Rhode Island.

Hird, C. C., Pyrah, I. C., and Russell, D. (1992). "Finite element modelling of vertical drains beneath embankments on soft ground". *Geotechnique*, 42(3), 499-511.

Hird, C. C., Pyrah, I. C., Russell, D., and Cinicioglu, F. (1995). "Modelling the effect of vertical drains in two-dimensional finite element analyses of embankments on soft ground". *Can. Geotech. J., Ottawa*, 32, 795–807.

Jia, N., Chen, R.P., Chen, Y.M., Xu, L.X., Yang, S.H. (2004). "Theoretical analysis and measurement for widening project of Hang-Yong Expressway". *Chinese Journal of Geotechnical Engineering*, 26(6), 755-760(in Chinese).

Roscoe, K. H., and Burland, J. B. (1968). "On the generalized stressstrain behavior of 'wet' clay.'' *Engineering plasticity*, J. Heyman and F. A. Leckie, eds., Cambrige University Press, Cambridge, U.K., 535-609.

Taylor, D. W. (1948). *Fundamentals of soil mechanics*, Wiley, New York.

Zhang, D.W., Liu, S.Y. (2006). "Numerical Analysis of Interaction Between Old and New Embankment in Widening of Freeway on Soft Ground". *China Journal of Highway and Transport*, 19(6),7-12(in Chinese).

Zhang, J.H., Huang, X.M., Peng, X. (2007). "Numerical Analysis of Expressway Widened with Two Sides on Soft Soil Foundation". *Journal of Highway and Transportation Research and Development*,24(3),20-29(in Chinese).

Improving Reinforced Soil Performance Incorporating Vertical Reinforcement

Binod Shrestha[1] and Hadi Khabbaz[2]

[1]PhD Candidate, Faculty of Civil and Environmental Engineering, University Technology of Sydney, Broadway, NSW 2007, Australia, binod.shrestha@eng.uts.edu.au
[2]Senior Lecturer, Faculty of Civil and Environmental Engineering, University Technology of Sydney, Broadway, NSW 2007, Australia, hadi.khabbaz@uts.edu.au

ABSTRACT: Reinforced soils have been widely used in different variety and range of applications. Applying vertical reinforcement along with conventional horizontal reinforcement, a new concept of soil reinforcement, is proposed in this paper. The primary difference between the general practice and the insertion of vertical reinforcement is that the latter provides passive resistance against shearing, making all the layers intact that will increase the strength and stability of the reinforced soil. Different modes of failure can be tackled by this improvement in reinforced soil technology. Vertical reinforcement cages the soils in different units along with layered by horizontal reinforcement and produce intact effects in soil mass. It enhances the tensile strength and provides bending effects. Likewise, implementing vertical reinforcement reduces the induced tensile stresses in horizontal reinforcement, which results in less length. The main objective of the vertical reinforcement is to stitch horizontal reinforcing layers to each other. This paper also presents possible methods of construction process. This technology can add numerous benefits to the current industry of soil reinforcement.

INTRODUCTION

Reinforced soils have been widely used in different variety and range of applications. Many studies, examined the reinforcement of soil, have mainly focused on soil reinforcing with conventional horizontal inclusions (Zhang et al. 2008). Most of the recent papers have been published on reinforced soil foundations (e.g. Alamshahi and Hataf 2009; Latha and Somwanshi 2009) and retaining walls (e.g. Huang and Luo 2009; Won and Kim 2007). A few studies have been carried out to investigate the strength of soil reinforced with multi-layer horizontal-Vertical orthogonal elements (Zhang et al. 2006; Zhang et al. 2008) and pullout response for cellular reinforcement (Khedkar and Mandal 2009; Wesseloo et al. 2009).

Khedkar and Mandal (2009) have conducted an experimental study as well as a numerical analysis for pullout response of cellular reinforcements, which are used in place of the horizontally placed conventional reinforcement. In this reinforcement,

members of equal heights are connected perpendicular to each other. The new dimension of reinforcement with height makes the cellular reinforcement stiffer and anticipates good bearing resistance in the pullout situations of cellular reinforcement. Zhang et al. (2006) have purposed three-dimensional reinforcing elements for reinforced soil applications. Triaxial test results showed the acceptability and better performance of three-dimensional reinforcement over two-dimensional, planar, reinforcement. Based on experimental results (Zhang et al. 2008), the interaction of reinforcing elements were analysed and compared with shear strength of the soil reinforced with horizontal reinforcements and orthogonal inclusions. A strength model was developed using theory of equilibrium and compared with the results of triaxial tests for soil reinforced with multi-layer orthogonal inclusions. It can be noted that these studies lacked to take the advantage of reinforcement connecting layers to each other.

This paper presents a new concept of soil reinforcement using vertical reinforcement designed for the connection of every two consecutive horizontal reinforcements. The primary difference between the general practice and the insertion of vertical reinforcement is that the latter not only provides passive resistances against shearing but also makes all the layers to remain intact increasing the strength and stability of the reinforced soil.

VERTICAL REINFORCEMENT CONCEPT

The concept of soil reinforcement, using vertical reinforcement, inserted into the conventional horizontal reinforcement (e.g. woven geotextiles or geogrids), is explained in this section. For this system, similar to conventional reinforcement, the selected granular material is compacted over horizontal reinforcement up to a given height and then another layer of horizontal reinforcement is laid down. Afterwards, the proposed vertical reinforcements are inserted vertically or in angle with vertical as per design. A typical soil structure reinforced with three dimensional reinforcing elements for in situ applications and its sectional elevation are shown in Fig. 1 (a) and Fig. 1 (b), respectively.

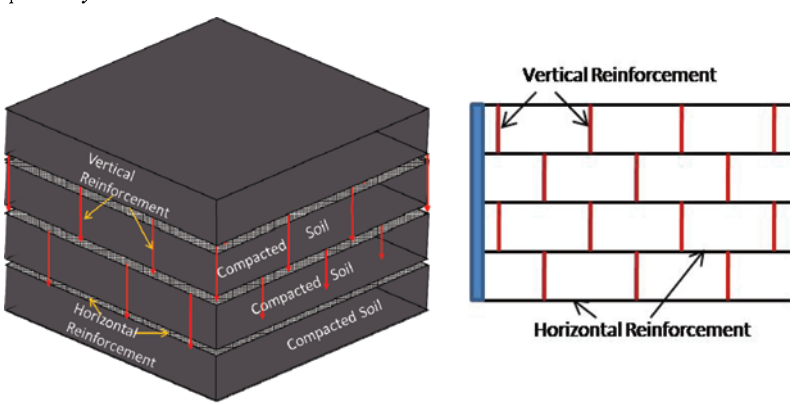

(a) (b)

FIG. 1. Typical use of vertical reinforcement: (a) 3D view, (b) Front Sectional view

ENHANCEMENT OF REINFORCED SOIL STRENGTH

Soil shearing resistance stems from frictional contact among soil particles subject to the effective compressive stress. Deformation in the soil causes tensile or compressive stresses to be developed in the reinforcement. The magnitude of stresses depends on the reinforcement inclination in the direction of tensile or compressive stresses in the soil. As reported by Jewell (1996), the mobilised reinforced force, ultimately limited by the available bond, acts to alter the force equilibrium in the soil mass.

Shear deformation in the soil will cause tensile force T_r, to be mobilised in the reinforcement, and provide two additional components of resistance in the slope (Fig. 2a). The tangential component of the reinforcement force, $T_r Sin\theta$ directly resists the disturbing shear force in the soil, while the normal component of the force, $T_r \cos\theta$, mobilises the additional frictional shearing resistance, $T_r \cos\theta \tan\phi$.

Vertical reinforcement adds two more components: $T_{vr} \cos\theta$ resisting the disturbing shear force, and $T_{vr} Sin\theta$, normal component of the force, providing extra frictional shearing resistance $T_{vr} Sin\theta \tan\theta$ as shown in Fig. 2b. In addition to this, it will cage soil in different units alongside, layered by horizontal reinforcement, and produce intact effect in soil mass.

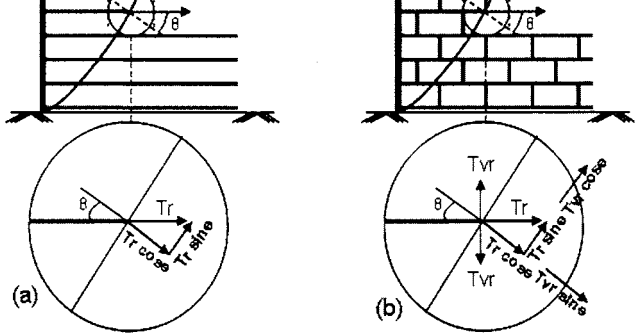

FIG. 2. Effect of reinforcement on equilibrium allowing for: (a) horizontal reinforcement, (b) horizontal and vertical reinforcement

IMPROVEMENT AGAINST MODES OF FAILURE

The design of reinforced soil retaining walls have two primary design requirements in current guidelines and specifications: (i) the external stability and (ii) the internal stability. The external modes of failure in the design of walls consist of base sliding, overturning, bearing capacity and excessive settlement, and global failures. The internal modes of failure comprise of tensile over-stressed, pullout and internal sliding failures of reinforcement. Beside these, there are a number of local failure criteria, such as those for

the connections of the reinforcement and facing units, column shear failure and toppling. Further instability modes should be considered in certain conditions such as: modes of failure could be governed by seismic or cyclic loading. The advantages from proposed reinforcement mechanisms against bearing capacity, tensile over-stress and pullout failures are analysed in this section.

a. Bearing capacity of foundation: Many experimental and analytical studies have been performed to investigate the behaviour of reinforced soil foundation for different soil types. The method of superposition can be used to include the contribution of reinforcement (Sharma et al. 2009) and the bearing capacity including increased bearing capacity can be given as $q_{u(R)} = q_{u(UR)} + \sum_{i=1}^{N} 4T_i[u+(i-1)h]/B^2$ where, T_i is the tensile force in the ith reinforcement layer, u is the depth of reinforcement location, $q_{u(UR)}$ is the bearing capacity of unreinforced soil foundation depending on the friction angle of soil.

Vertical reinforcement enhances the tensile strength and provides bending effects, which ultimately increases the bearing capacity with some modification in the above equation as follows:

$$q_{u(R)} = q_{u(UR)} + \sum_{i=1}^{N} 4(T_i + \Delta T_{vi})[u+(i-1)h]/B^2 + f(I) \quad (1)$$

Where, ΔT_{vi} is the increased tensile force due to the vertical reinforcement and $f(I)$ is the stress due to bending effect on reinforced soil as a function of the moment of inertia.

b. Tensile over stress: Rupture failure occurs in the reinforcement after the tensile force in the reinforcement becomes larger than the reinforcement strength. In current design, rupture failure is being checked and vertical spacing between reinforcement layers should be decreased if reinforcement strength is less than the tensile force or reinforcement with higher allowable tensile strength should be selected.

The failure envelop of unreinforced $c-\phi$ soil is given by $\sigma_1 = \sigma_3 N_\phi + 2c\sqrt{N_\phi}$, where c is the cohesion and N_ϕ can be defined as $N_\phi = \tan^2(45+\phi/2)$. This envelop modifies if we use horizontal reinforcement, which is given by $\sigma_1 = (\sigma_3 + R_T/S_Z)N_\phi$, where R_T is the tensile strength of reinforcing materials per unit length, S_z is the spacing of reinforcements. Comparing the last two equations gives, $c = R_T/2S_z\sqrt{N_\phi}$.

Therefore, the failure envelop of reinforced and unreinforced soil are parallel and exhibit the same angle of internal friction. The additional strength develops in the form of anisotropic apparent cohesion.

Vertical reinforcement unites the soil mass vertically as well as horizontally. First, tensile stresses are produced in the horizontal reinforcement and a corresponding compression in the soil element. Then, it extends tensile stresses in vertical reinforcement before the slippage between the soil and horizontal reinforcement. Those additional mechanisms enlarge apparent anisotropic cohesion and frictional angle, which is the supplementary strength in the soil over tensile stress, reduce the chance of rupture failure in the reinforcement arrangement.

c. Pullout: Pullout failure occurs when tensile force in reinforcement exceeds the friction force between the reinforcement and soil. A number of numerical and experimental tests have been carried out to identify the pullout strength behaviour for different types of reinforcement (e.g. Saran 2005).

For the slippage failure, the failure envelop is given by $\sigma_1 = \sigma_3 N_\phi^{'}$, where $N^{'}\phi = N_\phi / 1 - (2b_r . f^* / S_z) N\phi$. As $N^{'}{}_\phi > N_\phi, \phi_R > \phi$. The parameter N_ϕ can be expressed as: $N_\phi = \tan^2(45 + \phi_R / 2)$, where ϕ_R is increased frictional angle due to horizontal reinforcement and f* represents coefficient of internal friction between reinforcing material and soil.

As a result, in the case of failure of reinforcement due to slippage, the failure envelop of reinforced sand will also pass through the origin, and it indicates an increase of the angle of internal friction. Application of vertical reinforcement adds the total area of reinforcement, which enlarges internal friction angle, and ultimately enhance soil strength performance.

CONSTRUCTION PROCESS

As this proposed technique is a new concept, the construction process can be another major challenge. For stitching horizontal reinforcing layers to each other, different techniques can be employed. However, one practical and possible method, proposed by the authors, is shown in Fig. 3.

For this purpose, about 15 to 20 mm diameter high tensile rod/pipe with a cone tip can be used. As the spacing of reinforcement is generally not more than 500mm, the maximum insertion depth for this equipment will be around 1m. Hence, the required load for insertion and pull out of the rod is not substantial. The detailed features of the equipment can be designed after consultation with the manufacturer. Different steps are presented below to clarify the construction process.

Firstly, the reinforcement should be laid then the soil over the first layer of horizontal reinforcement should be compacted. Next, a fibre cord (vertical reinforcement) with a V-shape flexible tip, which should be opened as an umbrella beneath the first layer, will be inserted just below the lower reinforcement with the help of a metal hose, as shown in Fig 3. When the fibre cord is pulled out, the V-shape tip will be opened and then, this should be tied with the upper layer of horizontal reinforcement.

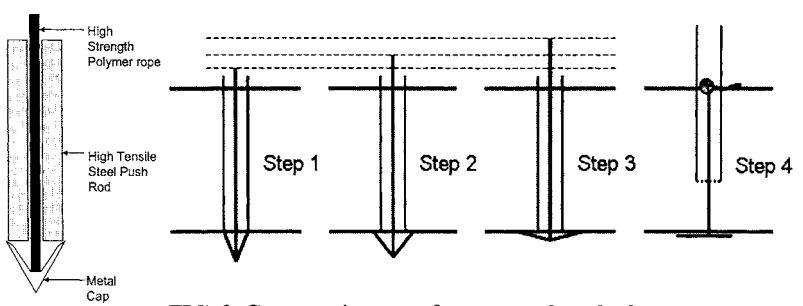

FIG. 3. Construction steps for proposed method

CONCLUSIONS

This paper summarises an innovative concept for the improvement of reinforced-soil performance. Vertical reinforcement not only ties each layer to another but also encounter some components of tensile forces and increases frictional resistance rising anisotropic cohesion and frictional angle. The theoretical analysis anticipates strength upgrading against bearing capacity, tensile over-stress and pullout failures. This technology has been largely driven by economics to get the optimum benefit of soil reinforcement. Consequently, employing this concept can bring substantial benefits to the current soil reinforcement industry.

As the proposed technique is in its initial stages, the findings acquired from these theoretical analyses necessitate further validation based on in situ performance. Further investigation based on large scale laboratory testing and numerical modeling would be required to extend the results for field applications. Additional research on reinforced soil behaviour incorporating vertical reinforcement using rigorous numerical modeling and experimental testing is carrying out by the authors and the results will be disseminated in the follow up papers.

REFERENCES

Alamshahi, S., and Hataf, N. (2009). "Bearing capacity of strip footings on sand slopes reinforced with geogrid and grid-anchor." *Geotextiles and Geomembranes*, Vol. 27 (3), 217-226.

Bilgin, Ö. "Failure mechanisms governing reinforcement length of geogrid reinforced soil retaining walls." *Engineering Structures*, In Press, Corrected Proof.

Huang, C.-C., and Luo, W.-M. (2009). "Behavior of soil retaining walls on deformable foundations." *Engineering Geology*, Vol. 105 (1-2), 1-10.

Jewell, R. A. (1996). *Soil reinforcement with geotextiles*, CIRIA and Thomas Telford.

Khedkar, M. S., and Mandal, J. N. (2009). "Pullout behaviour of cellular reinforcements." *Geotextiles and Geomembranes*, Vol. 27(4), 262-271.

Latha, G. M., and Somwanshi, A. (2009). "Bearing capacity of square footings on geosynthetic reinforced sand." *Geotextiles and Geomembranes*, Vol. 27(4), 281-294.

Saran, S. (2005). *Reinforced Soil and its Engineering Applications*, I.K. International Pvt. Ltd.

Sharma, R., Chen, Q., Abu-Farsakh, M., and Yoon, S. (2009). "Analytical modeling of geogrid reinforced soil foundation." *Geotextiles and Geomembranes*, Vol. 27(1), 63-72.

Wesseloo, J., Visser, A. T., and Rust, E. (2009). "The stress-strain behaviour of multiple cell geocell packs." *Geotextiles and Geomembranes*, Vol. 27 (1), 31-38.

Won, M.-S., and Kim, Y.-S. (2007). "Internal deformation behavior of geosynthetic-reinforced soil walls." *Geotextiles and Geomembranes*, Vol. 25 (1), 10-22.

Zhang, M. X., Javadi, A. A., and Min, X. (2006). "Triaxial tests of sand reinforced with 3D inclusions." *Geotextiles and Geomembranes*, Vol. 24 (4), 201-209.

Zhang, M. X., Zhou, H., Javadi, A. A., and Wang, Z. W. (2008). "Experimental and theoretical investigation of strength of soil reinforced with multi-layer horizontal-vertical orthogonal elements." *Geotextiles and Geomembranes*, Vol. 26 (1), 1-13.

Safety Problem of Freezing Projects in Saline Soils

HU Xiang-Dong[1], ZHAO Fei[2] and YU Rui-Zhi[3]

[1,a]Department of Geotechnical Engineering, Tongji University, Shanghai 200092, China, [1,b]Key Laboratory of Geotechnical and Underground Engineering of Ministry of Education, Tongji University, Shanghai 200092,China; anton.geotech@tongji.edu.cn
[2]Department of Geotechnical Engineering, Tongji University, Shanghai 200092, China; dafei336@163.com
[3]Department of Geotechnical Engineering, Tongji University, Shanghai 200092, China; ruizhiu@yahoo.com.cn

ABSTRACT: In recent years, underground projects are being extensively carried out at the coastal area in China. As a usual way of ground reinforcement, artificial ground freezing (AGF) method meets the challenge of saline soil. Presence of salt in pore water brings strong influence on freezing process in saline soils. Disadvantages including freezing temperature depression and frozen strength loss have direct relationships with the salinity of the pore water. These factors create unfavorable influence on the properties of the frozen soil structure and may cause safety problems. For the safety of freezing projects in saline soils, a research on dependence of saline soil's freezing temperature depression and frozen strength loss on the salinity of the pore water is conducted by laboratory experiment studies. Furthermore, an investigation on the relationship between decrease of frozen soil wall thickness and freezing temperature depression is carried out. Based on that, a calculation method of thickness and bearing capacity of frozen soil wall is established for saline soil.

INTRODUCTION

As a mature technique of ground reinforcement and temporary support for underground construction in soft soil, Artificial Ground Freezing (AGF) method has been more and more employed in construction and recovery projects under complicated geological conditions and special working conditions. With the development of utilization of urban underground space, AGF is much used in soft ground tunneling and related underground projects such as cross passage construction and launching/reception of shield machine. Emerging in recent years is AGF's application in engineering at estuary, off shore or even under sea, such as the Shanghai Yangtze

River Tunnel (Huang et al., 2008), the Hangzhou Qiantang River Tunnel, the Shiziyang Tunnel in the Guangzhou-Shenzhen-Hong Kong Express Rail Link and the undersea cable tunnel of Shantou Huaneng Power Station. Different from that in mining projects and ordinary geology, AGF in maritime soils is quite special due to high salinity and complicated salt composition introduced by seawater.

Compared with those of ordinary soils, freezing-borne properties of soil with high salinity bear distinctive characteristics, such as freezing temperature depression, frozen soil strength loss, influenced thermo-physical parameters and mitigated freeze-thaw effect. With the increasing salinity, frost heaving ratio and thaw settlement coefficient generally decrease, as is frost heaving force; and this is favorable for construction. However, other factors mentioned above have negative influence on freezing process and freezing effect. These disadvantages, including slowed growing, decreased thickness and reduced strength of frozen soil wall, may lead to safety problems.

FACTORS AFFECTING FREEZING PROCESS

Freezing Temperature Depression

The issue of freezing temperature depression in saline soils has been much studied. Solutes lower the freezing temperature of water. The freezing temperature depression in dilute solutions was given by the Van't Hoff equation (Lewis et al., 1961). Much research has been conducted thereafter to investigate the relationship between freezing temperature and salinity. Results of experiments on several common saline solutions and seawater generally supported the conclusion that freezing temperature depressed with rising salinity (Linke, 1965). For soils, the major factors influencing the freezing temperature are adherence of water to soil particles and solute concentration (Hoekstra, 1969, Anderson et al., 1973, Perfect et al., 1991, Frolov et al., 1993). It has been reported that the freezing temperature in soil also decreased, sometimes quite considerably, with increasing salt concentration (Patterson et al., 1983, Frolov et al., 1993, Cui, 1997, Xu et al., 2001).

Freezing temperature depression lengthens the time taken to reach the latent heat stage (Harris, 1995), making the boundary temperature of frozen soil wall below 0°C. This means the thickness of frozen soil wall obtained by conventional calculation is often too optimistic. This causes construction risk in overestimating the bearing capacity and (or) watertight range. Ignorance of these problems brought by freezing temperature depression will lead to great risk or even disaster. Water inrush due to unsatisfying freezing of marine sand at Xinli Mine of Cangshang Gold Mine, Laizhou is quite a lesson. Another case is the design alteration of freezing hole from single row to double in consideration of the influence of salt in pore water in the construction of the Oslofjord subsea tunnel, Norway, where AGF was used to cope with loose bed (Backer et al., 1999).

Strength Loss

The presence of salts in soils generally decreases mechanical strength (Tyutyunov et

al., 1970, Tsytovich et al., 1973, Mahar et al., 1982, Ogata et al., 1982, Chamberlain, 1983). This decline in mechanical strength with increasing salt concentration is generally attributed to a lowering of the freezing temperature and, as a consequence, an increase in unfrozen water content. In addition to unfrozen water films around soil particles, larger unfrozen brine pockets can form during especially rapid ground freezing of saline soils, which also decreases the mechanical strength of soils (Mahar et al., 1982, Chamberlain, 1983). Japanese scholars Takashi et al. (1981) investigated on the compressive strength of frozen saline soils and found, with increasing salt concentration, a first rapid and then slow decline in compressive strength for sandy soils and a relatively flat and mild decline for clayey soils. For each of the two soils, highest compressive strength is recorded near zero salinity.

LABORATORY RESEARCH ON AFFECTING FACTORS

Freezing Temperature Depression

Let's take the Shanghai Yangtze River Tunnel for example. Severe intrusion of saline water is reported at the estuary of the Yangtze River (Shen et al., 2003), hence the high salinity in the soils. According to the authors' investigation, average salinity of the pore water in riverbed soils at the estuary area of the Yangtze River reaches 14.35‰, the highest 18.37‰, much greater than that of fresh water.

Soil layers related to the Shanghai Yangtze River Tunnel are mainly gray mucky clay ([4]), gray clay ($[5]_1$), gray clayey silt ($[5]_2$), gray silty clay ($[5]_3$) and gray clayey silt ($[7]_{1\text{-}1}$) (Hu et al., 2008[b]). The test result of the freezing temperature of each layer is presented in Table 1. The difference between freezing temperatures of clayey soils and sandy soils is obvious in that clayey soils begin to freeze at a lower temperature. Plus, salinity has evident influence on freezing temperature of clayey soils in a way that higher salinity leads to lower freezing temperature; while this tendency is not so remarkably represented by sandy soils.

Table 1. Test Results of Freezing Temperature

Soil layer	Salinity (‰)	Freezing point (°C)
[4] gray mucky clay	18.37	-2.5
$[5]_1$ gray clay	17.39	-2.3
$[5]_2$ gray clayey silt	13.23	-1.7
$[5]_3$ gray silty clay	8.04	-2.1
$[7]_{1\text{-}1}$ gray clayey silt	14.74	-1.7

Strength Loss

Two typical soil layers common in Shanghai underground engineering, i.e. gray silty clay ($[5]_3$), which represents clayey soils, and gray-yellow silty sand ($[7]_2$) for sandy soils were tested. Specimens are reconstituted with NaCl solutions. Uniaxial compression tests are conducted on specimens with pore water salinity (S) at 0, 2, 5 and

20 (‰, ppt). FIG 1 shows the relation between compressive strength and salinity of pore water at various temperatures. Functional relation between frozen soil strength and pore water salinity at a given temperature can be achieved by data fitting with test result.

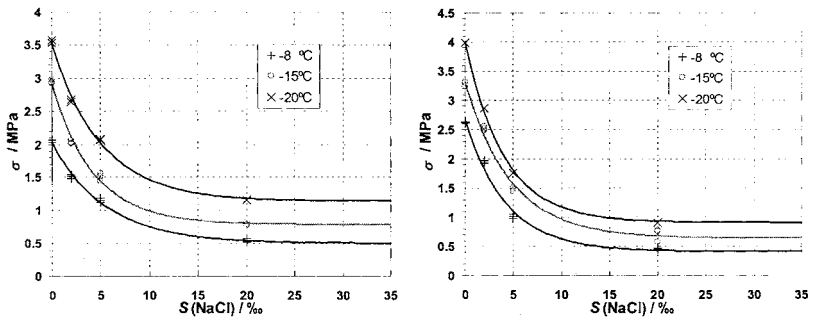

(a) Gray silty clay ($[5]_3$) **(b) Gray-yellow silty sand ($[7]_2$)**

FIG. 1. Relationship Between Uniaxial Compressive Strength and Salinity

It is illustrated in FIG 1 that, for frozen soil, uniaxial compressive strength is at its highest without the presence of salt, but when salt is introduced, strength declines rapidly with increasing salinity. Moreover, strength loss of sandy soil is more dramatic than that of clayey soil, i.e. sandy soil is more sensitive to the change of salt concentration. These conclusions coincide with those of the research by Ogata et al. (1982).

CALCULATION OF FROZEN SOIL WALL

Based on the temperature field of the frozen soil wall, the calculation is mainly about the thickness and the average temperature. Conventional calculation method all assume that the freezing temperature of soil is 0°C, disregarding factors those may lead to freezing temperature depression such as salinity. As a result, the calculated thickness and average temperature of the frozen soil wall could be quite away from the actual value (Hu et al., 2008[a]). In order to achieve more convincing result, a temperature field considering freezing temperature depression is proposed first and thereupon a new calculation approach.

Temperature Field

In China, conventional temperature field models widely accepted in engineering are Trupak's single-pipe model and single-row-pipe model; while the authors have been adopting Bakholdin's single-row-pipe model and double-row-pipe model (Bakholdin, 1963). It is verified both theoretically and practically that, although Trupak's

single-pipe model can accurately describe single-pipe freezing, when it comes to single-row-pipe freezing, Bakholdin's model better agrees with the real situation; and that, for double-row-pipe freezing, Bakholdin's double-row-pipe model is the only analytical solution available which also has favorable accuracy and fidelity. Therefore, Bakholdin's solutions are recommended here by the author. However, as Bakholdin's solutions, either, do not cover freezing temperature depression, remarkable error still exists when calculating for saline soils. After theoretical study and derivation (Hu et al., 2008[a]), below are modified temperature field solutions counting freezing temperature depression:

For Trupak's single-pipe model,

$$t(r) = t_{CT}\frac{\ln\frac{\xi}{r}}{\ln\frac{\xi}{r_0}} + t_0\frac{\ln\frac{r}{r_0}}{\ln\frac{\xi}{r_0}} \tag{1}$$

For Bakholdin's single-row-pipe model,

$$t(x,y) = \frac{t_{CT}-t_0}{\ln\frac{l}{2\pi r_0}+\frac{\pi\xi}{l}}\left\{\frac{\pi\xi}{l} - m_1(x,y)\right\} + t_0 \tag{2}$$

Where,

$$m_1(x,y) = \frac{1}{2}\ln\left[2\left(\mathrm{ch}\frac{2\pi}{l}y - \cos\frac{2\pi}{l}x\right)\right] \tag{3}$$

And for Bakholdin's double-row-pipe model,

$$t(x,y) = \frac{t_{CT}-t_0}{\ln\frac{l}{2\pi r_0}+\frac{2\pi\xi}{l}}\left[\frac{\pi(2\xi+L)}{l} - m_2(x,y)\right] + t_0 \tag{4}$$

Where,

$$m_2(x,y) = \frac{1}{2}\ln\left\{4\left[\mathrm{ch}\frac{2\pi}{l}\left(\frac{L}{2}-y\right) - \cos\frac{2\pi}{l}x\right]\left[\mathrm{ch}\frac{2\pi}{l}\left(\frac{L}{2}+y\right) + \omega\cos\frac{2\pi}{l}x\right]\right\} \tag{5}$$

In the above equations, t_{CT} is the temperature on the surface of freezing pipe, ξ is the distance from freezing tube to the outer surface of frozen soil wall (i.e. the flange extension of frozen soil wall), r_0 is the outer radius of freezing pipe, t_0 is the actual freezing temperature, l is the spacing of pipes in the same row, and L the distance between two rows. The factor ω is a flag indicating the layout of double-row-pipe freezing (1 for staggered arrangement and -1 for regular arrangement).

Thickness of Frozen Soil Wall

In engineering practice, based on the temperature measured in temperature holes and the temperature field models above, the thickness of frozen soil wall can be calculated as follows:

For Trupak's single-pipe model, the radius of ice column

$$\xi = \exp\left(\frac{t(r)\cdot \ln r_0 - t_{CT}\cdot \ln r + t_0 \cdot \ln \frac{r}{r_0}}{t(r) - t_{CT}}\right) \tag{6}$$

For Bakholdin's single-row-pipe model,

$$\xi = \frac{l}{\pi}\cdot \frac{[t(x,y)-t_0]\ln \frac{l}{2\pi r_0} + (t_{CT}-t_0)m_1(x,y)}{t_{CT}-t(x,y)} \tag{7}$$

And for Bakholdin's double-row-pipe model, the thickness of frozen soil wall

$$E = L + 2\xi \tag{8}$$

Where

$$\xi = \frac{l}{2\pi}\cdot \frac{[t(x,y)-t_0]\ln \frac{l}{2\pi r_0} + [t_{CT}-t_0]\left[m_2(x,y) - \frac{\pi L}{l}\right]}{t_{CT}-t(x,y)} \tag{9}$$

Average Temperature of Frozen Soil Wall

Bakholdin's models have favorable accuracy, but as for average temperature, only a solution for single-row-pipe freezing is given, yet quite rough. Based on Bakholdin's models, average temperature calculation methods considering freezing temperature depression are proposed below.

Equivalent triangle method is suggested to calculate the average temperature of single-row-pipe frozen soil wall. This method chooses the section *l*/6 away from the freezing pipe as the equivalent section and account the average temperature thereof (t_{CP}) as that of the whole frozen soil wall. Calculation of average temperature at the equivalent section is simplified by adopting an equivalent triangle whose base is the thickness of frozen soil wall and height the temperature at the axis plane (t_K). In equation:

$$t_{CP} = \frac{1}{2}(t_K - t_0) + t_0 \tag{10}$$

Where

$$t_K = \frac{\frac{\pi\xi}{l}}{\ln \frac{l}{2\pi r_0} + \frac{\pi\xi}{l}}(t_{CT} - t_0) + t_0 \tag{11}$$

For double-row-pipe freezing, equivalent trapezoid method is proposed. The section *l*/4 away from the freezing pipe is taken as the equivalent section and the average temperature is calculated by equivalent trapezoid. Its upper base is the distance between two rows of freezing pipes, lower base is the total thickness of the frozen soil wall and height the temperature at the axis plane. In equation:

$$t_{CP} = (t_K - t_0)\frac{L+\xi}{L+2\xi} + t_0 \tag{12}$$

where

$$t_K = \frac{t_{CT} - t_0}{\ln\frac{l}{2\pi r_0} + \frac{2\pi\xi}{l}}\left[\frac{\pi(2\xi + L)}{l} - \ln\left(2\mathrm{ch}\frac{\pi L}{l}\right)\right] + t_0 \quad (13)$$

Given functional relation between frozen soil strength and pore water salinity at different temperatures previously achieved by laboratory test, average strength of the frozen soil wall can thus be determined by average temperature obtained from equations above.

CONCLUSIONS

Freezing temperature depression and strength loss of frozen soil is investigated by laboratory work. Besides, new models and approaches considering freezing temperature depression are proposed to calculate the temperature field, thickness and average temperature of frozen soil wall. Hence, safety problems of freezing projects in saline soils such as thickness reduction and strength loss are solved.

ACKNOWLEDGMENTS

The authors appreciate the support of the National Natural Science Foundation of China (Grant No. 50578120) and the National High Technology Research and Development Project of China (863 Project) (Grant No. 2006AA11Z118).

REFERENCES

Anderson D.M. and Morgenstern N.R. (1973). "Physics, chemistry and mechanics of frozen ground." *A review. In Permafrost: The North American Contribution to the 2nd International Conference on Permafrost*, Yakutsk. Washington, D.C.: National Academy of Sciences: 257–288.

Backer, L. and Blindheim, O.T. (1999). "The Oslofjord subsea road tunnel. Crossing of a weakness zone under high water pressure by freezing." *Challenges for the 21st Century*, Alten et al. (eds) Balkema, Rotterdam. (*Proc. ITA World Tunnel Congress '99, Oslo.*)

Bakholdin B.V., *Selection of optimal mode soil freezing for construction*, Moscow: State Construction Press, 1963. (in Russian)

Chamberlain, E.J. (1983). "Frost heave of saline soils." *Proc. 4th Int. Conf. on Permafrost.* Fairbanks, Alaska. Washington, D.C.: National Academy Press: 121-126.

Cui G.X. (1997). "Study on Freezing Point of Wet Soil and Thickness Determining of Freezing Wall in Deep Alluvium." *J. China Univ. of Mining & Technology*, Vol. 26(3): 1-4. (in Chinese)

Frolov, A.D. and Komarov, I.A. (1993). "Characteristics of the thermophysical and electric property changes of saline frozen soils." *Proc. Fourth Int. Symp. on Thermal Eng. and Sci. for Cold Regions* (V.J. Lunardini and S.L. Bowen, Ed.). USA Cold

Regions Research and Engineering Laboratory, Special Report 93–22: 282-287.

Harris, J.S. (1995). *Ground freezing in practice.* Amer Soc of Civil Engineers.

Hoekstra P. (1969). "The physics and chemistry of frozen soils. National Research Council." *Highway Research Board, Special Report 103.*

Hu, X.D., Huang, F. and Bai, N. (2008[a]). "Models of artificial frozen temperature field considering soil freezing point". *J. China Uni. of Mining and Technology*, Vol. 37(4): 550-555. (in Chinese)

Hu, X.D. and Pi, A.R. (2008[b]). "Frozen soil properties for cross passage construction in Shanghai Yangtze River Tunnel." *Geotechnical Aspects of Underground Construction in Soft Ground.* The Sixth Int. Symp. on Geotechnical Aspects on Underground Construction in Soft Ground, Shanghai: 319-324.

Huang, Z.H., Hu, X.D., et al. (2008). "Key techniques in cross passage construction of Shanghai Yangtze River Tunnel by artificial ground freezing method." *The Shanghai Yangtze River Tunnel – Theory, Design and Construction*, Taylor & Francis Group, London: 205-210.

Lewis, G.N. and Randall M. (1961).*Thermodynamics.* 2nd edition, revised by K.S. Pitzer and L. Brewer. New York: McGraw-Hill.

Linke, W.F. (Ed.) (1965). *Solubilities: Inorganic and Metalorganic Compounds.* K–Z. Washington, D.C.: American Chemical Society, vol. II, 4th edition.

Mahar, L.J., Vinson, T.S. and Wilson, R. (1982)."Effect of salinity on freezing of granular soils." *Proc. 4th Int. Symp. on Ground Freezing*, Sapporo, Japan (S. Kinoshita and M. Fukuda, Ed.). Rotterdam, Netherlands: A.A. Balkema.

Ogata, N., Yasuda, M. and Kataoka, T. (1982). "Salt concentration effects on strength of frozen soils." *Proc. 3rd Int. Symp. on Ground Freezing*, Hanover, N.H., U.S.A. USA Cold Regions Research and Engineering Laboratory: 3-10.

Perfect, E., Groenevelt, P.H. and Kay B.D. (1991). "Transport phenomena in frozen porous media." *Transport Processes in Porous Media.* Dordrecht: Kluwer Academic Publishers: 243-270.

Patterson, D.E. and Smith, M.W. (1983). "Measurement of unfrozen water content in saline permafrost using time domain reflectometry." *Proc. 4th Int. Conf. on Permafrost*, Fairbanks, Alaska. Washington, D.C.: National Academy Press: 968-972.

Shen, H.T., Mao Z.H. and Zhu J.R. (2003). *Saltwater Intrusion in the Changjiang Estuary.* Beijing: China Ocean Press. (in Chinese)

Takashi, T, Ohrai, T., Yamaoto, H, Okamoto, J. (1981). "Experimental study of uniaxial compressive strength of homogeneously frozen clay." *Proc. of The Japan Society of Civil Engineers*, No315:83-93. (in Japanese)

Trupak N.G., *Ground freezing in shaft sinking*, Moscow: Coal Technology Press, 1954. (in Russian)

Tsytovich, N.A., Kronik, Y.A., et al. (1973). "Physical and mechanical properties of salinized soils." *Dokl. Soobshch. Mezhdunar. Konf. Merzlotoved*, 2nd edition: 40-52.

Tyutyunov, I.A. and Derbeneva, M.M. (1970). *Crushing strength of frozen saline soils in relation to the chemical composition of saturating solutions.* Sb., Nauch. Issled. Inst. Osn. Podzemn. Sooruzhenii, Report No. 59.

Xu, X.Z., Wang, J.C., Zhang, L.X. (2001). *Frozen Soil Physics.* Beijing: Science Press. (in Chinese)

Large Scale Test on Improving Ultra Soft Soil Using Electro-osmotic Method

Cao Yonghua[1] Yang Jingfang[2] Cheng Dongdong[3]

[1] CCCC-Tianjin port engineering institute, Ltd, 1002 Dagunan road,Tianjin, PRC, Key Laboratory of Geotechnical Engineering, Ministry of Communication, PRC, caoyonghua@126.com;

[2] CCCC-Tianjin port engineering institute, Ltd, 1002 Dagunan road,Tianjin, PRC, Key Laboratory of Geotechnical Engineering, Ministry of Communication, PRC, tpeiyjf2008@sina.com;

[3] Tianjin port industry investment & holding co., LTD, 66 Dong Ting Road, TEDA, Tianjin, PRC; aaronychan@yahoo.com.cn

ABSTRACT: Large scale laboratory test was conducted to study the feasibility of improving ultra soft soil with electro-osmotic method. Two layers of soil was prepared with different water content and placed in a big tank. The electro osmotic test was performed in a stable current. In the test, the electric resistance increased with the time, thus the electric voltage between the cathode and anode increased progressively. With the cutoff of current for 3 days and the reversal of the electrodes, the electric voltage between the electrodes fell significantly. It is helpful to reduce power consumption. Settlement and dissipation of pore water pressure were also observed. The test was ended after 25 days owing to the corrosion of the electrodes. For the soil in the upper layer, the water content decreased from 96% to 80%. For the soil in the lower layer, the water content decreased from 70% to 65%, and the vane shear strength increased from 4.5kPa to 9.0kPa. The test results indicated that the sole use of electro osmosis may not effectiveness of the electro osmotic method for improving ultra soft soil, thus it can be a better choice to use the electro osmotic method in combination with other soil consolidation methods.

INTRODUCTION

In present China, land reclamation has become a widely applied practice with the rapid development of the coastal areas. In some cases, ultra soft soil needs to be improved shortly after the completion of a dredging project because of the requirements of the construction period. Some soil-improvement projects have proved that the ultra soft soil is very difficult to improve with the conventional drainage consolidation methods, such as vacuum preloading or surcharge preloading. Electro osmosis is usually considered as an effective method for clayey soil even though the particles may be very fine. The ultra soft soil usually has very fine particles, hence the electro-osmosis may be an alternative method for this kind of soil.

Studies have been carried out on application of electro-osmosis for ground improvement. Esrig (1968) presented a one-dimensional consolidation theory of

electro-osmosis. Wan and Mitchell's (1976) one-dimensional consolidation theory of electro osmosis included the combined effect of electro-osmotic and direct loading consolidation and demonstrated the effectiveness of electrode reversal technique. Su and Wang (2003) deduced the two-dimensional consolidation theory of electro osmosis. Lewis and Chris (1973) provided a numerical analysis, which could consider the variation of electric flow in the process of electro osmosis. Many outstanding laboratory tests (Lo et al. 1991, Shang *et al.* 1996, Laursen *et al.* 1997, and Micic *et al.* 2001) were conducted to study the performance of electro osmosis, but these tests were in small scales, which may weaken their referential value for engineering application. Seldom studies were found to improve ultra soft soil with electro osmosis. In this paper, large scale laboratory tests were conducted to study the feasibility of improving ultra soft soil with electro osmosis.

EXPERIMENTAL DESIGN

The ultra soft soil in this study was taken from two land reclamation sites, Dalian and Qingdao, which are both coastal cities in Northern China. The ultra soft soil in this study had relatively low strength after they had been improved with vacuum preloading. This kind of ultra soft soil usually has high water content, high fines content and fine grain sizes. The soil was placed in two layers in a big test tank which was 2.0m (L)*2.0m(H)*1.5m(W). The upper layer was soil from Dalian with a thickness of 450mm while the lower layer was soil from Qingdao with a thickness of 1100mm. Thus, the effectiveness of the electro osmotic method for different soils could be studied. The major physical properties of the soils can be seen in Table 1 and Fig. 1.

Table 1. Physical properties of ultra soft soil

Soil	Water Content (%)	Unit Weight (kN/m^3)	Plastic Index	Fine Content (%)
Upper layer	96	1480	26	47.4
Lower layer	70	1610	29	31.3

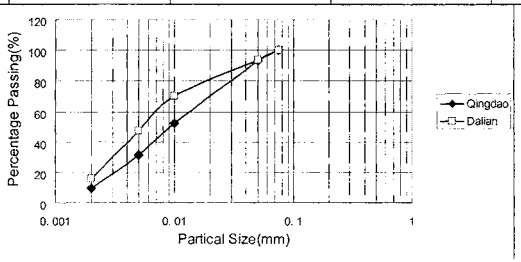

FIG. 1. Grain size distribution of ultra soft soil

The electrodes were made of steel tubes with perforated holes in the tube walls. To prevent the soil from entering the electrodes, the electrodes were wrapped with filter cloth. The external diameter of the steel tubes was 20mm and the thickness of the tube walls was 1mm. The electrodes were shown in FIG. 2.

The horizontal distance between the electrodes was 400mm and the length of the

electrodes in the soil was 1200mm. Pore water pressure gauges, electric potential sensors and mini settlement plates were used to monitor the process of the test. The layout plan of the test was shown in FIG. 3.

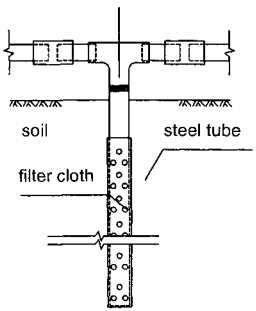

FIG. 2. Electrode

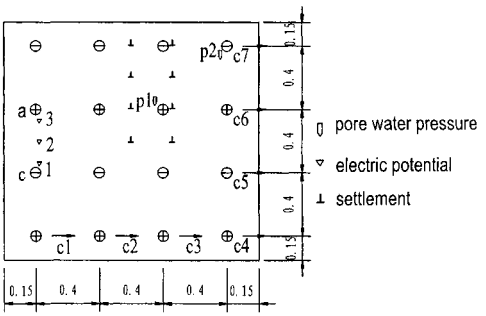

FIG. 3. Layout plan of testing instruments

The electro-osmotic test was performed in a stable current. When the voltage increased significantly, the current was cut off and the test was suspended. The water gathered at the cathodes was pumped away for 10 minutes per hour. To minimize the effect of vacuum on the soil, the vacuum was controlled below 20kPa. After a break of several days, the electro osmotic test was restarted and reversal of the electrodes was conducted. The effectiveness of the electro osmotic method was demonstrated by the decrease of water content and the increase of vane shear strength of the soil.

RESULTS AND DISCUSSION

As shown in FIG. 3., the electrodes were placed in four rows and the total current of the four rows was stabilized at 30A. After 17 days of electro osmotic improvement, the current was cut off for a break of 3 days. Then the cathodes and the anodes were inverted and the electro osmotic process was restarted. In the process of electro osmotic improvement, the current in these rows of electrodes had different change tendency owing to the physical and chemical changes in the test and their different plan position.

The electric currents of different rows of electrodes were shown in FIG. 4., in which, c7 and c5 were the currents of the two rows of cathodic electrodes which didn't corrode and the electric resistance remained stable, so c7 and c5 were relatively stable in the test. C5 was greater as this row of electrodes was in the middle of the test field. After the reversal of the electrodes, the electrodes in the two rows became anodes and corrosion took place, making c7 increase and c5 decrease.

C6 and c4 were the currents of the two rows of anodic electrodes which corroded and the electric resistance of which also changed, so c6 and c4 were changed in the test. C6 was greater because the electrodes in this row were located in the middle of the test field. The electrodes in the row, which had greater initial current, corroded faster and the electric resistance increased more quickly, therefore, before the reversal of the electrodes, c6 decreased significantly. To keep the total current stable, c4 was increased at the same time.

The distribution of current in one row can be seen in FIG.5. , in which, c1, c2, c3, and

c4 were currents at different positions in the same row of electrodes. The currents at different positions had fair regularity and increased from c1 through c4. This proved the uniformity of the electrodes and the soil.

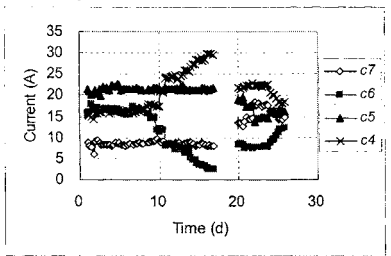

FIG. 4. Current of different branches

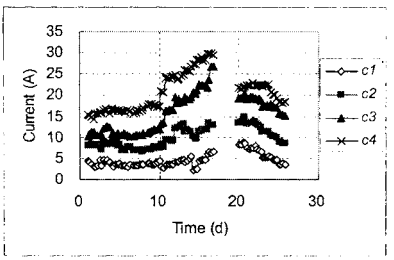

FIG. 5. Current in one branch

The electric potential of the cathode was zero. C-1 was the electric potential of the soil which was 5cm away from the cathode; C-2 was the electric potential of the soil which was 20cm away from the cathode; C-3 was the electric potential of the soil which was 5cm away from the anode; and C-a was the electric potential of the anode. As shown in Fig.6, the electric potential of the soil increased from a cathode to an anode and increased with the time. There was a sharp increase of c-a after the electro osmotic process continued for 12 days, but the electric potential at other positions decreased slightly. The reason was that the soil near the anode became dryer and the soil near the cathode became wetter in the test, which can also explain the phenomena shown in Fig.7. The distribution of electric potential was ranged from 0 to 1 in FIG.7. At the early stage of the test, the distribution of electric potential was fairly even in the soil because the difference between c-1 and c-2 and between c-2 and c-3 was close to each other. After the electro osmotic process continued for 12 days, the relative electric potential consumed in the soil from cathode to soil (c-1 to c-3) decreased sharply because the soil near the anode consumed most of the electric potential.

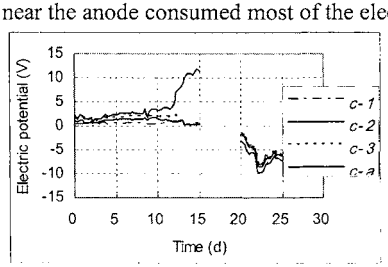

FIG. 6. Electric potential vs. time electrodes

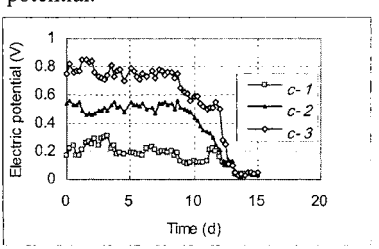

FIG.7. Electric potential between two

To avoid too much electric potential consumption near the anodes and improve the efficiency of the power, electrode reversal was an effective method. As shown in FIG.6, after reversal of electrodes, the electric potential decreased significantly. But they increased again in the electro osmotic process because the soil near the anode (a cathode before the reversal) became dryer.

Pore water pressure was monitored and measured in the test. P1 was measured at the depth of 0.6m and p2 was measured at the depth of 1.1m. As shown in FIG.8, the pore water pressure dissipated gradually in the test, indicating the increase of effective stress of the soil. The dissipation was not significant owing to the short period of electro osmosis.

Settlement of soil was measured with 8 mini settlement plates, which were made of aluminum to minimize their weight. As shown in FIG.9, the settlement developed gradually in the process of the test. There was an obvious slowdown of settlement in the intermission of 3 days (from the 17th day to the 19th day). The ultimate settlement was 46mm.

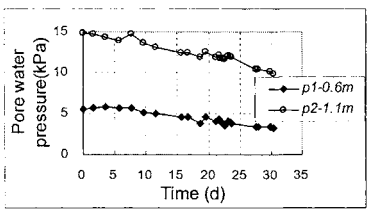

FIG.8. Pore water pressure vs. time

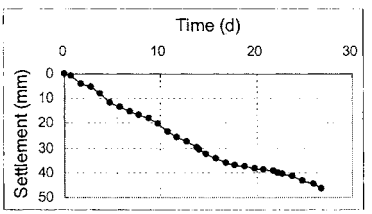

FIG. 9. Settlement vs. time

The initial water content of the soil in the upper layer was 96% and was reduced to 80% after the electro osmosis. Though the water content decreased significantly, it was still too high to make the soil achieve measurable strength.

The initial water content of the soil in the lower layer was 70% and it was reduced to 65% after the test. At the same time, the vane shear strength increased from 4.5kPa to 9.0kPa (FIG.10). Though the vane shear strength increased significantly, the development of strength was limited by the exhaustion of steel electrodes. But the test can still verify the effectiveness of electro osmotic process to improve ultra soft soil made of fine particles. If the steel electrodes worked longer, the vane shear strength of the soil would be higher.

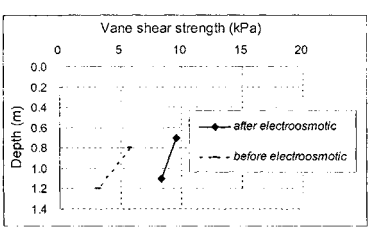

FIG.10. Comparison of vane shear strength

Based on the electric current and potential records, the power consumption during the test was 21.12kw.h/m^3, indicating that the electro osmotic process alone was not an economical method for improving ultra soft soil owing to the power consumption and corrosion of electrodes.

CONCLUSIONS

In the case of stable current, the electric potential increased gradually. In the later

time before the electrode reversal, most of the electric potential was consumed near the anode. After the electrode reversal, the electric potential decreased significantly. To avoid too much electric potential consumption near the anode and improve the efficiency of the power, electrode reversal was an effective method.

Though the water content of the soil in the upper layer was reduced obviously, the strength was still too low to be measured by vane shear test because of the high water content after the electro osmotic process. The water content of the soil in the lower layer was reduced obviously and the vane shear strength increased at the same time. The strength was not very high after the electro osmotic process because of the exhaustion of electrodes. But this increase of strength can verify the effectiveness of electro osmotic process for improving ultra soft soil.

The ultimate strength of soil improved with the electro osmotic process using steel electrodes was limited by the corrosion of anodes and the high initial water content in soil. Hence, to improve the strength of soil with the electro osmotic process, one way is to use electrodes made of in corrosive material while another way is to adopt other soil improvement methods in combination with. When a combined method is used, conventional soil improvement methods such as the vacuum preloading technique can be first used to reduce the high initial water content and then the electro osmotic process can be used to improve the ultimate strength of the soil.

REFERENCES

Esrig.M.I.(1968). "Pore Pressure, Consolidation and Electrokinetics." Journal of the SMFD, ASCE, 94(SM4), 899~921.

Laursen S.(1997). "Laboratory investigation of electroosmosis in bentonites and natural clays." Canadian Geotechical Journal, 34(5): 664-671.

Lewis,W.R. and Chris Humpheson(1973). "Numerical Analysis of Electroosmotic Flow in Soils." Journal of the SMFD, ASCE, 95(SM4), 603~616.

Lo K.Y., Ho K. S.(1991). "Electroosmotic strength of soft sensitive clays." Canadian Geotechical Journal, 28(1): 62-73.

Micic S., Shang J.Q.(2001). Lo K.Y., Lee Y.N., Lee S.W., "Electrokinetic strengthening of a marine sediment using intermittent current." Canadian Geotechical Journal, 38(22): 287-302.

Shang J. Q., Dunlap W. A.(1996). "Improvement of soft clays by high boltage electrokinetics." Geotechnical engineering Journal, 29(2):117-120.

Su, J.Q., Wang, Z.(2003). "The two-dimensional consolidation theory of electro-osmosis." Geotechnique, 53(8): 759-763.

Wan T.Y. and Mitchell J. K. (1976). "Electroosmotic Consolidation of Soils." Journal of the Geotechnical Engineering Division, GT5 (5), 473~491.

Finite Element Modeling Of A Field-Scale Shored Mechanically Stabilized Earth Wall

Cheng Chen[1], Louis Ge[2], and Jia Sheng Zhang[1]

[1]Central South University, School of Civil Engineering and Architecture, Changsha, China. E-mail: chencheng401@sina.com
[2]Missouri University of Science and Technology, Department of Civil, Architectural, and Environmental Engineering, 1401 N Pine Street, Rolla, MO 65409; PH (573) 341-7193; FAX (573) 341-4729; E-mail: geyun@mst.edu

ABSTRACT: The shored mechanically stabilized earth (SMSE) walls are typically used in steep terrain to allow construction of a new road or widening of an existing narrow road by constructing the wall on the outboard of the roadway. The state-of-practice suggests a minimum bench width and MSE reinforcement length equivalent to seventy percent of the design height of the MSE wall. It has been shown recently that shorter reinforcement length is sufficient when the SMSE wall system is constructed and the retaining benefits provided by the shoring component should be taken into consideration. In this paper, a finite element analysis is performed to model a tested field-scale SMSE wall. The finite element model including the constitutive models, boundary conditions, and staged construction procedure is discussed in detail.

INTRODUCTION

MSE walls are typically used to allow construction of a new road or widening of an existing narrow road by constructing the wall on the outward site of the roadway. They behave as a flexible coherent block which is capable of sustaining significant load due to the tensile strength provided by the reinforcement and the interface strength between the backfill material and the reinforcing elements. In steep terrain, a flat bench is normally excavated where the MSE wall is constructed. The state-of-practice suggests a minimum bench width and MSE reinforcement length equivalent to seventy percent of the design height of the MSE wall (Elias et al., 2001). Shoring walls often with soil nails have been used to stabilize the back slope for construction of the MSE wall. In other words, the MSE wall is designed and constructed in front of the shoring wall. When a composite MSE and shoring wall system is proposed for a project, the MSE wall component of the system should consider the long-term retaining benefits provided by the shoring wall, including reduction of lateral loads

on the MSE wall mass and significant contributions to global stability (Morrison et al., 2006).

This paper presents a finite element analysis procedure to model a tested field-scale SMSE wall with an instrumentation of strain gages, pressure cells, LVDTs, and potentiometers. The finite element model including the constitutive models, boundary conditions, and staged construction procedure is discussed in detail. Due to the space limitation, only the field measurement and numerical results of the vertical settlement and horizontal displacement at various loading condition are compared and discussed.

FIELD-SCALE SMSE WALL TEST

A field-scale testing of shored MSE (SMSE) wall system was performed at the Turner Fairbanks Highway Research Center of the Federal Highway Administration in McLean, Virginia. The field-scale test model consisted of a test wall with shore MSE reinforcements. The test wall was constructed using geogrid reinforcements with wire facing elements. Half of the wall was constructed as an unconnected system, while the other half of the wall incorporated reinforcements attached to the shoring wall. The finite element analysis in this paper simulates the latter one.

As shown in Fig. 1, the MSE wall was constructed with a facing batter of 1H:24V (horizontal:vertical) and the shoring wall was constructed at a batter of 1H:6V behind the reinforced section. The minimum geogrid reinforcement length (measured at the bottom of the wall) was 1.4 m, the reinforcement length increased from bottom to top, with the longest MSE reinforcement length (2.14 m). The vertical reinforcement spacing was set at a nominal 0.46 m. More detailed information is available in Morrison et al., 2006.

FINITE ELEMENT ANALYSIS

A plane-strain finite element model was constructed to mimic the construction process of the SMSE wall, followed by the static load test through a footing on the top of the wall. Fig. 2 below shows the geometry of the finite element model. The wall is 5.76 m high with a reinforcement base width of 1.40 m increasing to 2.12 m at the top. Lift thickness is 0.48 m, and additional geogrids were placed centrally in lifts 11 and 12. In the following discussion, the materials models, structure members including geogrids, facing unit, and wall facing, and boundary conditions are discussed in detailed. All the analyses were carried out by PLAXIS.

Constitutive Models

Initial attempt was made by using the Mohr-Coulomb model (linearly elastic and perfectly plastic) to simulate the compacted back fill materials. However, after several trials, the finite element analysis led to either excessive vertical settlement or failure of the wall system. Mohr-Coulomb model was found not adequate to model the back fills in the wall system so Hardening Soil model was adopted instead. The model parameters were first roughly estimated based on Allen et al., (2003) and then finely tuned through comparison between field measurement and numerical computation. It is assumed that the back fills were highly compacted so that a high

friction angle and secant moduli were chosen. Interface elements were applied along the soil-geogrid interface. As the material models for geogrid, footing, and MSE facing units, the values were adopted in Morrison et al. (2006). In Plaxis, a specific model is available for modeling geogrid, which is treated as an elastic material with an option of adding a maximum allowable tensile force. The Young's modulus E used in the geogrid model is normally available through the geogrid manufacturer's specification.

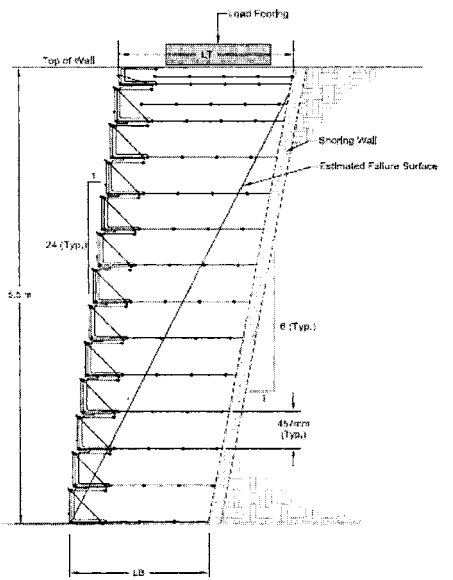

Fig. 1 – The field-scale test wall cross section with connected system (adopted from Morrison et al., 2006).

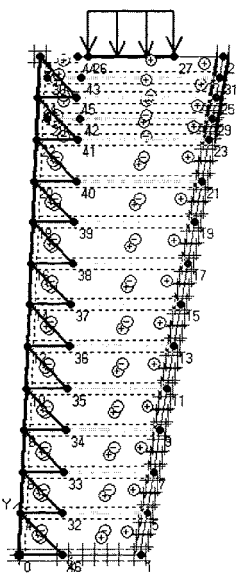

Fig. 2 – PLAXIS finite element model configuration

Boundary Conditions and Staged Construction Procedure

As depicted in Fig. 2, the nodes on the back of the wall along the shoring were fixed as well as those at the bottom of the wall except the nodes 0 and 2. The justification of releasing the horizontal and vertical fixities for nodes 0 and 2, respectively, is to avoid an unnecessary development of stress concentration during the staged construction and static load test through the footing. There were twelve lifts in constructing the wall, where in each lift the corresponding soil cluster, geogrid, and facing unit were activated. The accumulated deformation during the wall construction was reset to zero before the static load test was performed.

Table 1 – Soil model parameters

Parameter	Value
Unit weight (unsaturated), γ	15kN/m^3
Effective cohesion, c'	5 kPa
Effective friction angle, φ'	45 degrees
Dilatancy angle, ψ	12 degrees
Power for stress-level dependency of stiffness, m	0.5
Reference secant molulus for deviatoric loading, E_{50}^{ref}	50000 kPa
Reference secant molulus for primary compression, E_{oed}^{ref}	50000 kPa
Reference secant molulus for unloading/reloading, E_{ur}^{ref}	100000 kPa
Poisson's ratio for unloading/reloading, ν_{ur}	0.2
Reference pressure for stiffness, p^{ref}	100 kPa
Tension strength, $\sigma_{tension}$	2 kPa
Failure ratio, R_f	0.9
Interface ratio, R_{inter}	1.0

Table 2 – Model parameters for geogrid

Parameter	Value
Axial stiffness per unit strain, EA	1560 kN/m
Maximum tensile force, F	114kN/m

Table 3 – Model parameters for loaded footing

Parameter	Value
Axial stiffness per unit strain, EA	1.4 × 10^7 kN/m
Bending stiffness, EI	2.8 × 10^5 kN/m^2/m
Unit weight, γ	12 kN/m^3/m

Table 4 – Model parameters for MSE facing units

Component	Parameter	Value
Vertical Facing	Axial stiffness per unit strain, EA	4 kN/m
	Bending stiffness, EI	0.12 kN/m^2/m
	Moment capacity, M_p	2000 kN/m/m
	Axial force capacity, N_p	6 kN/m
	Possion's Ratio, ν	0.3
	Unit weight, γ	0.046kN/m^3/m
Support Strut	Axial stiffness per unit length, EA	10900 kN
	Maximum compressive force, $F_{max,comp}$	17 kN
	Maximum tensile force, $F_{max,tens}$	17 kN

Out of plane spacing, L	1.0 m

RESULTS

The finite element analysis of the SMSE wall was carried out iteratively until the numerical computation reasonably matched the field measurement. Fig. 3 shows such an outcome that the footing settlement was plotted against applied vertical stress. The computed maximum settlement was about 19 mm under the vertical stress 356 kPa while the field measurement was about 17 mm under the same vertical stress. However, the overall trend from finite element analysis fit well when compared to field-scale testing. As for the corresponding horizontal displacement of the footing due to the applied vertical stress, the computed maximum horizontal displacement was about 9.2 mm while the field measurement was about 8.7 mm as shown in Fig. 4. It is found from the computed horizontal deflection of the wall facing (not shown in the paper) was quite different than the field measurement, which is believed to lead to at 2.5 mm difference in horizontal displacement after the footing was fully unloaded.

CONCLUSIONS

It is demonstrated that the finite element analysis can be used to simulate the stage construction process in geotechnical engineering. The model presented here was calibrated against the measurement in a field-scale testing program. The calibration process is not trivial and requires better understanding of material behaviors and construction sequences. By and large, the finite element model performed well and shed lights on future sophisticated modeling geotechnical construction process.

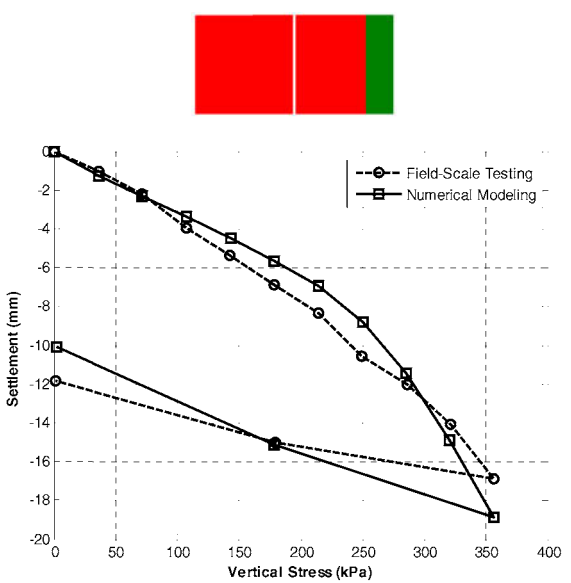

Fig. 3 – Comparison of settlement of load footings

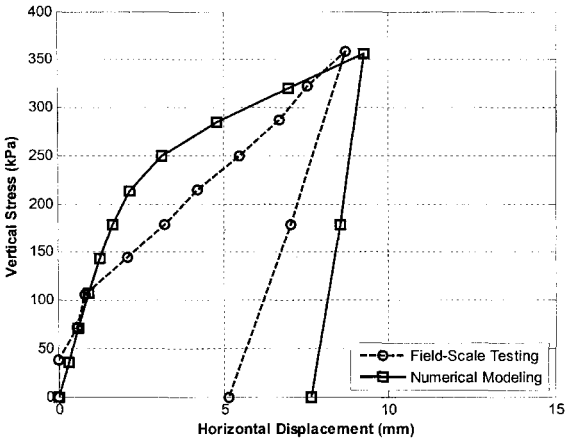

Fig. 4 – Comparison of horizontal displacement of load footings

REFERENCES

American Association of State Highway and Transportation Officials (AASHTO). (2002). Standard Specifications for Highway Bridges, Seventeenth Edition. HB-17.

Elias, V., Christopher, B. R., and Berg, R. R. (2001). Mechanically Stabilized Earth Wall and Reinforced Soil Slopes, Design & Construction Guidelines. *Report No.* FHWA-NHI-00-043. Federal Highway Administration, March. 394 pp.

Morrison, K. F., Harrison, F. E., Collin, J. G., Dodds, A, and Arndt, B. (2006). Shored Mechanically Stabilized Earth Wall Systems Design Guidelines. *Report No.* FHWA-CFL/TD-06-001. Federal Highway Administration, February. 212 pp.

PLAXIS b.v. (2002). PLAXIS 2D, Version 8, Finite Element Code for Soil and Rock Analyses, Netherlands.

Allen, T. M., Bathurst, R. J., Hotlz, R. D., Walters, D. and Lee, W. F. (2003). "A New Working Stress Method for Prediction of Reinforcement Loads in Geosynthetic Walls." *Canadian Geotechnical Journal*, 40: 976-994.

Bearing Capacities of Geogrid-reinforced Sand Bases under Static Loading

Yan-Li Dong[1], Jie Han[2], M. ASCE, and Xiao-Hong Bai[3]

[1] College of Architecture and Civil Engineering, Taiyuan University of Technology, Taiyuan 030024, P.R. China; Department of Civil, Environmental, and Architectural Engineering, the University of Kansas, Lawrence, Kansas 66045, USA; qianxinjie@ku.edu
[2] Department of Civil, Environmental, and Architectural Engineering, the University of Kansas, Lawrence, Kansas 66045, USA; jiehan@ku.edu
[3] College of Architecture and Civil Engineering, Taiyuan University of Technology, Taiyuan 030024, P.R. China; bxhong@tyut.edu.cn

ABSTRACT: Since geogrids with triangular apertures have a more symmetrical and therefore more stable structure than biaxial geogrids, they are expected to provide more uniform resistance in all directions. Laboratory model tests were performed in this study to evaluate the bearing capacities of triangular aperture geogrid-reinforced bases under static loading. Unreinforced bases and biaxial geogrid-reinforced bases were also tested for comparison purposes. In this study, the influence of aperture shape, location, and number of geogrids on the bearing capacity were investigated. The test results showed that all the reinforced sections performed better, when the geogrid was placed within the depth of 2/3 of the plate diameter, than the unreinforced section. Triangular aperture geogrids had higher capacity to weight ratios than biaxial geogrids.

INTRODUCTION

Geogrids have been increasingly used for soil reinforcement in the past 30 years. As a planar reinforcement, geogrids have been successfully used to improve soft subgrade and reinforce base courses by providing lateral confinement. The benefits of biaxial geogrid reinforcement on the increase in bearing capacity and reduction in settlement have been well recognized. Many papers have been published relating to the evaluation of bearing capacities and settlements of footings over geogrid-reinforced sand or clay. For example, Yetimoglu et al. (1994) investigated the bearing capacities of rectangular footings on geogrid-reinforced sand by performing laboratory model tests and finite-element analyses. Guido et al. (1987) performed 80 plate load tests using a 305mm×305mm square plate to study the effects of the location of the top geogrid layer and the width, the number, and the tensile strength of geogrid on the load-settlement responses. Gabr et al. (1998) conducted five plate load tests to investigate the effect of the geogrid depth on the stress distributions in geogrid-reinforced sand. DeMerchanta et al. (2002) performed 25 plate load tests in a large laboratory test pit (2.2×3.2×1.6m deep) using a 305mm diameter rigid steel

plate. In the DeMerchanta et al. (2002) study, five influence factors were investigated: the soil density (compacted and loose), the width of geogrid reinforcement, the location of the top geogrid layer, the number of geogrid layers, and the tensile strength of geogrid.

All the above-mentioned studies used biaxial geogrids. Due to the shape of apertures, biaxial geogrids are relatively strong in the machine and cross-machine directions; however, they are relatively weaker in other directions (for example, 45° to the machine direction). The numerical study done by Dong et al. (2010a) demonstrated such a strength distribution. The new triangular aperture geogrid products with a triangular aperture shape recently introduced into the market are expected to have a more stable grid structure, which can provide more uniform resistance in all directions. However, limited test data related to triangular aperture geogrid-reinforced bases has been published so far. Dong et al. (2010b) conducted six plate load tests to study the influence of the depth and type of triangular aperture geogrid on the reinforced sand bases. In this study, more plate loading tests were conducted to investigate the influence of aperture shape, location, and number of geogrid layers on the bearing capacity. The efficiency of the two geogrid products (biaxial and triangular aperture geogrids) will be evaluated based on the ratio of the bearing capacity to the weight of the geogrid.

PROPERTIES OF BASE AND GEOGRID MATERIALS

Kansas River sand was used as the granular base in this study. This sand is poorly-graded and sub-rounded with a minimum void ratio of 0.354, a maximum void ratio of 0.583, and a specific gravity of 2.65 at 20°C. The corresponding maximum and minimum unit weights of this sand are 19.5kN/m^3 and 16.4kN/m^3, respectively.

Three types of geogrid with a triangular aperture shape, named TX1, TX2, and TX3, were used in this study. Two types of biaxial geogrid with a rectangular aperture shape, named BX1 and BX2, were used for comparison purposes. All the geogrids used in this study were made of polypropylene by a punched-drawn manufacturing process and therefore are part of the punched and drawn geogrid family. Due to the triangular apertures, the tensile strengths of triangular aperture geogrids cannot be only defined in the machine and cross-machine directions. Appropriate mechanical properties of these products are still under development. In terms of their relative strength and stiffness, TX1 is the weakest while TX3 is the strongest among three triangular aperture geogrids. BX1 and BX2 have ultimate tensile strengths of 19.2kN/m and 27.0kN/m in the machine direction, respectively. The nodal thicknesses of TX1, TX2, and TX3 geogrids are 2.1, 3.1, and 4.1mm, respectively. The nodal thicknesses of BX1 and BX2 geogrids are 4.2 and 4.4mm, respectively. The size of the geogrids used in all the tests was 80cm in length by 80cm in width. Among these five products, TX1 geogrid is the lightest one while BX2 geogrid is the heaviest one.

TEST SETUP

Laboratory plate load tests were conducted in a medium-scale loading apparatus designed and fabricated at Department of Civil, Environmental, and Architectural Engineering at the University of Kansas. The loading system had a 15cm diameter air cylinder and could apply a pressure up to 1,000 kPa. The test box was square and had a plan area of 6400 cm^2 with an adjustable depth. The loading plate was selected based on the size of the test box to avoid a boundary effect and had the same diameter as the cylinder. The Kansas River sand was placed and compacted to 70% relative density by four layers, 5 cm each for all the four layers. The compaction to 70% relative density of the sand was maintained in all tests by using the same amount of sand in a fixed volume. No subgrade existed for all the tests because the primary purpose of this research was to evaluate the bearing capacities of the triangular and biaxial geogrid-reinforced bases under static loading. Both reinforced and unreinforced sections were tested by increasing the load in increments until failure using the maintained load test method. The load was applied through the air cylinder and the displacements were measured by three dial gauges. The next load increment was applied when no further displacement was noticed under the current load increment. The test was terminated when the total displacement became excessive (mostly greater than 20mm).

RESULTS AND DISCUSSIONS

Effect of aperture shape

This study investigated the effect of the aperture shape of geogrid on the bearing capacities of reinforced sand bases. Based on the previous study (Dong et al., 2010b), the geogrid showed the most benefit when placed at the depth of 5cm (i.e., 1/3 of the plate diameter). In this investigation, all the triangular and biaxial geogrids were placed at 5cm below the surface. An unreinforced base was also tested for comparison purposes. Figure 1 presents the test results of five reinforced bases and one unreinforced base. It is shown that the inclusion of a triangular or biaxial geogrid increased the ultimate bearing capacity and stiffness (i.e., the slope of the initial portion) as compared with the unreinforced base. During the tests, it was observed that the failure modes of the triangular and biaxial geogrids are different. No significant heaving was observed on the triangular aperture geogrid-reinforced bases, while larger heaving was observed on the biaxial geogrid-reinforced bases. The larger heaving indicates the lateral movement and failure of the sand above the biaxial geogrid. On the other hand, the failure of the triangular aperture geogrid-reinforced bases was due to the failure of sand below the triangular aperture geogrid, which minimized the heaving from that below the geogrid. This phenomenon implies that the triangular aperture geogrid has a higher interface shear resistance than the biaxial geogrid. The triangular shape of the triangular aperture geogrids may have contributed to the higher interface shear resistance.

Table 1 presents the bearing capacity, the bearing capacity ratio (BCR), and the capacity to weight ratio (CWR) of the base reinforced by a different type of geogrid.

The ultimate bearing capacity was determined based on the applied pressure after which a sudden and excessive displacement occurred. BCR is defined as the ratio of the ultimate bearing capacity of the reinforced base to that of the unreinforced base. CWR is referred to as the ratio of the ultimate bearing capacity of the reinforced base to the weight of the geogrid used to reinforce that base. Table 1 shows that the BCR values ranged from 1.5 to 2.1 and the triangular aperture geogrids had higher CWRs than the biaxial ones. The higher CWR implies higher efficiency of the triangular aperture geogrids than the biaxial geogrids.

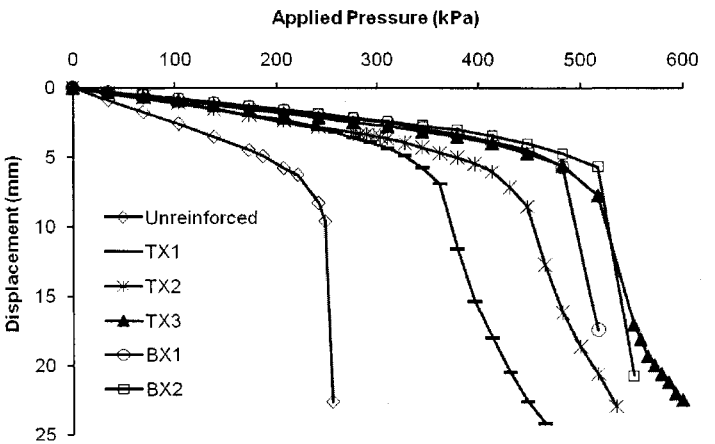

FIG. 1. Pressure vs. displacement curves for unreinforced and reinforced bases with different types of geogrid.

Table 1. Bearing Capacities of Bases Reinforced by Different Types of Geogrid

Type	TX1	TX2	TX3	BX1	BX2
Ultimate bearing capacity (kPa)	365	450	520	380	520
Bearing capacity ratio	1.5	1.8	2.1	1.9	2.1
Capacity to weight ratio ($kPa/m^2/kg$)	1750	1920	1830	1190	1330

Effect of geogrid location and layers

To study the effect of the geogrid location, one layer of TX2 geogrid was placed at a different position (5, 10, or 15 cm) in the Kansas River sand in each test (i.e., TX2-

5, TX2-10, or TX2-15). To investigate the effect of the number of geogrid layers, two layers of TX2 geogrid were placed at depths of 5 and 10cm in the Kansas River sand (i.e., TX2-5-10). The test results of four reinforced sections and one unreinforced section are plotted in Figure 2. Figure 2 shows that the ultimate bearing capacity and stiffness of a single layer geogrid-reinforced base decreased with an increase of the depth of the geogrid layer. The sand base reinforced by two layers geogrid had the highest ultimate bearing capacity. As compared with one layer of TX2 geogrid at the depth of 5cm, two layers of TX2 geogrid not only increased the bearing capacity and stiffness of the base but also changed the pressure-displacement relationship from the ductile to brittle behavior. It was observed that the base reinforced by the two layers of geogrid failed suddenly with larger heaving because the second geogrid layer at the depth of 10cm prevented the failure from occurring below the top geogrid and forced the failure occur above the top geogrid.

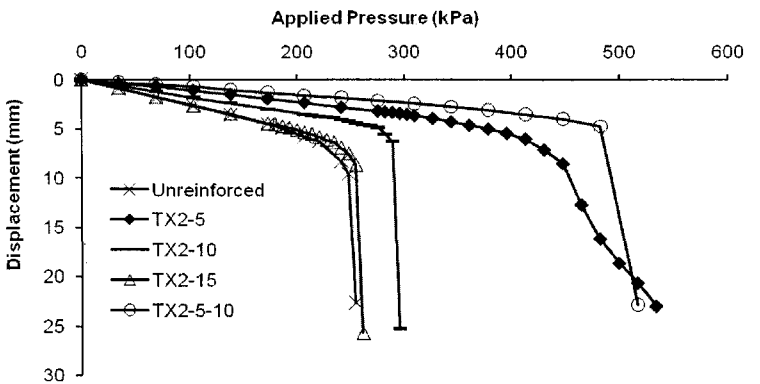

FIG. 2. Pressure vs. displacement curves for unreinforced and reinforced bases by TX2 geogrids at different locations.

Table 2 presents BCR and CWR values of sand bases reinforced by TX2 geogrids at different locations. It is shown that the BCR value of the sand base reinforced by a single layer of geogrid decreased from 1.8 to 1.0 with an increase of the geogrid depth. The sand base reinforced by two layers of geogrid had the largest BCR value but the lowest CWR value. The lowest CWR value implies that the two-layer geogrid system may not be efficient as compared with the one-layer geogrid system.

Table 2. Bearing Capacities of Sand Bases Reinforced by TX2 Geogrid at Different Positions

Type	TX2-5	TX2-10	TX2-15	TX2-5-10
Ultimate bearing capacity (kPa)	450	290	255	485
Bearing capacity ratio	1.8	1.2	1.0	1.9
Capacity to weight ratio ($kPa/m^2/kg$)	1925	1240	1090	1040

CONCLUSIONS

This paper presents the results of an experimental study conducted to investigate the bearing capacities of triangular aperture geogrid-reinforced bases as compared with biaxial geogrid-reinforced bases under static loading. The following conclusions can be drawn from this study:

- The reinforced sections were found to perform better than the unreinforced sections when the geogrid was placed at 5 or 10cm (1/3 or 2/3 of the plate diameter). The geogrid at the depth of 5cm performed the best.
- A heavier and stiffer geogrid resulted in higher ultimate bearing capacity and stiffness of the reinforced base.
- The observations implied that triangular aperture geogrids had a higher interface shear resistance than biaxial geogrids.
- Triangular aperture geogrids had higher capacity to weight ratios than biaxial geogrids.
- The use of the second layer of geogrid increased the ultimate bearing capacity but reduced the capacity to weight ratio or system efficiency.

ACKNOWLEDGMENTS

The first author was sponsored by the Chinese Scholarship Council to be a visiting scholar at the University of Kansas. The geogrid materials were supplied by the Tensar International, Inc. The authors are thankful for their great help.

REFERENCES

DeMerchant, M.R., Valsangkar, A.J., and Schriver, A.B. (2002). "Plate load tests on geogrid-reinforced expanded shale lightweight aggregate." *Geotextiles and Geomembranes,* Vol.20: 173–190.

Dong, Y.-L., Han, J., and Bai, X.-H. (2010a). "A numerical study on stress-strain responses of biaxial geogrids under tension at different directions." *Proceedings*

of ASCE Geo-Institute GeoFlorida 2010, West Palm Beach, Florida, February 20 to 24, in press.

Dong, Y.-L., Han, J., and Bai, X.-H. (2010b). "Behavior of triaxial geogrid-reinforced bases under static loading." *Proceedings of the 9th international Conference on Geosynthetics*, Guarujá, Brazil, May 23 to 27, in press.

Gabr, M.A., Dodson, R., and Collin, J.G. (1998). "A study of stress distribution in geogrid-reinforced sand." *Proceedings of geosynthetics in foundation reinforcement and erosion control systems. ASCE Geotechnical Special Publication,* Vol.76: 62–76.

Guido, V.A., Knueppel, J.D., and Sweeny, M.A. (1987). "Plate loading tests on geogrid-reinforced earth slabs." *Geosynthetics 87 Conf.*, New Orleans: 216–225.

Yetimoglu, T., Wu, T.H., and Saglamer, A. (1994). "Bearing capacity of rectangular footings on geogrid-reinforced sand." *Journal of Geotechnical Engineering,* Vol. 120(12): 2083-2099.

Performance Study of Geosynthetic Reinforced Soil Retaining Structures

Sao-Jeng Chao

Associate Professor, Department of Civil Engineering, Ilan University, Ilan, Taiwan; chao@niu.edu.tw

ABSTRACT: Geosynthetic reinforced soil retaining structures (GRSRS) have the benefits of low construction cost, hard to decay, and construction convenience. However, GRSRS are composed of backfill materials and reinforcements, which are relatively complex in considering of the soil-structure interaction. The complicated soil-reinforcement interaction and its effects on the behavior of GRSRS need to be investigated comprehensively. This paper follows the processes of cases description and numerical analysis to study the performance of the four major GRSRS built in Ilan County, Taiwan. The purpose of this paper is to validate a relatively reliable and economical technique to be adopted greatly at present in civil engineering practice.

INTRODUCTION

Geosysthetic reinforced soil retaining structures (GRSRS) were introduced into Taiwan around late 1980s. Since then, the geosynthetic reinforced soil retaining structures have been increasingly constructed in Taiwan. There are 4 major cases of large-scale land developing projects employed the technique of GRSRS to increase the geotechnical stability of slopes in Ilan County, Taiwan.

However, because the good-quality backfilled materials are in short supply and the principle of balancing cutting and filling is required to follow by the Soil and Water Conservation Legislation, the in-situ soils are used as the backfilled materials by nearly all civil engineering projects. Based on the reasons mentioned above, in the current technical manuals or design codes, the basic requirement of backfilled materials has been loosened up and thus the backfilled materials in a range from GW to CL may be used. In addition, GRSRS are composed of backfill materials and reinforcements, which are relatively complicated in considering of the soil-structure interaction, and thus need more comprehensive study to understand the mechanical behavior.

In this paper, the 4 most important cases of large-scale land developing projects employed the technique of GRSRS are illustrated in detail at the start. After that, with the aid of the finite element computer program PLAXIS, numerical simulation was performed to evaluate the stability of slopes and the potential failure surfaces. Numerical simulations of large-scale reinforced soil retaining structures with various backfill materials in Ilan County are performed to recognize the performance of

GRSRS. From the investigation of the safety factor and potential failure surface of GRSRS, we can have confidence to evaluate whether the GRSRS in Ilan County are in stable states.

CASES DESCRIPTION

GRSRS of Sheraton Yilan Resort

The Sheraton Yilan Resort is located in the Sanshing Town and was constructed at the middle of 2007. The resort covers about 10.2 ha. and situates at the elevation between 200 m ~ 280 m. The GRSRS of the Sheraton Yilan Resort can be divided into 4 different groups roughly. Figure 1(a) demonstrates a representative cross-section of the GRSRS, which is 15 m in height with 3 flat-stages. This representative cross-section is chosen to perform the numerical analysis in this paper.

GRSRS of Tamkang Langyang Campus

The Tamkang Langyang Campus is located in the Jiaosi Town and was constructed at the beginning of 2002. The campus contains a mountainous road on the slope with the length of 446.7 m and situates at the elevation between 228 m ~ 278.3 m. The GRSRS was built along the slope, which is inclined with the degree between 5° ~ 25°, as the component of road embankment. Figure 1(b) demonstrates a representative cross-section of the GRSRS, which is 20 m in height with a 5 m as stage high limit.

GRSRS of Yinghua Cemetery

The Yinghua Cemetery is located in the Yuanshan Town and was constructed at the year of 2003. The cemetery is surrounded by a dangerously steep road on the slope with the length of 8.5 km and situates at the elevation between 468 m ~ 715 m. The GRSRS of the Yinghua Cemetery was designed as the lower component of the slope to be the road foundation. Figure 1(c) demonstrates a representative cross-section of the GRSRS, which is 10 m in height with 2 flat-stages.

GRSRS of Foguang University

The Foguang University is also located in the Jiaosi Town and was constructed at the year of 1996. The campus covers about 56.6 ha. and situates at the elevation between 120 m ~ 435 m. The GRSRS was built along the slope with an average degree of 46.5° as the soil retaining structures. Figure 1(d) demonstrates a representative cross-section of the GRSRS, which varies between 6 m ~ 12 m in height.

NUMERICAL SIMULATION

In order to have more understanding on the complicated mechanical behavior and failure mechanism of GRSRS, the finite element computer program PLAXIS is used in this study. In the FEM simulation, the GRSRS is assumed to be plain strain condition. The backfill materials are simulated using the Mohr-Coulomb model while the reinforcements simply using the elastic tensile model.

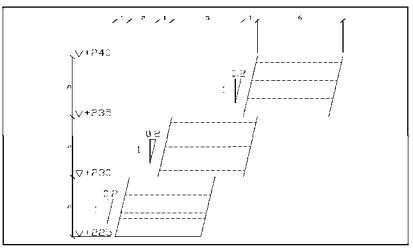

(a) Sheraton Yilan Resort

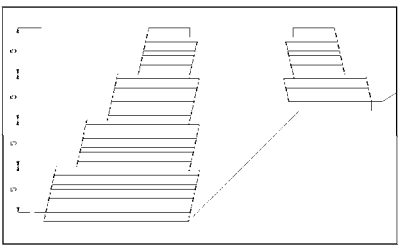

(b) Tamkang Langyang Campus

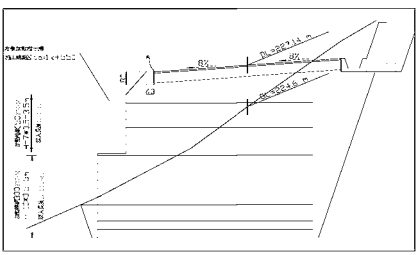

(c) Yinghua Cemetery

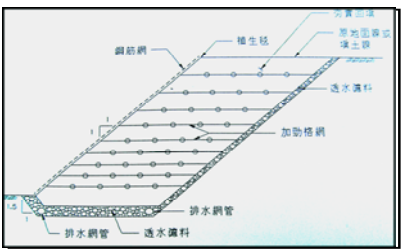

(d) Foguang University Campus

FIG. 1. Representative cross-sections for the GRSRS of the four cases

A special option termed as ϕ-c reduction approach is available in PLAXIS to calculate the safety factor. In the ϕ-c reduction approach, the soil shear strength parameters tanϕ and c of the backfill soils are successively reduced until failure of the GRSRS occurs. This approach resembles the method of calculation of safety factors conventionally adopted in slip-circle analyses, such as Stabl computer program. The 4 major projects are simulated using PLAXIS to predict their factors of safety as follows.

GRSRS of Sheraton Yilan Resort

The total number of the elements is 164 and the total number of the nodes is 387 for performing the FEM simulation for GRSRS of Sheraton Yilan Resort. The material properties used in the PLAXIS simulation are listed in Table 1. The material property of the geosynthetic reinforcement is set as EA = 4000 kN/m based on former tests.

The ϕ-c reduction approach is used to calculate safety factor and to locate potential failure surface. The predicted potential failure surface passes from the slope top through the slope toe, which is shown in Figure 2(a). The factor of safety for the GRSRS of the Sheraton Yilan Resort is 2.04 obtained from the PLAXIS simulation.

Table 1. Material properties of the GRSRS of Sheraton Yilan Resort

Parameter	γ (kN/m^3)	c (kN/m^2)	ϕ (°)	E (kN/m^2)	υ -
Reinfored soil	18.6	15	30	51750	0.38
Weathered rock	23.5	30	55	10^6	0.25

GRSRS of Tamkang Langyang Campus

The total number of the elements is 318 and the total number of the nodes is 721 for performing the FEM simulation for GRSRS of Tamkang Langyang Campus. The material properties used in the PLAXIS program are listed in Table 2. The predicted potential failure surface also passes from the slope top with some distance through the slope toe, which is shown in Figure 2(b). The factor of safety for the GRSRS of the Tamkang Langyang Campus is 1.97 obtained from the PLAXIS simulation.

Table 2. Material properties of the GRSRS of Tamkang Langyang Campus

Parameter	γ (kN/m^3)	c (kN/m^2)	ϕ (°)	E (kN/m^2)	υ -
Reinfored soil	18.3	2.9	30	51750	0.38
In-situ soil	23.5	49.1	30	10^6	0.25

GRSRS of Yinghua Cemetery

The total number of the elements is 153 and the total number of the nodes is 352 for performing the FEM simulation for GRSRS of Yinghua Cemetery. The material properties used in the PLAXIS program are listed in Table 3. The predicted potential failure surface passes from the slope top through the slope toe as well, which is shown in Figure 2(c). The factor of safety for the GRSRS of the Yinghua Cemetery is 2.35 obtained from the PLAXIS simulation.

Table 3. Material properties of the GRSRS of Yinghua Cemetery

Parameter	γ (kN/m^3)	c (kN/m^2)	ϕ (°)	E (kN/m^2)	υ -
Reinfored soil	19.6	0.1	30	51750	0.38
In-situ soil	19.6	5	45	10^6	0.25

GRSRS of Foguang University

The total number of the elements is 166 and the total number of the nodes is 373 for performing the FEM simulation for GRSRS of Foguang University. The material properties used in the PLAXIS program are listed in Table 4. The predicted potential failure surface is located inside of the reinforced region, which is shown in Figure 8. The factor of safety for the GRSRS of the Foguang University is 2.54 obtained from the PLAXIS simulation.

Table 4. Material properties of the GRSRS of Foguang University

Parameter	γ (kN/m^3)	c (kN/m^2)	ϕ (°)	E (kN/m^2)	υ -
Reinfored soil	19.6	20	35	51750	0.38
In-situ soil	19.6	20	32	10^6	0.25

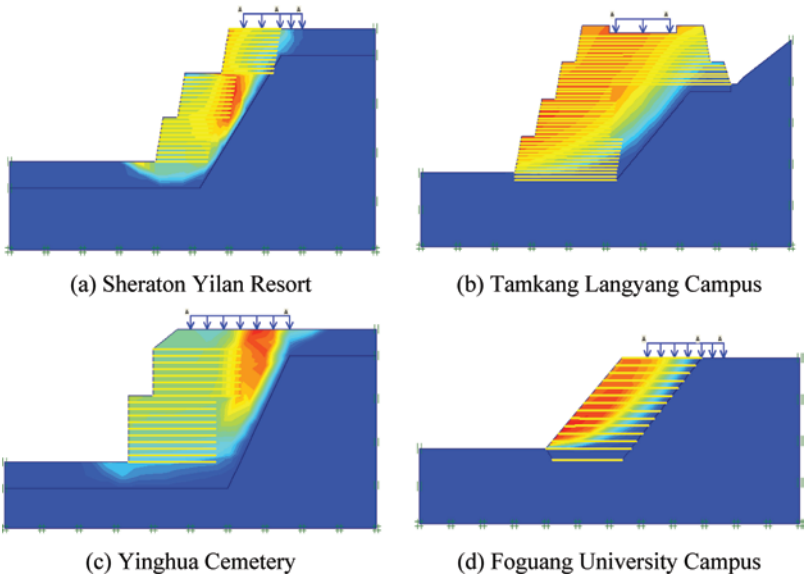

(a) Sheraton Yilan Resort (b) Tamkang Langyang Campus

(c) Yinghua Cemetery (d) Foguang University Campus

FIG. 2. Potential failure surfaces for the GRSRS of the four cases

CONCLUSIONS

Numerical simulations of the four most important large-scale geosynthetic reinforced soil retaining structures with various backfill materials in Ilan County are performed to understand the mechanical behavior of GRSRS. From the investigation of the safety factor and the potential failure surface, we recognize that the GRSRS in the Ilan County are all in stable states. The safety factor of the stability of slope for the four major projects are in the range of 1.97 ~ 2.54.

The predicted results demonstrate that the higher wall dimension provides lower FS slightly for the GRSRS. However, the author believe that the effect of the offset tiers plays a much more important role than the properties of the backfill materials on the FS of the GRSRS.

REFERENCES

Holtz, R.D. (2008). "Geosynthetics for soil reinforcement." *Proceedings of International Workshop on Frontier Technologies for Infrastructures Engineering*, Taiwan.

Leshchinsky, D. and Han, J. (2004). "Geosysthetic reinforced multitiered wall." *Journal of Geotechnical and Geoenvironmental Engineering*, Vol. 130 (12), pp. 1225-1235.

Villard, P., Kotake, N. and Otani, J. (2002). "*Modelling of reinforced soil in finite element analysis.*" Geosynthetics - 7 ICG - Delmas, Gourc & Girard (eds), pp. 39-95.

Stability Analysis of Geobelt-Reinforced Cushion Foundations

Xian-Zhi Huang[1], Jie Han[2], M.ASCE, Feng-Xiang Yan[3], and Jian-Zhou Fan[4]

[1] Professor, Engineering College of Shanxi University, Taiyuan, Shanxi 030024, P.R. China, Currently Visiting Scholar at the University of Kansas, huanxzh1@163.com

[2] Associate Professor, Department of Civil, Environmental, and Architectural Engineering, the University of Kansas, 1530 W.15th Street, Lawrence, KS66045, USA, jiehan@ku.edu

[3]Lecturer, Engineering College of Shanxi University, Taiyuan, Shanxi 030024, P.R. China, hebang9610@sina.com

[4]Associate, Engineering College of Shanxi University, Taiyuan, Shanxi 030024, P.R. China, tyfjz_1@163.com

ABSTRACT : Geobelt, one type of geosynthetics, can be included into soil to provide lateral confinement through geobelt-soil interface friction under loading. The lateral confinement increases the modulus of the soil cushion so that the modulus ratio of the reinforced cushion to the underlying soft soil stratum is increased. The increased modulus ratio results in a larger stress distribution angle and reduces the stresses distributed onto the underlying soft soil stratum and therefore the bearing capacity of the foundation is increased. Based on experimental and theoretical studies, this paper proposed a method for analyzing the bearing capacity of a geobelt-reinforced cushion foundation. This study found that the bearing capacity of the underlying soft soil can be evaluated using the theories of tensioned membrane and thin layer compression when the width of the foundation is larger than 6 meters. Case studies were selected to verify the effectiveness and accuracy of this method. This proposed method provides the guidance for the design of the geobelt-reinforced foundation.

INTRODUCTION

Geobelt, one type of geosynthetics, has been used to stabilize foundations in China since 1990s. Geobelt is formed by longitudinal and transverse belts and has square apertures with an aperture width (i.e., center-to-center spacing of two neighboring belts) of 3 to 4 times the width of the belts (typically 5cm wide).

Geobelt is made of fiberglass-plastic or steel-plastic composites. It is typically installed from the individual belts (Fig. 1a) delivered to the field, which are joined together and fixed by nails penetrating through the belt junctions into soil at a spacing of 16 to 20 times the belt width (Fig. 1b). These belts have textured surfaces on both sides to improve the interface resistance with the surrounding soil. Special measures are needed to place the geobelt at the end to provide enough anchorage to the geobelt as shown in Fig. 1c. Geobelt can be placed within a fill material to form a reinforced cushion to support foundation loading.

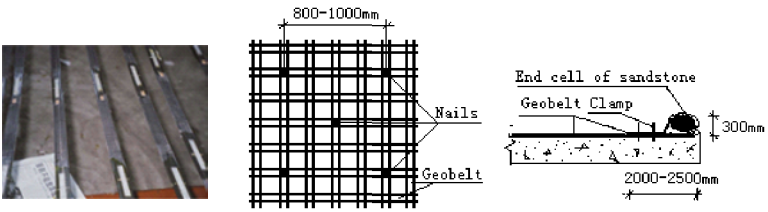

(a) Individual belts (b) Belt structures (c) End anchorage

FIG. .1 Geobelt structures and anchorage.

As compared with other improvement methods, the geobelt-reinforced cushion has the following advantages: easy for construction and quality control, flexible to superstructure deformations, and economic. The performance of the geobelt-reinforced cushion mainly depends on the ultimate strength and stiffness of the geobelt, the density of cushion fill, and the interface friction characteristics between geobelt and soil. The first project using the geobelt for foundation treatment was the multi-purpose education building in the Shanxi Transportation Academy College (Dong et al. 1996). This technology has been gradually adopted to treat soft soils, highly sensitivity clays, and non-uniform subsoils and has demonstrated its benefits. In most cases, the geosynthetic-reinforced cushion foundation is used to support large raft foundations. The finite element analysis by Huang (2005) showed that the influence depth of the reinforced foundation was approximately 2.0 times the foundation width. Past studies and experience have suggested that only the soil strength underneath the reinforced zone should be checked using the stress distribution method in the Chinese Code for Design of Foundations (GB50007-2002) if the width of the foundation is less than 6 m. The stress distribution angle of the geobelt-reinforced cushion in Shanxi is determined based on the following procedure: (1) 36°to 38°when gravel or sandy gravel is reinforced by two layers of geobelt, (2) 33°to 35°when lime-flyash stabilized soil is reinforced by two layers of geobelt, and (3) 26°when a single

layer of geobelt is used (Huang et al., 2004). However, when the width of the foundation is larger than 6 m, both the soil underneath the reinforced zone and the underlying soft soil should be checked against their strength and stability due to the existence of soft soil underneath the foundation. Based on experimental and theoretical results, this paper proposed a method for analyzing the stability of the geobelt-reinforced foundation larger than 6m in width. In this method, the theories of tensioned membrane and thin layer compression are used. Case studies were selected to verify the effectiveness and accuracy of this method.

STABILITY ANALYSIS OF GEOBELT-REINFORCED FOUNDATIONS

Geobelt can be included into soil to provide lateral confinement through geobelt-soil interface friction under loading. This lateral confinement increases the modulus of the soil cushion so that the modulus ratio of the reinforced cushion to the underlying soft soil is increased. The increased modulus ratio can result in a larger stress distribution angle and reduces the stresses distributed onto the underlying soft soil, therefore, the bearing capacity of the foundation can be increased (Huang et al., 2004). Wayne et al. (1998) summarized the possible failure modes of geosynthetic-reinforced foundations. The derivations of the solution for the stability of the underlying soft soil will be introduced below.

Additional stress on the top of soft soil

Assuming the reinforced cushion as a firm soil platform has a much higher modulus than the soft soil. Based on Terzaghi's (1943) soil arching theory and considering the reinforcement effect, the following equation was derived by Dong and Wang (1996) to calculate the additional stress at the base of the reinforced foundation (i.e., the top of the soft soil):

$$p_z = 2\gamma b\left(1 - e^{-0.5(\frac{Z}{b})}\right)\cdot k + pe^{-0.5(\frac{Z}{b})} \tag{1}$$

where γ = unit weight of the reinforced foundation; b = width of the footing; Z = thickness of the reinforced foundation; p = applied pressure at the base of the foundation; and k = influence coefficient of reinforcement (ranging from 1.2 to 1.5), which is related to the parameter of reinforcement, m_c (Niu, 2001):

when t≤3.0m and t/b≤0.2, $k = e^{1-(\frac{1}{m_c})}$ (2)

when t>3.0m and t/b>0.2, $k = e^{0.5-(\frac{1}{m_c})}$ (3)

$$m_c = \left(\sum_{i=1}^{n} l_i d_i + \sum_{j=1}^{n} l_j d_j \right) \cdot \frac{N}{F} \tag{4}$$

where t = thickness of the underlying soft soil; l_i, d_i and l_j, d_j = length and width of the geonelt in the longitudinal and transverse directions, respectively; N = number of reinforcement; and F = area of the foundation base.

Ultimate Bearing Capacity of Soft Soil

Due to the inclusion of the geobelt, the reinforced cushion has a higher stiffness than the soft soil. The possible failure of the soft soil can be considered being squeezed under the geobelt-reinforced cushion as a thin rigid slab. The ultimate bearing capacity $\bar{p}_u$ of the underlying soft soil can be calculated according to the thin layer squeezing theory described by Dong and Wang (1996). For a rectangular foundation, the ultimate bearing capacity $\bar{p}_u$ can be expressed as:

$$\bar{p}_u = N_{ct} \cdot C + N_{qt} \cdot \bar{\gamma} \cdot H \tag{5}$$

where C = cohesion of the soft soil; $\bar{\gamma}$ = average unit weight of the soil above the soft soil; H = depth from the ground surface to the top of the soft soil, $H = d + Z$, d = embedment depth of the footing; N_{ct} and N_{qt} = bearing capacity factors for the squeezing failure of the soft soil, in which

$$N_{ct} = \zeta_t \left(N_c + \frac{1}{\tan\varphi} \right) - \frac{1}{\tan\varphi} \tag{6}$$

$$N_{qt} = \zeta_t \cdot N_q \tag{7}$$

$$\zeta_t = \frac{2(b_0 + z \cdot \tan\theta)}{b} - \frac{t}{b \cdot \alpha} \left(1 - e^{(\frac{b-2b_0}{t})\alpha} \right) \tag{8}$$

$$\alpha = \tan\varphi \cdot (\frac{1+\sin\varphi}{1-\sin\varphi}) \tag{9}$$

where N_c and N_q = non-dimensional Hansen's bearing capacity factors as listed in

Table 1, φ = the internal friction angle of the soft soil, θ = the stress distribution angle of the reinforced cushion, and b_0 = the width of the edge zone at the constant pressure beyond the distributed area, which is related to the stiffness of the foundation and the rigidity and plasticity of the soil, generally, $b_0 = (0.5 \sim 1.0)\ t$.

Table1. Bearing Capacity Factors, N_c and N_q

$\varphi(^0)$	N_C	N_q	$\varphi(^0)$	N_C	N_q
0	5.14	1.00	22	16.88	7.82
2	5.63	1.20	24	14.32	9.60
4	6.19	1.43	26	22.25	11.85
6	6.81	1.72	28	25.80	14.72
8	7.53	2.06	30	30.14	18.40
10	8.38	2.47	32	35.49	23.18
12	9.28	2.97	34	42.16	29.44
14	10.37	3.59	36	50.59	37.75
16	11.63	4.34	38	61.35	48.93
18	13.10	5.26	40	75.31	64.20
20	14.83	6.40			

Factor of Safety against Bearing Failure of Soft Soil

The factor of safety against the bearing failure of the soft soil can be calculated based on Equation (10). The calculated factor of safety K should be greater than the allowable factor of safety K_a, which typically ranges from 2 to 3.

$$K = \frac{\overline{p_u}}{p_z + p_{cz}} \qquad (10)$$

where p_{cz} = the overburden stress of the reinforced cushion, i.e., $p_{cz} = \gamma Z$.

If $K \geq K_a$, the foundation would be stable. If $K < K_a$, the foundation would be unstable. To ensure the stability of the foundation, the following conditions should also be met (Huang et al., 2003): (1) the geobelt embedded in the cushion does not break and is not pulled out and (2) quality control of construction is necessary, for example, the minimum splice length of geobelt should not be less

than one meter, geobelt should be placed flat and not folded or twisted, the ends of geobelt should be fixed in a wrapped form, and appropriate compaction of fill should be achieved. When $K < K_a$ (due to the inappropriate resistance of the soft soil), the thickness of the cushion should be increased and re-design of the reinforced cushion is necessary until meeting the stability requirement, $K \geq K_a$.

DESIGN EXAMPLES

To illustrate the proposed method to be used for design, three projects are selected here as examples for the stability analysis of the geobelt-reinforced foundation over soft soil: (1) a main building in one coal factory in Qingxu, (2) a coal tower of the same coal factory in Qingxu, and (3) the multi-purpose education building at the Shanxi Transportation Academy College. In these three projects, the widths of the foundations, *b,* were 16, 8.2, and 17.5m, respectively and the depths of the foundations, d, were 1.0, 3.2, and 5.4m, respectively. Two layers of fiberglass-plastic geobelt were adopted in three projects. The thickness and width of the geobelt were 2.5mm and 50mm, respectively. Their ultimate tensile strength was 94.3MPa at the corresponding elongation of 0.87%.

The calculated additional stresses on the top of soft soils according to Eq. (1) are provided in Table 2, in which the influence coefficient of reinforcement, k = 1.5, was used. The calculated bearing capacity factors and the ultimate bearing capacities are provided in Tables 3 and 4 according to Eqs. (5), (6), (7), and (8). The stress distribution angle of the reinforced cushion θ=38°, was used. The width of the edge zone at a constant pressure, $b_0 = 0.5t$, was used. The allowable factor of safety, K_a = 3, was used. Based on the calculated ultimate bearing capacity and the applied pressure, the factors of safety of the geobelt-reinforced foundations calculated according to Eq. (9) are provided in Table 5. The stability analyses showed that Project No. (1) and (3) had stable foundations while Project No. (2) had an unstable foundation. Field measurements showed that Project No. (2) had excessive settlements with the maximum settlement at 200mm. Therefore, the calculated results are in agreement with the field measurements.

Table 2. Calculated Additional Stresses on Top of Soft Soils

Project No.	p (kPa)	γ (kPa)	z (m)	k	p_z (kPa)
(1)	150	20	1.5	1.5	97
(2)	250	19	1.5	1.5	183
(3)	260	21.5	2.5	1.5	159

Table 3. Bearing Capacity Factors of Soft Soils, N_{qt} and N_{ct}

Project No.	φ (^{0})	N_q	N_c	α	t (m)	b_0	ξ_t	N_{qt}	N_{ct}
(1)	12.0	2.97	9.28	0.32	4.0	4.0	1.31	3.88	11.52
(2)	6.0	1.72	6.81	0.13	2.7	2.7	1.03	1.77	7.06
(3)	14.03	3.59	10.4	0.41	2.5	3.75	2. 17	7.79	24.05

Table 4 .Ultimate Bearing Capacity of Soft Soil, $\overline{p}_u$

Project No.	C (kPa)	$\overline{\gamma}$ (kN/m^3)	H (m)	N_{qt}	N_{ct}	$\overline{p}_u$ (kPa)
(1)	18.0	19.0	2.5	3.88	11.52	422
(2)	30.0	19.0	4.7	1.77	7.06	292
(3)	8.5	16.9	7.9	7.79	24.05	1446

Table 5. Stability Analysis of the Foundation

Project No.	p_z (kPa)	p_{cz} (kPa)	$\overline{p}_u$ (kPa)	K	Stability assessment
(1)	97	30	422	$3.32 > K_a$	Stable
(2)	183	29	292	$1.38 < K_a$	Unstable
(3)	159	54	1446	$6.79 > K_a$	Stable

SUMMARY

For a large geobelt-reinforced cushion to support a raft foundation with a width of more than 6m, it is important to check the stability of the foundation due to the existence of soft soil underneath the foundation. Tensioned membrane and thin soil layer squeezing theories were used to develop the design method for the geo-belt reinforced foundation. The design parameters, such as the influence coefficient of reinforcement, k, and the width of the edge zone at a constant pressure, b_0, were determined based on the research carried out in Shanxi, China. They should be verified if used in other regions. The calculated results are compared well with the field performance of the reinforced foundations.

ACKNOWLEDGMENTS

The authors gratefully acknowledge the financial support through the research funds from the Shanxi Scholarship Council of China, the Shanxi College and University Science and Technology Research Development Project No. 20051273, and the Shanxi Natural Science Foundation Project No. 20041061.

REFERENCES

Chinese Code for Design of Foundations (GB50007-2002). China Architecture & Building Press, Beijing, 2002, in Chinese.

Dong, W.M. and Wang, B.Y. (1996). "A case history of the reinforced cushion foundation in an educational building at the Shanxi Transportation Academy College." *Proceedings of the fourth Chinese Geotechnical Case Histories Symposium*, Ordnance Industry Press, Beijing:, 424–431, in Chinese.

Huang, X.Z. (2005). *Experimental and Theoretical Studies and Applications of Geobelt-reinforced Graval Cushion Foundations*. Ph.D. Dissertation, Taiyuan University of Technology, in Chinese.

Huang, X.Z., Qi, L.S., and Bai, X.H. (2004). "A study of stress distribution in belt geosynthetic-reinforced gravel on soft soil." *Chinese Journal of Rock Mechanics and Engineering*, 23(17), 2992–2997, in Chinese.

Huang, X.Z., Qi, L.S., and Bai, X.H. (2003). "Experimental study on belt geosynthestic-reinforced gravel." *Proceedings of the Ninth Chinese Soil Mechanics and Geotechnical Engineering Conference*, Vol. 2, Tsinghua University Press, Beijing, 822–825, in Chinese

Niu, Z.R. (2001). "Application of reinforced sand - stone cushions for ground improvement. *Rock and Soil Mechanics*, Vol 22(2):195–198, in Chinese.

Terzaghi, K.(1943). *Theoretical soil mechanics*, J. Wiley and Sons, New York.

Wayne, M. H., Han, J., and Akins, K. (1998). "The design of geosynthetic reinforced foundations." *Design and Construction of Retaining Systems, ASCE Geo-Institute Geotechnical Special Publication*, No. 76, edited by John J. Bowders et al., 1-18.

Noise Barriers by Steep Vegetated Walls Reinforced with Geosynthetics – An Economical Alternative?

Harald Schoen[1], Franz Aschauer[2] and Wei Wu[3]

[1]Dipl.-Ing, Teerag-Asdag, Hafenstrasse 63, A-3500, Krems, Austria; harald.schoen@aon.at
[2]Doctor., Institute of Geotechnical Engineering, University of Natural Resources and Applied Life Sciences, Vienna, Feistmantelstrasse 4, A-1180 Vienna, Austria; franz.aschauer@boku.ac.at
[3]Professor, Institute of Geotechnical Engineering, University of Natural Resources and Applied Life Sciences, Vienna, Feistmantelstrasse 4, A-1180 Vienna, Austria; wei.wu@boku.ac.at

ABSTRACT: The use of reinforced steep walls in connection with mineral recycling materials as a protection against traffic noise is discussed as a technically innovative and economical solution observing the prescribed emission limit values for construction materials. The steep wall can be vegetated. With the help of a testing wall with a length of 70 m and a height of 4.5 m it is shown that such innovative solutions for noise protection may save energy and resources. Moreover, vegetated steep noise protection walls are also economically competitive with conventional noise protection systems.

INTRODUCTION

By the increase of traffic and the result of rising noise emissions in the last decade years, there was a higher need of noise protection measures, causing an enormous cost. Based on the prognoses of increasing needs of commercial and individual transport for the following years, protection measures should be considered for human beings to minimize the harmful impacts of the motorized traffic without great losses in life quality.

Lots of people as well as experts strongly criticize the installed monotonous noise protection systems. Mostly used methods for noise reduction are noise barriers made of aluminum, plastics, wood or concrete. Their needs for small space and little construction material seem to be a cost-saving method; however, on the other hand they have a deep impact on townscape and landscape. Traffic and transportation psychologists disagree with the releasing of so-called tunnel visions for drivers because of their negative effects on the moving traffic. These conventional systems exhibit deficits in dust protection and should be improved in regard to acoustic absorption.

Because of this history, the research project "Vegetated steep noise barriers with geosynthetics and recycling products" was initiated at the University of Natural Resources and Applied Life Sciences, Vienna. This project shows that a steep noise protection formed by the excavation materials from transportation engineering and recycled mineral construction waste contribute to the protection of environment with the help of new technologies.

MODEL TEST ON A SCALE 1:1

A test field was erected in a gravel quarry near Krems for analyzing the different construction systems, emplacement methods, fill and reinforcement materials, and surface designs, and developing an ecologically and economically optimum noise protection. This construction is permanent enabling phytosociological records, geotechnical, chemical and sound technological measurements over a lot of years.

Test construction

A vegetated steep noise protection wall with a length of 70 m and a height of 4.5 m (Fig. 1) was built with slope inclinations between 70° and 85° (widths at base between 2.60 and 4.90 m, widths at crown between 0.5 and 2.5 m). The steep noise protection wall is divided into seven test sections of each 10 m. In the construction, eight different shuttering systems were used, which were developed for the support of terraces and the protection of slopes and adapted to steep noise protection wall. High-strength geosynthetics were used as reinforcement in all sections.

FIG. 1. Finished test construction.

Fill material

Considering the protection of natural resources and landfill spaces, the specialty of this test is the use of recycling material as construction material. Six sections of the protection wall were constructed with recycled ballast RMH 0-45 (recycled broken granulate consisting of concrete, bricks and natural rock), the remaining section was filled with gravel for comparison purposes. According to the Austrian Act on Remediation of Confirmed Contaminated Sites (ALSAG), deposit fees must be paid for the construction waste and contaminated excavation materials (temporarily at least 7.20 €/T) except that the construction waste is given to a recycling plant (so-called ALSAG contributions). Considerable costs can be saved due to the non-use of more expensive primary construction material.

Fill material was emplaced in layers with a thickness of 0.5 m each and compacted by usual compaction equipment. Reinforcement consisting of geosynthetics was emplaced between these layers.

Substrate

The planting substrate with a thickness of 0.5 m forms the nutrition base for vegetation, and is simultaneously the surface and slope liner (Fig. 2) in order to avoid or reduce the pollutants for water and construction material from the deposit.

Impermeabilization measures

The individual sections were vertically divided by a cohesive layer with a thickness of ca. 1 m for the analyzing of occurring seepage waters in each section and enabling qualified conclusions for the assessment of possible long-term effects. The complete construction with a length of 70 m was sealed with a HDPE geomembrane (2 mm thick) against the underground and set on a zonal drainage with a thickness of 40 cm (Fig. 2).

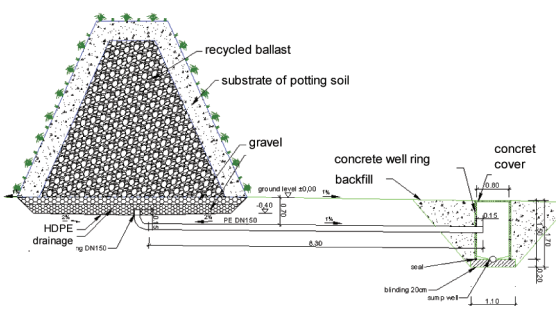

FIG. 2. Cross section test construction.

Vegetation

In this project, an innovative technique of the combination the steep wall with vegetation was developed, which shows an attractive and efficient way by the combination steep wall and vegetation comparing with the conventional noise protection measures.

The selection of suitable plants was made in regard to both the requirements for the vegetation (creative, ecological concerning and structural maintenance) and the structural requirements. In this project, only drought-tolerable plants and climbing plants were used.

Monitoring measurement techniques

Lack of experience in the system behavior, a voluminous measurement program

was executed in this project. The program includes a section-related characterization of kind, quantity and spacious distribution of possible seepage contaminations and measurements with sound technology for the analysis of sound insulation resp. sound absorption grade of the noise barrier complete the investigation program.

COST CALCULATION

Post-calculation had been done for the above mentioned project using the different systems. The estimate of activities bases partly on the calculated periods for the erection of the test construction and on the usual calculations in building industry. The geometry of the construction is 1000 m long, 4.5 m high, and crown width of 1.0 m and inclination of 80°. For personnel costs, 10 persons with the average wage of 31.15 €/h were considered. For equipment costs, crawler excavator (90 kW), plate compactor (DVH3010), 1 truck, 1 flat-bed truck, 1 skip, 1 bulldozer (CAT D5M XLP), 1 roller (Bomag213) were countered. The transport costs were depended on means of transport, distance (0-50 km) and route of delivery. For material costs, both costs of recycled mineral construction waste and costs of broken fill material were calculated. In most systems, a protection against fall was erected. The Costs of the protection were included in the on-site overhead and have not to be considered as additional costs.

Calculated systems

The following eight different systems were calculated (gabions, Ecowall, Polyslope S, Polyslope T, Vector Wall® Gabion, Vector Wall® Gruen and Terramesh®) (Fig. 3 – Fig. 9) and also a system where the gabions were delivered (Table 1).

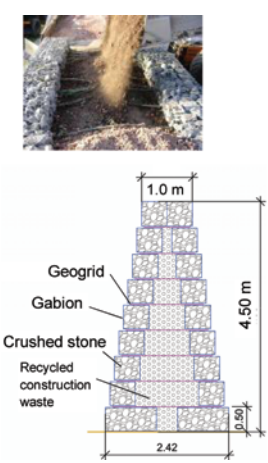

FIG. 3. Gabions.

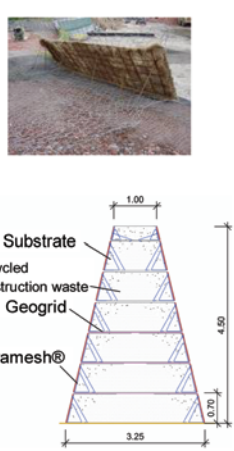

FIG. 4. Terramesh.

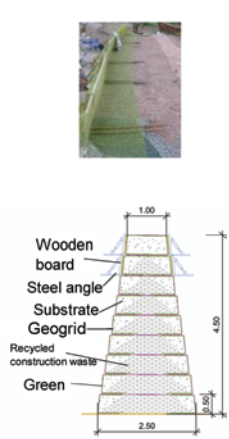

FIG. 5. Polyslope T.

Table 1. Calculated systems

System	Description
Gabions (Fig. 3)	In this system gabions were used which were folded on-site into a box, set onto the designed slope edge and manually filled with crushed stone 100/250. After closing of lid the core was filled and compacted.
Terramesh ® (Fig. 4)	The folded shutting elements were assembled and placed on the slope at closed quarters. Afterwards the core and the substrate wedge were filled in. Additional layers of geogrids were emplaced onto the three first layers after compaction.
Polyslope T (Fig. 5)	This shuttering system consisted of steel angles in a distance of ca. one meter and form work panels as infill. These components were drawn after completion of fill layer and brought into position for the next layer. The geogrids laid between the individual layers were folded on the front wall of the slope forming a so-called cushion. An additional grid (Green) for erosion protection was used.
Polyslope S (Fig. 6)	L-shaped wire meshes made of construction steel framework into the designed inclination were used. Erosion in the front area should be avoided by using products for erosion protection (Polymat).
Vector Wall (Fig. 7, Fig. 8)	At this shutting system a temporary timber shutting was erected outside of the bearing surface of the wall. Fixed on it were wire meshes made of construction steel. These wire meshes were fixed on anchor blocks with hook-ties in the course of the erection in layers. This system could be vegetated in dependence on the execution of the visible surface (Vector Wall® Gruen, Fig. 7). By the emplacement of rounded gravel in combination with galvanized wire meshes a gabion-like appearance could be reached (Vector Wall® Gabion). Vegetation was possible with climbing plants only (Fig.8).
Ecowall® (Fig 9.)	Two galvanized steel matt elements were combined by inserting a push-fastener, braced by hook-ties and adjusting of the designed inclination.

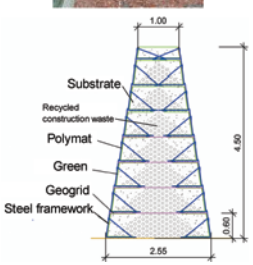

FIG. 6. Polyslope S.

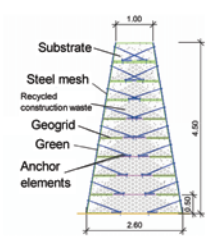

FIG.7. Vector Wall® Green

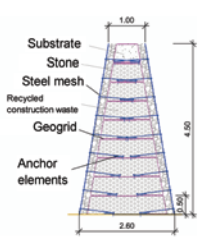

FIG. 8. Vector Wall® Gabion.

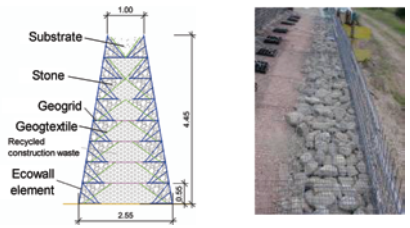

FIG. 9. Ecowall.

The Costs for vegetation were not considered in the calculation of the corresponding system; they had to be added additionally (Table 2).

Table 2. Possible measures for vegetation

System / Vegetation	Gabions	Ecowall	Polyslope S	Polyslope T	Terramesh®	Vector Wall® Gruen	Vector Wall® Gabion
Seedlings (6.00€/m²)	X		X	X	X	X	
Climbing plants (3.00€/m²)	X	X					X
Cuttings (2.00€/m²)	X		X	X	X	X	
Injected Vegetation (0.20€/m²)			X	X	X	X	

Comparison of erection costs

Fig. 10 shows the cost comparison of the conventional noise barriers and steep noise protection walls. Based on Fig 10, the construction costs for noise barriers can be listed as Table 3.

Table 3. Construction costs of noise barriers

Noise Barriers (height = 4.5 m)	Costs (€/m)	Costs (€/m²)
Wooden wickerwork elements	315.00	70.00
Timber concrete elements	412.00	91.56
Aluminium elements	442.00	98.22
Acryl glass elements	747.00	166.00

SUMMARY

Basing on post calculations of different systems it can be displayed that the erection costs of individual systems are lower than the costs of conventional systems. In comparison with today's most commonly used noise barriers made of aluminium elements systems Polyslope T, Ecowall and Vector Wall® Gruen offer an attractive and economical alternative when the roadway is on the same level as the surface of

terrain. A cost saving in the height of up to 50 % can be assumed when using Polyslope T (Green) and compared with conventional noise barriers.

For future research, the application area of vegetated steep-sided noise protection walls can be extended. An economical system price can be reached in comparison with conventional noise barriers by the replacement of expensive natural materials by excavation material and recycling material (roadway rubble, construction waste etc.), even in consideration of additional costs for larger bearing surfaces and vegetation.

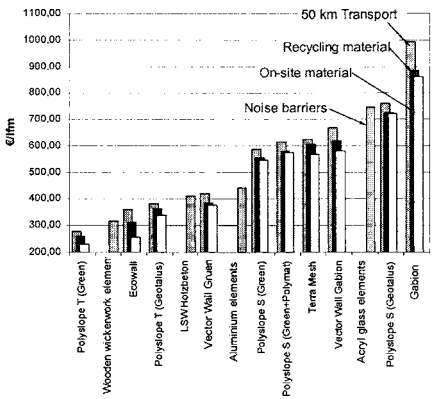

FIG. 10. Cost comparison of conventional noise barriers and steep noise protection walls.

REFERENCES

Bathurst, R.J., Walters, D., Vlachopoulos, N., Burgess, P. and Allen, T.M. (2000), Full Scale Testing of Geosynthetic Reinforced Walls, *ASCE Special Publication, Proceedings of GeoDenver 2000*, Denver, Colorado.

Bathurst, R. J., Blatz, J. A. and Burger, M. H. (2003). Performance of instrumented large-scale unreinforced and reinforced embankments loaded by a strip footing to failure, *Can. Geotech. J.* Vol. 40, 1067-1083.

Farnham, J and Beimborn, E. (1990) "Noise barrier design guide lines, Part 2: Noise Barrier Design Principles" at http://www.uwm.edu/Dept/CUTS//noise/noiseb.htm

Geosynthetics and Pavement Life Cycle: an Analysis through the M-E PDG

Filippo G. Praticò[1], Domenico Tramontana [2], Antonio Casciano [3], Antonella Attinà[4]

[1,2,3]*Mediterranea* University at Reggio Calabria - Via Graziella – Feo di Vito – 89100 Reggio Calabria – Italy - [1]filippo.pratico@unirc.it; [2]ratio85@libero.it; [3]casciano.antonio@libero.it; [4]antoat@hotmail.it

ABSTRACT: One of the most recurrent issues in hot mix asphalt (HMA) maintenance and rehabilitation is reflective cracking. Incorporating geosynthetics products into the pavement structure is a technique for reducing the severity and delaying the appearance of reflective cracking, reducing maintenance work and costs. Although many methods and procedures were developed to quantify and to predict the influence of geogrids in flexible pavements, the new Mechanistic-Empirical Pavement Design Guide (M-E PDG) contains no tool to account for the presence of a geogrid in flexible pavements. In the light of the above facts, the objectives of the paper were to research into the possibility to operate on some of the input parameters of the new M-E PDG in order to account for the modification of the expected life due to the geosynthetics. Several case-histories were considered and for each case-history attention was focused on the modification of M-E PDG inputs in order to account for the different expected life. Factors included in M-E PDG, such as layers thickness, Poisson coefficient and fatigue equation parameters were considered. The obtained results provided information and findings for practical benefit of the work.

PROBLEM STATEMENT

Incorporating geosynthetics into the pavement structure is a technique for reducing the severity and delaying the appearance of reflective cracking, therefore increasing the road working life due to retarding of crack propagation, increasing the tensile strength of the asphalt layer, reducing maintenance work and costs and reducing the formation of ruts in areas of high traffic loading. Areas of application include asphalt paved road, airport runway and taxiway, road widening. Since the 1970s, many methods, studies and procedures were developed to quantify and to predict the influence of geogrids. These studies were based on the following key-assumptions: i) reinforced layer: HMA layer or base; ii) geosynthetics main behaviour: membrane or separation. In many cases, results showed some specific benefits (Webster, 1977;

Chaddock, 1988; Fannin, 1996; Montanelli, 1996; Appea, 1997; Tingle, 2003): a) increase of expected life: + 82~134%; b) increase of traffic to failure: + 1.95~7.5 times; c) reduction of base thickness: -25~50%. On the other hand, the new Mechanistic-Empirical Pavement Design Guide (M-E PDG, 2007) contains no tool to account for the presence of a geogrid in flexible pavements. Other factors currently not included in M-E PDG are asphalt treated permeable base layers, semi-rigid pavements, pavement preservation programs. In the light of the above facts, the objectives of the paper were to research into the possibility to operate on some of the input parameters of the new M-E PDG in order to account for the modification of the expected life due to the geosynthetics. Next section investigates into the modification of M-E PDG and (AASHTO, 1993) inputs in order to account for the different expected life. Finally conclusions are drawn.

EXPERIMENTS AND RESULTS

Experimental Plan

Experiments were planned as follows (see figure 1): i) pavement design (unreinforced case, UR) according to M-E PDG and AASHTO 1993; ii) traffic data: transition from Average Annual Daily Truck Traffic (AADTT) to Equivalent Single Axle Load (ESAL); iii) Pavement design (UR), according to AASHTO -1993; iv) Estimate of the benefit in terms of Traffic Benefit Ratio (TBR), due to geosynthetic reinforcement. Two cases, termed A and B, were considered. In the case A the geosynthetic reinforcement was positioned between the subgrade and the base while in the case B it was embedded within the HMA layer; v) Assessing equivalent values for AASHTO-1993 and M-E PDG, in order to take into account for the effect of geosynthetic (see flowchart in Fig.1, R: reinforced case). The following variables were considered: υ, Poisson coefficient; D_1, thickness of the bituminous layer; D_2, thickness of the unbound base layer; k_2, fatigue law parameter (bituminous layer); a_1 structural layer coefficient of the bituminous layer.

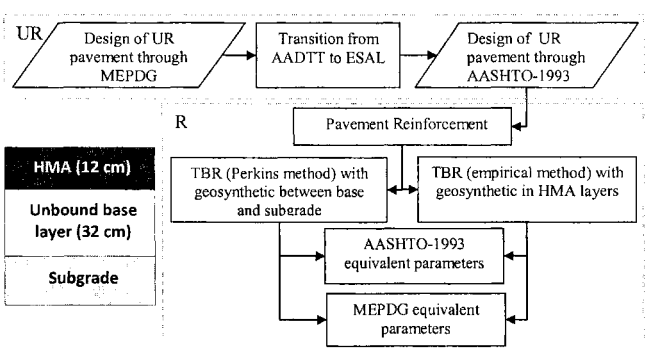

FIG. 1. Experimental plan and pavement structure.

Design of the unreinforced pavement according to M-E PDG and AASHTO Guide 1993

Table 1 summarizes the design of the unreinforced pavement according to M-E PDG. In order to perform the design through the AASHTO-1993 method, traffic data expressed in terms of AADTT were converted in ESALs. For the selected classes, 1800 vehicles per day were equivalent to 7,024 ESALs per day. An expected life of 20 years was obtained, both for the M-E PDG and the AASHTO-1993 (SN=4.36 inches).

Table 1. M-E PDG input data

Performance Criteria			
Terminal IRI (in/mi)		172	
AC Surface Down Cracking (Long. Cracking) (ft/mile):		2000	
AC Bottom Up Cracking (Alligator Cracking) (%):		25	
AC Thermal Fracture (Transverse Cracking) (ft/mi):		1000	
Chemically Stabilized Layer (Fatigue Fracture)		25	
Permanent Deformation (AC Only) (in):		0.25	
Permanent Deformation (Total Pavement) (in):		0.75	
Traffic			
Initial two-way AADTT		1800	
Number of lanes in design direction		2	
Percent of trucks in design direction(%)		50	
Percent of trucks in design lane(%)		95	
Operational speed (km/h)		90	
Structure			
Layer	L1	L2	L3
Material	HMA	A-1-a	A-7-a
Layer thickness (inch)	4.72	12.6	infinite
Poisson coefficient	0.35	0.35	0.35
Lateral Pressure coefficient K_0	/	0.5	0.5
Elastic Modulus (psi)	/	30000	10000

L1: Layer 1, Hot Mix Asphalt; L2: Layer 2, Granular Base; L3: Layer 3, Subgrade; IRI: International Roughness Index; AC: Asphalt Concrete; 1ft ≅ 30.34 cm; 1 in ≅ 25.4 mm; 1 mi ≅ 1.6 km; 1 psi ≅ 0.00689 N/mm^2.

Expected life of the reinforced pavement

Two different estimates of the expected life of the reinforced pavement (see figure 1) were carried out. Though out of scope of the paper, the first estimate was performed according to Perkins' model and termed case A. In this case TBR (traffic benefit ratio after Perkins S., 2001) was determined as follows (see table 2):

Table 2. TBR determination

I - Equivalent Thickness of the HMA layer	$D_{1\text{-}e}$	127 [mm]
I - Equivalent Thickness of the base layer	$D_{2\text{-}e}$	428.5 [mm]
I - Equivalent Structural Number	SN_e	5.3 [inch.]
I - Geo. Secant Tensile Mod. at 2% axial strain	$G_{SM\text{-}2\,\%}$	975 [kN/m]
O - Isotropic value of elastic Mod. for geo.	E_G	4,290,000 [kPa]
I - California Bearing Ratio	CBR	6.67
I - Reduction Factor geo. At Interface	RF_{GI}	1.00
I - Reduction Factor geo. P. ratio (base)	RF_{Gv}	1.00
I - Reduction Factor geo. P. ratio (subgrade)	RF_{Gv}	1.00
I - Reduction Factor geo. Shear Mod. (base)	RF_{GG}	1.00
I - Reduction Factor geo. Shear Mod. (subgrade)	RF_{GG}	1.00
I - Ratio of min. to max. 2% secant Mod. for geo.	G_{MR}	0.615
O - SN when $TBR_{S\text{-}GM}$=1	SN*	5.8
O - Model parameters	$Y_{1\text{-}GM}$; $Y_{2\text{-}GM}$	1.1; 1.4
O - Model parameters	m_1; m_2; y_{01}; y_{02}	0.05; -0.06; 0.94; 2.15
O -TBR for geo. isotropic secant Mod.-subgrade*	$TBR_{S\text{-}GM}$	1.07
O - TBR for geo. isotropic secant Mod. (base)*	$TBR_{B\text{-}GM}$	1.11
O -TBR for geo. modulus e Mod. ratio-subgrade°	$TBR_{S\text{-}GMR}$	1.06
O - TBR for geo. modulus e Mod. ratio (base) °	$TBR_{B\text{-}GMR}$	1.03
O - TBR for reinforcement effects (subgrade)	TBR_S	1.06
O - TBR for reinforcement effects (base)	TBR_B	1.03
O - TBR for reinforcement effects in total system	TBR_T	1.09
Note. * = it accounts for the influence of geosynthetics (geo.) isotropic elastic modulus on TBR; ° = it accounts for the influence of geosynthetics modulus anisotropy on TBR; I: Input; O: Output; Mod.: modulus; P. ratio: Poisson's ratio.		

From TBR_T and $W_{18\text{-}U}$, the $W_{18\text{-}R}$ was derived (40,138,228.63 ESALs). Finally the expected life of the reinforced pavement was derived (21.4 years). As above-mentioned, the determination of the expected life of a HMA pavement, in which a bituminous layer is reinforced, is a very complex task. From an empirical point of view, it is possible to obtain a rough estimate through nomograms, as shown in figure 2. In this case a TBR=2.5 was obtained. This case was termed B.

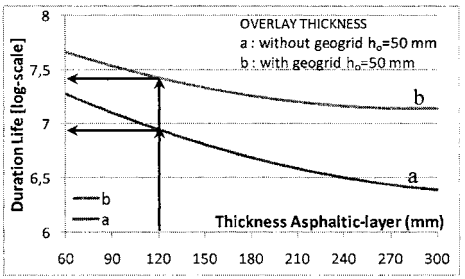

FIG. 2. Netherlands Pavements Consultants Nomogram (adapted).

Equivalent factors according to M-E PDG and AASHTO-1993

Table 3 refers to the determination of the equivalent thickness of the bituminous layer, carried out through the M-E PDG.

Table 3. HMA Equivalent thickness according to M-E PDG

	Expected Life (months)					
Thickness (in)	**Longitudinal**	**Alligator**	**AC Rutting**	**Total Rutting**	**IRI**	**Life**
4.7	243	302	255	260	450	**243**
5.2	328	382	415	455	504	**328**
5.7	493	494	482	592	545	**482**
6.2	780	573	526	716	575	**526**
6.7	1339	754	584	865	602	**584**
7.2	2572	944	626	1018	622	**622**
8.2	/	1390	712	1370	655	**655**

By interpolating the data reported in table 3, an equivalent thickness of 4.78 inch (=12.14cm) was obtained for the case A, while for the case B, an equivalent thickness of 6.95 inch = 17,65 cm was derived. As for Poisson coefficient, table 4 summarizes results. By interpolating the data reported in table 4, an equivalent Poisson coefficient of 0.37 was obtained for the case A, while for the case B, an equivalent Poisson coefficient of 0.68 was derived. As for fatigue law, table 5 summarizes results. By interpolating the data reported in table 5, an HMA equivalent fatigue law factor of 3.949 was obtained for the case A, while for the case B, an equivalent fatigue law coefficient of 4.08 was derived. Note that the higher k_2 (positive value) the closer to zero is the first derivative of the curve $N_f(\varepsilon)$, the higher, for a given ε, is the corresponding value of the number of cycles to failure. As for AASHTO-1993 equivalent factors they were easily derived by simple elaborations, based on the well known algorithm (AASHTO, 1993).

Table 4. HMA Equivalent Poisson Coefficient according to M-E PDG

	Expected Life (Months)					
Poisson coeff.	**Longitudinal**	**Alligator**	**AC Rutting**	**Total Rutting**	**IRI**	**Life**
0.20	189	276	191	205	412	**189**
0.25	201	282	225	235	424	**201**
0.30	220	291	291	307	436	**220**
0.35	245	302	254	352	450	**245**
0.40	277	315	388	384	462	**277**
0.45	322	331	404	404	473	**322**

Table 5. HMA Equivalent fatigue law coefficient according to M-E PDG

	Expected Life (Months)		
K_2 factor	**Longitudinal**	**Alligator**	**Life**
3.74	31	63	**31**
3.79	55	94	**55**
3.84	94	140	**94**
3.89	150	201	**150**
3.94	243	302	**243**
3.99	343	366	**366**

Fatigue law: $N_f = 0.00432 \cdot C \cdot \beta_1 \cdot k_1 \cdot \varepsilon^{-\beta 2 \cdot k2} \cdot E^{-\beta 3 \cdot k3}$; N_f = Number of repetitions to fatigue cracking; $C=10^M$; $M= 4.84 \cdot [V_b/(V_a+V_b)-0.69]$; V_b= effective binder content (%); V_a = air voids (%); β_1, β_2, β_3 = adjustment factors (default values: 1;1;1); k_1, k_2, k_3 = laboratory regression coefficients (default values: 0.007566; 3.9492; 1.281); E = stiffness of the material (psi); ε = tensile strain at the critical location.

Summary

Figures 3 and 4 summarize results (the *XOR* gate, exclusive-OR, was used). Figure 3 refers to AASHTO-1993 method and shows how the parameters a_1 or D_1 or D_2 can be modified in order to simulate the effects caused by the reinforcement in terms of expected life. It is interesting to remark that for the case A only an increase of 2% of a_1 is required, while for the case B an increase of 57% of the same a_1 is required . For the case A an increase of 2.5 % of D_1 is required, while for the case B an increase of 54.7% of the same D_1 is required. For the case A an increase of 2% of D_2 is required, while for the case B an increase of the 46 % of the same D_2 is required. Figure 4 refers to M-E PFG method and shows how ν_1 or D_1 or K_2 can be modified in order to simulate the effects caused by the reinforcement in terms of expected life. According to the M-E PDG method, for the case A an increase of 5% of υ_1 is required while, for the case B an increase of 94.3% of υ_1 is required. For the case A an increase of 1% of D_1 is required while, for the case B an increase of 47% of D_1 is required. For

the given fatigue law, for the case A an increase of 0.2% of parameter K_2 is required, while for the case B an increase of the 3.6% of the same K_2 is required.

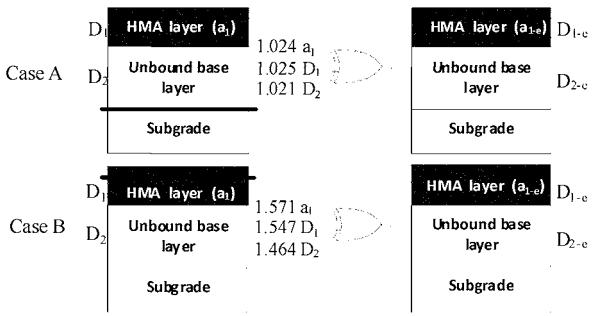

FIG. 3. Results derived according to AASHTO-1993 method.

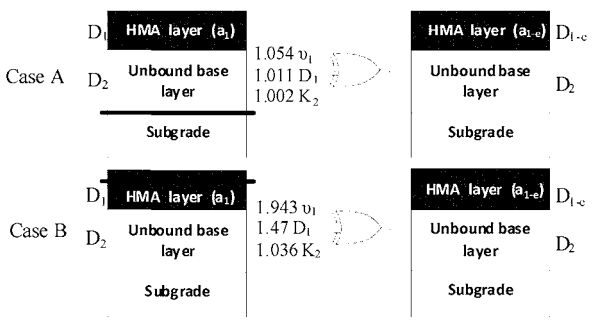

FIG. 4. Equivalent factors according to the method M-E PDG.

CONCLUSIONS

Many boundary hypotheses were needed in order to carry out the simulations and authors are aware that this fact can affect the general applicability of conclusions. However, in the light of the above-mentioned facts, the following conclusions may be drawn: i) Though many authors report an increase of performance due to the geosynthetics reinforcement, the rationale of such determinations is hard to be found due to many variables. Estimates have a very appreciable variance; ii) The increase in HMA thickness which is needed (in order to obtain the same expected life) ranges from 1% up to 55% c.a. This fact shows that uncertainties and variables play a very relevant role and more research is needed; iii) As for fatigue law, reinforcement seems to be well simulated through an increase in k_2 value which ranges from 0.2% up to 4%; iv) M-E PDG demonstrated to be able to provide a more exhaustive and rational answer to the issue of investigating on the expected life of reinforced *vs.*

unreinforced pavements. In particular, the potential for detecting the real failure mechanism and for fixing the various geometric and material inputs in order to obtain better performance both for reinforced and unreinforced conditions appeared as the key-determinant of M-E PDG.

Future research will aim at designing and carrying out an optimized experimental plan.

REFERENCES

AASHTO (1993). "AASHTO Guide for Design of Pavement Structures." *American Association of State Highway and Transportation Officials,* Washington, D.C.

AA.VV. (2003). "Guidelines for using geosynthetics with HMA overlays to reduce reflective cracking." Retrieved July 2009 from *ftp://ftp.dot.state.tx.us/pub/txdot-info/cmd/tech/1777-p2geobook.pdf.*

AA.VV. (2007). "Guide for Mechanistic-Empirical Design of New and Rehabilitated Pavement Structures." Retrieved May 2008 from www.trb.org/mepdg, *National Cooperative Highway Research Program,* Transportation Research Board, Washington, D.C.

Appea, A. K. (1997). "In-Situ Behavior of Geosynthetically Stabilized Flexible Pavement." *Master Thesis.* Virginia Polytechnic Institute & State University. Blacksburg.

Attinà, A.M.T. (2008). "Pavimentazioni flessibili rinforzate: Modellistica e specificazioni prestazionali." *Master thesis.* Mediterranea University of Reggio Calabria, Italy.

Chaddock, B.C.J. (1988). "Deformation of Road Foundations With Geogrid Reinforcement." *Research Report 140,* Transportation and Road Research Laboratory, pp. 1-8.

Fannin, R.J. and Sigurdsson, O. (1996). "Field Observations on Stabilization of Unpaved Roads with Geosynthetics." *ASCE Journal of Geotechnical Engineering*, Vol. 124, No. 7, pp. 544-55.

Montanelli, F., Zhao, A. and Rimoldi, P. (1997). "Geosynthetics-reinforced pavement system: testing and design." *Proceeding of Geosynthetics '97, IFAI,* Long Beach, pp. 619-632.

Netherlands Pavements Consultants (1990). "The influence of HaTelit reinforced asphalt in comparison with unreinforced asphalt." Hoevelaken, the Nederland.

Perkins, S.W. (2001). "Mechanistic-empirical modeling and design model development of geosynthetic reinforced flexible pavements." *Final Report,* Montana State University.

Tingle, J.S. and Webster, S.L. (2003). "Corps of Engineers Design of Geosynthetic-Reinforced Unpaved Roads." In *Transportation Research Record 1849*, Transportation Research Board, National Research Council, pp. 193-201.

Webster, S.L. and Watkins, J.E. (1977). "Investigation of Construction Techniques for Tactical Bridge Approach Roads Across Soft Ground." *Technical Report S-77-1,* U.S. Army Engineer Waterways Experiment Station, Vicksburg, MS, pp. 1-74.

Mechanical Behavior of Geosynthetic-reinforced Soil Retaining Wall

Mamoru Kikumoto[1], Teruo Nakai[2], Shahin Md. Hossain[3],
Kenji Ishii[4], Asami Watanabe[5] and Feng Zhang[2]

[1]Assistant Professor, Nagoya Institute of Technology, Gokiso-cho, Showa-ku, Nagoya 466-8555, Japan; kikumoto@nitech.ac.jp; [2]Professor, ditto.; [3]Associate Professor, ditto.; [4]Graduate Student, ditto.; [5]Engineer, Toho Gas Co. Ltd., Nagoya, Japan. (former Graduate Student, ditto.)

ABSTRACT: Mechanical behavior of geosynthetic-reinforced soil retaining wall is investigated and the reinforcing mechanism by geosynthetics is discussed through two-dimensional laboratory model tests and their corresponding finite element analyses. A series of mode tests and simulations are carried out varying arrangement, length and number of the reinforcements. It is revealed that the effectiveness of the geosynthetics mainly depends on the increase of internal stability, which is local stability within the reinforced ground, and external stability, which is overall stability of the surrounding backfill and subsoil. It is also indicated that the results of the numerical analyses show good agreement with the results of the model tests.

INTRODUCTION

Recently, reinforced soil method by geosynthetics such as geogrid or geotextile is usually applied in the actual field for reducing deformation of the ground, lightening earth pressure acting on soil structures or increasing bearing capacity of foundations. The deformation and failure mechanism of the ground reinforced with geosynthetics is, however, not fully understood because the reinforcing mechanism by geosynthetics is a typical problem of complicated mechanical interaction between ground, reinforcements and geostructures. In the previous research, Nakai et al. (2009) discussed the bearing capacity problem on the horizontal geosynthetic-reinforced soil ground and indicated that the effectiveness of reinforcements mainly depends on their position and skin friction. In the present study, mechanical behavior of geosynthetic-reinforced soil retaining wall subjected to vertical loading is investigated through two-dimensional laboratory model tests and their corresponding elastoplastic finite element simulations. Though Tatsuoka et al. (1989) have conducted similar experiments and have discussed effects of rigidity of the wall and lateral position of vertical loading, the deformation and failure behaviours of the ground including subgrade soil have not been considered. Through a series of tests and simulations in which arrangement, length and interval of geosynthetics-reinforcements are varied, the reinforcing mechanism by geosynthetics is discussed and a rational and effective use of reinforcements is investigated in this study.

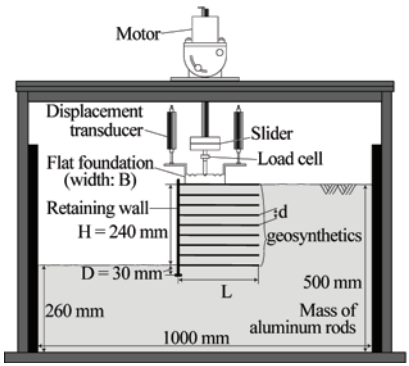

FIG. 1. Schematic diagram of apparatus for two-dimensional model tests.

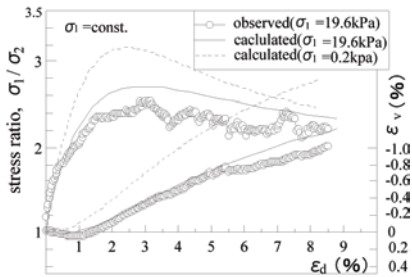

FIG. 2.Stress-strain-dilatancy relation of aluminum rods mass.

OUTLINE OF MODEL TESTS AND NUMERICAL ANALYSES

Bearing capacity tests of flat (strip) foundation are conducted on the backfill of the geosynthetic-reinforced retaining wall. Fig. 1 shows a schematic diagram of the apparatus for two-dimensional model test. Scales of the model structures are assumed to be 1/50 of the prototype, i.e., height of the wall H is 240 mm, embedment depth D is 30 mm and width of the model foundation B is 120 mm. Retaining wall and flat foundation are made by aluminum plates of 5 and 20 mm thickness, respectively. Geosynthetic-reinforcements are made by tracing paper having almost no bending stiffness, to which aluminum rods of 1.6 mm diameter are glued at 10 mm intervals to consider realistic frictional behavior between reinforcements and ground. Flat foundation is set up on the surface of the backfill at 20 mm spacing from the retaining wall. Mass of aluminum rods, having diameters of 1.6 and 3.0 mm mixed in a ratio of 3:2 in weight, is used as ground material. Stress-strain relationship of aluminum rods mass is similar to those of medium dense sand (Fig. 2). The unit weight of the aluminum rods mass is 20.4 kN/m^3, and the length is 50 mm. Vertical load is applied at the center of the flat foundation. A slider permits lateral movement of the loading rod, while a load cell for measuring the magnitude of load is set in the loading system. Vertical displacement and rotation of the foundation are measured with two displacement transducers at the both ends of the foundation. Taking digital photographs of the model ground and analysing them using PIV method, the deformation of the ground is captured.

The finite element analyses are carried out with FEMtij-2D considering plane strain, drained condition for the same scale of the model tests using elastoplastic subloading t_{ij} model (Nakai & Hinokio, 2004). An example of finite element mesh is shown in Fig. 3. Boundary conditions are the same as those of the model tests, namely, vertical sides of the mesh are free in the vertical direction and the bottom face is fixed. Isoparametric 4-noded element is used for soil element. The reinforcements are modeled by elastic beam elements having almost no flexural rigidity EI and having axial tensile rigidity EA of 1.31 x 10^3 N. The foundation and the retaining wall are assumed to be linear elastic materials of high stiffness. The frictional behaviors between the reinforcements and soil (angle of friction $\phi = 20°$), the retaining wall and soil ($\phi = 8°$) and the foundation and soil

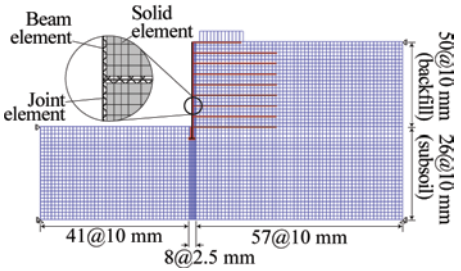

FIG. 3. An example of finite element mesh.

Table 1. Material parameters

l	0.008
k	0.004
$N = e_{NC}$ at $p = 98$ & $q = 0$ kPa	0.3
$R_{cs} = (s_1/s_3)_{cs}$	1.8
n_c	0.2
b	1.2

Table 2. Testing patterns

d/H (number of geosynthetics)	L/H = 7/12	L/H = 1	$L_1/H=1$, $L_2/H=7/12$	$L_1/H=7/12$, $L_2/H=1$
1/12 (13)	Case I	Case I	–	–
1/8 (9)	Case I	Case I	Case II	Case II
1/6 (7)	Case I	Case I	–	–
1/4 (5)	–	Case I	–	–
1/3 (4)	–	Case I	–	–

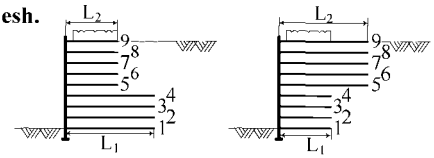

$L_1/H=1$, $L_2/H=7/12$ $L_1/H=7/12$, $L_2/H=1$

FIG. 4. Arrangements of reinforcements.

(ϕ = 15°) are modeled employing elastoplastic joint elements (Nakai, 1985), whose friction angles are determined by the results of preliminary tests. Material parameters for the aluminum rods mass are shown in Table 1. The meanings of parameters are fundamentally the same as those of the Cam clay model except the parameter a, by which the influence of density and confining pressure are considered. The parameter β represents the shape of yield surface. These parameters can easily be obtained from traditional laboratory tests. Results of the biaxial tests and the corresponding calculation are compared in Fig. 2. It is indicated from this figure that the strength and deformation behavior of ground material is suitably described by the subloading t_{ij} model. In the simulation, calculation of self-weight consolidation of subsoil layer is, firstly, conducted by assuming void ratio of 0.328 under very low confining pressure ($p = 9.8 \times 10^{-6}$ kPa) and applying nodal forces equivalent to body force (self-weight) of each element. Reinforced soil retaining wall and backfill layer are, then, set up by repeating installation of reinforcement (beam and joint elements), self-weight consolidation of backfill layer. After that the vertical load is applied to the center of the flat foundation.

In the present study, 10 patterns of tests are conducted (Table 2) varying length L, intervals d and arrangement (Fig. 4) of geosynthetics.

RESULTS AND DISCUSSIONS

Influence of interval of reinforcements (Case I): Relationships between vertical displacement and bearing capacity of the foundation for different intervals (numbers) of the reinforcement are shown in Fig. 5. In this figure, vertical displacement of the foundation normalised by its width B are plotted against vertical loads divided by $\gamma H / 2$. It is seen from Fig. 5 that the initial stiffness and the ultimate bearing capacity increase significantly when the reinforcements work effectively such as for the arrangement of d/H = 1/6 or less. On the other hand, the effects of reinforcements cannot be expected

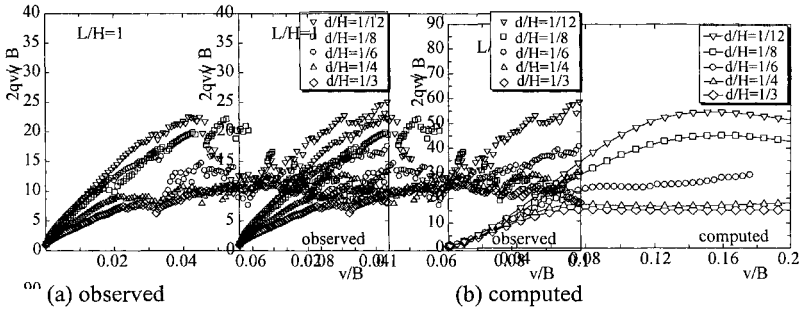

FIG. 5. Relationships between vertical load and vertical displacement of the foundation for different intervals of the reinforcements in case of L/H = 1.

when the interval of the reinforcements is larger than a certain distance (d/L is 1/4 or greater). The numerical analyses capture well the influence of the intervals of the reinforcements in the same way as the model tests though they overestimate the ultimate bearing capacity.

Fig. 6 shows the observed and computed shear strain distributions of the ground when the bearing capacity approaches to the peak value (for the model test it is at v/B = 0.04, while it is at v/B = 0.13 for the analysis). It is seen from this figure that, in the case when d/H is 1/4 or greater where the effects of the reinforcement cannot be expected, a zone of large shear strain concentrates especially in the vicinity of the right end of the foundation, and uneven settlement of the foundation with clockwise rotation is observed, which means that the internal stability of the reinforced backfill ground is not ensured. Meanwhile it is found that, in the case when d/H = 1/8 or less where a sufficient number of reinforcements is installed, shear deformation within the reinforced backfill ground is well restrained and shear band forms in a large area of both the backfill and the subsoil ground. The computed results describe well the differences of the formation of shear band due to the interval of the reinforcements as observed in the model tests.

It is indicated through the results in this section that, in order to increase the bearing capacity and to reduce the settlement of the foundation, the reinforcements should be installed within a proper interval so that the internal stability of the reinforced ground is ensured.

Influence of length of reinforcements (Case I): Bearing capacity of the foundation for different lengths and intervals of the reinforcement are shown in Fig. 7. It is seen from Fig. 7 that, regardless of the interval of the reinforcements, the initial stiffness and the ultimate bearing capacity for L/H = 7/12 are rather smaller than those for longer reinforcements (L/H = 1). In the experiments, the backfill ground of the reinforced soil retaining wall is totally collapsed before the normalized vertical displacement v/B of the foundation reaches 0.04 in the case of L/H = 7/12. It is also indicated from this figure that the numerical analyses properly predict the influence of the lengths of the reinforcements observed in the model tests.

Fig. 8 shows the shear strain distributions of the ground for different lengths of the reinforcements at normalized vertical displacement v/B is 0.02, where the interval d of the reinforcements is 1/8H. It is observed from this figure that, regardless of the length

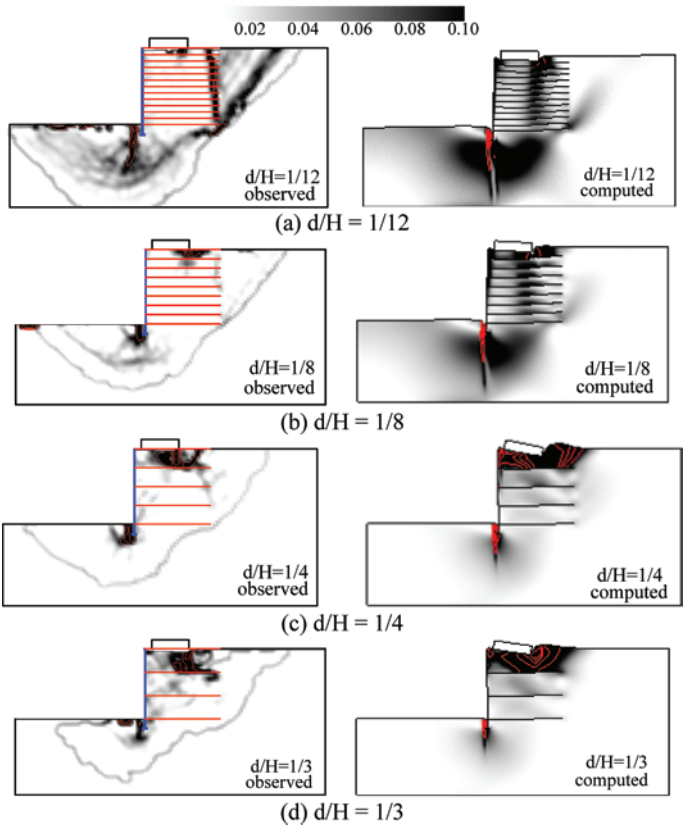

FIG. 6. Shear strain distributions for different intervals of the reinforcements in case of L/H = 1 (Left: observed, Right: computed).

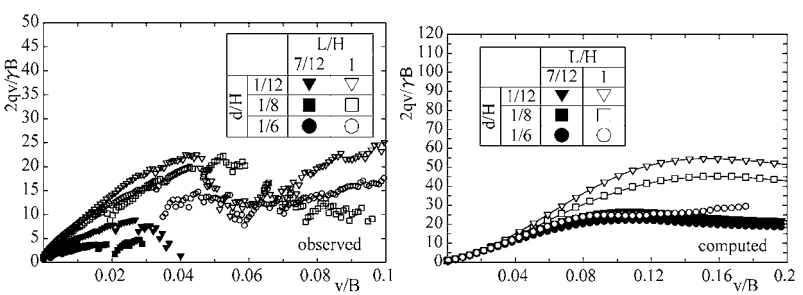

FIG. 7. Relationships between vertical load and vertical displacement of the foundation for different lengths and intervals of the reinforcements.

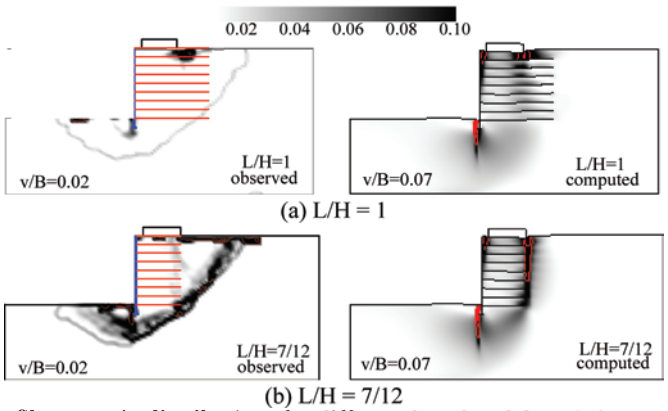

FIG. 8. Shear strain distributions for different lengths of the reinforcements in case of d/H = 1/8 (Left: observed, Right: computed).

of the reinforcements, the magnitude of the shear strain observed within the ground reinforced by the geosynthetics is not much significant and the local stability of the reinforced backfill ground is retained as the reinforcements are installed with a sufficiently small interval. However, in the case of shorter reinforcements (L/H = 7/12), shear band clearly forms a circular arc, which causes slippage failure of the ground containing the retaining wall, the foundation and the reinforced backfill ground. On the contrary, in the case of longer reinforcements (L/H = 1), the deformation of the ground surrounding the reinforced soil retaining wall is properly restricted because the reinforcements are installed up to the place where shear band forms in the case of L/H = 7/12. It is also indicated that, although the shape of the shear band formed in the case of L/H = 7/12 is different from one observed in the model tests, the effect of the reinforcement length on the deformation mechanism of the ground is well explained by the numerical analyses using elastoplastic subloading t_{ij} model.

From the discussions in this section, it is concluded that the effectiveness of the geosynthetic-reinforcements depends not only on their interval but also on their length, which determines the stability of the surrounding ground.

Influence of installation pattern (arrangement) of reinforcements (Case II): For the case where the interval of the reinforcements is 1/8H for which the reinforced ground is internally stable, effective arrangement of the reinforcements is examined by changing the lengths of the reinforcements according to location. In addition to the cases of L/H = 7/12 and 1, two kinds of arrangements which are shown in Fig. 4 are considered here. Fig. 9 shows the bearing capacity for four kinds of the arrangements of the reinforcements, while Fig. 10 indicates the observed and computed shear strain distributions of the ground when the bearing capacity is about to reach the ultimate value. It is indicated from Fig. 10 that a zone of large shear strain is not seen and the internal stability of the reinforced ground is ensured in every case. However, the characteristics of bearing capacity and the deformation behavior of the surrounding ground are totally different due to the arrangement of the reinforcements. When the reinforcement length in the lower part L_1 is equal to 7/12H and that in the upper part L_2

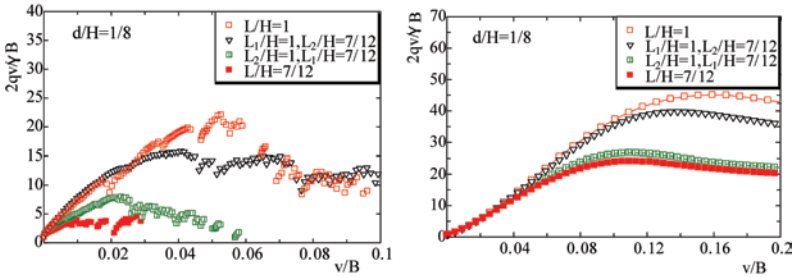

FIG. 9. Relationships between vertical load and vertical displacement of the foundation for different arrangements of the reinforcements.

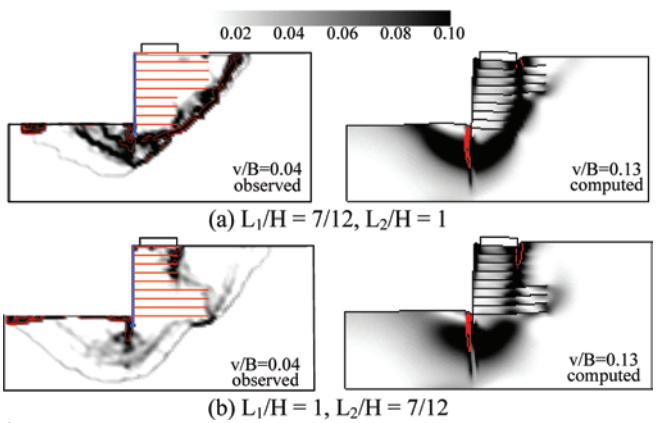

FIG. 10. Shear strain distributions for different arrangements of the reinforcements (Left: observed, Right: computed).

is equal to H (shorter reinforcements are installed in the lower part of the backfill), the initial stiffness and the ultimate bearing capacity are similar to those for the case of L/H = 7/12, which means that the backfill ground is not effectively reinforced by the geosynthetics. In this case, a zone of large shear deformation forms an arc-shaped shear band and slippage failure occurs. On the other hand, in the case when $L_1/H = 1$ and $L_2/H = 7/12$, the characteristic of bearing capacity is similar to that in the case of L/H = 1 (Fig. 9) and the formation of slippage surface is interrupted by the reinforcement installed in the lower part (Fig. 10). The calculated and observed shear strain distributions show very good agreement although the ultimate bearing capacity is overpredicted by the simulations.

It is concluded that a rational arrangement of the geosynthetic-reinforcements would be one which ensures the internal stability of the reinforced ground with a proper interval of reinforcements and increases the external stability of the overall ground with a proper length of the reinforcements.

CONCLUSIONS

In order to investigate the deformation and failure behaviors of reinforced earth retaining wall subjected to vertical loading and reinforcing mechanism of geosynthetics, two-dimensional model tests and their numerical analyses are conducted varying the length, intervals and arrangement of reinforcements. From a series of experiments and simulations, the following conclusions are revealed.

a) The effectiveness of geosynthetic-reinforcements mainly depends on whether they are able to increase both internal stability, which is local stability within the reinforced ground, and external stability, which is overall stability of the surrounding ground.
b) If the interval of the geosynthetics is not short enough to stabilize the reinforced ground, geosynthetic-reinforcements have little effects on the bearing capacity of the foundation.
c) Effect of reinforcements cannot be expected if the length of the reinforcements is not long enough to prevent the formation of the shear band in the backfill and subsoil ground.
d) By flexibly changing the length of the reinforcements according to location, the stability of the backfill ground of the retaining wall can be rationally increased. For the reinforced soil retaining wall focused on the present study, the reinforcements in the lower part of the retaining wall should be longer than a certain length in the sight of the external stability of the surrounding ground. It is, however, indicated by past experimental study (Ito et al., 2008) that sufficient lengths of the reinforcements in the upper part will also be necessary to increase the dynamic stability of the retaining wall against earthquake.
e) Numerical simulation in which stress strain characteristics of geomaterials, retaining wall and reinforcement are properly taken into account and frictional behaviors between retaining wall, foundation, reinforcements and ground are suitably modeled can predict well the effects of the interval, length and arrangement of the reinforcements.

REFERENCES

Ito, H., Saito, T., Ueno, M., Izawa, J. And Kuwano, J. (2008). "Development of rational design method for the geogrid reinforced soil wall combined with soil cement and its application." *New Horizons in Earth Reinforcement*, 661-666.

Nakai, T. (1985). "Finite element computations for active and passive earth pressure problems of retaining wall." *Soils & Foundations*, 25(3): 98-112.

Nakai, T. and Hinokio, M. (2004). "A Simple Elastoplastic Model for normally and over consolidated soil with unified material parameters." *Soils & Foundations*, 44(2): 53-70.

Nakai, T., Shahin, H.M., Watanabe, A. and Yonaha, S. (2009). "Reinforcing mechanism of geosynthetics on bearing capacity problems – model tests and numerical simulations." *Proc. of the 17th Int. Conf. on Soil Mech. and Geotech. Eng.*, 917-920.

Tatsuoka, F., Tateyama, M., and Murata, O. (1989) "Earth retaining wall with a short geotextile and a rigid facing", *Proc. 12th Int. Conf. on SMFE*, 1311-1314.

3D Parametric Study of Geosynthetic-Reinforced Column-Supported Embankments

Jie Huang[1], A.M. ASCE, PE, Jie Han[2], M. ASCE, PE, and Junjie Zheng[3], PE

[1]Transportation Engineer (civil), Office of Geotechnical Design South-1, Division of Engineering Services, California Department of Transportation, 100 South Main Street, 11th Floor, Los Angeles, California 90012, USA; huangjie966@hotmail.com
[2]Associate Professor, the University of Kansas, CEAE Department, 1503 W 15th Street, Lawrence, Kansas 66045, USA, jiehan@ku.edu
[3]Professor, Institute of Geotechnical and Underground Engineering, Huazhong University of Science and Technology, Wuhan 430074, China, zhengjj@hust.edu.cn

ABSTRACT: Column-supported geosynthetic-reinforced embankments have been increasingly designed and constructed. Since settlement analysis has not been well considered in current design methods, numerical modeling has been often adopted to predict the long-term serviceability of the embankment by coupling hydraulic and mechanical models. To assess the influence of various factors on the settlement of column-supported embankments, coupled 3D numerical analyses were performed using FLAC3D in this study. Once calibrated by a well-documented case history in Finland, the coupled 3D numerical modeling scenario was implemented in a parametric study to fulfill the objective of this study. In the parametric study, a prototype case with a typical configuration served as the baseline case. One parameter was changed at one time to investigate the influence of a certain factor on the settlement. In the analyses, the foundation soils including soft and firm soils, the embankment fill, and the columns were modeled as linearly elastic-perfectly plastic materials with Mohr-Coulomb failure criteria. The geosynthetic reinforcement was simulated by geogrid elements in the FLAC3D, which in realty are plane-triangular elements, sustaining in-plane forces only. The staged construction was approximated by building the embankment in lifts with duration equal to the construction time plus the lapse time between two consecutive stages. The computed settlements were presented, compared, and discussed in this paper.

INTRODUCTION

Geosynthetic-reinforced column-supported (GRCS) embankments have been widely constructed all over the world in the past decades, especially in soft soil areas. Meanwhile, a number of design methods have been proposed and applied, which were based on different assumptions. Researchers have identified great variations among existing design methods (Naughton and Kempton 2005; Steward and Filz 2005) and

advocated experimental and numerical studies to improve the understandings, which are expected to minimize the uncertainty of the GRCS embankment system (e.g. Demerdash 1996; Han and Gabr 2002; Abdullah and Edil 2007; Almeida and Spotti 2007; and Smith and Filz 2007). Relative to experimental studies, numerical studies are cost- and time- efficient as well as flexible. When it comes to the serviceability concern (i.e., short- and long-term performance), numerical modeling often becomes the only feasible option. Even though 3D coupled hydraulic and mechanical modeling has been conducted on some well-defined case histories to provide useful information on the consolidation (e.g. Huang and Han 2009), comprehensive 3D parametric studies, which can evaluate the influence factors on the serviceability of GRCS embankments, have not yet been well performed due to the complexity and time-consumption.

Considering the facts stated above, a 3D parametric study based on coupled mechanical and hydraulic modeling was conducted to assess the influence of various factors on the serviceability of the GRCS embankment. The discussion in this paper is limited to settlement, which is deemed the most direct indicator of the serviceability of GRCS embankments. The investigated factors include modulus, friction angle, and permeability of soft soil, modulus and spacing of columns, tensile stiffness of geosynthetic, and average construction rate. FLAC3D Version 3.1, three-dimensional finite difference software (Itasca 2006), was selected for this study. More information on the coupling process within FLAC3D should be referred to the Itasca manual of Fluid-Mechanical Interaction.

MODEL CALIBRATION

Prior to the parametric study, a model calibration was conducted to ensure a good representation of the numerical model for the GRCS embankment applications. The modeling calibration was based on a well-documented case history in Finland (Formans et al. 1999). The case history and the conclusion of the model calibration are briefed herein. The following two references should be referred for details: Forsman et al., (1999), and Huang and Han (2009).

The case history is a deep mixed column-supported and geotexitle-reinforced embankment with 2H:1V side slopes, which was extensively instrumented and monitored for up to 5 years after the completion of construction. The measured settlements at designated locations were compared with the results yielded by numerical modeling as presented in Fig. 1. Disregarding the dispensable fluctuation of the field measurements, the numerical results and field measurements exhibited good consistency, which was the basis for the following parametric study.

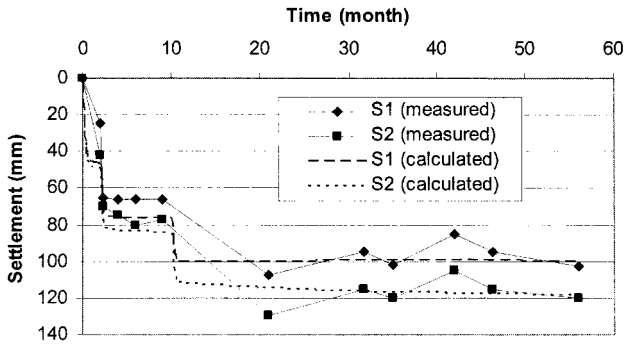

(a) Settlements at Locations S1 and S2

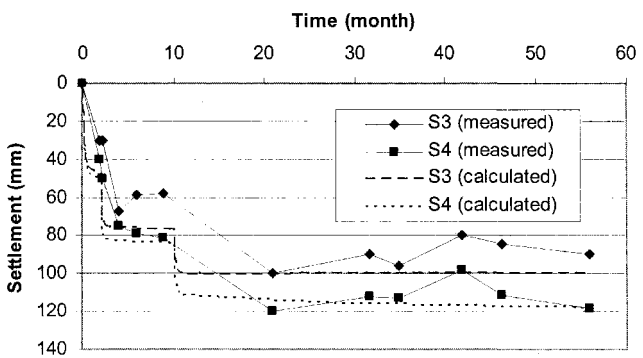

(b) Settlements at Locations S3 and S4

FIG. 1. Settlement versus time (Huang and Han 2009).

PARAMETRIC STUDY

The parametric study started with a baseline case, which was a pre-determined case with typical configurations as shown in Fig. 2. Due to its symmetry, only half of the embankment was modeled with a width of 10m at the crest. Widely adopted 2:1 (H:V) side slopes were assumed. The height of the embankment was 5m. The in-situ soils below the embankment were a layer of 10m thick soft clay and a layer of 2m thick firm soil. No settlement was allowed below the firm soil layer considering underlying intact bedrock. Since many column types are suitable for GRCS embankments and their properties vary greatly, deep mixed (DM) columns were exclusively studied. The DM columns in a square pattern were assumed to penetrate 1m into the firm soil. A geosynthetic layer was placed 0.25m above the columns. The

end of the geosynthetic sheet at the centerline was fixed laterally but free vertically and the other end toward the toe was free in both directions. The boundary effect was eliminated by extending the left boundary of the model far enough from the embankment. The ground water level was assumed at the ground surface. The mechanical boundary conditions are explicitly illustrated in Fig 2. The hydraulic boundary conditions are explained as follows. The right boundary in Fig. 2 (a) was assumed to be impervious, i.e., no water enters or leaves the plane of symmetry. The left boundary in Fig. 2 (a) was randomly set impervious, which was too far away from the embankment to have any influence. The front and back boundaries were set impervious to account for the repetition of the span. The bottom boundary was set impervious to keep compliance with the assumed intact bedrock layer.

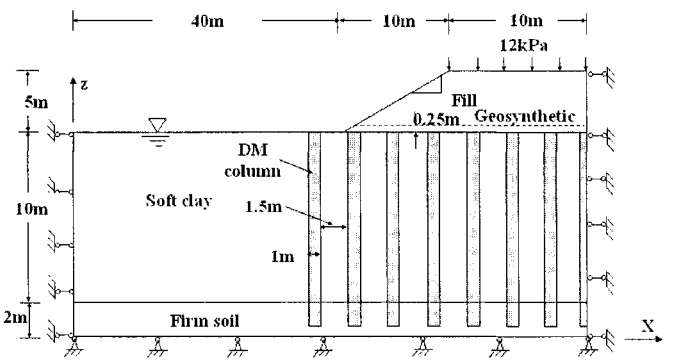

(a) Elevation view

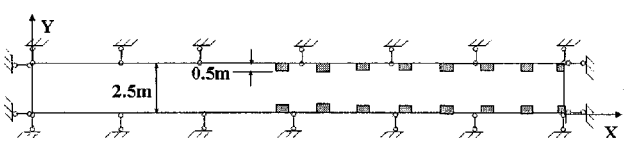

(b) Plane view

FIG. 2. Numerical model of the baseline case (modified from Huang 2007).

Since the baseline case served as a reference for comparisons when parameters were deviated, the variation ranges of the parameters were considered to cover their typical ranges in most actual projects. The properties of the DM columns, the soft soil, and the embankment fill of the baseline case were in the middle of their typical ranges to leave enough margins for property variations in the parametric study (EPRI 1990; Budhu 2000), which are listed in Table 1. The DM columns, the soft soil, the firm soil, and the embankment fill were modeled as linearly elastic-perfectly plastic

materials with Mohr-Coulomb failure criteria. The geosynthetic reinforcement layer was modeled by geogrid elements incorporated in FLAC3D, capable of sustaining in-plane tensile forces only. A reduction multiplier of 0.8 was used for the interface shear strength between the embankment fill and the geosynthetic reinforcement.

Table 1. Material Properties in the Baseline Case

Material	Properties
DM columns	$\gamma = 18kN/m^3$, $c = 1235kPa$, $\phi' = 0^o$, $E_c = 247MPa$, $\nu = 0.3$, $c_t = 247kPa$, $k = 1\times10^{-9}m/s$
Soft Soil	$\gamma = 18kN/m^3$, $c' = 0kPa$, $\phi' = 25^o$, $E_s = 2MPa$, $\nu = 0.3$, $k = 1\times10^{-9}m/s$
Firm Soil	$\gamma = 18kN/m^3$, $c' = 0kPa$, $\phi' = 30^o$, $E_{sf} = 100MPa$, $\nu = 0.3$, $k = 1\times10^{-9}m/s$
Embankment Fill	$\gamma = 18kN/m^3$, $c' = 5kPa$, $\phi' = 32^o$, $E_{se} = 30MPa$, $\nu = 0.3$,
Geosynthetics	$t = 0.002m$, $E_x = 500MPa$, $E_y = 500MPa$, $k_s = 20MN/m/m$, $c_a = 0kPa$, $\delta = 24.8^o$

Note: γ = unit weight; c = shear strength of soil-cement; c' = effective cohesion; ϕ' = effective friction angle; k = permeability; E = elastic modulus; ν = Poisson's ratio; c_t = tensile strength of soil-cement; t = thickness of geosynthetic reinforcement; E_r = elastic modulus of geosynthetic reinforcement; k_s = bond stiffness between geosynthetic and embankment fill; c_a = bond strength between geosynthetic and embankment fill; δ = bond friction angle between geosynthetic and embankment fill.

The simulation was advanced in three steps: the initiation of the ground stress field and the hydrostatic pore water distribution, the simulation of the staged construction of the embankment, and the application of the traffic load. Such simplification on staged construction was employed to limit the simulation with reasonable complexity and time as: each embankment lift was applied instantaneously, and a period of waiting time followed the lift to allow for partial dissipation of excess pore water pressure. The traffic load was uniformly distributed in a magnitude of 12kPa in numerical modeling. The modeling was continued to 4.5 years after traffic.

Upon the conclusion of the baseline case, the study was proceeded with changing one parameter from the baseline case one time to assess the influence of a certain factor on the settlement. The factors and their parameter values are listed in Table 2.

Table 2. Parameter and Variation Used in the Three-Dimensional Study

Influence Factors	Parameter Variation Range of value
Elastic modulus (MPa)	1.0, 2.0*, 4.0, 8.0
Friction angle (°)	15, 20, 25*, 30
Permeability (m/s)	10^{-8}, 10^{-9}*, 10^{-10}
Elastic modulus (MPa)	247*, 372, 497
Spacing (m)	2.0, 2.5*, 3.0
Tensile stiffness (kN/m)	0, 1000*, 5000, 10000
Average construction rate (meter/mon)	0.25, 1*, 4

* The parameters used in the baseline case

RESULTS AND COMPARISONS

As a direct indicator of serviceability, settlements at the crest of the embankment, at 1 month and 4.5 years after construction, are presented herein. Settlement occurring at 1 month is considered as a short-term settlement. The settlement of the column-supported embankment became stable within a few years after construction (Forsman et al. 1999; Huang et al. 2009). As a result, the settlement occurring at 4.5 years can be considered as a long-term settlement. The settlement at the base of the embankment is presented as well, since it is a very important reference when the strain in the geosynthetic is to be evaluated. Being of more practical significance, the maximum settlements are presented herein.

The influence of the soft soil modulus on the maximum settlement is presented in Fig. 3. Obviously, the increase of the soft soil modulus reduced the maximum settlement at the crest and base in short-term and long-term. However, the effect of the soft soil modulus decreased when the modulus continued increasing. The settlements at the crest and base both increased from 1 month to 4.5 years after service. The soil modulus did not show a noticeable influence on the difference in the settlements from 1 month to 4.5 years, which is evidenced by parallel curves.

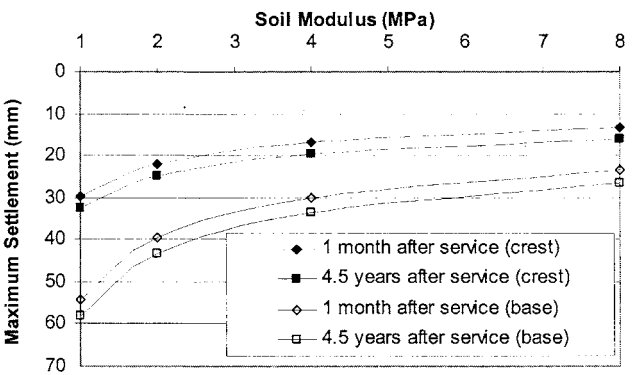

FIG. 3. Maximum settlement versus soil modulus.

The influence of the soil friction angle on the maximum settlement is shown in Fig. 4. The maximum settlement decreased almost linearly with the increase of the soil friction angle. The friction angle did not show an influence on the difference in the settlements from 1 month to 4.5 years, either.

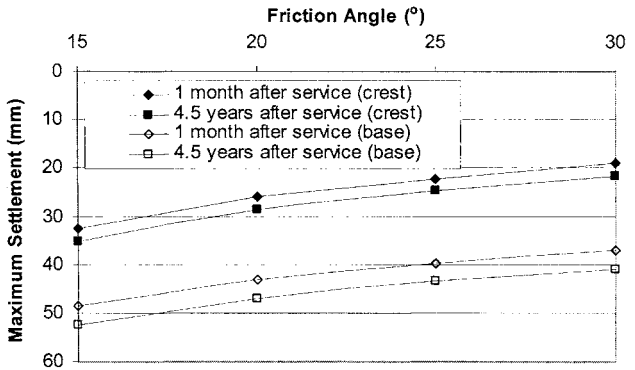

FIG. 4. Maximum settlement versus friction angle.

Soil permeability has been overlooked in the past studies. Since most GRCS embankment applications involve a high ground water table, not only the mechanical properties but also the hydraulic properties have an important influence on the GRCS embankment. The influence of the soil permeability on the maximum settlement is shown in Fig. 5. The lower soil permeability resulted in the higher maximum settlement both at the crest and the base. As the soil permeability was higher than 10^{-9}m/s, however, the influence of the soil permeability on the maximum settlement became less. In addition, the lower soil permeability resulted in a greater increase of the maximum settlement from 1 month to 4.5 years after service, which was attributed to less dissipation of excess pore water pressure during construction. Evidently, when the soft soil permeability is less than 10^{-9}m/s, according to this study other measures may be needed to avoid its detrimental effect on short-term and long-term serviceability.

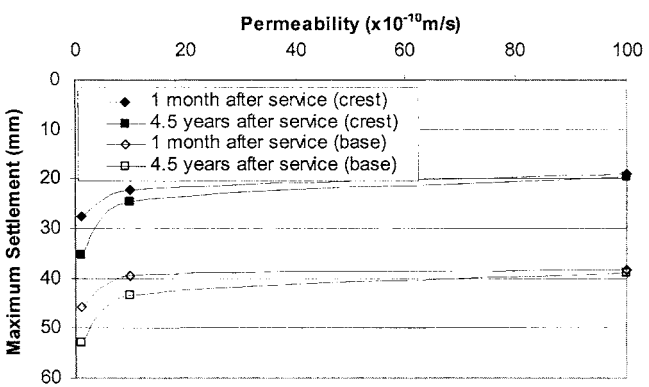

FIG. 5. Maximum settlement versus soil permeability.

The column spacing versus the maximum settlement is plotted in Fig. 6. The maximum settlement increased with the increase of the column spacing. It is also shown that the column spacing had more effect on the settlement at the base than that on the crest. The increase of the column spacing had another adverse effect, which resulted in a greater settlement increase from 1 month to 4.5 years.

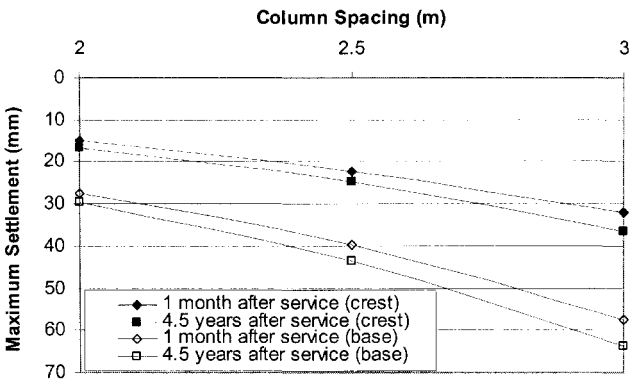

FIG. 6. Maximum settlement versus column spacing.

The column modulus and the geosynthetic tensile stiffness showed a limited influence on the settlement at the crest, therefore, the results are not presented herein. The limited influence of the column modulus and the geoysnthetic tensile stiffness may be attributed to the range of the column modulus investigated, within which the column modulus was higher enough as compared with the soft soil to ensure the efficiency of load transfer from the soil to the columns.

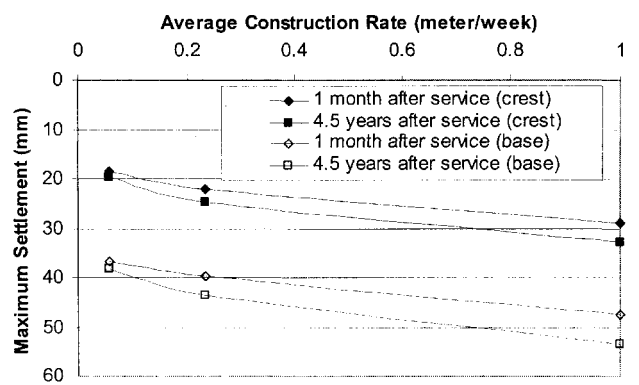

FIG. 7. Maximum settlement versus average construction rate.

Average construction rate is another factor having been overlooked so far. The maximum settlement against the average construction rate is plotted in Fig. 7, which justifies the importance of construction on the serviceability of the embankment. The decrease of the average construction rate led to a smaller maximum settlement and less increase in the settlement from 1 month to 4.5 years. High construction rate allows less time for excess water pressure dissipation, which in turn leads to more settlement and more post-construction consolidation. Within the range of the investigation, the maximum settlement is bi-linearly related to the construction rate with the turning point at 0.2meter/week.

CONCLUSIONS

Based on the parametric study conducted in this study, the following conclusions can be drawn:

1. The increase of the soil modulus and the friction angle reduced the maximum settlement at the crest and at the base. However, they did not have any significant influence on the post-construction consolidation within the property ranges of investigation.
2. The soil permeability had a significant influence on the settlement and the post-construction settlement due to consolidation after construction when the soil permeability was less than 10^{-9}m/s. Lower permeability resulted in higher settlement and post-construction settlement. Some measures may be needed to counteract these two adverse effects when the soil permeability is too low.
3. Provided the constant column size, larger column spacing induced larger settlement. This study also showed that the larger column spacing also resulted in a larger post-construction settlement increase from 1 month to 4.5 years.
4. The column modulus and the geosynthetic tensile stiffness had limited influence on the settlement on the crest, which may be attributed to the efficiency of load transfer from the soil to the columns.
5. Average construction rate had a noticeable influence on both the settlement and the settlement increase from 1 month to 4.5 years.

REFERENCES

Abdullah, C.H., and Edil, T.B. (2007). "Behavior of geogrid-reinforced load transfer platforms for embankment on rammed aggregate peirs." *Geosynthetics International*, 14(3): 141-153.

Almeida E. and Spotti M. (2007). "Embankment supported on piles with biaxial geogrids." *Geotechnical Engineering*, 160(4): 185-192.

Budhu, M. (2000). *Soil mechanics and foundations.* New York: John Wiley, 2000. p. 586.

Demerdash, MA. (1996). *An experimental study of piled embankments incorporating geosynthetic basal reinforcement.* Ph.D. Dissertation, University of Newcastle-Upon-Type; 1996. p. 158.

EPRI. (190). *Manual on estimating soil properties for foundation design.* Cornell University, p. 327.

Forsman, J., Honkala, A., and Smura, M. (1999). "Hertsby Case: A column Stabilized and Geotextile Reinforced Road Embankment on Soft Subsoil," *Dry Mix Method for Deep Soil Stabilization*, Bredenberg, Holm, and Broms (eds), Balkema, Rotterdam, pp. 263-268.

Han, J. and Gabr, M.A. (2002). "Numerical analysis of geosynthetic-reinforced and pile-supported earth platform over soft soil." *Journal of Geotechnical and Geoenvironmental Engineering*, 128(1): 44-53.

Huang, J. (2007). *Coupled mechanical and hydraulic modeling of geosynthetic-reinforced column-supported embankments.* Ph.D. dissertation, the University of Kansas, pp. 420.

Huang, J. and Han, J. (2009). "3D coupled mechanical and hydraulic modeling of a geosynthetic-reinforced deep cement column supported embankment." *Geotextiles and Geomembranes*, 27 (4): 272-280

Huang, J., Han, J., and Oztoprak, S. (2009). "Coupled mechanical and hydraulic modeling of geosynthetic-reinforced column-supported embankment." ASCE *Journal of Geotechnical and Geoenvironmental Engineering*, 135 (8): 1011-1021.

Itasca. (2006). *FLAC3D Fast Lagrangian Analysis of Continua in 3 Dimensions User's Guide.* p. 261.

Naughton, P.J. and Kempton G.T. (2005). "Comparison of analytical and numerical analysis design methods for piles embankment." *Geotechnical Special Publication, Geo-Frontiers*, p. 487-96.

Smith, M. and Filz, G. (2007). "Axisymmetric numerical modeling of a unit cell in geosynthetic-reinforced, column-supported embankments." *Geosynthetics International*, 14(1): 13-22.

Stewart, M.E. and Filz, G. M. (2005). "Influence of clay compressibility on geosynthetic loads for bridging layer for column supported embankments." *Geotechnical Special Publication*, No. 130-142, pp. 447-460.

Prediction of Settlements of Geocell Reinforced Sand Foundations

[1]Sireesh Saride, A.M. ASCE, [2]T. G. Sitharam and [3]Anand J. Puppala, M. ASCE

[1]Lecturer (adjunct), Department of Civil Engineering, The University of Texas at Arlington, Arlington, Tx 76019; sireesh@uta.edu
[2]Professor, Department of Civil Engineering, Indian Institute of Science, Bangalore, India 560012; sitharam@civil.iisc.ernet.in
[3]Professor, Department of Civil Engineering, The University of Texas at Arlington, Arlington, Tx 76019; anand@uta.edu

ABSTRACT: Utilization of geosynthetics as a reinforcement material to improve the weak subgrades is gaining popularity over decades. The evaluation of the improvement achieved from these foreign materials is always a difficult task. It is also necessary to have a quantitative assessment of the improvement achieved from these techniques to adopt them in the new designs. This paper presents the results of two prediction models such as artificial neural networks (ANNs) and non-linear multiple regression models to estimate the bearing capacity of a foundation resting on geocell reinforced sand beds. Modeling results are compared with the experimental results to address the efficacy of these models. Overall, results obtained from both models showed good agreement with the experimental measurements up to about 10% of the footing settlements. At higher settlements, ANNs prediction is better than the multiple regression models.

INTRODUCTION

The decreasing availability of good construction sites has led to the increased use of the marginal ones. In view of this, the requirement for in-situ treatment of foundation soil to improve its bearing capacity has risen markedly, and soil reinforcement is one such method of treatment often used to improve bearing capacity of virgin soil beds (Ingold, 1982; Saride, 2006). Apart from economic advantages, the reinforced soil bed opens up the possibilities of founding civil engineering structures on soil conditions hitherto not suitable. Introduction of reinforced soil below the footing can increase the bearing capacity substantially, thus obviating the necessity of a combined footing or a raft foundation (Sireesh, 2006).

The basic concept of soil reinforcement is to impart apparent tensile strength to the soil, which is otherwise weak in tension. This is achieved by the restraining effect

produced by the reinforcement and also due to the transfer of stresses from soil to reinforcement (Ingold, 1982). The more recent advancement in this field is to provide three-dimensional confinement to the soil using geocells. Several investigations have been reported highlighting the reinforcing efficacy of geocells (Rea and Mitchell, 1978; Bush et al. 1990; Krishnaswamy et al. 2000; Dash et al. 2001; Sitharam and Sireesh, 2005). All these results are based on scale model tests on reinforced soil beds.

Laboratory model studies provide a clear insight of the general behavioral trend of reinforced soil beds (Sitharam et al. 2005). However, to extend these model-test results for prototype practical applications, one should use suitable scaling laws with careful consideration of different parameters as discussed by Butterfield (1990), Fakher and Jones (1996).

As an alternate choice, large scale model tests are more encouraged, yet, the general mechanisms and behavior observed in the model tests are reproduced at large scale (Milligan et al. 1986). Cost and time involved in performing these large scale model tests is considerably very high. Other approaches involving numerical simulation of reinforced soil beds to predict the bearing capacity also provide useful solutions. Lately, Sireesh et al. (2009) have closely predicted the bearing capacity of geocell reinforced sand and clay beds using FLAC3D. However, the involved complexity of simulating the soil-reinforcement coherent mass properties is yet to understand completely. As a result, alternative methods are always needed, which provide more accurate bearing capacity predictions.

The main objectives of this paper are to predict the bearing capacity of the geocell reinforced sand bed at given footing settlement(s) and the general behavioral trend of entire load settlement curve for a specific geometry of the geocell mattress.

This study employs two methods, Artificial Neural Networks (ANNs) and non-linear multiple regression models to predict the behavior of geocell reinforced sand beds. Model predictions are compared with measured test results to evaluate the prediction capacities of these models.

BACKGROUND

Artificial Neural Networks (ANNs), in general, simulates the biological structure of human brain by mean of their architecture. ANNs is an emerging technique that has been applied to many geotechnical engineering applications successfully by many researchers (Shahin et al. 2001). Transportation Research Board (TRB) has summarized the state-of-the-art ANN applications in geotechnical engineering (TRB, 1999). Recently, Shahin et al. (2002) used ANNs to predict the settlements of shallow foundations. Padmini et al. (2008) adopted neurofuzzy models to predict the ultimate bearing capacity of shallow foundations on cohesionless soils. The approaches employed in ANNs are almost similar to that used in conventional statistical models. The purpose of both the models is to predict the relationship between the model inputs and corresponding output(s) (Shahin et al. 2002). This is obtained by repeatedly feeding the known examples of input/output relationships to the model and minimizing the error function defined between the measured and predicted outputs by the model (Shahin et al. 2002).

Extensive literature search shows that the empirical formulation to predict the bearing capacity of reinforced soil beds has not gained much attention, though the

empirical estimation methods are common in all specialties in Civil Engineering field. In empirical formulation, a function is assumed to estimate the relation between the dependent variables and independent variables. The coefficients of the function are estimated by least squares—regression analysis using the observed data.

A detailed discussion on regression analysis can be found in Dielman (2001). Bera et al. (2005) presented the regression model to predict the bearing capacity of square footing on reinforced pond ash.

EXPERIMENTAL STUDIES

The detailed explanation of the laboratory model test results used in this study is presented by Sitharam and Sireesh (2005). Relevant information required in this study is only presented here. The model tests were conducted in a test bed loading frame assembly in the laboratory. The soil beds were prepared in a test tank with inside dimensions of 900 mm × 900 mm × 600 mm. The model circular footing used in this investigation was made of a rigid steel plate and measured 150 mm diameter (D) and 30 mm thickness (t). The base of the model footing was made rough by cementing a thin layer of sand to it with epoxy glue.

The soil used was dry sand with coefficient of uniformity (Cu) of 2.22, coefficient of curvature (Cc) of 1.05, effective size of particle (D10) 0.36 mm, and specific gravity of 2.63. The soil was classified as poorly graded sand with letter symbol SP according to the Unified Soil Classification System (USCS). In all tests the average unit weight (γd) and relative density (Dr) of sand was kept at 16.8kN/m3 and 70% respectively. Pluviation technique was used to prepare the sand beds. In this technique, the height of fall to achieve the desired relative density was determined a priori by performing a series of trials with different heights of fall. The friction angle of the sand at 70% relative density as determined from standard triaxial compression tests is found to be 41°.

The geocell layers were formed using a biaxial geogrid having aperture-opening size of 35 mm × 35 mm. The properties of the geogrid as obtained from standard multi-rib tension test (ASTM, 2001) were: Ultimate tensile strength of 20 kN/m, Initial modulus of 183 kN/m and Secant modulus (5% strain) of 160 kN/m. The geocell mattress was prepared by cutting the geogrids to required length and height from full rolls and placing them in transverse and diagonal directions with bodkin joints (plastic strips) inserted at the connections (Bush et al. 1990).

The geometry of the problem is shown in Figure 1. The pocket size (dp) of the geocells is taken as the diameter of an equivalent circular area of the geocell pocket opening. In all the tests the pocket size of geocells (dp/D) was kept constant at 0.8. Dash et al. (2001) have shown that the optimum pocket size of geocells is 0.8 times the footing width (to obtain maximum performance improvement) to avoid the excess heave on the fill surface.

The footing was loaded by a hand operated hydraulic jack supported against the reaction frame. The load transferred to the footing was measured through a pre-calibrated proving ring placed between the ball bearing and the hydraulic jack. Each load increment was maintained constant until the footing settlement stabilized. Footing settlements were measured through two dial gauges placed on either side of the centre

line of the footing.

A series of model tests were performed by varying the depth of placement of geocell mattress (u), width of geocell mattress (b) and the height of geocell mattress (h). All these parameters are expressed as non-dimensional forms by dividing these values with footing width. These details are summarized in Table 1.

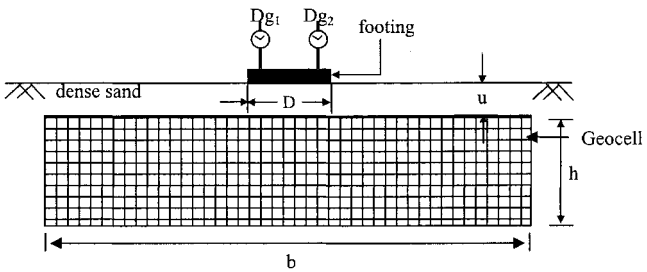

FIG. 1. Geometry of geocell reinforced foundation bed.

Table 1. — Details of model tests carried out on sand beds

Test series	Type of reinforcement	Details of test parameters
A	Unreinforced	Constant parameters: Dr = 70 %, γd = 16.8 kN/m3
B	Geocell	Constant parameters: Dr = 70 %, γd = 16.8 kN/m3, b/D = 3.1, h/D = 1.2 Variable parameters: u/D = 0.0, 0.05, 0.1, 0.25, 0.5, 1.0
C	Geocell	Constant parameters: Dr = 70 %, γd = 16.8 kN/m3, u/D = 0.05, h/D = 1.2 Variable parameters: b/D = 1.3, 1.9, 3.1, 3.7, 4.3, 4.9,5.5
D	Geocell	Constant parameters: Dr = 70 %, γd = 16.8 kN/m3, u/D = 0.05, b/D =4.9 Variable parameters: h/D = 0.6, 1.2, 1.8, 2.4

PREDICTION MODEL STUDIES

In order to obtain the accurate prediction of bearing capacity of geocell reinforced foundation beds, it is important to understand the factors/parameters that affect most the bearing capacity of the reinforced soil bed. These parameters should include the characteristics of material properties, size of the geocell mattress, and that of soil-

reinforcement interaction properties.

Sitharam and Sireesh (2005) demonstrated through a series of model tests that the bearing capacity of reinforced bed was influenced by the bearing capacity of unreinforced bed (qu), footing settlement ratio (s/D), width of the geocell mattress (b/D), and height of the geocell mattress (h/D). The direct influence of the soil-reinforcement interaction on the bearing capacity of the geocell reinforcement bed was not studied. However, Farrag et al. (1993) demonstrated through pullout tests on compacted geogrid-sand beds that the pullout resistance of the geogrid is based on the soil-grid interaction characteristics and the particle shape of the sand particles. Therefore, the friction angle ratio, δ_μ/ϕ (defined as the ratio of soil-grid interfacial friction angle, δ_μ to peak angle of shear resistance of sand, ϕ) is also considered as one of the influencing parameters in this study. From experimentally obtained pressure-settlement curve for a set of constant parameters and one variable parameter, the bearing pressure of reinforced bed corresponding to different footing settlement ratios (i.e. s/D = 1%, 3%, 5%, 10%, 15%, 20%, 25%, 30%, 35%, and 40%) was selected. Similarly, from each performed with different variable parameter (Table 1), a huge data base was generated to develop the prediction models. Following sections describe the development of ANN and multiple regression models using the generated data base from the experimental studies.

ANN MODEL DEVELOPMENT

The development of neural network model consists of selecting model input/out parameters, data pre-processing, designing appropriate model architecture, model training and model validation. The data used to train and validate the neural network model were obtained from a series of experimental tests carried out on geocell reinforced sand beds as explained before. A total of 350 data sets were obtained from these model test results out of which, 60% of the data was used to train the selected model and 20% of the data was used for the testing and the remaining 20% was used for model validation.

The segregated database is divided into three subsets, a training set and a testing set, to develop the neural network model and a validation set to check the accuracy of the predictions. Both the training set and the validation set contain all the patterns to represent the entire data set. After data preprocessing the next hurdle is arriving at versatile model architecture. In this step the number of hidden layers and their corresponding nodes in each hidden layer are determined. According to Hornik et al. (1989) a network with a single hidden layer provided with enough connection weights can be used to approximate any continuous function. Accordingly, a network with single hidden layer was trained with different number of nodes (varying from 1 through 15). Finally, the network with a single hidden layer having three nodes is accepted as the best network architecture for this study. The input layer has 6 nodes and the output layer has one node in this particular network as shown in Figure 2.

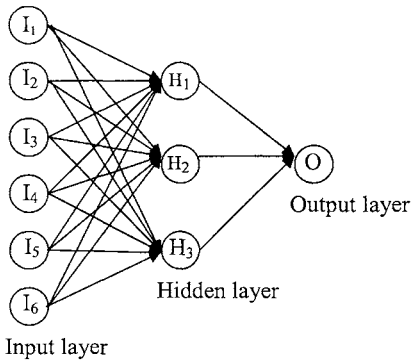

FIG. 2. Optimized network architecture.

As defined by Shahin et al. (2002) training process is the step in which the connection weights are optimized. There are a variety of algorithms available to train the neural network models, but in geotechnical engineering (Goh, 1994) it is a common practice is to use the back-propagation algorithm. However, when the number of weights in a network is less than 300, Levenberg-Marquardt algorithm is proven to be effective. This method often performs considerably faster than other algorithms and finds better optima than other algorithms. Hence this algorithm has been adopted to train the above described network in this study.

After the training stage is completed, the functioning of the trained model is ascertained using the validation test data which has not been used during the training and the testing stages. The idea behind validating the process is to guarantee the models prediction ability for a generalized data (in place of the training data) instead of simply memorizing the input/output relationships that are contained in the training data. Figure 3a presents the correlation obtained between the predicted and measured bearing pressures corresponding to footing settlement ratios, s/D = 5%, 10%, and 25%. In this research study the coefficient of determination (R^2) is used to evaluate the performance of the developed model. The R^2 value for the selected ANN model is found to be 0.98, which indicates the model provided accurate prediction of measured bearing pressures of the geocell reinforced foundation beds.

MULTIPLE REGRESSION ANALYSIS

From the experimental pressure-settlement plots, extensive data on bearing pressure at different settlements of footing, for different factors (i.e. height and width of geocell layer), were obtained that provided a large database for the regression analysis. Out of 350 numbers of data sampled over the whole range of database, 70% of the data was randomly taken and used in the regression analysis and the rest was used in the validation of the derived regression equation. Through a series of trial and error, the

following functional form was fitted to the present test data:

$$q_c = q_u^{\alpha_1} * \left(\frac{s}{D}\right)^{\alpha_2} * \left(\frac{b}{D}\right)^{\alpha_3} * \left(\frac{h}{D}\right)^{\alpha_4} * \alpha_5^{\left(\frac{u}{D}\right)} * \alpha_6^{\left(\frac{\delta_\mu}{\phi}\right)} \quad (1)$$

Where, qc = bearing pressure of geocell reinforced bed (kN/m2), qu = bearing pressure of unreinforced bed (kN/m2), s/D = footing settlement ratio (%), b/D = width of the geocell mattress, h/D = height of the geocell mattress, u/D = depth of placement of geocell mattress from the base of the footing, δ_μ/ϕ = friction angle ratio i.e. ratio of soil-grid interfacial friction angle to peak angle of shear resistance of sand. α1, α2, α3, α4 , α5 and α6 are the regression coefficients. Theses coefficients were found out through nonlinear regression analysis (Dielman, 2001). The final form of the proposed model, for predicting the bearing pressure of sand foundation is expressed by the following equation:

$$q_c = q_u^{0.9838} * \left(\frac{s}{D}\right)^{0.3576} * \left(\frac{b}{D}\right)^{0.3176} * \left(\frac{h}{D}\right)^{0.3260} * 0.5261^{\left[\frac{u}{D}\right]} * 0.8623^{\left(\frac{\delta_\mu}{\phi}\right)} \quad (2)$$

This was validated using the data samples which were not used in the regression analysis. The correlation between the measured and predicted value of the bearing pressure (qc) corresponding to the settlement ratios, s/D = 5%, 10%, and 25% is shown in Figure 3b. The R^2 of this model is found to be 0.95, which indicates that the model provides good predictions. It should be noted that the bearing pressures are regarded as bearing capacities of the reinforced foundations when s/D ratios are close to 25%.

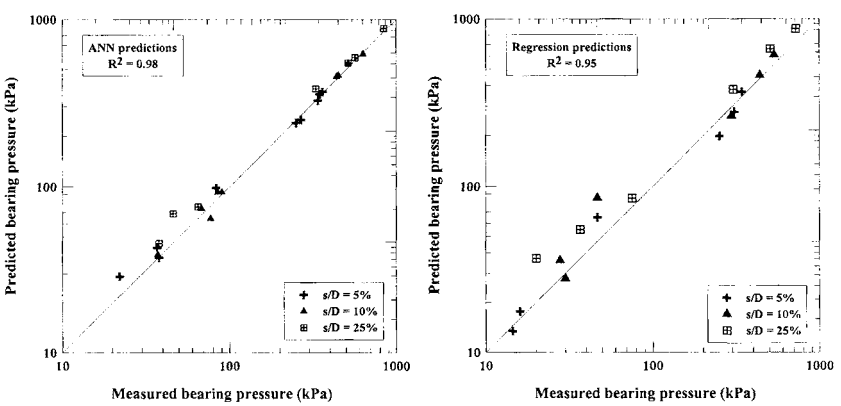

a) ANN model predictions **b) Regression model predictions**

FIG. 3. Variation of predicted bearing pressure with measured bearing pressure.

DISCUSSION

Earlier analysis in the previous section showed that both predictive models (ANNs and multiple regressions) presented in this paper provided very good prediction of measured bearing pressures at different footing settlement ratios. An attempt is made here to predict a typical laboratory loading - settlement behavior of geocell reinforced sand bed. The geometry of the geocell mattress chosen for this prediction is: b/D = 3.1, h/D = 1.2, u/D = 0.0, and δ_μ/ϕ = 0.92. Figure 4 depicts both the predicted behaviors of geocell reinforced sand bed using the present ANNs and multiple regression models. Laboratory measured test data has also been included in the same figure for comparisons. Results in Figure 4 demonstrate that both models have predicted the load – settlement behavior very well up to a footing settlement ratio of 10%. Beyond this ratio, both models have over predicted the loading behavior by 18 to 23%. This could be attributed to the unavailability of test data in some test cases at such high footing settlements. In unreinforced bed conditions, tests as shown in series A of Table 1 have yielded failures that have occurred at footing settlement ratios, s/D less than or equal to 15%. The lack of data at this footing settlement range would have reflected in predicted behavior variations by both these models. It should be noted that the failure here is defined as that an increase in settlement did not produce any increase in bearing pressure.

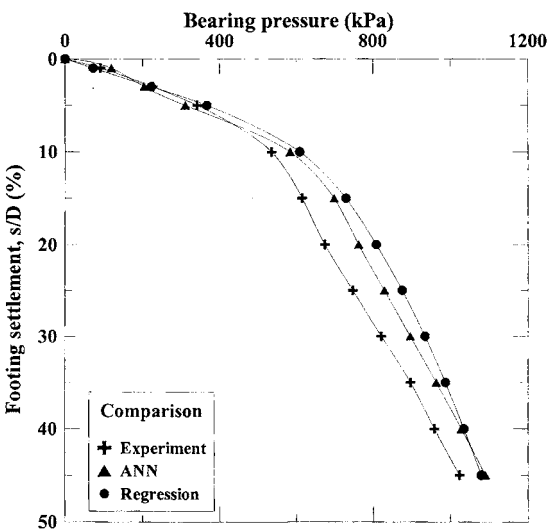

FIG. 4. Variation of bearing pressure with footing settlement: a comparison.

The ultimate bearing capacities obtained from the experiment, ANNs and regression models are computed to be 530kPa, 625 kPa, and 650 kPa respectively. ANNs and multiple regression models over predicted the measured ultimate bearing capacity by

18% and 23% respectively. This shows that the ANNs are slightly better than the regression models in predicting the loading behavior of geocell reinforced sand beds.

In general practice, foundations are designed according to either bearing capacity failure criteria or settlement failure criteria. Latter one dominates the design criteria if the foundations are expected to locate in sand beds due to higher initial settlements. In such cases, the allowable footing settlements are decided based on the type and function of the structure. For example, if the super structure is a bridge or a high rise building, the allowable footing settlement is much smaller (s/D < 5%). In contrary, the allowable foundation settlements are considerably high in the case of foundations for oil storage tanks or foundations for structures such as loading platforms. Taking these points into consideration, it can be concluded that both the predictive models employed in this study can be used to evaluate the behavior of the geocell reinforced foundation beds with reasonable confidence.

CONCLUSIONS

This paper presents the results of both experimental and predictive models viz. ANNs and multiple regressions to compare the predictive results with the experimental test data. The practical problems in performing large scale model tests along with the difficulties associated with experimental study are also discussed. The analysis of results concludes that both the predictive models are very well predicted the behavior of geocell reinforced foundation beds. The predicted bearing capacities of geocell reinforced sand beds are observed to be on conservative side at footing settlement ratios higher than 10%. However, ANNs are observed to be slightly superior to regression models to predict the behavior at higher footing settlements.

These models should be well trained with variety of test data including large scale model tests to prototype field tests to improve the predictive behavior of both models. Further research is needed to extend these predictive models to estimate the bearing capacities of soft clay and mixed soil systems when reinforced with geocells.

REFERENCES

American Society for Testing and Materials (ASTM), "Standard test method for determining tensile properties of geogrids by single or multi-rib tensile method". ASTM D6637: 2001.

Bera, A. K., Ghosh, A. and Ghosh, A. (2005). "Regression model for bearing capacity of a square footing on reinforced pond ash". *Geotextiles and Geomembranes*, Vol. 23, 261-285, 2005.

Bush D.I., Jenner C.G. and Bassett R.H., (1990). "The design and construction of geocell foundation mattress supporting embankments over soft ground", *Geotextiles and Geomembranes*, Vol. 9, 83-98.

Butterfield, R. (1999). "Dimensional analysis for geotechnical engineers." *Geotechnique*, Vol. 49(3), 357-366.

Dash S.K., Krishnaswamy, N.R. and Rajagopal K. (2001). "Bearing capacity of strip footings supported on geocell-reinforced sand", *Geotextiles and Geomembranes*, Vol. 19, 235-256.

Dielman, T.E. (2001). "Applied Regression Analysis for Business and Economics". Duxbury. Thomson Learning, Inc., USA.

Fakher, A. and Jones, C.J.F.P. (1996). "Discussion of bearing capacity of rectangular footings on geogrid reinforced sand", by Yetimoglu, T., Wu, J.T.H. and Saglamer, A. *ASCE Journal of Geotechnical Engineering Division*, Vol. 122(4), 326-327.

Farrag, K., Acar, Y.D., and Juran, I. (1993). "Pullout resistance of geogrid reinforcements", *Geotextiles and Geomembranes*, Vol. 12, 133-159.

Goh, A. T. C. (1994). ''Seismic liquefaction potential assessed by neural networks.'' *J. Geotechnical & Geoenv. Engrg.* ASCE, Vol. 120(9), 1467–1480.

Hornik, K., Stinchcombe, M., and White, H. (1989). ''Multilayer feed-forward networks are universal approximators.'' Neural Networks, Vol. 2, 359–366.

Ingold, T. S. (1982). "Reinforced Earth", Thomas Telford Ltd., London, 1982.

Krishnaswamy N.R., Rajagopal K. and Madhavi Latha G. (2000). "Model studies on geocell supported embankments constructed over soft clay foundation", *Geotechnical Testing Journal*, ASTM, Vol. 23, 45-54.

Milligan, G.W.E., Fannin, R.J., Farrar, D.M. (1986). "Model and full-scale tests of granular layers reinforced with a geogrid". *Proceedings of Third International Conference on Geotextiles*, Vienna, Vol, 1, 61-66.

Padmini, D., Illumpathi, K. and Sudheer, K. P. (2008). "Ultimate Bearing Capacity Prediction of Shallow Foundation on Cohesionless Soils using Neurofuzzy Models", *Computers and Geotechnics*, Vol. 35, 353-46, 2008.

Rea C. and Mitchell J.K. (1978). "Sand reinforcement using paper grid cells", ASCE Spring Convention and Exhibit, Preprint 3130, Pittsburgh, PA, 24-28.

Sireesh, S. (2006). "Behavior Geocell Reinforced Foundation Beds", PhD thesis Submitted to the Indian Institute of Science, Bangalore, India.

Sireesh, S., Srilakshmi, G., Sitharam, T. G., and Anand, J. P (2009). '3D numerical simulation of geocell reinforced soil beds' *Proceedings of ICE, Ground Improvement*, Vol. GI 162, No. 4, pp 185-198.

Shahin, M. A., Maier, H. R., and Jaksa, M. B. (2001). "Artificial Neural Network Applications in Geotechnical Engineering", *Australian Geomechanics*, Vol. 36 (1), 49-62.

Shahin, M. A., Maier, H. R., and Jaksa, M. B., "Predicting Settlement of Shallow Foundations using Neural Networks", *J. Geotechnical & Geoenv. Engrg.* 128(9), 785-793, 2002.

Sitharam, T. G. and Sireesh, S. (2005). "Behaviour of Embedded Footings Supported on Geocell Reinforced Foundation Beds". *Geotechnical testing Journal*, ASTM, Vol. 28 (5), 452-463.

Sitharam, T.G., Sireesh, S. and Dash, S.K. (2005). "Model Studies of a Circular Footing Supported on Geocell-Reinforced Clay". *Canadian Geotechnical Journal*, Vol. 42 (2), 693-703.

Transportation Research Board. (1999). ''Use of Artificial Neural Networks in Geomechanical and Pavement Systems'', Transportation Research Circular, December (E-C012), 1–18.

Investigation of Tire Chips-Sand Mixtures as Preventive Measure against Liquefaction

Hemanta Hazarika[1], A.M. ASCE, Masayuki Hyodo[2] and Kazuya Yasuhara[3]

[1]Associate Professor, Akita Prefectural University, 84-4, Tsuchiya, Yurihonjo, Akita, Japan 015-0055; hazarika@akita-pu.ac.jp

[2] Professor, Yamaguchi University, Ube, Japan; hyodo@yamaguchi-u.ac.jp

[3] Professor, Ibaraki University, Hitachi, Japan; yasuhara@mx.ibaraki.ac.jp

ABSTRACT: This paper presents results of a series of element testing and model testing in which tire derived geosynthetics such as tire chips are utilized as liquefaction preventive backfill material. Undrained cyclic shear tests were conducted on tire chips and sand mixed tire chips for various percentages of mixtures, and the liquefaction potentials of the mixtures were evaluated. The best mixing percentage of tire chips was found to be close to 50% by the total volume of sand. Also, a model shaking table test on a caisson type quay wall was conducted on liquefaction prevention measures for backfill sand reinforced with tire chips. The test results have demonstrated that, despite the fact that the tire chips reinforced composite backfill has a very low relative density, there was no liquefaction in the backfill. Also, the earth pressure on the wall and its residual displacement could be substantially reduced, implying a good performance of the soil-structure system during earthquake loading.

INTRODUCTION

Growing emphasis on cost, environment and structural performance, have led to an increasing attention to research on alternative reinforcing materials. Scrap tire derived recycle materials (such as tire chips and tire shreds) are such alternative materials, which have applications similar to those found in other conventional geosynthetics. The applications include: drainage, leachate, reinforcement, soil stabilization, bearing capacity improvement, erosion control, thermal insulation and noise barrier etc. Use of scrap tires derived recycle materials also reduces the adverse environmental impact from scrap tires, which until now were used for thermal recycling purposes producing greenhouse gases such as CO_2. Recent researches by Hazarika et al. (2008) has shown that such recycled materials can be used as a protective cushion for reducing the earthquake induced lateral deformation of geotechnical structures. A comprehensive collection of papers on recent researches and applications worldwide can be found in Hazarika and Yasuhara (2007) that includes the state of art reports by Edil (2007),

Humphrey (2007) and Yasuhara (2007). Various applications of tire derived geomaterials can also be found in Bosscher et al. (1997), Humphrey (1998), Tweedie et al. (1998), and Hazarika et al. (2009). Due to their potential economic and environmental benefits for developing disaster preventive technique that can enhance the structural performances during earthquakes, tire derived recycled material can be used as reinforcing materials.

The joint report (JSCE/JGS, 1996) of the Japanese Geotechnical Society (JGS) and the Japan Society of Civil Engineers (JSCE) after the 1995 Hyogoken-Nanbu earthquake, Kobe has concluded that there were mainly two geotechnical aspects that led to the devastating damages to retaining structures during the earthquake. One of the aspects was backfill and subsoil liquefaction. Liquefaction related damages such as subsidence and lateral spreading are evident in almost every earthquakes affecting the performance of geotechnical structures (Hamada et al. 1996). The performances of many structures improved by various existing liquefaction prevention methods during the 1995 Hyogoken Nanbu Earthquake have been reported in Yasuda et al. (1996). The geotechnical engineering professional continue to put their effort on developing cost-effective and environmentally friendly disaster mitigation techniques.

In this research an attempt has been made to improve seismic performance of structures by using an emerging geosynthetics (tire chips) by mixing it with sand. A series of element testing on tire chips and sand mixed tire chips were conducted. Also, model testing of utilizing sand mixed tire chips as a non-liquefied material in a retaining wall backfill is described.

UNDRAINED CYCLIC SHEAR TESTING

Specimen setup and physical properties of the materials used

Tire chips, No. 5 Soma silica sand and a mixture of the two were used in the undrained cyclic triaxial testing. The maximum grain size of the tire chips was 1mm. Tire chips and Soma silica sand were mixed in various proportions, i.e., the mix ratios of sand to tire chips by volume were set at 10:0, 9:1, 8:2, 7:3, 6:4, 5:5, 3:7 and 0:10. The tire chips-sand mixture specimen was prepared by moist tamping method. The test specimen was prepared by placing the mixture inside the mold (10 cm in height and 5 cm in diameter) in five layers to control the compaction energy.

Table 1. Physical Properties of soil samples

Sand fraction	ρ_s(g/cm^3)	ρ_{dmin}(g/cm^3)	ρ_{dmax}(g/cm^3)	e_{max}	e_{min}	D_{50}(mm)	U_c
sf=1(Soma sand)	2.645	1.273	1.574	1.077	0.680	0.395	1.65
sf=0.9	2.576	-	-	-	-	0.399	1.67
sf=0.8	2.498	-	-	-	-	0.403	1.67
sf=0.7	2.410	0.939	1.234	1.565	0.953	0.407	1.69
sf=0.6	2.309	-	-	-	-	0.414	1.72
sf=0.5	2.192	0.744	0.988	1.948	1.218	0.423	1.75
sf=0.3	1.892	0.563	0.735	2.361	1.576	0.453	1.91
sf=0 (Tire chips)	1.150	0.347	0.442	2.318	1.600	0.655	2.72

Table 1 summarizes the physical properties of the soil mixture, including density of soil particles (ρ_s), minimum and maximum dry densities (ρ_{dmin} and ρ_{dmax}), maximum

and minimum void ratios (e_{max} and e_{min}), mean diameter (D_{50}) and coefficient of curvature (U_c), respectively, of the samples used in the experiments. In the table, *sf* (sand fraction) indicates the proportion by volume occupied by Soma silica sand in the tire chip-sand mixture. Thus, *sf* = 1 indicates samples consisting of sand only, while *sf* = 0 represents sample with tire chips only.

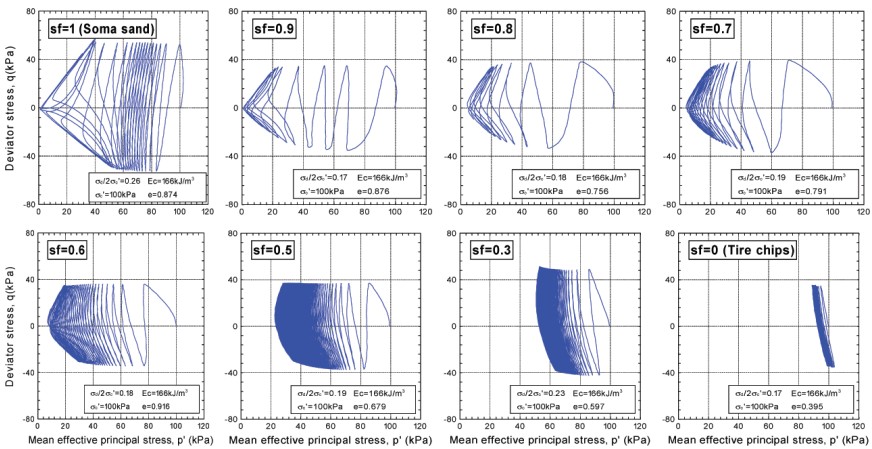

(a) Effective stress paths

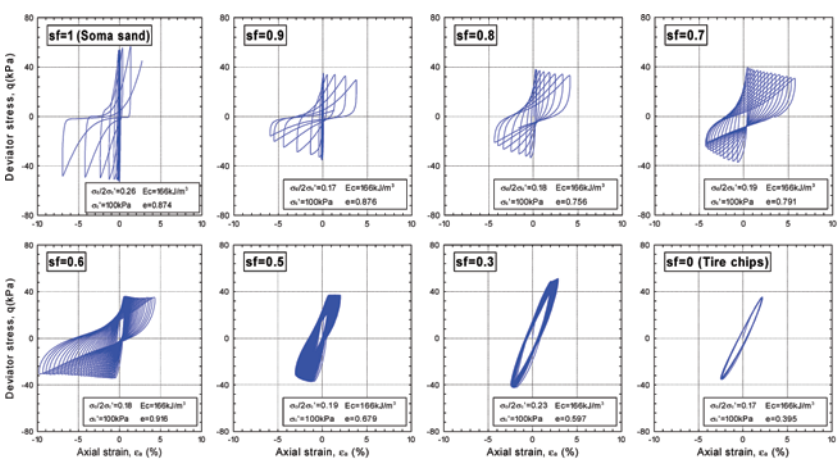

(b) Deviator stress vs. axial strain

FIG. 1. Typical results of undrained cyclic shear tests.

Test results

Typical results obtained from undrained cyclic triaxial tests for tire chips-sand mixtures are shown in Figures 1(a) and (b) in terms of the stress paths and the corresponding deviator stress q – axial strain ε_a relations, respectively. For specimens with $sf = 1$ and 0.9, the excess pore water pressure accumulated as the cyclic shear loading progresses until the effective stress completely dropped to zero. Moreover, since the amplitude of axial strain suddenly increased at a particular time, it is understood that liquefaction took place. For specimens with $sf = 0.8$, 0.7 and 0.6, the effective stress did not disappear completely and reached a steady state at the end, with the amplitude of axial strain showing gradual increase. For specimens with $sf \leq 0.5$, the decrease in effective stress with the cyclic loading was controlled, while for specimen with $sf = 0$ (pure tire chips), the decrease in effective stress was very minimal. Moreover, the relation between deviator stress and axial strain for $sf = 0$ showed visco-elastic behavior, with large axial strain generated during the first cycle of loading followed by small increase in axial strain during subsequent loading. For specimens with $sf = 0.3$ and 0.5, the amplitude of axial strain appeared to show gradual increase, but in the end, the stiffness was maintained and followed a regular loop. Thus, the undrained cyclic shear behavior of specimens with $sf \leq 0.5$ clearly differed from that of specimens with $sf = 0.6$~0.9, with the characteristics of tire chips dominant when $sf \leq 0.5$.

Figure 2 shows the relation between the maximum excess pore water pressure ratio, $\Delta umax/\sigma c'$, and sand fraction, sf, for all the test cases considered in this research. From the figure, although there was scattering of data points for each individual soil mixture, it can be said that $\Delta umax/\sigma c' > 0.9$ for soil mixtures with sf = 1~0.6, while for mixtures with sf < 0.5, a trend of lower $\Delta umax/\sigma c'$ for smaller sf was evident. In addition, the two lines connecting the average $\Delta umax/\sigma c'$ for each individual sf, which correspond to different compaction energies Ec, were practically the same. Based on these results, the tire chips have the effect of controlling the accumulation of excess pore water pressure, and the effect was significant for specimens with lower sf. However, because the stiffness of the tire chip is very small, specimens with low sf have low stiffness and they deform easily for the prescribed loading.

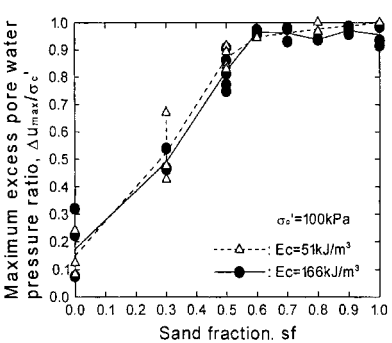

FIG. 2. Relation between maximum excess pore water pressure ratio and sand fraction.

DESCRIPTION OF SHAKING TABLE TESTING PROGRAM

In this testing program 1G shaking table test was conducted on a model quay wall for two different backfill conditions shown in Figure 3.

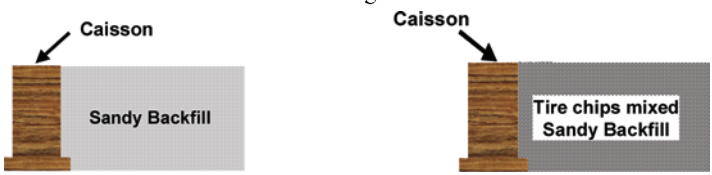

(a) Structure with conventional backfill (b) Structure with tire chips reinforced backfill

FIG. 3. Test cases.

Test Model and Materials

Figure 4 shows the cross section and front view of the model caisson and the locations of various devices used in the testing program. The soil box was made of a steel container 0.85 m long, 0.36 m wide and 0.55 m deep. The model caisson is 20 cm high and 10 cm wide as shown in the figure.

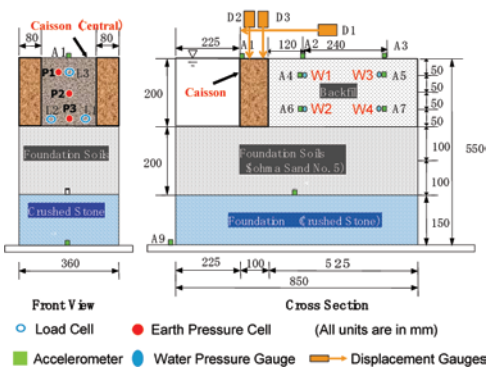

FIG. 4. Cross section of the test setup.

(a) Soma sand No. 5 and tire chips (c) Tire chips mixed sand (50% by volume)

FIG. 5. Materials used in the tests.

For the conventional backfill, No. 5 Soma sand was used. For reinforced backfill, tire chips similar to those used in the element testing described above was used. The mixing percentage of tire chips was set at 50% of the total volume of the backfill sand based on the experimental findings of Hyodo et al. (2007). Figure 5 shows the sand and reinforcing materials used in the model testing and the state of the mixture after mixing. Thus, the adopted mixing percentage in this model test was reasonable from the liquefaction and practical point of view.

Model Preparation and Testing Procedures

The dense saturated foundation sand was prepared in four layers using vibratory compaction technique. After preparing each layer, the whole assembly was shaken with 300 Gal of vibration of frequency 7 Hz for 4 sec. The process was repeated for 4 to 8 times depending on the requirements. Backfill (under submerged condition) was prepared in five layers using free falling technique. Compaction was achieved by shaking the soil box and the wall assembly 3 to 4 times (as needed) with 200 Gal of vibration of frequency 7 Hz for 4 sec. The achieved relative densities of the foundation soil were 95 % to 100 %. In the case of tire chips mixed backfill the mixing percentage were tire chips = 50% and sand = 50% by volume (achieved backfill relative density, D_r =Approx. 40%). In the case of conventional backfill without reinforcement, the backfill relative density, D_r = Approx. 40%, implying that the backfill is liquefiable.

A sinusoidal acceleration was imparted to the soil-structure system for a period of 1 sec (frequency = 20 Hz). They were applied in several stages starting with 100 Gal and increasing up to 600 Gal at an increment of 100. For a given acceleration, the response accelerations, the dynamic load on the wall, displacement of the caisson, and the pore water pressures at various locations were measured.

RESULTS FROM MODEL TESTING

Liquefaction Potential of the Backfill

Figures 6(a)~(b) show the excess pore water pressure measured (at acceleration = 300 Gal) in the backfill at locations, W2 and W4 (Refer to Figure4). The thick dotted lines in the figures represent the overburden pressures at the locations. It can be seen that while the conventional backfill shows the increase of the excess pore water pressure with time, the tire chips reinforced backfill shows almost no increase in the pore water pressure. This is, in spite of the fact that the two backfill were having almost the same relative density (40%). The presence of tire chips in the sand could control the buildup of the excess pore water pressure and thus prevent any liquefaction related damages. It can be inferred from these test results that the tire chips acts as a good earthquake resistant geosynthetic material.

Performance of the Structure

Figure 7 shows the relationship between the residual displacement of the structure at the end of each dynamic load and the input acceleration for the two test cases. The figure indicates that with increasing acceleration amplitude, while conventional caisson experiences higher residual displacement, the caisson with the tire chips mixed backfill with same relative density, shows only a mild increase. The residual displacement could

be reduced to more than half, even at higher level of acceleration. This implies that even at higher acceleration levels, the adopted countermeasure could enhance the performance of a soil-structure system.

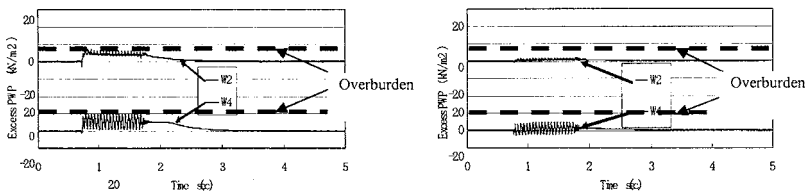

(a) Conventional backfill (b) Tire chips reinforced backfill

FIG. 6. Liquefaction behavior of the backfill (Acceleration = 300 Gal).

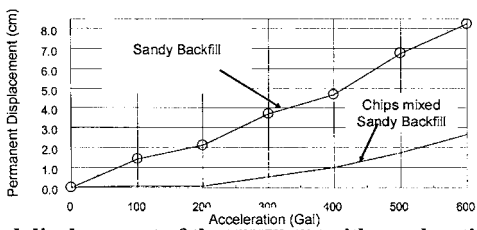

FIG. 7. Residual displacement of the structure with acceleration amplitude.

CONCLUSIONS

Undrained cyclic shear testing of tire chips and tire chips sand mixtures have demonstrated that pure tire chips have very small stiffness and displacements are easily generated during cyclic shear loading, resulting in visco-elastic stress-strain relation. Moreover, excess pore water pressure was not generated during cyclic loading and liquefaction did not occur. The occurrence of liquefaction was confirmed for specimens with sand fraction greater than 0.5, but for specimens with sand fraction less than 0.5, liquefaction was not clearly observed. Tire chips appear to control the build-up of excess pore water pressure of the mixture during shearing, and for specimens with sand fraction less than 0.7, such effect was remarkable for low values of sand fraction.

The model shaking table test results on liquefaction prevention measures, using tire chips as reinforcing agent by mixing it with sand, have revealed that tire chips mixed sand does not undergo liquefaction, if proper mixing percentage is selected. The reinforcing action of the tire chips embedded into the backfill soil could prevent the liquefaction of the backfill. The test results have also demonstrated that the liquefaction prevention measures could substantially reduce the earthquake induced permanent displacement of structures.

ACKNOWLEDGEMENTS

The authors gratefully acknowledge the financial support for this research provided by the Japan Society of Promotion of Science (JSPS) and Ministry of Education,

Culture, Sports, Science and Technology (MEXT), Japan under the Grant-in-Aid for scientific research (Grant No. 18206052, Principal Investigator: Hemanta Hazarika).

REFERENCES

Bosscher, P.J., Edil, T.B., and Kuraoka, S. (1997). Design of highway embankments using tire chips, *Journal of Geotechnical and Geoenvironmental Engineering, ASCE*, Vol. 123(4): 295-304.

Edil, T.B. (2007). A Review of Environmental Impacts and Environmental Applications of Shredded Scrap Tires, Keynote Paper, *Proc. Int. Workshop on Scrap Tire Derived Geomaterials. -Opportunities and Challenges- Hazarika & Yasuhara (eds).* Taylor & Francis, London, 3-18.

Hamada, M., Isoyama, R., and Wakamatsu, K. (1996): Liquefaction Induced Ground Displacement and Its Related Damage to Lifeline Facilities, *Special Issue of Soils and Foundations*, Vol. 1: 81-98.

Hazarika, H., Kohama, E., and Sugano, T. (2008). Underwater Shake Table Tests on Waterfront Structures Protected with Tire chips Cushion, *Journal of Geotechnical and Environmental Engineering, ASCE*, USA, Vol. 134(12): 1706-1719.

Hazarika, H. and Yasuhara, K. (2007). *Scrap Tire Derived Geomaterials - Opportunities and Challenges* -, Taylor & Francis, London, UK.

Hazarika, H., Yasuhara, K., Karmokar, A.K., Kikuchi, Y., and Mitarai, Y. (2009). Multifaceted Potentials of Tire Derived Three Dimensional Geosynthetics in Geotechnical Application and Their Evaluation, *Geotextiles and Geomembranes*, Special Volume, (In Press).

Humphrey D.N. (1998): *Civil Engineering Applications of Tire Shreds*, Manuscript Prepared for Asphalt Rubber Technology Service, SC, USA.

Humphrey, D. N. (2007). Tire derived aggregates as lightweight fill for embankments and retaining walls, *Special Invited Paper, Scrap Tire Derived Geomaterials. -Opportunities and Challenges- Hazarika & Yasuhara (eds).* Taylor & Francis, London, 56-79.

Hyodo, M., Yamada, S., Orense, R.P., Okamoto, M., and Hazarika, H. (2007). Undrained Cyclic Shear Properties of Tire Chip-Sand Mixtures, *Proc. Int. Workshop on Scrap Tire Derived Geomaterials. -Opportunities and Challenges- Hazarika & Yasuhara (eds).* Taylor & Francis, London, 187-196.

Japanese Geotechnical Society (JGS) and Japan Society for Civil Engineers (JSCE) (1996): *Joint Report on the Hanshin-Awaji Earthquake Disaster* (In Japanese).

Tweedie, J.J., Humphrey, D.N., and Standford, T.C. (1998). Tire Shreds as Retaining Wall backfill, Active Conditions, *Journal of Geotechnical and Geoenvironmental Engineering*, ASCE, Vol. 124(11): 1061-1070.

Yasuda, S., Ishihara, K., Harada, K., and Shinkawa, N. (1996): Effect of Soil Improvement on Ground Subsidence Due to Liquefaction, *Special Issue of Soils and Foundations*, Vol. 1: 99-108.

Yasuhara, K. (2007). Recent Japanese experiences on scrapped tires for geotechnical applications, Keynote Paper, *Proc. Int. Workshop on Scrap Tire Derived Geomaterials. -Opportunities and Challenges- Hazarika & Yasuhara (eds).* Taylor & Francis, London, 17-40.

Design Method for Flat Geotextile Tubes

Yan Yue[1], Yan Shuwang[1], Qiu Changlin[1]and Zheng Gang[1]

[1]Schoool of civil engineering, Tianjin University, Tianjin China, 300072; yanshuwang@tju.edu.cn

ABSTRACT: Using geotextile tubes to construct dikes for land reclamation has been widely applied. The tubes are usually filled with slurry made of sand, silt or clay. Since the dimensions of the tube are quite large, the tube usually takes a very flat shape. The circumference tensile force is a dominant factor for constructing a safe geotextile tube dike. The existing design methods are suitable for sausage shaped tubes but not for the flat ones. Based on the flat tubes features, an iterative procedure was compiled. The shape of the large size geotextile tube, as well as the relationship among tube size, pumping pressure, unit weight of the slurry and tensile stress developed in the geotextile tube were determined. The soil heterogeneity was also considered in the procedure.

INTRODUCTION

The technique of using geotextile tubes to construct dikes for land reclamation has been widely applied in the coastal areas of China, such as Tianjin harbor and Tangshan harbor. The tubes can be filled with soils having better permeability, such as sand and silt (Bogossian, et al, 1982; Ockels, 1991; and Sprague, 1993). Therefore, the construction cost can be much lower than that using other methods (Pilarczyk, 1994). To design a geotextile tube dike, it is necessary to know the circumference tensile force developed in the geotextile during filling slurry and stacking up to make sure the tensile force will not exceed the strength of the geotextile. Therefore, it is important to know the relationship among tube size, pumping pressure, unit weight of the slurry and circumference tensile force. Several design methods have been presented (Leshchinsky, 1992; Carroll, 1994; and Kazimierowicz, 1994) and reasonable solutions were given to analyze the sausage tube, or with a perfect height herein. In practice, the tube is usually designed to take a very flat shape and the corresponding height is far less than the perfect height (Fig.1), because the tube perimeter is quite large (more than 20 m). So the existing methods cannot be directly used to design a geotextile tube with flat segment. The heterogeneity resulting from grain sediment velocity will also influence the tube shape and should be considered in calculating the tensile stress (AASHTO, 1990).

In this paper, a procedure for designing a flat or not fully inflated geotextile tube was developed base on the existing methods. The slurry heterogeneity was also included in the program. The program can be used to help designers to select suitable geotextile and

reasonable dike profiles.

a) A flat tube being filled

b) A filled flat tube

FIG. 1. Formation of a plate geotextile tube.

DESIGN METHODS FOR SAUSAGE SHAPED TUBE

Basic Theory and Solutions

The tubes are usually made of sewn geotextile sheets. The calculation of the circumferential tensile force is base on the equilibrium of the encapsulating flexible shell (Leshchinsky, 1996). The analysis diagram is shown in FIG.2.

Since the problem is two-dimensional and no shear stresses developed between the slurry and the geotextile, the tensile force, T, must be constant along the circumference. Eq.(1) can be derived from the force equilibrium at the infinitesimal arc, ds:

$$r(x)=T/p(x) \tag{1}$$

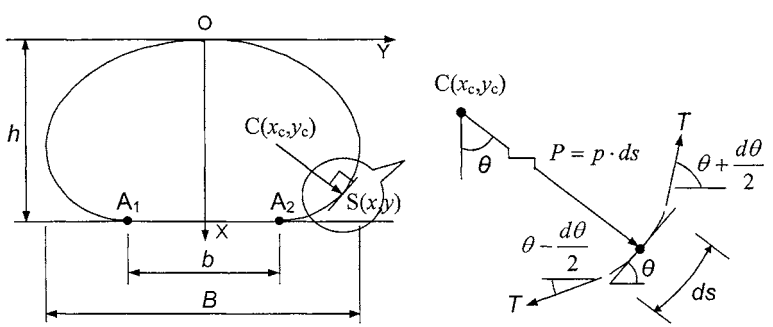

FIG. 2. Cross-sectional view of geotextile tube-convention and notation.

The slurry pressure $p(x)$ at any point S(x, y) is related to the pumping pressure p_0:

$$p(x)=p_0+\gamma_0 \cdot x \tag{2}$$

As well known, differential calculus gives the curvature radius as

$$r(x)=[1+(y')^2]^{\frac{3}{2}}/y'' \tag{3}$$

Substituting Eq.(3) and Eq.(1) into Eq.(2) yields

$$T\cdot|y''|-(p_0+\gamma_0\cdot x)\cdot[1+(y')^2]^{\frac{3}{2}}=0 \tag{4}$$

Eq.(4) has to be solved numerically and its solution can be presented by

$$y = f[x(0 < x < h)\,|\,T, p_0, h, \gamma_0] \tag{5}$$

Since the unit weight γ_0 is known, $y(x)$ can be determined when one of T, p_0, or h is given and the other two parameters will be parts of the solution. To obtain such an explicit solution, two physical constraints must be specified. One constraint is that the geotextile at O should be horizontal to assure symmetry of the problem. That is

$$1/y'(0)=0 \tag{6}$$

Since the tube is sewn up using a certain amount of geotextile sheets, it is more practical to control the second constraint by specifying the tube perimeter L which can be expressed as following:

$$L = b + \int_s ds \tag{7}$$

The flat base length b can be derived from vertical force equilibrium and the second part on the right of Eq.(7) is the well known arc length formula. Then

$$L=\frac{2}{p_0+\gamma_0\cdot h}\int_0^h \gamma_0\cdot y\cdot dx+2\int_0^h[1+(y')^2]^{\frac{1}{2}}dx \tag{8}$$

The relationship between T, p_0 or h, and $y(x)$ can be obtained by solving simultaneous Eq.(4), Eq.(6) and Eq.(8). Then, the numerical process should be involved (Leshchinsky, 1992; and Kazimierowicz, 1994).

A computer program DFGT (Design Flat Geotextile Tube) was developed allowing the user to specify various safety factors related to the geotextile strength. Normally, the axial tensile force T_{axial} is smaller than T and hence can be ignored.

INFLUENCE OF INHOMOGENEOUS SLURRY ON GEOTEXTILE TUBE

Sediment of different sized grains will induce slurry heterogeneity. It is reasonable to assume that the unit weight of the slurry increases linearly with the depth, i.e.,

$$\gamma(x)=\gamma_0+m_\gamma\cdot x \tag{9}$$

Where, γ_0 and $\gamma(x)$ are the unit weights at depth x=0 and x=x respectively, and m_γ is a constant.

The heterogeneity of the slurry can be taken into account by substituting γ_0 with $\gamma(x)$ in Eq.(1) through Eq.(8). . As an example, let γ_0 =12kN/m3 and L=9m, the calculated results for the inflated tubes with different m_γ are listed in Table 1. It can be seen that the height of the tube will decrease and the tensile force will increase when m_γ becomes larger, but the amount of these changes is not obvious.

Table 1. Results for fully inflated tubes (P_0=0 kPa)

m_γ	Tube Height h (m)	Bottom Width b (m)	Section Width B (m)	Tensile Force T (kN/m)
0	0.90	3.60	4.05	2.56
2	0.89	3.62	4.07	2.60
4	0.88	3.64	4.09	2.63
6	0.87	3.67	4.10	2.65
8	0.86	3.69	2.65	2.68

DESIGN A FLAT GEOTEXTILE TUBE WITH A HEIGHT LESS THAN THE PERFECT HEIGHT

Based on the discussion above, the design parameters of the sausage typed tube can be determined using DFGT. From Table 1 it can be seen that when the pumping pressure is equal to zero, the tube can be filled to the perfect height, denoted as h_p, which is about 0.9 m. In practice, however, the perimeter of the tube is more than 30 m and the tube height for constructing a dike is usually designed to be 0.5 m, much less than the perfect height, causing the tube to take a flat shape customarily. Therefore, the aforementioned procedure shall not be used and should be improved for analysis of the flat tube.

A Procedure for Designing a Flat (Not Fully Inflated) Tube

When a smaller amount of slurry is filled into a tube, the tube will expand to a height, h, which is less than the perfect height. From FIG.3 it can be derived that the geometry of the two side parts of the tube can be put together to form a sausage shape and its feature it can be determined using DFGT. Analysis results show that, if h is less than the perfect height under p_0=0 condition, the calculated perimeter of the patched sausage tube will be much less than designed. It is logical to think that there must be a flat segment between the two side parts, which can be usually observed in practice, as shown in FIG.1.

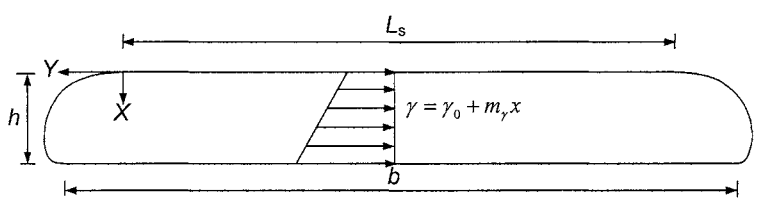

FIG. 3. The loading and boundary conditions of a tube that is not fully inflated.

The program DFGT has been improved to find out the shape of a flat tube base on the following iteration procedure.

(1) Determine the parameters for design: the unit weight of the slurry γ_0 and m_γ, the

desired height h and the perimeter of the tube L;

(2) Assume a fully inflated trial tube having a perimeter of L_c ($L_c < L$);

(3) With the given γ_0 and assumed L_c, letting $p_0 = 0$, calculate the perfect height, h_p, of the trial tube by using the program DFGT;

(4) If $h_p \neq h$, repeat step (2) to (3), until $h_p = h$ is reached. Record L_c and the tensile force, T;

(5) The length of the line segment, denoted as L_s, is one half of the difference between the perimeter of the designed tube, L, and that of the trial tube, L_c (refer to FIG.3):

$$Ls = (L - L_c)/2 \tag{10}$$

(6) Once the L_s is found, the shape of the designed tube can be defined.

The following example demonstrates the use of the program. Let $\gamma_0 = 12 kN/m^3$ and L=25 m. The analysis results for a flat tube with different tube heights that are less than the perfect height (h_p =0.9 m) were summarized in Table 2. It indicates that the calculated tensile force of the flat tube is much less than the strength of the geotextile (about 24 kN/m).

Table 2. Calculation results for a flat tube

Tube Height H (m)	Bottom Width b (m)	Line Segment L_s (m)	Section Width B (m)	Tensile Force T (kN/m)	Section Area A (m^2)
0.3	4.2	3.3	4.36	0.29	1.27
0.5	4.0	2.3	4.26	0.78	2.02
0.7	3.8	1.2	4.17	1.50	2.67
0.9	3.6	0	4.04	2.50	3.30

USING FLAT GEOTEXTILE TUBES TO CONSTRUCT A DIKE FOR HYDRAULIC BACKFILL

The flat geotextile tubes have been used to construct dikes for confining the hydraulic backfill for land reclamation in Tianjin. A typical profile of the dike is shown in FIG.4. Silt slurry is filled to the geotextile tubes (or mats) of about 0.5 m thick. Since the permeability of the filled material is quite good (greater than 10^{-3}cm/s), it can consolidate within a few hours. By filling the tubes one after another, the core of the dike is formed (FIG.5a). The naked core is then covered and protected with a concrete geotextile mattress to complete the dike construction FIG.5b).

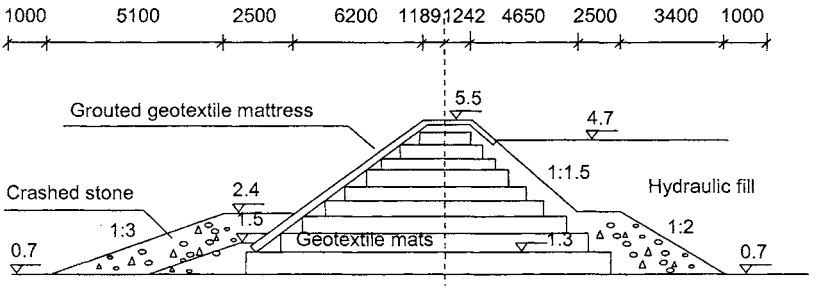

FIG. 4. A design profile for using geotextile tubes to construct a dike.

a) Filled geotextile tubes **b) The constructed dike**

FIG. 5. The geotextile tube core and the constructed dike.

CONCLUSIONS

An improved iterative procedure has been presented in this paper to determine the relationship among the tube size, the pumping pressure, the unit weight of the slurry and the tension stress developed in the geotextile sheets. The program can be used to design both fully inflated tubes and flat tubes. The slurry heterogeneity which may slightly increase the geotextile tensile stress was also considered in the program.

REFERENCES

Bogossian, F. Smith, R.T., Vertematti, J.C., and Yazbek, O. (1982) "Continuous retaining dikes by means of geotextiles" *Proc. 2nd Int. Conf. on Geotextiles, Las Vegas*: 211-216.

Silverster R. (1986) "Use of grout-filled sausages in coastal structures". *J. Wtrwy. Port, Coast., and Oc. Engrg.*, ASCE: Vol. 112(1):95-114.

Ockels R. (1991) "Innovative hydraulic engineering with geosynthetics" *Geosynthetics World*, Vol. 2(4):26-27.

Sprague C. J. (1993) "Dredged material filled fabric tubes" *Rep. submitted to the Constr, Products Div., Project No. CJS-92-008, Nicolon Corporation, Atlanta, Ga.*

Leshchinsky, D. (1992) "Issues in geosynthetic-reinforced soil" *Balkema, Proceeding of international symposium on earth reinforcement practice. Kyushu, Japan,*: 871-897.

Carroll, R.P. (1994) "Submerged geotextiles flexible forms using noncircular cylindrical shapes" *Geotech. Fabrics Rep., IFAI, St. Paul, MN*, Vol. 12(8):4-15.

Kazimierowicz, K. (1994) "Simple analysis of deformation of sand-sausages" *Proceedings of 5th International Conference On Geotextiles, Geomembranes and Related Products. Southeast Asia Chapter of the International Geotextile Society*, Singapore: 775-778.

Leshchinsky, D., et al. (1996) "Geosynthetic tubes for confining pressureized slurry: some design aspects" *J. of Geotechnical Engineering*, ASCE, Vol. 122(8):682-690.

Laboratory Model Tests for a Strip Footing Supported on Geocell Reinforced Sand Bed

S. N. Moghaddas Tafreshi[1] and A. R. Dawson[2]

[1]Associate Professor, K.N. Toosi University of Technology, Tehran, Iran; nas_moghaddas@kntu.ac.ir
[2]Associate Professor, University of Nottingham, Nottingham, UK; andrew.dawson@nottingham.ac.uk

ABSTRACT: This paper describes laboratory tests results on the strip footing supported on the geocell reinforced sand bed under monotonic load. The various parameters studied in this testing program include the reinforcement width (2.1, 3.2 and 4.2 times of footing width) and height of the reinforcement (0.33, 0.66, 1 and 1.33 times of footing width) below the footing base. The results indicate that, with increase in the height of reinforcement and reinforcement width of the geocell, the load carrying capacity of the footing significantly increases and the footing settlement decreases as compared with the unreinforced one while the efficiency of the reinforcement was decreased by increasing the height and width of the reinforcement. It should be noted that only one type of geotextile, one type of sand and one size of footing width are used in laboratory tests.

INTRODUCTION

Due to its cost savings, ease of construction and ability to improve the visual appearance, reinforced soil has been widely used in geotechnical engineering applications such as construction of road and railway embankments, stabilization of slopes, and improvement of soft foundation bed. Numerous studies have been examined the planar reinforcement of soil for different purposes by Yoon et al. (2004), Ghosh et al. (2005), Patra et al. (2006), El Sawwaf (2007), Alamshahi and Hataf (2009) and etc. In the case of geocell reinforcement, several researchers such as Cowland and Wong (1993), Jenner et al. (1988) and Krishnaswamy et al. (2000) have highlighted the beneficial use of geocell reinforcement in the construction of foundations and embankments. Dash et al. (2001) investigated the reinforcing efficacy of the geocell mattress within a homogeneous sand bed supporting a strip footing. Dash et al. (2003) also reported load test results from a model circular footing supported on geocell-reinforced sand overlying soft clay. Sireesh et al. (2009) carried out a series of laboratory scale model tests on a circular footing supported by geocell reinforced sand beds overlying clay bed with a continuous circular void. They reported the beneficial ability of geocell constructions to improve the bearing capacity of

footings. Most researches have considered the improvement in bearing capacity due to the provision of reinforcement at an unrealistically high range of footing settlement level, up to 40%-50% of footing width (Krishnaswamy et al. 2000; Dash et al. 2003; Sitharam et al. 2007), while this range of settlement level is not acceptable for the design of the footings in most practical circumstances.

Hence, in this research and in order to develop a better understanding of the geocell reinforcement concept, a series of different laboratory, pilot scale tests were performed to evaluate the bearing pressure and settlement of a strip footing supported by reinforced relatively dense sand with geocell (formed of geotextile) with special emphasis on the reduction of footing settlement and on the improvement in bearing capacity of footings at the range of low to medium settlement level (less than 12% of footing width), similar to those of interest in practice. The various parameters studied in this testing program include the width and height of geocell reinforcement below the footing base.

MATERIAL USED

The soil used is relatively-uniform silica sand with grain sizes between 0.85 and 2.18 mm and with a specific gravity, G_s, of 2.68. It has a Coefficient of uniformity, C_u, of 1.35, Coefficient of curvature, C_c, of 0.95, Effective grain size, D_{10}, of 1.2 mm, Medium grain size, D_{50}, of 1.53. The maximum and minimum void ratio (e_{max} and e_{min}) of the sand were obtained as 0.82 and 0.54, respectively. According to the Unified Soil Classification System, the sand is classified as poorly graded sand with letter symbol SP.

The geocells used were made of a type of a planar geotextile thermo-welded to form a honeycomb structure with an open top and bottom – an innovative approach for use in ground stabilization. The type of geotextile used to form the geocell is non-woven. The engineering properties of this geotextile as listed by manufacturer (DuPont de Nemours, Luxembourg) are: thickness 0.57 mm, mass per unit area 190gr/m2, ultimate tensile strength 13.1kN/m and effective opening size 0.08mm. Fig. 1 shows the view of the geocell used in the experiments.

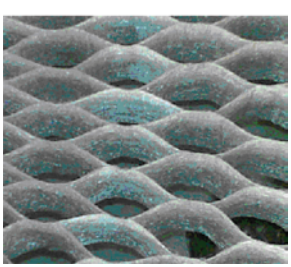

FIG. 1. Isometric view of the geocell.

TESTING TANK AND TEST PROCEDURE

The testing tank is designed as a rigid box (as the plane strain conditions were

achieved), 750mm in length, 375mm in height, and 150mm in width, encompassing the reinforced soil and model foundation (see Fig. 2). To prepare the test and in order to provide experimental control and repeatability of the tests, the raining technique (Kolbsuzewski, 1948) was used to deposit the soil in the testing tank at a known and uniform density. Sand was then rained from a pre-calibrated height of raining to consistently maintain a relative density of 72% and to the predetermined depth using depth-marking on the sides of the tank as guides. Then the geocell was placed on the top of the levelled sand bed. After that the cell pockets were filled with sand using the raining technique which continued up to the footing level. The model footing used was made of a steel rigid plate and measured, 148 mm in length, 75 mm in width and 20 mm in thickness.

A load cell with an accuracy of ±0.01% full scale was placed on the loading shaft to record the applied loads. A LVDT with an accuracy of 0.01% of full range (750 mm) was placed on the footing model accurately to measure the settlement of the footing during the loading. The static load was applied at a rate of 1.0 kPa per second until reaching failure at a maximum load which after that decreasing in carrying capacity observes. In the absent of a no clear failure point, the footing was loaded to reach a constant value of applied stress. To ensure an accurate reading, all of the devices were calibrated prior to each series of tests.

TEST PARAMETERS AND TESTING PROGRAM

The geometry of the test configurations for the geocell reinforcement considered in these investigations is shown in Fig. 2. Also, the details of the tests are given in Table 1. In the case of the reinforced bed, two series of tests (Test series 2 and 3) were conducted by varying the depth to the top of geocell layer below the footing (u or u/B), the height of geocell (H or H/B) and the width of the geocell (b or b/B).

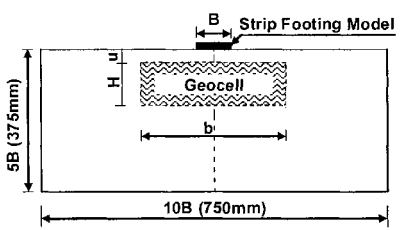

FIG. 2. Geometry of the geocell reinforced foundation bed.

It should be noted that many of the tests described in Table 1 were repeated carefully at least twice to examine the performance of the apparatus, the accuracy of the measurements, the repeatability of the system, reliability of the results and finally to verify the consistency of the test data. The results obtained depicted a close match between results of the two or three trial tests with maximum differences in results of around 8%. This difference was considered to be small and is acceptable in geotechnical engineering applications (Moghaddas Tafreshi and Khalaj, 2008). The presentation of the result figures of tests repeated would have made the paper lengthy.

Table 1. Scheme of tests for unreinforced and reinforced sand

Test Series	Type of reinforcement	H/B	u/B	b/B	No. of Tests	Purpose of the tests
1	Unreinforced	--------	------	--------	1+2*	To quantify the improvements due to reinforcements
2	Geocell Reinforced	H/B = 0.33	0, 0.1, 0.25, 0.5, 1	b/B= 4.2	5+2*	To obtain the optimum value of u/B
3	Geocell Reinforced	H/B = 0.33, 0.66, 1, 1.33	0.1	b/B= 2.1, 3.2 and 4.2	12+4*	To study the effect of the H/B and b/B

**the tests which were performed two or three times to verify the repeatability of the test data*

RESULTS

The performance improvement due to the provision of reinforcement is represented using two non-dimensional improvement factors:

(1) Improvement in bearing pressure of footing (IF: Improvement Factor) which compares the bearing pressure of geocell reinforcement bed ($q_{geocell}$) to that of the unreinforced bed (q_{unrein}) at a given settlement, s_i.

(2) Improvement in footing settlement (PRS: Percentage Reduction in Footing Settlement) which compares the settlement of the geocell reinforcement bed ($s_{geocell}$) to that of the unreinforced bed (s_{unrein}) at the same bearing pressure. The values of bearing pressures selected are those that cause the indicated amount of settlement in the unreinforced case, s_{unrein}. They are defined as follows:

$$IF = \frac{q_{geocell}}{q_{unrein.}} \qquad s_i/B = 2\%, 4\%, 6\%, 8\%, 10\% \text{ and } 12\% \qquad (1)$$

$$PRS = \left(1 - \frac{s_{geocell}}{s_{unrein.}}\right) * 100 \qquad s_{unrein}/B = 2\%, 4\%, 6\%, 8\%, 10\% \text{ and } 12\% \qquad (2)$$

Fig. 3 presents the bearing pressure-settlement behaviour of the geocell foundation beds for two geocell-reinforcement widths (b/B=3.2 & b/B=4.2) at different height of the geocell; H/B. In these tests, according to the results obtained from tests Series 2 in Table 3, which the details have not been presented here, the value of u/B was used 0.1. From Fig. 3, it may be clearly observed that, with increasing the mass of reinforcement (increase in the height of the geocell reinforcement; H/B); both stiffness and bearing pressure (bearing pressure at a specific settlement) considerably increase. Also, it shows clear evidence of failure at around s/B = 10% in all the graphs. After s/B = 10%, the slope of the curve is drastically decreased, which is evident of clear cut failure. In the case of the unreinforced sand beds, it is apparent that the bearing

capacity failure has taken place at a settlement equal to 12% of footing width while in case of both the geocell-reinforced sand beds; no clear failure point is evident for the larger masses of reinforcement (H/B≥0.66). Beyond a settlement of 10-16% there is a reduction in the slope of the pressure-settlement curve. However, when lightly reinforced (H/B=0.33) failure is observed at settlements of 16-18% with clear post-failure reductions in bearing capacity.

At this range of settlement, heave of the fill surface starts. It is attributable to that the soil-reinforcement composite material breaking locally in the region under and around the footing, because of high deformation induced by the large settlement under the footing. This leads to a reduction in the load carrying capacity of the footing indicated by the softening in the slope of the pressure-settlement responses (Fig. 3). Beyond this stage, the slope of the moderately and heavily reinforced cases remains almost constant while the footing bearing pressure continuously increases. The foundation bed continues to take additional load through mobilization of its rigidity and anchorage derived from the adjacent stable soil mass, thereby giving rise to the improved performance. No clear bearing capacity failure has been observed, even at a settlement of 25%, it is probable that no yield condition is to be found at conventional stress levels.

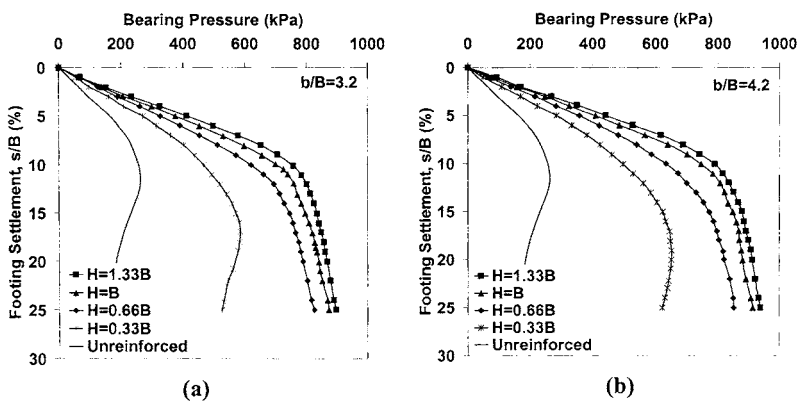

FIG. 3. Variation of bearing pressure with settlement for the reinforced and unreinforced sand bed (a) b/B=3.2 and (b) b/B=4.2.

THE ROLE OF HEIGHT OF THE GEOCELL

The variation of the value of bearing pressure improvement factor (IF) and percentage reduction settlement (PRS) with height of geocell (H/B) for reinforcement width of 4.2 (b/B=4.2) are shown in Fig. 4. Generally, from this figure, it is of interest to note that improvement in bearing pressure (IF) and the percentage reduction in settlement (PRS) are higher at higher settlement of footing, irrespective of the height of geocell reinforcement (H/B). This indicates that the reinforcing efficacy increases

with increase in footing penetration. This means that the internal confinement provided by the soil reinforcement increases with increase in the imposed settlement level on the reinforced system.

Likewise, it can be seen that the values of IF and PRS increase steadily with increase in the height of the geocell (H/B). The reason is that more reinforcement considerably increases the stiffness of the reinforced sand bed compared to the unreinforced sand. The rate of reduction in footing settlement and the rate of enhancement in load carrying capacity of the footing can also be seen to reduce and can be anticipated that the improvement rates would be vanished with increase in the height of the geocell (H/B). The reason is that the zone of soil influenced by the footing loading extends to a depth of about 1-2 times the footing width.

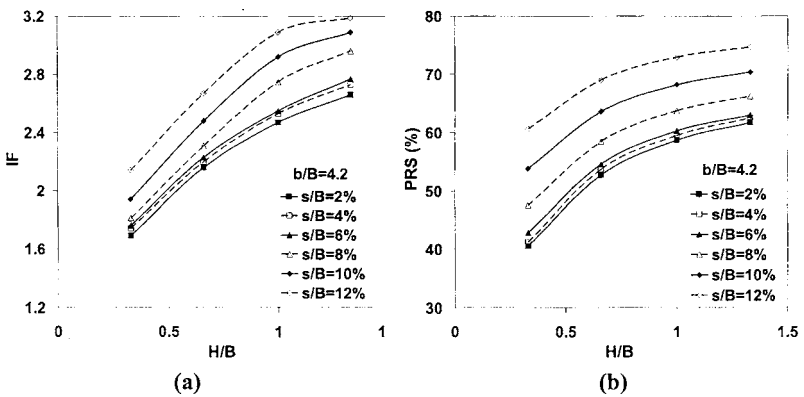

FIG. 4. Variation of the bearing capacity improvement factor (IF) and the percentage reduction in settlement (PRS) with height of geocell (for b/B=4.2), (a) IF and (b) PRS.

THE ROLE OF RIENFORCED WIDTH

Fig. 5 shows the variation of IF and PRS with reinforcement width for height of gecell of 1.0 (H/B=1). It is clear that the performance of the footing in terms of bearing pressure (IF) and reduction in settlement (PRS) are significantly improved with increase in the width of reinforcement. This improvement continues to around 4-5 times of footing width. Consider, for example for the geocell case with H/B=1 at settlement ratio of s/B=4%, the bearing pressure increases 64%, 133% and 153% (IF=1.64, 2.33, and 2.53) for reinforcement width of 2.1, 3.2 and 4.2, respectively. These values imply that the percent increase in bearing pressure for variation of b/B between 2.1 and 3.2 is substantially greater than those for variation of b/B between 3.2 and 4.2, confirming that with increase in the value of b/B more than 4.2 further substantial increased bearing capacity can not be expected. A similar pattern can be observed in increasing the values of PRS (decreasing the footing settlement), with increases in the reinforcement width.

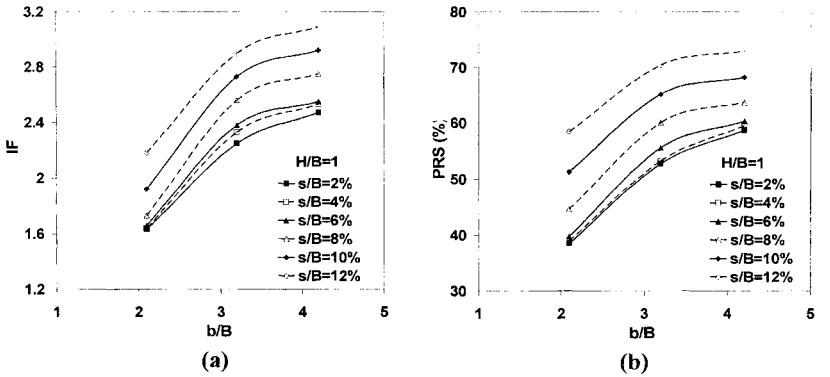

FIG. 5. Variation of the bearing capacity improvement factor (IF) and the percentage reduction in settlement (PRS) with geocell width (H/B=1), (a) IF and (b) PRS.

CONCLUSION

In this research, laboratory model tests results were used to investigate the potential benefits of reinforcing foundation sand with geocell-reinforcement in increasing bearing capacity and in decreasing settlement of a strip footing subjected to a monotonically increasing load. Based on the results obtained, the following conclusions can be extracted:

(1) Provision of the geocell reinforcement in reinforcing the sand layer significantly increases the load carrying capacity, reduces the footing settlement.

(2) Overall, when the height of geocell reinforcement (H/B) and the reinforcement width (b/B) increase, the bearing pressure of the foundation bed increases and the footing settlement decreases.

(4) The tests performed with different reinforcement widths indicate that increasing the reinforcement width more than 4.2 (approximately) times of footing width would not provide much additional improvement in bearing pressure and additional reduction in footing settlement.

(5) The values of IF and PRS increase steadily with an increase in the height of the geocell (H/B). The rate of reduction in footing settlement and the rate of enhancement in the load carrying capacity of the footing can also be seen to reduce with increase in the value of H/B.

(6) For the amounts of settlement that are tolerated in practical applications, improvements in bearing capacity greater than 200% and reductions in settlement by 75% can be achieved with the application of geocell reinforcement.

Although, the results presented herein provide encouragement for the application of geocell-reinforcement, the results of this study may be somewhat different to full-scale foundation behaviour in the field while the general trend may be similar.

REFRENCES

Alamshahi, S., Hataf, N. (2009). "Bearing capacity of strip footings on sand slopes reinforced with geogrid and grid-anchor." *Geotextiles and Geomembranes.* 27 (3): 217–226.

Cowland, J.W., Wong, S.C.K. (1993). "Performance of a road embankment on soft clay supported on a geocell mattress foundation." *Geotextiles and Geomembranes.* 12 (8): 687–705.

Dash, S.K., Krishnaswamy, N.R., Rajagopal, K. (2001). "Bearing capacity of strip footings supported on geocell-reinforced sand." *Geotextiles and Geomembranes.* 19 (4): 235–256.

Dash, S. K, Sireesh S, Sitharam, T. G. (2003). "Model studies on circular footing supported on geocell reinforced sand underlain by soft clay." *Geotextiles and Geomembranes.* 21 (4): 197–219

El Sawwaf., M.A. (2007). "Behaviour of strip footing on geogrid-reinforced sand over a soft clay slope." *Geotextile and Geomembranes.* 25 (1): 50-60.

Ghosh, A., Ghosh, A., Bera, A.K. (2005). "Bearing capacity of square footing on pond ash reinforced with jute-geotextile." *Geotextile and Geomembranes.* 23 (2): 144-173.

Jenner, C.G., Basset, R.H., Bush, D.I. (1988). "The use of slip line fields to asses the improvement in bearing capacity of soft ground given by cellular foundation mattress installed at the base of an embankment." *Proceedings of International Geotechnical Symposium on Theory and Practice of Earth Reinforcement. Balkema, Rotterdam:* 209–214.

Kolbsuzewski, J. (1948). "General investigation of the fundamental factors controlling loose packing of sands." *Proc. of the 2nd Int. Conf. on Soil Mech. And Found. Eng., Rotterdam.,* Vol. VII: 47-49.

Krishnaswamy, N.R., Rajagopal, K., Madhavi Latha, G. (2000). "Model studies on geocell supported embankments constructed over soft clay foundation." *Geotechnical Testing Journal.* ASTM 23 (1): 45–54.

Moghaddas Tafreshi, S.N., Khalaj, O. (2008). Laboratory tests of small-diameter HDPE pipes buried in reinforced sand under repeated load. Geotextiles and Geomembranes 26 (2), 145-163.

Patra, C.R., Das, B.M., Bohi, M., Shin, E.C. (2006). "Eccentrically loaded strip foundation on geogrid-reinforced sand." Geotextile and Geomembranes 24 (4): 254-259.

Sitharam, G., Sireesh, S. (2005). "Behavior of embedded footings supported on geogrid cell reinforced foundation beds." *Geotechnical Testing Journal.*, 28 (5), 452-463.

Sitharam, G., Sireesh, S., Dash, S.K. (2007). "Performance of surface footing on geocell-reinforced soft clay beds." *Geotech. Geol. Eng.* 25 (5): 509-524.

Sireesh, S., Sitharam, T.G., Dash, S.K. (2009). "Bearing capacity of circular footing on geocell–sand mattress overlying clay bed with void." *Geotextiles and Geomembranes.* 27 (2): 89–98.

Yoon, Y. W., Cheon, S. H., Kang, D. S. (2004). "Bearing capacity and settlement of tire-reinforced sands." *Geotextile and Geomembranes.* 22 (5): 439-453.

Macro-Mesoscopic Study Of The Interface Between Sand And Geogrid

Wang[1], J.Q.; Zhou, J.[2]; Deng, Y.B.[3]

[1]Doctor, Department of Civil Engineering, Guangxi University of Technology, Liuzhou, China; wjquan1999@163.com

[2]Professor, Key Laboratory of Geotechnical and Underground Engineering of Ministry of Education, Tongji University, Shanghai,China.; tjuzj@vip.163.com

[3] Doctor, Department of Ocean Environment&Engoneering Traffic,Shanghai Maritime University, Shanghai, China; dybing2000@163.com

ABSTRACT: The visual pullout model box was built, and a series of geogrid pullout tests were conducted to study the micro-macro feature of the soil/geogrid interface. Associating with image visual tracing technique and non-target measuring technique, displacement and shear strain field in the process of pullout was obtained. The results show that the apparent friction coefficient was related with the vertical stress. the sand particles show high gradient changes of displacement and concentration of shear strain in the interface region; the thickness of standard soil/geogrid interface is 6.5 times the average particle size. The study results contribute to providing a new understanding for more in-depth study on the mechanism of the reinforcement interface.

INTRODUCTION

Pullout test of geosynthetics has been studied for the purpose of making clear the pull-out mechanism of the reinforced soils by many researchers, and for understanding various factors affecting the pullout results, i.e., box size, sample size, sleeve length, front as well as side wall conditions, test speed, etc. (Palmeira and Milligan, 1989; Farrag et al., 1993; Sugimoto et al., 2001; Moraci and Recalcati, 2006). Experimental results (Moraci and Recalcati, 2006) showed that the reinforcement extensibility influences the peak pullout resistance. In particular, extensibility effects were more evident in long reinforcements and in high vertical confining stresses. Moraci and Gioffre (2006) proposed a theoretical method for determining peak and residual pullout resistances of extruded geogrids embedded in a compacted cohesionless soil.

Many scholars also conducted a micro-study of the interaction on the soil-structure interface. Yin et al. (1994) used a tiny "periscope" device buried in the concrete specimen to observe the relative displacement distribution along the contact surfaces, and pointed out that contact surface damage was a gradual development from the edge to the internal process. Zhang et al. (2006) used a newly developed micro-measurement techniques for measuring the shear interface test particle movement and pointed out that

the movement of soil particles significantly reduced with increasing distance from the structure, and the interface thickness is about 5 times the average particle diameter.

The purpose of this paper is to study the micro-macro feature of the soil/geogrid interface by conducting a series of pullout tests. The characteristics of macro-interface parameters of pullout test are reported. At the same time, using Olympus stereomicroscope, associating with image visual tracing technique and non-target measuring technique, the influence scope of size soil/geogrid interface and the law of sand particles movement are studied from mesoscopic view.

PULLOUT TEST APPARATUS

The visual model box size of 60cm × 40cm × 40cm (length × width × height), frame with angle iron welded together. In order to reduce the side wall friction, the tempered glass of 5mm thick was glued in the three iron inner side, and glass surface coated with a layer of silicone. To facilitate shooting micro-and macro picture of soil/geogrid interface during the course of pullout, the obverse side of model box is 12mm thick tempered glass. Loading system consists of vertical load and horizontal loading system.

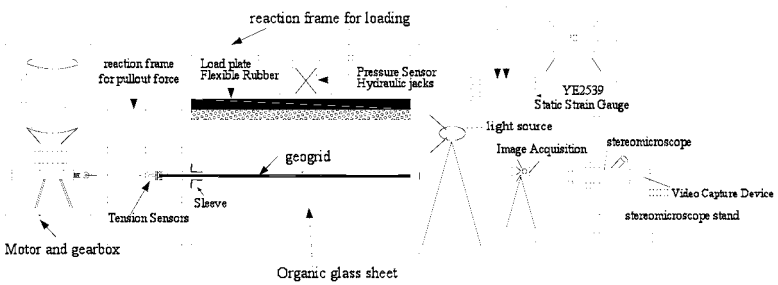

FIG. 1. pullout tests apparatus.

IMAGE CAPTURE DEVICE

The images of pullout test contain the macro and micro pictures. Macroscopic features was observed by using high-resolution digital photo capture, as shown in FIG.2, with 8 million pixels digital photos, 8-optical zoom Canon SLR 350D (image maximum resolution of 3456 × 2304) shooting. Auxiliary camera equipments are news lights, tripod, remote controller. The micro-observation system consists of the stereomicroscope, iodine-tungsten lamp light source, camera and computer, for observing soil particles characteristics.

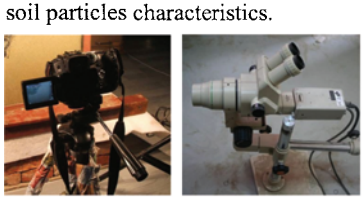

FIG. 2. Image Capture Device.

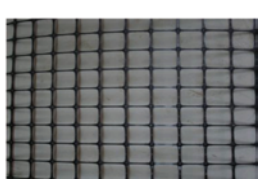

FIG. 3. Geogrid.

SOIL SAMPLES AND PREPARATION

SOIL SAMPLES AND PREPARATION

Soil samples of pullout test are used standard sand in Fujian,china. Sand specific density $\rho_s = 2.643$; maximum dry density and minimum dry density, respectively $\rho_{dmax} = 1.74 g/cm^3$, $\rho_{dmin} = 1.43 g/cm^3$; the maximum and minimum void ratio, respectively $e_{max} = 0.848$, $e_{min} = 0.519$; size composition of characteristic parameters: $d_{50} = 0.34mm$, $Cu = 1.542$, $Cc = 1.104$; the friction angle of sand: $\varphi=27.3°$.

Standard sand with falling rain method (falling height 60cm) layered into model box in order to prepare a homogeneous sand sample. Dense sand samples with a mean relative density of 66% by this method. After placing sand up to the pullout opening level, geogrid was placed on the top of the leveled sand and the front end of the geogrid was firmly connected to the loading shaft by the clamp. Sand was then placed in layers up to the top level.

In the course of pullout tests, using the digital camera to shoot continuously the entire pull-out test from the front wall of the model box, received a series of high-resolution digital photos that reflect the process of tests. At the same time, the micro-images of the reinforced soil interface particles can be obtained by using stereomicroscope to obtain.

MACRO-ANALYSIS OF TEST RESULTS

The biaxial geogrids were used in the test series(see FIG.3), and the geogrid properties is shown in Table 1. Pullout curve of geogrid is shown in FIG.4. We can see that the pullout resistance shows softening properties under low normal stress; and shows the trend of sustained growth when the normal stress is greater than 30kPa. The main reason is that on greater normal pressure (> 30kPa), the sand particles with each other is more compact, the friction of geogrid and the sand as well as the passive resistance of transverse ribs is significantly increasing, thus pullout curves showed the trend of sustained growth.

Table 1. Geogrid Physical Characteristics

Unit weight	Tensile strength of 2%	Tensile strength of 5%	Yield tensile strength	Yield elongation	Minimum carbon content
kg/m^2	KN/m	KN/m	KN/m	%	%
0.450	13.5	16.5	35	10.5	2

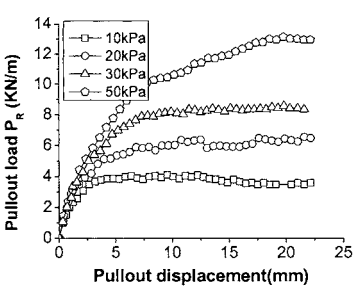

FIG. 4. Pullout curve of geogrid in standard sand.

In order to assess the interaction of reinforced soil interface, the reinforced soil interface friction coefficient is defined as the shear stress and normal stress ratio by many scholars(Moraci and Gioffre 2006; Moraci and Recalcati 2006), namely:

$$\mu_{sg} = \tau_{sg} / \sigma_v = P_R / (2\sigma_v LB) \quad (1)$$

where P_R is the pullout resistance (per unit width); L is the reinforcement length in the anchorage zone; B is the reinforcement width; σ_v is the vertical stress; τ_{sg} is the soil–geosynthetic interface shear stress; μ_{sg} is the soil–geosynthetic interface apparent coefficient of friction;

FIG.5 is the curve of normal stress and shear stress. The normal stress and shear stress are in good agreement with the linear, consistent with Mohr-Coulomb strength theory. The interface friction angle is 11.52°and the cohesion c of geogrid and soil is 1.22kPa. Relatively speaking, the interface friction angle is too small, it is because the sand particles uniform and smooth, and thus less friction with the geogrid.

FIG.6 shows change feature of the apparent friction coefficient vs vertical stress. We can find the apparent friction coefficient reduces with the vertical stress increasing. Before 30kPa of vertical stress, the apparent friction coefficient decreases fast, and after 30kPa, the change of apparent friction coefficient becomes slowly. The trend of changes betweenμ_{sg} and σ_v can be fitted into the following power function:

$$\mu_{sg} = 0.6803\sigma_v - 0.2772, \quad R^2 = 0.8632 \quad (2)$$

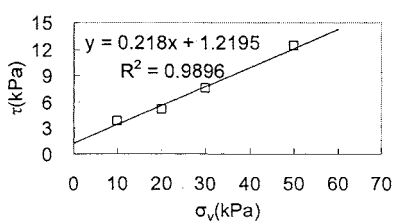

FIG. 5. Normal stress vs shear stress.

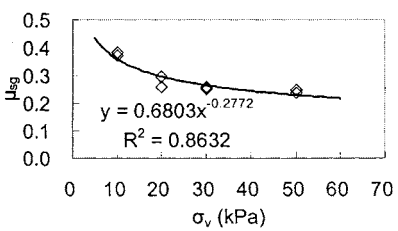

FIG. 6. μ_{sg} vs σ_v.

MICRO-ANALYSIS OF TEST RESULTS

Figure 7 is showed the displacement evolution of interface particle, combined with the video captured by stereomicroscope, we can observe: (1) With the geogrid be gradually pulled out, the thickness of the reinforced soil interface gradually thicken, and then tends to a stable values. (2) In the reinforced soil interface region of about 7 times the average particle size, the particles arises obviously displacement and rotation during pullout process, and the particles displacement of upper interface more obvious than lower interface particles. (3) In Figure 7, we can find that mark 1 on the upper interface does horizontal displacement and counterclockwise rotation with the grid pullout, and in the lower interface, the No. 2 mark points is mainly as translational motion, and

clockwise rotation.

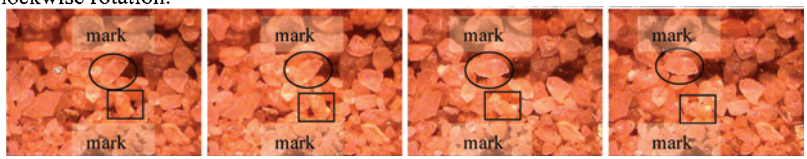

(a) at the beginning (b) Pullout 25s (c) Pullout 50s (d) Pullout 75s

FIG. 7. Interface particle displacement evolution map.

The deformation process of reinforced soil interface can be acquired by using non-target measuring technique to deal with continuous digital photo. FIG.8 shows the displacement field evolution law of the interface particles: (1) Sand displacement of the upper part of geogrid is greater than sand displacement of the lower part of geogrid. (2) At the beginning stage of pullout test, the geogrid develops displacement from the front to the back-end, and promote the sand particles of the interface rotary movement, which embodies ductile characteristics of the geogrid. When pullout displacement is 1.5mm, the reinforced soil interface displacement field has become quite obvious, and the upper and lower reinforced soil interface region has taken shape. (3) When the pullout displacement of 5mm or greater, the reinforced soil interface region has formed a relatively stable displacement zone, its thickness and this is reinforced soil interface of region. (4) The thickness of stable reinforced soil interface region is not the same along the interface, the overall thickness is slightly fluctuated in a constant value.

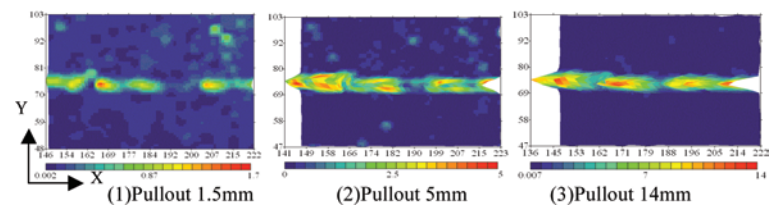

FIG. 8. Displacement field evolution map of reinforced soil interface.

The maximum shear strain development of the Y-cross-section was analyzed through the pictures that have formed the apparent stable interface region. FIG.9 shows the maximum shear strain of Y-section of the standard sand under the normal stress 20kPa. We can see that the interface region is the highest concentration region of shear strain. The interface shear strain of Y-section has formed two distinct peaks region. The peak region is the location of the interface region, interface thickness of reinforced soil can be acquire by quantitatively analyzing the region. Based on the test results of the analysis, the interface thickness is 2.0 ~ 2.6mm, approximately equivalent to 6.5 times the average particle size of the standard sand under the normal stress 20kPa.

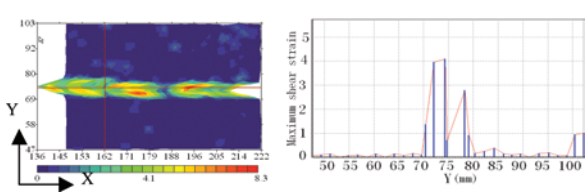

FIG. 9. The change of maximum shear strain along the Y-profile.

CONCLUSIONS

The main conclusions that can be drawn from this investigation are as follows:

(1) pullout resistance shows softening properties under low normal stress; and shows hardening characteristics when the normal stress is greater than 30kPa. The interface characteristic parameter like the apparent friction coefficient is not a constant. On analysis and comparison of the role of geosynthetics, we can not cast aside the vertical pressure and evaluate reinforcing effect only by the friction coefficient.

(2) Through stereomicroscope observation, standard soil/geogrid interface region is about 7 times the average particle size, in which the particles take place displacement and rotation during pullout process.

(3) When the pullout displacement is 5mm or greater, the reinforced soil interface has formed a relatively stable region of displacement and shear strain concentration zone with a stable reinforced soil interface thickness. The thickness of standard soil/geogrid interface is roughly equivalent to 6.5 times the average particle size of the standard sand.

ACKNOWLEDGMENTS

The authors appreciate the support of the Natural Science Foundation of China, Grant No.50879059.

REFERENCES

Farrag, K., Acar, Y.B., and Juran, I. (1993). "Pull-out resistance of geogrid reinforcements." *Geotextiles and Geomembranes*, 12, 133-159.

Moraci, N., and Gioffre, D. (2006). "A simple method to evaluate the pullout resistance of extruded geogrids embedded in a compacted granular soil." *Geotextiles and Geomembranes*, 24, 116-128.

Moraci, N., and Recalcati, P. (2006). "Factors affecting the pullout behaviour of extruded geogrids embedded in a compacted granular soil." *Geotextiles and Geomembranes*, 24, 220-242.

Palmeira, E. M., and Milligan, G.W.E. (1989). "Scale and other factors affecting the results of pull-out tests of grids buried in sand." *Geotechnique*, 39(3), 511-524.

Sugimoto, M., Alagiyawanna, A. M. N., and Kadoguchi, K. (2001). "Influence of rigid and flexible face on geogrid pullout tests." *Geotextiles and Geomembranes*, 19, 257-277.

Yin, Z., Zhu, H., and Xu, G. (1994). "Numerical Simulation of the Deformation in the Interface between Soil and Structural Material." *Chinese Jounal Of Geotechnical Engineering*, 16(3), 14-22.

Zhang, G., Liang, D., and Zhang, J. (2006). "Image analysis measurement of soil particle movement during a soil-structure interface test." *Computers and Geotechnics*, 33, 248-259.

Triaxial Compression and Extension Tests for Fiber-Reinforced Silty Sand

Cheng-Wei Chen [1], Ph.D.

[1] Director of Geotechnical Testing Laboratory, TRI/Environmental, Inc., 9063 Bee Caves Road, Austin, TX 78733, USA; cchen@tri-env.com

ABSTRACT: Inclusion of fibers to improve the engineering properties of compacted soil is becoming an increasingly common practice in geotechnical engineering projects. This study provides a better understanding of the engineering properties of fiber-reinforced soil to confirm the response with different loading conditions. An experimental study for consolidated-undrained ($\overline{CU}$) and consolidated-drained (CD) type triaxial compression and extension tests were performed on comparable unreinforced and fiber-reinforced specimens of silty sand to evaluate the effective stress-strain-pore pressure and effective stress-strain-volume change behavior. The results show that fibers increase the effective stress cohesion intercept (c') and effective stress friction angle (φ') in both triaxial compression and extension tests. In addition the fiber-reinforced silty sand specimens required a higher pore pressure to maintain the zero volume change in $\overline{CU}$ triaxial compression tests. The shear strength increases due to the fibers in triaxial extension test was significantly smaller than the strength increases in the triaxial compression test for both undrained and drained loading conditions. Moreover, the reinforced specimens begin to mobilizing the resistance at lower strains in both CD triaxial compression and extension tests. The results also indicate a rational way to evaluate the behavior of the fiber-reinforced silty sand, and therefore certainly warrant a better knowledge along diverse loading paths.

INTRODUCTION

The behavior of fiber-reinforced soils has been studied by several investigators over the last two decades. Fiber-reinforced soil is becoming a viable soil improvement method for geotechnical engineering problems. Fiber-reinforced soils are currently being used or considered for applications that include stabilization of shallow slope failures (Gregory and Chill 1998), construction of new embankments with marginal soils, reduction of shrinkage cracking in compacted clay liners (Rifai 2000), and to reinforce roadway subgrades (Santoni et al. 2001).

Fiber-reinforced soil is a mixture of soil and synthetic fibers. Synthetic fibers can be made of different materials, shapes and lengths. Polypropylene and polyester are the most common materials used to manufacture fibers. Fibers can be flat or round and

continuous or discrete. Discrete fibers are manufactured in several lengths, ranging from 12 mm to 76 mm, and are available in different types such as monofilament, fibrillated, tape, and mesh.

Significant research has been performed over the last few decades to evaluate basic shear strength properties and deformation characteristics of fiber-reinforced soils. Previous work has shown that an increase in fiber content generally increases the shear strength of soil. Most investigators have found that shear strength increases in direct proportion to fiber content or area ratio (Gray and Ohashi 1983, Gray and Al-Refeai 1986, Maher and Gray 1990, and Bauer and Oancea 1999). However, Shewbridge and Sitar (1989) observed that increase in strength was not proportional to the reinforcement concentration.

Some previous research has shown that inclusion of fibers increases both the cohesion intercept and angle of internal friction values as compared to values for unreinforced soil (Kumar et al. 1999, and Gregory and Chill 1998). However, Gray and Ohashi (1983) and Gray and Al-Refeai (1986) found that inclusion of fibers did not significantly affect the angle of internal friction, but rather that fiber-reinforced specimens exhibited bi-linear failure envelopes as a result of the existence of a critical confining stress below which the fibers tended to slip or pull-out. Consoli et al. (1998) observed an increase in the angle of internal friction but a decrease in the cohesion intercept. Bauer and Oancea (1999), and Consoli et al. (2003) found the friction angle to be barely affected by fiber inclusion whereas the cohesion intercept increased with increasing fiber content. As it can be seen, it is not clear that which statement is correct. Therefore, additional tests of fiber-reinforced soil are needed to confirm the response with different loading conditions.

TESTING MATERIALS AND PROGRAM

The soil used in the triaxial testing program was a loessial silty sand from Mound City, Missouri. The soil has a liquid limit of 27 and a plastic limit of 25 (plasticity index of 2). Grain size analyses show the soil contains a clay size fraction (passing #200 sieve) of 16 %. The soil classifies as silty sand (SM) according to the Unified Soil Classification System (ASTM D2487) and the specific gravity of the soil solids is 2.66. The maximum dry unit weight and optimum moisture content of the soil are 17.3 kN/m^3 and 16 %, respectively, according to the standard Proctor test (ASTM D698).

The fibers utilized in the testing program are commercially available 50 mm fibrillated polypropylene fibers with a specific gravity of 0.91. The ultimate tensile strength and modulus of elasticity of the fibers are 310 MPa and 4830 MPa, respectively.

Soil samples for all tests were prepared in the same manner to ensure consistency between the reinforced and fiber-reinforced specimens. After mixing of the soil, water, and reinforcing fibers (0.4 % by dry soil weight), all specimens were compacted in a 74 mm diameter by 145 mm tall cylindrical mold using a compactive effort that is approximately equal to that used in the standard Proctor (600 $kN\text{-}m/m^3$). The compactive effort was held constant for all molding water content of 18 %, which was 2 % wet of optimum moisture content. Following compaction, the specimens were extruded from the compaction mold and immediately set up in the triaxial cell. Again,

the initial densities were measured for each specimen of 17.2 kN/m^3, nominally. More details on the samples preparation and compaction were reported by Chen (2007).

Table 1 summarized the testing program for the silty sand used to evaluate the stress-strain behavior of unreinforced and reinforced specimens in terms of effective stresses. An experimental study for consolidated-undrained ($\overline{CU}$) and consolidated-drained (CD) type triaxial compression and extension tests were performed on comparable unreinforced and fiber-reinforced specimens of silty sand to evaluate the effective stress-strain-pore pressure and effective stress-strain-volume change behavior. All specimens were back-pressure saturated according to the procedures suggested in the ASTM D4767. Skempton's pore pressure coefficient, B, (Skempton, 1954) was checked (at least 0.95) on a regular basis to make sure that the specimens were saturated before consolidation and shearing. Following saturation, specimens were isotropically consolidated in one load increment to the desired effective stress of 69 kPa and 276 kPa. All specimens were sheared to failure at a strain rate of 1.25 %/hr (deformation rate of 1.8 mm/hr) up to a maximum axial strain of 30 % to permit evaluation of the post-peak stress-strain behavior.

Table 1. A List of Triaxial Tests of Unreinforced and Reinforced Specimens

Type of Triaxial Testing	Fiber Content (%)	Triaxial Compression Effective Confining Stress 69 kPa	Triaxial Compression Effective Confining Stress 276 kPa	Triaxial Extension Effective Confining Stress 69 kPa	Triaxial Extension Effective Confining Stress 276 kPa
$\overline{CU}$	0	1	1	1	1
	0.4	1	1	1	1
CD	0	1	1	1	1
	0.4	1	1	1	1

STRESS-STRAIN-PORE PRESSURE RESPONSES

The stress-strain observed for unreinforced and fiber-reinforced silty sand specimen for both triaxial $\overline{CU}$ compression and extension tests is shown in Fig 1. The test results are plotted as deviatoric stress (q) versus triaxial shear strain (ε_q), where

$$q = \sigma_v' - \sigma_h' \qquad (1)$$

in which σ_v' and σ_h' are the principal effective stresses in the vertical and horizontal direction.

$$\varepsilon_q = \varepsilon_a - \frac{1}{3}\varepsilon_v \qquad (2)$$

in which ε_a is the axial strain and ε_v is the volumetric strain.

As shown in Fig. 1, the typical stress-strain behavior observed for all fiber-reinforced silty sand specimens in triaxial compression tests is a strain-hardening response with no noticeable peak stress at strains up to 30 %. This has been noted in numerous previous investigations. However, the stress-strain responses for the unreinforced and reinforced specimen in triaxial extension are similar and showed a slightly higher perk deviatoric stress at moderate strains (10 %).

In undrained loading conditions, the pore pressures in the soil specimens are known

to change during shearing to maintain a zero volume change condition. The pore pressure change versus shear strain responses for unreinforced and reinforced silty sand specimens are shown in Fig. 2 for specimens compacted at 18 % water content. In general, the pore pressures increase at small strains (up to 2 %); significantly decrease with additional strains (from 2 % to 20 %) for the unreinforced specimens. The initial increases in pore pressure at small strains are similar or slightly greater for reinforced specimens than for unreinforced specimens in triaxial compression tests. More importantly, the decrease in pore pressures observed for the reinforced specimens tend to level off at intermediate strains and was significantly less than that observed for the unreinforced specimens in triaxial compression tests.

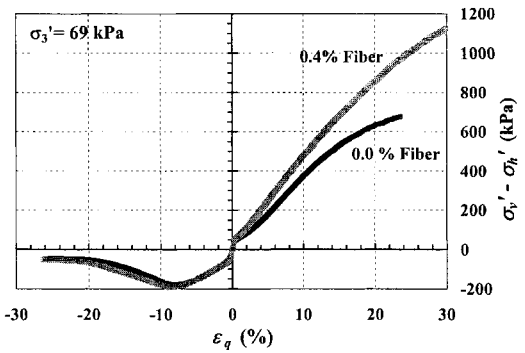

FIG. 1. Deviatoric stress versus triaxial shear strain curves from $\overline{CU}$ compression and extension tests.

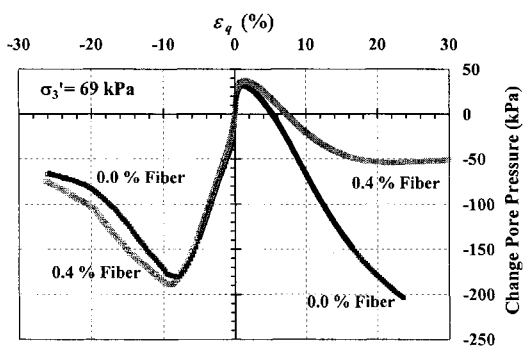

FIG. 2. Pore pressure changes versus triaxial shear strain curves from $\overline{CU}$ compression and extension tests.

In contrast, the pore pressures decrease at moderate strains (up to 8 %), start increasing with additional strains (from 10 % to 20 %t), and tend to level off at very large strains for the unreinforced specimens in triaxial extension tests. The initial decrease in pore pressure at small strains are followed the same path for reinforced

specimens in triaxial extension tests. However, the increase in pore pressures observed for the reinforced specimens at intermediate strains was slightly less than that observed for the unreinforced specimens in triaxial extension tests.

STRESS-STRAIN-VOLUME CHANGE RESPONSES

The typical volumetric strain versus triaxial shear strain response from CD triaxial compression and extension tests for the unreinforced and reinforced silty specimens are shown in Fig. 3. The volumetric strain (ε_v) was calculated.

$$\varepsilon_v = \frac{\Delta V}{V_c} \qquad (3)$$

where ΔV is the volume change measured during shearing and V_c is the specimen volume after the isotropic consolidation, which is

$$V_c = V_0 - \Delta V_c \quad (4)$$

where V_0 is the initial volume of specimen and ΔV_c is the volume change caused by consolidation and measured on the volume-change burette.

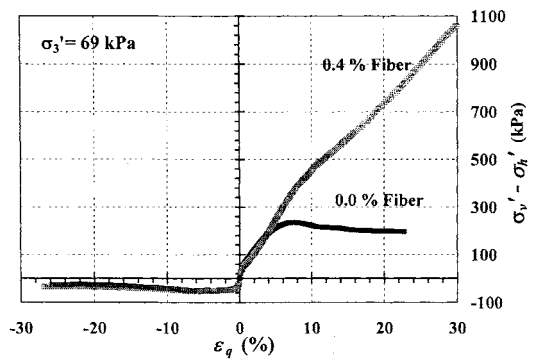

FIG. 3. Deviatoric stress versus triaxial shear strain curves from *CD* compression and extension tests.

For CD triaxial compression, unreinforced specimens consolidated to low effective stresses of about 69 kPa or less showed peak stresses at 5 % strain or less, while those consolidated to higher effective stresses required greater strain to reach the peak stress. The fiber-reinforced silty sand specimens show a strain-hardening behavior similar to that of the undrained tests for the reinforced specimens. In these tests, there was generally no noticeable peak stress observed except at the highest effective confining stresses, where peak stresses were observed at approximately 25 % strain. However, the peak stress didn't increased significantly for the reinforced specimens under extension loading condition, which is similar for those tested in the undrained tests.

As seen in Fig. 3, the stress-strain responses of fiber-reinforced silty sand specimens begin to deviate from that of the unreinforced specimens at 5 % strains for specimens compacted at 18 % water content. Note that the difference in terms of unreinforced

and reinforced specimens are greater in drained tests than for those tested in undrained tests (Fig. 1) at the same level of triaxial shear strain. This suggests that fibers in the specimen mobilize resistance at lower strains in drained tests. This is presumably due to the volume change that is allowed in drained tests, more details can be found in Romero (2003) and Chen (2007).

Volumetric strain versus the triaxial shear strain responses observed in the *CD* test for unreinforced and reinforced silty sand specimens are shown in Fig. 4. The unreinforced specimens revealed classical response in triaxial compression tests for compacted soils compression at small strains followed by significant dilation as they reached larger strains. The amount of dilation was observed to decrease with increasing effective confining stresses. Fiber-reinforced silty sand specimens revealed similar volumetric strain response with initial compression at small strains followed by dilation. However, the amount of dilation observed for the reinforced specimens was significantly less than that of the unreinforced specimens.

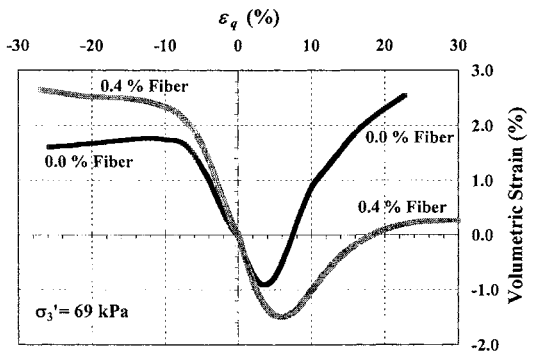

FIG. 4. Volumetric strain versus triaxial shear strain curves from *CD* compression and extension tests.

In Fig. 4, the unreinforced specimens in triaxial extension tests shown a significant initial dilation at small strains and tend to level off or slightly decease as they reached moderate strain. Fiber-reinforced specimens demonstrated higher volumetric strain response at very small strain and tend to level off or slightly increase as they reached moderate strain of 10 %. The volumetric strain for fiber-reinforced silty sand specimens began to deviate from that of the unreinforced specimens at strains of 1 to 4 % in both triaxial compression and extension loading conditions. This, in turn, again suggests that volumetric strain plays an important role in mobilization of fiber resistance.

Values of the effective stress cohesion intercept, c', and the effective stress friction angle, ϕ', for these envelopes are summarized in Table 2. The shear strength of the fiber-reinforced silty sand specimens compacted at 18 % moisture content can be represented by an effective stress cohesion intercept of 0 kPa and angle of internal friction of 54.4° in triaxial $\overline{CU}$ compression tests, while the effective stress cohesion intercept of 0 kPa and angle of internal friction of 26.5° in triaxil $\overline{CU}$ extension tests.

The results show that the shear strength increases due to the fibers in triaxial extension test was significantly smaller than the strength increases in the triaxial compression test. It is also observed for both undrained and drained loading conditions.

Table 2. Mohr-Coulomb Strength Parameters, c' and ϕ', for Triaxial Tests of Unreinforced and Reinforced Specimens

Type of Triaxial Testing	Fiber Content (%)	Triaxial Compression		Triaxial Extension	
		c' (kPa)	ϕ' (deg)	c' (kPa)	ϕ' (deg)
$\overline{CU}$	0	0	33.7	0	25.1
	0.4	0	54.4	0	26.5
CD	0	12	36.1	0	25.6
	0.4	142	44.5	0	26.2

Typical failure modes for the unreinforced and fiber-reinforced specimens from triaxial extension tests are shown in Fig. 5. It was observed that the middle bottom of the both unreinforced and reinforced specimens reveal localized deformation in the form of necking failure. In addition, the unreinforced specimen developed smaller area of necking failure than the fiber-reinforced specimens tested in the same loading condition.

(a) 18 % water content, 0 % fiber

(b) 18 % water content, 0.4 % fiber

FIG. 5. Typical failure modes of the $\overline{CU}$ extension tests for silty sand specimens consolidated to 276 kPa effective consolidation stress.

CONCLUSIONS

The results of the triaxial tests performed on silty sand show that inclusion of fibers can improve the strength of soils under undrained and drained loading conditions. Shear strength parameters of effective stress cohesion intercept and friction angle increase significantly in the $\overline{CU}$ and CD triaxial compression tests, due to the addition of fibers. The shear strength increases due to the fibers in triaxial extension test was significantly smaller than the strength increases in the triaxial compression test for both undrained and drained loading conditions.

It is noted the reinforcing fibers alter the pore pressure response of specimens tested under undrained loading conditions and the volume change response of specimens

tested under drained loading condition for both compression and extension tests. The fiber-reinforced specimens required a higher pore pressure to maintain the zero volume change in triaxial compression tests. Moreover, resistance due to the fiber reinforcement is mobilized at lower strains in drained tests than in undrained tests. This suggests that volumetric strain plays an important role in mobilization of fiber resistance. The results also indicate a rational way to evaluate the behavior of the fiber-reinforced silty sand, and therefore certainly warrant a better knowledge along diverse loading paths.

ACKNOWLEDGMENTS

The experimental work was carried out in the Geotechnical laboratory in the Department of Civil and Environmental Engineering, University of Missouri-Columbia. The encouragement and support of Dr. J. Erik Loehr is always appreciated.

REFERENCES

Bauer, G., and Oancea, A. (1999). "Soils reinforced with discrete synthetic fibers." Geosynthetics'99– Specifying Geosynthetics and Developing Design Detail, IFAI, Boston, MA, 465-475.

Chen, C-W. (2007). "A constitutive model for fiber-reinforced soils." Dissertation submitted in partial fulfillment for the requirements of the Doctoral Degree, University of Missouri-Columbia.

Consoli, N.C., Prietto, P.D.M., and Ulbrich, L.A. (1998). "Influence of fiber and cement addition on behavior of sandy soil." Journal of the Geotechnical and Geoenvironmental Engineering, 124(12), 1211-1214.

Consoli, N. C., Casagrande, M.D.T., Prietto, P.D.M., and Thome, A. (2003). "Plate load test on finer-reinforced soil." Journal of the Geotechnical and Geoenvironmental Engineering, 129(10), 951-955.

Gray, D.H., and Ohashi, H. (1983). "Mechanics of fiber reinforcement in sand." Journal of the Geotechnical Engineering, 109(3), 335-353.

Gray, D.H., and Al-Refeai, T. (1986). "Behavior of fabric- versus fiber-reinforced sand," Journal of the Geotechnical Engineering Division, ASCE, 112(8), 804-820.

Gregory, G.H., and Chill, D.S. (1998) "Stabilization of earth slopes with fiber reinforcement." Proceedings of the Sixth International Conference on Geosynthetics, Atlanta, Georgia, 1073-1078.

Kumar, R., Kanaujia, V.K., and Chandra, D. (1999). "Engineering Behaviour of Fibre-Reinforced Pond Ash and Silty Sand," Geosynthetics International, 6(6), 509-518.

Maher, M.H., and Gray, D.H. (1990). "Static response of sands reinforced with randomly distributed fibers." Journal of the Geotech. Eng., 116(11), 1661-1677.

Rifai, S.M. (2000). "Impact of polypropylene fibers on desiccation cracking and hydraulic conductivity of compacted clay liners." Dissertation submitted in partial fulfillment for the requirements of the Doctoral Degree, Wayne State University,Detroit, Michigan.

Romero, R.J. (2003). "Development of a constitutive model for fiber-reinforced soils." Dissertation submitted in partial fulfillment for the requirements of the Doctoral

Degree, University of Missouri-Columbia.
Santoni, R.L., Tingle, J.S., and Webster, S.L. (2001). "Engineering properties of sand-fiber mixtures of road construction." Journal of the Geotechnical and Geoenvironmental Engineering, 127(3), 258-268.
Shewbridge, S.E., and Sitar, N. (1989). "Deformation characteristics of reinforced soil in direct shear." Journal of the Geotechnical and Geoenvironmental Engineering, 115(8), 1134-1147.
Skempton, A.W. (1954). "The pore pressure coefficient A and B." Geotechnique, 4, 143-47.

This page intentionally left blank

Author Index

Page number refers to the first page of paper

Adams, Tiffany E., 119
Ahmed, Aly, 165
Archeewa, Ekarut, 255
Asaoka, Akira, 149
Aschauer, Franz, 295
Atapek, B. Alp, 131
Attin, Antonella, 302

Bai, Xiao, 275

Cali, Peter R., 119
Cao, Yanbo, 44
Cao, Yonghua, 263
Casciano, Antonio, 302
Chao, Sao, 282
Chen, Cheng, 269, 367
Chen, Yekai, 239
Cheng, Dongdong, 263
Chikyala, Srujan R., 155

Dawson, A. R., 353
Deng, An, 113
Deng, Y. B., 361
Deng, Yongfeng, 107
Ding, J., 220
Dong, Yan, 275
Du, Yanjun, 65
Dubey, Himanshu, 38

Egan, Derek, 197

Fan, Jian, 287
Feng, Weijiang, 107
Filz, George M., 119

Ge, Louis, 269
Gong, Nenghe, 65

Hamidi, Babak, 87
Han, Jie, 99, 275, 287, 318
Han, Jinping, 212
Hara, Takashi, 53, 205
Harris, Pat J., 155
Hazarika, Hemanta, 338
He, Jie, 79
He, Yufei, 31
Hong, Liao S., 181
Horpibulsuk, Suksun, 137
Hossain, Shahin Md., 310
Hu, Da, 79
Hu, Xiang, 255
Huang, Jie, 318
Huang, Xian, 287
Hyodo, Masayuki, 338

Ilamparuthi, K., 174
Ishii, Kenji, 310
Ivanetich, Ken, 125

Jiang, Geng Bo, 187
Jing, Fei, 65, 107

Kalita, Ajanta, 143
Kamei, Takeshi, 165
Khabbaz, Hadi, 249
Kikuchi, Yoshiaki, 1
Kikumoto, Mamoru, 310
Knott, R., 220

Li, Xiaobing, 71
Li, Xin, 59
Lin, Yong, 59
Liu, Jie, 79
Liu, Li, 99
Liu, Songyu, 65, 107

Lou, Xiao Ming, 187

McCabe, Bryan A., 197
Min, Chang, 79
Muttharam, M., 174

Nagatome, Takeshi, 1
Nakai, Teruo, 310
Nakano, Masaki, 149
Nasrizar, Amir Asad, 174
Nazarian, Soheil, 255
Nikraz, Hamid, 87

Pan, Linyou, 71
Peng, Fangle, 44
Praticò, Filippo G., 302
Puppala, Anand J., 155, 255, 328

Qiu, Changlin, 346

Raksachon, Yuttana, 137
Ren, Chao, 239
Roy, Debasis, 38

Saride, Sireesh, 155, 255, 328
Sawada, Kazuhide, 53
Schoen, Harald, 295
Schwanz, Neil T., 119
Shahin, Mohamed A., 181
Shao, Lisheng, 125
Shrestha, Binod, 249
Siddiquee, M. S. A., 44
Singh, Baleshwar, 93, 143
Singh, Raghvendra, 38
Sitharam, T. G., 328
Sun, Kai, 149

Tafreshi, S. N. Moghaddas, 353
Tan, Ke, 44
Tatta, Naoki, 53
Teymur, Berrak, 131
Tramontana, Domenico, 302
Tsuji, Shinichiro, 53, 205

Ugai, Keizo, 165

Varaksin, Serge, 87
Vester, R., 220
Vinot, V., 93

Wang, J. Q., 361
Wang, Mingwu, 212
Wang, Yimin, 239
Watanabe, Asami, 310
Williammee, Richard, Jr., 255
Woodward, Mark L., 119
Wu, Wei, 295

Xiao, Jie, 31
Xu, Hong Yue, 187
Xu, Shi, 113

Yamada, Eiji, 149
Yan, Feng, 287
Yan, Shuwang, 346
Yan, Yue, 346
Yang, Heping, 31
Yang, Jingfang, 263
Yashima, Atsushi, 53, 205
Yasuhara, Kazuya, 338
Yi, Yaolin, 65
Yoshida, Masaki, 205
Yu, Chuang, 71
Yu, Rui, 255

Zhang, Feng, 310
Zhang, Jia Sheng, 269
Zhang, Ke, 79
Zhang, Meng, 59
Zhao, Fei, 255
Zheng, Gang, 99, 346
Zheng, Junjie, 318
Zhou, J., 361

Subject Index

Page number refers to the first page of paper

Asphalt pavements, 302

Barriers, 295
Bridges, 255
Buildings, 79

Case studies, 255
Cement, 1, 65, 125, 131, 137, 143, 181
China, 71, 113, 255, 263, 287
Clays, 1,107, 137, 181
Columns, 65, 125, 197, 318
Composite materials, 79
Concrete construction, 87
Construction, 220
Construction materials, 31, 155, 197, 346
Cracking, 302

Differential settlement, 239
Dikes, 346
Drainage, 220
Dredging, 113, 149

Earthquake loads, 338
Economic factors, 31, 295
Elasticity, 187
Embankments, 38, 65, 99, 187, 220, 239
Emissions, 87
Estimation, 38
Expansive soils, 174
Experimentation, 79, 93

Failures, 44
Falling bodies, 205
Fences, 205
Fiber reinforced materials, 367
Field tests, 205
Finite element method, 269
Fly ash, 137, 143
Foam, 1
Footings, 353
Foundations, 107, 287, 328
Freezing, 255

Geogrids, 275, 361
Geomaterials, 1, 149, 282, 287, 295, 302, 310, 318, 346
Grouting, 125
Gypsum, 165

Harbors, 149
Highways and roads, 107, 205

Infrastructure, 71

Japan, 149, 205

Laboratory tests, 353
Lateral loads, 99
Layered soils, 65, 263
Life cycles, 302
Limit analysis, 59
Load bearing capacity, 79, 275
Load transfer, 187

Mechanical properties, 131, 149, 310
Micro piles, 212
Microstructures, 137
Mixing, 65, 125
Mixtures, 131, 338
Model tests, 353

Noise pollution, 295
Numerical analysis, 99, 205
Numerical models, 212

Optimization, 119
Organic matter, 155, 174

Parameters, 318
Pavements, 93, 239, 255
Pile foundations, 53, 71, 187
Piles, 79, 99, 119
Predictions, 328
Prefabrication, 220
Preloading, 31
Procurement, 87
Pullout, 361

Reinforcement, 53, 59, 249, 282, 318
Retaining walls, 44, 282, 310
Rocks, 205
Rubber, 181

Safety, 255
Sand, material, 338
Sand, soil type, 31, 44, 93, 131, 165, 275, 328, 353, 361, 367
Sediment, 220
Settlement, 107, 197, 328
Shear strength, 38, 93
Shear walls, 119
Slope stability, 220
Slopes, 59
Soft soils, 31, 71, 107, 239, 263
Soil compaction, 113
Soil compression, 367
Soil consolidation, 38, 113, 263
Soil deformation, 44
Soil liquefaction, 212, 338
Soil stabilization, 87, 143, 212, 249, 255
Soil structures, 53, 59, 269, 282, 310
Soils, 125, 143, 155, 255
Stabilization, 287
Static loads, 275
Stiffness, 181
Subgrades, 155

Temperature effects, 174
Texas, 255
Tires, 131, 181
Traffic volume, 239
Tubes, 346

Vegetation, 295
Vertical loads, 44

Walls, 119, 269, 295
Waste management, 165
Water content, 174, 263
Waterfront structures, 1